

# **Cable Supported Bridges**

# **Cable Supported Bridges**

Concept and Design, Third Edition

**NIELS J. GIMSING**  
**CHRISTOS T. GEORGAKIS**

Department of Civil Engineering  
Technical University of Denmark



A John Wiley & Sons, Ltd., Publication

This edition first published 2012  
© 2012, John Wiley & Sons, Ltd

First Edition published in 1983  
Second Edition published in 1997

*Registered office*

John Wiley & Sons Ltd, The Atrium, Southern Gate, Chichester, West Sussex, PO19 8SQ, United Kingdom

For details of our global editorial offices, for customer services and for information about how to apply for permission to reuse the copyright material in this book please see our website at [www.wiley.com](http://www.wiley.com).

The right of the author to be identified as the author of this work has been asserted in accordance with the Copyright, Designs and Patents Act 1988.

All rights reserved. No part of this publication may be reproduced, stored in a retrieval system, or transmitted, in any form or by any means, electronic, mechanical, photocopying, recording or otherwise, except as permitted by the UK Copyright, Designs and Patents Act 1988, without the prior permission of the publisher.

Wiley also publishes its books in a variety of electronic formats. Some content that appears in print may not be available in electronic books.

Designations used by companies to distinguish their products are often claimed as trademarks. All brand names and product names used in this book are trade names, service marks, trademarks or registered trademarks of their respective owners. The publisher is not associated with any product or vendor mentioned in this book. This publication is designed to provide accurate and authoritative information in regard to the subject matter covered. It is sold on the understanding that the publisher is not engaged in rendering professional services. If professional advice or other expert assistance is required, the services of a competent professional should be sought.

*Library of Congress Cataloguing-in-Publication Data*

Gimsing, Niels J.

Cable supported bridges : concept and design / Niels J. Gimsing, Christos T. Georgakis. — 3rd ed.  
p. cm.

Includes bibliographical references and index.

ISBN 978-0-470-66628-9 (cloth)

I. Cable-stayed bridges. 2. Suspension bridges. I. Georgakis, Christos T.  
II. Title.

TG405.G55 2012

624.2'38—dc23

2011024092

A catalogue record for this book is available from the British Library.

Set in 9/11pt, Times Roman by Thomson Digital, Noida, India

# Contents

|  |           |
|--|-----------|
| <i>Preface to the Third Edition</i>                            | <i>ix</i> |
| <b>Introduction</b>  | <b>1</b>  |
| <b>1 Evolution of Cable Supported Bridges</b>                  | <b>7</b>  |
| <b>2 Cables</b>  | <b>85</b> |
| 2.1 Basic Types of Cables                                      | 85        |
| 2.1.1 Helical bridge strands (spiral strands)                  | 85        |
| 2.1.2 Locked-coil strands                                      | 87        |
| 2.1.3 Parallel-wire strands for suspension bridge main cables  | 88        |
| 2.1.4 New PWS stay cables                                      | 90        |
| 2.1.5 Parallel-strand stay cables                              | 91        |
| 2.1.6 Bar stay cables  | 93        |
| 2.1.7 Multi-strand stay cables                                 | 94        |
| 2.1.8 Parallel-wire suspension bridge main cables              | 97        |
| 2.1.9 Comparison between different cable types                 | 101       |
| 2.2 Corrosion Protection                                       | 102       |
| 2.2.1 Suspension bridge main cables                            | 102       |
| 2.2.2 Stay cables  | 105       |
| 2.3 Mechanical Properties                                      | 109       |
| 2.3.1 Static strength  | 109       |
| 2.3.2 Relaxation   | 111       |
| 2.3.3 Fatigue strength   | 111       |
| 2.3.4 Hysteresis of helical strands                            | 113       |
| 2.4 The Single Cable as a Structural Element                   | 115       |
| 2.4.1 Transversally loaded cable                               | 115       |
| 2.4.2 Axially loaded cable                                     | 126       |
| 2.5 Static Analysis of Cables                                  | 131       |
| 2.5.1 Equation of state for a cable subjected to vertical load | 132       |
| 2.5.2 Stay cable under varying chord force                     | 135       |
| 2.5.3 Limit length and efficiency ratio of a stay cable        | 143       |
| 2.6 Bending of Cables  | 148       |
| 2.7 Dynamic Behaviour of the Single Cable                      | 157       |

|          |   |            |
|----------|---|------------|
| <b>3</b> | <b>Cable System</b>   | <b>165</b> |
| 3.1      | Introduction  | 165        |
| 3.1.1    | Pure cable systems  | 165        |
| 3.1.2    | Cable steel quantity comparison   | 170        |
| 3.1.3    | Stability of the cable system   | 173        |
| 3.2      | Suspension System   | 179        |
| 3.2.1    | Dead load geometry  | 179        |
| 3.2.2    | Preliminary cable dimensions  | 180        |
| 3.2.3    | Quantity of cable steel   | 182        |
| 3.2.4    | Quantity in the pylon   | 184        |
| 3.2.5    | Total cost of cable system and pylon  | 185        |
| 3.2.6    | Optimum pylon height  | 185        |
| 3.2.7    | Size effect   | 187        |
| 3.2.8    | Structural systems  | 188        |
| 3.3      | Fan System  | 202        |
| 3.3.1    | Anchor cable  | 202        |
| 3.3.2    | Preliminary cable dimensions  | 205        |
| 3.3.3    | Quantity of cable steel   | 206        |
| 3.3.4    | Quantity in the pylon   | 208        |
| 3.3.5    | Simplified expressions  | 208        |
| 3.3.6    | Total cost of cable systems and pylons                                      | 209        |
| 3.3.7    | Comparison between suspension and fan system                                | 209        |
| 3.3.8    | Inclined pylons   | 210        |
| 3.3.9    | Deformational characteristics   | 213        |
| 3.3.10   | Structural systems  | 217        |
| 3.3.11   | Reduction of sag variations   | 221        |
| 3.4      | Harp System   | 222        |
| 3.4.1    | Dead load geometry  | 225        |
| 3.4.2    | Intermediate supports   | 226        |
| 3.4.3    | Preliminary cable dimensions  | 227        |
| 3.4.4    | Quantity of cable steel   | 229        |
| 3.4.5    | Quantity of the pylon   | 229        |
| 3.4.6    | Simplified expressions  | 231        |
| 3.4.7    | Total cost  | 231        |
| 3.4.8    | Structural systems  | 231        |
| 3.5      | Hybrid Suspension and Cable Stayed System                                   | 235        |
| 3.6      | Multi-Span Cable System   | 239        |
| 3.6.1    | True multi-span cable supported bridges                                     | 241        |
| 3.6.2    | Non-traditional multi-span suspension bridges                               | 246        |
| 3.6.3    | Fixing of column-type pylons to piers                                       | 249        |
| 3.6.4    | Triangular pylon structures   | 250        |
| 3.6.5    | Horizontal tie cable between pylon tops                                     | 258        |
| 3.6.6    | Comparison between deflections of different multi-span cable stayed systems | 261        |
| 3.7      | Cable Systems under Lateral Loading   | 265        |
| 3.8      | Spatial Cable Systems   | 272        |
| 3.9      | Oscillation of Cable Systems  | 278        |
| 3.9.1    | Global oscillations   | 278        |
| <b>4</b> | <b>Deck (Stiffening Girder)</b>   | <b>287</b> |
| 4.1      | Action of the Deck  | 287        |
| 4.1.1    | Axial stiffness   | 287        |

|          |  |            |
|----------|--|------------|
| 4.1.2    | Flexural stiffness in the vertical direction                             | 287        |
| 4.1.3    | Flexural stiffness in the transverse direction                           | 289        |
| 4.1.4    | Torsional stiffness  | 291        |
| 4.2      | Supporting Conditions  | 291        |
| 4.3      | Distribution of Dead Load Moments  | 299        |
| 4.3.1    | The dead load condition  | 302        |
| 4.4      | Cross Section  | 310        |
| 4.4.1    | Bridge floor   | 310        |
| 4.4.2    | Cross section of the deck  | 310        |
| 4.4.3    | Cross section of stiffening trusses                                      | 328        |
| 4.5      | Partial Earth Anchoring  | 339        |
| 4.5.1    | Limit of span length for self-anchored cable stayed bridges              | 343        |
| 4.5.2    | Axial compression in the deck of the self anchored cable stayed bridge   | 344        |
| 4.5.3    | Lateral bending of the deck  | 346        |
| 4.5.4    | Partial earth anchoring of a cable stayed bridge                         | 346        |
| 4.5.5    | Improving the lateral stability  | 348        |
| 4.5.6    | Construction procedure for partially earth anchored cable stayed bridges | 349        |
| <b>5</b> | <b>Pylons</b>  | <b>353</b> |
| 5.1      | Introduction   | 353        |
| 5.2      | Structural Behaviour of the Pylon  | 353        |
| 5.3      | Pylons Subjected Primarily to Vertical Forces from the Cable System      | 367        |
| 5.4      | Pylons Subjected to Longitudinal Forces from the Cable System            | 399        |
| 5.5      | Cross Section  | 405        |
| <b>6</b> | <b>Cable Anchorage and Connection</b>                                    | <b>413</b> |
| 6.1      | Anchoring of the Single Strand   | 413        |
| 6.2      | Connection between Cable and Deck  | 427        |
| 6.3      | Connection between Main Cable and Hanger                                 | 433        |
| 6.4      | Connection between Cable and Pylon                                       | 442        |
| 6.5      | Connection between Cable and Anchor Block                                | 452        |
| <b>7</b> | <b>Erection</b>  | <b>463</b> |
| 7.1      | Introduction   | 463        |
| 7.2      | Construction of Pylons   | 463        |
| 7.3      | Erection of Suspension Bridge Main Cables                                | 472        |
| 7.4      | Erection of Stay Cables  | 486        |
| 7.5      | Deck Erection - Earth Anchored Suspension Bridges                        | 489        |
| 7.6      | Deck Erection - Self Anchored Cable Stayed Bridges                       | 501        |
| <b>8</b> | <b>Aerodynamics</b>  | <b>517</b> |
| 8.1      | Historical Overview  | 517        |
| 8.1.1    | Nineteenth-century bridge failures                                       | 517        |
| 8.1.2    | Tacoma Narrows Bridge collapse   | 517        |
| 8.1.3    | The Carmody Board  | 520        |
| 8.1.4    | The Fykkesund Bridge   | 520        |
| 8.2      | The Bridge Deck and Pylon  | 520        |
| 8.2.1    | Torsional divergence   | 520        |
| 8.2.2    | Coupled flutter  | 524        |
| 8.2.3    | Buffeting  | 526        |

|          |   |            |
|----------|---|------------|
| 8.2.4    | Vortex-shedding                             | 531        |
| 8.2.5    | Wind tunnel testing                         | 532        |
| 8.2.6    | During construction                         | 537        |
| 8.2.7    | Effects of vehicles                         | 538        |
| 8.2.8    | Pylon aerodynamics                          | 538        |
| 8.2.9    | Vibration control                           | 541        |
| 8.2.10   | Future trends                               | 543        |
| 8.3      | Cables                                      | 544        |
| 8.3.1    | Introduction                                | 544        |
| 8.3.2    | Incidences of wind-induced cable vibrations | 544        |
| 8.3.3    | Rain-wind-induced vibrations                | 545        |
| 8.3.4    | Dry galloping                               | 546        |
| 8.3.5    | Scruton number                              | 549        |
| 8.3.6    | Wake galloping                              | 550        |
| 8.3.7    | Aerodynamic countermeasures                 | 551        |
| 8.3.8    | Mechanical damping                          | 583        |
| 8.3.9    | Cable aerodynamic damping                   | 557        |
| 8.3.10   | Cross ties                                  | 557        |
| <b>9</b> | <b>Particular Issues</b>                    | <b>559</b> |
| 9.1      | Pedestrian-Induced Vibrations               | 559        |
| 9.1.1    | Lateral vibrations                          | 559        |
| 9.1.2    | Vertical vibrations                         | 562        |
| 9.1.3    | Serviceability limit states                 | 565        |
| 9.1.4    | Vibration control                           | 567        |
| 9.2      | Seismic Design                              | 568        |
| 9.2.1    | Earthquake intensity                        | 569        |
| 9.2.2    | Pylon design                                | 569        |
| 9.2.3    | Deck design                                 | 571        |
| 9.2.4    | Foundations                                 | 571        |
| 9.2.5    | Seismic analysis                            | 572        |
| 9.3      | Structural Health Monitoring                | 573        |
| 9.3.1    | Equipment                                   | 573        |
| 9.4      | Snow and Ice Removal and Prevention Systems | 575        |
| 9.4.1    | Mechanical removal                          | 575        |
| 9.4.2    | Thermal systems                             | 577        |
| 9.4.3    | Passive protection                          | 577        |
|          | <b>References</b>                           | <b>579</b> |
|          | <b>Index</b>                                | <b>587</b> |

# Preface to the Third Edition

The decision to prepare a manuscript for a book titled CABLE SUPPORTED BRIDGES was taken by Niels J. Gimsing in 1980 following his three year affiliation as an adviser on bridge technology to *Statsbroen Store Bælt*—the client organization established to design and construct a bridge across Storebælt (Great Belt) in Denmark. During the design period from 1976 to 1979, a large number of different designs for cable stayed bridges (with spans up to 850 m) and suspension bridges (with spans up to 1800 m) were thoroughly investigated and it was during that period the idea matured to write a book covering both cable stayed bridges and suspension bridges. The chance to prepare the manuscript came in 1979 when the Danish Government decided to postpone the construction of the Storebælt Bridge and to keep the design work at rest for a period of five years.

The manuscript for the First Edition was completed in 1982 and the book was published in 1983.

The decision to prepare a manuscript for a Second Edition was taken in 1994 when Niels J. Gimsing was involved in the design of both the 1624 m main span of the Storebælt East Suspension Bridge and the 490 m main span of the Øresund cable stayed bridge. Both bridges were under construction during the writing of the manuscript (from 1994–1996) and so useful information on construction issues could be collected.

The Second Edition was published in 1997; fourteen years after the First Edition appeared.

The Second Edition was sold out from the publisher after only 5 years on the market, so a Third Edition became desirable, and initially it was anticipated that this would be just a simple updating of the Second Edition. However, when digging deeper into the matter it became evident that a considerable evolution had taken place during the decennium following the publishing of the Second Edition. Very notable cable supported bridges had been constructed and a number of design issues related primarily to dynamic actions had gained in prominence.

It was, therefore, realized that the Third Edition had to be more than just a simple updating of the Second Edition. To emphasize the importance of issues pertaining to dynamic actions and health monitoring it was decided that two new chapters would be added. With his years of experience within the field, Christos T. Georgakis was entrusted with this task.

The Third Edition is published in 2011; fourteen years after the Second Edition appeared.

Besides revisions and additions in the text it was also decided to update the figures by preparing them in electronic versions that could be more easily edited to appear in a uniform manner throughout the publication. The financial support to cover the expenses for the figure updating came from the *COWI Foundation*. The figures were updated by Kristian Nikolaj Gimsing.

In the process of preparing the Third Edition, highly appreciated contributions came from Professor Yozo Fujino of the University of Tokyo, on matters relating to structural health monitoring and structural control, and from Professor Francesco Ricciardelli of the University of Reggio Calabria, on matters pertaining to bridge aerodynamics. PhD student Joan Hee Roldsgaard helped greatly with the preparation of elements of Chapters 8 and 9 and for the proof correcting of the book. Our great appreciation is also extended to all those who provided pictures, figures and copyright permissions. They are too many to mention here.

**Niels J. Gimsing and Christos T. Georgakis**  
*Technical University of Denmark*  
June 2011

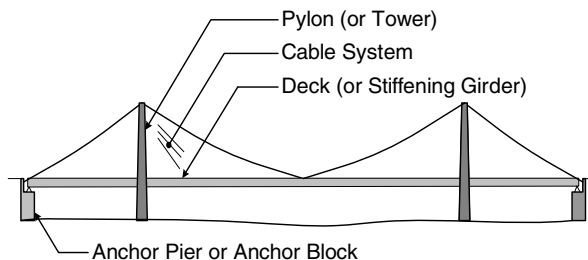


# Introduction

In the family of bridge systems the cable supported bridges are distinguished by their ability to overcome large spans. At present, cable supported bridges are enabled for spans in the range from 200 m to 2000 m (and beyond), thus covering approximately 90 per cent of the present span range.

For the vast majority of cable supported bridges, the structural system can be divided into four main components as indicated in Figure 0.1:

- (1) the deck (or stiffening girder);
- (2) the cable system supporting the deck;
- (3) the pylons (or towers) supporting the cable system;
- (4) the anchor blocks (or anchor piers) supporting the cable system vertically and horizontally, or only vertically, at the extreme ends.



**Figure 0.1** Main components of a cable supported bridge

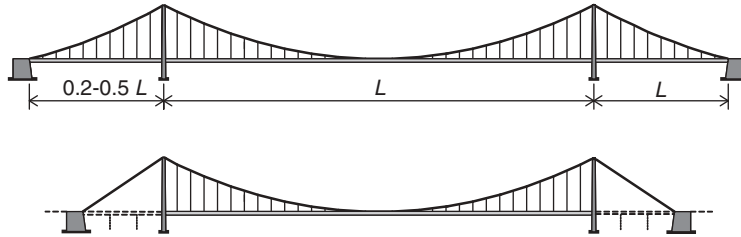
The different types of cable supported bridges are distinctively characterized by the configuration of the cable system.

The suspension system (Figure 0.2) comprises a parabolic main cable and vertical hanger cables connecting the deck to the main cable. The most common suspension bridge system has three spans: a large main span flanked by shorter side spans. The three-span bridge is in most cases symmetrical with side spans of equal size, but where special conditions apply, the side spans can have different lengths.

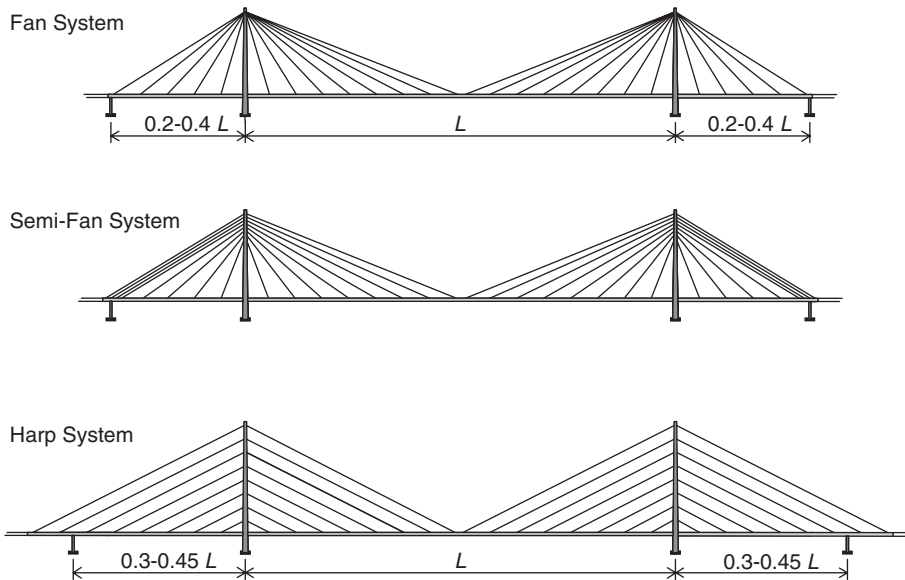
In cases where only one large span is needed, the suspension bridge may have only the main span cable supported. However, to transmit the horizontal component of the main cable pull acting at the pylon tops, the main cable will have to continue as free backstays to the anchor blocks.

A single-span suspension bridge will be a natural choice if the pylons are on land or close to the coasts/river banks so that the traffic lanes will continue on viaducts outside the pylons.

## 2 Cable Supported Bridges: Concept and Design



**Figure 0.2** Suspension bridge systems with vertical hangers and cable support of three spans (top) or only the main span (bottom)



**Figure 0.3** Cable stayed bridge systems: (top) pure fan system; (centre) semi-fan system; (bottom) harp system

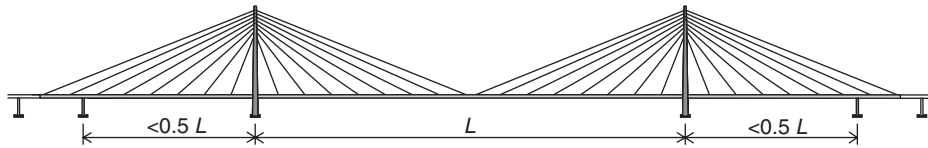
The cable-stayed system (Figure 0.3) contains straight cables connecting the deck to the pylons. In the fan system, all stay cables radiate from the pylon top, whereas parallel stay cables are used in the harp system.

Besides the two basic cable stayed systems (the fan system and the harp system), intermediate systems are often found. In the semi-fan system, the cable anchorages at the pylon top are spread sufficiently to separate each cable anchorage and thereby simplify the detailing. With cable anchorages positioned at minimum distances at the pylon top, the behaviour of the semi-fan system will be very close to that of the pure fan system.

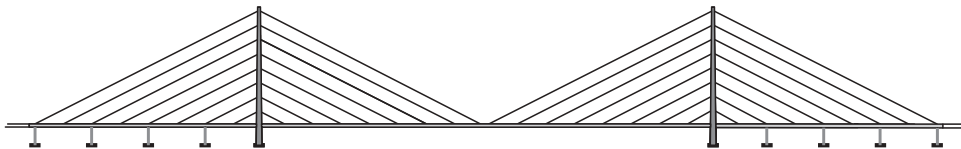
The stay cable anchorages at the deck will generally be spaced equidistantly so in cases where the side spans are shorter than half of the main span, the number of stay cables leading to the main span will be greater than the number of stay cables leading to the side span. In that case the anchor cable from the pylon tops to the anchor piers will often consist of several closely spaced individual cables (as shown for the semi-fan system).

In the harp system, the number of cables leading to the main span will have to be the same as in the side spans. With the anchor pier positioned at the end of the side span harp, the length of the side span will be very close to half of the main span length. That might prove inconvenient in relation to the overall stiffness of the system. It can then be advantageous to position the anchor pier inside the side span harp as indicated in Figure 0.3.

The position of the anchor pier closer to the pylon can also prove favourable in a fan system, if designed with fans of equal size in the main and side spans (Figure 0.4).



**Figure 0.4** Semi-fan system with side span pier inside the fan

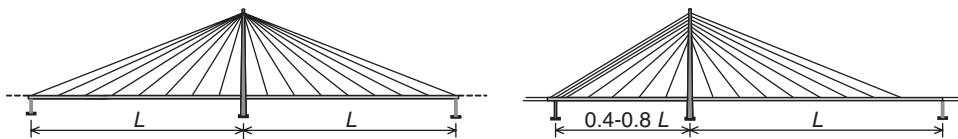


**Figure 0.5** Harp system with intermediate supports in the side spans

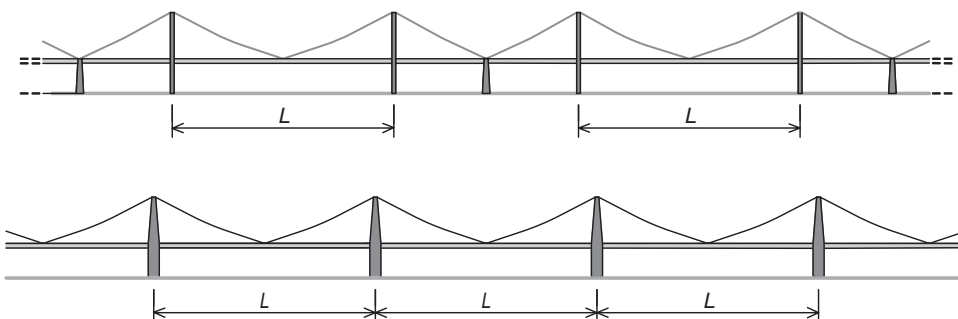
For the harp system the most efficient structural system will be achieved if a number of intermediate piers can be positioned under the side span harps (Figure 0.5). This will be the preferred solution if the side spans are on land or in shallow water.

The most common type of cable supported bridge is the three-span bridge with a large main span flanked by two smaller side spans. However, especially within cable stayed bridges, there are also examples of a symmetrical arrangement with two main spans of equal size or an asymmetrical two-span arrangement with a long main span and a somewhat shorter side span (Figure 0.6). If the two spans are of equal size, it will be necessary to stabilize the pylon top with two anchor cables whereas the asymmetrical arrangement often can be made with only an anchor cable in the shorter span.

The vast majority of cable supported bridges are built with three or two spans, but in a few cases this has not been sufficient. A straight forward solution that maintains the advantages of the three-span configuration is then to arrange two or more three-span bridges in sequence, as shown in Figure 0.7 (top). In appearance, the bridge will have every second opening between pylons without a central pier and the other openings with a central anchor pier (or anchor block).

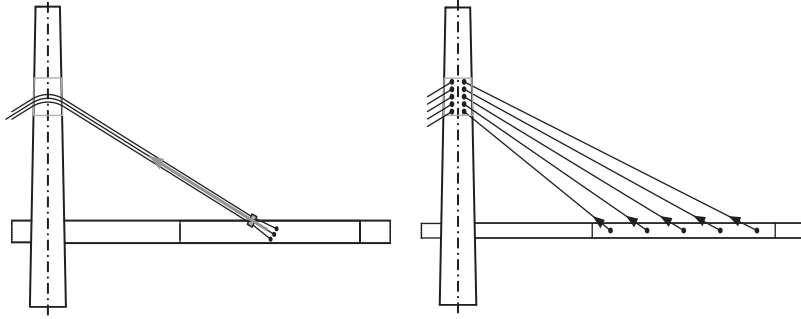


**Figure 0.6** Two-span cable stayed bridges



**Figure 0.7** Multi-span cable supported bridges

#### 4 Cable Supported Bridges: Concept and Design



**Figure 0.8** Cable stayed system with few multi-strand cables (left) and a multi-cable system (right)

A true multi-span cable supported bridge will consist of a number of main spans back-to-back as shown in Figure 0.7 (bottom).

In many cases, a true multi-span cable stayed bridge (bottom) will be preferable to a series of three-span bridges (top) from the point of view of appearance and function. However, from a structural viewpoint, the true multi-span arrangement presents a number of problems.

Due to the lack of anchor cables leading from vertically fixed points at the deck level to the pylon tops, the pylon must possess a considerable flexural stiffness to be able to withstand (with acceptable horizontal displacement at the top) a loading condition with traffic load in only one of the two spans adjacent to the pylon. In such a loading condition, the cable pull from the loaded span will be larger than from the unloaded span so the pylon must be able to withstand the difference between the horizontal force from the cable system in the loaded span and in the unloaded span.

In the early cable stayed bridges built from the mid-1950s to the mid-1970s, the distance between cable anchorages at deck level was generally chosen to be quite large and as a consequence each stay cable had to carry a considerable load. It was therefore necessary to compose each stay of several prefabricated strands joined together (Figure 0.8, left).

It was necessary to let the multi-strand cable pass over the pylon on a saddle as the space available did not allow the splitting and individual anchoring of each strand, and at the deck the anchoring of the multi-strand cable made it absolutely necessary to split it into individual strands.

In modern cable stayed bridges, the number of stay cables is generally chosen to be so high that each stay can be made as a mono-strand. This will ease installation, and particularly replacement, and it will render a more continuous support to the deck (Figure 0.8, right).

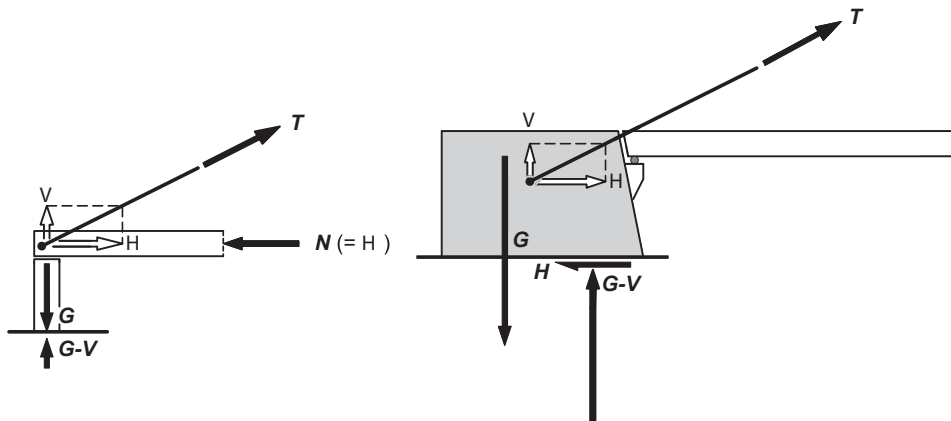
With the multi-cable system it will be possible to replace the stays one by one if the deck is designed for it, which will often be required in the Design Specifications. The advantages gained in relation to erection, maintenance and replacement have to some extent been set against an increased tendency for the stays in a multi-cable system to suffer from wind-induced vibrations.

Besides the configuration of the cables, cable supported bridges can also be distinguished by the way the cable system is anchored at the end supports. In the self-anchored system, the horizontal component of the cable force in the anchor cable is transferred as compression in the deck, whereas the vertical component is taken by the anchor pier (Figure 0.9, left). In the earth anchored systems, both the vertical and the horizontal components of the cable force are transferred to the anchor block (Figure 0.9, right).

In principle, both earth anchoring and self-anchoring can be applied in suspension bridges as well as in cable stayed bridges. However, in actual practice, earth anchoring is primarily used for suspension bridges and self-anchoring for cable-stayed bridges.

For the suspension bridges, self-anchoring is especially unfavourable in relation to structural efficiency and constructability. In modern practice, self-anchored suspension bridges are therefore only seen when the decision to use the system is taken by people without structural competence and who are not concerned about construction costs.

In the transverse direction of the bridge, a number of different solutions for the arrangement of the cable systems can be found. The arrangement used traditionally in suspension bridges comprises two vertical cable planes supporting the deck

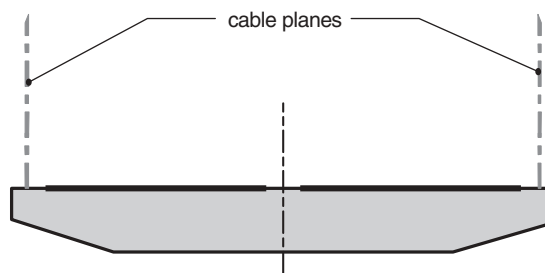


**Figure 0.9** Connection between the side span cable and the anchor pier/block in a self-anchored system (left), and in an earth-anchored system (right)

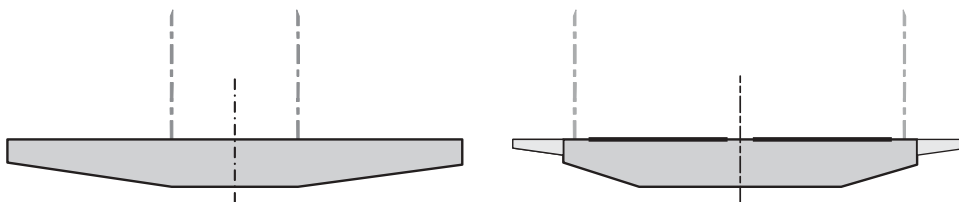
along the edges of the bridge deck (Figure 0.10). In this arrangement (which is also seen in many cable stayed bridges), the deck is supported by the cable systems both vertically and torsionally.

In cases where the bridge deck is divided into three separate traffic areas, e.g. a central railway or tramway area flanked by roadway areas on either side, the two vertical cable planes might be positioned between the central area and the outer areas (Figure 0.11, left). This arrangement is especially attractive if the central area is subjected to heavy loads that would induce large sagging moments in the transverse girders if the cable planes were attached along the edges of the bridge deck. On the other hand, with the cable planes moved in from the edges towards the centre of the deck, the torsional support offered by the cable system will be drastically reduced. A more moderate displacement of the cable planes from the edges of the deck is found in bridges with cantilevered lanes for pedestrians and bicycles (Figure 0.11, right).

The application of more than two vertical cable planes (Figure 0.12) was seen in some of the large American suspension bridges from the end of the nineteenth century and the beginning of the twentieth century. In bridges with a wide

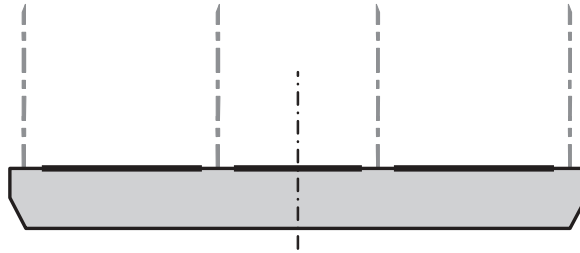


**Figure 0.10** System with two vertical cable planes attached along the edges of the bridge deck

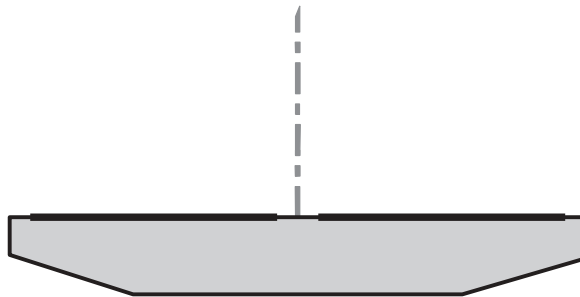


**Figure 0.11** Systems with two vertical cable planes positioned between three separate traffic lanes

## 6 Cable Supported Bridges: Concept and Design



**Figure 0.12** System with four vertical cable planes positioned outside and between three separate traffic lanes



**Figure 0.13** System with one central cable plane



**Figure 0.14** System with two inclined cable planes

bridge deck, more than two cable planes could still be considered, as the moments in the transverse girders will be significantly reduced.

Only one vertical cable plane (Figure 0.13) has been widely used in cable stayed bridges. In this arrangement, the deck is only supported vertically by the cable system, and torsional moments must therefore be transmitted by the deck. Consequently, the deck must be designed with a box-shaped cross-section.

Inclined cable planes (Figure 0.14) attached at the edges of the bridge deck and converging at the top are found in cable stayed bridges with A-shaped pylons. In this arrangement the deck is supported both vertically and torsionally by the cable system.

Two inclined cable planes converging at the top can also be supported on a single vertical pylon penetrating the deck in the central reserve or in the gap between two individual box girders.

# 1

## Evolution of Cable Supported Bridges

The principle of carrying loads by suspending a rope, chain or cable across an obstacle has been known since ancient times. However, it was not until 1823 that the first permanent bridge supported by cables composed of drawn iron wires was built in Geneva by the Frenchman Marc Seguin, one of five brothers who, in the following two decades, built hundreds of suspension bridges around Europe. All of these bridges were of modest size but they marked an important step on the way to the more impressive structures that followed.

The application of thin wires in the main load-carrying elements gave rise to a number of problems especially in relation to durability, as an efficient method for corrosion protection had not been found at that time. Therefore, some of the leading engineers preferred to construct suspension bridges with the main load-carrying elements, the catenaries, composed of pin-connected eye-bars forming huge chains.

This principle was applied by the British engineer Thomas Telford in the world's first bridge to cross a strait used by ocean-going vessels, the Menai Bridge between the British mainland and the Isle of Anglesey (Figure 1.1). Opened to traffic in 1826, this bridge had its 176 m long main span supported by chains assembled from wrought iron eye-bars, each with a length of 2.9 m.



**Figure 1.1** *The suspension bridge across the Menai Strait (UK)*

## 8 Cable Supported Bridges: Concept and Design

The chain support was generally preferred by the British engineers of the nineteenth century and a number of notable bridges were built, among these the famous Clifton Suspension Bridge, initially designed by Isambard Kingdom Brunel, but not actually constructed until after his death. The bridge was opened to traffic in 1864 and it comprised a main span of 214 m – an impressive span, considering that the strength-to-density ratio of the wrought steel in the chains was less than one-fifth of the ratio of modern cable steel (Figure 1.2).

To erect the eye-bar chains, a temporary footway had to be established between the supporting points on the pylon tops and at the anchor blocks. In the case of the Clifton Suspension Bridge, this temporary footway was supported by wire ropes, so the principle of cable support was actually applied, although only in the construction phase.

A most unusual bridge based on application of eye-bar chains is the Albert Bridge across the Thames in London (Figure 1.3). The bridge was built from 1871 to 1873 and it is characterized by combining the cable stayed and the suspension system. A part of the deck load is transferred to the strong top chain through hangers and the rest is carried by a number of straight chains radiating from the pylon tops. The system is statically indeterminate to such a degree that it was impossible with the available tools to calculate forces and moments to get even close to the exact values. Nevertheless the bridge with its 122 m-long main span is still in service although there are restrictions on the traffic allowed to pass over it (Figure 1.4).

Chain support was also applied in a number of bridges on the European continent, but here it was to a larger extent in competition with cable supported suspension bridges. Thus the longest free span in Europe was for several decades found in the wire supported *Grand Pont Suspensu* across the Sarine Valley at Fribourg in Switzerland. The bridge was completed in 1834 and it had a main span of 273 m. In the Grand Pont Suspensu, each of the four main cables was composed of over 1000 wires, grouped in 20 strands, each assembled on the ground and lifted individually into position. The bridge was in service for almost a century until it was finally demolished in 1923.

On a global level, the Swiss span record was beaten in 1849 by the completion of the Wheeling Suspension Bridge across the Ohio River in the USA. This bridge had a main span of 308 m, carried by a total of 12 parallel-wire cables, six on either side of the roadway.

The Wheeling Bridge is still in existence, although not in its original version. Five years after its completion, in 1854, a violent gale blew the bridge down. Subsequently it was reconstructed and later, in 1872, further strengthened by a fan-shaped system of stays. The principle of strengthening the suspension system with stays was originally introduced during the construction of the suspension bridge across the Niagara Gorge. This bridge was designed by the famous bridge designer John A. Roebling, who was born in Germany but emigrated to the United States of America at the



**Figure 1.2** Clifton Suspension Bridge (UK)





**Figure 1.3** Albert Bridge across the Thames (UK)

age of 25. The Niagara Bridge was constructed in the period from 1851 to 1855 and it was the first major suspension bridge to have air-spun wire cables, a system invented by Roebling.

The span of the Niagara Bridge was not quite as long as for the largest suspension bridges of that time but, due to the fact that the bridge carried both a railroad track and a roadway, its span of 250 m was still a very impressive achievement. As a most unusual feature the truss of the Niagara Bridge had the railroad track on the upper deck and the roadway on the lower, inside the two trusses.

Another unusual feature of the Niagara Bridge was the use of wood in the truss. This might today seem to be an awkward combination of structural materials but it must be remembered that in the early days of railroad building in North America, wood was the preferred material for bridges across rivers and gorges. For the Niagara Bridge, the application of a wooden truss resulted in a relatively short lifespan as the bridge had to be replaced in 1897 after 42 years of service.



**Figure 1.4** Traffic restrictions on the Albert Bridge (UK)



*Figure 1.5* The suspension bridge across the Ohio River between Cincinnati and Covington (USA)

The largest of Roebing's bridges completed during his lifetime, the Cincinnati–Covington Bridge across the Ohio River, was completed in 1866 with a record-breaking span of 322 m (Figure 1.5). In this bridge he tested many advanced features before they were adopted in his most sublime achievement: the design for the Brooklyn Bridge across the East River in New York.

### **Brooklyn Bridge**

The Brooklyn Bridge across the East River between Manhattan and Long Island (Figure 1.6) is justifiably regarded as the ancestor of all modern suspension bridges and it was to a large degree detailed by Roebing before his death in 1869 shortly after the start of construction of this, the greatest bridge of his career. Opened to traffic in 1883, the Brooklyn Bridge had a centre span of almost 500 m (486 m) and side spans of 286 m, i.e. a total cable supported length of 1058 m.



*Figure 1.6* Brooklyn Bridge across the East River in New York (USA)



*Figure 1.7* The cable system of the Brooklyn Bridge at the pylon (USA)

Based on his experience during design and construction of several suspension bridges, and through his investigations into accidents such as the collapse of the Wheeling Bridge in 1854, Roebling had acquired a profound understanding of the aerodynamic problem. This is clearly indicated in his own description of the Brooklyn Bridge concept:

But my system of construction differs radically from that formerly practised, and I have planned the East River Bridge [as the Brooklyn Bridge was initially called] with a special view to fully meet the destructive forces of a severe gale. It is the same reason that, in my calculation of the requisite supporting strength so large a proportion has been assigned to the stays in place of cables.

This description proves that Roebling knew very well that a cable stayed system is stiffer than the suspension system, and the fact that the stays of the Brooklyn Bridge carry a considerable part of the load can be detected by the configuration of the main cable having a smaller curvature in the regions where the stays carry a part of the permanent load than in the central region, where all load is carried exclusively by the main cable.

The efficiency of the stay cables (Figure 1.7) is clearly demonstrated by the following remark by Roebling: ‘The supporting power of the stays alone will be 15 000 tons; ample to hold up the floor. If the cables were removed, the bridge would sink in the center but would not fall.’

Roebling had started his engineering career at a time when the design of bridges was still more of an art, requiring intuition and vision, than a science. Therefore, he had to acquire a profound understanding of the structural behaviour of cable supported bridges through observations and by experience. He gradually learned how to design structures of great complexity, as he could combine his intuitive understanding with relatively simple calculations, giving adequate dimensions for all structural elements.

In the case of the Brooklyn Bridge, the system adopted is one of high indeterminateness as every stay is potentially a redundant. A strict calculation based on the elastic theory with compatibility established between all elements would involve numerical work of an absolutely prohibitive magnitude, but by stipulating reasonable distributions of forces between elements and always ensuring that overall equilibrium was achieved, the required safety against failure could be attained.

After Roebling, the next generation of engineers was educated to concentrate their efforts on the calculations, which required a stricter mathematical modelling. As systems of high statical indeterminateness would involve an insuperable amount of numerical work if treated mathematically stringently, the layout of the structures had to be chosen with due respect to the calculation capacity, and this was in many respects a step backwards. Consequently, a cable system such as that used in the Brooklyn Bridge had to be replaced by much simpler systems.

The theories available for the calculation of suspension bridges in the second half of the nineteenth century were all linear elastic theories, such as the theory by Rankine from 1858, dealing with suspension bridges where the deck comprised



**Figure 1.8** Williamsburg Bridge, second bridge to span the East River in New York (USA)

two- and three-hinged girders. The theory was the first to take into account rationally the interaction between the cable and the deck. Later, in 1886, the linear elastic theory was further developed by Maurice Levy in his paper, ‘*Mémoires sur le calcul des ponts suspendus rigides*’.

### Williamsburg Bridge

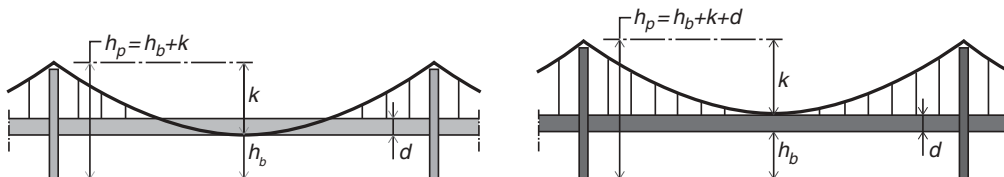
The trend to let the calculations influence the layout of the structure is clearly seen in the Williamsburg Bridge, the second bridge to span the East River in New York (Figure 1.8). Opened to traffic in 1903, this bridge had a main span of 488 m, just 2 m more than the Brooklyn Bridge.

The structural system with unsuspended side spans and only one well-defined, simply supported suspended main span without any additional stays, clearly shows the strive towards a practicable mathematical model. Also, the extreme depth of the stiffening truss, one-fortieth of the span, can be seen as a result of the attempt to match the behaviour of the real structure to agree with the mathematical model that took only linear elastic effects into account (i.e. neglecting the change of geometry due to node displacements).

That the final result will often be less satisfactory when calculations govern the design is well demonstrated by the Williamsburg Bridge, especially in comparison with the Brooklyn Bridge. In his book, *Bridges and Their Builders* [57.1], D. B. Steinman wrote about the Williamsburg Bridge:

With the ungainly tower design and the excessively deep trusses, the structure presents an appearance of angularity and clumsiness. It marked one extreme of the swing of the pendulum; thereafter there was a reversal of trend, toward progressively increasing slenderness and grace in the design of suspension bridges.

One feature that the Brooklyn Bridge and the Williamsburg Bridge has in common is the arrangement of the main cables at midspan in relation to the stiffening truss. In both bridges, the cables pass beneath the top chord of the truss and are led down to the bottom chord at the centre of the main span. This arrangement is very well justified from an economic point of view as the height of towers and the length of hangers, for a given sag of the main cable, are reduced by a distance equal to the depth of the truss, as illustrated in Figure 1.9. In modern suspension bridges the main cable will in general be positioned



**Figure 1.9** Position of the main cable in relation to the stiffening truss: (left) position favoured in the early suspension bridges; (right) position preferred today



**Figure 1.10** Manhattan Bridge, third bridge to span the East River in New York (USA)

entirely above the deck, which undoubtedly is preferable with regards to the appearance, as the cable curve is more easily perceived. Also, in modern bridges with slender decks, the savings would be smaller than in the Williamsburg Bridge where the truss depth corresponds to as much as 25% of the main cable sag.

### Manhattan Bridge

The third suspension bridge to span the East River was the Manhattan Bridge designed by L. S. Moisseiff and opened to traffic in 1909 (Figure 1.10).

In the evolution of cable supported bridges, the Manhattan Bridge is notable for the fact that it was the first major suspension bridge to be analyzed by the so-called ‘deflection theory’ which had been developed by Professor Melan in Vienna in 1888. The deflection theory is a nonlinear elastic theory that takes into account the displacements of the main cable under traffic load when calculating the bending moments in the stiffening truss. Thus, equilibrium is established more correctly for the deflected system than for the system with the initial dead load geometry.

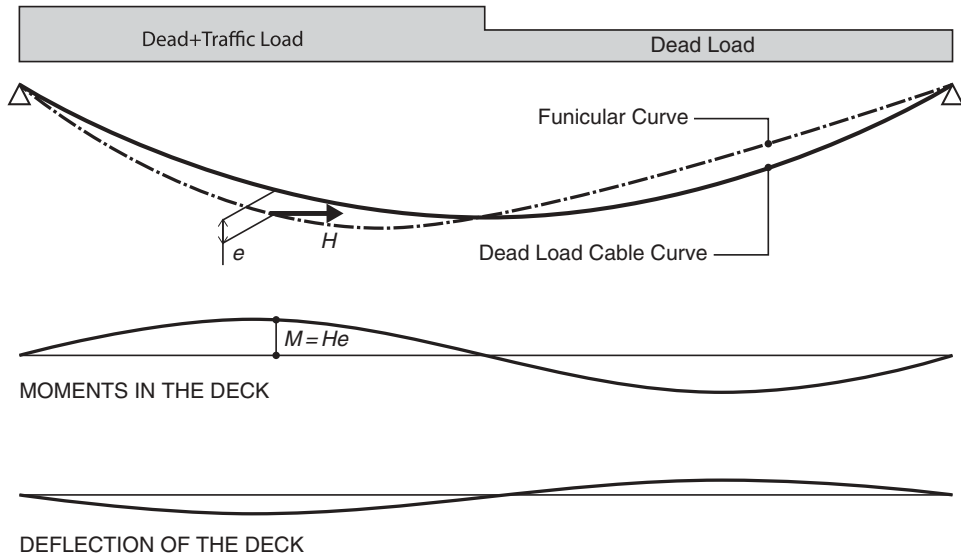
To get a phenomenological understanding of the deflection theory, a suspension bridge main span subjected to traffic load in the left half of the span may be considered. As indicated in Figure 1.11, the funicular curve of the applied dead plus traffic load does not coincide with the cable curve of the dead load condition, so moments will be induced in the deck.

With a linear elastic theory based on the assumption that the change in geometry due to deflections caused by the applied traffic load can be ignored, the moments to be taken by bending in the deck can be expressed by  $He$ , where  $H$  is the horizontal force (related to the funicular curve) and  $e$  is the vertical distance from the cable axis to the funicular curve.

The moments induced in the stiffening truss will be positive in the span half with traffic load and negative in the remaining part of the span. This means that the deck will deflect into an S-shape, as indicated at the bottom of Figure 1.11.

However, due to the hangers linking the deck to the main cable, the deflection of the deck will cause a change in the geometry of the main cable. In Figure 1.12, the full line indicates the shape of the cable when deflections of the deck are taken into account. It will be seen that the cable moves towards the funicular curve, and as equilibrium must exist in the deflected system, the real moments in the deck will be represented by the horizontal force  $H$  multiplied by the vertical distance  $e - \delta$  from the funicular curve to the distorted cable.

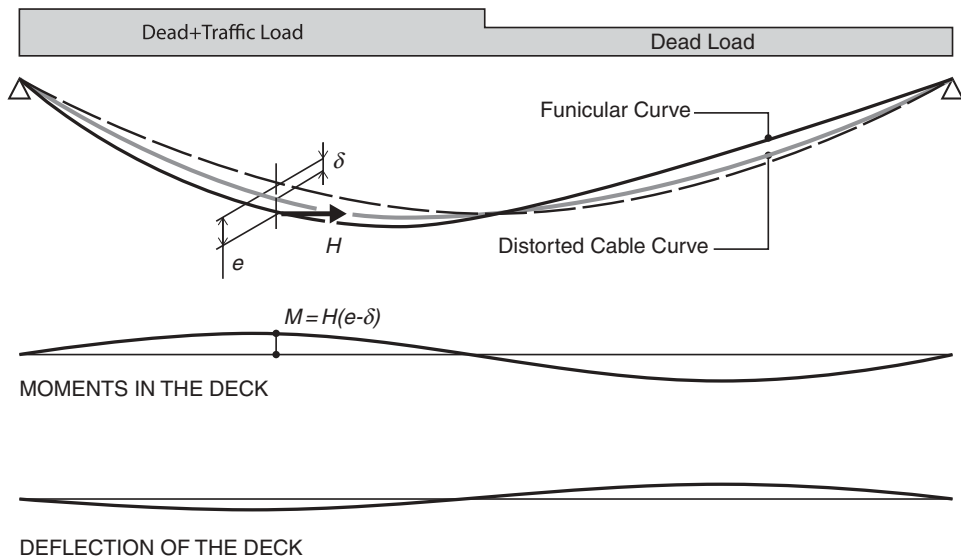
When taking into account the nonlinear elastic effect related to the displacement of the cable, the bending moments in the deck will be reduced, often to less than half of that found by a linear elastic theory. Actually, there are no limits to the reduction that can be achieved, as a suspension bridge with a very slender deck and therefore insignificant flexural stiffness will deflect under asymmetrical loading until the displaced cable and the funicular curve coincide. Then  $e - \delta = 0$  which



**Figure 1.11** Moments in the deck when assuming equilibrium of the system with the dead load geometry (linear elastic or 'elastic' theory)

implies  $M = 0$ . This also follows from the fact that the funicular curve by definition is the curve followed by a perfectly flexible string subjected to the action of the applied load.

As equilibrium can be attained without any stiffness of the deck, the deflection theory does not assure a minimum flexural stiffness – in contrast to a linear elastic theory. However, in the early applications of the deflection theory the authorities



**Figure 1.12** Moment in the deck when assuming equilibrium of the system in the deflected state (nonlinear elastic or 'deflection' theory)

specified a minimum depth of the stiffening truss in the interval from one-sixtieth to one-ninetieth of the span length and thereby actually introduced a lower limit for the bending stiffness.

At the time when the deflection theory was introduced, the calculation capacity was limited so the solution procedure for the nonlinear differential equation was complicated and tedious for the practising engineer. Consequently, simplifications had to be introduced in the form of charts, tables, and correction curves by which the results of the simpler, linear elastic theory could be corrected to approximate those of the deflection theory.

Besides the new analytical approach, the Manhattan Bridge also introduced several new construction techniques, such as pylon erection by vertically travelling derrick cranes, and cable wrapping by a self-propelling machine.

After the opening of the Manhattan Bridge, only modest progress was made in the design of cable supported bridges for a period of more than 20 years, although some bridges with spans slightly exceeding the span of the Manhattan Bridge were constructed.

### George Washington Bridge

Then, in 1931, came a suspension bridge which almost doubled the free spans of all previous bridges: the George Washington Bridge across the Hudson River (Figure 1.13). With a main span of 1066 m, this was the first bridge to span more than 1 km between supports.

Designed by O.H. Ammann, the George Washington Bridge was planned from the beginning to have two decks with a roadway on the upper deck and tracks for commuter trains on the lower deck. However, due to the economic Depression at the end of the 1920s, the original project was reduced so that only the upper deck was constructed initially. Thus, from the beginning the bridge was virtually unstiffened as only roadway stringers with insignificant bending stiffness were present in the longitudinal direction at deck level.

Despite the absence of a genuine stiffening truss, the George Washington Bridge proved to be adequately stable due to the large dead load from the heavy concrete floor and to the great width of the roadway with eight traffic lanes. Also, the short side spans, with a length of less than one-sixth of the main span, increased the efficiency of the cable system and compensated thereby to a certain extent for the lack of flexural deck stiffness.

In the early suspension bridges like the Brooklyn Bridge, the Williamsburg Bridge, and the Manhattan Bridge, four vertical cable planes were arranged across the whole width of the bridge to reduce the spans of the cross beams and establish a direct transmission of the load from the roadway to the cable systems. In the George Washington Bridge, the cable planes were to be positioned in pairs outside the edges of the roadway to achieve a continuous bridge floor across the whole width. The choice of four cable planes was mainly based on considerations regarding the spinning of the



**Figure 1.13** George Washington Bridge across the Hudson River (USA)

cables, as working on four cables instead of two would speed up the erection considerably. This was especially important as very large cable cross sections were required to carry the load from the wide bridge decks.

The cable system, the anchor blocks and the pylons were designed for the full double-deck structure and they were not reduced in size when the lower deck was initially omitted.

### **The three-dimensional deflection theory**

An interesting development in the process of analyzing suspension bridges appeared in 1932 when L. S. Moisseiff and F. Lienhard presented a theory for the calculation of suspension bridges under lateral load [32.1]. Actually the theory can be regarded as an extension of the nonlinear elastic deflection theory (that had so far only been developed for vertical in-plane loading) to cover horizontal forces also. Thus, the inclination of the cable planes caused by the lateral deflection of the deck could now be taken into account when calculating the moments and shear forces in the horizontal wind girder.

The new theory led to a substantial reduction of the lateral load to be carried by the deck itself, and the reduction became more and more pronounced with increasing slenderness of the wind girder. It would even be possible to create lateral equilibrium without any wind girder at all.

It earlier was mentioned how the two-dimensional deflection theory developed by Melan had removed the lower bound for the flexural stiffness of the deck in the vertical direction, and now the extension of the deflection theory to cover the three-dimensional behaviour implied that a lower bound for the lateral flexural stiffness also disappeared.

In the hands of engineers deprived of the intuitive understanding found in the previous century, and now trained to trust blindly the results of the calculations, these analytical achievements could, and should, lead to serious mistakes.

The 1930s became a decade of great achievements in the field of cable supported bridges in the United States: the George Washington Bridge was followed by such impressive structures as the San Francisco–Oakland Bay Bridge, designed by Moisseiff, and the Golden Gate Bridge, designed by J. B. Strauss.

### **San Francisco–Oakland Bay Bridge**

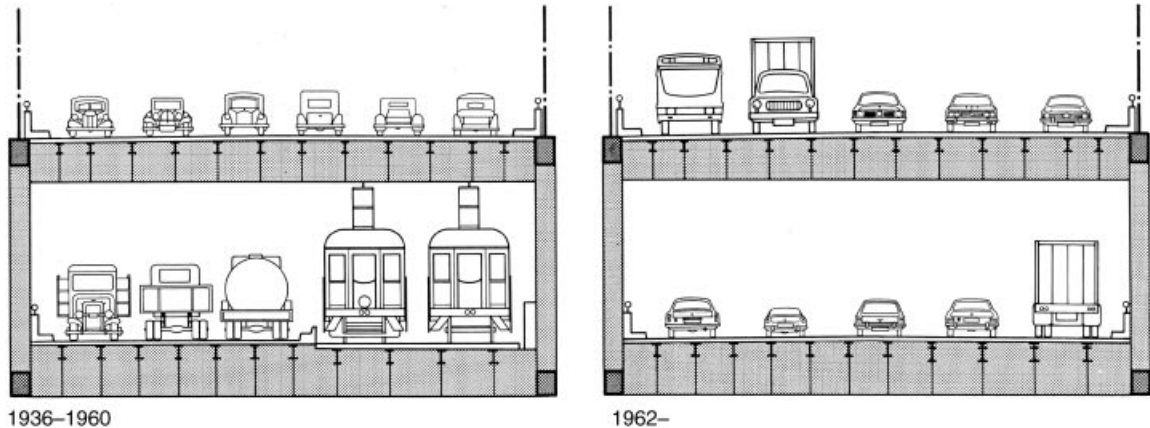
The San Francisco–Oakland Bay Bridge actually consists of two bridges, the East Bay Crossing from Oakland to the small island of Yerba Buena, and the West Bay Crossing from that island to San Francisco. However, in relation to the topic of cable supported bridges, the original East Bay Crossing is not relevant. But the West Bay Crossing consists of twin suspension bridges placed end to end with a separating anchor pier at the centre (Figure 1.14).

Each of the two suspension bridges has a main span of 704 m and side spans of 352 m, e.g. the side span length is exactly half of the main span length. This means that the central double span with the anchor pier has the same dimensions in the



**Figure 1.14** *The West Bay crossing of the San Francisco–Oakland Bay Bridge (USA)*





**Figure 1.15** Traffic lanes on the Bay Bridge in the original configuration (left), and in the converted configuration (right)

superstructure as the adjoining main spans. For this reason, the heavy anchor pier might at first seem unnecessary: why an anchor pier in the central span when the adjoining spans do not need any?

Considering at first only a constant load such as dead load, the anchor pier is actually inactive as the horizontal component of the cable force is constant from end anchorage to end anchorage. But in the case of traffic load applied to only one of the two main spans, the horizontal force in that part of the double bridge will be increased. The anchor pier must therefore be able to resist the difference between the horizontal force from the span with dead load plus traffic load and the horizontal force from the span with dead load only.

During the preliminary investigations, solutions without the central anchor pier were studied [33.1] but none of these more unconventional solutions reached the stage of detailed planning (Figures 3.136 and 3.166).

The Bay Bridge was from the beginning constructed with two floors, at the upper level with a six-lane roadway for cars and on the lower level a three-lane roadway for heavy traffic (trucks and buses) as well as two tracks for commuter trains. Despite the heavy loading from the two decks, the Bay Bridge could be made with only two main cables due to the smaller spans.

In the early 1960s, the Bay Bridge was converted to carry only automobile traffic with five lanes at each level (Figure 1.15).

Besides the problems facing the engineers in designing the superstructure of the Bay Bridge, problems related to the substructure were also of an unknown magnitude as the deepest pier had to go down to a depth of 73 m below water level. Despite these difficulties the Bay Bridge was built in only 40 months with actual construction beginning in July 1933 and opening to traffic in November 1936. Even today this stands as a most remarkable achievement.

### Golden Gate Bridge

Coinciding with the construction of the Bay Bridge was that of the Golden Gate Bridge where construction started in January 1933 and terminated in May 1937 (Figure 1.16). The Golden Gate Bridge has a main span of 1280 m, 20% more than the George Washington Bridge. Despite this, the bridge could be made with only two main cables, each 930 mm in diameter, compared to the four main cables each 910 mm in diameter used in the George Washington Bridge. The reason for this was partly that the Golden Gate Bridge had only a bridge floor at one level (and without any provisions for later additions) and partly that the sag ratio of the Golden Gate Bridge main cables was larger than for the George Washington Bridge.

The stiffening truss of the Golden Gate Bridge represented an extreme in slenderness as the depth-to-span ratio was only 1:168. At the same time, the space truss comprised only three plane trusses, two vertical under the cable planes and one horizontal directly below the bridge floor. This configuration resulted in an insignificant torsional stiffness of the total truss section, but at the time when the Golden Gate Bridge was designed, the importance of torsional stiffness for achieving aerodynamic stability was not fully appreciated.



**Figure 1.16** Golden Gate Bridge across the inlet to the San Francisco Bay (USA)

### **Tacoma Narrows Bridge**

A few years later the extreme slenderness of the Golden Gate Bridge was substantially surpassed by the next major suspension bridge on the American West Coast: the Tacoma Narrows Bridge.

This bridge, with a main span of 853 m, had the deck made up of plate girders with a depth-to-span ratio of only 1:350. This extreme slenderness was actually the ultimate result of the designer Moisseiff's application of the deflection theory, which – as has already been described – gave ever decreasing bending moments as the flexural stiffness was reduced. Besides the small depth-to-span ratio, the width-to-span ratio of 1:72 (compared to 1:47 for the Golden Gate Bridge and 1:33 for the George Washington Bridge) also went beyond previous practice. The extreme slenderness of the wind girder was also made possible by Moisseiff's own extension of the deflection theory to cover the three-dimensional behaviour. Furthermore, the deck of the Tacoma Bridge had virtually no torsional rigidity as only one lateral bracing was present. Despite the extreme slenderness of the deck, the bridge possessed an adequate safety margin against the action of the traffic load and the static wind pressure (drag), when taking full advantage of the nonlinear effects.

In less than 40 years from the Williamsburg Bridge of 1903 to the Tacoma Narrows Bridge of 1940, the pendulum had swung from one extreme to the other with a reduction of the relative girder depth by a factor of almost 10. However, shortly after the opening of the Tacoma Bridge, nature gave a clear demonstration of the fact that the trend towards increasing slenderness had gone too far.

Right from its opening, the bridge had shown a tendency to oscillate in the wind, but during the first four months these oscillations were vertical, with no twist of the cross section, and the oscillations were always damped down after reaching an amplitude of about 1.5 m.

Then, after a few months in service, following the breaking of inclined tie cables that had prevented mutual displacements between the deck and the main cables at midspan, the type of oscillation suddenly changed. The oscillations then took the form of twisting movements with the main span oscillating asymmetrically in two segments with a node at midspan (Figure 1.17). The torsional movements became more and more violent with a tilting of the roadway at the quarter points from  $+45^\circ$  to  $-45^\circ$ . After approximately one hour of these violent self-excited oscillations, caused by negative damping of the aerodynamic forces, the hangers began to break in fatigue at the sockets and a large portion of the deck fell into the water.

During the final oscillations of the Tacoma Bridge the wind speed (18 m/s) was by no means extreme, and far below the maximum wind speed the bridge had been designed to withstand. However, when analyzing the structure for the action of wind, only a static pressure had been considered – and in this respect, the bridge was completely safe.



**Figure 1.17** *The fatal twisting oscillation of the First Tacoma Bridge*

No attempts had been made to investigate the dynamic action related to the pulsating wind eddies formed at the sharp corners of the plate girders, and so it happened that the chosen design with its extreme slenderness proved to be subject to aerodynamic instability.

#### **Focus on aerodynamic behaviour**

After the Tacoma Bridge disaster, aerodynamic studies became an important part of the design process for all suspension bridges to come and suspension bridges already built were also investigated to reveal if there was any danger of aerodynamic instability.

One of the bridges investigated was the Bronx–Whitestone Bridge designed by Amman with a main span of 701 m. The bridge was opened to traffic in 1939 and it had a deck composed of two plate girders with a depth-to-span ratio of 1:209. Although not as extreme as the Tacoma Bridge, it still represented an unusual slenderness that was combined with solid web girders promoting the formation of pulsating wind eddies.

On the other hand, the width-to-span ratio of 1:31 for the Bronx–Whitestone Bridge was larger than the corresponding ratios for both the George Washington Bridge and the Golden Gate Bridge. It could therefore be stated that the Bronx–Whitestone Bridge was safer than the Tacoma Bridge, but was it safe enough?

Oscillations had been observed on the Bronx–Whitestone Bridge but they were always of the non-catastrophic vertical type and with small amplitudes. Nevertheless, in 1946, it was decided to strengthen the Bronx–Whitestone Bridge by adding a Warren truss on top of the plate girders to double the depth of the deck, and by erecting stays from the pylon tops to the deck (Figure 1.18).

More recent analyses have revealed that the addition of inclined stays only had a marginal effect on the vibrational characteristics, probably due to the relatively long side spans of the Bronx–Whitestone Bridge. Therefore, the measures taken did not completely eliminate the vibrations, so further measures had to be taken, and in the 1980s large tuned mass dampers were installed.

In 2003 the heavy Warren truss added in 1946 was removed and substituted by fiber glass fairings attached to the original plate girders of the deck structure. That did not only improve the aerodynamic properties but also gave the bridge back its original elegance. Furthermore the supplementary stay cables were removed.

The Golden Gate Bridge had also shown a tendency to wind-excited oscillations of the non-catastrophic vertical type. In December 1951, during a four-hour gale, these oscillations reached a vertical amplitude of 3.3 m and the bridge had to be closed to traffic for three hours.

After this severe warning of an unsatisfactory aerodynamic stability, it was decided to make provisions to increase safety. As theoretical investigations revealed that the lack of torsional rigidity could lead to catastrophic torsional oscillations, it

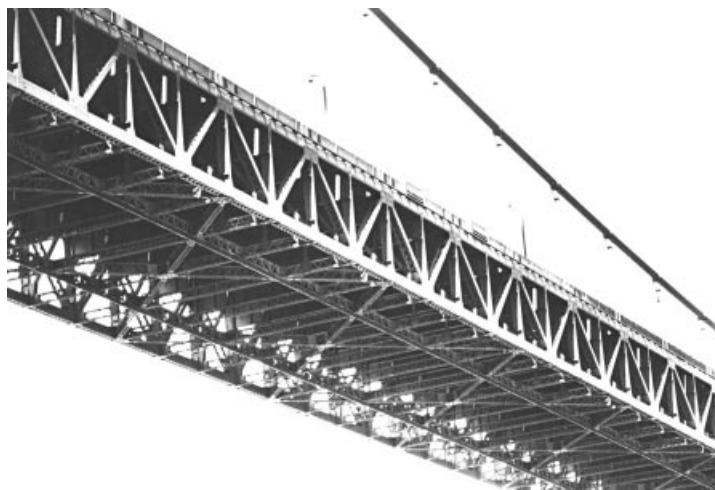


**Figure 1.18** Bronx–Whitestone Bridge after the first strengthening to improve the aerodynamic stability (USA)

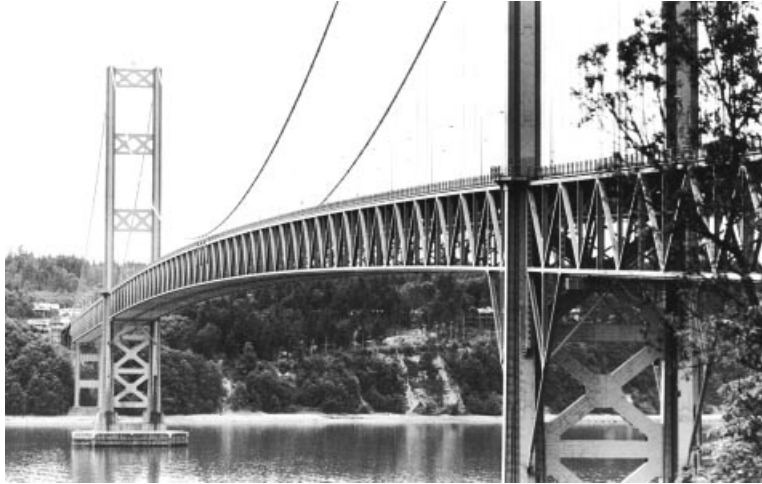
was decided to add a lower lateral bracing between the bottom chords of the vertical trusses (Figure 1.19). The space truss was then changed from an open section with three plane trusses to a closed section with four plane trusses, two vertical and two horizontal.

After World War II, it was decided to rebuild the Tacoma Narrows Bridge, but with significant changes in the overall dimensions and the structural system to achieve a very high degree of resistance against wind-excited oscillations (Figure 1.20).

In a comparison between the original and the rebuilt Tacoma Bridge (Figure 1.21), it can be seen that the 2.4 m deep plate girders were replaced by 10 m deep trusses and the width has increased by more than 50% – from 11.9 m to 18.3 m. Furthermore, in the new design, slots were introduced in the deck and different damping devices were built into the bridge.



**Figure 1.19** The stiffening truss of the Golden Gate Bridge after addition of the lower lateral bracing (USA)

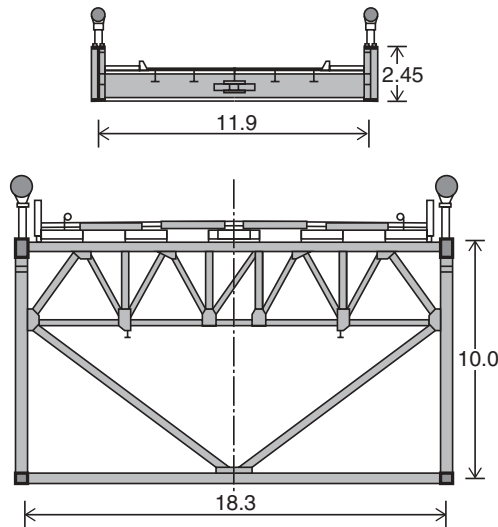


**Figure 1.20** Second Tacoma Bridge (USA)

With hindsight, the Second Tacoma Bridge seems to have unnecessarily large dimensions to achieve the required degree of safety. However, this tendency to overreact when collapsed structures are redesigned is so common that it undoubtedly reflects a basic characteristic of the human nature.

The flurry of activity in the construction of suspension bridges during the 1930s also led to the introduction of new analytical methods. Thus, in 1938, Hardesty and Wessman presented a method where the results were obtained by initially calculating the displacement of the main cable acting alone, and subsequently modifying these results due to the presence of the deck [39.1]. This method was well suited for preliminary calculations, especially of bridges with relatively flexible decks (such as those built more recently).

Another method was presented by F. Bleich in 1940. This method was based on a linearization of the deflection theory by omitting the non-linear terms of the differential equations [50.1]. This method proved to be well suited



**Figure 1.21** Cross section of the First Tacoma Bridge (top) and the Second Tacoma Bridge (bottom)

for studying the dynamic behaviour of suspension bridges, a topic brought into sharp focus by the collapse of the Tacoma Bridge.

In general, the Tacoma Bridge disaster focused designers' attention on the vibrational characteristics of suspension bridges and their response to aerodynamic excitations. The problem was treated theoretically or experimentally by several researchers such as F. Farquharson, F. Bleich, T. Von Kármán and A. Selberg [45.1]. Based on these investigations, procedures for the design of suspension bridges for aerodynamic excitations were set up, and became an important part of the design process for all major cable supported bridges to be built in the years to follow.

After World War II, the design and construction of cable supported bridges resumed, partly to restore bridges that had been destroyed during the war and partly to establish new bridge links.

#### **D.B. Steinman's design for a bridge across the Messina Strait**

In 1950, D. B. Steinman worked out a design for a bridge across the Strait of Messina [51.1]. With a main span of 1524 m and side spans of 732 m, this bridge would have surpassed all existing suspension bridges (Figure 1.22). The Messina Strait Bridge had to carry both road and railway traffic, so a considerable stiffness was required and, according to Steinman, this would lead to a depth of the stiffening truss corresponding to 1/40 of the main span length, or 38 m! As this would give the bridge a very clumsy appearance, he decided to vary the depth of the truss according to the principle he had applied in the chain-supported Florianapolis Bridge in Brazil built during the period 1922–26 with a main span of 340 m.



**Figure 1.22** *Design from 1950 for a bridge across the Strait of Messina*

In the Messina Bridge design, the depth of the truss was varied between 13 m and 50 m, with the largest depth present at the locations where the maximum flexural stiffness was required: at the quarter points of the main span and the mid-points of the side spans.

To further increase the stiffness, it was proposed to have stays radiating upwards from the points where the deck and the pylon intersect and to a number of points on the main cable. The action of these stays was primarily to reduce the displacement of the main cables under the asymmetrical traffic load.

In comparison with the stays of the Brooklyn Bridge radiating from the pylon top and anchored to the deck in the span, it will be seen that the stays of the Messina Bridge increase the downward load on the main cable, whereas this load is decreased with the stay arrangement of the Brooklyn Bridge. Due to this difference in the load-carrying performance of the stays, the Brooklyn Bridge stays might be denoted 'positive stays' and the stays of Steinman's Messina Bridge design 'negative stays'.

With the main dimensions chosen for the Messina Bridge, the application of negative stays is well justified, as the long side spans and the flexible pylons imply that relatively large longitudinal displacements of the pylon tops will occur and significantly reduce the efficiency of positive stays (as was the case for the stays added to stabilize the Bronx–Whitestone Bridge). In the Brooklyn Bridge the massive pylons had a flexural stiffness of such a magnitude that the pylon tops were restrained sufficiently against longitudinal displacements. The same restraint could be found in bridges with relatively short side spans, so that in these bridges the application of positive stays would generally be preferable.

The Messina Strait Bridge design from 1950 never got even close to the construction stage but in the following decades this bridge project became the object of numerous in-depth studies and investigations, many of which led to a better understanding of problems to be encountered when moving into an extreme span range.

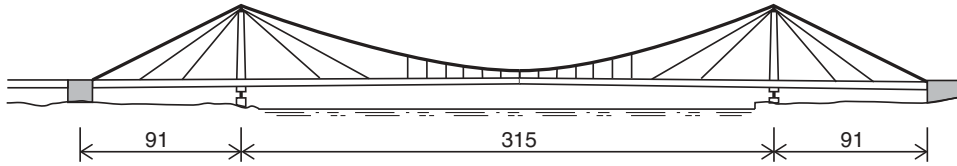
### **Mackinac Bridge**

The first post-war suspension bridge with dimensions equal to those of the bridges constructed in the 1930s was the Mackinac Bridge opened to traffic in 1957 (Figure 1.23). With a main span of 1158 m and side spans of 549 m, this bridge had a total cable supported length of 2256 m exceeding any previous suspension bridge. Although the Golden Gate Bridge had a longer main span, the side spans were considerably shorter so that the total cable supported length for this bridge was only 1966 m.

For the Mackinac Bridge, the designer D.B. Steinman carried the attempt to achieve a high degree of aerodynamic stability even further than in the case of the Second Tacoma Bridge. For the Mackinac Bridge, the critical wind speed for the first design was determined to be 995 km/h, more than 10 times the critical wind speed of existing suspension bridges built before the war. Later in the design process, the roadway in the two central lanes was changed to open grids, and this was claimed to result in an increase of the critical wind speed to infinity!



**Figure 1.23** Mackinac Bridge in Michigan (USA)



**Figure 1.24** Bridge system proposed by Dischinger (design for the reconstruction of the Köln–Mühlheim Bridge across the Rhine River) (Germany)

The high degree of aerodynamic stability was achieved by a thorough investigation of all the parameters affecting the aerodynamic stability of the traditional suspension bridge with vertical hangers and a simply supported stiffening truss. It resulted in quite large dimensions of the stiffening truss having a depth of 11.60 m (corresponding to one-hundredth of the main span length) and a width of 20.70 m, 6 m more than the roadway width.

Although the feat of designing a bridge with such enormous critical wind speeds stands as an impressive achievement, on the other hand, it was also unnecessary as these wind speeds will never occur in the real world and a perfectly safe structure could therefore have been designed with smaller and more harmonious dimensions.

The Mackinac Bridge and the Second Tacoma Bridge marked a new extreme in the swing of the pendulum, and – as was the case after the Williamsburg Bridge half a century earlier – in the following period a reversal of the trend occurred towards progressively increasing slenderness and grace in the design of suspension bridges.

#### **Dischinger's proposal for a combined suspension and cable stayed system**

The idea of combining the suspension system with stays to achieve more efficient structural systems had not been completely forgotten after the days of the Brooklyn Bridge. Thus, in 1938, Dischinger proposed a system in which the central part of the span was carried by a suspension system whereas the outer parts were carried by stays radiating from the pylon top. This system was proposed for a cable supported bridge with a 750 m main span to be built across the Elbe River in Hamburg.

In connection with the reconstruction of German bridges after the war, the Dischinger system was proposed on several occasions but it was never used for actual construction (Figure 1.24). One of the reasons is undoubtedly the pronounced discontinuity of the system, both with respect to structural behaviour and to appearance.

Strangely enough, although Dischinger adopted the idea of combining the suspension system and the cable stayed system, he did not appreciate the original solution of Roebling with the much more continuous lay-out. In the publication of his own system [49.1], Dischinger simply stated that the stays of Roebling's bridges had proved to be completely inefficient!

The contribution to the evolution of cable supported bridges by the system proposed by Dischinger turned out to be a considerable influence on the subsequent introduction of the pure cable stayed bridge.

#### **Cable stayed bridges**

The principle of supporting a bridge deck by inclined tension members leading to towers on either side of the span has been known for centuries but it did not become an interesting option until the beginning of the nineteenth century when wrought iron bars, and later steel wires, with a reliable tensile strength were developed. A limited number of bridges based on the stayed girder system were built – and more proposed – but the system was never generally accepted at that time.

In 1823, the famous French engineer and scientist Claude Navier published the results of a study on bridges with the deck stiffened by wrought iron chains and with a geometry as shown in the original drawing in Figure 1.25.

It is interesting to note that Navier considered both a fan-shaped and a harp-shaped system in configurations that today would be denoted multi-cable systems. So the cable systems were actually up-to-date, but in contrast to the present practice the backstays were assumed to be earth anchored, as seen in the lower half of Figure 1.25.

Navier's final conclusion was that the suspension system should be used instead of the stayed system. This conclusion was to a large extent based on observations of stayed bridges that had failed.

In the early stayed bridges it proved very difficult to arrive at an even distribution of the load between all stays. Thus imperfections during fabrication and erection could easily lead to a structure where some stays were slack and others



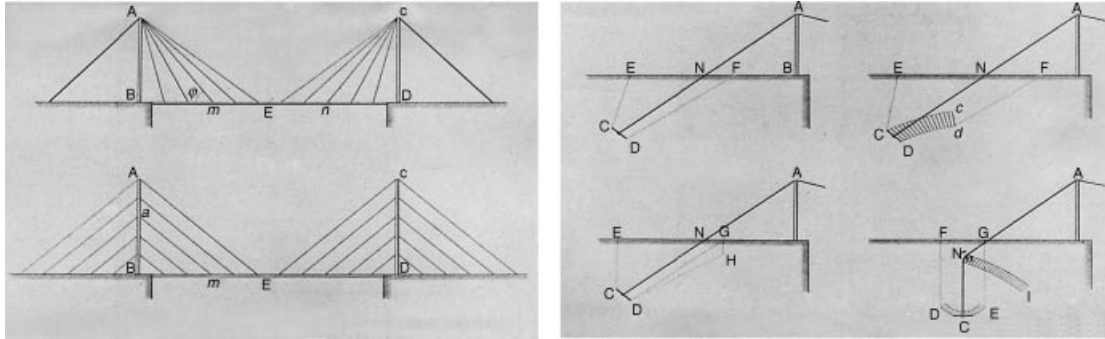


Figure 1.25 Bridge systems investigated by Claude Navier in 1823

overstressed. The stays were generally attached to the girder and pylon by pinned connections that did not allow a controlled tensioning.

### Strömsund Bridge

It was not until the mid-twentieth century that the first modern cable stayed bridge, the Strömsund Bridge in Sweden, opened to traffic in 1956 (Figure 1.26). The bridge was of the three-span type, a system generally used for suspension bridges, and it had a main span of 183 m flanked by two side spans of 75 m. The stays were arranged according to the pure fan system with two pairs of stays radiating from the pylon top. The pylons were of the portal type supporting the two vertical cable systems arranged on either side of the bridge deck. The stiffening girder contained two plate girders positioned outside the cable planes to allow an ‘invisible’ anchoring of the stays inside the plate girders.

The start of a new era for cable stayed bridges was to a large extent due to the improved technique of structural analysis allowing calculation of cable forces throughout the erection period and thereby assuring the efficiency of all cables in the final structure. Such calculations were made systematically for the first time in connection with the erection of the Strömsund Bridge.

Regarded as a plane system, the Strömsund Bridge is statically indeterminate to the eighth degree, but by dividing the loading into a symmetrical and an antisymmetrical part, the number of redundants could be reduced to four. This was well



Figure 1.26 Strömsund Bridge (Sweden)



**Figure 1.27** Duisburg–Ruhrort Bridge across the Rhine (Germany)

within acceptable limits for the numerical work that could be performed by the slide rule and the mechanical calculators available at the beginning of the 1950s.

In the case of the Strömsund Bridge the design could be based, with sufficient accuracy, on a plane analysis for each cable system, as the stiffening girder with its two I-shaped plate girders had an insignificant torsional stiffness allowing the forces acting on the bridge deck to be distributed transversally onto the two cable planes by the lever arm principle.

It is clearly seen that the general layout of the structural system of the Strömsund Bridge reflects the calculation capacity existing at the time, and that good agreement between the real structure and the mathematical model was intended.

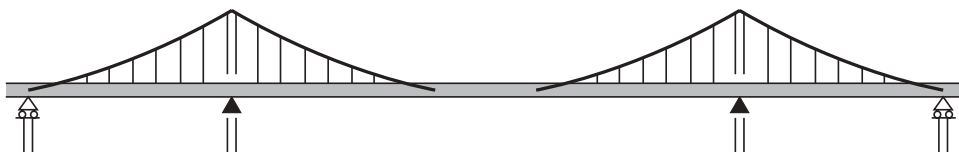
### Duisburg-Ruhrort Bridge

Coinciding with the construction of the Strömsund Bridge was the reconstruction of the Duisburg–Ruhrort Bridge across the Rhine River (Figure 1.27). Although not a real cable stayed bridge but a kind of transition system between a self anchored suspension bridge and a cable stayed bridge, the Duisburg–Ruhrort Bridge had a considerable influence on the introduction of cable stayed bridges in Germany.

In direct translation the cable system of the Duisburg–Ruhrort Bridge is designated a ‘rein chord system’ comprising a concave main cable anchored to the deck at the end supports of the side spans and near the main span centre. Between the main cable and the stiffening girder vertical hangers are arranged, as in a suspension bridge.

It will be seen from Figure 1.28 that the main cable can be regarded as a stay, connecting the stiffening girder to the pylon top, but in contrast to the pure cable stayed bridge, the main cable of the rein chord bridge also carries some vertical load in the regions between the pylon and the anchor point in the deck due to the transmission of loads through the hangers to the sagging main cables.

However, the influence of the Duisburg–Ruhrort Bridge on future cable stayed bridges was mainly due to the erection procedure prescribed by the requirement to avoid temporary piers in the main span. With a depth of



**Figure 1.28** Structural system of a ‘rein chord bridge’



**Figure 1.29** Theodor Heuss Bridge across the Rhine at Düsseldorf (Germany)

approximately 4 m, the stiffening girder could not be cantilevered to the main cable anchor point situated 125 m from the pylon, and a temporary supporting system was therefore required. This temporary system was made as a cable stayed system very similar to the one adopted in the Strömsund Bridge. And so the Duisburg–Ruhrort Bridge was born with a pure cable stayed system, but this was subsequently replaced by the rein chord system after completion of the deck erection.

Afterwards, it seemed obviously irrational first to build a bridge with a completely sensible cable stayed system and then replace it by a less efficient and more complicated cable system such as the rein chord system. In the years to come the cable stayed system was therefore preferred for all bridges with main dimensions equal to those of the Duisburg–Ruhrort Bridge.

### **Theodor Heuss Bridge**

After the Strömsund Bridge the next true cable stayed bridge to be erected was the Theodor Heuss Bridge across the Rhine River at Düsseldorf, opened to traffic in 1957 (Figure 1.29). With a main span of 260 m and side spans of 108 m, this, the second modern cable stayed bridge, was considerably larger than the Strömsund Bridge [58.1]. The Theodor Heuss Bridge also gave a clear indication of the cable stayed bridges' potential, initiating an impressive development of cable stayed bridges first in Germany and later throughout the world in the decades to follow.

In the case of the Theodor Heuss Bridge, new ideas were introduced in the cable system and in the design of the pylons. The cable system was of the harp configuration with parallel stays connected to the pylons at different levels. The pylons were made as free-standing posts fixed to the main girders and to a transverse girder between the bearings on the main piers. The configuration was chosen primarily for aesthetic reasons giving a more pleasant appearance of the two cable systems when viewed from a skew angle. However, the harp-shaped cable system is structurally less efficient than the fan system, as the global load transmission to a larger degree depends on the flexural stiffness of the deck (and the pylons).

Regarded as a plane system, the Theodor Heuss Bridge is statically indeterminate to the tenth degree but by splitting it into part systems and using symmetry and antisymmetry, it was possible to limit the number of redundants to a maximum of four in each step of the calculation.

### **Tancarville Bridge**

Until the end of the 1950s, the evolution of all major suspension bridges (with main spans exceeding 500 m) had been a completely American undertaking. But in 1959 the opening of the Tancarville Bridge with a main span of 608 m marked the beginning of the large suspension bridge era in Europe (Figure 1.30).

The Tancarville Bridge in France showed a number of novel features not derived from American practice. Thus, the stiffening truss was made continuous at the pylons and the cable in the main span was clamped to the truss at midspan. In connection with the application of a fixed bearing between the stiffening truss and one of the anchor blocks, this significantly increased the efficiency of the cable system for asymmetrical loading. The pylons of the Tancarville Bridge were made of reinforced concrete, a natural choice for these structural elements subjected mainly to compressive forces. In American bridges, steel pylons had been used for all major suspension bridges built in the twentieth century.



**Figure 1.30** *Tancarville Bridge across the Seine (France)*

### **Severins Bridge**

The second cable stayed bridge to be erected in Germany was the Severins Bridge in Köln (Figure 1.31). This bridge featured the first application of an A-shaped pylon combined with transversally inclined cable planes, and it was the first to be constructed as an asymmetrical two-span bridge with the pylon positioned at only one of the river banks. The cable



**Figure 1.31** *Severins Bridge across the Rhine at Köln (Germany)*



**Figure 1.32** George Washington Bridge after addition of the lower deck (USA)

system of the Severins Bridge was of the efficient fan-shaped type, which is in good harmony with the A-shaped pylon. The cross section of the deck was essentially the same as that used in the Theodor Heuss Bridge with two box girders connected by the orthotropic steel floor. Because of the large compression in the deck due to the one-sided arrangement of the pylon, the application of a steel floor was particularly advantageous in the Severins Bridge, as the axial compression could be distributed over a large cross sectional area. At both ends of the cable stayed portion, the deck was made continuous into the adjacent box girder spans. For this reason the structural system of the cable stayed portion was regarded as a plane system, was statically indeterminate to the ninth degree and, as the system was completely asymmetrical, the advantages of splitting into symmetrical and antisymmetrical loading could not be utilized. The task of analyzing the bridge in the final stage, as well as during erection, was therefore of considerable magnitude at the time it had to be performed.

Although it was one of the very first cable stayed bridges, the Severins Bridge still stands as a most successful bridge of this type. The design of the pylon with its pronounced dimensions and the way the deck ‘floats’ through the pylon constitute fine solutions to the design problems faced.

#### **Addition of the lower deck on the George Washington Bridge**

At the beginning of the 1960s, the George Washington Bridge had its lower deck added and at the same time the stiffening truss between the upper and the lower levels was established (Figure 1.32). The top chord and its gusset plates had already been included in the original structure from 1931 and this measure naturally eased the erection of the remaining part of the stiffening truss. But more importantly, the reconstruction was eased by the fact that the cable system, the pylons, and the anchorages were initially designed for the full load from the two decks. The stiffening truss of the George Washington Bridge was made with a depth of 9.12 m, corresponding to 1/117 of the main span length.

#### **Maracaibo Bridge**

A cable stayed bridge of unusual proportions (and based on a very different design philosophy) had been completed in 1962: the Maracaibo Bridge in Venezuela, designed by Riccardo Morandi (Figure 1.33).

In the Maracaibo Bridge both the pylons and the deck were made of concrete, thereby introducing a structural material that had not been used in the main elements of cable supported bridges. Furthermore, it was the first multi-span cable stayed bridge.

To allow one-way traffic of ships in and out of Lake Maracaibo, it was decided to build a bridge with five 235 m long main spans. Each of the five main spans contains a double cantilever arm supported by one pair of stays radiating from a



*Figure 1.33* Maracaibo Bridge (Venezuela)

triangular pylon structure designed to stabilize the system also for asymmetrical loads. Between the ends of the cantilever arms small drop-in spans were arranged, so that the system regarded as a plane system was externally determinate. The application of only one set of stays necessitated a heavy box girder to span from the pylon to the cable supported points. In later developments of the cable stayed system, the number of stays was gradually increased to give a more continuous support of the deck, which could then be made more slender and lighter.

The Maracaibo Bridge was later followed by two other major cable stayed bridges designed by Morandi: the Polcevara Viaduct in Genova and the Wadi Kuf Bridge in Libya.

### **Norderelbe Bridge**

The third German cable stayed bridge, the Norderelbe Bridge at Hamburg, was of a quite bizarre design with a pylon twice as high as required for structural reasons and with a cable system looking as if the main task was to support the pylon and not the deck (Figure 1.34). For the evolution of cable supported bridges the Norderelbe Bridge must however be included, as it was the first cable stayed bridge with a single cable plane arranged above the central reserve of the motorway. This system had already earlier been proposed by bidders for the Theodor Heuss Bridge and the Severins Bridge, but in both cases it had not been able to compete with the double cable plane system.

For a long period after the Norderelbe Bridge the single plane cable system became the preferred system for the majority of cable stayed bridges to be constructed in Germany – as well as in several other countries. In the case of the Norderelbe Bridge, the deck was composed of a central box girder 7.8 m wide and two outer plate girders, all with the same depth, and connected by a relatively larger number of primary transverse girders. This gave a high degree of indeterminateness, but the analysis of this complicated structural system was made easier by the application of one of the early computer programs for continuous girders on elastic supports. Therefore, only the plane cable system had to be analyzed by hand calculation.

The Norderelbe Bridge had to go through a major rehabilitation programme in the mid-1980s and as part of this the cable system was modified to a more sensible configuration. So today the Norderelbe Bridge looks less peculiar (Figure 1.35).

### **Verrazano Narrows Bridge**

In 1960, construction started on the largest bridge in the New York area: the Verrazano Narrows Bridge across the entrance to the port of New York (Figure 1.36). With a main span of 1298 m, this bridge was to have the largest free span of any bridge in the world, exceeding the Golden Gate Bridge span by 18 m!

In many of its design principles the Verrazano Narrows Bridge resembles the George Washington Bridge, both bridges being designed by Amman. Thus, they have in common the two closely spaced cable planes on either side of the roadway



*Figure 1.34* Norderelbe Bridge in its initial form (Germany)

area. As in the case of the George Washington Bridge, the Verrazano Narrows Bridge initially had only the upper deck prepared for carrying traffic. But in contrast to the George Washington Bridge, the Verrazano Narrows Bridge had the entire stiffening truss erected right from the beginning.

The depth of the stiffening truss was chosen to be 7.30 m, giving a depth-to-span ratio of 1:178, which is slightly more slender than in the Golden Gate Bridge, and considerably more slender than the stiffening trusses of other post-war suspension bridges in the USA such as the Second Tacoma Bridge and the Mackinac Bridge.

### **Firth of Forth Road Bridge**

Following the Tancarville Bridge, the suspension bridge across the Firth of Forth in Scotland was completed in 1964 (Figure 1.37). With a main span of 1006 m, this bridge ranked fourth in the world with respect to the main span length, and it was the first bridge to span more than 1 km outside the USA. With its steel pylons and simply supported stiffening trusses, the Forth Road Bridge appeared to be closer in its main layout to American practice than the Tancarville Bridge. However,



**Figure 1.35** Norderelbe Bridge in its renovated form (Germany)

in many details, the Forth Road Bridge showed important innovations. The depth of the stiffening truss of the Forth Road Bridge was chosen to be 8.4 m, corresponding to a depth-to-span ratio of 1:120.

### **Leverkusen Bridge**

After the Norderelbe Bridge came the Leverkusen Bridge (opened in 1964) across the Rhine (Figure 1.38). This bridge had the same centrally arranged cable plane, but here the cable system was of the harp configuration with two sets of stays connected to each pylon. Each stay comprised two individual cables composed of 19 locked-coil strands.

The orthotropic deck of the Leverkusen Bridge comprises a central 4.2 m deep box girder with large overhangs of the roadway. To reduce the moments in the cantilevered cross beams, inclined struts are added from the bottom of the main box girder to the cross beam near its tip.



**Figure 1.36** Verrazano Narrows Bridge in New York (USA)





*Figure 1.37 Firth of Forth Road Bridge in Scotland (UK)*

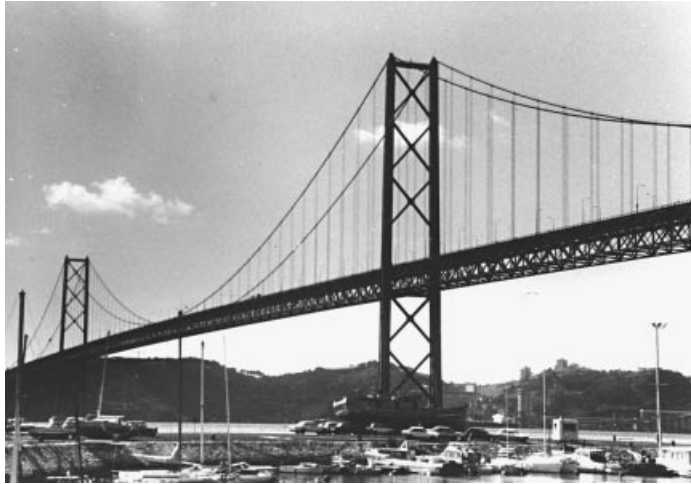
#### **20th April Bridge (Tagus River Bridge)**

Although built in Europe, the 20th April Bridge (Tagus River Bridge) in Portugal (Figure 1.39) is a product of American expertise on suspension bridges as both the designers (Steinman, Boynton, Gronquist and London) and the main contractors (US Steel, American Bridge Division) were American firms. Despite this fact, the 20th April Bridge shows some deviations from previous American practice. These deviations are mainly due to the requirement of preparing the bridge (initially built with a four-lane roadway) for a later addition of two railway tracks on a lower deck inside the stiffening truss. This made it necessary to make the stiffening truss continuous not only from the main span to the side spans but also further into adjacent beam spans of approximately 100 m length. Only by this continuity could unacceptable angular deflections in the track profile be avoided.

To limit the initial investment in the 20th April Bridge, it was required that only the anchorage and the pylons should be designed for the final loading from both the roadway and the railway, whereas the cable system and the stiffening truss were



*Figure 1.38 The bridge across the Rhine at Leverkusen (Germany)*



**Figure 1.39** 20th April Bridge (Tagus River Bridge) at Lisbon (Portugal)

to be strengthened when the railway tracks were added. The assumed solution was to supplement in the planned second stage the initial pure suspension system by a number of stays, and to utilize the railway stringers to transmit the horizontal components of the stay forces.

Many years would pass before the addition of the railway deck on the 20th April River Bridge reached the final design stage, and when that happened in the mid-1990s, the concept was changed so instead of adding a cable stayed system, the original suspension system was maintained but strengthened by an extra set of main cables above the existing system.

With a main span of 1014 m, the 20th April Bridge overtook by a small margin the Firth of Forth Road Bridge as the bridge with the longest free span outside the USA.

In connection with the opening of the 20th April Bridge in 1966, a Symposium on Suspension Bridges, organized by the International Association for Bridge and Structural Engineering (IABSE), was held in Lisbon. At this symposium many papers indicated the great possibilities for static and dynamic analysis offered by the electronic computer, and so the day was in sight when bridge designers could throw off the trammels placed upon them for three-quarters of a century by their limited calculation capacity. Naturally this freedom to choose the most appropriate structural system, without anxiously counting the degree of indeterminateness, gradually led to a new generation of cable supported bridges.

Along with these analytical advances, the 1960s also brought some new techniques that would decisively influence the future of cable supported bridges. One such technique was introduced during the construction of the Newport Bridge in the USA, and the other in the Severn Bridge in Great Britain.

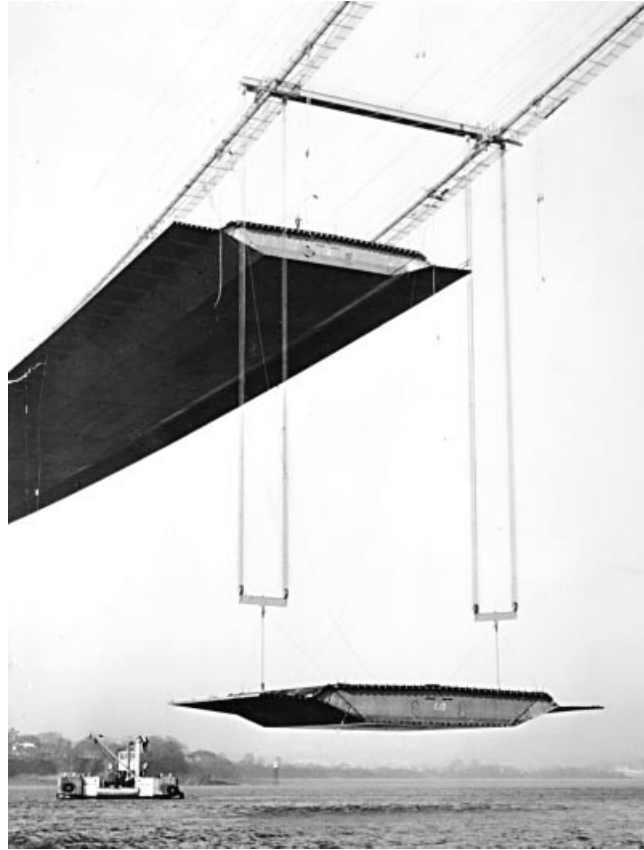
### **Severn Bridge**

During the design of the Severn Bridge, new concepts were introduced for the configuration of the deck and the hangers (Figure 1.40). Since the Tacoma Bridge disaster, the aerodynamic stability of all major suspension bridges had been achieved by the application of large trusses where the necessary resistance was achieved by a considerable flexural and torsional stiffness.

In the Severn Bridge concept, the designer Sir Gilbert Roberts substituted the truss by a slender box girder with a depth of 3 m, corresponding to a depth-to-span ratio of only 1:324, very close to the First Tacoma Bridge ratio of 1:350.

However, in the Severn Bridge design, the two main causes of the Tacoma Bridge disaster had been eliminated: the sharp edges of the plate girders were replaced by a streamlined shape determined by wind tunnel tests, and the insignificant torsional stiffness of the Tacoma Bridge was substituted in the Severn Bridge by the large torsional stiffness of a wide box girder.

The application of a streamlined box girder gave a noticeable saving in the construction cost, which was clearly demonstrated as both a conventional truss design and the new box design had been put out for tendering. The savings were



**Figure 1.40** Severn Bridge under construction (UK)

to a large extent due to the more efficient fabrication that could be obtained by the use of automatic welding especially suited for manufacturing the stiffened panels of the box girder.

Due to the large torsional stiffness of the box-shaped deck, torsional oscillations could be eliminated completely for actual wind speeds, whereas some vertical oscillations could still occur. To improve the damping characteristics of the cable system, it was decided to use inclined hangers, forming a zigzag net between the main cable and the deck. By this, the hysteresis of the helical ropes forming the hangers could be activated to damp oscillations.

### **Friedrich Ebert Bridge**

In the field of cable stayed bridges the breakthrough in computer-aided analysis led, in the second half of the 1960s, to the introduction of the multi-cable system where each stay is made of a single prefabricated strand.

The first of these multi-cable bridges was the Friedrich Ebert Bridge designed by H. Homberg and built across the Rhine north of Bonn (Figure 1.41). In this bridge, completed in 1967, a central cable plane with two pylons, each supporting 40 stays, was applied. Each stay was made of a single locked-coil strand with diameters ranging from 91 to 123 mm, depending on the position of the actual stay.

Multi-cable systems lead to a more continuous support of the deck, and at the same time the cable forces to be transmitted at each anchor point are reduced, so that a local strengthening of the deck at the anchorages can often be avoided. During erection, advantages are to be found due to the much shorter length of the cantilevers required to reach from one anchor point to the next, and in the final structure the smaller stay units will ease a replacement.



**Figure 1.41** Friedrich Ebert Bridge across the Rhine at Bonn (Germany)

The explanation for the fact that the multi-cable system with its clear merits first appeared 12 years after the introduction of the modern cable stayed bridge, is undoubtedly that this system involves a high degree of indeterminateness. With the multi-cable system of the Friedrich Ebert Bridge, containing a total number of 80 stays, even the plane system is indeterminate to the 82nd degree. With the electronic computer the analysis was well within reach, but with calculations by hand the amount of numerical work would be impossible.

In the Friedrich Ebert Bridge the application of a central cable plane made it necessary to use a rather large box section to ensure the necessary torsional stiffness. Full advantage of the continuous support from the multi-cable system to reduce the dimensions of the deck was therefore not achieved.

### **Rees Kalkar Bridge**

In the Rhine Bridge at Rees, constructed almost simultaneously with the Friedrich Ebert Bridge, two cable planes, each containing a harp-shaped multi-cable system, were used. Thus, the deck could be composed of two plate girders located at the edges of the orthotropic bridge floor (Figure 1.42).



**Figure 1.42** Rees Kalkar Bridge (Germany)



**Figure 1.43** Danube Canal Bridge in Vienna (Austria)

Both the Friedrich Ebert Bridge and the Rees Kalkar Bridge are characterized by relatively long portions of the girder unsupported by stays at midspan and adjacent to the pylon.

#### **Early cable stayed bridges with concrete girders**

In the first two decades after the completion of the Strömsund Bridge, the evolution of cable stayed bridges was dominated by steel bridges with orthotropic steel floors, plate or box girders and cellular pylons. Only the remarkable bridges by Riccardo Morandi showed an application of concrete for this bridge type. However, the designs of Morandi were of such a personal style that they did not serve, to any large extent, as models for the cable stayed concrete bridges to come.

A pioneer among cable stayed bridges made of concrete was the Danube Canal Bridge in Vienna (Figure 1.43) with a main span of 119 m. The deck consists of a concrete box girder and the stays are composed of parallel mono-strands. The Danube Canal Bridge has a pleasing appearance and harmonious proportions, and the construction procedure was quite unique as the bridge was cast in two halves on either side of the canal and subsequently turned around a vertical axis into position after installation and tensioning of the stay cables.

#### **Clairborne Pell Bridge (Newport Bridge)**

In the Clairborne Pell Bridge, the principle of using prefabricated parallel-wire strands (PPWS) for the erection of the main cables was applied for the first time in the construction of a major suspension bridge (Figure 1.44).

Since the days of Roebling, all major suspension bridges have had their main cables fabricated on site by the air-spinning method, where the wires are drawn one by one across the spans and successively placed in a bundle forming the entire cable. Although the air-spinning method had proved its efficiency during the construction of such notable bridges as the George Washington Bridge, the Golden Gate Bridge, and the Mackinac Bridge, it could cause problems due to its weather sensitivity and to its labour consumption. For some time therefore a procedure had been investigated where a large number of parallel wires forming a multi-wire strand were pulled over at a time, as this could make the operation more stable and reduce the required labour force.

The principle of hauling prefabricated strands across from one end anchorage to the other had long been utilized in the construction of smaller suspension bridges, but in these cases the strands were always of the helical wire type. By using parallel-wire strands, the properties of the final cable would be exactly the same as if the air-spinning method had been used [71.1].



**Figure 1.44** Hauling of a prefabricated parallel-wire strand during construction of the Clairborne Pell Bridge (Newport Bridge)

In the case of the Clairborne Pell Bridge, each main cable consists of 4636 wires, requiring 1159 runs of the spinning wheel if four wires were carried across in each run. With the prefabricated strands, each containing 61 wires, the number of runs could be kept as low as 76.

The introduction of the parallel-wire strand method took place during the last phase of the great American suspension bridge era, so the many potentials of the method could not be fully developed in continuation of the Clairborne Pell Bridge construction. Instead the developments took place in Japan, where the parallel-wire strand method soon became the preferred system for the erection of the main cables in the large Japanese suspension bridges.

### **Knie Bridge**

In 1969, a notable cable stayed bridge, the Knie Bridge, was opened to traffic in Düsseldorf (Figure 1.45). In this bridge the cable system was of the harp configuration with parallel stays, but in contrast to earlier bridges with this system, intermediate supports were arranged under every cable anchor point in the side span. This increased the efficiency of the double harp system to such an extent that it was possible to use a slender deck with an open cross section, i.e. with insignificant torsional stiffness.

In the Knie Bridge an asymmetrical layout similar to that of the Severins Bridge is used with the pylon located on one of the river banks only. Despite the considerable height of the steel pylon (114 m), it was possible to construct it as two free-standing posts without any cross beams or bracings to stabilize laterally.

### **Papineau Bridge**

A pioneer among cable stayed bridges in North America was completed in Montreal in 1969: the Papineau Bridge (Figure 1.46) with a main span of 241 m. In several of its design features this bridge resembled the Leverkusen Bridge and other German bridges with a central cable plane and a deep, but relatively narrow, box girder under the wide orthotropic bridge floor. The cable system was of the fan type with only two sets of stays radiating from each pylon top. Each stay cable



**Figure 1.45** Knie Bridge across the Rhine at Düsseldorf (Germany)

was composed of several helical bridge strands of galvanized wires. As a novelty each strand was covered with a hot extruded polyethylene coating with a minimum cover of 5 mm.

#### **Lillebælt Suspension Bridge**

For suspension bridges the application of the streamlined box as a deck became more widespread during the 1970s. In 1970, the Lillebælt Suspension Bridge in Denmark, designed by C. Ostenfeld, was the second, after the Severn Bridge, to use the streamlined box (Figure 1.47). However, because the Lillebælt Bridge was to carry only automobile traffic, the footpaths extending from the leading and trailing edges of the Severn box were omitted in the Lillebælt box.

The main cables of the Lillebælt Bridge were made of helical strands as they had proved to be the cheaper solution although the total cable length was close to 1500 m. In the Lillebælt Bridge the cable system was – in contrast to the solution adopted for the Severn Bridge – of the conventional configuration with vertical hangers. The pylons were made of concrete as in the Tancarville Bridge built ten years earlier with similar main dimensions.



**Figure 1.46** Papineau Bridge at Montreal (Canada)



**Figure 1.47** Lillebælt Suspension Bridge (Denmark)

An important contribution to the development of large steel bridges was the installation of dehumidification units inside the box girder of the Lillebælt Bridge. By keeping the relative air humidity below 40%, it was possible to avoid any corrosion on the interior steel surfaces and thereby avoid interior repainting that had become more and more costly due to health issues. In the years to follow the construction of the Lillebælt Bridge the principle of dehumidification spread to steel bridge around the world not only for new constructions but also as a retrofit of existing bridges.

### **Erskine Bridge**

In 1971, the Erskine Bridge in Scotland was completed (Figure 1.48). This bridge moved in the opposite direction of the trend towards the application of multi-cable systems, as only one stay leads from each of the two pylons to the deck in the 305 m long main span. Consequently, the deck had to span more than 100 m without support from the cable systems. Despite this fact, the deck was designed with a depth of only 3.05 m, which is of the same magnitude as used in cable stayed bridges with several stays supporting the deck at much smaller intervals. As the stay had to be made with a very large cross section, it was composed of 24 helical strands, each 76 mm in diameter.

During erection of the system with only one permanent stay from each pylon it was necessary to use two temporary stays to reduce the cantilever moment in the deck when advancing from the pylon to the cable anchor point in the main span.



**Figure 1.48** Erskine Bridge in Scotland (UK)





**Figure 1.49** The cable-stayed bridge across the Rhine between Mannheim and Ludwigshafen (Germany)

### **Mannheim-Ludwigshafen Bridge**

In 1972, the completion of the Mannheim-Ludwigshafen Bridge across the Rhine marked the first application of a parallel-wire strand in a major cable stayed bridge (Figure 1.49). Each strand with 295 wires of 7 mm diameter was anchored by a new type of socket denoted by a HiAm socket with increased fatigue resistance due to the application of a cold filling material containing an epoxy compound.

The Mannheim-Ludwigshafen Bridge also showed an interesting combination of materials as the deck in the main span was made entirely of steel and the deck in the side span entirely of concrete. This combination was very well justified, as the side span (through the application of an intermediate pier) had a maximum free span of 65 m, whereas the main span had a free length of 287 m. Actually, the higher dead load of the side span proved advantageous as it reduced the requirement for a vertical anchoring of the deck.

The combination of a concrete deck in the side spans and a steel deck in the main span was subsequently applied in several notable cable stayed bridges to be constructed in the years to follow.

### **First Bosphorus Bridge**

The third suspension bridge with the streamlined box was the First Bosphorus Bridge in Turkey (Figure 1.50). Here the cross section of the deck was very similar in its main layout to the one used in the Severn Bridge, whereas the structural system differs, as the Bosphorus Bridge had only the main span cable suspended. At completion in 1973, the 1073 m span of the Bosphorus Bridge was the longest outside the USA.

### **Kanmonkyu Bridge**

In Japan, the construction of major suspension bridges was initiated in 1973 with the completion of the Kanmonkyu Bridge between Honshu and Kyushu (Figure 1.51). This bridge has a main span of 712 m and carries a six-lane motorway.

In its design, the Kanmonkyu Bridge was very much influenced by the American tradition characterized by a deep stiffening truss, a non-participating bridge floor and cross-braced steel pylons. However, in the construction process, the Kanmonkyu Bridge contributed to the evolution of the suspension bridge, by use of the parallel-wire method for main cable erection.

### **Köhlbrand Bridge**

The cable stayed Köhlbrand Bridge in the port of Hamburg shows the first application of the multi-cable system in a bridge with double cable planes supported by diamond-shaped pylons (Figure 1.52). Each stay was made of an individual helical strand with diameters ranging from 54 mm to 110 mm.



**Figure 1.50** First Bosphorus Bridge at Istanbul (Turkey)

The cable system of the Köhlbrand Bridge is one of high efficiency with its modified fan configuration and short side spans. This gave advantages not only in the design of the final structures but also during erection as no temporary supports or temporary stays were required.

### **St Nazaire Bridge**

In France, the completion of the Saint Nazaire Bridge across the Loire River marked a further step for the cable stayed bridges as it was the first cable stayed bridge to span more than 400 m (Figure 1.53).

The pylons of the Saint Nazaire Bridge consist of an upper part in the form of an inverted V made of steel and a lower pier shaft of concrete. The cable system is of the multi-cable fan type where each stay consists of a single locked-coil strand.



**Figure 1.51** Kanmonkyu Bridge (Japan)



**Figure 1.52** Köhlbrand Bridge in the port of Hamburg (Germany)

**Rokko Bridge**

In Japan, cable stayed bridges had already begun to appear in the late 1950s but the first bridges of this type were not characterized by special design features so they had little influence on further development.

All cable stayed bridges built around the world in the period up to the second half of the 1970s had decks with solid web girders positioned below the bridge floor. In contrast to this, the decks of suspension bridges had traditionally been made as deep trusses and in a number of cases with two floors positioned at the top and the bottom chords of the truss. For cable stayed bridges, the high flexural stiffness of a truss was not required due to the efficiency of the cable support, but in the case of a double-deck structure the truss could be well justified.

The first double-deck cable stayed bridge – the Rokko Bridge – was completed in Japan in 1977 with a main span of 220 m (Figure 1.54). In this bridge the deck is formed as a truss with a depth of approximately 8 m to give ample headroom, daylight, and fresh air at the lower level. The cable system was of the multi-cable type, with each stay composed of two mono-strand cables.



**Figure 1.53** Saint Nazaire Bridge with a 404 m long main span across the Loire (France)



*Figure 1.54 Rokko Bridge at Kobe (Japan)*

### **Brotonne Bridge**

The application of a multi-cable system in a cable stayed concrete bridge was first seen in the Brotonne Bridge designed by J. Muller (Figure 1.55). Here a central cable plane was combined with a box-shaped deck, made partially of prefabricated elements.

The stays were made of parallel seven-wire strands of the type used for tendons in post-tensioned concrete. Corrosion protection was achieved by inserting the parallel strands in stainless steel tubes to be subsequently filled with cement grout. The anchoring of the seven-wire strands was initially made by wedge anchorages as used in tendons for pre-stressed concrete, but to increase the fatigue strength, especially for pulsating loads, a supplementary anchoring was established after application of the dead load. This supplementary anchoring was made by filling with epoxy resin a steel tube extending from the wedge anchorage.



*Figure 1.55 Brotonne Bridge across the Seine (France)*



**Figure 1.56** *Indiano Bridge across the Arno near Firenze. First major cable-stayed bridge with an earth anchored cable system (Italy)*

### **Indiano Bridge**

The first major cable stayed bridge with a fully earth anchored cable system was the Indiano Bridge built across the Arno River near Firenze (Figure 1.56). Designed by F. de Miranda [78.5], this bridge has a 206 m long main span supported by two fans radiating from the tops of 45 m high pylons leaning slightly backwards. From the pylons, earth anchored back stays are led to anchor blocks transmitting both the vertical and the horizontal component of the cable force to the soil.

The special problems related to the construction of cable stayed bridges with earth anchored cable systems were overcome in the Indiano Bridge by erecting the deck on temporary piers before adding the pylons and the cable system.

### **Pasco–Kennewick Bridge**

Another example of the use of the multi-cable system in a cable stayed concrete bridge was seen in the Pasco–Kennewick Bridge designed by F. Leonhardt in collaboration with Arvid Grant Associates (Figure 1.57). Here, the double cable plane systems are of the fan configuration, assuring an efficient support of the deck both vertically and torsionally.



**Figure 1.57** *Pasco–Kennewick Bridge across the Columbia River (USA)*



**Figure 1.58** Zarate-Brazo Largo Bridge across the Parana River (Argentina)

The stays, each made of a parallel-wire strand, are placed inside grouted polyethylene tubes for corrosion protection, and the anchorages are of the HiAm type. The deck was erected by the segmental method based on heavy prefabricated elements with the full width of the roadway.

### **Zarate-Brazo Largo Bridges**

Two cable stayed bridges across the Parana River in Argentina (Figure 1.58) were designed by a group comprising F. de Miranda from Italy, F. Leonhardt from Germany, and Techint of Buenos Aires. The bridges that were completed in 1978 are in many ways similar to the Pasco–Kennewick design. However, the decks of the Zarate-Brazo Largo Bridges are made of steel.

The Zarate-Brazo Largo Bridges are remarkable for the fact that they are the first cable stayed bridges to carry a track with heavy railway loading. Naturally this gave special design problems which were, to a certain extent, accentuated by the one-sided position of the track, thus subjecting the two vertical cable systems to traffic loads of different intensity. For this reason it was necessary to use different dimensions for the stays in the two sides, with the heavier cables required for the railway side.

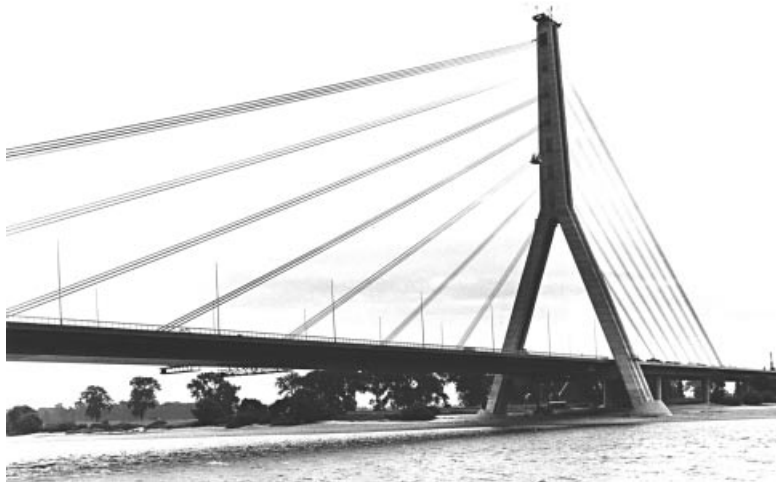
The stays of the Zarate-Brazo Largo Bridges are made of parallel-wire strands with 7 mm wires varying in number between 103 and 337, depending on the position of the stay. All strands have HiAm anchors at the ends – a feature of special importance in these bridges where a large fatigue resistance is essential to cope with the pulsating loads from passing trains. The cable systems of the Parana Bridges are of the efficient fan configuration with relatively short side spans. The pylons are made of concrete and the dimensions are chosen to allow a double-sided free cantilevering of the deck without requiring temporary supports.

### **Düsseldorf–Flehe Bridge**

The Düsseldorf–Flehe Bridge with a 367 m long main span across the Rhine River was built with only one pylon with a height of 150 m on one of the river banks. In contrast to the German practice at the time, the pylon was made of concrete, and its lambda ( $\lambda$ ) configuration was chosen to give support to the central cable plane with a harp-shaped cable system in the side span and a semi harp in the main span (Figure 1.59). In its appearance the pylon of the Flehe Bridge is not very convincing, especially when compared to other, more recent  $\lambda$ -shaped pylons.

### **Humber Bridge**

In 1981, the Humber Bridge in England (Figure 1.60) was completed with the largest clear span in the world, 1410 m, exceeding the Verrazano Narrows Bridge main span by more than 100 m.



**Figure 1.59** The cable-stayed bridge across the Rhine between Düsseldorf and Flehe (Germany)

The Humber Bridge is of a design similar to that used in the Severn Bridge and the Bosphorus Bridge, e.g. with a streamlined, box-shaped deck and with inclined hangers in the suspension system. However, the pylons of the Humber Bridge are made of concrete, whereas its two predecessors had steel pylons. An unusual feature of the Humber Bridge is the huge difference between the length of the two side spans, one being 280 m long and the other 530 m. Such asymmetry had not been found previously in any major suspension bridge.

In the Humber Bridge the air-spinning method was used for the erection of the main cables. Due to severe climatic conditions and the weather sensitivity of the air-spinning process, the time for cable erection was prolonged considerably beyond schedule. The delays experienced during air-spinning of the main cables of the Humber Bridge to many bridge designers were seen as an indication of the inadequacy of this traditional method so there was a feeling that the future belonged to the parallel-wire strand method.



**Figure 1.60** Humber Bridge (UK)



**Figure 1.61** *The first Tjörn Bridge under construction in 1959 (Sweden)*

### **Tjörn Bridge**

From the very beginning the principle of cable support has been applied not only in the final stage but also to give temporary support to bridges and other structures during erection. Thus, the principle of support by stay cables was actually used in the temporary stages before it was widely introduced as a part of the final bridge structure.

The application of a suspension system to give temporary support during construction of a major bridge was seen in the First Tjörn Bridge in Sweden constructed at the end of the 1950s as a steel arch with a span of 280 m. Due to the huge water depths and clearance requirements during construction, it was decided to erect the arch by application of a temporary cable system of the suspension bridge type (Figure 1.61).

After twenty years of service the choice of an arch bridge for the final structure proved to be fatal as a total collapse of the main span occurred when a misnavigated ship collided with one of the thin-walled tubular steel arches. To avoid a similar disaster in the future it was decided to rebuild the Tjörn Bridge as a cable stayed bridge with a 366 m main span, allowing both pylons to be positioned on land (Figure 1.62).



**Figure 1.62** *The second Tjörn Bridge under construction in 1981 (Sweden)*



Thus, the Tjörn Bridge constitutes a good illustration of the superiority of cable supported bridges in cases where navigable waters are to be spanned. With its load-carrying elements positioned above the roadway, the cable supported bridge is considerably less likely to suffer damage from ship collisions.

The Tjörn Bridge belongs to the group of cable stayed bridges with different structural materials in the side spans and the main span. The side spans are designed as continuous concrete girders with intermediate column supports at each cable anchor point whereas the main span is made as a steel box with orthotropic steel floor overhangs.

During the 1980s, the activity within the field of cable stayed bridges was considerably reduced in Europe compared to the previous decades, and most of the bridges that were actually built did not deviate much in size or design features from those already constructed.

### **Innoshima Bridge**

After the Kanmonkyu Bridge the construction of suspension bridges in Japan was to a very great extent associated with the construction of bridges between Honshu and Shikoku. In the early 1970s it was decided to build three routes: an eastern route between Kobe and Naruto, a central route between Kojima and Sakaide, and a western route between Onomichi and Imabari. The total number of major suspension bridges in these three routes was originally planned to be 11 and among these was the longest suspension bridge in the world, the Akashi Kaikyo Bridge.

Many of the bridges had to carry both road and railway traffic with the cars running on an upper deck and trains on a lower deck. From the beginning all the larger bridges (with spans exceeding 500 m) were planned to be built as suspension bridges with conventional stiffening trusses and suspension systems with vertical hangers. The design of the suspension bridges between Honshu and Shikoku was initially based entirely on the principles found in the Second Tacoma Bridge and the Mackinac Bridge.

Very thorough investigations were carried out to study the behaviour of long span suspension bridges under the action of fast running trains, seismic actions, and high wind speeds (typhoons). Furthermore, the problems related to fatigue in the elements subjected to railway loading were investigated both theoretically and experimentally.

It had originally been decided to construct the three routes simultaneously (to avoid favouring one region over another), but after the Energy Crisis following the Middle East War in 1973, the original decision was changed and priority was given to the central route where the chain of bridges between Kojima and Sakaide became known as the Seto Ohashi. However, on the two other routes a few bridges of local importance were to be included in the first phase of bridge construction between the many islands situated along the routes from Honshu to Shikoku.

The first suspension bridge to be completed by the Honshu–Shikoku Bridge Authority was the Innoshima Bridge of the Onomichi–Imabari Route (Figure 1.63). Opened to traffic in 1984, this bridge has a main span of 770 m and it is to a large



**Figure 1.63** *Innoshima Bridge (Japan)*



*Figure 1.64* Barrios de Luna Bridge (Spain)

extent based on the same design principles as seen in the Kanmon Bridge. The Innoshima Bridge was constructed to carry just a four-lane road as the western route will be for automobile traffic only.

### **Barrios de Luna Bridge**

In 1984, the completion of the Barrios de Luna Bridge in Spain gave an indication of the competitiveness of concrete as structural material not only in the pylons but also in the deck of cable stayed bridges (Figure 1.64).

With a main span of 440 m, the Barrios de Luna Bridge surpassed the span of the Saint Nazaire Bridge by a margin of almost 10% and became for a couple of years the record holder among cable stayed bridges.

The bridge is characterized by a large torsional stiffness due to the application of a wide multi-cell girder supported by efficient cable systems along both edges.

### **Ohnaruto Bridge**

The second suspension bridge to be completed in the Honshu Shikoku complex after the Innoshima Bridge was a bridge to carry both road and railway traffic, the Ohnaruto Bridge in the Kobe–Naruto Route.

Ohnaruto Bridge with a main span of 876 m was opened to traffic in 1985 but initially only with the upper roadway deck in operation. The lower deck was planned to accommodate two tracks for the high speed trains, the Shinkansen, but these tracks were not to be laid before the entire route was completed.

In contrast to the Portuguese 20th April Bridge that was also designed for a later addition of railway tracks on a lower deck (but only after additional strengthening of the cable system), the Ohnaruto Bridge was built from the beginning with a main structure designed for the full load from both road and railway traffic so that only railway tracks and the stringers beneath had to be added to allow trains to pass. Consequently, the Ohnaruto Bridge became the first major suspension bridge to be completed with a main structure ready to carry both road and rail traffic.

It would, however, take some time before the ability to carry the Shinkansen was utilized, as it was decided in the mid-1980s to construct the other bridge in the Kobe–Naruto Route, the Akashi Kaikyo Bridge, as a pure road bridge with no provision for a later addition of railway tracks. So trains would not be passing over the Ohnaruto Bridge until completion of a railway tunnel between Honshu and Awajishima (the island between the Akashi Strait and the Ohnaruto Strait) or of a combined road and railway bridge east of Osaka. In any case we will be far into the twenty-first century before any of these projects can materialize.

The Ohnaruto Bridge showed the application of larger parallel-wire strands than ever used before for suspension bridge main cables, as each strand was composed of 127 wires with a diameter of 5.37 mm. The strands for the Kanmonkyu Bridge had 91 wires with a diameter of 5.04 mm. So in the Ohnaruto Bridge, strands with a 60% higher unit weight than in



*Figure 1.65* Ohnaruto Bridge (Japan)

the Kanmonkyu Bridge had to be handled during construction. This marked a further step in the evolution of the parallel-wire method – an evolution that had now become entirely a Japanese undertaking.

The Ohnaruto Bridge followed the design principles of the Kanmonkyu Bridge and the Innoshima Bridge with basically the same configuration of the stiffening truss and the pylons. However, in the Ohnaruto Bridge, the depth of the stiffening truss is to some extent governed by the clearance requirements of the trains, and this in combination with the relatively low altitude of the superstructure gives the bridge a somewhat sturdy appearance (Figure 1.65).

#### **Meiko Nishi Bridge**

A much more elegant cable stayed bridge was completed in Japan in 1985 across the port of Nagoya: the Meiko Nishi Bridge with a 406 m long main span [87.13]. Here the deck is designed as a semi-streamlined box girder supported by two inclined cable planes radiating from the top of A-shaped pylons. With the chosen pylon shape and the fan-shaped cable systems, the Meiko Nishi Bridge constitutes a fine example of a highly efficient cable stayed bridge (Figure 1.66).

#### **Farø Bridge**

The Farø Bridge in Denmark was opened in 1985 and it comprised a 290 m long main span supported by a central cable plane. The deck had originally been designed by the owner as a concrete box but a steel box alternative



*Figure 1.66* Meiko Nishi Bridge at Nagoya (Japan)



**Figure 1.67** Farø Bridge (Denmark)

(designed by COWI) proved to be competitive and was chosen for construction. The concrete pylons form a further development of the diamond-shaped pylons originally introduced in the Köhlbrand Bridge in Hamburg. Thus, in the Farø Bridge the lower triangle is extended all the way down to the water surface (Figure 1.67) rather than being supported by pier shafts.

The overall shape of the Farø pylon is well justified in the actual case where the pylon is founded on a single caisson. The shape has, however, been copied in other bridges where it is less evident that the diamond shape should be preferred.

### **Sunshine Skyway Bridge**

In North America the activity in construction of cable stayed bridges had been negligible during the 1960s and the 1970s, but from the beginning of the 1980s the situation would change dramatically.

In Florida, a ship collision accident had given a clear indication of the inadequacy of the navigation opening in the 250 m long main span of the Sunshine Skyway. It was therefore decided to replace the existing two parallel bridges by a single bridge with a 360 m long cable stayed main span. Two designs were prepared for the bridge, one based on a



**Figure 1.68** Sunshine Skyway Bridge in Florida (USA)



**Figure 1.69** Alex Fraser Bridge in Vancouver (Canada)

composite deck and two cable planes along the edges of the roadway, and the other with a pure concrete box and a single central cable plane. Both designs were put out for tender and the result showed a very close race between the two options.

The final choice was to construct the concrete bridge with a design based on the principles initially introduced during design and construction of the Brotonne Bridge in France. With its main span of 366 m, the Sunshine Skyway was on its completion in 1986 the longest cable stayed bridge in the USA (Figure 1.68).

The composite girder alternative for the Sunshine Skyway was based on a system with two longitudinal plate girders directly under the cable planes and a large number of transverse girders to give support to the deck slab of reinforced concrete. This concept was to be known as a 'ladder deck' in its main features applied to another North American bridge constructed at the same time, the Alex Fraser Bridge (Annacis Island Bridge) in Vancouver in Canada.

### **Alex Fraser Bridge**

The potential of a composite girder deck was clearly demonstrated during the construction of the Alex Fraser Bridge in Canada. Thus, to cantilever from one cable anchor point to the next is easily accomplished by the relatively light steel girders, prior to installation of the new stay cables. Then on the subsequent addition of the heavy concrete slab, the stays at the tip of the new segment are already in place. As the cantilever process continues, the concrete slab will be most efficient in transferring the axial compression induced in the deck by the horizontal components of the stay cable forces.

The advantages of applying composite girders in cable stayed bridges would, in the years following the construction of the Alex Fraser Bridge, lead to a situation where this system was gradually preferred for the majority of cable stayed bridges in North America.

With its main span of 465 m, the Alex Fraser Bridge (Figure 1.69) became the record-holder among cable stayed bridges for a period of five years.

### **Katsushika Harp Bridge**

In Tokyo, a tricky design problem was overcome in the late 1980s by constructing an S-curved cable stayed bridge [87.14] with two pylons of different height (Figure 1.70). It was the first major cable stayed bridge with a horizontally curved deck which was made possible by the opposite curvature of the deck on the two sides of each pylon in such a way that each set of stay cables induced only a vertical force into the free-standing post-shaped pylon. Without such a point symmetry, a pylon will be subjected to a lateral force that will induce an unfavourable bending – especially if the pylon is formed like a post.



*Figure 1.70* Katsushika Harp Bridge in Tokyo (Japan)

### **Rama IX Bridge (Chao Phrya Bridge)**

In cable stayed bridges both the type with a central cable plane above the median reserve and the type with two cable planes outside the roadway area were extensively applied in the first three decades of the modern evolution. To some extent the choice between the two options seemed to depend on the designer's preference rather than on a rational, unbiased comparison between advantages and drawbacks.

H. Homberg had clearly preferred the central cable plane concept wherever it was applicable, i.e. where the road to be carried had dual carriageways. It is therefore not a surprise that Homberg's largest cable stayed bridge, the Rama IX Bridge in Bangkok, was designed with a central cable plane, despite the span of 450 m (Figure 1.71).

The cable system is of the multi-cable, semi fan configuration and all stays are made of single locked-coil strands, among these the largest diameter locked-coil strand with a diameter of 174 mm. The deck in the main span is a quasi-trapezoidal,



*Figure 1.71* The Rama IX Bridge in Bangkok (Thailand)



**Figure 1.72** Shimotsui Seto Bridge (Japan)

five-cell box with the full width of the bridge deck (32.5 m) and with a depth of only 4 m. In the side spans the box girder is made with only three cells as intermediate supports significantly reduce the torsion induced in these spans.

### Seto Ohashi

After the omission of the railway line across the Ohnaruto Bridge, the first major suspension bridges to actually carry railway traffic became the three suspension bridges on the Kojima–Sakaide route: the Shimotsui Seto Bridge, the Minami Bisan Seto Bridge, and the Kita Bisan Seto Bridge.

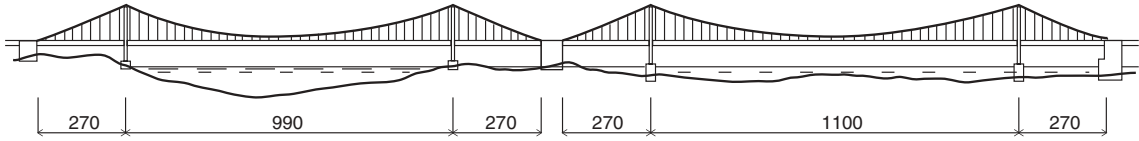
The Kojima–Sakaide route was opened to traffic in its entirety in 1988 and right from the beginning the double-deck truss carried automobile traffic at the upper level and ordinary trains at the level deck with two railway tracks. The bridges had originally been designed to carry four railway tracks on the lower deck, two for ordinary trains and two for the Shinkansen. However, due to the high costs of establishing the Shinkansen lines on land, only the tracks for ordinary trains were initially laid on the lower deck. But the ordinary trains also comprised freight trains with a relatively high load intensity.

During construction of the Kojima–Sakaide route it was decided to perform a full-scale comparative test of the two methods for main cable erection: the air-spinning method and the parallel-wire strand method. It was, therefore, chosen to let the main cables of the Shimotsui Seto Bridge be erected by the air-spinning method and the two Bisan Seto Bridges by the parallel-wire strand method.

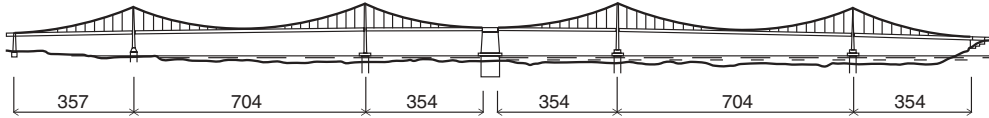
The Shimotsui Seto Bridge is a single-span suspension bridge as only the main span is cable supported (Figure 1.72). With a main span of 940 m, the Shimotsui Seto Bridge is the smallest of the suspension bridges of the Kojima–Sakaide route. Due to the fact that it has the same cross section of the stiffening truss as the Bisan Seto Bridges, but a considerably smaller clearance below, the appearance resembles that of the Ohnaruto Bridge. However, the Shimotsui Seto Bridge shows the first deviation from the application of cross-braced pylons previously found in all Japanese suspension bridges. In the Shimotsui Seto Bridge the pylons are of the portal configuration with two cross beams connecting the pylon legs above the bridge deck.

The Kita Bisan Seto Bridge and the Minami Bisan Seto Bridge together form a twin suspension bridge as they are only separated by a central anchor block as in the case of the San Francisco–Oakland Bay Bridge.

The two Bisan Seto Bridges are longer than their San Francisco counterpart, as is seen from Figure 1.73. Here it is also seen that, whereas the two suspension bridges of the Bay Bridge have long side spans corresponding to half the main span length, the Bisan Seto Bridges have relatively short side spans corresponding to approximately 25% of the main span length. This implies that the central anchor pier immediately appears to be more justified in the Bisan Seto Bridges because



BISAN SETO BRIDGE



SAN FRANCISCO-OAKLAND BAY BRIDGE

**Figure 1.73** Comparison between the San Francisco–Oakland Bay Bridge and the Bisan Seto Bridges

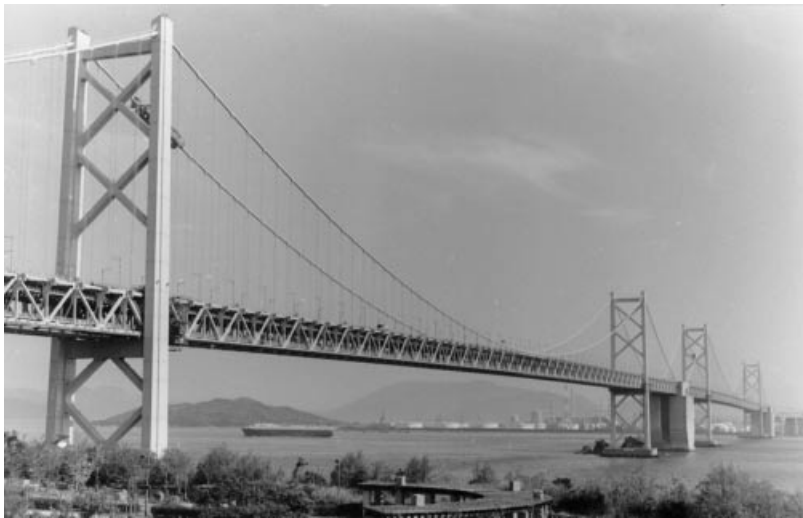
the central portion of the bridge, i.e. the two side spans flanking the central anchor block, is quite different from the adjacent main spans both in length but also in the main cable geometry.

Although twins, the two Bisan Seto Bridges are not identical as the main span is 1100 m for the Minami Bisan Seto Bridge and 990 m for the Kita Bisan Seto Bridge. This difference is, however, difficult to detect when looking at the bridges due to the perspective distortion (Figure 1.74).

The main cables of the Minami Bisan Seto Bridges have a diameter of 1.04 m – the largest found in any existing bridge at that time. The double-deck concept was also used for the twin cable stayed bridges, the Iwagurojima and the Hitsuishijima Bridges, that form a part of the Seto Ohashi between Honshu and Shikoku.

Each of the two cable stayed bridges has spans of 185 m–420 m–185 m and they are placed end to end. As in the suspension bridges on the same route, the traffic will be running on a two-level stiffening truss carrying at the upper level a four-lane expressway and at the lower level a double track railway with provisions for the later addition of two more tracks.

The cable systems are of the modified fan configuration with two vertical cable planes positioned directly above the stiffening trusses. This implies that an efficient support is achieved for both vertical and torsional loading.



**Figure 1.74** Bisan Seto Bridges (Japan)





*Figure 1.75 Iwagurojima and Hitsuishijima Bridges (Japan)*

The Iwagurojima and Hitsuishijima Bridges are remarkable structures although they are not exactly elegant in their appearance due to the heavy trusses imposed by the clearance and stiffness requirements of the railways (Figure 1.75).

#### **Ohshima Bridge**

Shortly before the opening of the Kojima–Sakaide Route an interesting suspension bridge named the Ohshima Bridge on the Onomichi–Imabari Route had been completed. This bridge deviated in a number of features from the tradition that had developed in Japan since the design of the Kanmonkyu Bridge.

The Ohshima Bridge was built with a streamlined box girder deck in the European style and the pylons were formed as portals in an elegant shape with a single cross beam at the top (Figure 1.76). From the point of view of appearance and adaption to the landscape, the Ohshima Bridge appears to outperform the other Japanese suspension bridges.



*Figure 1.76 Ohshima Bridge (Japan)*



**Figure 1.77** *Fatih Sultan Mehmet Bridge (Second Bosphorus Bridge) (Turkey)*

### **Fatih Sultan Mehmet Bridge (Second Bosphorus Bridge)**

The attitude towards the air-spinning method changed in the 1980s after the construction of the Fatih Sultan Mehmet Bridge where the method was improved by introduction of the low-tension procedure that eliminated the need for an individual sag adjustment of each wire and only required a sag adjustment of a full multi-wire strand, i.e. composed of 500 wires. The low-tension procedure was developed by Japanese engineers and it proved its efficiency by allowing the main cables (comprising 9500 tons of wires) to be spun in only four months. This gave back to the air-spinning method its former reputation and in the following years this method proved to be very competitive for cable erection outside Japan.

The Fatih Sultan Mehmet Bridge was designed by the same consulting engineers as the Severn Bridge, the First Bosphorus Bridge and the Humber Bridge so it is not surprising that it has a streamlined box beneath the roadway – and in this case a wider box than in any of the previous bridges of this type (Figure 1.77).

In one aspect, the Second Bosphorus Bridge deviates from its predecessors of the British suspension bridge concept as it has vertical hangers. This can be seen as an indication of the fact that the inclined hangers had actually given rise to more problems (e.g. in relation to fatigue) than they solved.

The structural system of the Fatih Sultan Mehmet Bridge corresponds in many ways to that of the First Bosphorus Bridge. Thus, it is a single span suspension bridge with only the main span supported by the cable system – a feature that is further emphasized by the position of the pylons at the top of the steep slopes on either side of the strait. So the road is at ground level all the way to the pylons and the abutments are integrated in the pylon foundations.

### **Yokohama Bay Bridge**

In Japan, the double-deck configuration was again applied in the Yokohama Bay Bridge [91.17] opened to traffic in 1989. With its main span of 460 m, the bridge was only 5 m shorter than the Alex Fraser Bridge in Canada – at that time the record-holder among cable stayed bridges.

From the point of view of appearance, the Yokohama Bay Bridge is quite successful as the truss is well proportioned and the pylons have a clear and simple geometry (Figure 1.78). The Yokohama Bay Bridge would eventually carry 12 lanes of vehicular traffic at two levels but initially only the upper level was opened to traffic.

The stiffening truss of the Yokohama Bay Bridge has its top chord made as a 39 m wide and 3 m deep, streamlined box girder, whereas the bottom chord and the diagonals are of more conventional bluff box sections. The total depth of the truss is 12 m corresponding to 1/38 of the main span length.



**Figure 1.78** Yokohama Bay Bridge (Japan)

#### **Napoleon Bonaparte Broward Bridge (Dames Point Bridge)**

In the USA, the general trend throughout the 1980s was to simplify the design of the decks especially in cable stayed bridges. Within concrete bridges a good example on this trend is the Napoleon Bonaparte Broward Bridge at Jacksonville in Florida. With a main span of 396 m, the bridge surpassed the Sunshine Skyway Bridge as the longest concrete cable stayed bridge in North America.

The cable system is a multi-cable harp system supported by concrete pylons with a considerable flexural stiffness in the longitudinal direction. This gave the cable system very good deformational characteristics so that the deck could be made with a depth of only 1.5 m corresponding to 1/260 of the main span length (Figure 1.79).

In principle, the layout of the deck in the Dames Point Bridge corresponds to that of the Alex Fraser Bridge, i.e. with two longitudinal edge girders beneath the cable planes and numerous cross beams. However, in the Napoleon Bonaparte Broward Bridge the longitudinal girders are made of solid concrete edge beams with a depth of 1.5 m and a width of 2.5 m, that allows the most efficient anchoring of the stay cables.

Seen in comparison with the Pasco–Kennewick Bridge, the Napoleon Bonaparte Broward Bridge clearly shows a simplification in the design of a concrete deck.



**Figure 1.79** Napoleon Bonaparte Broward Bridge (Dames Point Bridge) at Jacksonville in Florida (USA)



**Figure 1.80** Nanpu Bridge in Shanghai (China). (Courtesy of Bridge Magazine)

### **Nanpu Bridge**

In the People's Republic of China, a considerable number of cable stayed bridges had been built since the mid-1970s but they were all of moderate size. However, with the completion in 1991 of the Nanpu Bridge at Shanghai (Figure 1.80), China joined the group of nations with long span cable supported bridges and in the following decennia China would gradually be the country with most activity in construction of long span suspension and cable stayed bridges.

The 423 m main span of the Nanpu Bridge as well as its 150 m high concrete pylons were impressive in the early 1990s and gave a clear indication of the fact that the Chinese bridge technology had reached a high level. The deck of the Nanpu Bridge is in composite construction with a concrete slab on top of a steel girder grid often referred to as a 'ladder deck'.

### **Kvarnsund Bridge**

In the early 1990s, two remarkable Norwegian cable stayed bridges in concrete, the Helgeland Bridge and the Kvarnsund Bridge were constructed. In comparison with most other cable stayed bridges, the Norwegian bridges are characterized by very small width-to-span ratios as the bridges only have to carry two lane roads.

The Kvarnsund Bridge with its main span of 530 m was, for a period of slightly over two years, the record-holder for free spans of cable stayed bridges. This was a most remarkable achievement taking into account the limited deck width and the use of concrete in the entire structure. The Kvarnsund Bridge has a pleasing appearance with a slender A-shaped pylons and a simple deck geometry (Figure 1.81).

### **Askøy Bridge**

Numerous suspension bridges had been built in Norway throughout the twentieth century but most of these bridges were small and narrow, but in 1992 a remarkable suspension bridge, the Askøy Bridge, with a main span of 850 m, was completed (Figure 1.82).

During the construction of the many suspension bridges with moderate spans, a special Norwegian tradition had developed regarding the configuration of the main cables. The cables were composed of several individual locked-coil strands clamped together only at the points of hanger attachment.

In the Askøy Bridge, each of the two main cables comprised 21 locked-coil strands arranged in three layers, each with seven strands. The total ultimate breaking load of each main cable is 190 MN. With this size, the traditional Norwegian design of cable clamps and saddles appears to be somewhat primitive. Thus, the strands are pressed against flat plates inserted between and outside the three layers.



**Figure 1.81** Kvarnsund Bridge at Trondheim (Norway)

The most remarkable feature of the Askøy Bridge was the erection procedure for the steel box deck made up of segments with a length of 36 m or 24 m. Using a large floating crane, the entire deck with a length of 850 m was erected in just five working days!

#### **Alamillo Bridge**

Throughout the evolution of cable stayed bridges, a large number of variants regarding cable configuration, span arrangement, pylon shape, etc., have appeared, but in the early 1990s it was demonstrated by the construction of the Alamillo Bridge in Spain that there was still scope for innovative designs (Figure 1.83).

Designed by Santiago Calatrava, the Alamillo Bridge comprises a 200 m long steel span supported by stay cables in a harp configuration anchored at the other end to a backwards leaning concrete pylon. With the combination of a lightweight steel deck and a heavy concrete pylon, it was possible to balance the dead load of the two main structural elements but traffic



**Figure 1.82** Askøy Bridge at Bergen (Norway)



**Figure 1.83** Alamillo Bridge in Seville (Spain)

load has to be transferred by bending of the deck and the pylon. Therefore, the structural system is not one of very high efficiency but the bridge has a striking appearance and it certainly stands out as an unusual specimen of cable stayed bridges from the end of the twentieth century.

#### **Higashi Kobe Bridge**

The Higashi Kobe Bridge was completed in 1993. In this bridge with a main span of 484 m the deck is constructed as a double-deck truss supported by a harp-shaped cable system (Figure 1.84). In its main features the truss of the Higashi Kobe Bridge is considerably more modern in its design than most other cable supported trusses in Japan. Thus, the trusses are pure Warren trusses without verticals and the orthotropic bridge floors are incorporated in the chords, i.e. a system of high structural efficiency.

#### **Tsurumi Tsubasa Bridge**

A remarkable Japanese cable stayed bridge, Tsurumi Tsubasa Bridge, was completed in 1994 [94.13] on the Bay Shore Route between Tokyo and Yokohama just a short distance from the Yokohama Bay Bridge. The spans of the cable stayed



**Figure 1.84** Higashi Kobe Bridge (Japan)



**Figure 1.85** Tsurumi Tsubasa Bridge (Japan)

portion of the Tsurumi Tsubasa Bridge are 255 m, 510 m and 255 m, i.e. a most unusual ratio of 0.5 between side and main span length (Figure 1.85). In almost all other cable stayed bridges, the span ratio is less than 0.4 unless there are intermediate supports in the side span. With the long side spans, a considerable unloading of the initial dead load force in the anchor cables will occur.

The Tsurumi Tsubasa Bridge is also extreme by having only a single central cable support of the 38 m wide box girder. So it surpasses by 60 m the span of the bridge that was formerly the longest with only one central cable plane: the Rama IX Bridge in Bangkok.

The pylons of the Tsurumi Tsubasa Bridge constitute an interesting variant of the diamond-shaped pylons, and the combination of an upper steel part with a lower pier shaft in concrete is more aesthetically pleasing than in most other examples with this combination, e.g. the Köhlbrand Bridge or the Saint Nazaire Bridge.

### **Clark Bridge**

An interesting cable stayed bridge in the USA from the mid-1990s is the Clark Bridge across the Mississippi River, north of St. Louis. In this bridge a central pylon in the median reserve of the roadway was for the first time combined with two inclined cable planes with stay cables anchored along both edges of the roadway area. In all other bridges with a one post-shaped pylon, only one central and vertical cable plane was used.

The arrangement of pylons and cable planes in the Clark Bridge gave a new and exciting appearance (Figure 1.86), but it did lead to an additional width of the bridge deck to give room for the central pylon and to have sufficient vertical clearance under the inclined cable planes.

### **Yangpu Bridge**

In 1994, the world record for free spans of cable stayed bridges was conquered by the Yangpu Bridge in Shanghai [95.2] with its free span of 602 m (Figure 1.87). The Yangpu Bridge has a composite deck similar to that of the Nanpu Bridge and its H-shaped pylons (with a height of 208 m) are also of concrete.

### **Fred Hartman Bridge**

Among American cable stayed bridges with a composite deck, the most remarkable specimen is the Fred Hartman Bridge [94.9] across the Houston Ship Canal in Texas. Due to the extreme width of the bridge deck, approximately 47 m, the bridge is constructed with two independent decks, each containing two longitudinal plate girders, a large number of transverse girders and on top a concrete floor slab (ladder deck). Each of the two decks is supported by two inclined cable planes attached to the tops of the double diamond pylons (Figure 1.88).



**Figure 1.86** *Clark Bridge across the Mississippi (USA)*



**Figure 1.87** *Yangpu Bridge in Shanghai (China). (Courtesy of Bridge Magazine)*





**Figure 1.88** Fred Hartman Bridge at Houston (USA)

In contrast to the decks, the two diamond-shaped pylon structures do not act independently but are joined at the deck level. This leads to a most efficient truss action under lateral loading, completely eliminating the drawbacks of the single diamond-shaped pylon.

### **Normandy Bridge**

At the end of the 1980s, it became evident that great achievements would be experienced within the field of cable supported bridges in the last decade of the twentieth century. The first of these achievements was the construction of the record-breaking Normandy Bridge with its cable stayed span of 856 m across the Seine River in France [91.2].



**Figure 1.89** Normandy Bridge (France)



**Figure 1.90** *Erasmus Bridge in Rotterdam (Netherlands)*

The start of construction of the Normandy Bridge marked a much more innovative step from existing spans of this bridge type than any earlier steps, and at the same time a number of new design features were introduced. With a main span across the main navigation channel of the Seine River, there would be no need for larger spans outside the pylons and it was therefore decided to continue the short approach spans with lengths of 43.5 m throughout the cable stayed side span until a point 96 m from the pylons. It even proved advantageous to continue the concrete box girder through the 96 m span and 116 m into the navigation span so that only the central 624 m of the 856 m main span was to be made as a steel box (Figure 1.89).

As a most unusual feature, the bridge girder is fixed to the pylons at both ends so that strains in the main span girder due to temperature variations will induce an axial force in the girder and bending moments in the pylon legs.

The pylons of the Normandy Bridge are made of concrete in a  $\lambda$ -shape so that the top part, where the stays of the multi-fan system are anchored, has the form of a vertical column.

### **Erasmus Bridge**

Cable supported bridges are in general mainly recognizable by the shape of their pylons so if a bridge of a unique design is required, it is often attempted to give the pylon an unusual shape.

The Erasmus Bridge in Rotterdam from 1996 is a good example of this feature as in elevation the 139 m high  $\lambda$ -shaped pylon has a kink between the top part and the straddling legs (Figure 1.90). The cable system in the 280 m long main span is of a semi-fan configuration and in the side span a large, steep backstay stabilizes the pylon.

### **Shantou Bridge**

In the beginning of the 1990s, a number of major suspension bridges began to appear in China, and one of these was the unconventional medium-span Shantou Bridge of 1995. The Shantou Bridge with its 452 m long main span is unique by having the deck made of pre-stressed concrete segments. This was the first application of a pure concrete deck in a major suspension bridge where it was generally found that the increased weight of a concrete deck would lead to an unacceptable increase in the quantity of cable steel used. However, in the case of the Shantou Bridge, the chosen design turned out to compete favourably against a suspension bridge with a steel deck as well as a cable stayed bridge with a concrete deck.

The Shantou Bridge is a three-span suspension bridge with side spans of 154 m, approximately one-third of the main span and with a main span sag of 46 m (Figure 1.91).

The application of a concrete deck in a suspension bridge does not seem to have been convincingly demonstrated by the Shantou Bridge, so it is not to be expected that the combination of a concrete deck and a suspension system will be repeated in future.



**Figure 1.91** *The Shantou Bridge (China). (Courtesy of Bridge Magazine)*

### **Höga Kusten Bridge**

In 1993, construction began on the Höga Kusten Bridge in Sweden [94.5] – a suspension bridge with a main span of 1210 m, the second longest bridge span in Europe at its completion. The design of the Höga Kusten Bridge was in accordance with the modern European tradition, i.e. a streamlined box girder with continuity from anchor block to anchor block and concrete pylons. For the main span the width-to-span ratio is quite extreme with a value of  $20.8/1210 = 1/58$ .

The side spans, with lengths of 317.5 m and 287.5 m, are almost entirely on land and it was initially assumed that these spans should be made as girder spans acting independently of the cable supported main span, but for architectural reasons it was decided to build a three-span suspension bridge with cable support throughout. Also for architectural reasons, the pylons have been given a somewhat awkward shape with legs having a width that increase laterally from the deck level to the top (Figure 1.92).

Since 1997, the Höga Kusten Bridge has been the world's longest toll-free bridge.

### **Tsing Ma Bridge**

In Hong Kong, the fixed traffic links between the mainland and Hong Kong Island, which were constructed in the early 1970s, were all tunnels, but for the link to the new Chek Lap Kok Airport off the coast of Lantau Island, it was



**Figure 1.92** *Höga Kusten Bridge. (Photo credit: Staffan Gillusson, Swedish Road Administration)*



**Figure 1.93** *Tsing Ma Bridge (Hong Kong SAR)*

decided to build three major cable supported bridges. The largest of these bridges is the Tsing Ma Bridge [95.7], built in 1997. It is a suspension bridge with a free span of 1377 m and carrying both road and rail traffic at two levels (Figure 1.93).

The deck is designed in quite a unique (but also quite complicated) way with two longitudinal trusses positioned some distance from the vertical cable planes, and with non-participating corrugated plates of stainless steel added to give the desired overall shape of the deck and to give protection against the side wind on the lower level.

In elevation, the Tsing Ma Bridge was unusual by having one of the side spans suspended whereas the main cables in the other side span are continued from the pylon saddles to the anchor blocks as straight backstays. Among major suspension bridges, the Tsing Ma Bridge was probably the first to have such an asymmetric layout but this model has since then been applied to other large suspension bridges, e.g. in the Kurushima Bridges and the Xihoumen Bridge.

The main cables of the Tsing Ma Bridge have a diameter of 1.1 m, which makes them the largest diameter suspension bridge cables in the world. The main cables were erected by the traditional high-tension air-spinning method.

### **Kap Shui Mun Bridge**

In almost direct continuation of the Tsing Ma Bridge is the Kap Shui Mun Bridge [94.12], a cable stayed bridge with a main span of 430 m and carrying the same traffic lanes and railway tracks as the Tsing Ma Bridge.

The deck of the Kap Shui Mun Bridge has the same two level arrangement as the Tsing Ma Bridge but the structural configuration is somewhat simpler, e.g. in the main span, the longitudinal trusses are replaced by webs of stiffened steel plates and the bridge floors are made of concrete in composite action with the main girders and the cross beams. In the side spans with intermediate supports, the deck is made entirely of concrete. The cable system is of the modified fan configuration and is supported by concrete pylons (Figure 1.94).

### **Akashi Kaikyo Bridge**

In Japan, the main achievement of the 1990s was the completion of the Akashi Kaikyo Bridge in 1998 [94.2] with a record span of almost 2 km.

The design of the Akashi Kaikyo Bridge is based on the traditions of the great American suspension bridges built around the mid-twentieth century, i.e. with the deck composed of three simply supported trusses with a non-participating orthotropic floor and separated by expansion joints at the pylons (Figure 1.95).

The bridge is characterized by very long side spans with a length of 960 m, almost half of the main span length of 1990 m (1990.8 m after the Hanshin Earthquake in January 1995). As a consequence of the large side-to-main span ratio, the cable system has rather poor deformational characteristics, and this is undoubtedly one of the reasons for ending up with a heavy truss to achieve aerodynamic stability.

In the Akashi Kaikyo Bridge, the pylons with their record-breaking height of 297 m are of the traditional cross-braced type found in American suspension bridges from the first half of the twentieth century and later favoured in most of the Japanese suspension bridges from the 1970s and 1980s.



**Figure 1.94** Kap Shui Mun Bridge (Hong Kong SAR)

An innovative feature of the Akashi Kaikyo Bridge was the system of dehumidifying the main cables to increase the durability of these structural elements. In the years to follow, dehumidification of suspension bridge main cables has been used in several other bridges and the system has also been developed to be used to prolong the life of existing main cables where start of corrosion has been observed.



**Figure 1.95** Akashi Kaiko Bridge (Japan)



**Figure 1.96** Storebælt East Bridge (Denmark)

### **Storebælt East Bridge (Great Belt Bridge)**

A fixed traffic link across the Storebælt (Great Belt) in Denmark had been in the planning stage since the 1930s, and throughout the 1970s and the 1980s many different schemes for the main span across the eastern channel had been investigated, among these a double-deck cable stayed bridge with a main span of 780 m and a suspension bridge with a main span of 1416 m.

These bridge designs from the late 1970s were designed as bridges for both road and railway traffic, but in the final legislation from 1987 it was specified that the link across the eastern channel should be split into a railway tunnel and a road bridge (the latter designed by CBR JV).

Relieved of the strict strength and stiffness requirements for a bridge carrying heavy train loads, it became possible to increase the main span for the benefit of navigational safety. So the final choice was for a suspension bridge that opened in 1998 with a 1624 m long main span flanked by side spans of 535 m, i.e. a total cable suspended length of almost 2700 m.

The span of the Storebælt East Bridge is 15% longer than that of the Humber Bridge, but despite this, it proved feasible to have practically the same depth of the box girder forming the deck. One of the reasons for this was the improved efficiency of the structural system due to the continuity of the box girder from the main span to the side spans, the clamping of the main cables to the deck at midspan, and the addition of hydraulic buffers between the deck and the anchor blocks.

The 254 m high pylons of the Storebælt East Bridge are made of concrete in a simple geometry with only two cross beams between the pylon legs. Of special significance is the omission of a cross beam beneath the deck – a feature made possible by the continuity of the box girder (Figure 1.96).

The main cables of the Storebælt East Bridge were erected by the air-spinning method in an improved version called the controlled tension method. The 19,700 tons of cable wires were spun in just 136 days, which constituted a new record with a daily progress of almost twice that achieved in the erection of the main cables of the Second Bosphorus Bridge.

### **Mariánský Bridge**

A notable cable stayed bridge was completed in 1998 across the Labe River in the Czech Republic. With a main span of 123 m, the bridge is of modest size but it shows an attractive shape of the steel pylon in a monolithic form that also incorporates the side span (Figure 1.97).

With the backwards leaning pylon and the lack of a backstay, the Mariánský Bridge appears to be somewhat similar to the Alamillo Bridge in Spain, but through the moment rigid connection between the pylon and the side span, the overturning moment from the one-sided cable pulls is more efficiently transferred to the ground in the Mariánský Bridge.

In 2001, the Mariánský Bridge was ranked one of the ten most beautiful constructions of the twentieth century in an international survey by the well-known *Structural Engineering International Magazine*.



**Figure 1.97** *Mariánský Bridge (Czech Republic)*

### **Ting Kau Bridge**

The third cable supported bridge in the Hong Kong area was the Ting Kau Bridge [95.9] of 1998. This bridge was of quite an unconventional design with three single post-shaped pylons and four cable supported spans with lengths of 127 m, 448 m, 475 m and 127 m (Figure 1.98).

The single-level deck consists of two separate 18.5 m wide composite girder decks connected by transverse girders at the cable anchor points. Each of the two bridge halves are supported by two transversally inclined cable planes. To stabilize the central, 200 m high pylon, two very long and heavy anchor cables are arranged from the top of this pylon to the outer pylons at deck level. From the point of view of appearance, the solution with a very heavy anchor cable that crosses the fans from the outer pylons is not very convincing.

### **Jiangyin Bridge**

The largest of the Chinese suspension bridges in the 1990s was the Jiangyin Bridge with a main span of 1385 m – at completion in 1999, the fourth longest in the world. In this bridge only the main span is cable suspended (Figure 1.99)



**Figure 1.98** *Ting Kau Bridge (Hong Kong SAR)*



**Figure 1.99** Jiangyin Bridge across Yangtze River (China). (Courtesy of Bridge Magazine)

and the bridge deck is designed as a shallow steel box with a width of 32 m and a depth of only 3 m. The pylons are made of concrete so in its main features the Jiangyin Bridge followed the modern European suspension bridge concept.

### **Tatara Bridge**

With a main span of 890 m, the cable stayed Tatara Bridge in Japan surpassed in 1999 the Normandy Bridge by a margin of 4%, i.e. a relatively modest step further on the way to cable stayed bridges with spans of more than 1 km. In its main features, the Tatara Bridge appears to be more modern than the Akashi Kaikyo Bridge, as it has a slender box to form the deck.

In the Tatara Bridge the deck is also – as in the Normandy Bridge – made partly in concrete and partly in steel. However, in the Tatara Bridge, steel is used not only in the entire main span but also in the major part of the side spans so that the concrete is confined to the outer parts of the deck where it mainly acts as counterweight to reduce the uplift from the anchor cables (backstays). The pylons of the Tatara Bridge with heights of 216 m are made of steel in quite an elegant diamond shape with a low bottom part (Figure 1.100).



**Figure 1.100** Tatara Bridge (Japan)





**Figure 1.101** Kurushima Kaikyo Bridges in the final construction phase (Japan)

With the completion of the three routes between Honshu and Shikoku including the world's largest suspension bridge and the largest cable stayed bridge, the Japanese bridge construction programme of the twentieth century was concluded, but plans were already being worked out for even larger bridges to be built in the next century. These plans included a bridge across the mouth of Tokyo Bay where a span of more than 2500 m would be required, a bridge between Shikoku and Kyushu, and as the most ambitious project, a bridge between Honshu and Hokkaido across the 14 km wide and 140 m deep Tsugaru Strait. This strait is today crossed by the 54 km long Seikan Railway Tunnel, but an additional highway link could be beneficial.

At present it does not seem likely that the large bridges envisaged at the end of the twentieth century will reach the construction stage in the near future – if ever.

### **Kurushima Kaikyo Bridges**

Together with the Tatara Bridge three suspension bridges across the Kurushima Kaikyo were completed in 1999. The Kurushima Kaikyo Bridges consist of three consecutive suspension bridges with two intermediate anchor blocks and one at each of the two ends. All three bridges have a deck of slender orthotropic steel boxes and all pylons are in steel with two cross beams above the deck and one below (Figure 1.101).

The first suspension bridge on the way from Honshu to Shikoku is (as could be expected) called the First Kurushima Bridge and it is a relatively small suspension bridge with a main span of only 600 m and side spans of 140 m and 170 m, respectively. All three spans are suspended and the depth of the steel box forming the deck is only 2.5 m.

The Second Kurushima Bridge has a larger main span of 1020 m and an asymmetrical layout with only one 250 m long side span suspended. The main span of the Third Kurushima Bridge has a length of 1030 m and in this bridge only the main span is suspended. The depth of the steel box in both the Second and the Third Kurushima Bridge is 4.3 m.

### **Øresund Bridge**

Across the Øresund between Denmark and Sweden, construction began in 1995 of the 15 km long fixed traffic link that comprises a 7.8 km long bridge with a cable stayed main span.

The Øresund Bridge, designed by the ASO Group, carries a four-lane motorway as well as a double track railway line for both high-speed passenger trains travelling at 200 km/h and heavy freight trains – a feature that gave rise to special problems during the design of the cable stayed bridge with its 490 m long main span (Figure 1.102).

The Øresund Bridge was built with a double-deck arrangement where the two railway tracks are positioned on a lower level with vertical trusses on either side. This ensures a large flexural stiffness of the deck, and in combination with an efficient harp-shaped cable system with intermediate supports in the side spans, favourable static and dynamic properties are achieved.



**Figure 1.102** Øresund Bridge between Denmark and Sweden

With its main span of 490 m, the Øresund Bridge surpassed both the Iwagurojima and Hitsushijima Bridges with their main span of 420 m as well as the Kap Shui Mun Bridge with its 430 m main span, so when completed in 2000, it had the longest span of any cable stayed bridge carrying both road and rail traffic.

### **Youngjong Bridge**

A most unusual cable supported bridge was constructed in Korea at the end of the twentieth century and opened to traffic in 2000: the Youngjong Bridge. The bridge has a 550 m long cable supported section designed as a self anchored suspension bridge with a main span of 300 m and side spans of 125 m. As a unique feature the pylons are diamond-shaped and the two cable planes are transversally inclined (Figure 1.103).

The deck comprises a two-level truss with a six-lane expressway at the upper level and a four-lane roadway plus a double-track railway on the lower level. The top chord of the truss is formed as a wide closed box with a depth of 3 m and the total depth of the truss is approximately 12 m. With such a depth the side spans could easily do without cable support



**Figure 1.103** Youngjong Bridge (Korea)



**Figure 1.104** London Millennium Bridge across the Thames (UK)

and the depth-to-span ratio of the main span is  $1/25$  – a value that is about four times greater than generally found in suspension bridges.

### **London Millennium Bridge**

In the present chapter on the evolution of cable supported bridges, the emphasis has been on a description of the evolution related to major bridges for road and rail traffic. However, cable support is also found in many pedestrian bridges and some of these are of interest for the evolution because they have drawn the attention of bridge designers to phenomena that were not fully understood before they were observed in actual structures.

As a single example in this category a short description of the London Millennium Bridge is included. The design for the new pedestrian bridge across the Thames was selected from 220 designs submitted for a competition in 1996. The design chosen for construction was in almost every aspect unusual and beyond previous practice.

Thus, the three-span suspension bridge had three spans of 81 m, 144 m and 108 m, i.e. with both side spans longer than half the main span length. The span-to-sag ratio of the suspension cables in the main span was 60 (Figure 1.104) – compared to the ratio of 9–12 found in all previous suspension bridges. The deck of the bridge was without flexural and torsional stiffness as the lightweight aluminium deck was subdivided into relatively short segments separated by hinged expansion joints. This had proved necessary as the connection between the main cables and deck was by rigid half-frames and not by hanger cables as in existing suspension bridges. With the rigid frame connection the deck would be subjected to almost the same strains as the suspension cables and that was not acceptable as the axial stress in the high strength cables would be several times greater than the allowable stress in the longitudinal members of a continuous deck. By eliminating the flexural and torsional stiffness, the traditional action of the deck as a stiffening girder was completely lost. So in almost every aspect the design of the London Millennium Bridge ignored the suspension bridge technology that had developed over two centuries.

On the opening day and the following day, a large number of people walked over the bridge and, as it turned out, this caused the bridge to oscillate in what was called ‘unexpected’ lateral vibrations. The phenomenon that occurred is called synchronous lateral excitation and it is caused by the sway motion of people walking on a deck with lateral movements (‘sailors’ walk’).

Two days after its opening the ‘wobbly bridge’, as it was nicknamed, was closed and in the following 20 months the bridge was retrofitted with a large number of dampers (Figure 1.105) to avoid the initial lateral movements that would start the sailors’ walk when people were using the bridge.

In the original Competition Brief of 1996, the budget for the Millennium Bridge was fixed at £8 million but before the initial opening in 2000 the construction costs had risen to £18.2 million. On top of this was added the sum of £5 million for



**Figure 1.105** London Millennium Bridge with dampers

the retrofit so the final cost for the 325 m long and 4 m wide bridge was £23.2 million, corresponding to a unit price per square metre of deck amounting to almost £18,000!

### **Second Nanjing Bridge**

The very first bridge to be built across the Yangtze River was completed in 1968 at Nanjing. It was a double-deck truss bridge carrying both road and rail traffic.

The Second Nanjing Bridge came 33 years later and it was a cable stayed bridge for road traffic only. With its main span of 628 m, on completion, the bridge ranked as the third longest among cable stayed bridges, surpassed only by the Tataru Bridge and the Normandy Bridge (Figure 1.106). The main span of the Second Nanjing Bridge has both the deck and the 195 m high pylons made of steel. The shape of the pylons is clearly inspired by the pylons of the Tataru Bridge.



**Figure 1.106** Second Nanjing Bridge (China). (Courtesy of Bridge Magazine)



**Figure 1.107** Rion-Antirion Bridge. (Photo credit: Francis Vigouroux/Photothèques Vinci et filiales)

#### **Charilaos Trikoupis Bridge (Rion-Antirion Bridge)**

A very demanding bridge construction was undertaken at the beginning of the twenty-first century when a bridge was built across the Gulf of Corinth in Greece. The 2252 m long main part of the bridge had to be built in a highly active seismic zone and with four piers founded on a seabed of loose sediments at a water depth of 65 m.

The chosen solution was a multi-span cable stayed bridge with three main spans of 560 m and two side spans of 286 m supported by four pylons with a height of 141–164 m above the water level (Figure 1.107).

The deck of the bridge is in composite construction with two main girders and numerous cross beams (ladder deck). The four concrete pylons have a pyramidal, four-legged top part above the deck level.

To allow mutual movements between the deck and the pylons in the event of an earthquake, the deck has no rigid connection to the piers.

#### **Runyang Bridge**

For the crossing of the Yangtze River by the Beijing-Shanghai Expressway, two bridges, the cable stayed North Runyang Bridge, and the suspension South Runyang Bridge, were built. Upon completion in 2005 the suspension bridge, with its main span of 1490 m, ranked as the third longest in the world as it surpassed the main span of the Humber Bridge by 80 m (Figure 1.108).

The South Runyang Bridge is a very fine example of a modern no-nonsense suspension bridge where all structural elements are functional and without any ornamentation. Only the main span is cable supported as the viaducts on land are continued all the way to the pylons. Between the saddles on the pylon tops and the anchor blocks the main cables act as backstays, and as a matter of fact the South Runyang Bridge is actually the longest suspension bridge with only the main span suspended.

It is interesting to compare the Runyang Bridge and the Høga Kusten Bridge as both bridges have their pylons on land and only the main span crossing over water. However, for the Høga Kusten Bridge the architect demanded that the side spans be suspended despite the fact that there was no need for it and made the construction more complex.

The deck of the South Runyang Bridge is in the form of an orthotropic steel box 39 m wide and only 3 m deep. So it was proved that a 3 m depth could be maintained even though the span of the suspension bridge was increased beyond previous limits. In the case of the Humber Bridge, the depth of the box was increased to 4.5 m when proceeding from existing bridges with 3 m deep box girders and spans around 1000 m. Keeping the depth of the box girder as small as possible has the advantage that the drag on the deck is kept low.



**Figure 1.108** *Runyang Suspension Bridge (China)*

### **Millau Viaduct**

In Central and Western Europe the first decennium of the twenty-first century was generally characterized by a very modest activity in the construction of long span suspension and cable stayed bridges. However, as a unique exception, the Millau Viaduct in southern France was built from 2001 to 2005.



**Figure 1.109** *Millau Viaduct (France)*



**Figure 1.110** Sutong Bridge across the Yangtze River (China). (Courtesy of Bridge Magazine)

The bridge crosses the 2.5 km wide Tarn Valley at a height of 270 m above the Tarn River and it is thereby the longest and highest valley crossing in Europe (Figure 1.109).

The bridge is a multi-span cable stayed bridge with six 342 m long main spans and two 204 m long side spans. The orthotropic steel deck is continuous over the full length from one abutment to the other.

The piers from the valley bottom to the deck are made of concrete and the tallest is 245 m high. Adding to this the height of the triangular steel pylon above the deck, the total height of the tallest pier-pylon becomes 343 m, substantially taller than the Eiffel Tower in Paris.

### Sutong Bridge

The great achievements in the construction of cable supported bridges in China reached a climax in 2008 when the first cable stayed bridge with a span of more than one km, the Sutong Bridge, was completed (Figure 1.110).

The 41 m wide orthotropic steel box is supported along the two edges by semi-fan cable systems attached to the vertical top of the 306 m high  $\lambda$ -shaped concrete pylons. The length of the main span is 1088 m and each of the two side span fans reach 500 m out from the pylons. On either side of the pylons the spans are 300 m, 100 m and 100 m, so besides the end support there are two intermediate supports under the side-span fan. This ensure very high efficiency of the cable system and it also limited the double cantilever deck erection from the pylon to  $2 \times 300$  m until the first side span pier was reached.

The Sutong Bridge, that has a total length of 8.2 km including approach spans, was constructed in just five years from June 2003 to June 2008.

### Jiangdong Bridge

An unusual cable supported bridge was opened to traffic in 2008 across the Qiantang River at Hangzhou. The total length of the bridge is 4.3 km and it contains two navigation spans, each 260 m long and with long side spans on either side.

In the main spans the deck is supported by two transversally inclined cable planes, each with a parabolic main cable and hangers attached along the edges of the 47 m wide deck (Figure 1.111). The pylons are of the vertical column-type positioned in the central reserve of the eight-lane expressway. The span-to-sag ratio of the suspension cables in the main span is as high as 4.5 – a value that has probably been chosen to limit the transverse slope of the cable planes.

### Stonecutters Bridge

The Stonecutters Bridge in Hong Kong was for some time planned to be the first cable stayed bridge to span more than 1 kilometre but it was overtaken by the Sutong Bridge and did not open until the very end of 2009.



**Figure 1.111** *Jiangdong Bridge (China)*

In 2000, the Highways Department in Hong Kong announced an International Design Competition for a bridge across the entrance to the new container port in Hong Kong. No piers would be allowed in the water so the span should be at least 1 km and in initial feasibility studies it had been anticipated that this would require a suspension bridge to be constructed. However, the soil conditions did not at all favour a suspension bridge with large horizontal forces to be transferred from the anchor blocks to the ground.

In the Competition Brief it was therefore pointed out that it was desirable to provide designs based on a self anchored cable stayed bridge. It was also emphasized that the design should lead to a landmark structure as the bridge would be



**Figure 1.112** *Stonecutters Bridge (Hong Kong SAR)*



visible from many locations in Hong Kong. On the other hand, it was also clearly stated that the structure should be structurally sound and be constructable. Therefore, priority was given to the Technical Evaluation before the Aesthetical Evaluation.

Despite the clear emphasis on structural efficiency, quite a few of the entries could only be classified as crazy, and of the 27 entries, 16 were eliminated by the Technical Evaluation Committee before the remaining 11 were passed on to the Aesthetical Evaluation Committee.

The winning design comprised a cable stayed bridge with a twin box deck (vented deck) in steel in the main span and concrete in the multi-pier side spans. The 300 m high pylons were of the single free-standing configuration and the cross section was circular. As a special architectural feature, the 125 m top parts of the pylons were in composite construction with a 20 mm-thick stainless steel plate forming the exterior surface.

The main span of the Stonecutters Bridge is 1018 m long so the fans from the two pylons reach 500 m out into the main span (Figure 1.112). Due to local conditions the side span fans could only be 300 m long. It was, therefore, well justified to have a heavy concrete deck in the side spans to balance the longer half span deck in the main span.

The deck is composed of two boxes separated by a 14 m wide gap imposed by the space required for the pylon shaft to pass between. The twin box configuration proved to have a very positive influence on the aerodynamic stability but a single box could actually have fulfilled the specified design wind speed for onset of flutter (also clearly demonstrated by the single box deck of the Sutong Bridge).

### Incheon Bridge

The construction of long span cable supported bridges in the Far East started in Japan in the 1970s and continued in China during the 1990s. From the beginning of the 21st century the activity in Japan was considerably reduced whereas the activity in China surpassed that of all other countries around the world. But also in Korea the construction of large cable stayed bridges showed impressive results in the first decennium of the third millennium.

As an example Figure 1.113 shows the Incheon Bridge opened in 2009 on the route from Seoul to the international airport at Incheon. The main span is 800 m long which made it the fifth longest cable stayed span at completion.

The design followed the general trend with pylons of concrete and the deck made as a wide streamlined box girder in steel. The semi-fan cable system includes beside the fans in the main span also two 340 m fans outside the pylons. Under the side span fans an intermediate pier support is arranged 80 m from the outer anchor pier. This makes the cable system highly efficient.

### Xihoumen Bridge

At the end of 2009, the Xihoumen Bridge in China took the lead as the world's second longest suspension bridge. The 1650 m main span was 26 m longer than the main span of the Storebælt East Bridge, but 341 m shorter than the main span of



**Figure 1.113** Incheon Bridge in Korea (courtesy of H. Tanaka, Samsung C&T)



**Figure 1.114** *Xihoumen Bridge (China)*

the Akashi Kaikyo Bridge. The bridge is asymmetric as only the northern side span is suspended, whereas on the south side the access to the pylon is via a horizontally curved ramp composed of 60 m continuous box girder spans in concrete (Figure 1.114). The asymmetry of the alignment has also resulted in a different configuration of the 211 m high pylons, as the southern pylon has three cross beams, two above and one below the deck, whereas the northern pylon does not have a cross beam below the deck (as in the Storebælt East Bridge). From a structural point of view, the difference in pylon design is well justified as the deck is continuous and with only lateral support at the northern pylon, whereas the transition from the main span steel deck to the concrete ramp required an expansion joint at the southern pylon.

For the orthotropic steel deck it was studied whether a single box would give sufficient aerodynamic stability but due to the rather strict requirement of a design wind speed of 78.7 m/sec for the onset of flutter this proved not to be possible. This result was actually in accordance with the result of the Storebælt East Bridge wind tunnel tests where the critical wind speed for the single box was determined to be around 72 m/sec.

The final solution for the steel deck was, therefore, a twin box composed of two box girders, each 15 m wide and 3.5 m deep, separated by a 6 m wide gap. With this concept the critical wind speed was determined to be around 88 m/sec, comfortably above the specified design wind speed for the onset of flutter.

### **Third Bridge across the Firth of Forth**

The largest bridge built in the 19th century was the impressive railway bridge across the Firth of Forth in Scotland. It was in the 1960s joined by the Forth Road Bridge constructed as a suspension bridge with a main span of slightly more than 1 kilometer.

During inspections in the beginning of the 21st century it was revealed that the Forth Road Bridge showed signs of deterioration and it was estimated that the suspension bridge would need either a total replacement or an in-depth renovation that would involve erection of new main cables. However, as a replacement of the main cables would seriously affect the traffic flow across the bridge during the replacement period it was decided to go for a new Replacement Crossing west of the existing road bridge.

The alignment of the third bridge across the Forth of Forth was chosen so that a central support could be established on the small Beamer Rock and that led to a bridge with two main spans (as in the old railway bridge). Due to navigational requirements the main spans each had to be 650 m long which clearly pointed towards a cable stayed bridge with three pylons.

A cable stayed bridge with two main spans of equal length require special attention in its design to achieve sufficient stiffness as the central pylon will be without a back stay leading to an anchor pier where the cable system is vertically supported. The problem has in some existing cable supported bridges been overcome by having a central pylon in an A-shape, but in the case of the Third Forth Bridge this was not an attractive solution as it was not possible to arrange two foundations on the small Beamer Rock.

The final solution was to apply, as shown in Figure 1.115, the concept of overlapping fans in the two main spans – a concept that was introduced initially in the Second Edition of this book.



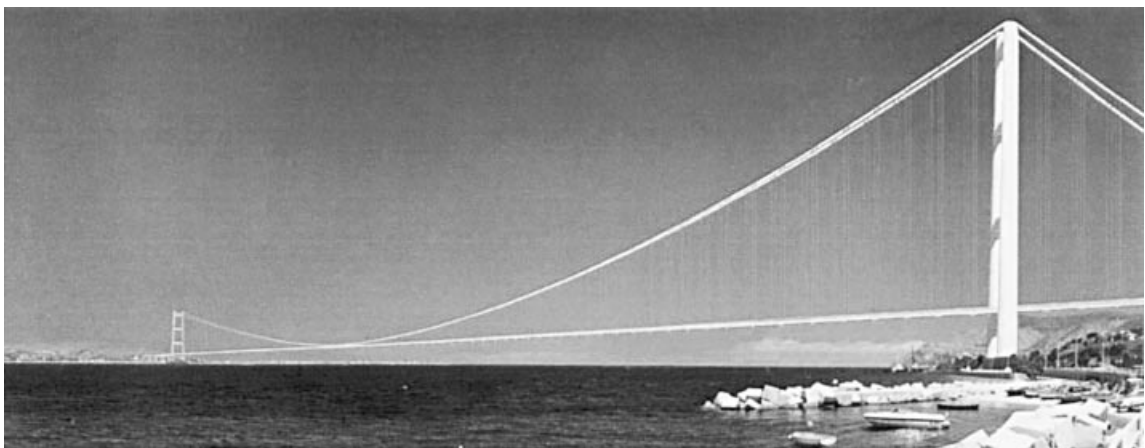
**Figure 1.115** Third Bridge across the Firth of Forth in Scotland (visualisation by Dissing+Weitling Architecture)

### Messina Strait Bridge project

Outside Japan the most realistic plan for a bridge to go beyond the present span limits is the Messina Strait Bridge [94.16] between Sicily and the Italian mainland. This bridge has been thoroughly investigated for several decades and an impressive effort has been made to study all the problems related to the construction of a bridge with a free span of up to 3300 m carrying both road and rail traffic.

In 1992, the 'Progetto definitivo' was presented by Stretto di Messina SpA (the state-controlled company formed to prepare the design for the link) and the design comprised a 'traditional' suspension bridge with a 3300 m long main span reaching from coast to coast (Figure 1.116).

The important issue of aerodynamic stability was addressed in the Messina design by composing the bridge deck of three individual streamlined box girders separated by wide slots covered with open grids. In this design it was shown by intensive wind tunnel testing that an adequate margin against catastrophic wind-induced oscillations could be achieved – and in a much more elegant way than by constructing a large and heavy truss.



**Figure 1.116** Messina Strait Bridge Project (courtesy of E. Vullo, Stretto di Messina)

**Table 1.1** *Longest suspension bridge spans since 1826*

| Period    | Name of bridge        | Span   | Deck material | Pylon material | Country     |
|-----------|-----------------------|--------|---------------|----------------|-------------|
| 1826–1834 | Menai Bridge          | 176 m  | Iron          | Stone          | Wales       |
| 1834–1849 | Grand Pont Suspendu   | 273 m  | Iron          | Stone          | Switzerland |
| 1849–1866 | Wheeling Bridge       | 308 m  | Iron          | Stone          | USA         |
| 1866–1883 | Cincinnati Bridge     | 322 m  | Iron          | Stone          | USA         |
| 1883–1903 | Brooklyn Bridge       | 486 m  | Iron          | Stone          | USA         |
| 1903–1924 | Williamsburg Bridge   | 488 m  | Steel         | Steel          | USA         |
| 1924–1926 | Bear Mountain Bridge  | 497 m  | Steel         | Steel          | USA         |
| 1926–1929 | Benjamin Franklin     | 533 m  | Steel         | Steel          | USA         |
| 1929–1931 | Ambassador Bridge     | 564 m  | Steel         | Steel          | USA         |
| 1931–1937 | George Washington Br. | 1067 m | Steel         | Steel          | USA         |
| 1937–1964 | Golden Gate Bridge    | 1280 m | Steel         | Steel          | USA         |
| 1964–1981 | Verrazano Narrows Br. | 1298 m | Steel         | Steel          | USA         |
| 1981–1998 | Humber Bridge         | 1410 m | Steel         | Concrete       | England     |
| 1998–     | Akashi Kaikyo Bridge  | 1990 m | Steel         | Steel          | Japan       |

**Table 1.2** *Longest cable stayed bridge spans since 1955*

| Period    | Name of bridge         | Span   | Deck material | Pylon material | Country |
|-----------|------------------------|--------|---------------|----------------|---------|
| 1955–1959 | Strömsund Bridge       | 183 m  | Steel         | Steel          | Sweden  |
| 1959–1961 | Theodor Heuss Bridge   | 260 m  | Steel         | Steel          | Germany |
| 1961–1969 | Severins Bridge        | 302 m  | Steel         | Steel          | Germany |
| 1969–1970 | Knie Bridge            | 320 m  | Steel         | Steel          | Germany |
| 1970–1975 | Duisburg-Neuenkamp Br. | 350 m  | Steel         | Steel          | Germany |
| 1975–1983 | St. Nazaire Bridge     | 404 m  | Steel         | Steel          | France  |
| 1983–1986 | Barrios de Luna Bridge | 440 m  | Concrete      | Concrete       | Spain   |
| 1986–1991 | Alex Fraser Bridge     | 465 m  | Composite     | Concrete       | Canada  |
| 1991      | Iguchi Bridge          | 490 m  | Steel         | Steel          | Japan   |
| 1991–1993 | Kvarnsund Bridge       | 530 m  | Concrete      | Concrete       | Norway  |
| 1993–1995 | Yangpu Bridge          | 602 m  | Composite     | Concrete       | China   |
| 1995–1999 | Normandy Bridge        | 856 m  | Steel/Cone    | Concrete       | France  |
| 1999–2008 | Tatara Bridge          | 890 m  | Steel         | Steel          | Japan   |
| 2008–     | Sutong Bridge          | 1088 m | Steel         | Concrete       | China   |

### Record spans

As a conclusion to this chapter on the evolution of cable supported bridges, two tables are shown to illustrate the increase of span length for both suspension and cable stayed bridges.

In suspension bridges the major steps (more than 25% increase over previous record span) were taken by the Grand Pont Suspendu in 1834 (+55%), the Brooklyn Bridge (+50%), the George Washington Bridge (+89%), the Golden Gate Bridge (+25%) and the Akashi Kaikyo Bridge (+41% over the Humber Bridge) (Table 1.1).

The Golden Gate Bridge was the record holder for the longest period, 27 years from 1937 to 1964. The second longest record holder has, quite astonishingly, been the Williamsburg Bridge with its marginal record span from 1903 to 1924, i.e. a period of 21 years. The shortest record-holding periods before 1996 was those of the Bear Mountain Bridge and the Ambassador Bridge – 2 years from 1924 to 1926 and 1929 to 1931, respectively.

For cable stayed bridges the relative span increases have been more moderate than for suspension bridges. Only the Theodor Heuss Bridge (+42%) and the Normandy Bridge (+42% over the Yangpu Bridge, but +84% over the Alex Fraser Bridge) have increased the previous record by more than 25%.

For cable stayed bridges the record-holding periods have also been shorter than within suspension bridges (Table 1.2). Thus, the longest record-holders have been the Tatara Bridge with 9 years followed by the Severins Bridge and the St. Nazaire Bridge, each with an 8-year record-holding period. The shortest record-holding period was that of the Iguchi Bridge with only a few weeks in 1991.

# 2

## Cables

The basic element for all cables to be found in modern cable supported bridges is the steel wire characterized by a considerably larger tensile strength than that of ordinary structural steel.

In most cases, the steel wire is of cylindrical shape with a diameter between 3 and 7 mm. Typically, a wire with a diameter of 5–5.5 mm is used in the main cables of suspension bridges whereas wires with diameters up to 7 mm are used for parallel wire strands in cable stayed bridges.

The steel material for the wires is manufactured by the Siemens–Martin process or as electro steel, with a chemical composition characterized by a higher carbon content than allowed for structural steel.

Table 2.1 shows a comparison between different properties of cable steel and structural steel. It appears that the strength of the cable steel is approximately four times that of mild structural steel and twice that of high-strength structural steel. This increased strength is, however, paid for by a noticeable decrease of the ductility as the strain at breaking is only about one-fifth of that found for structural steel.

In the chemical composition, the high carbon content of cable steel, about four times that of structural steel, is of special significance. This high content of carbon makes the cable steel unsuited for welding.

### 2.1 Basic Types of Cables

Although the single wire forms the basic element for cables, several wires are often shop-assembled to form pre-fabricated strands, subsequently used in the shop or at the site as basic elements for the construction of the final cable.

The simplest strand to be found within cable supported bridges is the seven-wire strand as used extensively in tendons for pre-stressed concrete. For cables, the strand is normally made from seven 5 mm wires giving the strand a nominal diameter of 15 mm (Figure 2.1).

The most common seven-wire strands comprise wires with tensile strengths between 1770 and 1860 MPa. The seven-wire strand consists of a single straight core wire surrounded by a single layer of six wires, all with the same pitch and direction of helix. As the pitch is relatively large, the inclination of the wire axis in respect to the strand axis is small, and this means that the stiffness of the seven-wire strand is close to that of straight wires. Typically, the nominal modulus of elasticity for the seven-wire strand will be only 6–8% lower than for the wires themselves, i.e. a typical modulus of elasticity of  $E = 190$  GPa.

#### 2.1.1 Helical bridge strands (spiral strands)

Multi-wire helical strands are fabricated by successive spinning of layers generally with opposite direction of helix, starting out with a straight core (Figure 2.2). As a smaller pitch is used in multi-wire strands, the decrease of the stiffness is more pronounced than for the seven-wire strand. The nominal modulus of elasticity for the multi-wire helical strand will often be

**Table 2.1** Comparison between cable steel and structural steel (based on typical values)

|                                  | Conventional cable steel |                   | Structural steel |               |
|----------------------------------|--------------------------|-------------------|------------------|---------------|
|                                  | Unity                    | (5 or 7 mm wires) | Mild             | High strength |
| Yield stress (= 2% proof stress) | MPa                      | 1180              | 240              | 690           |
| Tensile strength                 | MPa                      | 1570              | 370              | 790           |
| Strain at breaking               | %                        | 4                 | 24               |               |
| Modulus of elasticity            | GPa                      | 205               | 210              | 210           |
| Typical chemical composition     | C                        | 0.80%             | 0.20%            | 0.15%         |
|                                  | Si                       | 0.20%             | 0.30%            | 0.25%         |
|                                  | Mn                       | 0.60%             |                  | 0.80%         |
|                                  | Cu                       | 0.05%             | 0.20%            | 0.30%         |
|                                  | Ni                       | 0.05%             |                  | 0.80%         |
|                                  | Cr                       | 0.05%             | 0.30%            | 0.50%         |
|                                  | P                        | 0.03%             | 0.04%            | 0.03%         |
|                                  | S                        | 0.02%             | 0.04%            | 0.03%         |



**Figure 2.1** Seven-wire strand



**Figure 2.2** Multi-wire helical strand (Lillebælt Bridge)

15–25% below the value for straight wires. A typical value for the nominal modulus of elasticity of the helical strand then becomes  $E = 170$  GPa.

The twisting of the wires also leads to a reduction of the strength compared to straight wires. Typically the strength of a helical strand is approximately 10% lower than the sum of the breaking strengths of the individual wires. Therefore, the design stress for helical strands is generally chosen as  $0.9f_{cbd}$  where  $f_{cbd}$  is the design stress of a parallel-wire strand made of the same wires.

When the helical strand is subjected for the first time to axial tension, the elongation will be due not only to the elastic strain in the wires, but also to an irreversible elongation caused by the compaction of the strand. To remove this non-elastic contribution to the strand elongation, a pre-stretching is often performed to make the strand act in a nearly ideal elastic manner in the final structure. This requires a pre-stretching with a force exceeding the maximum tensile force to be expected in the final service condition. Consequently, an overloading of 10–20% is generally used during pre-stretching.

Due to the twisting of the layers, the helical strand becomes self-compacting. It is therefore unnecessary to wrap or apply bands around the strand to hold the wires together.

### 2.1.2 Locked-coil strands

Locked-coil strands are composed of two types of twisted wire: in the core, regular round wires arranged as in a normal helical strand, and in the outer layers, wires of a special Z-shape (Figure 2.3). The Z-shape is chosen so that the wires interlock which, in combination with the self-compacting effect from the spiral arrangement, ensures a tight surface. Also, the fit of the Z-wires leads to a very small void ratio inside the strand. The locked-coil strands are, therefore, more compact than any other type of strand. A locked-coil strand with an outer diameter of 150 mm has a metallic cross section of  $15\,900\text{ mm}^2$  corresponding to a void ratio of only  $1 - 15\,900/(\pi \times 75^2) = 0.10$ .

The wires used for locked-coil strands generally have tensile strengths of 1370–1570 MPa.

In modern locked-coil strands all wires are galvanized and traditionally this corrosion protection is only combined with a surface treatment by painting. This implies that the additional weight of the corrosion protection becomes modest. For a strand composed of heavy galvanized wires the equivalent density  $\gamma_{eq}$ , (defined as the weight per unit length divided by the steel cross section) is approximately  $88\text{ kN/m}^3$ .

The Z-shaped wires of the outer layers also make the locked-coil strand less sensitive to side pressures at saddles and anchorages, as the wires have a genuine surface contact and not just a point contact between intersecting wires as in the case of round wires.

Locked-coil strands are always manufactured in full length and full cross section, and delivered with sockets on large reels. The longest locked-coil strands (used for suspension bridge main cables) have had a length of approximately 1250 m.

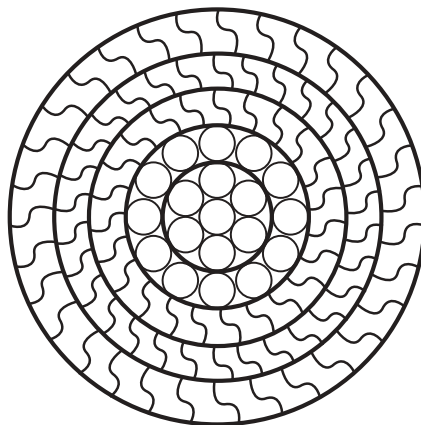


Figure 2.3 Cross section of a locked-coil strand

Locked-coil strands for bridges are fabricated with diameters in the range from 40 mm to 180 mm. One of the largest yet fabricated had a diameter of 174 mm and was installed in the Rama VIII Bridge in Bangkok. Generally the largest locked-coil strands are found in cable stayed bridges with multi-cable systems where each stay is made as a mono-strand cable, whereas locked-coil strands of smaller size with diameters from 60 mm to 80 mm were used in cable stayed bridges (and suspension bridges) where the final cable was composed of several strands. This was common practice in early cable stayed bridges but it is hardly done any longer.

Locked-coil strands are characterized by a nominal modulus of elasticity slightly higher than found for helical strands, i.e. typically 180 GPa, which corresponds to a reduction of the axial stiffness by approximately 12%. However, due to the fact that the cross section has to be increased by 10% to compensate for the lower breaking strength of locked-coil strands compared to parallel-wire strands, the elongation due to the strain in the cable wires will increase by only 2%.

### 2.1.3 Parallel-wire strands for suspension bridge main cables

The reduction of strength and stiffness associated with the twisted wires in the helical strands promoted the development of the pre-fabricated parallel-wire strand where all the wires were straight from one end to the other. The advantages of using strands with parallel wires had been recognized for a long time, but for many years the problems related to the reeling process excluded the introduction of these strands in actual construction. The reeling problem is associated with the fact that the curving of a parallel-wire strand with undistorted cross sections would require an elongation of the wires at the outside and a contraction of the wires at the inside of the curve. With reels of realistic dimensions, the required strains in the wires would result in unacceptable stresses.

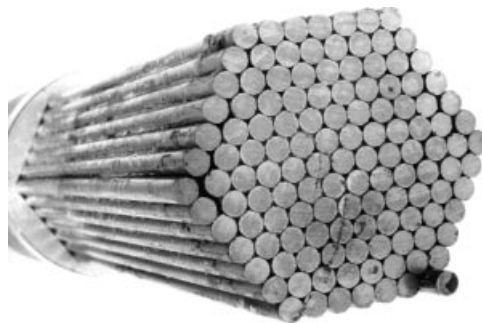
However, in the early 1960s, actual tests on the reeling possibilities were undertaken in the USA, and it was shown that the parallel-wire strand, through a local distortion of the wires inside the bundles, could actually be reeled and unreeled without creating unacceptable permanent distortions. From a description of the pilot test with a 37-wire strand [66.1], the following can be quoted:

When this strand was reeled on an 80 in (2 m) diameter drum, it was observed to rotate about its own axis first one way and then the other, and to flatten out or ‘birdcage’ to some degree between bindings, thus automatically equalizing individual wire lengths locally in each turn around the drum. Furthermore, the strand was found to resume substantially its original shape upon being unreeled, and subsequent strength tests showed that repeated reeling did not affect the physical properties of the strand.

The tests with a 37-wire strand were followed by tests with 61-, 91- and 127-wire strands, all with a hexagonal pattern (Figure 2.4).

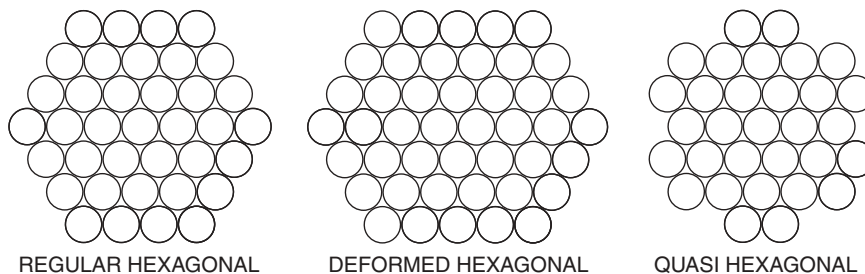
In present practice parallel-wire strands to be built into suspension bridge main cables comprise 5–5.5 mm wires, whereas 7 mm wires are more common in stay cables. Parallel-wire strands are generally fabricated with the wires in a regular hexagonal pattern, but also deformed hexagonal or a quasi-hexagonal patterns (Figure 2.5) have been used in a few cases.

In Japan where suspension bridge main cables with parallel-wire strands were adopted early, a trend towards larger wire or strand sizes was seen in the first years after the introduction of the system. Thus, Figure 2.6 shows the parallel-wire



**Figure 2.4** *Parallel-wire strand with 127 nos. 5 mm wires (Bisan Seto Bridges)*





**Figure 2.5** Patterns of parallel-wire strands: (left) regular hexagonal; (middle) deformed hexagonal; (right) quasi hexagonal

strands used in the Kanmonkyo Bridge, the Ohnaruto Bridge and the Akashi Kaikyo Bridge. In the Kanmonkyo Bridge the wire diameter was 5.04 mm and the number of wires 91, whereas the corresponding figures for the Ohnaruto Bridge were 5.37 mm and 127. For the Akashi Kaikyo Bridge the number of wires was also chosen to be 127, but the wire diameter of 5.23 mm was slightly smaller than in the Ohnaruto Bridge. Due to these differences and the increased lengths, the transportation weight of the parallel-wire strand (including reel) has increased from 17.5 tonnes via 41 tonnes to 85 tonnes in the Akashi Kaikyo Bridge.

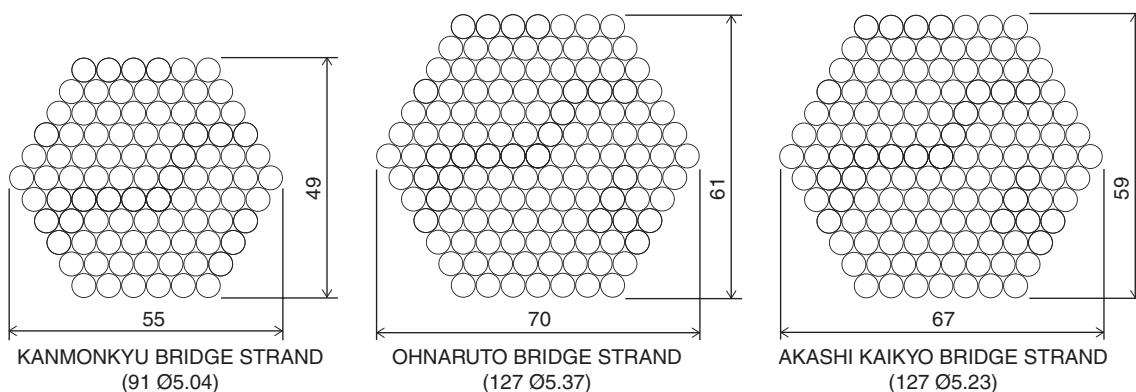
### 2.1.3.1 Parallel-wire stay cables

In cable stayed bridges, parallel-wire cables are generally composed of a larger number of wires than found in parallel-wire strands for suspension bridge main cables. Thus, as an example Figure 2.7 shows the largest of the parallel-wire strands used in the Zarate-Brazo Largo Bridges in Argentina (337 Nos. 7 mm wires).

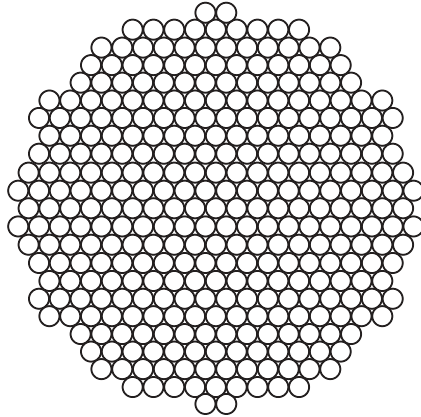
With parallel wires the integrity of the wire bundle forming the cable would not be ensured as in the case of a helical strand. Therefore, the wires had to be kept in place by additional means, e.g. by twisting a steel rope around the bundle. Furthermore to give adequate corrosion protection the parallel-wire cable had to be surrounded by a tube and the void filled with a corrosion inhibitor.

In the early bridges with parallel-wire cables the tube was made of polyethylene (PE) or stainless steel, the inhibitor of cement grout, and the wires were blank, i.e. ungalvanized. However, today it is regarded as mandatory to use galvanized wires and to have an inhibitor of a non-cracking, ductile material.

The main disadvantage of the early parallel-wire stay cable was the large outer diameter resulting from the spiral rope, the void for the corrosion inhibitor and the PE tube. Thus, a traditional parallel-wire stay cable with an outer diameter of 200 mm had a metallic cross section of maximum 14 584 mm<sup>2</sup> corresponding to a void ratio of  $1 - 14\,584 / (\pi \times 100^2) = 0.54$ . This implied that less than half of the area inside the surface of the PE tube was metallic.



**Figure 2.6** Parallel-wire strands used in major Japanese suspension bridges



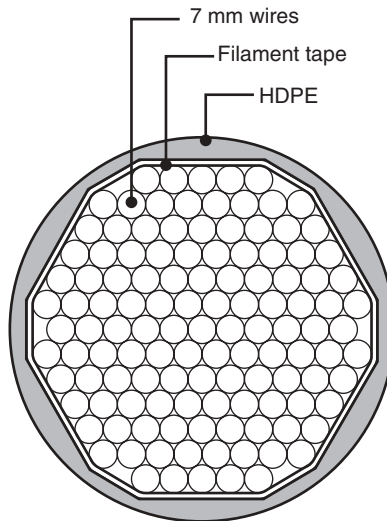
**Figure 2.7** Parallel-wire strand used in the largest stays of the Zarate-Brazo Largo Bridges in Argentina (337 nos. 7 mm wires)

The additional weight of the spiral rope, the corrosion inhibitor and the polyethylene tube also had the unfavourable effect of increasing the equivalent density  $\gamma_{eq}$ . For the original parallel-wire stay cables with a covering PE tube and cement grout as inhibitor the equivalent density was as high as  $\gamma_{eq} = 115\text{--}120 \text{ kN/m}^3$ . For the type with a tighter tube and a greasy corrosion inhibitor the equivalent density was reduced to  $\gamma_{eq} = 85\text{--}90 \text{ kN/m}^3$ .

According to supplier information, parallel-wire stay cables can be fabricated in sizes ranging from 19 Nos. 7 mm wires up to 499 Nos. 7 mm wires.

#### 2.1.4 New PWS stay cables

A variant of the parallel-wire stay cable with straight wires was introduced in the 1990s under the designation 'New PWS Cable' (Figure 2.8). In this cable the wire bundle is slightly twisted with a long lay to ease reeling and unreeling and make the strand self-compacting when subjected to axial tension.



**Figure 2.8** New PWS Cable

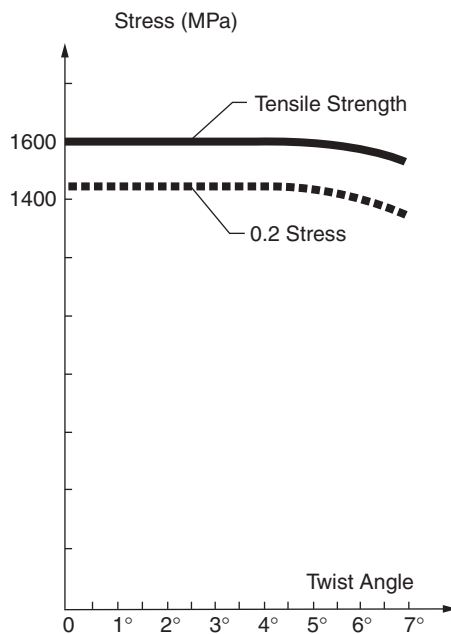


Figure 2.9 Tensile strength versus twist angle

In connection with the development of the New PWS Cable – a development that took place mainly in Japan – the relation between the twist angle and the tensile strength as well as the modulus of elasticity was carefully investigated. From the tests, the plots in Figure 2.9 were derived and it is seen that both the tensile strength and the axial stiffness are almost unaffected by twist angles up to 3–4°.

Besides the slight twist of the wire bundle the New PWS Cables are also characterized by having the protecting polyethylene cover extruded directly onto the wire bundle so that no void will exist between the wires and the surrounding pipe.

With the elimination of the spiral rope and the voids for cement grouting the New PWS Cable is more compact than traditional PWS cables. Thus, a New PWS Cable with an outer diameter of 175 mm has a metallic cross section of 16 202 mm<sup>2</sup> corresponding to a ‘void’ ratio of  $1 - 16\,202 / (\pi \times 87.5^2) = 0.33$ .

The elimination of the spiral rope and the cement grout also leads to a reduction of the equivalent density  $\gamma_{eq}$  which typically has a value around 82 kN/m<sup>3</sup>.

New PWS Cables are fabricated in sizes ranging from 7 Nos. 7 mm wires to 421 Nos. 7 mm wires.

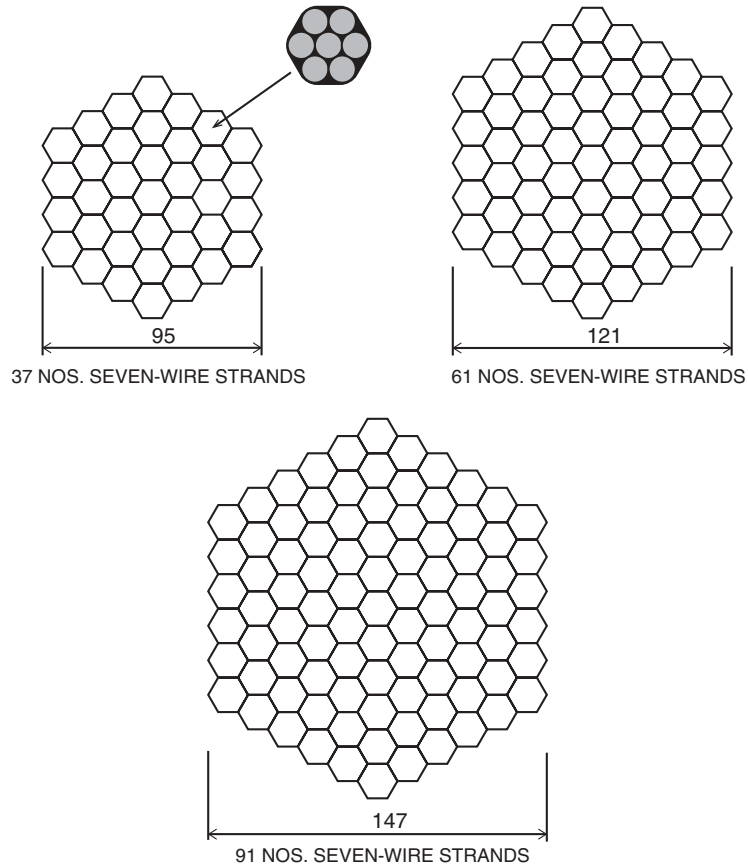
### 2.1.5 Parallel-strand stay cables

Parallel-strand cables are in principle composed in the same way as parallel-wire cables, with the exception that the individual 7 mm wires are replaced by seven-wire strands.

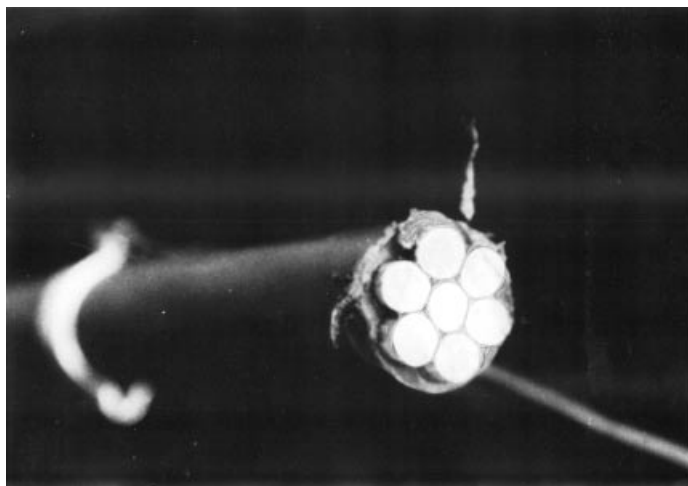
The most common arrangements of parallel-strand cables are shown in Figure 2.10. It is, however, easy to apply intermediate sizes by leaving out some of the seven-wire strands, and it is also indicated by some of the suppliers that parallel-strand cables can be made with up to 127 seven-wire strands.

A parallel-strand cable might be manufactured as a complete unit, as described for a parallel-wire cable, but it is much more common to insert and stress the seven-wire strands one by one (the ‘Isotension method’). This will substantially reduce the size of the stressing equipment, but increase somewhat the amount of work to be carried out on site.

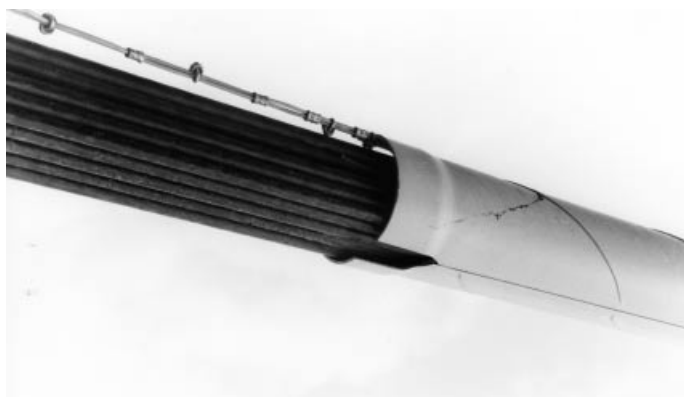
The seven-wire strands are generally made of galvanized wires and in the present standard version the seven wires are furthermore protected by an extruded high density polyethylene (HDPE) sheath (Figure 2.11). With an individual HDPE protection of each seven-wire strand the completed stay cable might be made as a parallel-strand bundle without further protection. It will, however, be necessary to add binders around the bundle at intervals of approximately 40 m to ensure integrity and avoid individual oscillations of the single wires.



**Figure 2.10** Parallel-strand cables comprising seven-wire strands



**Figure 2.11** Seven-wire strand with an extruded high density polyethylene (HDPE) sheath



**Figure 2.12** Parallel-strand cable surrounded by a cylindrical two-piece pipe to give a smoother surface (Normandy Bridge)

A stay cable composed of individually protected seven-wire strands will be characterized by a relatively large drag coefficient due to the grooved surface. It is, therefore, in many cases decided to add a cylindrical pipe around the strand bundle to give a smoother surface (Figure 2.12). In the case of an individual HDPE sheathing of each seven-wire strand, it will not be necessary to add any compound in the void between the strand bundle and the covering pipe.

Without an individual HDPE sheathing, the entire bundle of seven-wire strands had to be protected by a surrounding polyethylene tube with a corrosion inhibiting compound in the voids.

Parallel-strand stay cables with a surrounding polyethylene tube will be characterized by a large void ratio. Thus, a cable composed of 109 Nos. 0.6 in strands will have an outer diameter of 315 mm and a metallic cross section of  $109 \times 140 = 15\,260 \text{ mm}^2$  leading to a void ratio of  $1 - 15\,260 / (\pi \times 157.5^2) = 0.804$ . This means that only about one-fifth of the total area inside the surface of the PE tube is metallic.

The standard version with individually sheathed seven-wire strands is the preferred solution for stay cables in short to medium span bridges, but for long span bridges the large external diameter of the surrounding tube becomes a problem due to the increased drag on the stay cable. In a recent development the individual sheathing of the seven-wire strands has therefore been abandoned and to maintain a high degree of corrosion protection the interior of the much tighter PE tube is dehumidified.

Without the individual strand sheathing and the tighter PE tube a cable with 109 seven-wire strands can be made with an exterior diameter of 200 mm compared to 315 mm as mentioned above. The void ratio is thereby reduced to  $1 - 15\,260 / (\pi \times 100^2) = 0.514$  and the drag to less than  $2/3$ .

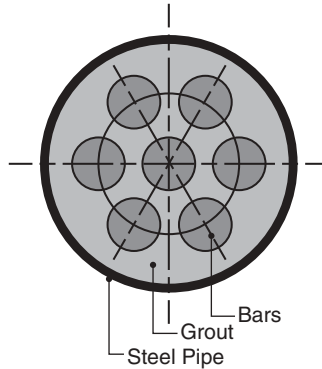
### 2.1.6 Bar stay cables

Bar stay cables where 5–7 mm wires are replaced by high strength round bars have been used in a limited number of cable stayed bridges but the system is hardly used any longer.

Standard bar stay cables contained 7–10 round steel bars, each with a diameter of 26.5 mm, 32 mm or 36 mm, made from steel with a yield stress of 1080 MPa and a tensile strength of 1230 MPa. The bars were delivered in lengths of typically 12 m and joined by threaded couplers. The bar bundle was placed inside a genuine steel tube that was finally filled with cement grout (Figure 2.13).

The application of threaded bars resulted in a relatively low fatigue resistance, but this was to some extent counteracted by the interaction with the external steel tube, as the external steel tube was incorporated in the cable cross section when the bridge became subjected to traffic load. The stress variations under traffic load were, therefore, determined by taking both the cross sectional area of the bars and the steel tube into account.

In a bar cable the bars were all arranged in a parallel configuration so that the modulus of elasticity became as for the steel itself. Bar cables were characterized by a relatively large void ratio of the same magnitude as found for parallel-strand cables with sheathed seven-wire strands. A bar cable composed of ten 36 mm bars inside a steel tube with an external diameter of 241 mm had a metallic cross sectional area of the bars of  $10\,178 \text{ mm}^2$  leading to a void ratio of  $1 - 10\,178 / (\pi \times 120.5^2) = 0.78$ . However, if the void ratio is calculated on the basis of the total steel area comprising round bars and steel tube, then the void ratio became approximately 0.66.



**Figure 2.13** Bar cable

For bar cables with cement grout inside the steel tube the equivalent density related to the total steel cross section had a value around  $125 \text{ kN/m}^2$ .

### 2.1.7 Multi-strand stay cables

Where large cable sections are required, the application of multi-strand cables composed of several multi-wire helical strands has been used both within cable stayed and suspension bridges.

In the first modern cable stayed bridge, the Strömsund Bridge, each stay cable was composed of four helical strands placed separately, as can be seen in Figure 2.14.

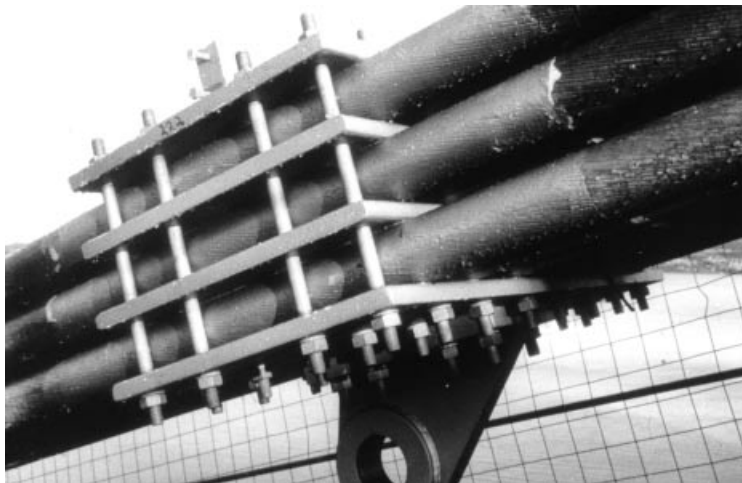
A similar arrangement was for many years used in Norway for suspension bridge main cables, as illustrated in Figure 2.15. For smaller main cables with a limited number of individual strands, this configuration seems quite adequate but for larger main cables it appears to be too primitive.

In the field of cable stayed bridges it was preferred in the early days to assemble all helical strands of larger stay cables into a single compact section.

Figure 2.16 shows some typical sections of multi-strand stay cables used in cable stayed bridges built in the 1960s and 1970s. As can be seen, the pattern of the strands in the cable differed significantly as both hexagonal, square, and flat



**Figure 2.14** Stay cable composed of four individual helical strands (Strömsund Bridge)



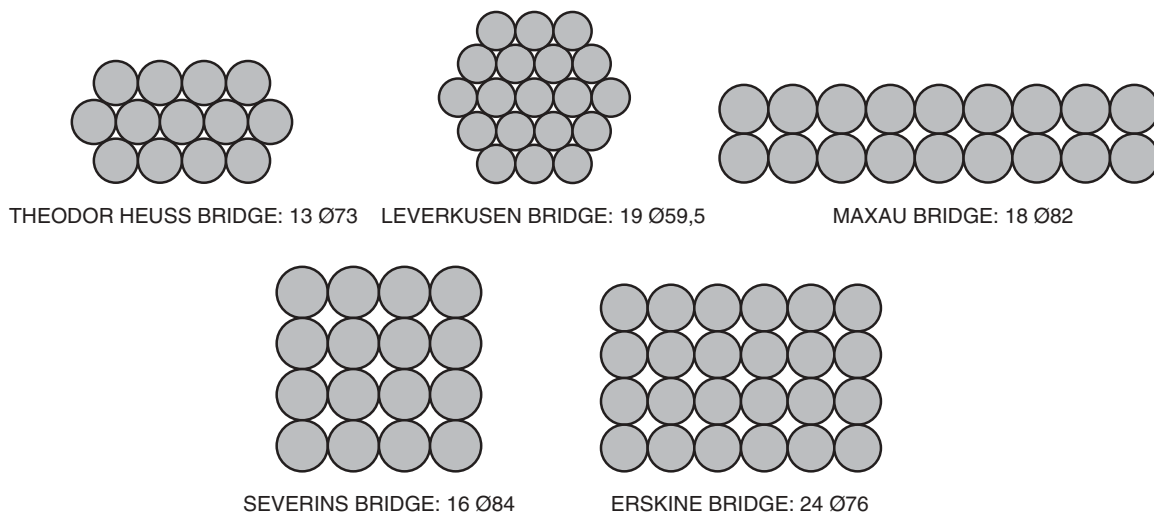
**Figure 2.15** Multi-strand suspension bridge main cable composed of individual locked-coil strands (Askøy Bridge)

rectangular shapes were used. Compact, multi-strand cables of the type illustrated in Figure 2.16 have not been used for stay cables recently mainly due to the rather complicated anchorage details and the inability to replace individual strands.

In suspension bridges with main cables made from helical strands, a hexagonal shape of the completed cable has been used, as illustrated in Figure 2.17 by the original main cable of the Tancarville Bridge from 1959. Here, the individual strands were kept in position in each cable band and this excluded the individual oscillation of the single strands, so it was decided to do without a wrapping.

The wires in the original Tancarville Bridge main cables were made from ungalvanized wires. That resulted in a poor durability so in the late 1990s it became necessary to perform a costly replacement of the two deteriorated main cables by four new ones.

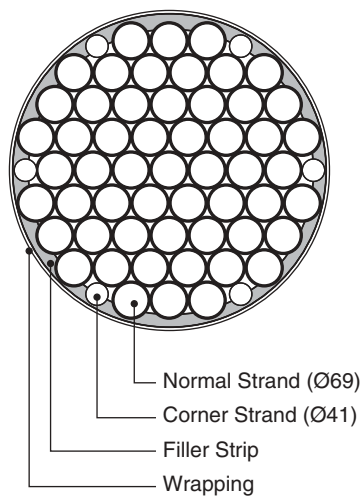
In the Lillebælt Bridge the main cables were also made from helical strands, but here a quasi-circular shape was achieved by the use of special corner strands with a smaller diameter than used for the normal strands (Figure 2.18). After erection of



**Figure 2.16** Multi-strand stay cables used in cable stayed bridges built in the 1960s and 1970s



**Figure 2.17** Suspension bridge main cable composed of tightly spaced locked-coil strands (original Tancarville Bridge)



**Figure 2.18** Cross section of the main cable in the Lillebælt Bridge





**Figure 2.19** Lillebælt Bridge main cable with polyethylene fillers to achieve a circular shape

the strands, a complete circular shape was achieved by adding polyethylene fillers (Figure 2.19) followed by a wrapping of the entire cable by a mild steel wire. By this procedure, the final cable showed the same circular shape as found in cables erected by the air-spinning method and it could therefore be wrapped by a spiral wire in the conventional way. At the same time, an increased corrosion protection was to be expected. However, after some years of operation it was noted that the wrapping wire had lost most of its pre-tension, probably due to creep in the polyethylene fillers. As this would affect the durability of the main cables, it was decided to improve the corrosion protection by adding a dehumidification system to this bridge that was the first in the world to use dehumidification for corrosion protection of the box girder interior.

In the Lillebælt Bridge, the helical strands to be used in the main cables had a length of approximately 1500 m, the longest ever used in suspension bridge construction.

The principle of composing a multi-strand stay cable of individual strands, as used originally in the Strömsund Bridge, has again appeared in some modern cable stayed bridges (Figure 2.20) as this arrangement will allow the strands to be replaced one by one while the bridge is still in operation. Note that in the modern application the strands are separated to such an extent that all surfaces can easily be inspected and maintained. Also the spacing allows all strand anchorages to be arranged individually so that each strand can be stressed and de-stressed without affecting the other anchorages.

### **2.1.8 Parallel-wire suspension bridge main cables**

For suspension bridges with larger cable lengths, the main cables are made either by the air-spinning method (AS method) or by the pre-fabricated parallel-wire strand method (PPWS method).

For more than a century, the AS method was the preferred method for erection of suspension bridge main cables. By this method, the total cable section containing up to 30 000 Nos. 5 mm wires (Figure 2.21) is assembled on site from individual wires pulled across from one anchorage to the other over the pylon saddles. After erection of all wires, the cable is compacted into a circular shape by a compacting machine and the total cable is then wrapped by a soft annealed galvanized steel wire. To ensure that the cable keeps its compacted form, the wrapping is made under tension and this leads to the occurrence of frictional forces between the individual wires. This influences the flexural stiffness of the cable and increases to some extent the bending stresses induced at the cable saddles and the cable bands. Figure 2.22 shows the main cable of the Severn Bridge after the circular shape was achieved but before wrapping.

Pre-fabricated parallel-wire strands have been introduced for the erection of suspension bridge main cables to reduce the labour involved as well as the weather sensitivity, and thereby to speed erection. Basically the difference between the AS method and the PPWS method is that in the former the wires are pulled across individually, whereas they are pulled across in bundles (the pre-fabricated strands) in the latter, as illustrated in Figure 2.23. Due to the larger weight per unit length of the parallel-wire strand, this becomes more stable and less affected by wind action than the individual wires. Also, with the



**Figure 2.20** Stay cables composed of individual locked-coil strands (renovated Norderelbe Bridge)



**Figure 2.21** Mock-up of the Golden Gate Bridge main cable composed of 27 572 wires



**Figure 2.22** Main cable of the Severn Bridge after compaction



**Figure 2.23** PPWS supported on a roller at the catwalk when pulled across from anchor block to anchor block (Akashi Kaikyo Bridge)

PPWS method the sag adjustment performed during erection can be made for the whole bundle in one operation, whereas it has to be done individually for each wire in the case of the conventional AS method.

The limiting factor for the application of the PPWS method is the weight of the strand, as this has to be fabricated in full length corresponding to the distance from one anchorage to the other along the main cable. However, the maximum allowable weight and outer dimensions of the reels with the pre-fabricated strand will depend strongly on local conditions, especially the transportation facilities available. If transportation from the shop to the site can take place entirely by sea, considerably larger and heavier reels can be allowed than if transportation over land is required. In this connection it should be mentioned that in special cases it might be possible to fabricate the parallel-wire strands at a work site area adjacent to the bridge location to eliminate or considerably reduce the transportation problem.

The pioneering effort to introduce the pre-fabricated PPWS method for erection of suspension bridge main cables actually took place in the USA at the end of the American suspension bridge era but further development of the method has mainly taken place in Japan.

The first major Japanese suspension bridge to have the main cables erected by the PPWS method was the Kanmonkyu Bridge with its main span of 712 m.

A European attempt to introduce the PPWS method took place in 1969 during the tender for the First Bosphorus Bridge as the consulting engineers had based their design on this method for erection of the main cables. However, the lowest bid received was for an alternative application of the AS method, and consequently this method was chosen for the actual construction.

During the 1980s the PPWS method was developed further in Japan at the construction of the main cables in the two Bisan Seto Bridges (Figure 2.24) forming a major part of the Seto Ohashi between Honshu and Shikoku. These bridges have main spans of 990 m and 1100 m, respectively, requiring parallel-wire strands with a length of up to 1780 m and a weight of 40 tonnes for strand, sockets and reel.

Besides the Bisan Seto Bridges the Seto Ohashi also comprised a third suspension bridge, the Shimotsui Seto Bridge, and for this bridge it was decided to use the AS method in a modified form where the wires were pulled across with a lower tension than used traditionally. This proved to give a number of advantages especially in relation to the sag adjustments that could now be made for an entire wire bundle (the *in situ* strand) comprising 552 wires instead of an individual sag adjustment of each wire.

The method developed for the Shimotsui Seto Bridge was later used by Japanese contractors during erection of the main cables of the Fatih Sultan Mehmet Bridge (Second Bosphorus Bridge). Here this 'low-tension method' proved to be a most efficient method as the two main cables comprising 9500 tonnes of steel wire were erected in just four months.

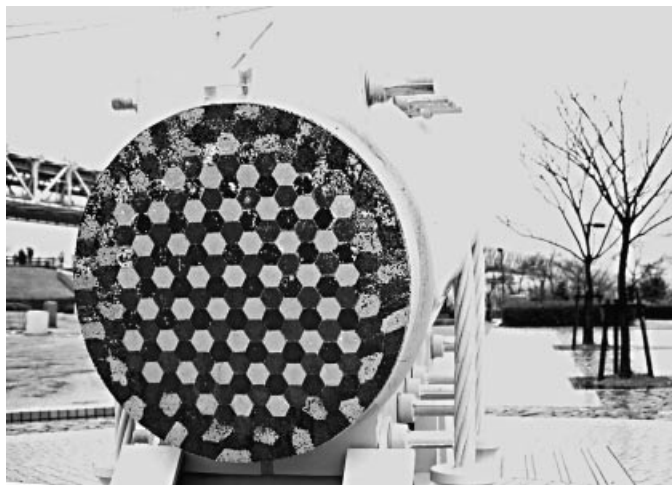
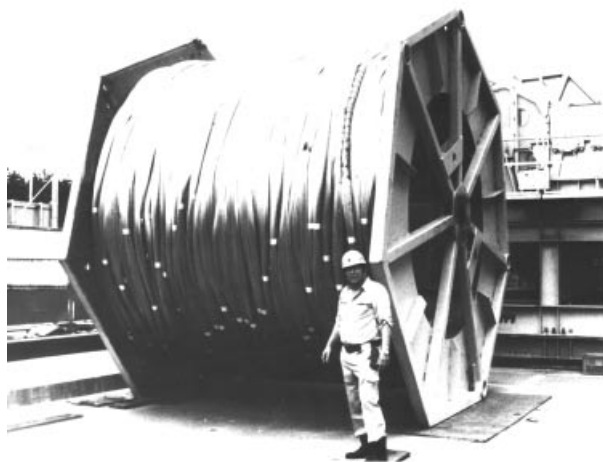


Figure 2.24 Mock-up of a main cable in the Bisan Seto Bridges



**Figure 2.25** Strand reel for the 4000 m long PPWS used in the Akashi Kaikyo Bridge

In the tender designs from 1990 for the Storebælt East Bridge, both the AS method and the PPWS method were investigated and, as they were found to be equally acceptable, the contractors were free to base their bids on either of the two methods.

When bids were received, it turned out that the cost of erecting the main cables by the PPWS method would be substantially higher than for the AS method. So despite the fact that it was believed that the PPWS method would imply a number of advantages and give cables of a slightly superior quality, it was chosen to base the contract on the AS method. The deciding factor here was that past experience had proved that the quality achieved by the AS method was fully acceptable and the durability comparable.

A somewhat similar scenario was experienced during tendering for the Tsing Ma Bridge in Hong Kong with the exception that for this bridge only the PPWS method was indicated in the tender documents. However, the contractor offered as an alternative bid to erect the main cables by the AS method at a lower price so also here the PPWS method was ousted.

Meanwhile in Japan the PPWS method was further developed to overcome the difficulties of erecting the main cables of the record-breaking Akashi Kaikyo Bridge requiring strands with a length of 4000 m and a strand, sockets and reel weight of 95 tonnes (Figure 2.25). However, in Japan, the decision to use either the AS method or the PPWS method is generally taken by the client prior to tendering, and alternatives are not permitted.

### 2.1.9 Comparison between different cable types

A comparison based on typical values for some of the cables described above is given in Table 2.2. The highest strength-to-density values are found for suspension bridge main cables and New PWS cables, whereas grouted cables show the smallest values.

The void ratio is smallest for locked-coil strands and suspension bridge main cables, whereas the grouted stay cables are characterized by the highest values.

The efficiency of the cable support in a cable stayed system is reflected by the axial stiffness  $AE_{eq}$  of the cables. In Table 2.2 the axial stiffness is illustrated by the index  $4(E_{tan}/f_{cbd})10^{-3}$ , where  $E_{tan}$  is the equivalent tangent modulus corresponding to a cable stress of  $\sigma = 0.75f_{cbd}$ .

The axial stiffness index is given for cables with a horizontal projection of 100 m and 500 m, respectively. It is seen that for  $a = 100$  m the lowest axial stiffness is found for parallel-strand cables due to their 7% lower modulus of elasticity. For the locked-coil cable the even lower basic modulus of elasticity is almost entirely balanced out by the reduced design stress, leading to an increased cross section.

**Table 2.2** Modulus of elasticity  $E$ , design stress  $f_{cbd}$ , equivalent density  $\gamma_{eq}$ , strength-to-density ratio  $f_{cbd}/\gamma_{eq}$ , 'void' ratio, and axial stiffness index for seven different types of cable

| Cable type                        | $E$<br>(GPa) | $f_{cbd}$<br>(MPa) | $\gamma_{eq}$<br>(kN/m <sup>3</sup> ) | $f_{cbd}/\gamma_{eq}$<br>(km) | Void ratio | Stiffness index $4(E_{tan}/f_{cbd})10^{-3}$ |             |
|-----------------------------------|--------------|--------------------|---------------------------------------|-------------------------------|------------|---|-------------|
|                                   |              |                    |                                       |                               |            | $a = 100$ m                                 | $a = 500$ m |
| Suspension bridge main cable      | 205          | 800                | 84                                    | 9.52                          | 0.20       |   |             |
| Locked-coil strand                | 180          | 720                | 88                                    | 8.18                          | 0.10       | 0.99  | 0.85        |
| PWS (grouted) for stay cables     | 205          | 800                | 120                                   | 6.67                          | 0.54       | 1.01  | 0.80        |
| New PWS for stay cables           | 200          | 800                | 82                                    | 9.76                          | 0.33       | 1.00  | 0.88        |
| Parallel seven-wire strand cables |              |                    |                                       |                               |            |   |             |
| Grouted                           | 190          | 800                | 130                                   | 6.15                          | 0.75       | 0.94  | 0.72        |
| HDPE sheathed seven-wire strands  | 190          | 800                | 90                                    | 8.89                          | 0.80       | 0.94  | 0.83        |
| Dehumidified for stay cables      | 190          | 800                | 85                                    | 9.41                          | 0.51       | 0.94  | 0.84        |

For stays with a horizontal projection of 500 m the more pronounced sag effect of the heavy grouted cables result in a larger axial stiffness of the locked-coil cables than of the PWS cables.

The values given in Table 2.2 are calculated under the simplifying assumption that the weight of the cables does not influence the design force in the cables. This tends to slightly underestimate the effect of having lighter cables.

## 2.2 Corrosion Protection

The large number of wires, each with a small diameter, implies that the cable will be extremely vulnerable to surface corrosion. Adding to this that most of the wires in the completed cable will be inaccessible to direct inspection and maintenance, that cavities often are present between wires, and that the steel material in the wires is sensitive to stress corrosion further emphasizes the seriousness of the corrosion problem.

In Figure 2.26 a comparison is made between four different load-carrying elements with almost the same cross sectional area: a solid round bar with a diameter of 100 mm, a rolled H-section, a square hollow section and a cable composed of 400 Nos. 5 mm wires.

For the round bar and the H-section the entire surface can be visually inspected, whereas the hollow section has only the exterior surface accessible for such an inspection. For the multi-wire cable only approximately half of the surface of the outer wires will be directly visible. This corresponds to only approximately 8% of the total surface of all wires.

In case of a surface corrosion of 1 mm the cross sectional area of the solid round bar will be reduced by only 4% of its initial value and such a reduction will be amply covered by the general safety margin so that there will be no danger of a collapse of the entire structure.

For the H-section and the hollow section the reduction of cross sectional area will be approximately 15% and 25%, respectively. These values could be more critical for the safety of the structure, but in most cases they would not lead to an immediate collapse.


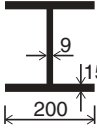
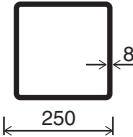

Finally for the cable the reduction of the cross sectional area due to a 1 mm surface corrosion will be 64% – a value that will definitely not be covered by the safety margin used during the design of the structure.

The sensitivity to corrosion illustrated in Figure 2.26 has from the very beginning concentrated the attention of structural engineers on the importance of an efficient surface protection and still today great effort is put into developing improved protective systems.

For the single wire, the most efficient corrosion protection is obtained by hot galvanizing, typically with a zinc weight of 3 N/m<sup>2</sup>. For a 5 mm wire, this corresponds to a zinc weight of approximately 0.05 N/m or 3.5% of the steel weight of the wire. So in this case the equivalent density of the galvanized wire will be  $1.035 \times 77 = 80$  kN/m<sup>2</sup>.

### 2.2.1 Suspension bridge main cables

Galvanized wires are today generally used in suspension bridge main cables whether they are made by the AS method or by the PPWS method. To further increase the corrosion protection after compaction into a circular shape, the completed cable has traditionally been treated with zinc dust paste (earlier with red lead paste, now abandoned due to health problems)

| TYPE OF STRUCTURAL ELEMENT   | RATIO BETWEEN VISIBLE SURFACE AND TOTAL SURFACE | RESIDUAL STRENGTH AFTER 1mm SURFACE CORROSION |
|--|---|---|
| <p><math>\phi</math> 100      <math>A=7850 \text{ mm}^2</math></p>  | 1   | $0.96 \times F_u$                             |
| <p>HE 200 B      <math>A=7810 \text{ mm}^2</math></p>               | 1   | $0.85 \times F_u$                             |
| <p>RHS 250x250x8      <math>A=7920 \text{ mm}^2</math></p>          | 0.52  | $0.75 \times F_u$                             |
| <p>400 nos. 5mm wires      <math>A=7850 \text{ mm}^2</math></p>    | 0.08  | $0.36 \times F_u$                             |

**Figure 2.26** Comparison between a solid round bar, an H-section, a rectangular hollow section and a multi-wire cable in relation to visual inspection and sensitivity to surface corrosion

before being wrapped by a soft-annealed galvanized wire. By this procedure, a double corrosion protection is achieved, and if executed with the necessary care durable protection will result.

This was clearly indicated during the first in-depth inspection of the Brooklyn Bridge main cables in 1946. Here, the 65-year-old cables proved to be in an acceptable condition (except in some parts of the anchorage zones), and later inspections have given almost the same result even now when the cables have been exposed to a quite aggressive atmosphere for more than 125 years.

The wrapping of suspension bridge main cables by a soft steel wire was replaced in some American bridges by a plastic cable covering in the mid-1960s. This covering typically consisted of the following components:

- (1) a covering with polyester film;
- (2) an initial coating with acrylic resin;
- (3) a layer of non-woven glass mat pressed into place;
- (4) a second coating with acrylic resin;
- (5) a layer of woven 150 mm wide glass cloth spiral wound on the cable;
- (6) a third coating with acrylic resin;
- (7) a final coating with a mixture of acrylic resin and sand to give the surface a rough texture.



**Figure 2.27** Cross section of a Z-shaped wrapping wire

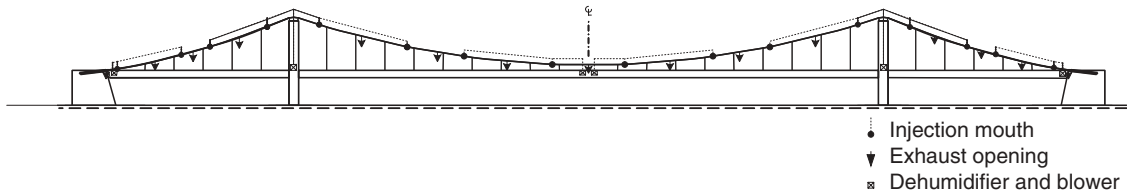
The plastic covering did not at the time fulfil all expectations, so steel wire wrapping continued to be used in the years to follow. However, as the main cable elongates under the strains caused by traffic load, the paint has in several cases cracked and given access for water to penetrate. Improved behaviour can be obtained if flexible paint systems are applied but even these might become brittle as time goes by.

For the main cables of the Kurushima Kaikyo Bridges in Japan a new wire was used for the wrapping. In stead of the round wire a Z-shaped wire with a cross section as shown in Figure 2.27 was used. With this wire shape gaps will not occur and the exterior surface will be smoother and thereby make the paint more durable.

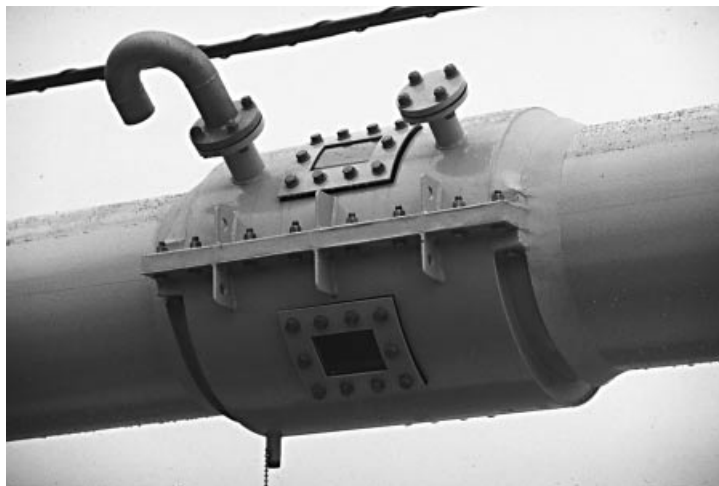
The most important step in recent years to improve corrosion protection of suspension bridge main cables was taken during the construction of the Akashi Kaikyo Bridge. Here the system of dehumidification by dry air injection was for the first time used to protect the main cables against corrosion.

The dehumidifiers are positioned in the deck at the pylons, at the anchor blocks and at midspan. From these locations the dry air is pumped through air supply pipes to special cable clamps with injection mouths (Figure 2.28). Halfway between the injection clamps exhaust clamps are positioned so that the air flows from the air supply pipes through the voids between the wires to the exhaust openings (Figure 2.29).

If cable dehumidification is to be used, it is essential that an efficient air tightness of the exterior is provided, whereas the traditional application of zinc paste under the wrapping should be omitted to ease the air flow through the voids.



**Figure 2.28** Location of dehumidifiers, supply pipes and injection mouths



**Figure 2.29** Cable clamp with exhaust opening





**Figure 2.30** Wrapping with polyethylene strips to achieve air tightness (Photo credit: Ove Sørensen, COWI)

Past experience indicates that the desired air tightness can be achieved with an elastomeric wrapping where two 150 mm wide neoprene strips are wrapped around the main cable with a 50% overlap. Subsequently an air curing coating is applied to the surface after sprinkling of gritty material to give the top of the cable an anti-slip surface.

Another system ('Cableguard') uses polyethylene strips for the airtight wrapping that is 'welded' together by application of heating blankets around the cable (Figure 2.30). This seems to give a very reliable and durable watertight cover.

In most cases the elastomeric wrapping is added on top of the traditional spiral wire wrapping but it has also been tried to add the elastomeric wrapping directly on the wires of the main cable. However, neither the strength nor the stiffness of an elastomeric wrapping is equal to that of a steel wire wrapping.

### 2.2.2 Stay cables

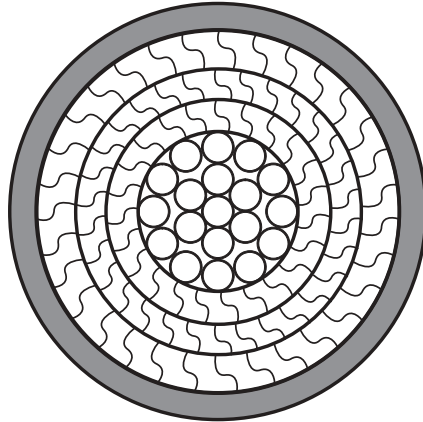
For stay cables, in the beginning often ungalvanized wires were used but today only galvanized wires are regarded as acceptable.

In some cases the entire corrosion protection of the stay cable has had to depend on galvanizing of the single wires, as was the case for some of the early British cable stayed bridges. Here, the stay cables were composed of helical strands with all wires galvanized. Although the corrosion protection based solely on galvanizing of the wires cannot be as effective as the double protection used for suspension bridge main cables, it could give adequate protection for a number of years, but today it is generally agreed that stay cables should have at least two barriers against corrosion so, besides using galvanized wires, a second barrier must be added.

Locked-coil strands were in earlier times often made with varying corrosion protection in the different layers. Thus, it was quite common that the outer Z-shaped wires were galvanized, whereas all the inner wires were ungalvanized. To eliminate or reduce the inner cavities between the round wires, a filling with red lead was made during fabrication of the strands. If combined with a final paint layer on the surface of the locked-coil strand, it could be argued that a double barrier system was in place as the outer wires were protected by the galvanizing and the final surface paint whereas the inner wires were protected by the outer wire layers and the red lead filling.

In the past, locked-coil strands with all wires ungalvanized have been used occasionally. In these cases the only corrosion protection of the outer wires was a normal painting of the strand surface, i.e. a single barrier protection. This was the case for the strands used in the Köhlbrand Bridge in Germany, but here a breaking of wires began to appear after only three or four years of service, and a costly replacement of all strands had to be made [82.3].

As is often the case when accidents occur in structures, the very early deterioration of the Köhlbrand Bridge strands seemed to have been caused by a combination of factors; the bridge was situated in an industrialized area with high contents of sulphur and phosphorus in the air; the red lead protection of the inner wires had been damaged in the heat-affected zone near the sockets; notches were found in several of the outer wires; the strands were anchored in the deck in such a way that angular changes were concentrated at the socket, introducing maximum bending in the strand at this location. Furthermore,



**Figure 2.31** Locked coil strand with 7 mm thick HDPE sheathing

the lower parts of the stays were exposed to salt water splashed up from the roadway in the winter time, and the painting of the strands suffered in some places from bad workmanship.

For the replacement, strands with galvanized wires either in all layers or in the two outer layers were used. At the same time the lower part of the strands (in the ‘splash’ zone) were protected by a polyethylene tube and dampers were installed to reduce the wind-induced oscillations. The cost of the strand replacements amounted to 28% of the initial cost of the entire cable stayed portion of the Köhlbrand Bridge.

Similar problems were experienced in the Maracaibo Bridge, the Norderelbe Bridge and probably a few more, and in all cases the replacement costs have been substantial. This is one of the reasons for the present preference for mono-strand cables that can easily be replaced.

In modern locked-coil strands all wires are galvanized and the second barrier is established by a sealing compound (such as metal coat) which fills the voids and provides excellent corrosion and abrasion protection.

An improved corrosion protection of locked-coil strands can be achieved by an HDPE sheathing extruded around the entire length of the strand. That will certainly constitute an efficient two-barrier protective system as used for e.g. the hangers of the Storebælt East Bridge where the sheathing is 7 mm thick (Figure 2.31),

The combination of a helical strand with galvanized wires and a PE tube was used for the first time during the construction of the Papineau–Leblanc Bridge in Canada back in the 1960s. In recent times the principle has been further developed in the New PWS Cables.

At the introduction of the parallel-wire strands (PWS), the corrosion protection was generally made by placing the wires inside a tube subsequently injected with cement grout, which was believed to give a corrosion protection similar to that found inside ducts in pre-stressed concrete. Therefore, the wires were generally ungalvanized as in tendons.

The tube was made of either stainless steel or polyethylene (PE). Stainless steel offered the advantage of a well-known and long-lasting protection, but it gave rise to complications during erection as the thin-walled tubes had to be kept straight (or very modestly curved) during installation due to the material’s high modulus of elasticity. With PE tubes the complete stay cable with wires, sockets, and tube was completed in the shop and reeled for transportation (Figure 2.32). After erection in the bridge, the grout is injected when the cable was under full dead load stress to suppress the formation of cracks in the grout. As described earlier the wires were kept tight together during transportation and erection by twisting a small helical strand around the wire bundle and this strand also acted as a spacer between the wire bundle and the PE tube, thus improving the embedding of all wires by the cement grout (Figure 2.33).

In the early parallel-wire strands the double barrier protection was assumed to be established by, first, the external tube and, second, the cement grout so that it should be unnecessary to use galvanized wires.

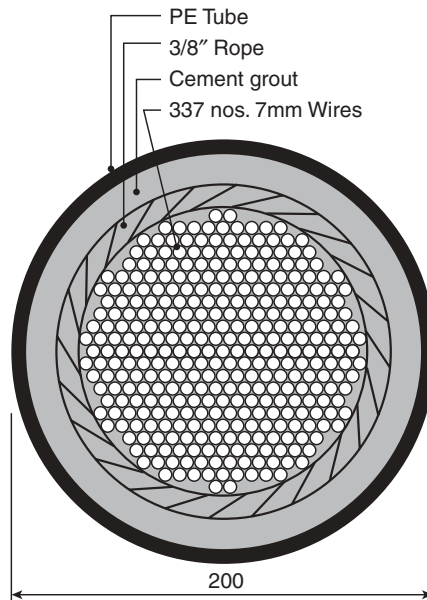
Although applied in several major cable stayed bridges, the corrosion protection achieved by grouted PE tubes was questioned by a growing number of bridge engineers fearing that cracks in the PE tube and in the cement grout due to environmental and dynamic actions would in the long run reduce the efficiency of this protection. Actually, mishaps have occurred in some cases, such as in the Zarate-Brazo Largo Bridges, where cracks were observed in the PE tubes.



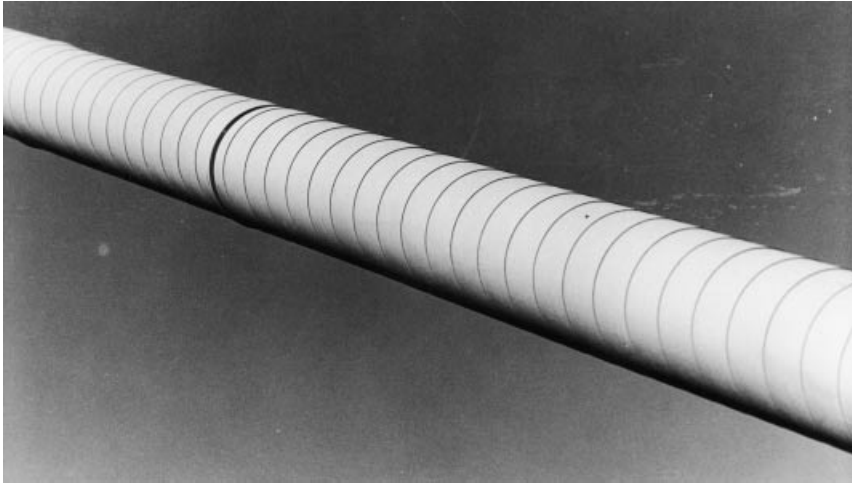
**Figure 2.32** PWS with PE tube reeled for transportation (Farø Bridge)

Consequently, the expected efficiency of the corrosion protection was not achieved. The problems in the Zarate-Brazo Largo Bridges could be traced back to the fact that the strands had been stored on reels for a very long period, giving rise to creep in the tube material.

In a test series carried out on full-scale parallel-wire strands at the University of Texas at Austin, it was detected by observations through transparent tubes that both transverse and longitudinal cracks occurred in the grout as soon as the axial tension was increased from the level of dead load to the level of dead + traffic load. Subsequently it was observed during accelerated corrosion tests with test specimens where the tube was removed, that the cement grout gave virtually no protection against corrosion due to the presence of the many cracks. It could, therefore, be concluded that the assumed double barrier protection was in fact only a single barrier protection relying entirely on the integrity of the PE tube.



**Figure 2.33** PWS inside a grouted PE tube (Zarate-Brazo Largo Bridges)



**Figure 2.34** Parallel-wire strand of the Pasco–Kennewick Bridge wrapped in a white plastic cover

With these experiences it was recommended to avoid an application of cement grouted strands in the future, and also to carefully inspect the existing cable stayed bridges with these types of strands in order to detect as early as possible any disintegration of the protecting tubes and then take immediate action, e.g. by an additional wrapping around the damaged part of the tube.

Wrapping has in some cases also been used to give the completed cable a colour different from the black that has to be used for the PE tube to protect it from UV radiation. Such a supplementary wrapping was for the first time used in the Pasco–Kennewick Bridge where the PE tubes were wrapped in a white plastic cover (Figure 2.34). However, on that occasion the experience was not too promising as the cover deteriorated within a period of a few years. Later applications of plastic wrapping in the form of laminated Tedlar tapes have been more convincing but long-term experiences to prove the durability are still not at hand.

A later application of an additional coloured cover is seen in Figure 2.35 showing one of the stays in the Second Severn Bridge. Here the cover sheaths are curved directly onto the tube surface instead of being wrapped spirally around.



**Figure 2.35** Parallel-strand cable of the Second Severn Bridge with plastic cover

After realizing the drawbacks of the grouted stay cables the manufacturers made an effort to develop new and more reliable types of stay cables. An obvious step seemed to be to replace the cement grout by a more suitable material such as a polymer cement grout with a sufficient tensile ductility. Compared to grout of normal Portland cement, the grout with polymer added would give a material that is 20 times more ductile in elongation and highly resistant to cracking under dynamic loading. Furthermore, with polymer cement grout there would be no shrinking and no bleeding during grouting, and no special technique or equipment was required. Finally, with a polymer cement grout there would be no danger of a chemical reaction between the zinc layer on galvanized wires and the cement. The disadvantage of polymer cement grout was the high material cost.

A grout of resin material based on polybutadiene was used during construction of the Hitsuishijima and Iwagurojima Bridges in Japan. In these bridges built to carry railway traffic it was regarded as paramount to have a crack-free grout.

A two-component material was also tried, with one liquid consisting of polybutadiene polyurethane polyol resin and the other of an isocyanate hardener. This resulted in a material with very low viscosity during pouring so that all voids would be easily filled. After hardening, the material was very flexible with an ultimate elongation of 280% and its density was only half of that of cement grout. However, the cost of material and execution was high, handling was delicate, and it was highly temperature dependent and flammable [95.1].

Another alternative to cement grout was petroleum wax injected in a liquid state at temperatures of 85–105 °C where after it solidified at ambient temperatures. During cooling the material shrank and at lower temperatures cracks might develop. It was therefore doubtful whether the wax in itself constitutes a barrier even if this was improved by corrosion-inhibiting additives. In any case, with petroleum wax as filler, the wires must be galvanized to constitute one of the corrosion-inhibiting barriers. With petroleum wax the completed stay cable with wires, PE tube, filler and sockets would be sufficiently flexible to allow transportation on large reels, thus reducing site work to a minimum.

Another possibility was to extrude a PE sheathing directly onto the wire bundle, i.e. leave out any intermediate layer of grout or wax.

For parallel-strand stay cables the same protective systems as described above can be used if the seven-wire strands are made from galvanized wires. However, with the seven-wire strand as the basic element it is also possible to extrude a HDPE sheath directly onto each strand after it has been internally waxed. In that case both barriers will be present on each individual seven-wire strand.

It should finally be mentioned that, instead of galvanizing, an epoxy coating of the individual wires or seven-wire strands has also been used to form one of the corrosion barriers. If manufactured and handled with sufficient care the epoxy coating will undoubtedly give a long-lasting protection but it is extremely important that the epoxy layer is intact over the entire surface as even the smallest hole in the layer can permit corrosion at that spot.

## 2.3 Mechanical Properties

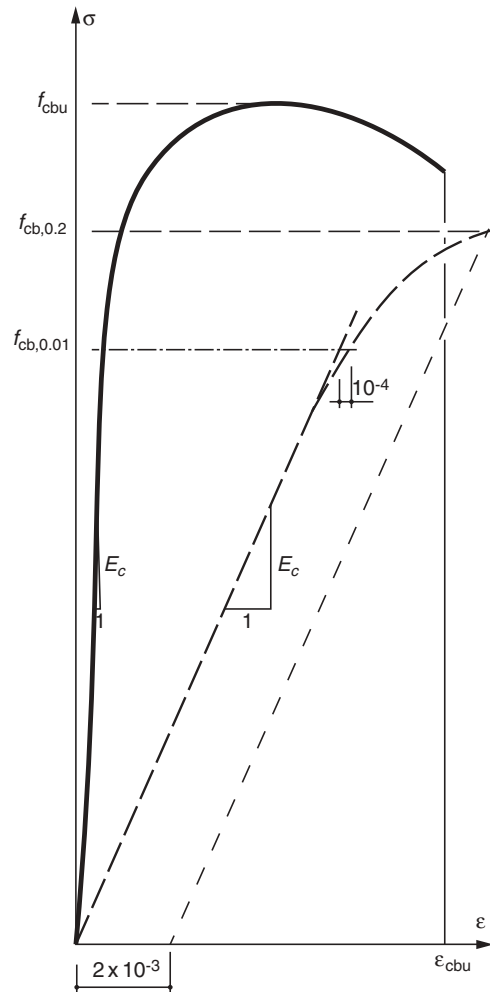
### 2.3.1 Static strength

A typical stress–strain relationship for a galvanized wire as used in cables is shown in Figure 2.36. Here the most important parameters for the designer are indicated:

|  |                     |
|--|---------------------|
| the modulus of elasticity:                   | $E_c$               |
| the 0.2% proof stress:                       | $f_{cb,0.2}$        |
| the limit of proportionality (0.01% stress): | $f_{cb,0.01}$       |
| the ultimate tensile strength:               | $f_{cbu}$           |
| the total elongation at rupture:             | $\varepsilon_{cbu}$ |

The modulus of elasticity is slightly smaller than for ordinary structural steel. Thus for design purposes, a value of  $E_c = 205$  GPa is generally applied in the design process.

For the wires most commonly used for cables the guaranteed minimum tensile strength will be 1570 MPa and the guaranteed 0.2% proof stress 1180 MPa. The limit of proportionality (0.01% proof stress) will typically have a value of 65–70% of the tensile strength. For the design the limit of proportionality is of significance as this stress indicates an absolute upper limit for the stresses in the service condition due to the fact that it is unacceptable to have permanent



**Figure 2.36** Typical stress–strain diagram for a wire used in cables (the dotted curve has a ten times larger horizontal scale than the solid curve)

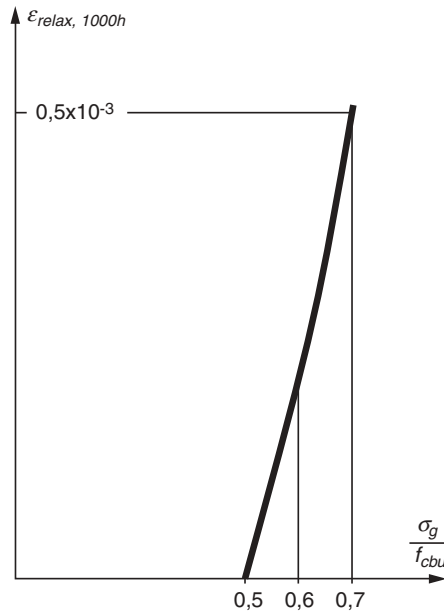
(irreversible) elongation of the wires for loads that will occur with a large number of repetitions throughout the lifetime of the bridge.

Wires with a higher minimum tensile strength of 1770 MPa have been available from several suppliers for some time, and wires with a minimum tensile strength of 1960 MPa are being developed [95.18].

In Japan a steel wire with an improved tensile strength was developed for the main cables of the Akashi Kaikyo Bridge as the manufacturers agreed to guarantee a minimum tensile strength of 1800 MPa. The increased strength was mainly achieved by adding silicon (Si) to the conventional low-alloy steel, and it also proved possible to control the loss of strength due to heating in the galvanization process.

For the 2005 Messina Strait Bridge tender one of the bidders had based his bid on application of wires with a minimum tensile stress of 1860 MPa.

As seen from the stress–strain diagram the cable steel does not show a plastic plateau and the elongation at rupture is considerably smaller than for ordinary structural steel. The available plastic strains (characterized by a minimum elongation at rupture  $\sim 4\%$  in a 250 mm gauge length) are generally sufficient to allow a local redistribution of forces



**Figure 2.37** Irreversible strain due to relaxation in a cable wire (normal relaxation grade) subjected to a constant stress  $\sigma_g$  for 1000 hours

between wires with different initial stresses due to imperfections during erection. Also, the plasticity will reduce peak stresses from bending under permanent loads. On the other hand, the plastic strains of the cable steel will generally not be sufficient to allow a plastic design of the entire structure based on mechanisms assuming a radical redistribution of loads between the cable system and the deck.

### 2.3.2 Relaxation

For the stipulation of the allowable stress level in cable steel, the effect of relaxation must also be taken into account. As shown in Figure 2.37, the relaxation accelerates significantly when the permanent stress  $\sigma_g$  is chosen to take a value larger than 50% of the tensile strength. The stresses from permanent loads should therefore not exceed a value of  $0.45 f_{cbu}$  unless a special low relaxation grade of steel is used.

It should be mentioned that with the present total safety factor of typically 2.2 against breaking, the condition of a dead load stress below 45% of the ultimate strength will be fulfilled automatically as the total stress from dead + traffic load will be kept below  $f_{cbu}/2.2 \sim 0.45 f_{cbu}$ . However, if the trend towards lowering the (partial) safety factors continues, then relaxation could be decisive for the dimensioning.

### 2.3.3 Fatigue strength

As the fatigue strength of steel does not increase proportionally with the ultimate tensile strength, it becomes essential to consider fatigue in the design of cables subjected to pulsating forces. However, the fact that the cables are main load-carrying elements with relatively large forces from the permanent loads and that the concentrated forces from the vehicular traffic acting on the bridge deck are distributed efficiently by the deck, to some extent reduces the fatigue problems.

Thus, in road bridges the fatigue strength will in most cases only govern the dimensions of a few cables even in structures with light decks of steel. With concrete decks the dead load forces will be of such a magnitude that fatigue will hardly ever have to be considered.

In railway bridges the fatigue effect will be more decisive due to the larger ratio between traffic load and dead load.

The fatigue resistance is generally represented by a Wöhler curve showing the relation between the number  $N$  of load cycles and the corresponding stress range  $\Delta\sigma$  that the actual structural element or joint can withstand. On a

**Table 2.3** Wöhler curves according to PTI Recommendations, 1986

| Number $N$ of cycles   | Allowable stress range $\Delta\sigma$ (MPa) |   |
|------------------------|---|---|
|                        | Parallel-wire cable                         | Parallel-strand cable                     |
| $N < 3 \times 10^6$    | $\log\Delta\sigma = -0.253 \log N + 3.815$  | $\log\Delta\sigma = -0.301 \log N + 4.01$ |
| $N \geq 3 \times 10^6$ | $\Delta\sigma = 150$                        | $\Delta\sigma = 115$                      |

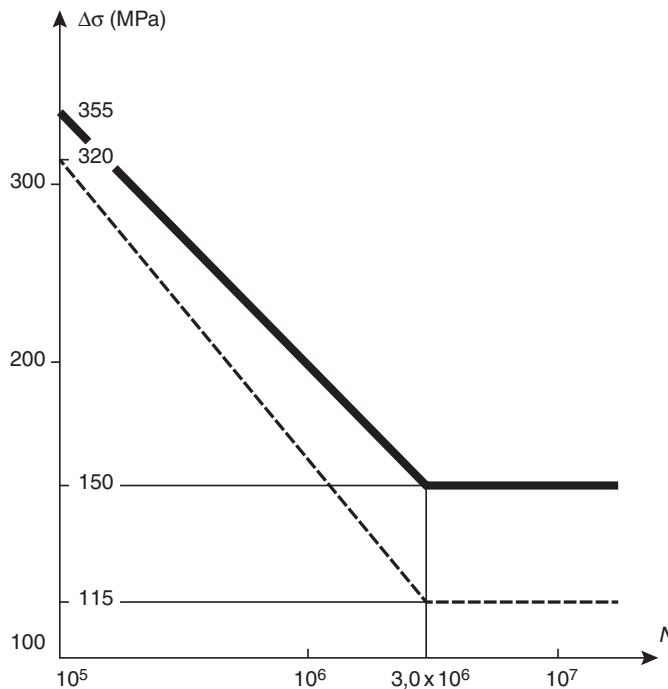
log–log scale the Wöhler curve is generally assumed to be composed of straight lines, i.e. corresponding to the following equation:

$$\log \Delta\sigma = C_1 \log N + C_2 \tag{2.1}$$

In [86.1] the Ad-Hoc Committee on Cable stayed Bridges at the Post-Tensioning Institute in the USA recommended the values for parallel-wire and parallel-strand cables as given in Table 2.3 and shown on the Wöhler curves in Figure 2.38. It should be emphasized that the specified values correspond to allowable stress ranges so they are to be used without additional safety or load factors.

The values of Table 2.3 and the plots in Figure 2.38 are valid for redundant load path structures where a single fracture in a member cannot lead to a collapse. For non-redundant load path structures it is indicated in [86.1] that the allowable stress ranges shall be considerably smaller, typically only 60% of the values in Table 2.3. However, in the present practice with multi-cable systems the structure can generally be classified as a redundant load path structure.

In this connection it should be emphasized that the choice of a specific Wöhler curve for design purposes is closely related to the degree of conservatism applied when stipulating traffic loads and safety factors in an actual case.



**Figure 2.38** Wöhler curves for parallel-wire and parallel-strand cables according to the PTI recommendations 1986



When checking the structure for fatigue, the ultimate state loadings found in specifications cannot generally be used as these are extreme loadings that will occur very few times, if any, during the lifetime of a bridge.

The specified loads on the roadways correspond to a situation with congested traffic and a high percentage of heavy vehicles. This load can, therefore, only appear if the traffic has come to a total standstill, i.e. in connection with a serious traffic accident.

In most specifications the lane loading is stipulated as being between 9 and 30 kN/m but for a moving passenger car occupying a length of approximately 10 m and a width corresponding to the lane width, the load will hardly exceed 2 kN/m. Taking into account that the percentage of passenger cars in most cases is between 70% and 90%, it is evident that the loading to appear with a large number of repetitions is only a small fraction of the load specified for the static strength check.

Bridges carrying railway traffic differ from road bridges by being subjected to traffic loads of much higher intensity. Thus, for a double-track bridge carrying an ordinary railway line (in Europe) the distributed traffic load will be 160 kN/m and this corresponds to the distributed traffic load on 10–16 roadway lanes each with a lane loading of 10–16 kN/m. Also, on a railway bridge the structure will be subjected to a traffic load which is close to the design load each time a fully loaded freight train passes. So fatigue will play a much more dominant role for the design of railway bridges.

For the Øresund Bridge, designed as a combined bridge with a four-lane motorway and a double-track railway, the fatigue check of cables was made primarily for the railway loading, and to give a realistic picture of the stress ranges to appear under passing trains, nine different train categories were defined as shown in Figure 2.39. It is seen that the train with the largest number of passages is Passenger Train II, but this train is characterized by a quite modest load intensity of only 21.4 kN/m. The largest load per unit length of track, 150 kN/m, is found for Heavy Rail Train III, but this train is very short so in structures with an efficient load distribution between stay cables, the stress ranges will be manageable, and as the number of train passages is very small, this train will have a very modest effect on the fatigue life. Therefore, the trains with the most pronounced effect on the fatigue life will be some of the trains with medium load intensities, but a considerable number of passages, such as Freight Train I and III.

For a bridge carrying a double-track railway, like the Øresund Bridge, the calculation of stress ranges from the combined action of simultaneous train loads on both tracks will naturally have to be based on a stochastic approach.

When the stress spectrum has been determined, the design check is generally based on the Palmgren–Miner formula:

$$\sum_{i=1}^n \frac{N_{p,i}}{N_i} \leq 1 \quad (2.2)$$

where  $N_{p,i}$  is the actual number of repetitions of load no.  $i$ , and  $N_i$  the number of repetitions that can be allowed for the stress range  $\Delta\sigma_i$  produced by load no.  $i$  according to the specified Wöhler curve.

Although the Palmgren–Miner formula is widely used for the fatigue check, it is also well known that the fatigue problem is of such complexity that it is only roughly described by this simple formula. In an actual case it is therefore highly recommended to make a number of fatigue tests with cables (or realistic cable models) being subjected to the anticipated stochastic stress spectrum.

It should be emphasized that the calculated stress range for the fatigue check must take into account all stresses, primary as well as secondary. Thus, bending stresses in the cables at sockets and saddles, caused by variation of the cable configuration or by wind-excited oscillations must be included.

### 2.3.4 Hysteresis of helical strands

A mechanical property of interest in special cases is the hysteresis found in helical strands. Figure 2.40 shows the hysteresis curve for the strands that were used for the hangers of the Severn Bridge [66.5]. The effect of the hysteresis was, for this bridge, especially linked to the anticipated increase of the damping due to the absorption of energy in the strands when subjected to cyclic stresses.

For the Severn Bridge it was calculated that the damping to be achieved by the hysteresis of the strands of the inclined hangers was of the same magnitude as found in bridges with riveted trusses. Therefore, the reduced damping caused by the use of welding instead of riveting was expected to be counteracted by the application of inclined hangers made of helical strands.

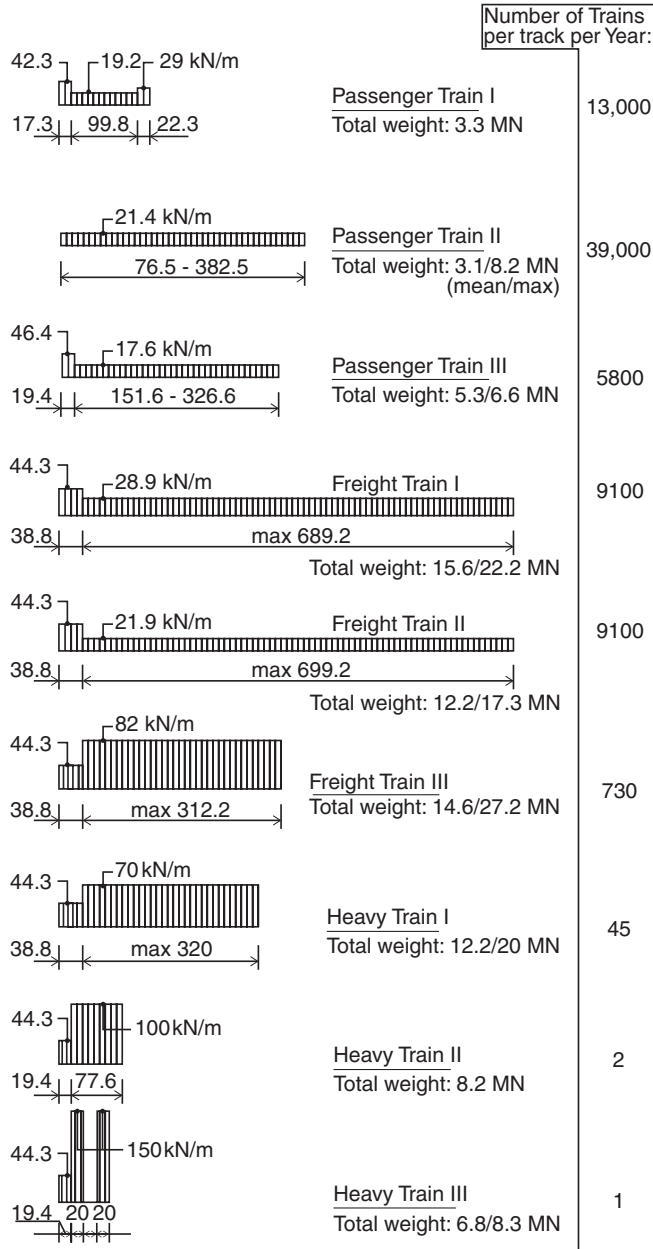
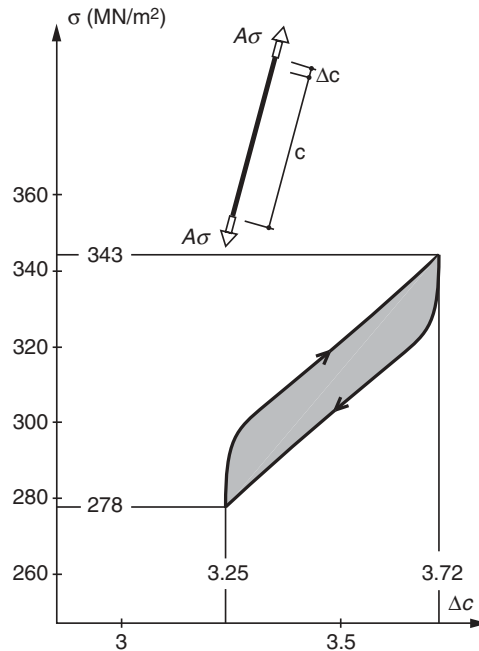


Figure 2.39 Idealized train loads specified for the Øresund Bridge

In parallel-wire strands the hysteresis is insignificant, and it has also been questioned whether the hysteresis of the helical strands will remain at its initial value or vanish as time goes by.

In the case of the Severn Bridge the inclined hanger arrangement might have introduced some damping but they also resulted in such large stress variations under moving traffic that fatigue cracking began to appear in the hangers at an early date, and consequently they all had to be replaced after less than 25 years of service.



**Figure 2.40** Hysteresis of helical strands for the hangers in the Severn Bridge

## 2.4 The Single Cable as a Structural Element

To understand the behaviour of cable supported bridges it is essential to know how the basic element, the single cable, responds to different loadings. In this context it is important to realize that many engineers' intuitive understanding of structural behaviour is linked to the response of beams and columns in a load-carrying system. However, in a number of aspects the cable will show a behaviour that is quite different from that of beams and columns.

In cable supported structures a single cable is used either to carry an axial load or to carry a transverse load. A typical example of a cable carrying axial load is the stay cable in a cable stayed bridge. Here the load transfer is very similar to that found in a tension diagonal of a truss, as indicated in Figure 2.41 on the left.

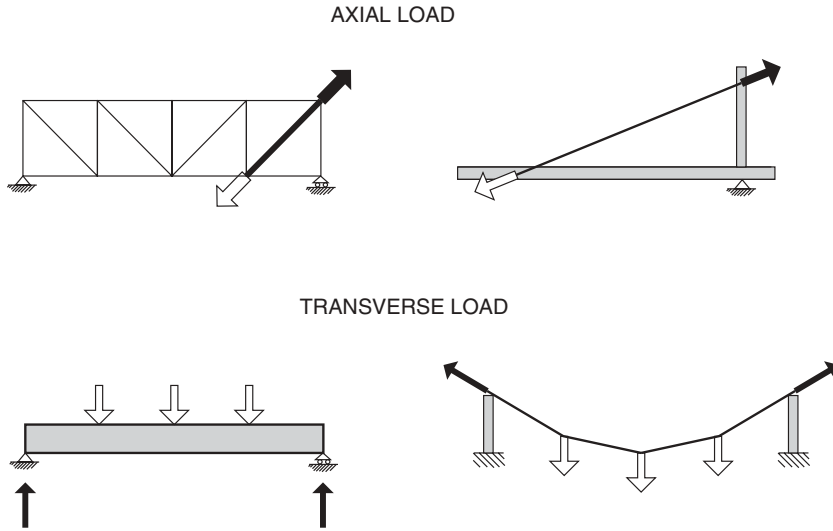
A typical example of a cable carrying transverse load is the suspension bridge main cable. Here the load-carrying performance is similar to that of a beam, as illustrated in Figure 2.41 on the right.

### 2.4.1 Transversally loaded cable

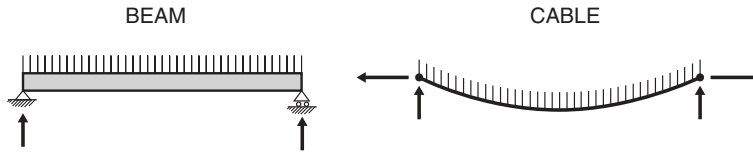
When comparing a beam and a cable carrying transverse load a pronounced difference applies to the supporting conditions. A horizontal beam under vertical load will only require vertical support at the ends whereas the corresponding cable (i.e. a cable with its two end supports at the same level) will have to be supported both vertically and horizontally at the ends (Figure 2.42), and in most cases the horizontal reactions will have to be substantially larger than the vertical reactions.

For a cable carrying transverse load the geometrical configuration is decisive due to the fact that the axial force at mid-span (the horizontal force) is inversely proportional to the sag (Figure 2.43). From this follows that a straight cable is unable to carry any transverse load as zero sag will imply an infinitely large cable force.

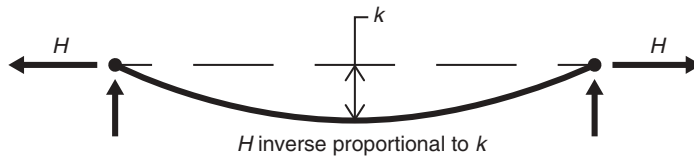
For a beam the geometrical configuration is of much less importance so in most cases the beam is made straight from support to support – and this is also the optimum form from a purely structural viewpoint. However, minor deviations from the straight line will have almost no effect on the required dimensions of the beam. Under similar loading a convex, a straight or a concave beam will be subjected to an equal bending moment at midspan – the decisive internal force for the design of a beam (Figure 2.44).



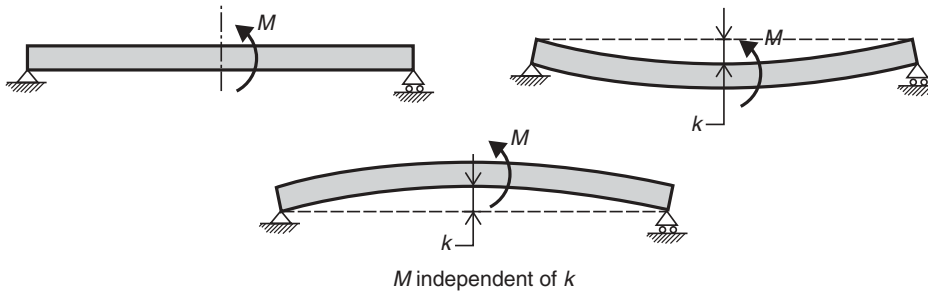
**Figure 2.41** Axially and transversally loaded cable compared to other structural elements with a similar function



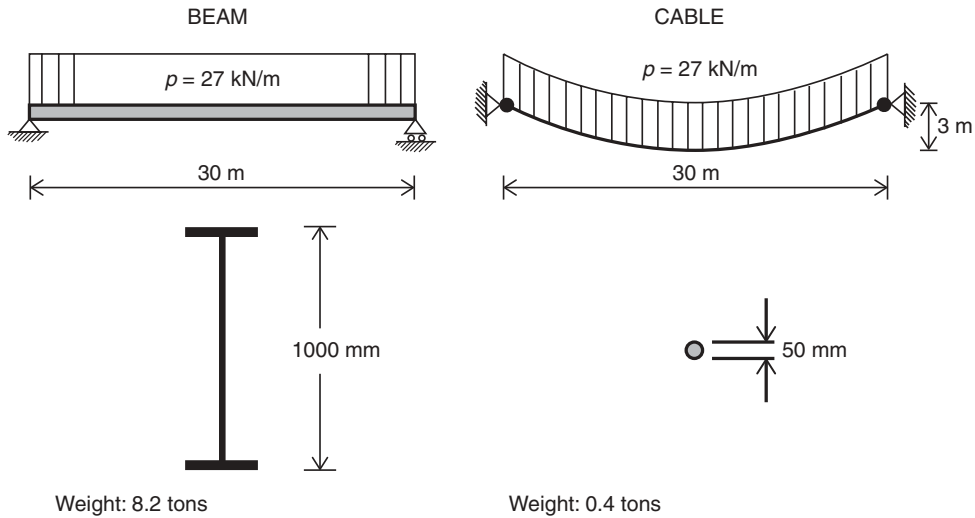
**Figure 2.42** Reactions at the supporting points of a beam and a cable



**Figure 2.43** Sag of a transversally loaded cable



**Figure 2.44** Midspan moment in straight and curved beams

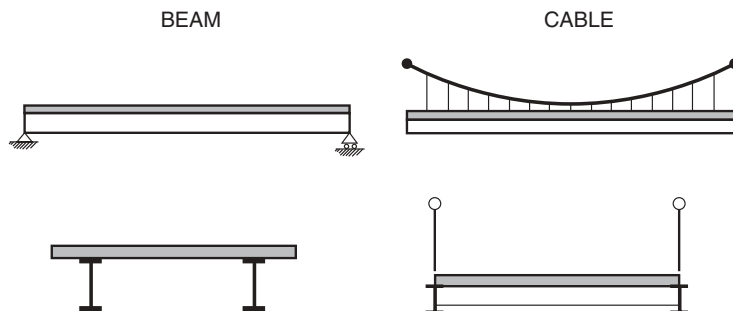


**Figure 2.45** Comparison between a beam (plate girder) and a cable both capable of carrying a uniform load of  $12 \text{ kN/m}$  over a span of  $30 \text{ m}$

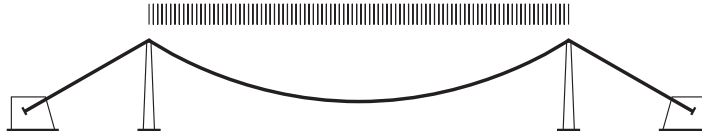
The main advantage of using a cable as a load-carrying element lies in the most efficient load transfer by pure tension. To illustrate this, Figure 2.45 shows a comparison between a beam and a cable both with a modest span of  $30 \text{ m}$  and subjected to an external load of  $27 \text{ kN/m}$ . The beam will have to be made with a depth of  $1 \text{ m}$  and its total weight will be  $8.2 \text{ tonnes}$  whereas a cable with a sag of  $3 \text{ m}$  can be made with a diameter of  $50 \text{ mm}$  and a weight of  $0.4 \text{ tonnes}$ . So under the given assumptions the weight of the cable will be only one-twentieth of the weight of a beam with the same load-carrying capacity. With this result the immediate reactions would be that cables should be preferred as structural elements in almost all cases. However, the simple comparison illustrated in Figure 2.45 does not give the full picture.

First of all, in real structures, and especially in bridges, the cable cannot be used to directly support the deck so a number of supplementary elements are needed. This is illustrated in Figure 2.46 where the floor in the beam bridge is directly supported by the main girders whereas a grid of cross beams and longitudinal girders as well as vertical hanger cables are needed to transfer the roadway loading to the main cables. So in a realistic comparison these secondary elements should of course be included, and this will – especially for smaller spans – change the picture completely.

Another disadvantage for the cable support is the fact that the supporting points will have to be positioned way up in the air whereas the beam can be supported directly under the roadway. Furthermore the large horizontal reactions required at the supporting points of the main cables will make it impossible to support them on vertical columns only – as is possible in



**Figure 2.46** Bridge floor supported directly by beams (main girders), or via transverse and longitudinal, secondary beams and hangers to parabolic main cables



**Figure 2.47** Vertically loaded cable supported by columns (pylons) and by backstays attached to anchor blocks

the beam case. It will be necessary to continue the main cables as backstays to anchor blocks positioned in some distance from the vertical columns under the main supporting points (the pylons), as indicated in Figure 2.47. So if the load only has to be carried across a single span, then the main cable will be substantially longer than the corresponding beam.

The extra length of main cable needed to reach the anchor blocks can be considerably reduced in case of a three-span structure as illustrated in Figure 2.48. Here the cable structure corresponds to the traditional three-span suspension bridge.

Summing up, a comparison between using beams or cables as main load-carrying elements will give the following result: With beams as the main load-carrying elements:

- large quantities of structural material required in the beams;
- direct support of the bridge floor;
- main supporting points positioned under the girders below the roadway;
- axially loaded vertical columns can be used below the supports as the vertical load results in vertical reactions only;
- foundations will be subjected primarily to vertical forces.

With cables as the main load-carrying elements:

- small quantities of structural material required in the cables;
- grid of secondary beams and vertical hanger cables required to transfer the roadway loading to the main cables;
- main supporting points of the main cables high above the bridge deck;
- high vertical columns (pylons) required to carry the load from the main cable supporting points to the ground;
- continuation of the main cables required outside the main supporting points;
- heavy foundations (anchor blocks) required to transfer the horizontal components of the cable forces to the soil.

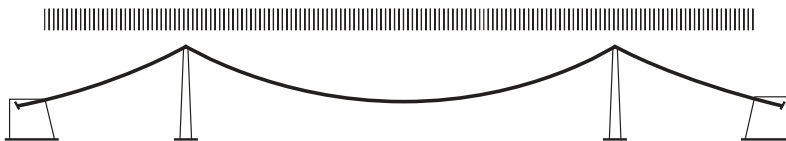
As will be seen from this comparison the only decisive advantage of using cables as the main load-carrying elements is related to the low consumption of structural material (cable steel) in the cables themselves. As this feature will be more and more dominating when spans are increased, it is to be expected that suspension bridges will dominate in the upper span range whereas beams in the form of plate and box girders are to be preferred in the lower span range.

In a comparison between a horizontal cable under vertical load and a beam, it is also interesting to consider the deformational characteristics.

One important difference between a cable and a beam is the response to a concentrated force (Figure 2.49). In the case of a cable a sharp bend will appear under the concentrated force, but in the beam only a continuous curvature will result (ignoring the insignificant deflections from shear in the beam).

In general, a transversally loaded cable will show a more pronounced change of geometry under non-uniform load than a beam. The reason for this is that the cable will have to take the form of the funicular curve corresponding to the applied load.

In the initial stage the cable curve will correspond to the funicular curve of the dead load which in general is uniform or at least quasi-uniform. Then when the live load is added, the cable will deflect partly due to the elastic strain in the



**Figure 2.48** Three-span cable supporting the deck in the main span and the flanking side spans

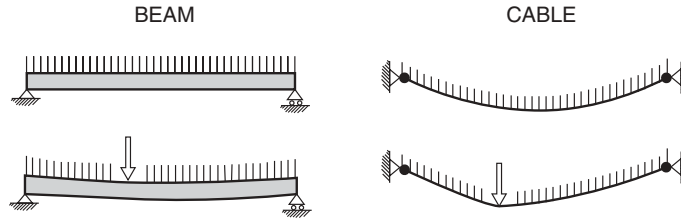


Figure 2.49 Deflection of a cable and a beam subjected to a concentrated force

cable material and partly due to the change of geometry. Which of these two contributions will dominate depends on the non-uniformity of the live load. To illustrate this effect the deflection of a horizontal cable with a length of 1000 m and a cross sectional area of  $0.56 \text{ m}^2$  subjected to a non-uniform, symmetrical live load will be shown.

In the initial stage the cable is assumed to be subjected to a uniform dead load of  $220 \text{ kN/m}$  and to have the form of a second order parabola with a sag of  $100 \text{ m}$ . The live load with an intensity of  $80 \text{ kN/m}$  is applied symmetrically in the mid-span region over a length of  $b$ , as indicated in Figure 2.50. For different values of the ratio  $b/a$  between the live loaded length  $b$  and the span of the cable  $l$  the midspan deflection is plotted in Figure 2.51. In the plot the total deflection is shown by a solid line and the deflection due to the cable displacement (change of geometry) by a dotted line. The dotted line can also be interpreted as the deflection of an inextensible cable with zero strain and therefore no elongation.

It appears from the plot in Figure 2.51 that the maximum deflection of  $3.12 \text{ m}$  will occur for a value of  $b/l = 0.4$ , corresponding to a case where the live load is acting over a length of only  $400 \text{ m}$  or  $40\%$  of the span. For live load acting over the entire span ( $b/l = 1.0$ ) the midspan deflection will be  $1.65 \text{ m}$  close to half of the maximum value.

From the plot it can be deduced that for  $b/l = 0.4$  the displacement of the cable accounts for approximately  $2/3$  of the total deflection and the elongation only for  $1/3$ . For  $b/l = 1.0$ , i.e. live load acting over the full span length, the deflection is entirely due to the elongation of the cable.

It is also interesting to note that for a live loaded length of only  $10\%$  of the span length ( $b/l = 0.1$ ), the midspan deflection will be the same as for live load acting over the entire span. This clearly illustrates the effect of the change of geometry (cable displacement) which accounts for almost the entire deflection in case of  $b/l = 0.1$ .

For a beam the maximum deflection will occur under maximum live load, i.e. live load over the entire span, and for a case with live load in only the central  $40\%$  of the span the deflection will be reduced to approximately  $70\%$  of the maximum value, as illustrated in Figure 2.52 where the deflections of the cable are also indicated. It is seen that, if experiences based on the behaviour of beams were transferred uncritically to the cable case, then it would be assumed that the maximum deflection had occurred under live load acting in the entire span and this would lead to an underestimation by a factor of close to  $0.5$  as the most critical non-uniform loading case will increase the midspan deflection of the cable to almost twice the value for uniform live load across the entire span.

The importance of considering non-uniform live load will be very clear if the midspan deflection  $\delta_y$  is plotted against the sag ratio  $k/2a$ , as shown in Figure 2.53. It appears that, if only uniform live load over the entire span ( $b/l = 1.0$ ) was considered (from a 'beam' experience), then it would be concluded that the sag should be chosen as large as possible to give the smallest deflection. However, when considering the non-uniform case with  $b/l = 0.4$  then the opposite conclusion will

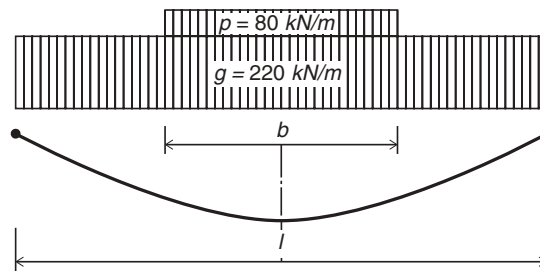
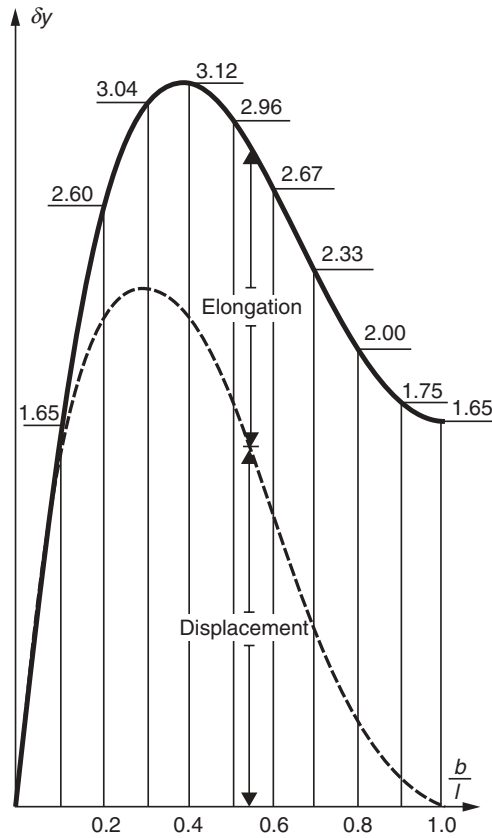


Figure 2.50 Cable subjected to uniform live load applied symmetrically in the central region of the main span



**Figure 2.51** Variation of the midspan deflection  $\delta_y$  with the live loaded length  $b$

be reached, and it will be seen that the deflection start to grow significantly when the sag ratio goes beyond 0.1–0.12. So this is one of the main reasons for choosing a sag ratio between 1/9 and 1/11 for the main span cable in a suspension bridge.

Before leaving the case of cables subjected to non-uniform symmetrical load it should be emphasized that the results plotted in Figures 2.51–2.53 are all based on the assumption that the supporting points of the cable are completely fixed both vertically and longitudinally. In real structures the supporting points will often have some flexibility in the longitudinal direction (e.g. in the suspension bridge case due to elongation and displacement of the side span cables) and this will to some extent influence the results. Thus, a longitudinal flexibility of the end supports will tend to increase the length to be loaded by live load beyond  $0.4 l$  to give maximum midspan deflection.

A load case with asymmetrical live load on half of the span can be used to illustrate the stabilizing effect of dead load in the cable case. Thus, in Figure 2.54 is shown how doubling the dead load will reduce the maximum deflection of a cable to 55% whereas there will be no reduction from increased dead load in the case of a beam. This is all based on the assumption that the cross sections of the load-carrying elements (area of the cable, moment of inertia of the beam) are kept constant irrespective of the dead load intensity.

The explanation of the fact that increased dead load results in a reduction of the live load deflections of a cable is that the deviation between the funicular curves for dead load alone and for dead plus live load will be smaller as the dead load increase.

In Figure 2.55 is shown the deflection curves of a cable with a traffic load of 80 kN/m in one half span and dead load of 110 kN/m, 220 kN/m and 440 kN/m, respectively over the entire span.



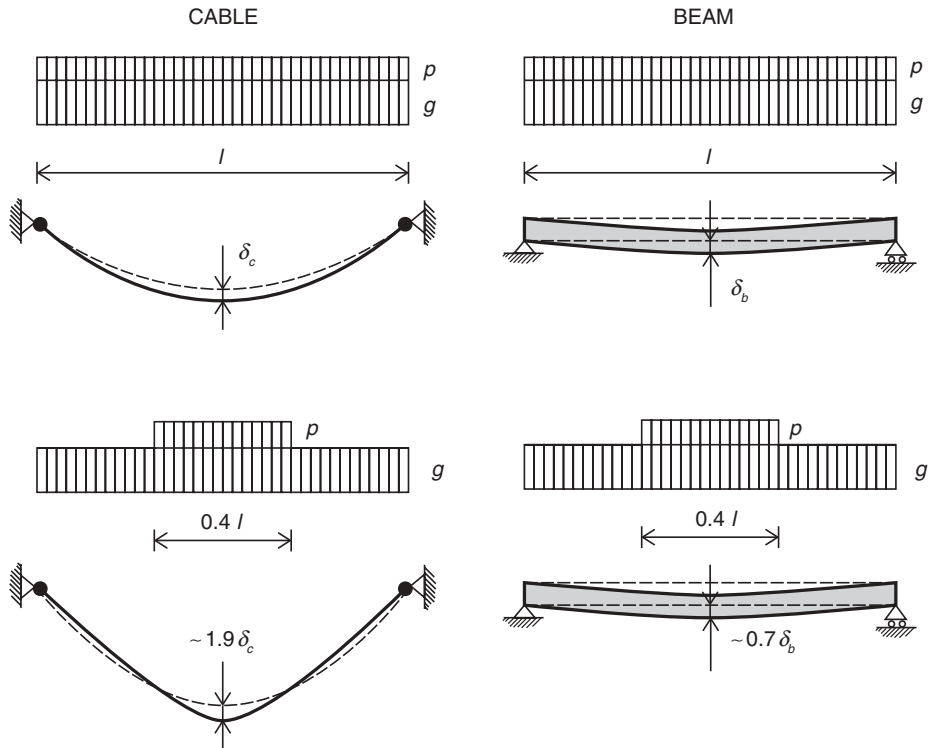


Figure 2.52 Comparison between deflections of a beam and a cable with total and partial live load

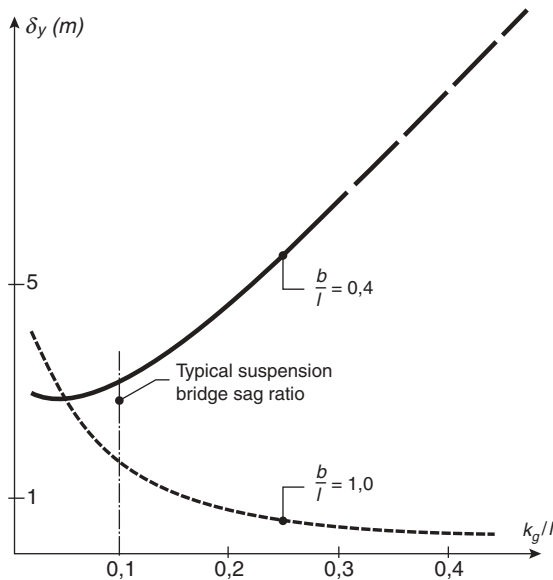


Figure 2.53 Relation between the sag ratio  $k_g/l$  and the midspan deflection  $\delta_y$  of a symmetrically loaded, horizontal cable with uniform live load over the entire span length ( $b/l = 1.0$ ) and over the central 40% of the span length ( $b/l = 0.4$ ). The cable area is adjusted to the different sag ratios

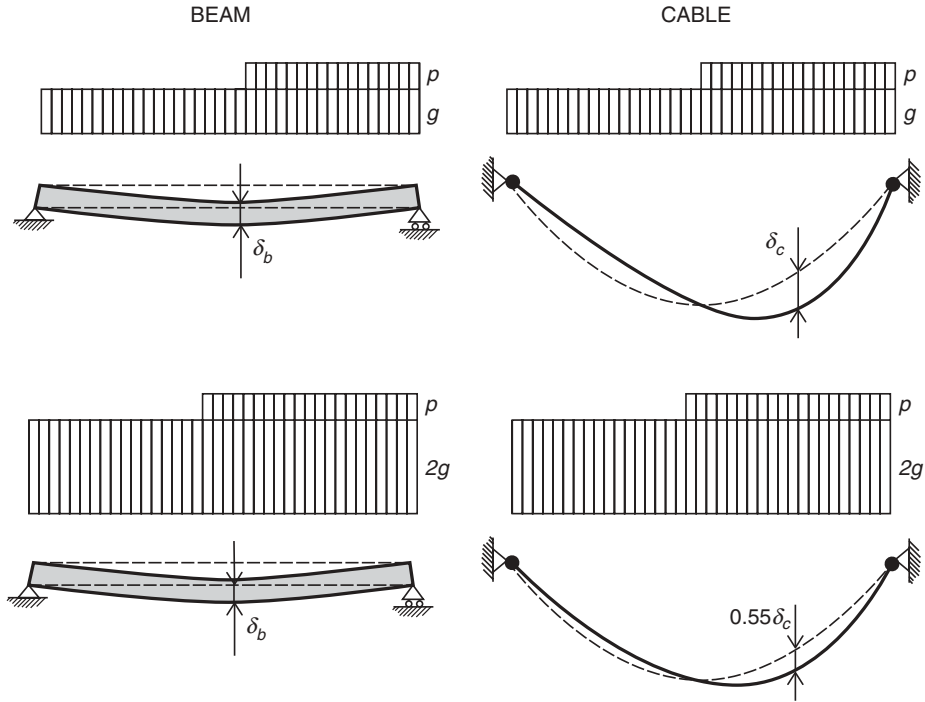


Figure 2.54 Stabilizing effect of the dead load for an asymmetrically loaded cable

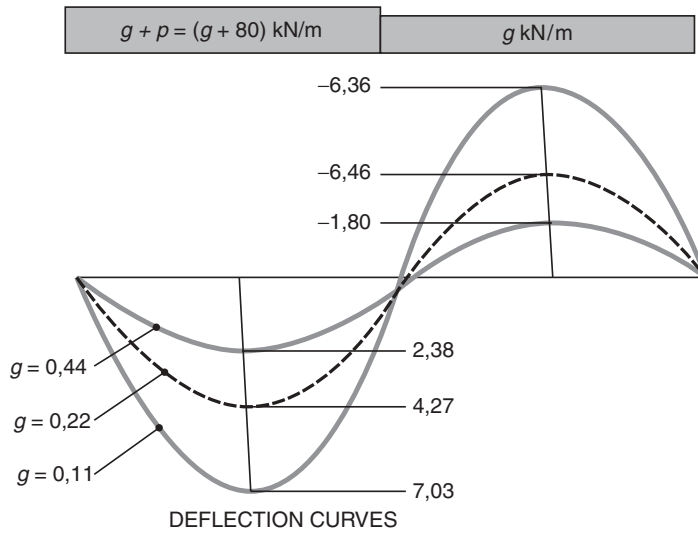
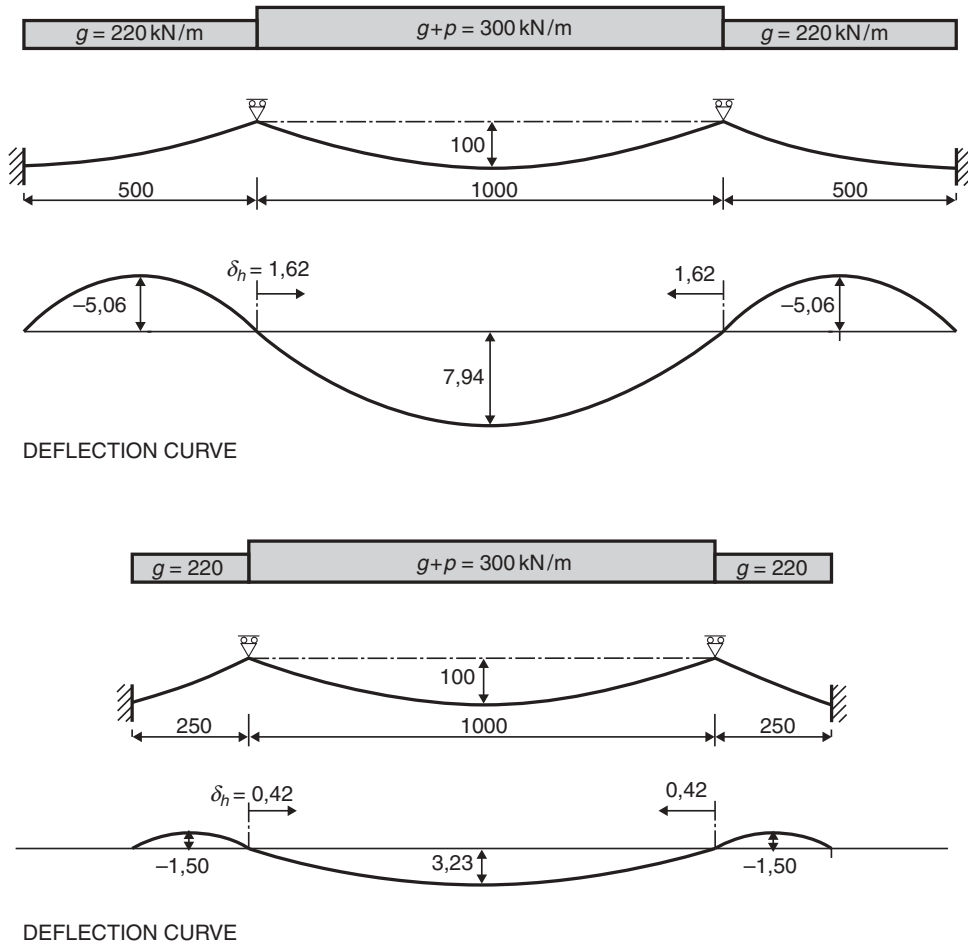


Figure 2.55 Deflection curves for an asymmetrical loaded cable with different dead load intensity



**Figure 2.56** Deflection curves for two three-span cables with different side span lengths

For the design of suspension bridges it is important to carefully consider the consequences of reduced dead load on the deformational characteristics of the cable system. In fact with the modern lightweight steel box girders the deflections will be larger than for the old suspension bridges with heavy steel trusses and concrete floors.

In the basic comparisons between beam and cable behaviour presented above, only the single span case was considered. However, suspension bridges are most commonly constructed as three-span structures with a long main span and relatively short side spans. It can therefore be argued that it would be more relevant to study the behaviour of a three-span cable than a single-span cable.

An important observation in the case of a three-span cable is the pronounced influence of the side span length on the deflections of the main span, as illustrated in Figure 2.56 where the deflections of two three-span cables with spans of either 500 m, 1000 m and 500 m, or 250 m, 1000 m and 250 m are compared. In both cases the deflection curves are drawn for a live load of 80 kN/m acting in the main span only, but combined with a dead load of 220 kN/m acting over the entire length.

It is seen that the midspan deflection in the main span will be reduced to almost 40% if the side span length is reduced from 500 m to 250 m. In the case of a continuous beam with a constant moment of inertia, the midspan deflection under live load in the main span would be reduced to only 79% if the side span length was changed from half to one quarter of the main span length.

So again it is seen how the chosen geometry has a much stronger influence on the deformational characteristics of a cable than of a beam.

The explanation of the pronounced influence of the side span length on the main span deflection is to be found when looking at the longitudinal displacements of the supporting points between side and main spans (the pylon tops). From Figure 2.56 it is seen that the longitudinal displacement is reduced from 1.62 m to 0.42 m when changing from long to short side spans. So the variation in longitudinal displacement is about twice as large as would be expected if it was only governed by the elastic strain of the side span cable.

To further illustrate the deformational characteristics of the side span cable, Figure 2.57 shows the relation between the relative side span length  $\alpha$  and the longitudinal displacement of the upper support (the pylon top) for a change of the horizontal force from 275 MN to 375 MN. The plot is based on a cable area that will lead to a stress of 720 MPa in the side span cable under maximum tension.

It is seen that for shorter side span lengths ( $\alpha < 0.5$ ) the longitudinal displacement is not too far from being proportional to the length, but for longer side span lengths there is a clear progression of the longitudinal displacement. This is due to the effect of sag reduction appearing when the cable tension is increased.

In relation to Figure 2.55 it was described how an increased dead load would improve the deformational characteristics of the single span cable. However, in the case of a side span cable the dead load will have the opposite effect as illustrated in Figure 2.58 for a side span cable with a span of 250 m. A doubling of the dead load from 220 kN/m to 440 kN/m will more than double the longitudinal displacement, which again is due to the sag variations as the initial sag will be larger when the side span dead load is increased.

Throughout the comparisons made above between a cable and a beam it has been assumed that the cable acts as a perfectly flexible string which is a good approximation for the cable itself but less evident for a suspension system where the cable interacts with the deck. However, for modern suspension bridges with slender decks the global deflections are only to a small extent influenced by the flexural stiffness of the deck.

This feature is illustrated in Figure 2.59 showing the deflections of three different systems: (1) the cable alone; (2) a suspension bridge with a deck composed of three simply supported spans; and (3) a suspension bridge with a continuous deck, all having the same cable dimensions and subjected to dead and traffic load of the same intensity.

For the suspension bridge systems the moment of inertia of the deck is chosen to be a typical value as found for a 3 m-deep box girder section.

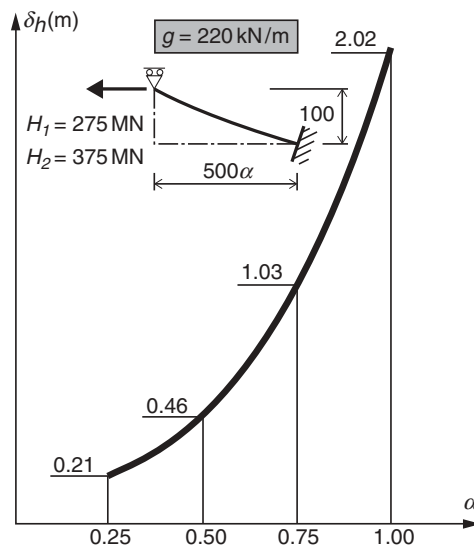
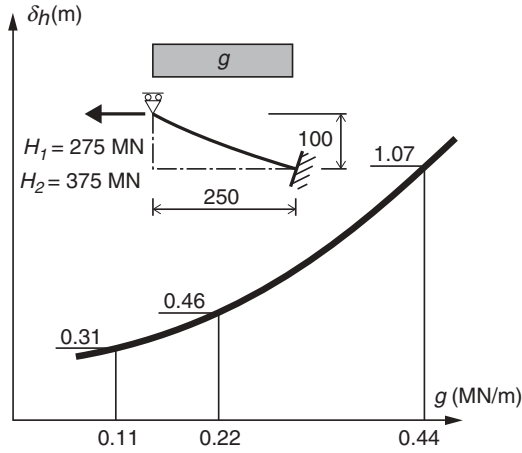
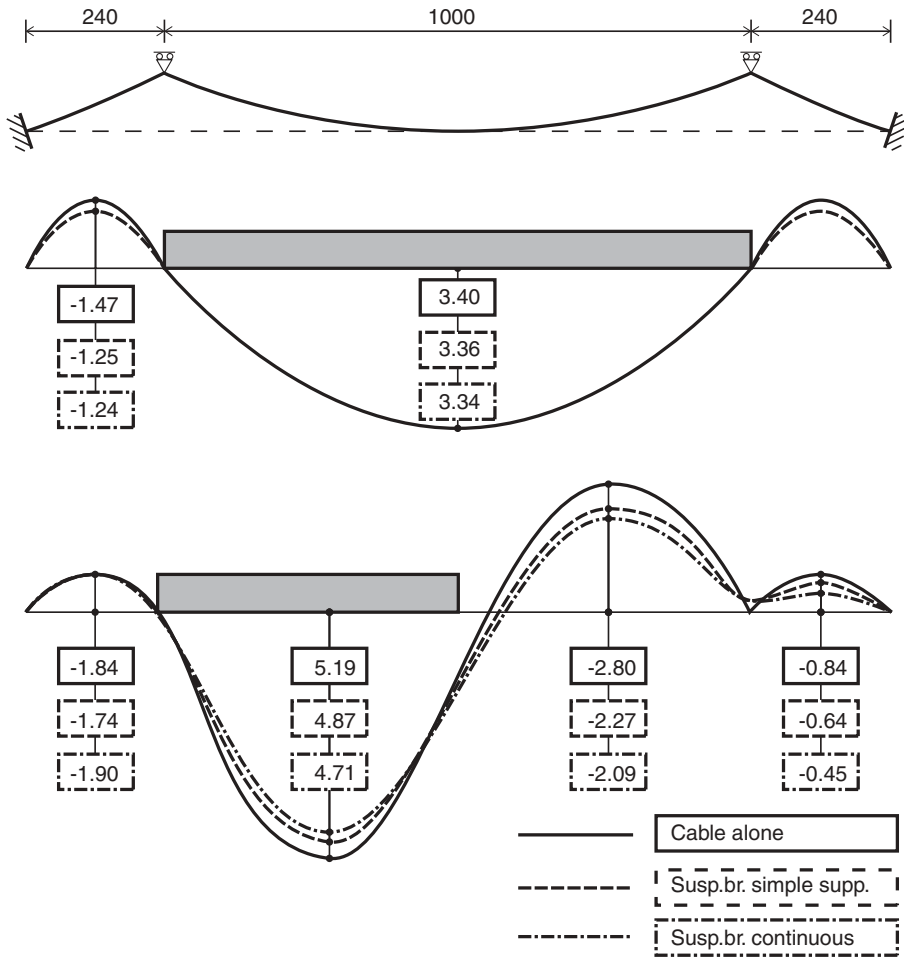


Figure 2.57 Relation between the horizontal distance  $500\alpha$  and the displacement  $\delta_h$  of the pylon top



**Figure 2.58** Relation between the dead load intensity and the displacement  $\delta_h$  of the pylon top



**Figure 2.59** Comparison between deflections of a cable, a suspension bridge with a simply supported deck and a suspension bridge with a continuous deck

It is seen that for traffic load in the entire main span the difference between the deflections of the three systems is insignificant as regards the main span whereas the uplift of the side spans is smaller for the suspension bridges as the bending stiffness of the deck is more pronounced for the shorter spans.

For asymmetrical traffic load the deflections of the three systems deviate to a larger degree, but the overall shape of the deflection curves are still astonishingly alike, taking into account the pronounced differences between the structural systems.

### 2.4.2 Axially loaded cable

For the cable under transverse load it was described how the sag was indispensable for the load-carrying performance as the cable force was practically inversely proportional to the sag. So a small sag will result in large forces and uneconomic cable dimensions.

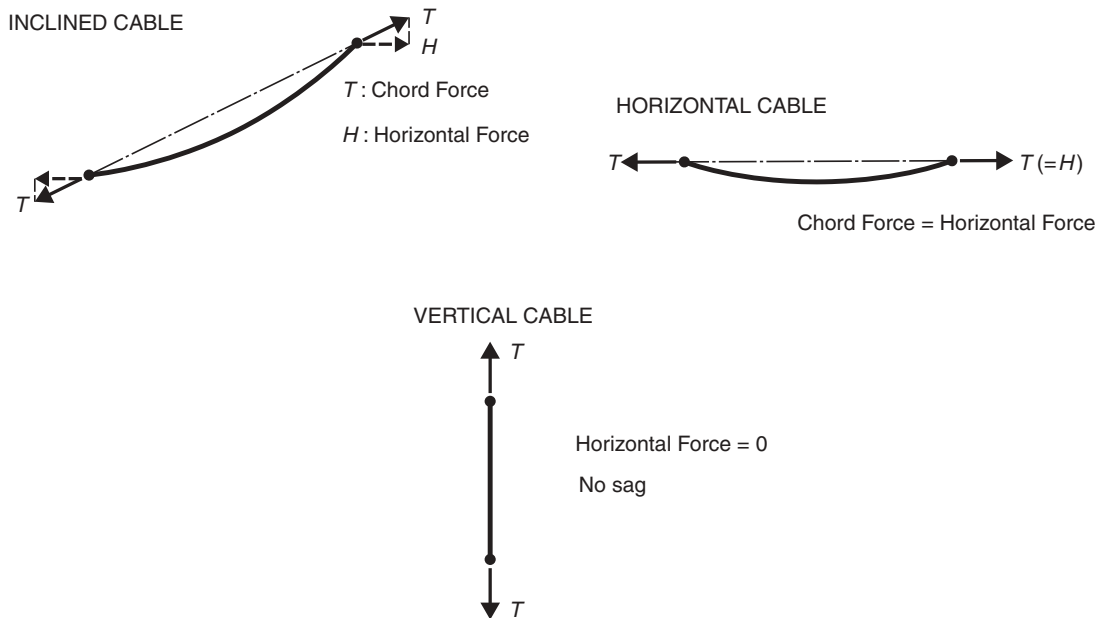
For the cable under axial load a sag is not required to carry the load and is, therefore, basically undesirable. However, the only case where an axially loaded cable will be without a sag is when the cable is vertical (Figure 2.60). As soon as the cable is inclined (or horizontal) the weight of the cable will create a sag.

In the following only the case of an inclined or horizontal cable will be treated, so when the characteristics of a ‘cable’ are described, then it is to be understood that these characteristics do not necessarily apply to a vertical cable.

Due to the relatively modest intensity of the cable’s weight the sag of an axially loaded cable will be difficult to detect when the cable is viewed in elevation from some distance. Therefore, cables in cable stayed bridges appear to be straight from most viewing positions. Only if the stay cable is viewed along its chord will the sag be clearly visible (Figure 2.61).

As described earlier, the sag of a transversally loaded cable, such as the suspension bridge main cable, will typically have a sag ratio around 0.1 – a value chosen as a compromise between material minimization (that could favour a larger sag) and stiffness optimization (that could favour a smaller sag).

In axially loaded cables the sag is created by the weight of the cable so the sag will be proportional to the density of the cable material and inversely proportional to the strength. To keep the undesired sag small it is therefore important to use materials with large strength-to-density ratios.



**Figure 2.60** Inclined, horizontal and vertical cable subjected to a chord force  $T$  and the weight of the cable



**Figure 2.61** Visible sag of a stay cable in the Stonecutters Bridge

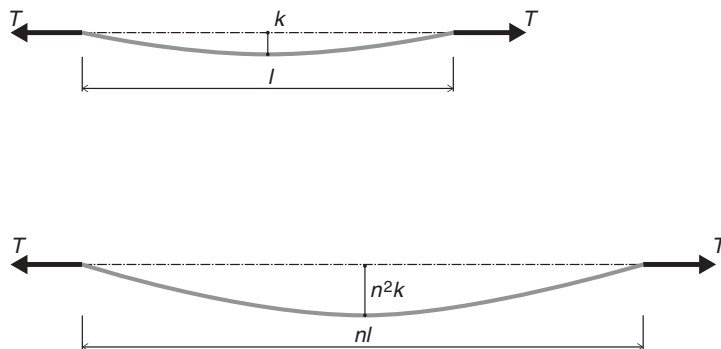
For a stay cable of high strength wires the sag ratio will typically be in the order of 0.01 or about one-tenth of what is found in suspension bridge main cables, and this is the reason why the sag of a suspension bridge main cable is easy to detect from any viewing position whereas the sag of a stay cable will remain unnoticed by most spectators.

For a stay cable with a given cross section and a given axial force the sag will be proportional to the square of the length as illustrated in Figure 2.62. The sag ratio  $k/l$  will then be proportional to the length of the stay cable and all effects related to the sag ratio will consequently become more dominant as the free length is increased.

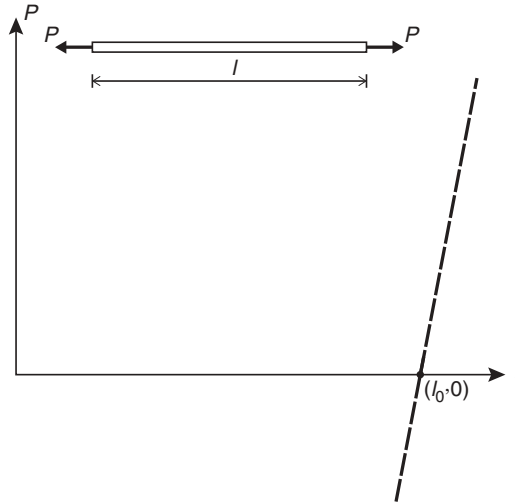
In the case of the transversally loaded cable a number of comparisons were made to a beam to show the differences in behaviour. For an axially loaded cable it will similarly be relevant to make a comparison with a straight bar.

For the straight bar the force/deflection curve will be as shown in Figure 2.63. For zero force the bar will have its stress-free length  $l_0$  and for an axial tensile force it will elongate whereas it will shorten for an axial compressive force.

For the corresponding cable, i.e. a cable with the same cross sectional area and the same modulus of elasticity, the force/deflection curve will be quite different as illustrated in Figure 2.64. For zero force the distance between the end supports of the cable will be zero as the cable will be hanging absolutely slack along two (coinciding) vertical lines. Then, when the cable is subjected to tension it will, for even a small force, start to stretch out and take the form of a catenary. For larger tensile forces the force/deflection curve will start to become steeper and eventually it will go asymptotic towards the corresponding curve for the straight bar under tension (the force/deflection curve from Figure 2.63 is shown with a dotted line in Figure 2.64).



**Figure 2.62** Variation of sag with the length of an axially loaded cable

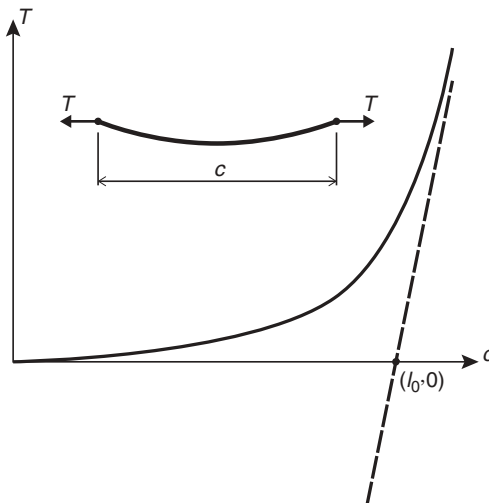


**Figure 2.63** Force/deflection curve for a straight bar

From the force/deflection curve for the cable it can be seen that for any distance between the supporting points the cable will still be in tension, and consequently the cable will not be unloaded even if it is shortened to a length that would induce a considerable compression in the corresponding straight bar.

From the plot in Figure 2.64 it is seen that the force/deflection curve of the cable is very flat in the lower range where the cable force is close to zero. Consequently, in this range the cable will be very flexible and show large elongations even for small force increments. This feature is further illustrated by the example in Figure 2.65 where a horizontal cable with a stress-free length of 100 m is considered.

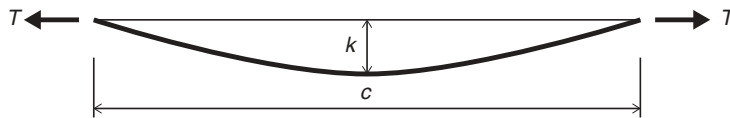
From the table in Figure 2.65, it is seen that already for a force of one-thousandth of the breaking strength (the ultimate strength) the distance between the supporting points will be 66.4 m or approximately  $2/3$  of the stress-free length. However, for such a small force the cable will still be characterized by a substantial sag of 33.5 m.



**Figure 2.64** Force/deflection curve for a horizontal cable



EXAMPLE:  
HORIZONTAL CABLE WITH STRESS-FREE LENGTH 100 m.



| $T/T_{ult}$ | $c$ (m)  | $k$ (m) |
|-------------|----------|---------|
| 0.001       | 66.44    | 33.53   |
| 0.01        | 99.03    | 14.33   |
| 0.05        | 100.00   | 2.86    |
| 0.1         | 100.07   | 1.45    |
| 0.5         | 100.38   | 0.29    |
| 1.0         | (100.76) | (0.15)  |

**Figure 2.65** Sag and chord length of a horizontal cable with a stress-free length of 100 m and a varying chord force

For a force of one-hundredth of the ultimate strength the cable will already have stretched out to a length of 99 m between end supports, but the sag will still be substantial, i.e. 14.3 m which is more than the normal sag ratio of 0.1 for suspension bridge main cables.

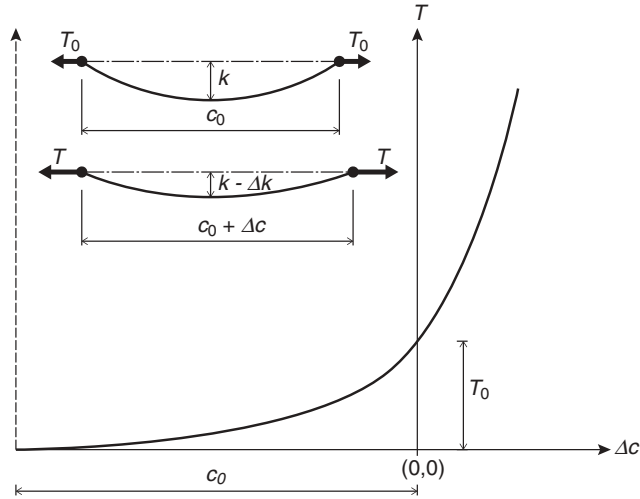
A force corresponding to 5% of the ultimate strength will, under the given assumptions, stretch the cable so much that the distance between end supports will be the same as the stress-free length of 100 m. So in this condition the strain in the cable material will give rise to a total elongation that is exactly the same as the difference between the curve length of the sagging cable and the stress-free length (= the chord length).

For a force of half the ultimate strength the distance between supporting points will be 100.4 m, i.e. a further elongation of only 0.4 m. In real structures the value for  $T/T_{ult} = 0.5$  is quite realistic as the safety factor on material strength typically is chosen to a value around 2.

The extreme flexibility of the cable in the lower force range is clearly illustrated by the values in the table. Thus, an increase of the relative cable force  $T/T_{ult}$  from 0.001 to 0.01 corresponding to a tenfold increase will change the distance between supporting points by 32.6 m, whereas a further tenfold increase from 0.01 to 0.1 changes the distance by only 0.11 m. For a straight bar the elongation for a force increment of  $0.09T_{ult}$  (from  $0.01T_{ult}$  to  $0.1T_{ult}$ ) would be ten times larger than for a force increment of  $0.009T_{ult}$  (from  $0.001T_{ult}$  to  $0.01T_{ult}$ ).

It has already been mentioned that a cable never can get 'unloaded' but will remain in tension for any distance between the end supports, and even for a cable with a chord length corresponding to the stress-free length the cable tension will by no means be insignificant. Thus, for a cable with an initial force of  $0.3T_{ult}$  in the dead load condition the force for a chord length equal to the stress-free length will still be one-sixth of the initial force ( $0.05T_{ult}$ ), whereas a straight bar would be completely unloaded to zero force.

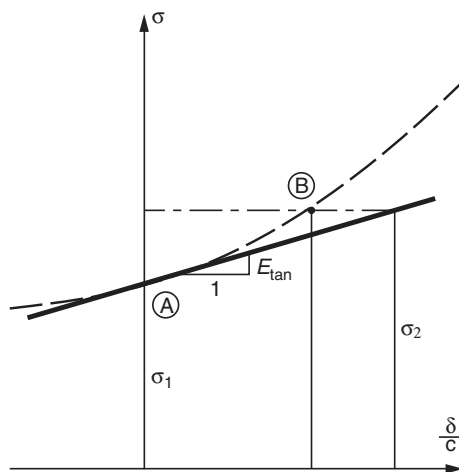
The load/deflection curves shown in Figures 2.63 and 2.64 are plotted with the origin at zero length between end supports. However, in structural applications it is not advantageous to link the force to the total length but rather to the elongation from a given initial condition. In straight members under axial force the elongation is commonly measured from the stress-free length so that a linear relationship will exist in elastic materials  $P = EA(\Delta/l)$ , or if the stress  $\sigma = P/A$  and the strain  $\varepsilon = \Delta/l$  are inserted then  $\sigma = E\varepsilon$ , where  $E$  is the modulus of elasticity of the actual material.



**Figure 2.66** Force/deflection curve for a cable with origin at the dead load condition

For cables it will be most convenient to measure elongations from the initial dead load condition as it is illustrated in the force/deflection diagram of Figure 2.66. Here  $T_0$  is the cable force in the dead load condition and  $c_0$  the corresponding chord length of the cable. For a cable force  $T > T_0$  the chord length will increase by  $\Delta c$  and at same time the sag  $k$  of the cable will decrease by  $\Delta k$ . This change of the sag is actually the cause of the curved force deflection diagram of the cable.

The non-linear behaviour of the sagging cable will, to some extent, complicate the structural calculations, especially if the available frame analysis programs are based on an elastic behaviour of each member. In such cases it will therefore be advantageous to linearize the force/elongation relation of the cable. A simple linearization can be made by substituting the curve by the tangent at the point that corresponds to the initial dead load condition, as illustrated in Figure 2.67. With this linearization the cable is replaced by a straight bar with a modulus of elasticity  $E_{tan}$  corresponding to the tangent slope in a stress/(relative elongation) diagram.



**Figure 2.67** Definition of the tangent modulus for cable stiffness

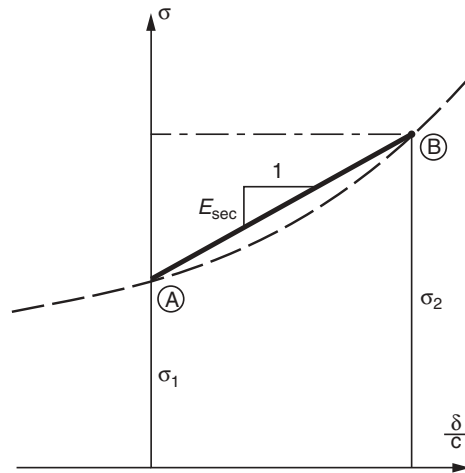


Figure 2.68 Definition of the secant modulus for cable stiffness

The tangent modulus will generally give sufficiently accurate results when the live-to-dead load ratio is small so that the cable stresses will only vary modestly from the dead load stress. However, for larger stress variations the tangent approach will overestimate the flexibility of cables with increased tension and underestimate the flexibility of cables with reduced tension.

In cases where the linearization based on a tangent modulus will lead to unacceptable deviations from the real behaviour a secant modulus can be introduced.

With the secant modulus approach the curve leading from point A (corresponding to the initial dead load stress  $\sigma_1$ ) to point B (corresponding to the dead plus live load stress  $\sigma_2$ ) is replaced by the straight line (the secant) between these two points, as illustrated in Figure 2.68. With this approach the cable elongation will be the correct one so no errors will be introduced in the calculation of the structure as a whole. However, to base the calculations on the secant modulus will be more complicated than to use the tangent modulus.

The tangent modulus will depend only on the well-known dead load condition whereas the secant modulus requires that both the stress in the initial condition (dead load only) and in the final condition (dead plus live load) is known. However, the stress from dead plus live load will not be known until after the analysis has been performed, and to perform this analysis the moduli of elasticity of the individual cables must be known.

To solve this dilemma it will be necessary to iterate and, strictly speaking, this iteration will have to be made individually for all stay cables and for all loading conditions. It will, however, be sufficient in many cases for the regular stay cables to calculate the secant modulus corresponding to the maximum cable force and then to use this value also for other loading cases although they produce somewhat smaller cable forces.

For the anchor cable it is generally seen that some loading cases will increase the initial cable force and others decrease it. Consequently, it will be advisable to determine two different secant moduli: one to be used when the anchor cable force will be increased and another when it will be decreased.

It should finally be mentioned that in many of the modern frame analysis computer programs, cable elements can be specified. So when such programs are used the iterations leading to the correct axial cable stiffness are performed as an integral part of the computer calculations.

## 2.5 Static Analysis of Cables

When analyzing the main structural system it will generally be sufficient to assume that the cables act as completely flexible strings able to resist forces only. Under this assumption the cable curve will coincide with the funicular curve of the load applied to the cable.

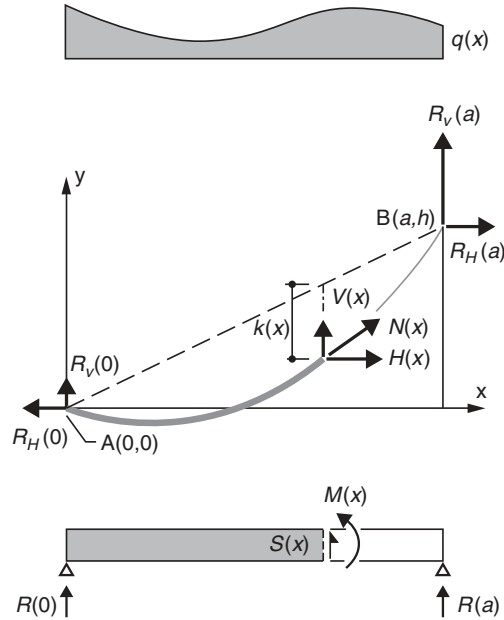


Figure 2.69 Forces and reactions acting on a cable and a simply supported beam with equal load and span

### 2.5.1 Equation of state for a cable subjected to vertical load

Simple expressions for the forces in a cable supported at two points A and B can be found by using as reference the reactions, moments, and shear forces of a simply supported beam with the same span and load [37.1]. With a notation as indicated in Figure 2.69 the following expressions can be derived by applying the general equilibrium conditions:

$$\begin{aligned} R_H(0) &= R_H(a) = H(x) = H(\text{constant}) \\ R_V(0) &= R(0) - H(h/a) \\ R_V(a) &= R(a) + H(h/a) \\ V(x) &= S(x) + H(h/a) \end{aligned}$$

$$N(x) = \sqrt{H(x)^2 + V(x)^2} = H \sqrt{\left(\frac{S(x)}{H} + \frac{h}{a}\right)^2 + 1} \quad (2.3)$$

The cable curve A-B is determined by the equation:

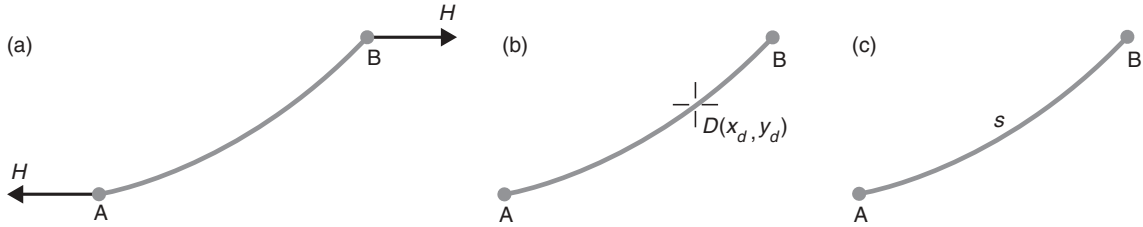
$$y = -M(x)/h + h/a \quad (2.4)$$

As  $y = (h/a)x$  represents the straight line A-B, the sag  $k = k(x)$  of the cable curve is affine with the bending moment curve  $M(x)$  of the simply supported beam with  $(-1/H)$  as the factor of affinity:

$$k(x) = M(x)/H \quad (2.5)$$

It appears that the sag  $k(x)$  is inversely proportional to the horizontal force  $H$  and proportional to the moment  $M(x)$  (which in turn is proportional to the load intensity).

For a cable with a specified load and given positions of the supporting points the cable curve will be determined by the magnitude of the horizontal force  $H$ . However, in some cases the cable curve will be determined by other conditions such as a specified position of point D on the cable or a specified curve length  $s$ . Thus, the commonly found conditions leading to the



**Figure 2.70** Cable configuration specified by: (a) size of horizontal force; (b) position of point  $D$  on cable; (c) length  $s$  of cable specific cable curve are shown in Figure 2.70. In case (a) the cable curve is directly determined by (2.4). In case (b) the horizontal force  $H$  is found by inserting the coordinates  $(x_d, y_d)$  of the specified point  $D$  into (2.4):

$$H = \frac{M(x_d)}{(hx_d/a) - y_d}$$

$$y = \left( y_d - \frac{h}{a}x_d \right) \frac{M(x)}{M(x_d)} + \frac{h}{a} \tag{2.6}$$

Case (c), a specified curve length  $s$ , is the most troublesome to handle since the corresponding horizontal force  $H$  cannot be found explicitly in most cases. The curve length  $s$  is determined by:

$$s = \int_0^a \sqrt{1 + \left( \frac{dy}{dx} \right)^2} dx = \int_0^a \sqrt{1 + \left( \frac{h}{a} - \frac{1}{H} \frac{dM}{dx} \right)^2} dx \tag{2.7}$$

which shows that, for a given position of the cable supports  $(a, h)$  and the load  $(\rightarrow M)$ ,  $s = s(H)$  is a function of  $H$ . To solve the problem, the inverse function  $H = H(s)$  must be found.

Generally, the cable must be studied under different load conditions, each characterized by a different elongation  $\Delta s$  of the cable from the unstressed condition.

The elastic strain  $\varepsilon(x)$  at the cable point  $(x, y)$  is given by:

$$\varepsilon(x) = \frac{N(x)}{EA} = \frac{H}{EA} \sqrt{1 + \left( \frac{dy}{dx} \right)^2}$$

so the total elongation  $\Delta s$  becomes:

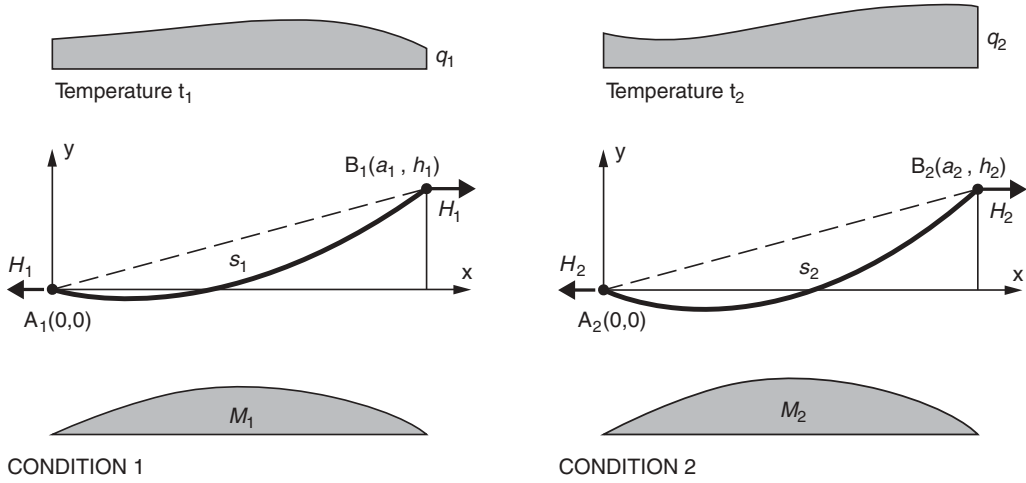
$$\Delta s = \int_0^a \varepsilon(x) \frac{\partial s}{\partial x} dx = \frac{H}{EA} \int_0^a \left[ 1 + \left( \frac{dy}{dx} \right)^2 \right] dx \tag{2.8}$$

As each load condition leads to a specific cable curve, the transition from one load condition to another implies a change of the cable geometry.

Within cable supported bridges the three main causes for change of the cable geometry are:

- (a) change in load intensity or position;
- (b) change in position of supporting points;
- (c) change in temperature.

To set up an equation of state for the cable, two conditions are investigated, as shown in Figure 2.71. In Condition 1 the cable is supported at points  $A_1(0, 0)$  and  $B_1(a_1, h_1)$ , subjected to the load  $q_1$  with the corresponding moment curve  $M_1$ , and exposed to temperature  $t_1$ . In Condition 2 the supporting points are  $A_2(0, 0)$  and  $B_2(a_2, h_2)$ , the load  $q_2$  with the corresponding moment curve  $M_2$ , and temperature  $t_2$ .



**Figure 2.71** Two conditions of a cable subjected to vertical load

For Condition 1 the curve length  $s_1$  is found from (2.7):

$$s_1 = \int_0^{a_1} \sqrt{1 + \left(\frac{dy_1}{dx}\right)^2} dx = \int_0^{a_1} \sqrt{1 + \left(\frac{h_1}{a_1} - \frac{1}{H_1} \frac{dM_1}{dx}\right)^2} dx \quad (2.9)$$

and the total elongation from a stress-free condition at temperature  $t_0$  by:

$$\Delta s_1 = \frac{H_1}{EA} \int_0^{a_1} \left[ 1 + \left(\frac{dy_1}{dx}\right)^2 \right] dx + \beta(t_1 - t_0)s_0 \quad (2.10)$$

where the first term is found from (2.8), and the second expresses the elongation due to a temperature difference  $t_1 - t_0$  ( $t_0$  is an arbitrarily chosen reference temperature).  $s_0$  is the length of the unstressed cable (at temperature  $t_0$ ), and  $\beta$  the coefficient of thermal expansion.

For Condition 2 the corresponding equations are

$$s_2 = \int_0^{a_2} \sqrt{1 + \left(\frac{dy_2}{dx}\right)^2} dx \quad (2.11)$$

$$\Delta s_2 = \frac{H_2}{EA} \int_0^{a_2} \left[ 1 + \left(\frac{dy_2}{dx}\right)^2 \right] dx + \beta(t_2 - t_0)s_0 \quad (2.12)$$

As compatibility requires  $s_2 - s_1 = \Delta s_2 - \Delta s_1$ , the following equation is derived:

$$\int_0^{a_2} \sqrt{1 + \left(\frac{dy_2}{dx}\right)^2} dx - \int_0^{a_1} \sqrt{1 + \left(\frac{dy_1}{dx}\right)^2} dx = \frac{H_2}{EA} \int_0^{a_2} \left[ 1 + \left(\frac{dy_2}{dx}\right)^2 \right] dx - \frac{H_1}{EA} \int_0^{a_1} \left[ 1 + \left(\frac{dy_1}{dx}\right)^2 \right] dx + \beta(t_2 - t_1)s \quad (2.13)$$

With  $b(t_2 - t_1) s_0 \sim bt_2 s_2 - bt_1 s_1 s_0$ , (2.13) can be written:

$$(1 - \beta t_2) \int_0^{a_2} \sqrt{1 + \left(\frac{dy_2}{dx}\right)^2} dx - \frac{H_2}{EA} \int_0^{a_2} \left[1 + \left(\frac{dy_2}{dx}\right)^2\right] dx = (1 - \beta t_1) \int_0^{a_1} \sqrt{1 + \left(\frac{dy_1}{dx}\right)^2} dx - \frac{H_1}{EA} \int_0^{a_1} \left[1 + \left(\frac{dy_1}{dx}\right)^2\right] dx \quad (2.14)$$

or in brief:

$$(1 - \beta t_2) s_2 - \Delta s_2 = (1 - \beta t_1) s_1 - \Delta s_1 \quad (2.15)$$

For cables with a maximum inclination of approximately 0.8 (maximum  $dy/dx < 0.8$ ), the following approximation might be applied to simplify (2.14):

$$\int_0^{a_1} \sqrt{1 + \left(\frac{dy_1}{dx}\right)^2} dx \simeq \int_0^{a_1} \left[1 + \frac{1}{2} \left(\frac{dy_1}{dx}\right)^2\right] dx = a_1 + \frac{1}{2} \int_0^{a_1} \left(\frac{dy_1}{dx}\right)^2 dx \quad (2.16)$$

With this approximation (2.14) becomes:

$$\left(1 - \beta t_2 - \frac{H_2}{EA}\right) a_2 + \left(\frac{1}{2} - \frac{1}{2} \beta t_2 - \frac{H_2}{EA}\right) \int_0^{a_2} \left(\frac{dy_2}{dx}\right)^2 dx = \left(1 - \beta t_1 - \frac{H_1}{EA}\right) a_1 + \left(\frac{1}{2} - \frac{1}{2} \beta t_2 - \frac{H_1}{EA}\right) \int_0^{a_1} \left(\frac{dy_1}{dx}\right)^2 dx \quad (2.17)$$

If all parameters of condition 1, i.e.  $a_1, h_1, q_1 (\rightarrow M_1), H_1$  and  $t_1$  as well as those of condition 2, i.e.  $a_2, h_2, q_2 (\rightarrow M_2)$ , and  $t_2$ , are known, then (2.14) or (2.17) can be used to determine  $H_2$  and thereby the cable geometry of condition 2.

### 2.5.2 Stay cable under varying chord force

In cable stayed bridges where the cables are subjected to axial tension the most relevant deformational characteristic is the relationship between the chord force  $T$  and the chord length  $c$  (Figure 2.72).

With the cable dead load distributed uniformly along the curve, the correct cable curve is a catenary, but – as shall be shown later – a parabolic approximation might be used in most cases without introducing an unacceptable error [70.2].

The investigation of the catenary configuration versus the parabola configuration shall be made initially by considering a horizontal stay cable as shown in Figure 2.73. Here two conditions, characterized by the chord forces  $T_1$  and  $T_2$ , are considered.

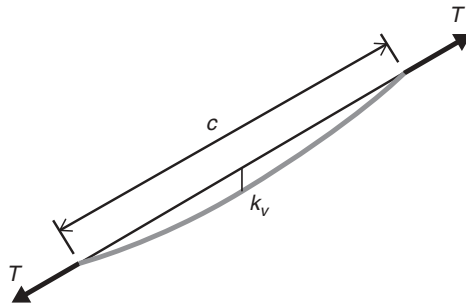
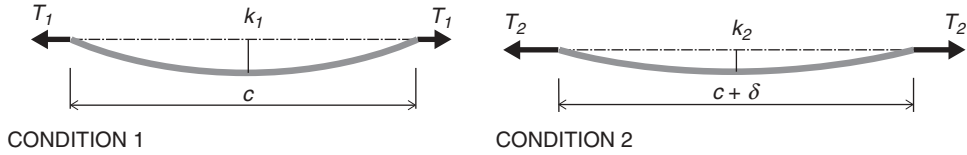


Figure 2.72 Chord force  $T$  and chord length  $c$  of stay cable



**Figure 2.73** Two conditions for horizontal stay cable with chord forces  $T_1$  and  $T_2$ , respectively

In Condition 1 the equation of the catenary is given by:

$$y = \frac{T_1}{g_{cb}} \left[ \cosh \left( \frac{g_{cb}}{T_1} \left( x - \frac{1}{2}c \right) \right) - \cosh \left( \frac{g_{cb}c}{2T_1} \right) \right] \quad (2.18)$$

and in Condition 2:

$$y = \frac{T_2}{g_{cb}} \left\{ \cosh \left[ \frac{g_{cb}}{T_2} \left( x - \frac{c + \delta}{2} \right) \right] - \cosh \left( \frac{g_{cb}(c + \delta)}{2T_2} \right) \right\} \quad (2.19)$$

where  $g_{cb}$  is the cable dead load per unit length and  $\delta$  the cable elongation, defined as the increase of the distance between the supporting points.

The cable lengths  $s_1$  and  $s_2$  are determined by

$$s_1 = \int_0^c \sqrt{1 + \left( \frac{dy}{dx} \right)^2} dx = 2 \frac{T_1}{g_{cb}} \sinh \left( \frac{g_{cb}c}{2T_1} \right) \quad (2.20)$$

$$s_2 = 2 \frac{T_2}{g_{cb}} \sinh \left( \frac{g_{cb}(c + \delta)}{2T_2} \right) \quad (2.21)$$

The total elongations from the unstressed condition,  $\Delta s_1$  and  $\Delta s_2$ , are found from (2.8):

$$\Delta s_1 = \frac{T_1}{EA} \int_0^c \left[ 1 + \left( \frac{dy}{dx} \right)^2 \right] dx = \frac{T_1^2}{2EA g_{cb}} \left[ \sinh \left( \frac{g_{cb}c}{T_1} \right) + \frac{g_{cb}}{T_1} \right] \quad (2.22)$$

$$\Delta s_2 = \frac{T_2^2}{2EA g_{cb}} \left[ \sinh \left( \frac{g_{cb}c}{T_2} \right) + \frac{g_{cb}c}{T_2} \right] \quad (2.23)$$

Here it is utilized that  $\delta \ll c$ . For the same reason the expression for  $s_2$  in (2.21) might be replaced by

$$s_2 = 2 \frac{T_2}{g_{cb}} \sinh \left( \frac{g_{cb}c}{2T_2} \right) + \delta \cosh \left( \frac{g_{cb}}{2T_2} \right) \quad (2.24)$$

The equation of state  $s_2 - s_1 = \Delta s_2 - \Delta s_1$  for the cable now leads to the following expression for  $\delta$ :

$$\delta = \frac{\frac{(T_2 - T_1)c}{2EA} + \frac{1}{2EA g_{cb}} \left[ T_2^2 \sinh \left( \frac{g_{cb}c}{T_2} \right) - T_1^2 \sinh \left( \frac{g_{cb}c}{T_1} \right) \right]}{\cosh \left( \frac{g_{cb}c}{2T_2} \right)} + \frac{\frac{2}{g_{cb}} \left[ T_1 \sinh \left( \frac{g_{cb}c}{2T_1} \right) - T_2 \sinh \left( \frac{g_{cb}c}{2T_2} \right) \right]}{\cosh \left( \frac{g_{cb}c}{2T_2} \right)} \quad (2.25)$$



Introducing  $T_1 = A \sigma_1$ ,  $T_2 = A \sigma_2$  and  $g_{cb} = A \gamma_{cb}$  yields:

$$\frac{\delta}{c} = \frac{(\sigma_2 - \sigma_1)\gamma_{cb} + \frac{1}{c} \left[ \sigma_2^2 \sinh\left(\gamma_{cb} \frac{c}{\sigma_2}\right) - \sigma_1^2 \sinh\left(\gamma_{cb} \frac{c}{\sigma_1}\right) \right] + 4 \frac{E}{c} \left[ \sigma_1 \sinh\left(\gamma_{cb} \frac{c}{2\sigma_1}\right) - \sigma_2 \sinh\left(\gamma_{cb} \frac{c}{2\sigma_2}\right) \right]}{2E\gamma_{cb} \cosh\left(\frac{\gamma_{cb} c}{2\sigma_2}\right)} \quad (2.26)$$

where  $\sigma_1$  is the cable stress in Condition 1,  $\sigma_2$  the cable stress in Condition 2, and  $\gamma_{cb}$  the density (weight per unit volume) of the cable material.

(2.26) expresses the elongation based on the correct catenary configuration. An approximate solution can be based on a parabolic configuration and the corresponding expression can be deduced from (2.26) by substituting  $\sinh x$  by  $x + x^3/6$  and  $\cosh x$  by 1.

This will lead to:

$$\frac{\delta}{c} = \frac{\sigma_2 - \sigma_1}{E} + \frac{\gamma_{cb}^2 c^2}{24} \left( \frac{1}{\sigma_1^2} - \frac{1}{\sigma_2^2} \right) + \frac{\gamma_{cb}^2 c^2}{12E} \left( \frac{1}{\sigma_2} - \frac{1}{\sigma_1} \right) \quad (2.27)$$

As  $E \gg \sigma$  the last term might be omitted without significant loss of accuracy:

$$\frac{\delta}{c} = \frac{\sigma_2 - \sigma_1}{E} + \frac{\gamma_{cb}^2 c^2}{24} \left( \frac{1}{\sigma_1^2} - \frac{1}{\sigma_2^2} \right) \quad (2.28)$$

It is evident that the parabola-based solution, (2.28), is considerably easier to use than the exact catenary-based solution, (2.26).

For the inclined stay cable the sag-creating transverse load has an intensity of  $g_{cb} \cos \phi$ , as indicated in Figure 2.74. The deformational characteristics of the inclined cable will be very close to those of a horizontal cable with the same chord length  $c$ , but subjected to a vertical dead load  $g_{cb} \cos \phi$ . Substituting  $g_{cb}$  by  $g_{cb} \cos \phi$  (or  $\gamma_{cb}$  by  $\gamma_{cb} \cos \phi$ ) and  $c$  by  $a/\cos \phi$  in (2.28) yields:

$$\frac{\delta}{c} = \frac{\sigma_2 - \sigma_1}{E} + \frac{\gamma_{cb}^2 a^2}{24} \left( \frac{1}{\sigma_1^2} - \frac{1}{\sigma_2^2} \right) \quad (2.29)$$

In this equation the first term expresses the elastic elongation of the cable and the second the effect of the sag variations.

For large values of  $\sigma_2$  the curve described by (2.29) will approach an asymptote with the equation

$$\frac{\delta}{c} = \frac{\sigma_2 - \sigma_1}{E} + \frac{\gamma_{cb}^2 a^2}{24\sigma_1^2} \left( = \frac{\sigma_2}{E} \right) \quad (2.30)$$

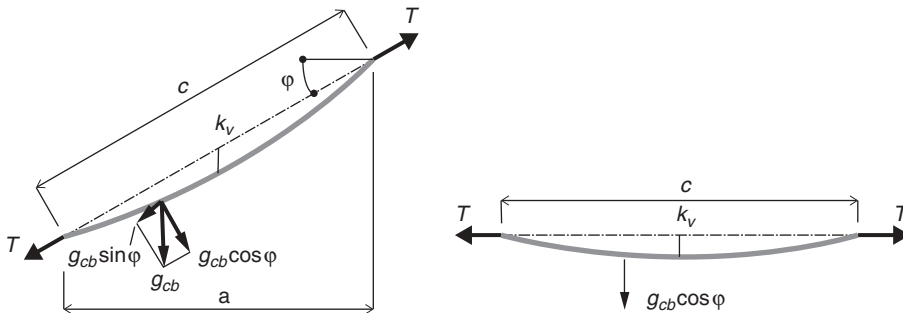
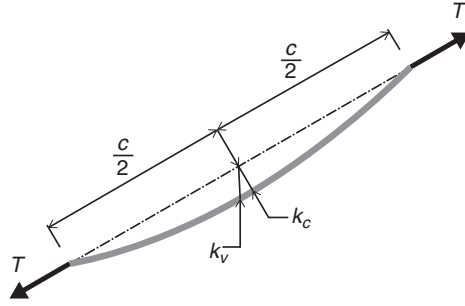


Figure 2.74 Inclined stay cable and equivalent horizontal stay cable with equal deformational characteristics



**Figure 2.75** Sag of stay cable measured perpendicular to the chord ( $k_c$ ) and vertical ( $k_v$ )

which is the stress–strain relationship of a straight bar with the same unstressed length as the cable. Considering that the sag is inversely proportional to the cable stress, it is very well understandable that, for large values of  $\sigma_2$ , the sag effect will eventually vanish and the cable behave more and more like a straight bar.

The vertical sag  $k$  of a horizontal stay cable is determined by:

$$k = \frac{g_{cb}c^2}{8T} = \frac{\gamma_{cb}c^2}{8\sigma} \quad (2.31)$$

It appears that the relative sag  $k/c$  is proportional to the cable length  $c$  with a proportionality factor of:  $\gamma_{cb}/8\sigma$

Typically, the factor  $\gamma_{cb}/8\sigma$  has a value of around  $25 \times 10^{-6}$  in the dead load condition, so that the relative sag  $k/c$  remains below 1/100 for cable lengths up to 400 m. Thus, the relative sag of a stay cable is less than one tenth of the relative sag in suspension bridge main cables.

For an inclined stay cable (Figure 2.75), the sag  $k_c$  perpendicular to the chord is given by:

$$k_c = \frac{g_{cb}c^2 \cos \phi}{8T} = \frac{\gamma_{cb}c^2}{8\sigma} \cos \phi \quad (2.32)$$

and the vertical sag  $k_v$ :

$$k_v = \frac{k_c}{\cos \phi} = \frac{\gamma_{cb}c^2}{8\sigma} \quad (2.33)$$

Note that the vertical sag  $k_v$  is independent of the inclination of the stay cable.

The effect of the changing sag under different loading conditions implies that a linear relation between force and deformation does not exist, as seen from (2.29) or Figure 2.64, but as earlier described, a linearization can be made by introducing a secant modulus of elasticity,  $E_{sec}$ , defined by:

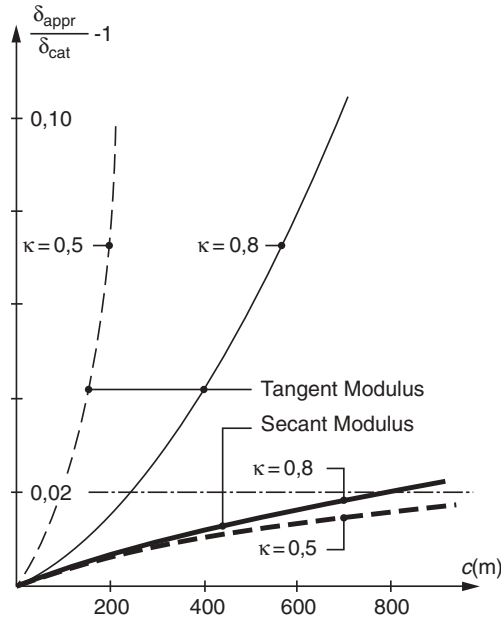
$$E_{sec} = \frac{\Delta\sigma}{\Delta\varepsilon} = \frac{\sigma_2 - \sigma_1}{\delta} c \quad (2.34)$$

By substituting the value of  $\delta/c$  from (2.30) into (2.34) the following expression for  $E_{sec}$  is derived:

$$\frac{1}{E_{sec}} = \frac{1}{E} + \frac{\gamma_{cb}^2 a^2}{24} \left( \frac{\sigma_1 + \sigma_2}{\sigma_1^2 \sigma_2^2} \right) \quad (2.35)$$

For cable stayed bridges with small traffic-to-dead load ratios, the secant modulus might be replaced by a tangent modulus  $E_{tan}$  found from (2.35) with  $\sigma_2 = \sigma_1$ :

$$\frac{1}{E_{tan}} = \frac{1}{E} + \frac{\gamma_{cb}^2 a^2}{12\sigma_1^3} \quad (2.36)$$



**Figure 2.76** Error ( $\delta_{appr}/\delta_{cat}-1$ ) by application of the tangent modulus or the secant modulus for stay cables with the following parameters:  $E=205\text{ GN/m}^2$ ,  $\gamma_{cb}=0.08\text{ MN/m}^3$  (including corrosion protection),  $\sigma_2=720\text{ MN/m}^2$ ,  $\kappa=0.5$  and  $0.8$ , respectively

To illustrate the effect of applying an equivalent modulus of elasticity based on the parabolic approximation instead of the correct catenary solution, Figure 2.76 shows for cables with stress ratios of  $\kappa=0.8$  and  $\kappa=0.5$ , respectively; the error defined as  $\delta_{appr}/\delta_{cat}$  where  $\delta_{appr}=(\sigma_2-\sigma_1)c/E_{eq}$  for a horizontal cable with varying length.

It appears that the secant modulus gives a very good approximation as the error remains below 1% for cable lengths up to 300 m and below 2% for cable lengths up to 750 m. Considering that the modulus of elasticity of the cable steel material hardly is known to an accuracy of more than 2–3%, it is evident that the secant modulus approach will be adequate for all practical purposes.

Generally, it is easier to use the tangent modulus than the secant modulus as only the cable stress in the initial condition has to be known. On the other hand, the use of the tangent modulus might give quite erroneous results for large cable lengths and large traffic-to-dead load ratios, as is seen in Figure 2.76.

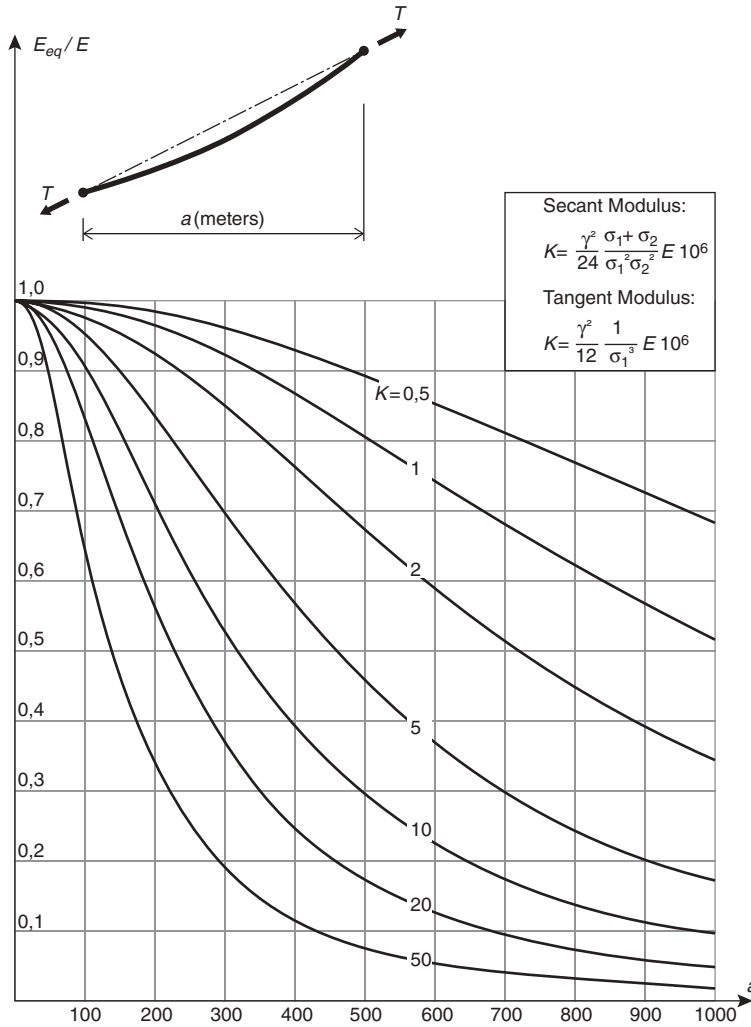
Based on (2.35) and (2.36) Figure 2.77 shows a plot of the relation between the equivalent modulus of elasticity and the horizontal cable projection. The diagram applies to both the secant modulus and the tangent modulus when the following expressions are used for calculating the curve parameter  $K$ :

$$K = \begin{cases} \frac{\gamma_{cb}^2(\sigma_1 + \sigma_2)}{24\sigma_1^2\sigma_2^2} E \times 10^6 & \text{for the secant modulus} \\ \frac{\gamma_{cb}^2}{12\sigma_1^3} E \times 10^6 & \text{for the tangent modulus} \end{cases} \quad (2.37)$$

For a modern parallel-wire cable the curve parameter  $K$  will typically have a value in the range from 0.5 to 1.0.

If the cable was made of ordinary mild steel the curve parameter would (due to the strong dependability of the stress level) increase to a value of about 20. This would lead to a drastic reduction of  $E_{eq}$  with increasing cable length. With  $a=300\text{ m}$  the ratio  $E_{eq}/E$  is equal to 0.96 if  $K=0.5$ , but 0.36 if  $K=20$ .

The fact that  $K$  is inversely proportional to the third power of the stress level has often led to the conclusion that the largest axial cable stiffness is achieved by applying the highest possible stress level. However, the axial stiffness is not governed



**Figure 2.77** Diagram showing the variation of the equivalent modulus of elasticity  $E_{eq}$  with the horizontal cable projection  $a$  and the curve parameter  $K$

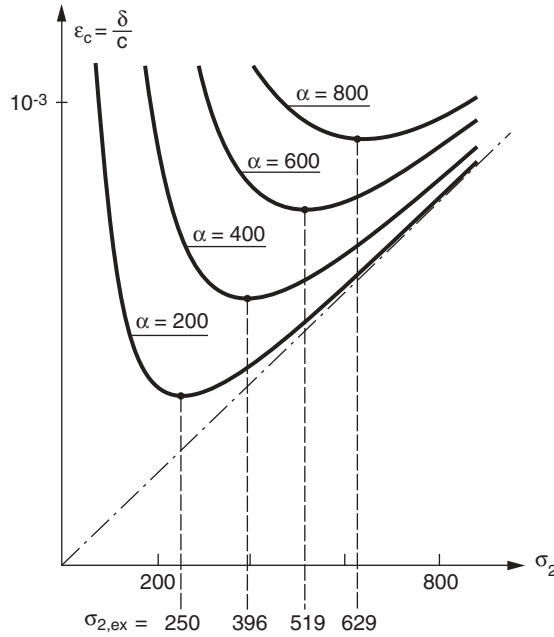
exclusively by the modules of elasticity, but by the product  $E_{eq}A_{cb}$ , and as  $A_{cb}$  increases with decreasing stress level the product  $E_{eq}A_{cb}$  might very well increase although  $E_{eq}$  decreases.

The cable strain  $\varepsilon_c = \delta/c = (\sigma_2 - \sigma_1)/E_{sec}$  is found from (2.35), which after introduction of the stress ratio  $\sigma_1/\sigma_2 = \kappa$  might be written:

$$\varepsilon_c = \frac{\delta}{c} = \frac{1 - \kappa}{E} \sigma_2 + \frac{\gamma_{cb}^2 a^2}{24} \left( \frac{1}{\kappa^2} - 1 \right) \frac{1}{\sigma_2^2} \tag{2.38}$$

The minimum  $\varepsilon_c$  is determined by equating  $\partial \varepsilon_c / \partial \sigma_2$  to zero:

$$\frac{\partial \varepsilon_c}{\partial \sigma_2} = \frac{1 - \kappa}{E} - \frac{\gamma_{cb}^2 a^2}{12} \left( \frac{1}{\kappa^2} - 1 \right) \frac{1}{\sigma_2^3} = 0$$



**Figure 2.78** Relation between the upper stress  $\sigma_2$  and the unit cable elongation  $\epsilon_c = \delta/c$  for stay cables with stress ratio  $\kappa = 0.8$  and horizontal projections 200, 400, 600, and 800 m, respectively

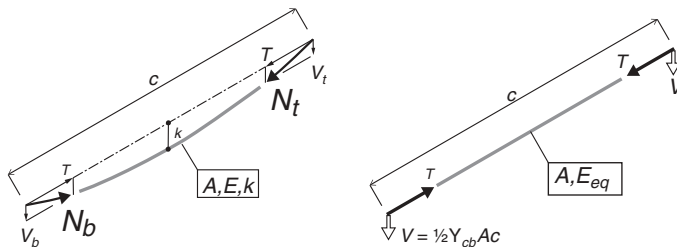
from which the stress  $\sigma_{2,ex}$  giving maximum axial stiffness is found

$$\sigma_{2,ex} = \left( \frac{1}{12} \gamma_{cb}^2 a^2 E \frac{1 + \kappa}{\kappa^2} \right)^{1/3} \tag{2.39}$$

The variation of  $\epsilon_c$  with the stress  $\sigma_2$  is indicated in Figure 2.78.

However, it should be emphasized that the increased axial stiffness that could be achieved by choosing a lower stress level generally leads to a more expensive structure due to the increased quantity of cable steel. Only if the lower stress level makes it possible to use less expensive steels for the cables will it be economically sound to increase the stiffness by enlarging the cable cross sections.

The idealization introduced by the equivalent modulus of elasticity is illustrated in Figure 2.79. The real cable, characterized by its cross sectional area  $A_{cb}$ , the modulus of elasticity  $E$ , and the sag  $k$ , is replaced by a straight, linear element with the same cross section  $A_{cb}$ , but an equivalent modulus of elasticity  $E_{eq}$  ( $E_{sec}$  or  $E_{tan}$ ). Then the idealized element can go into a conventional structural analysis requiring elastic behaviour of all elements.



**Figure 2.79** Real and idealized stay cable

In the real cable the line of action of the tangential force  $N$  at the supporting points can be decomposed into the chord force  $T$  and a vertical force  $V$ . The vertical force is found by taking moments about the other supporting point:

$$V = \frac{1}{2} g_{cb} c = \frac{1}{2} \gamma_{cb} A_{cb} c \tag{2.40}$$

As  $g_{cb}c$  represents the total self weight of the cable, it is seen that each of the vertical forces  $V$ , defined as indicated in Figure 2.79, equals half of the cable weight.

When substituting for the cable the idealized straight member with a force equal to the chord force  $T$ , the vertical forces  $V = \frac{1}{2} g_{cb}c$  should at the same time be applied at the supporting points. These vertical forces will then go into the analysis of the main structural system in the same way as other dead loads.

After analyzing the structural system and determining the forces  $T$  in the idealized cable elements, the maximum tensile force in the real cable has to be found to determine the cable area  $A_{cb}$ .

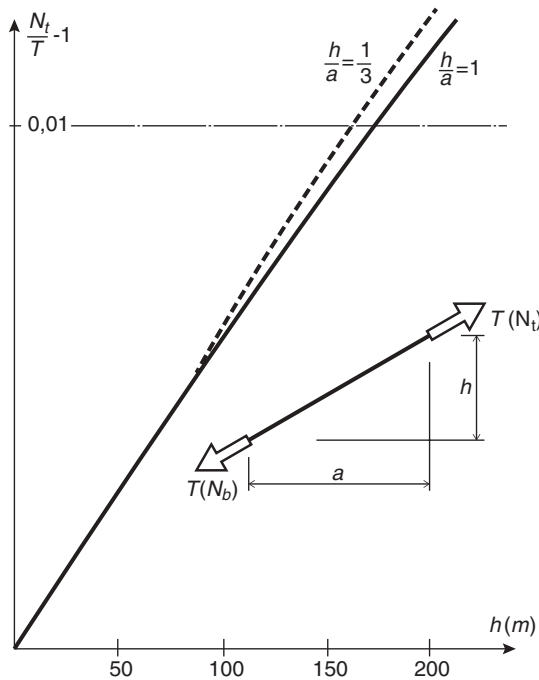
For the maximum normal force  $N_t$ , acting at the upper supporting point B, the following expression can be found:

$$N_t = \sqrt{\left(T^2 + V^2 + 2TV \frac{h}{\sqrt{a^2 + h^2}}\right)} \tag{2.41}$$

Introducing  $V = \frac{1}{2} \gamma_{cb} A_{cb} \sqrt{a^2 + h^2}$  and  $A = N_t / \sigma$  leads to

$$\frac{N_t}{T} = \left( \sqrt{4 - \frac{\gamma_{cb}^2}{\sigma^2} a^2 + \frac{\gamma_{cb}}{\sigma} h} \right) \left( 2 - \frac{\gamma_{cb}^2 (a^2 + h^2)}{2\sigma^2} \right)^{-1} \tag{2.42}$$

With  $\gamma_{cb} = 0.09 \text{ MN/m}^3$  and  $\sigma = 720 \text{ MPa}$  Figure 2.80 shows for stay cables with  $h/a = 1$  and  $h/a = 1/3$  the error  $(N_t/T - 1)$  when using the chord force  $T$  rather than the maximum tensile force  $N_t$  for the design of the cable. It appears that for cables



**Figure 2.80** Error  $(N_t/T - 1)$  by application of chord force  $T$  instead of maximum normal force  $N_t$  for stay cables with slope  $h/a = 1$  and  $h/a = 1/3$

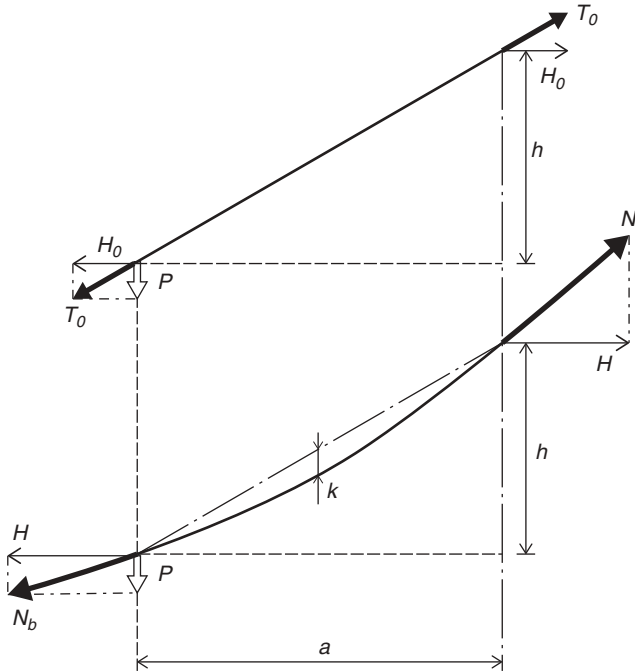


Figure 2.81 Forces induced in a straight and a sagging cable

with vertical projections up to 150 m the error remains so small that it will be acceptable to use the chord force  $T$  throughout the design – and vertical stay cable projections of up to 150 m will correspond to main spans of more than 600 m for traditional three-span cable stayed bridges.

### 2.5.3 Limit length and efficiency ratio of a stay cable

It has earlier been emphasized that the sag occurring in a stay cable basically is undesirable as it reduces the efficiency of the load transfer and increases the axial flexibility.

The adverse effect on the load-carrying performance is illustrated in Figure 2.81 showing at the top the forces acting on a straight cable and at the bottom those acting on the sagging cable, both cables carrying the same vertical force  $P$  at the deck level.

As the relative sag  $k/a$  of the stay cable is proportional to the length of the stay (refer to Figure 2.62) the effect illustrated in Figure 2.81 will be more and more pronounced the longer the stay cable becomes.

The ultimate length of a stay cable will be reached when the cable tangent at the bottom becomes horizontal in which case the vertical force  $P$  would induce an infinitely large force in the stay.

To calculate the maximum horizontal projection  $a_{\max}$  a cable with a horizontal tangent at the origin and with the correct catenary configuration, as illustrated in Figure 2.82, shall be considered.

The value of  $a_{\max}$  will depend on the equivalent density  $\gamma_{eq}$  of the cable material, the design stress  $f_{cbd}$  and the ratio  $h/a$  equal to the inclination  $\alpha$  of the chord.

The equation for the actual catenary will be:

$$y = \frac{H}{\gamma_{cb}A_{cb}} \left( \cosh \frac{\gamma_{cb}A_{cb}}{H} x - 1 \right) \quad (2.43)$$

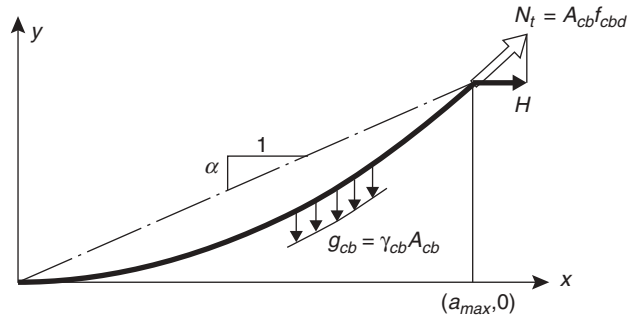


Figure 2.82 Stay cable at its limit length

From this equation the following expression for the tangential force  $N$  at the top can be derived:

$$N = H \cosh\left(\gamma_{cb} \frac{A_{cb}}{H} x\right) \quad (2.44)$$

With this equation and the conditions:

$$\begin{aligned} x &= a_{\max} \\ N_t &= A_{cb} f_{cbd} \\ y &= \alpha a_{\max} \text{ for } x = a_{\max} \end{aligned}$$

the following expression can be derived:

$$\cosh \frac{a_{\max}}{(f_{cbd}/\gamma_{cb}) - \alpha a_{\max}} = \frac{f_{cbd}/\gamma_{cb}}{f_{cbd}/\gamma_{cb} - \alpha a_{\max}} \quad (2.45)$$

It appears that this equation has only  $a_{\max}$  as an unknown when the cable properties and the chord inclination are known.

Based on (2.45) Figure 2.83 shows a plot of the limit length  $a_{\max}$  with the chord inclination  $\alpha$  varying between 0 and 1.0. The plot is based on the typical values of  $f_{cbd} = 720 \text{ MPa}$  and  $\gamma_{cb} = 0.09 \text{ MN/m}^3$ .

It is seen that for smaller values of the chord inclination  $\alpha$  ( $\alpha < 0.3$ ) the limiting length  $a_{\max}$  is almost proportional to the chord inclination but for larger values of  $\alpha$  the limit length starts to curve downwards and a maximum is reached for  $\alpha = 0.68$  where  $a_{\max} = 5,300 \text{ m}$ .

The plot in Figure 2.83 can also be used to determine the maximum span of a suspension system if the stay is considered as one half of a suspension bridge main cable. Thus, with the given cable material properties the maximum span of a main cable for a suspension bridge (i.e. the span where the cable will be able to carry just its own weight) will be 10 600 m. However, this length will require that the cable is suspended with a sag ratio of  $k/l = \frac{1}{2} 0.68 = 0.34$  which is a much larger sag than used in existing suspension bridges. For the typical sag ratio of  $k/l = 0.1$  corresponding to a chord inclination of  $\alpha = 0.2$  the maximum span will be approximately  $2 \times 2,900 \text{ m} = 5,800 \text{ m}$ .

Figure 2.83 also shows with a dotted line the relation between  $a_{\max}$  and  $\alpha$  in case the correct catenary is replaced by a second order parabola (parabolic approximation). It is seen that for chord inclinations  $\alpha$  below 0.3 the difference between the results obtained by assuming a catenary or a parabola is insignificant, but for larger values the difference becomes more pronounced. Thus, with the parabolic approximation the limit length will remain under 5,000 m even for the optimum chord inclination.

For both the catenary and the parabolic configuration it is assumed that the cable has a constant cross section which implies that the design stress will only be fully reached at the upper supporting point whereas all other cable cross sections will have smaller stresses. It would, however, be theoretically possible to vary the cable cross section in such a way that the design stress was reached in any position along the cable.



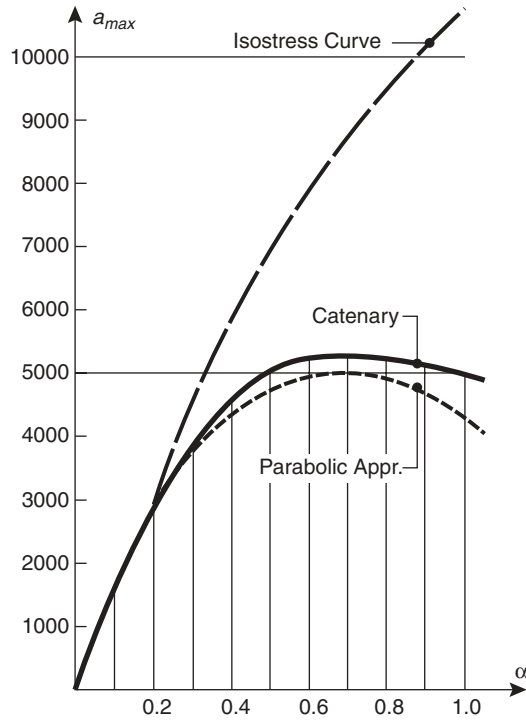


Figure 2.83 Plot of the relation between the limit length  $a_{max}$  and the chord inclination  $\alpha$  of a stay cable

The equation for the ‘isostress’ cable curve can be found by considering an infinitesimal cable element with a horizontal projection of  $dx$ , as indicated in Figure 2.84.

For this element the cross section  $A_{cb}(x)$  will be:

$$A_{cb}(x) = \frac{H}{f_{cbd}} \sqrt{1 + \left(\frac{dx}{dy}\right)^2} \tag{2.46}$$

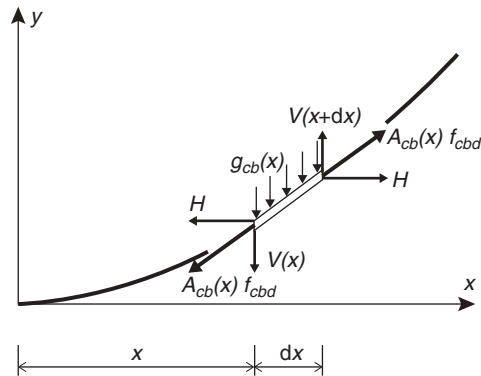


Figure 2.84 Isostress cable with design stress in all cross section

and the weight of the element:

$$g_{cb}(x)dx = \gamma_{cb}A_{cb}(x)\sqrt{1 + \left(\frac{dy}{dx}\right)^2} = \frac{\gamma_{cb}}{f_{cbd}}H\left(1 + \left(\frac{dy}{dx}\right)^2\right) \quad (2.47)$$

Expressing vertical equilibrium yields:

$$H\left(\frac{dy}{dx} + \frac{d^2y}{dx^2}dx\right) - H\frac{dy}{dx} = \frac{\gamma_{cb}}{f_{cb}}H\left(1 + \left(\frac{dy}{dx}\right)^2\right)dx \quad (2.48)$$

Leading to the differential equation for the isostress cable:

$$\frac{d^2y}{dx^2} - \frac{\gamma_{cb}}{f_{cbd}}\left(\frac{dy}{dx}\right)^2 - \frac{\gamma_{cb}}{f_{cbd}} = 0 \quad (2.49)$$

With the relevant boundary conditions the solution to (2.49) can be expressed:

$$y = -\frac{f_{cbd}}{\gamma_{cb}}\ln\left(\cos\frac{\gamma_{cb}}{f_{cbd}}x\right) \quad (2.50)$$

Based on this equation the corresponding curve has been plotted with a dot-and-dash line in Figure 2.83 and it is seen that for larger chord inclinations the isostress cable can be much longer than the catenary cable. However, for chord inclinations below 0.2, the difference is rather marginal.

The isostress curve will have no maximum but it will reach an asymptotic value for  $(\gamma_{cb}/f_{cbd})x = \pi/2$ . With  $f_{cbd} = 720$  MPa and  $\gamma_{cb} = 0.09$  MN/m<sup>3</sup> the asymptotic value for  $a_{\max}$  becomes 12 566 m.

In real structures it will of course not be possible to get even close to the limit length of a stay cable as the efficiency of the support offered by stay cables of such extreme lengths will be unacceptably small.

A stay cable of more reasonable length can always be regarded as a part of a stay cable with the limiting length, as illustrated in Figure 2.85. Here the parabolic approximation is used and based on this the following expressions for the stay cable with a horizontal projection  $a$  can be derived:

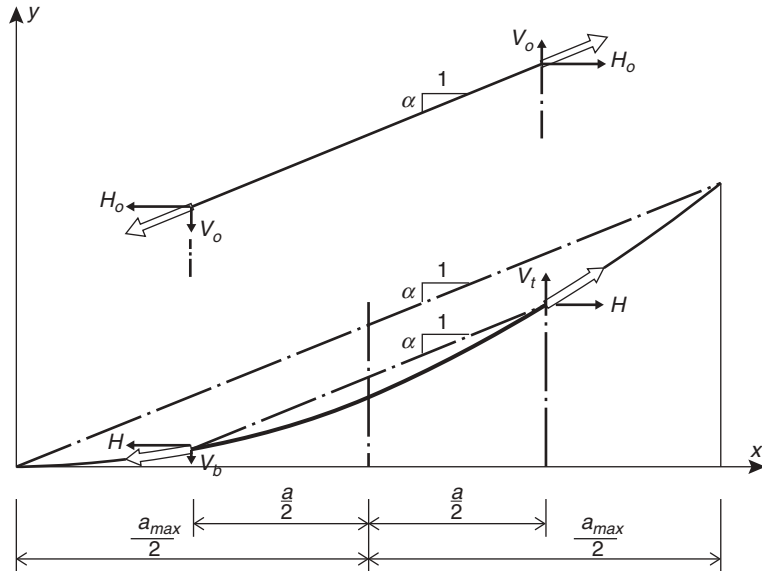
$$H = A_{cb}f_{cbd}\frac{1}{\sqrt{1 + \alpha^2\left(1 + \frac{a}{a_{\max}}\right)^2}} \quad (2.51)$$

$$V_b = A_{cb}f_{cbd}\frac{\alpha\left(1 - \frac{a}{a_{\max}}\right)}{\sqrt{1 + \alpha^2\left(1 + \frac{a}{a_{\max}}\right)^2}} \quad (2.52)$$

For an idealized straight cable as shown above the sagging cable in Figure 2.86 the horizontal force  $H_o$  and the vertical force  $V_o$  becomes:

$$H_o = A_{cb}f_{cbd}\frac{1}{\sqrt{1 + \alpha^2}} \quad (2.53)$$

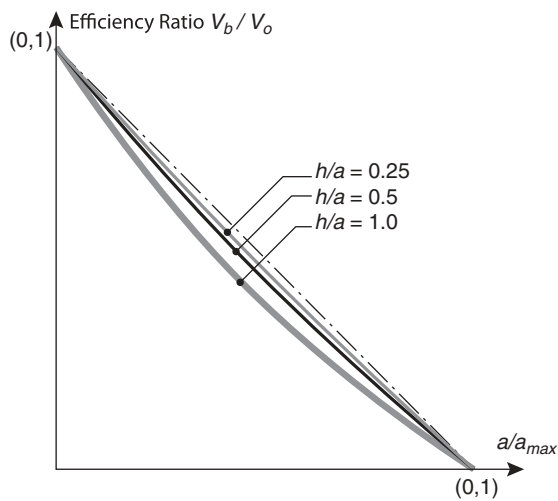
$$V_o = A_{cb}f_{cbd}\frac{\alpha}{\sqrt{1 + \alpha^2}}$$



**Figure 2.85** Stay cable with horizontal projection  $a$  and chord inclination  $\alpha$  forming a portion of a stay cable with the limit length  $a_{max}$

The efficiency ratio of the sagging cable can now be defined as  $V_b/V_o$  as this expresses how much the load carrying capacity is reduced due to the cable sag:

$$\frac{V_b}{V_o} = \frac{\left(1 - \frac{a}{a_{max}}\right) \sqrt{1 + \alpha^2}}{\sqrt{1 + \alpha^2 \left(1 + \frac{a}{a_{max}}\right)^2}} \quad (2.54)$$



**Figure 2.86** Efficiency ratio of a stay cable as function of the relative horizontal projection  $a/a_{max}$

In Figure 2.86 the relation between the relative horizontal projection  $a$  and the efficiency ratio  $V_b/V_o$  is shown for three different values of the chord inclination. The longest existing stay cables have an inclination of approximately 0.4 and a length of approximately 550 m which is less than 12% of the limit length ( $\sim 4.700$  m) so even for these stay cables the efficiency ratio is close to 90%.

## 2.6 Bending of Cables

With its composition of relatively thin wires the cables are generally assumed to be without any bending stiffness, and therefore acting as completely flexible strings.

For the calculation of the main structure, the assumption of perfectly flexible strings will be adequate for all practical purposes, but in the study of local effects it might be necessary to take into account the actual bending stiffness of the cables.

The fact that the bending stresses even in the wires can be of a magnitude that should not be neglected is illustrated by the example in Figure 2.87 showing a parallel-wire cable passing over a saddle with a radius of  $R = 7$  m – a typical value for a pylon saddle of a suspension bridge. The bending stress  $\sigma_b$  induced in a wire with a diameter of  $d$  is determined by:

$$\sigma_b = E(d/2R) \quad (2.55)$$

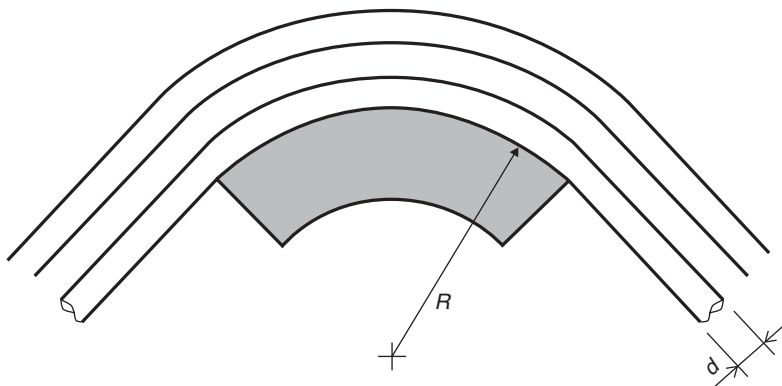
With  $E = 205$  GPa,  $d = 5$  mm and  $R = 7000$  mm,  $\sigma_b$  becomes 73 MPa, corresponding to approximately 10% of the design stress for cable steel.

A much smaller radius  $R$  is generally used in the strand shoes where the wires of air-spun cables are anchored to the anchor blocks. Thus, in the Storebælt East Bridge the 5.38 mm wires are anchored to strand shoes with a radius of  $R = 400$  mm. Consequently, the bending stress induced in the wires will be  $\sigma_b = 205 (5.38/800) \times 10^3 = 1,380$  MPa – a value that far exceeds the design stress of the wires. However, experience from a large number of suspension bridges built over a period of more than 100 years seems to indicate that this apparent overloading does not affect the overall safety of the bridge. This might be explained by the fact that plastification and relaxation in the wire material will diminish the initial bending stresses in the curvature around the strand shoes.

(2.55) can also be applied to determine the minimum reeling radius for the wires to avoid irreversible strains induced during transportation and storage. For normal wire material this will require that the bending stress is kept below a value around 600 MPa, which for a 5 mm wire leads to a minimum reeling radius  $R_{\min}$  of:

$$R_{\min} = Ed/(2\sigma_b) = 875 \text{ mm}$$

Figure 2.88 shows the wire reels with a mean diameter of 1500 mm for the Storebælt East Bridge.



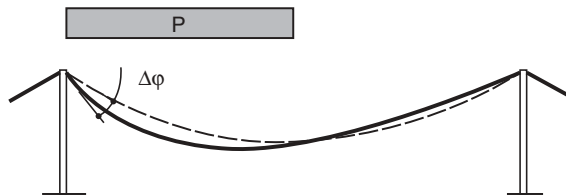
**Figure 2.87** Wire with diameter  $d$  passing over a saddle with radius  $R$



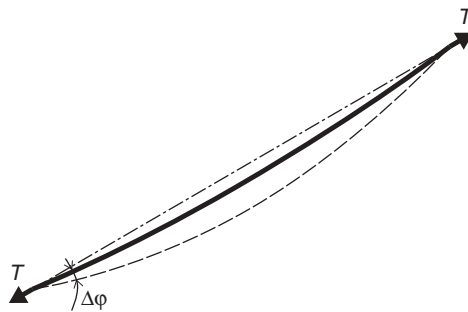
**Figure 2.88** Wire reels for the Storebælt East Bridge

Under the action of traffic load, wind load, and temperature changes the shape of the cables will vary and this induces angular changes at the cable supports, as illustrated in Figure 2.89 for a suspension bridge main cable under asymmetric load and in Figure 2.90 for a stay cable with varying axial force.

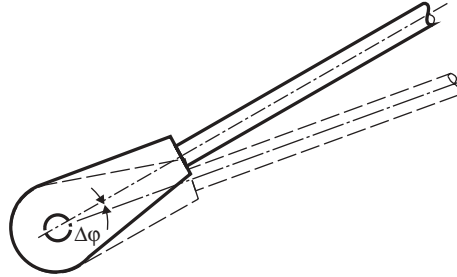
If the cable was pin-connected at the ends and no friction was present then the cable end would be free to rotate (Figure 2.91), and the stresses due to the change of curvature would be absolutely insignificant and would not have to be taken into account. However, in real structures the friction will be so large that in the final stage when the cable is under full tension from dead load a rotation will only take place under extreme angular changes. So even with a pin-connection as shown in Figure 2.91 secondary stresses due to the action of traffic load or wind load should be calculated by assuming a fixed connection to the adjacent structure.



**Figure 2.89** Angular change  $\Delta\phi$  at the cable saddle occurring under asymmetrical traffic load on a suspension bridge



**Figure 2.90** Angular change  $\Delta\phi$  at the cable end under varying sag of a stay cable



**Figure 2.91** Cable socket allowing angular changes at the cable end

If the cable, as indicated in Figure 2.92, contains bearing sockets resting against structural parts rigidly connected to the adjoining structure, then the cable cross section will be prevented from rotating in all conditions so a concentrated change of curvature must therefore occur at the ends.

For a cable subjected to an angular change  $\Delta\phi$  at the end (Figure 2.93) the following expressions can be derived:

$$M(x) = EJ_c \frac{d^2y}{dx^2} = Ty \tag{2.56}$$

$$y = \Delta\phi \sqrt{\frac{EJ_{cb}}{T}} \exp\left[-x\sqrt{\frac{T}{EJ_{cb}}}\right] \tag{2.57}$$

$$M(x) = Ty = \Delta\phi \sqrt{EJ_{cb}T} \exp\left[-x\sqrt{\frac{T}{EJ_{cb}}}\right] \tag{2.58}$$

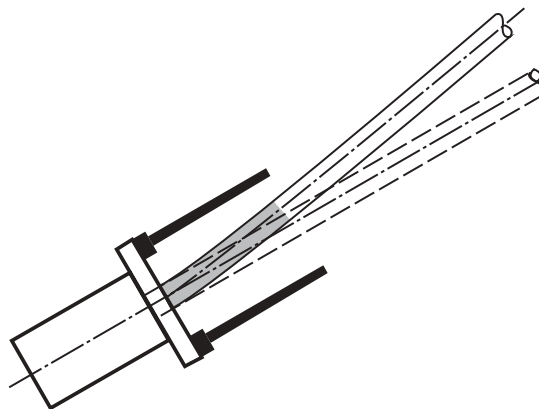
where  $J_{cb}$  is the moment of inertia of the cable.

The maximum moment occurs at the cable end ( $x=0$ ):

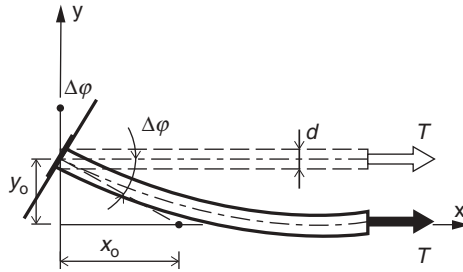
$$M(0) = \Delta\phi \sqrt{EJ_{cb}T} \tag{2.59}$$

inducing a local bending stress  $\sigma_{bl}$ :

$$\sigma_{bl} = \frac{1}{2}d\Delta\phi \sqrt{ET/J_{cb}} \tag{2.60}$$



**Figure 2.92** Cable socket in fixed connection with the adjoining structure



**Figure 2.93** Cable subjected to an angular change  $\Delta\phi$  at the end

Inserting  $J_{cb} = A_{cb}d^2/16$  as found for a circular cable section yields:

$$2\Delta\phi\sqrt{ET/A_{cb}} = 2\Delta\phi\sqrt{E/\sigma_{cb}} \quad (2.61)$$

where  $\sigma_{cb}$  is the axial cable stress.

It is now interesting to note that the bending stress  $\sigma_{bm}$  is independent of the cable diameter, as seen from (2.61).

For a stay cable with a horizontal projection  $a$  and a stress variation from  $\sigma_1$  to  $\sigma_2$  the following expression for the angular change  $\Delta\phi$  at the ends might be found:

$$\Delta\phi = \frac{1}{2} \gamma_{cb} (1/\sigma_1 - 1/\sigma_2) \quad (2.62)$$

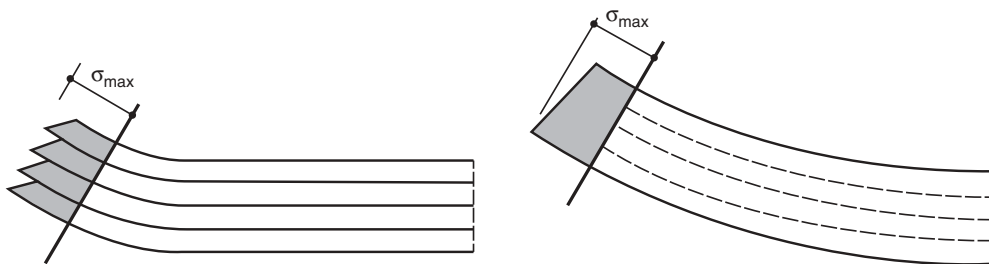
For a cable with a horizontal projection  $a = 300$  m, a density  $\gamma_{cb} = 0.09$  MN/m<sup>3</sup>, and the axial stress varying from  $\sigma_g = 540$  MPa to  $\sigma_{g+p} = 720$  MPa (2.62) yields:

$$\Delta\phi = 6.25 \times 10^{-3} \text{ MPa}$$

With this value the local bending stress from (2.60) becomes  $\sigma_{bl} = 152$  MPa, which means that the maximum cable stress is increased by more than 20% when taking the cable bending into account.

At first glance this 20% increase might not seem to be very serious, but it should be noted that the stress range from the dead load condition to the traffic load condition is increased from 180 MPa to 332 MPa when including the cable bending. This indicates a much more pronounced influence on the fatigue resistance.

The fact that the bending stress does not depend on the cable diameter implies that the same stress develops in cables where the wires are free to slide mutually and in cables where no slip occurs between wires. This feature is illustrated in Figure 2.94 showing at the top the stresses in a cable with four layers of wire sliding freely and at the bottom the stresses in the same cable with no sliding between wires. In the latter case the cable can be assumed to have a homogeneous cross section.



**Figure 2.94** Variation of stresses in a cable with slip between wires (left), and without slip (right)

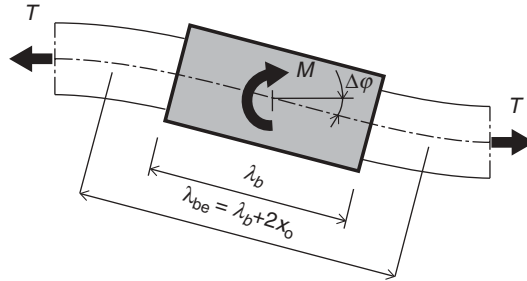


Figure 2.95 Cable clamp subjected to an angular change

As indicated in Figure 2.94 the curvature of the cable will be concentrated in a smaller zone when the wires act independently. This can be seen by determining the distance  $x_0$  from the  $y$  axis to the intercept between the cable tangents at  $x = 0$  and  $x = \infty$  (as shown in Figure 2.93):

$$x_0 = \sqrt{EJ_{cb}/T} = \frac{1}{4} d \sqrt{E/\sigma_{cb}} \quad (2.63)$$

which shows that the distance  $x_0$  is proportional to the cable/wire diameter  $d$ , but independent of the angular change  $\Delta\phi$ .

In cables with clamps as on suspension bridge main cables, the combined action of cable tension and slip prevention due to the friction leads to the occurrence of bending stresses when the cable distorts.

For a cable clamp, as shown in Figure 2.95, the relation between the moment  $M$  and the angular change  $\Delta\phi$  is determined by:

$$M = T\lambda_{be}\Delta\phi \quad (2.64)$$

where  $\lambda_{be}$  is the effective cable clamp length:

$$\lambda_{be} = \lambda_b + 2x_0 = \lambda_b + \frac{1}{2} d \sqrt{E/\sigma_{cb}} \quad (2.65)$$

As the effective cable band length  $\lambda_{be}$  is independent of the angular change, the cable with its clamp might be represented by a system as shown at the bottom of Figure 2.96 where a stiff body with the length  $\lambda_{be}$  is hinge-connected to bars representing the wires.

With this model, the behaviour of a cable with length  $2c_b$  ( $c_b \gg \lambda_{be}$  and a central clamp (as shown in Figure 2.97) will be studied.

Under symmetrical deformation (b) characterized by angular changes  $\Delta\phi_s$  at both ends the cable clamp remains in its original position and a constant moment  $M_s$  occurs in the cable:

$$M_s = (EJ_{cb}/c_b)\Delta\phi_s \quad (2.66)$$

where  $J_{cb}$  is the moment of inertia for the entire cable cross section.

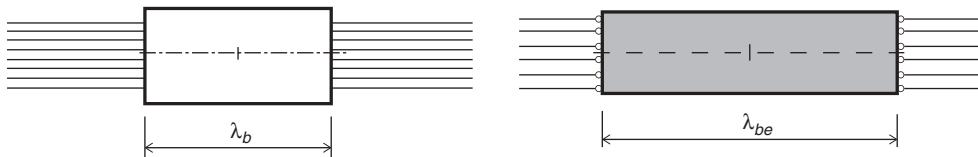


Figure 2.96 Real and idealized cable clamp



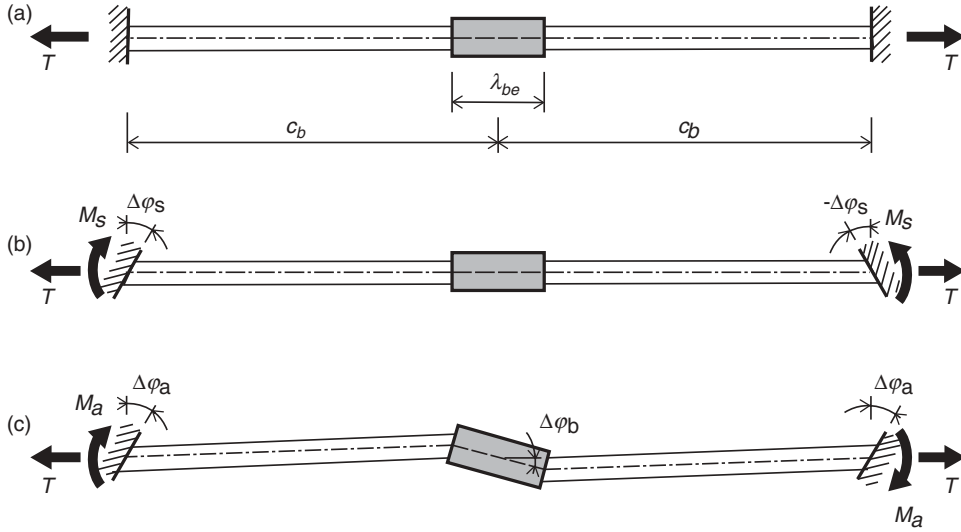


Figure 2.97 Cable with a central cable band subjected to symmetrical and asymmetrical rotation of supports

Under asymmetrical deformation (c) with angular changes  $\Delta\phi_a$  at both ends the cable clamp rotates an angle  $\Delta\phi_b$  determined by:

$$2 \frac{EJ_{cb}}{c_b} (\Delta\phi_a - \Delta\phi_b) = T\lambda_{be}\Delta\phi_b \quad (2.67)$$

leading to

$$\Delta\phi_b = \frac{2EJ_{cb}}{2EJ_{cb} + T\lambda_{be}c_b\Delta\phi_a} \quad (2.68)$$

and

$$M_a = \frac{EJ_{cb}T\lambda_{be}}{2EJ_{cb} + T\lambda_{be}c_b} \Delta\phi_a \quad (2.69)$$

Note that  $M_a$  is a function of the cable tension  $T$  (in contrast to  $M_s$  being independent of  $T$ ).

In a general case where the cable with a central clamp is subjected to angular changes  $\Delta\phi_1$  at one end and  $\Delta\phi_3$  at the other, a subdivision into a symmetrical case and an anti-symmetrical case can be made by introducing:

$$\Delta\phi_s = \frac{1}{2}(\Delta\phi_1 - \Delta\phi_3) \text{ and } \Delta\phi_a = \frac{1}{2}(\Delta\phi_1 + \Delta\phi_3)$$

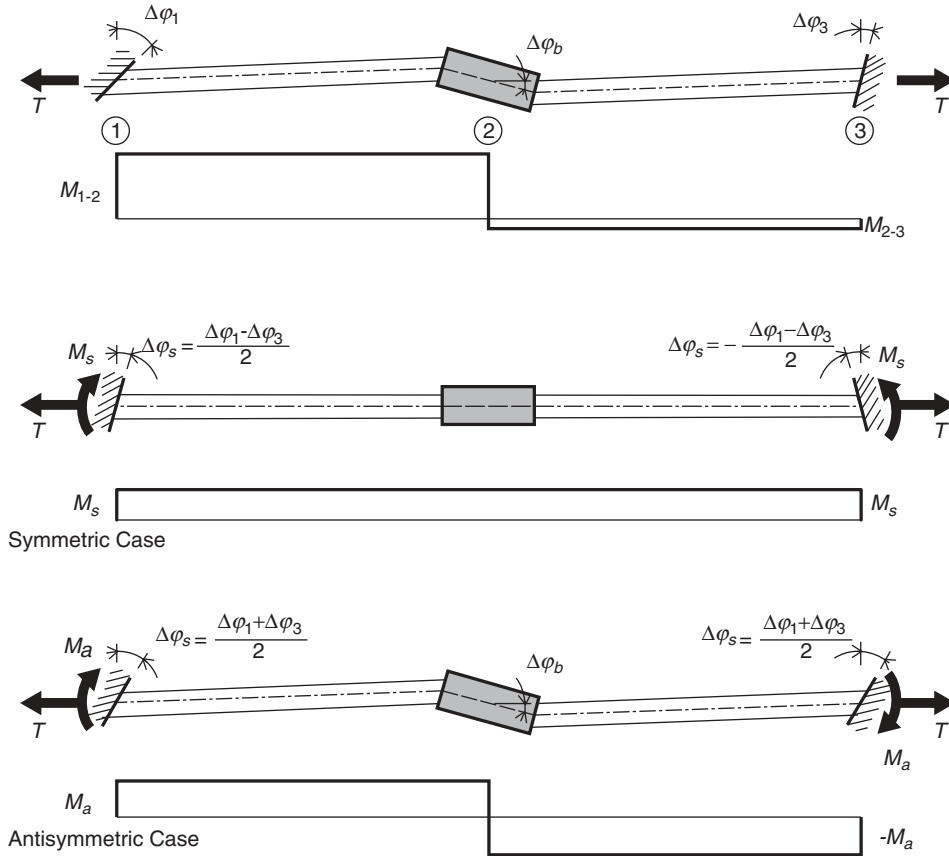
as shown in Figure 2.98.

The angular change  $\Delta\phi_b$  of the cable clamp is determined by considering the anti-symmetrical case only (2.68):

$$\Delta\phi_b = \frac{2EJ_{cb}}{2EJ_{cb} + T\lambda_{be}c_b} \left( \frac{\Delta\phi_1 + \Delta\phi_3}{3} \right) \quad (2.70)$$

The bending moments in the cables are found by combining (2.66) and (2.69):

$$\begin{aligned} M_{1-2} &= \frac{EJ_{cb}}{c_b} \left( \frac{\Delta\phi_1 - \Delta\phi_3}{2} \right) + \frac{EJ_{cb}T\lambda_{be}}{2EJ_{cb} + T\lambda_{be}c_b} \left( \frac{\Delta\phi_1 + \Delta\phi_3}{2} \right) \\ &= \frac{1}{2} \left( \frac{EJ_{cb}T\lambda_{be}}{2EJ_{cb} + T\lambda_{be}c_b} + \frac{EJ_{cb}}{c_b} \right) \Delta\phi_1 + \frac{1}{2} \left( \frac{EJ_{cb}T\lambda_{be}}{2EJ_{cb} + T\lambda_{be}c_b} - \frac{EJ_{cb}}{c_b} \right) \Delta\phi_3 \end{aligned} \quad (2.71)$$



**Figure 2.98** Cable with a central cable clamp subjected to angular changes  $\Delta\phi_1$  and  $\Delta\phi_3$  at the supports

$$\begin{aligned}
 M_{2-3} &= \frac{EJ_{cb}}{c_b} \left( \frac{\Delta\phi_1 - \Delta\phi_3}{2} \right) - \frac{EJ_{cb}T\lambda_{be}}{2EJ_{cb} + T\lambda_{be}c_b} \left( \frac{\Delta\phi_1 + \Delta\phi_3}{2} \right) \\
 &= \frac{1}{2} \left( -\frac{EJ_{cb}T\lambda_{be}}{2EJ_{cb} + T\lambda_{be}c_b} + \frac{EJ_{cb}}{c_b} \right) \Delta\phi_1 + \frac{1}{2} \left( \frac{EJ_{cb}T\lambda_{be}}{2EJ_{cb} + T\lambda_{be}c_b} + \frac{EJ_{cb}}{c_b} \right) \Delta\phi_3
 \end{aligned} \tag{2.72}$$

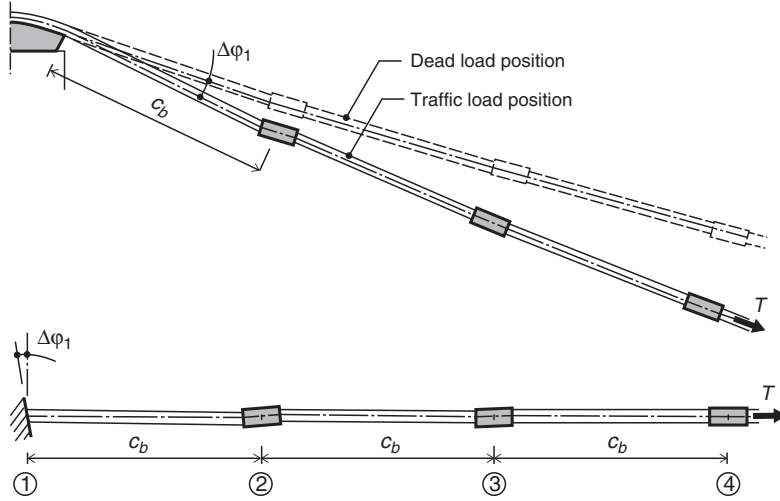
It should be emphasized that the moments  $M_{1-2}$  and  $M_{2-3}$  determined above include only the pure cable clamp effect in accordance with the idealized mathematical model indicated to the right in Figure 2.96. Thus, to arrive at the total stress in the cable due to the rotation of the cable clamp a contribution from the local cable bending as expressed by (2.60) or (2.61) will be added.

For a suspension bridge main cable the maximum bending is induced in the region at the pylon where the largest angular change occurs.

Figure 2.99 shows at the top the situation when the main cable distorts from the dead load position to the traffic load position.

For long span bridges with a large number of hangers (clamps) the calculation might be based on the following idealizations without introducing unacceptable errors:

- (1) The cable is assumed to be straight in the initial state.
- (2) The distortion of the entire cable is replaced by a rotation  $\Delta\phi_1$  of the cable end.
- (3) The clamps are assumed to be positioned equidistant.



**Figure 2.99** Suspension bridge main cable distorted under traffic load. At the bottom is shown the idealization based on investigation of a straight cable subjected to the angular change  $\Delta\phi_1$  at the end

This implies that the real situation, illustrated at the top of Figure 2.99, is replaced by the idealized situation at the bottom of the figure.

Considering the cable 1–2–3 and applying (2.70) leads to:

$$\Delta\phi_2 = \frac{2EJ_{cb}}{2EJ_{cb} + T\lambda_{be}c_b} \left( \frac{\Delta\phi_1 + \Delta\phi_3}{2} \right) \quad (2.73)$$

With the supplementary condition:

$$\Delta\phi_1/\Delta\varphi_2 = \Delta\varphi_2/\Delta\varphi_3 \quad (2.74)$$

the following expression for  $\Delta\varphi_2$  might be derived:

$$\Delta\phi_2 = \left[ 1 + \frac{T\lambda_{be}c_b}{2EJ_{cb}} - \sqrt{\left( 1 + \frac{T\lambda_{be}c_b}{EJ_{cb}} \right)^2 - 1} \right] \Delta\phi_1 \quad (2.75)$$

The moment  $M_{1-2}$  in the cable adjacent to the cable saddle is determined by:

$$M_{1-2} = \frac{EJ_{cb}}{c_b} (\Delta\phi_1 - \Delta\phi_2) \quad (2.76)$$

Inserting  $\Delta\varphi_2$  from (2.75) yields:

$$M_{1-2} = \left[ \sqrt{\frac{1}{4}T^2\lambda_{be}^2 + EJ_{cb}T\frac{\lambda_{be}}{c_b}} - \frac{1}{2}T\lambda_{be} \right] \Delta\phi_1 \quad (2.77)$$

The moment  $M_{2-3}$  between cable clamps 2 and 3 is determined by

$$M_{2-3} = \frac{\Delta\phi_2}{\Delta\phi_1} M_{1-2} \quad (2.78)$$

so that the moment change  $\Delta M_2$  at cable clamp 2 becomes

$$\Delta M_2 = M_{1-2} - M_{2-3} = (1 - \Delta\phi_2/\Delta\phi_1)M_{1-2} \quad (2.79)$$

To get an indication of the magnitude of moments and bending stresses induced in a suspension bridge main cable, the following realistic values will be inserted in the relevant expressions derived above:

$$\lambda_b = 1.5 \text{ m}; d_{cb}c_b = 22 \text{ mm}; E = 205 \text{ GPa}; \sigma_{cb} = 720 \text{ MPa}$$

where  $d_{cb}$  is the diameter of the cable. Assuming 20% voids inside the cable leads to:

$$\begin{aligned} A_{cb} &= \frac{1}{4} \pi \times 0.75 \times 0.8 = 0.353 \text{ m}^2 \\ J_{cb} &= (\pi/64) \times 0.75^4 \times 0.8 = 12.4 \times 10^{-3} \text{ m}^4 \\ T &= A_{cb}\sigma_c = 254 \text{ MN} \end{aligned}$$

The effective cable clamp length  $\lambda_{be}$  is determined by (2.65). Assuming that the wires are free to slide in the regions between the cable clamps implies that  $d$  is equal to the wire diameter (5 mm):

$$\lambda_{be} = 1.5 + \frac{5 \times 10^{-3}}{2} \sqrt{\frac{205 \times 10^3}{720}} = 1.54$$

With  $\Delta\varphi_1 = 1.5 \times 10^{-3}$  rad (2.75) yields:

$$\Delta\varphi_2 = 0.193\Delta\varphi_1 = 2.89 \times 10^{-3} \text{ rad}$$

and from (2.76) and (2.78):

$$M_{1-2} = 1.40 \text{ MNm}; M_{2-3} = -0.27 \text{ MNm}; M_{3-4} = 0.5 \text{ MNm}$$

It appears that the moment occurring between the cable saddle and the first cable clamp rapidly is ‘damped’ when passing through a few cable clamps.

The bending stress  $\sigma_{bc}$  due to the cable clamp effect now becomes:

$$\sigma_{bc} = \frac{M_{1-2}d_{cb}}{2J_{cb}} = 42 \text{ MN/m}^2$$

To this stress should be added the local bending stress introduced in the curved part of the cable in accordance with (2.61).

At the first cable clamp (where  $\Delta\varphi = \Delta\varphi_2 = 2.89 \times 10^{-3}$  rad) is found:

$$\sigma_{bl} = 2\Delta\varphi_2\sqrt{E\sigma_c} = 70 \text{ MN/m}^2$$

so that the total stress  $\sigma_{br}$  due to the cable clamp rotation becomes:

$$\sigma_{br} = \sigma_{bc} + \sigma_{bl} = 112 \text{ MN/m}^2$$

At the cable saddle the local bending is generally controlled by extending the saddle length so that the cable will have a curved support in the distorted state also. Then the total bending stress in the wires can be determined by (2.55), which was shown to give a local stress of  $\sigma_{bl} = 73 \text{ MPa}$  for a saddle with a radius of 7 m.

It appears that the total bending stresses occurring in the suspension bridge main cable are of the same magnitude as found for the bending of the stay cable.

The calculation of the bending due to the cable clamp effect has so far been based on the following two basic assumptions:

- (1) The wires are free to slip outside the cable clamps.
- (2) Any slip between wires is prevented inside the cable clamps.

In suspension bridge main cables wrapped by a wire under tension assumption 1 is not strictly valid as friction will develop between wires. However, the limiting friction shear stress is quite small as shown by T. A. Wyatt [63.1]. For a cable with a

diameter of 600 mm wrapped with a soft annealed 4 mm wire, the limiting friction shear stress is only 0.23 MPa (whereas the shear stress for a homogeneous material with a tensile strength of 1600 MPa would be approximately 920 MPa or 4000 times larger).

If slipping was prevented completely outside the cable clamps, the effective cable clamp length  $\lambda_{be}$  should be determined by inserting  $d = d_{cb} = 750$  mm in (2.65):

$$\lambda_{be} = 1.5 + \frac{0.75}{2} \sqrt{\frac{205 \times 10^3}{720}} = 7.83 \text{ m}$$

which is five times the value found when assuming wire slipping between cable clamps.

However, the value of  $\lambda_{be}$  does not have a very significant influence on the moments induced in the cable as the moment  $M_{1-2}$  merely is increased from 1.40 MN m to 1.64 MNm and  $M_{2-3}$  decreased from 0.27 MN m to 0.09 MN m when changing the value of  $\lambda_{be}$  from 1.52 m to 7.83 m.

Assumption 2 requires that the clamping force on the cable clamp is sufficient to prevent slip between the wires. According to Wyatt the maximum moment change at the band can be expressed by:

$$\max \Delta M = 1.5 \mu_c d_{cb} N_{cl} \quad (2.80)$$

where  $N_{cl}$  is the total clamping force and  $\mu_c$  the coefficient of friction between wires. For the actual case where the bulging of the cable adjacent to the band also gives a certain effect, Wyatt recommends a value of  $\mu_c$  equal to 0.25. With  $\Delta M_2 = 1.40 - 0.27 = 1.13$  MNm and  $\mu_c = 0.25$  the required clamping force to prevent wire slip will be:

$$N_{cl} = 4.02 \text{ MN} \quad (2.81)$$

A clamping force of this magnitude will often be required simply to prevent sliding of the cable clamp under the action of the hanger force, and in this case Assumption 2 will be fulfilled. However, if the clamping force is smaller than the value required to prevent wire slip due to the moment change, the calculations can be made in two steps assuming a linear relation between  $\Delta\varphi_1$  and  $\Delta M_2$  up to  $\Delta M_2 = 1.5 \mu_c d_{cb} N_{cl}$ , and subsequently neglecting clamp No. 2 for  $\Delta\varphi_1$  values above the limiting value. This implies that the additional moments remain constant from the cable saddle (point 1) to the second cable clamp (point 3).

## 2.7 Dynamic Behaviour of the Single Cable

The high stress level resulting in a small cross section, and consequently a small mass per unit length, in combination with the lack of bending stiffness, makes the individual cables sensitive to oscillations.

For the inextensible taut string under constant tension the natural vibrations are characterized by a number of equidistant nodes along the length, as illustrated in Figure 2.100.

The lowest natural frequency  $n_1 = \sqrt{g_a T / g_{cb} l^2}$  ( $g_a$  acceleration due to gravity and  $g_{cb}$  the weight per unit length of the cable) is found for the first symmetric mode vibrating in one wave with nodes at the supports only. The natural frequency  $\omega_n$  of all other modes of higher order is recovered by  $n_i = i n_1$  where  $n = 1, 2, 3, \dots$  is the number of half waves in the vibration. Thus, the symmetric modes are characterized by odd numbers and the asymmetric modes by even numbers

In reality a straight cable corresponding to the taut string can – as already emphasized before – only be found if the cable is vertical, as gravity always introduces a sag and a curvature of horizontal or inclined cables.

For the cable suspended between two points and having a vertical sag  $k$ , two basic types of vibrations exist: the sway vibration characterized by movements perpendicular to the cable plane, and the in-plane vibration (Figure 2.101) [77.1].

The natural frequencies of the sway vibration for a horizontal cable are determined by  $n_i = i \sqrt{(g_a H / g_{cb} l^2)}$  where  $i = 1, 2, 3, \dots$ . Thus the sway vibration of the sagging horizontal cable with a horizontal force  $H$  shows the same natural frequencies as the taut string with a tension  $T = H$ .

The natural in-plane vibrations of an inextensible cable suspended horizontally between fixed supports will be as shown in Figure 2.102. When comparing with the vibration of the taut string it is interesting to note that the lowest frequency is

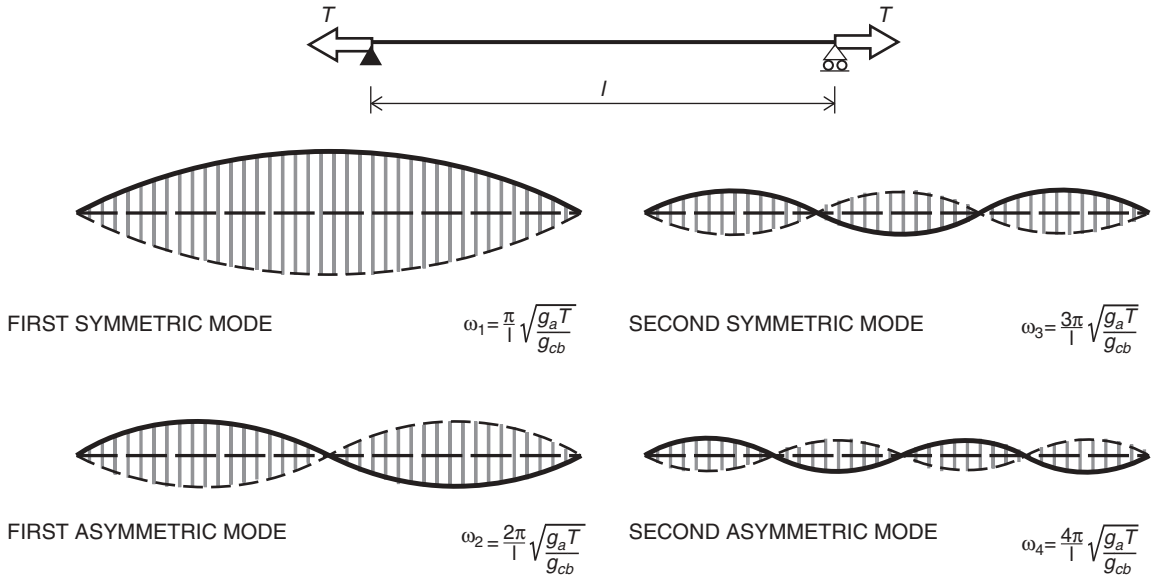


Figure 2.100 Modes of vibration for the taut string

found for an antisymmetric mode. This is due to the fact that the symmetric mode with only one half wave cannot exist if the sagging cable is inextensible and the supports are fixed.

For real cables the assumption of inextensibility leads to erroneous results especially for the symmetric modes as these will be characterized by varying tension. Thus, in the elastic cable a continuous transition from the results found for the taut string to those of the sagging cable will take place as the sag is increased. This has been shown by H. M. Irvine [81.1] and the plot in Figure 2.103 is based on his investigations.

The abscissa  $P_{ge} = (8k/l)^3 EA/g_{cb}l$  is a characteristic geometric and elastic parameter that governs the dynamic behaviour of the cable in question. It is seen that  $P_{ge}$  will take small values for long and shallow cables (large  $l$ , small  $k/l$  ratios) having small axial stiffness ( $EA_{cb}$ ).

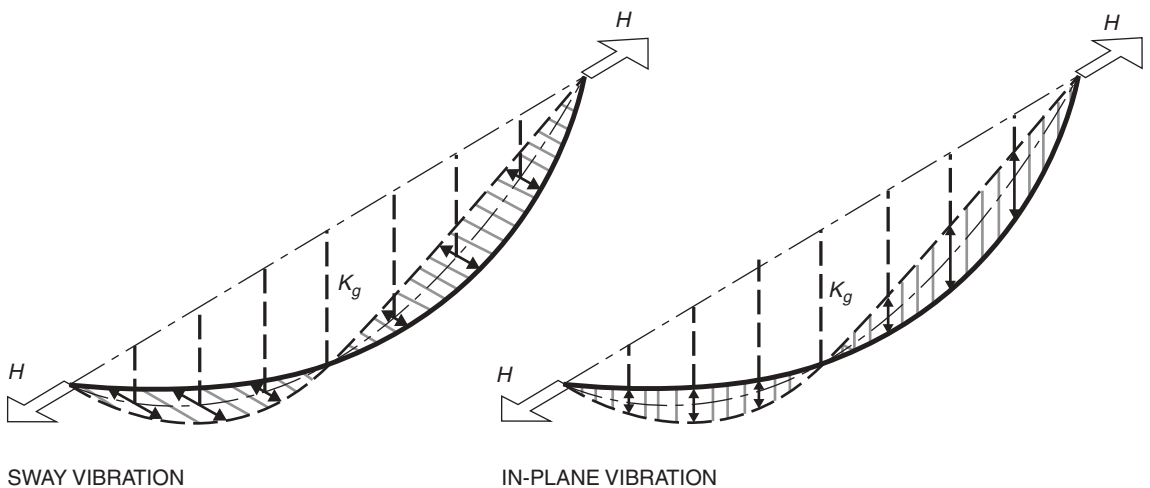


Figure 2.101 Sway vibration and in-plane vibration of a sagging cable

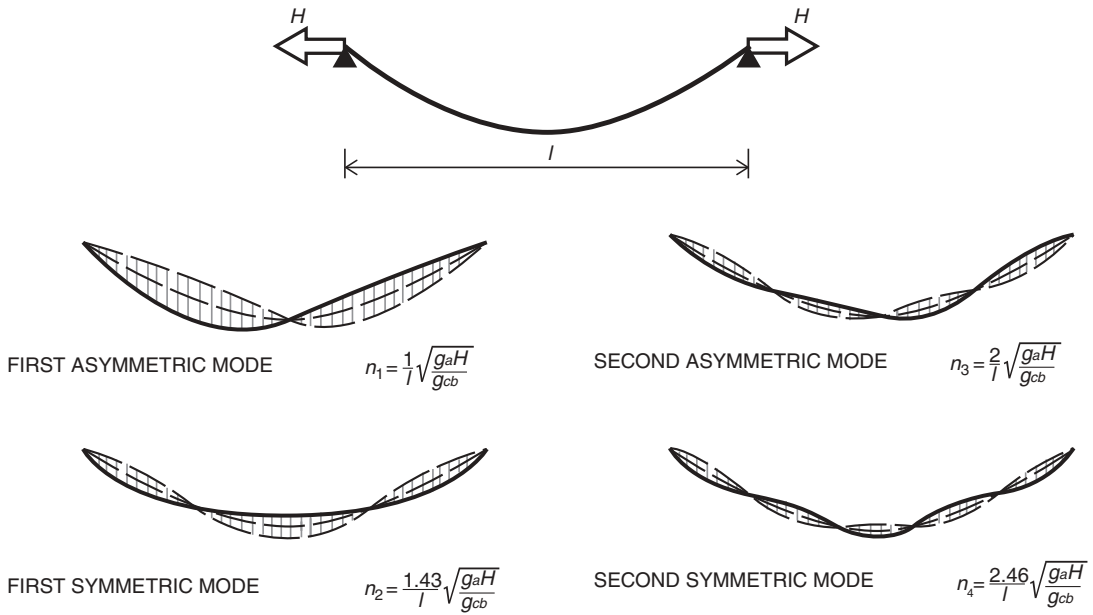


Figure 2.102 Modes of in-plane vibration for the sagging cable

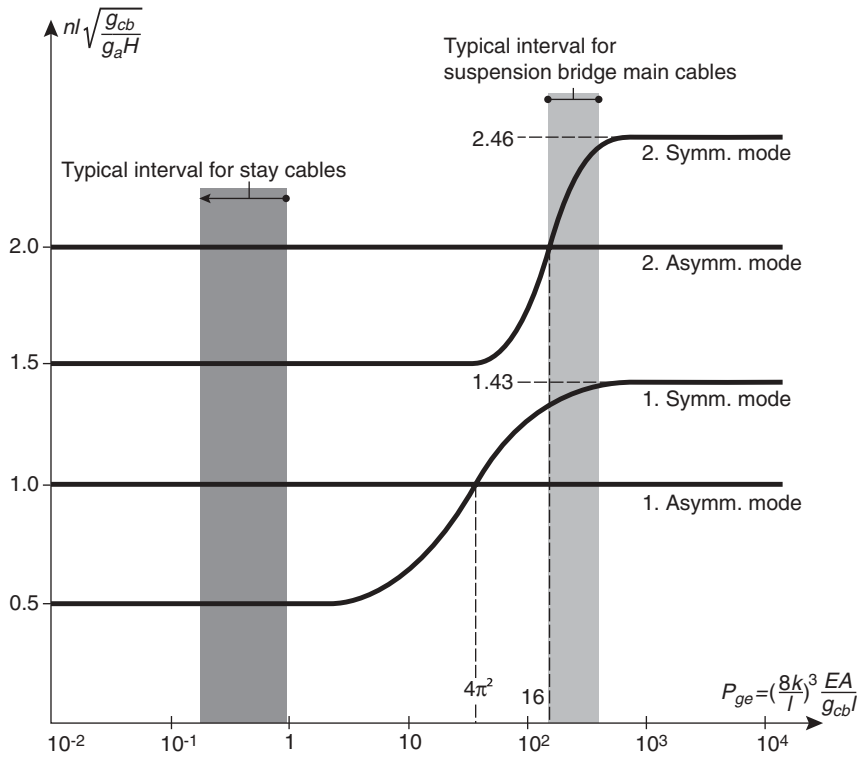
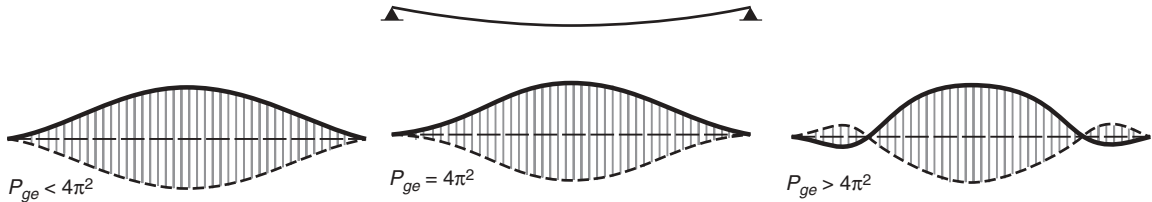


Figure 2.103 Dimensionless curves for the first four natural frequencies of a sagging cable



**Figure 2.104** Change of the first symmetric mode as the parameter  $P_{ge} = (8k/l)^3 EA_{cb}/(g_{cb}l)$  passes the value  $4\pi^2$  (the cross-over point)

For small values of  $P_{ge}$  the cable acts like a taut string with the lowest frequency found in the first symmetric mode. However, for  $P_{ge} = 4\pi^2$  the natural frequencies of the first symmetric and the first antisymmetric modes are the same, and for larger values of  $P_{ge}$  the lowest frequency is found for the first antisymmetric mode. For the second symmetric and second antisymmetric modes a similar behaviour is found. However, for these modes the cross-over point is situated at  $P_{ge} = 16\pi^2$ .

The change in the frequency of the first symmetric mode when passing the cross-over point ( $P_{ge} = 4\pi^2$ ) is reflected in the form of the vertical modal component, as shown in Figure 2.104.

For  $P_{ge} < 4\pi^2$  the first symmetric mode has no internal nodes along the span and angular changes occur at the supporting points. For  $P_{ge} = 4\pi^2$  the first symmetric mode is characterized by no angular changes at the supporting points (the tangent of the vertical modal component is fixed and horizontal). For  $P_{ge} > 4\pi^2$  the first symmetric mode has two internal nodes in a relatively small distance from the supporting points. If  $4\pi^2 < P_{ge} < 16\pi^2$  both the first and the second symmetric modes will have two internal nodes, but the nodes of the second symmetric mode will be positioned further from the supports.

For the suspension bridge main span the parameter  $P_{ge}$  can be determined by the following formula:

$$P_{ge} = 4 \frac{E}{\sigma_{cb}} \left( 1 + \frac{p}{g_{cb}} \right) \left( \frac{2k_g}{a} \right)^2 \sqrt{1 + \left( \frac{2k_g}{a} \right)^2} \quad (2.82)$$

A lower bound for the parameter  $P_{ge}$  can be found by using the following values:  $E = 170$  GPa (helical strand cables),  $\sigma_{cb} = 800$  MPa,  $p/g_{cb} = 0.2$ , and  $k_g/a = 0.18$ , and an upper bound by using  $E = 205 \times 10^3$  (parallel-wire cables),  $\sigma_{cb} = 700$  MPa,  $p/g_{cb} = 0.4$ , and  $k_g/a = 0.22$ .

Thus, the typical interval of  $P_{ge}$  for suspension bridge main span cables is determined by:

$$140 < P_{ge} < 350 \quad (2.83)$$

For stay cables the parameter  $P_{ge}$  is determined by:

$$P_{ge} = \left( \frac{\gamma_{ge}}{\sigma_{cb}} \right)^3 \frac{E}{\gamma_{eq}} \frac{a^3}{c} \quad (2.84)$$

An upper bound of  $P_{ge}$  for stay cables can be found by inserting the following values;  $E = 205$  GPa,  $\sigma_{cb} = 700$  MPa,  $\gamma_{eq} = 0.1$  MN/m<sup>3</sup>, and  $a = c = 400$  m. The lower bound of  $P_{ge}$  will be found for a vertical stay cable with  $a = 0$ . Thus, the typical interval of  $P_{ge}$  for stay cables becomes

$$0 < P_{ge} < 1 \quad (2.85)$$

In Figure 2.105 these typical intervals are indicated and it is seen that the stay cables act as taut strings with the first symmetric mode having the lowest frequency, whereas suspension bridge main span cables generally will have the lowest



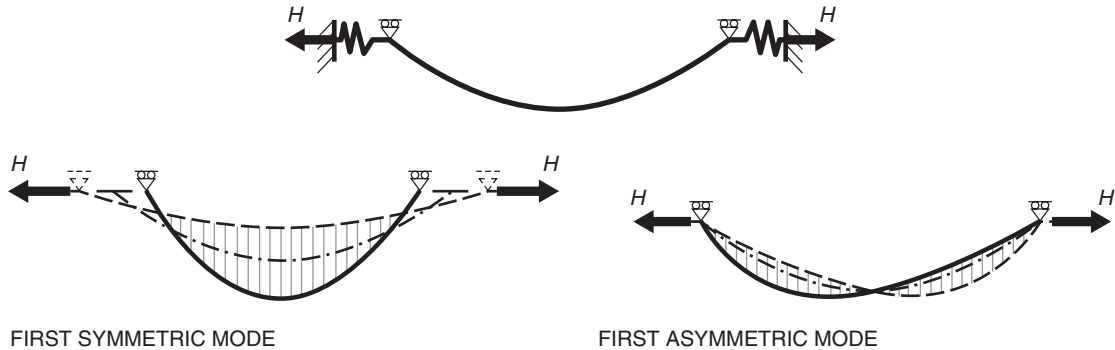


Figure 2.105 Modes of vibration for the sagging cable with flexible supports

frequency in the first antisymmetric mode. Consequently, the suspension bridge cable acts more like an inextensible, sagging cable.

A relatively simple way to determine the symmetric in-plane circular frequencies,  $\omega_{i=1,3,5,\dots}$ , of a sagging inclined stay cable for small displacements is through the evaluation of the roots of (2.86) [05.1].

$$\tan \frac{\omega_1}{2v_t} - \frac{\omega_1}{2v_l} + \frac{(\omega_1 v_t)^3}{2v_l^2} = 0 \quad (2.86)$$

where  $v_t$  and  $v_l$  are the non-dimensional transverse and longitudinal wave propagation velocities, respectively. These are defined as:  $v_t = \sqrt{T/g_{cb}l \cos \theta}$  and  $v_l = \sqrt{EA/g_{cb}l \cos \theta}$ , with  $\theta$  the angle between cable chord and the horizon.

In real structures the assumption of completely fixed supporting points, used when determining the modes of the sagging cable in Figure 2.102, is not applicable, as the pylon tops will always be characterized by a certain horizontal flexibility. Thus, the dynamic behaviour of the suspension bridge main span cable is better simulated by a structural system as shown at the top of Figure 2.105, characterized by horizontal springs at the supports.

The modes of the horizontal cable with flexible supports depend decisively on the stiffness of the springs. With springs having a large stiffness the modes will in principle be as shown in Figure 2.105 with the lowest frequency of the first antisymmetric mode. For springs with a smaller stiffness the modes will change so that the lowest frequency is found for the first symmetric mode characterized by horizontal movements of the supports and a single half wave in the span, as indicated in Figure 2.105.

It has earlier been shown that the horizontal restraint of the pylon tops depends strongly on the ratio between the side span and the main span. Consequently, short side spans correspond to large stiffness of the horizontal springs at the supporting points and long side spans to small stiffness of the horizontal springs. This difference in stiffness is reflected in the natural vibrations of the three-span cable, as shown in Figure 2.106.

With short side spans the lowest frequency is found for the first asymmetric mode with the motion concentrated in the main span so that the pylon tops practically act as fixed supports during this mode of vibration.

The second mode of the three-span cable with short side spans will be symmetrical but with two nodes in the main span and with some motion in the side spans.

With long side spans the lowest frequency corresponds to a symmetric mode with all of the three spans vibrating in single half waves, and with a considerable longitudinal movement of the intermediate supports (pylon tops).

In the given example on a three-span cable with long side spans both the second and the third modes are asymmetrical, and with a considerable motion in the side spans.

In the second mode the side span is vibrating in phase with the adjacent half of the main span and this introduces a large longitudinal movement of the cable at the main span centre, whereas the third mode is characterized by an out-of-phase motion of the side span and the adjacent main span half. This implies a much smaller movement of the cable at the main span centre.

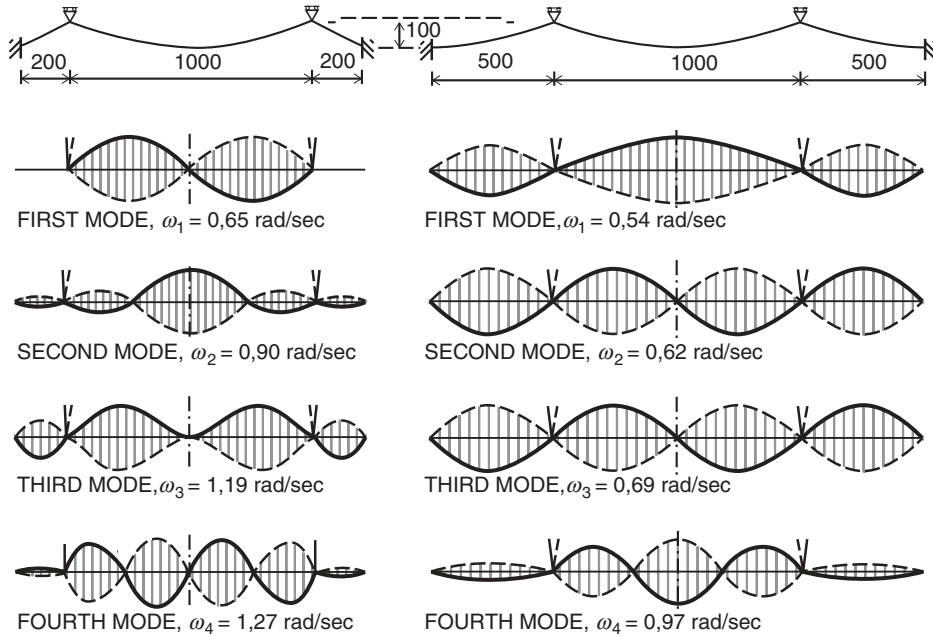


Figure 2.106 Modes of vibration for three-span cables with short side span (left) and long side spans (right)

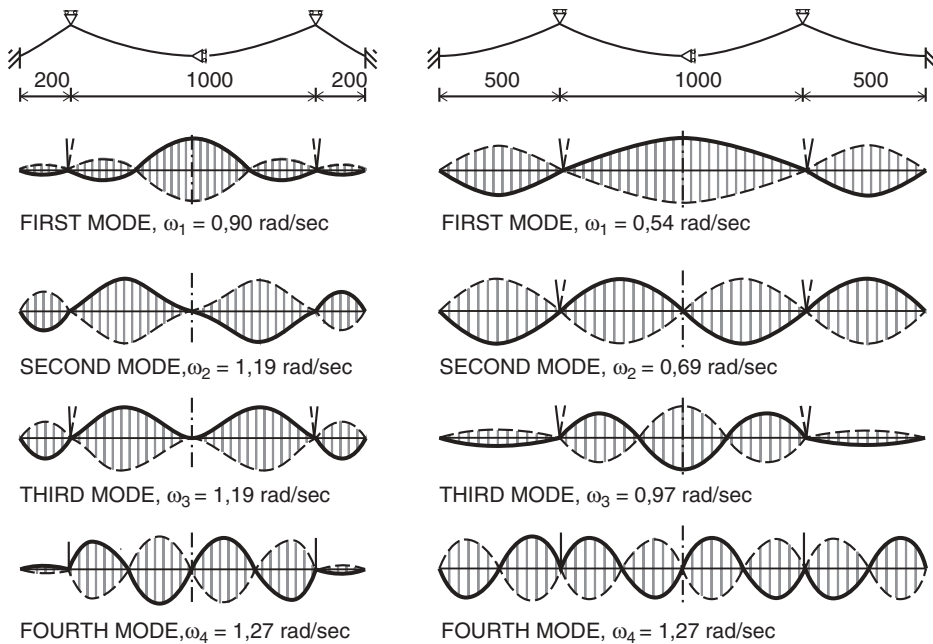


Figure 2.107 Modes of vibration for three-span cables with a central clamp

Note that the lowest frequency is increased by 20% when changing from the system with long side spans to the system with short side spans.

A central clamp restraining the main cable against longitudinal movements at the main span centre has a significant influence on the dynamic of the three-span cable with a central clamp, shown in Figure 2.107, with those of the free cable, shown in Figure 2.106.

For the cable with short side spans a central clamp excludes the formation of the symmetric mode that gave the lowest frequency of the free cable. Thus, the first mode of the centrally clamped cable becomes symmetrical, corresponding to the second mode of the free cable. This implies an almost 40% increase of the lowest frequency.

For the cable with long side spans, the introduction of a central clamp does not give any increase of the lowest frequency due to the fact that the first mode of the free cable was symmetrical. On the other hand, the central clamp excludes the second mode of the free cable as this mode was characterized by a large longitudinal movement at the main span centre. The third mode of the free cable, although asymmetrical, was characterized by small longitudinal movements at the main span centre due to the out-of-phase motion of the side span and the adjacent main span half. Consequently, the third mode of the free cable is not influenced by the introduction of a longitudinal restraint at midspan, and the third mode of the free cable therefore becomes the second mode of the centrally clamped cable.

When comparing the frequencies of the free cable (Figure 2.106) with those of the centrally clamped cable (Figure 2.107), it is evident that the introduction of the central clamp is much more advantageous with short side spans than with long side spans.

# 3

## Cable System

### 3.1 Introduction

For a cable supported bridge, the choice of the cable system is probably the most decisive factor in the design process, and it is therefore important to evaluate the characteristic behaviour of different cable systems.

Of vital importance is the quantity of cable steel required, so the description of the different cable systems shall begin with an investigation of the theoretical quantity of cable steel for some basic cable systems [80.2].

The theoretical quantity of cable steel  $Q_{cb,1}$  for a single cable with length  $l_{cb}$  and axial force  $T_{cb}$  is defined by:

$$Q_{cb,1} = \frac{\gamma_{cb}}{f_{cbd}} T_{cb} l_{cb} \quad (3.1)$$

where  $f_{cbd}$  is the design stress (allowable cable stress) and  $\gamma_{cb}$  the density of the cable material.

For a cable system composed of  $n$  cable elements the theoretical quantity for the total system is found by a summation:

$$Q_{cb} = \sum_{i=1}^n \frac{\gamma_{cb}}{f_{cbd}} T_{cb,i} l_{cb,i} = \frac{\gamma_{cb}}{f_{cbd}} \sum_{i=1}^n T_{cb,i} l_{cb,i} \quad (3.2)$$

In this summation the normal force of each cable is the maximum force corresponding to the most critical loading condition for that particular cable. However, for the most commonly used cable systems the maximum axial forces in the major part of the cables occur for loading in the entire span. Consequently, in cases where concentrated forces are of minor importance, a comparison between different cable systems can be based on only one load condition corresponding to a uniform loading of maximum intensity across the entire span.

#### 3.1.1 Pure cable systems

To arrive at some conclusions on the material consumption, the following three basic cable systems will be considered: (a) the suspension system; (b) the fan system; and (c) the harp system; as shown for a single symmetrical span in Figure 3.1. Initially, the cable systems will be treated as pure cable systems, with all elements made as cables in tension. This requires, as indicated in Figure 3.1, that the cable stayed systems (b) and (c) contain not only the inclined stay cables but also a horizontal cable connecting all points of load application.

For the suspension system loaded uniformly with  $2n$  vertical forces  $P$  acting on constantly spaced hangers in a horizontal distance of  $\lambda = l/(2n+1)$  the theoretical quantity of cable steel can be determined by a summation of the quantities in the hanger  $i-i'$  and in the main cable element  $i'-(i+1)'$ , as shown in Figure 3.2 for the right half of the system.

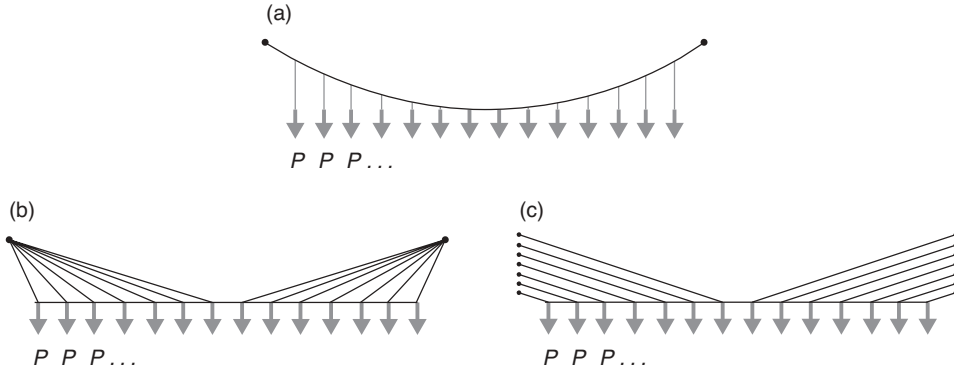


Figure 3.1 Three basic cable systems as pure cable systems with all elements in tension

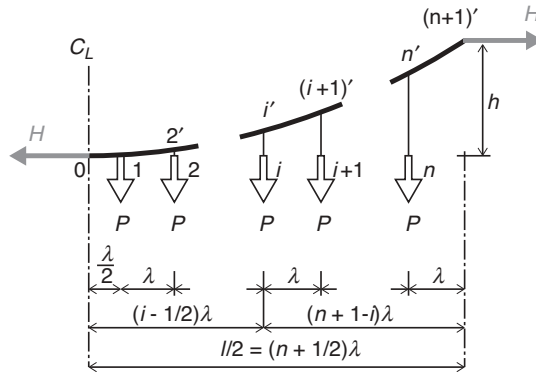


Figure 3.2 Geometry and nomenclature of the suspension system

The theoretical quantity of cable steel  $Q_{cbS}$  is now determined by:

$$Q_{cbS} = 2 \frac{\gamma_{cb}}{f_{cbd}} P \left[ \frac{1}{4} n(n+1) \frac{\lambda^2}{h} + \sum_{i=1}^n \frac{i(i-1)}{n(n+1)} h + \sum_{i=1}^n \frac{n(n+1)}{2h} \left( \lambda^2 + \frac{4h^2}{n^2(n+1)^2} i^2 \right) \right] \quad (3.3)$$

where the first term is the quantity of the cable 0–1, the second term the quantity of the hangers (summation of  $i-i'$ ) and the third term the quantity of the main cable 1– $(n+1)'$  (summation of  $i'-(i+1)'$ ).

The following expression for  $Q_{cbS}$  can now be derived:

$$Q_{cbS} = 2nP \left( h + (n+1)(2n+1) \frac{\lambda^2}{4h} \right) \frac{\gamma_{cb}}{f_{cbd}} \quad (3.4)$$

or, with  $\lambda = l/(2n+1)$ :

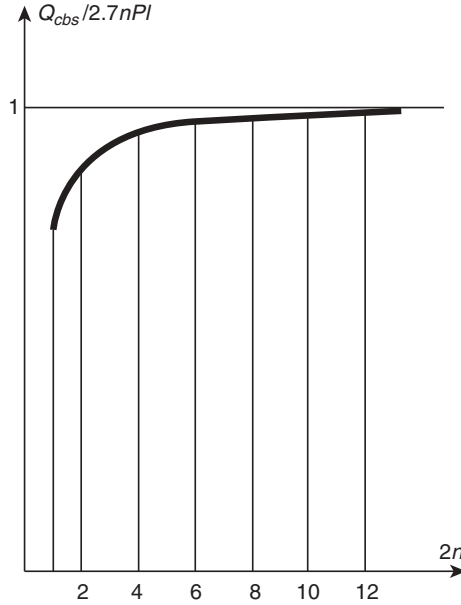
$$Q_{cbS} = 2nP \left( h + \frac{n+1}{2n+1} \frac{l^2}{4h} \right) \frac{\gamma_{cb}}{f_{cbd}} \quad (3.5)$$

Assuming a large number of hangers, the asymptotic value of  $Q_{cbS}$  (for  $n \rightarrow \infty$ ) can be used:

$$Q_{cbS} = pl \left( h + \frac{l^2}{8h} \right) \frac{\gamma_{cb}}{f_{cbd}} \quad (3.6)$$

where  $p (= P/\lambda)$  is the load per unit length.

The variation of the theoretical cable steel quantity with the number of hangers can be studied by plotting the ratio  $q_{cbS}$  between  $Q_{cbS}$  from (3.5) and  $Q_{cbS}$  from (3.6).



**Figure 3.3** Influence of hanger spacing on the quantity of cable steel  $Q_{cbs}$  for a suspension system with  $h/l = 0.1$  ( $2n$  is the number of hangers)

With  $P = p\lambda = pl/(2n + 1)$  replaced into (3.5) the ratio  $q_{cbs}$  becomes:

$$q_{cbs} = \frac{\frac{n}{2n+1}h + \frac{n(n+1)}{(2n+1)^2} \frac{l^2}{4h}}{h + \frac{l^2}{8h}} \quad (3.7)$$

For a suspension system with  $h/l = 0.1$ , the variation of  $q_{cbs}$  with the number of hangers is plotted in Figure 3.3. From this plot it appears that the theoretical quantity of cable steel shows a very moderate variation with the number of hangers, and already for systems with 10 hangers the difference between  $Q_{cbs}$  from (3.5) and  $Q_{cbs}$  from (3.6) is less than 1.5%. Consequently, the asymptotic value is adequate for all practical applications.

For the fan system shown in Figure 3.4 the theoretical quantity  $Q_{cbF}$  is determined by:

$$Q_{cbF} = 2 \frac{\gamma_{cb}}{f_{cbd}} P \left( \sum_{i=1}^n (n-i+1) \left( i - \frac{1}{2} \right) \frac{\lambda^2}{h} + \sum_{i=1}^n [(n-i+1)^2 \lambda^2 + h^2] \frac{l}{h} \right) \quad (3.8)$$

the first term includes the summation of the horizontal cable elements  $0-i$  and the second the summation of the inclined elements  $i-(n+1)'$ .

The following expression for  $Q_{cbF}$  can now be derived:

$$Q_{cbF} = 2nP \left( h + (n+1)(2n+1) \frac{\lambda^2}{4h} \right) \frac{\gamma_{cb}}{f_{cbd}} \quad (3.9)$$

which is exactly the same expression as found for the suspension system.

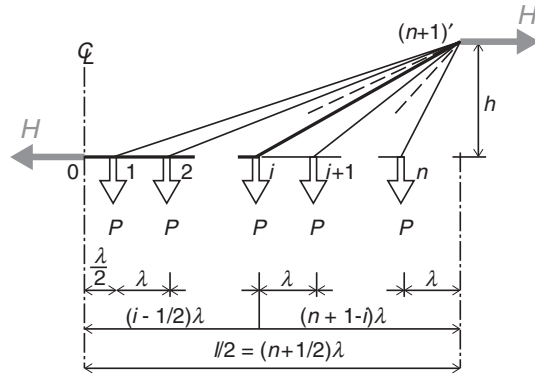


Figure 3.4 Geometry and nomenclature of the fan system

For the harp system shown in Figure 3.5 the following expression for the theoretical quantity  $Q_{cbH}$  is found correspondingly:

$$Q_{cbH} = 2nP \left( \frac{n+1}{2n} h_H + n \left( n + \frac{1}{2} \right) \frac{\lambda^2}{h_H} \right) \frac{\gamma_{cb}}{f_{cbd}} \quad (3.10)$$

where  $h_H$  is the height of the harp system. The horizontal force  $H_H$  of the harp system, defined as the sum of the horizontal cable components, can be expressed by:

$$H_H = nP \frac{n\lambda}{h_H} = n^2 P \frac{\lambda}{h_H} \quad (3.11)$$

The horizontal force  $H_S$  of the suspension system is found from:

$$H_S = \frac{n(n+1)}{2} P \frac{\lambda}{h_S} \quad (3.12)$$

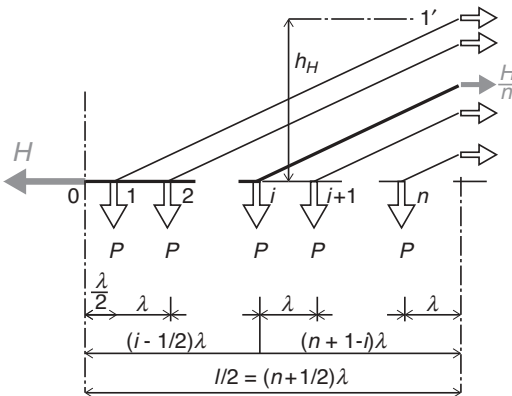
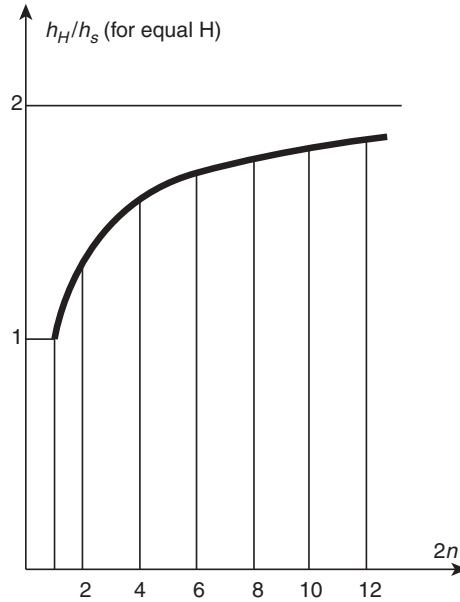


Figure 3.5 Geometry and nomenclature of the harp system



**Figure 3.6** Variation of the ratio between the height  $h_H$  of a harp system and the height  $h_S$  of a suspension system with equal horizontal force ( $2n$  is the number of loading points = number of hangers)

Equal horizontal force for the suspension system and the harp system leads to the following ratio  $h_H/h_S$ :

$$\frac{h_H}{h_S} = \frac{2n}{n+1} \quad (3.13)$$

In Figure 3.6 is shown the variation of the ratio  $h_H/h_S$  (for equal horizontal force  $H$ ) with the number  $2n$  of loading points. It appears that the ratio increases with the number of loading points and that the asymptotic value is 2. Consequently, for multi-cable systems, the height of the harp system should be chosen to be twice the height of the suspension system to achieve equal horizontal force.

Introducing  $h_H = 2nh_S/(n+1)$  from (3.13) into (3.10) yields:

$$Q_{cbH} = 2nP \left( h_S + (n+1)(2n+1) \frac{\lambda^2}{4h_S} \right) \frac{\gamma_{cb}}{f_{cbd}} \quad (3.14)$$

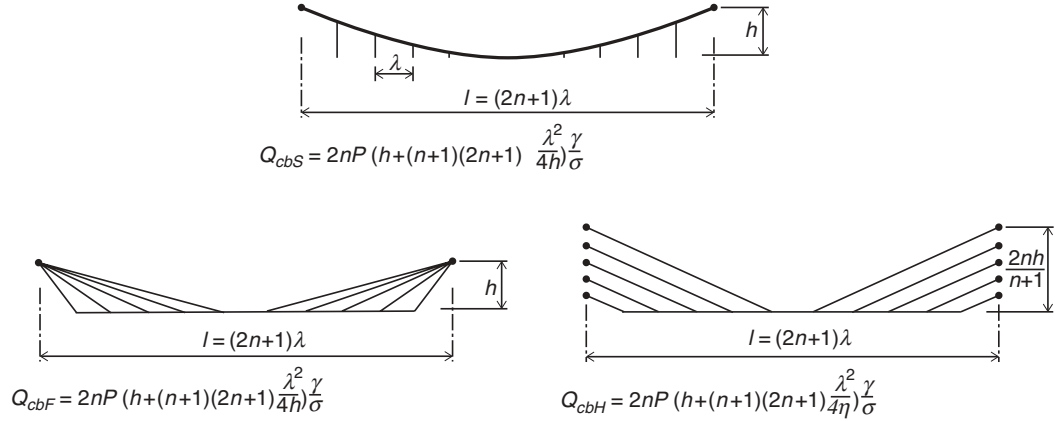
again exactly the same expression as found for the suspension system (refer to (3.4)). So the same theoretical quantity of cable steel will be found for a pure harp system and a pure suspension system if they have the same horizontal force at midspan.

The above results are summarized in Figure 3.7 showing the three basic cable systems with configurations leading to equal horizontal force. Note that the height of the suspension system and the fan system is the same, whereas the harp system is higher in accordance with the previous investigation.

As the theoretical quantity of cable steel is exactly the same for the three cable systems, the following theorem on the constancy of cable steel quantity can be deduced:

For pure cable systems (with all elements as cables in tension), subjected to uniform load, the theoretical cable steel quantity is the same for the suspension system, the fan system, and the harp system with equal horizontal force.





**Figure 3.7** Theoretical quantity of cable steel for the three basic cable systems with equal horizontal force

This theorem constitutes an important link in the understanding of the characteristics of the cable systems. However, the theorem is only of theoretical interest as pure cable systems are not applied in cable stayed bridges. Here the horizontal cable elements connecting the points of load application are replaced by the deck and the cable steel quantity should consequently only include the inclined stay cables.

### 3.1.2 Cable steel quantity comparison

The theoretical quantity  $Q_{cbFs}$  of cable steel in the stay cables of the fan system is found by including only the second term in (3.8) in the summation. This leads to the following expression:

$$Q_{cbFs} = 2nP \left( h_F + \frac{1}{6} (n+1)(n+2) \frac{\lambda^2}{h_F} \right) \frac{\gamma_{cb}}{f_{cbd}} \quad (3.15)$$

For multi-cable systems with a large number of stay cables the asymptotic value for  $n \rightarrow \infty$  can be used with sufficient accuracy:

$$Q_{cbFs} = pl \left( h_F + \frac{l^2}{12h_F} \right) \frac{\gamma_{cb}}{f_{cbd}} \quad (3.16)$$

Correspondingly, the theoretical quantity  $Q_{cbHs}$  of cable steel in the stay cables of the harp system can be expressed by:

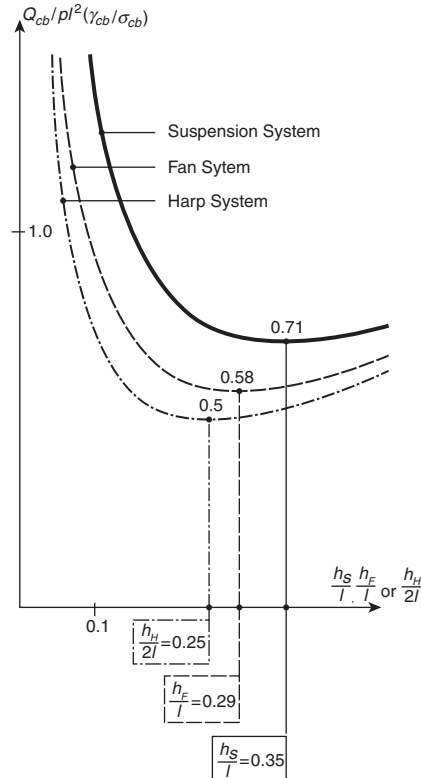
$$Q_{cbHs} = 2nP \left( \frac{n+1}{2n} h_H + \frac{n(n+1)}{2} \frac{\lambda^2}{h_H} \right) \frac{\gamma_{cb}}{f_{cbd}} \quad (3.17)$$

with the asymptotic value:

$$Q_{cbHs} = pl \left( \frac{h_H}{2} + \frac{l^2}{8h_H} \right) \frac{\gamma_{cb}}{f_{cbd}} \quad (3.18)$$

For the suspension system, the deck cannot be used to replace any cable element and the theoretical quantity of cable steel is therefore determined by (3.6):

$$Q_{cbS} = pl \left( h_S + \frac{l^2}{8h_S} \right) \frac{\gamma_{cb}}{f_{cbd}} \quad (3.19)$$



**Figure 3.8** Variation of the cable steel quantity with the relative pylon height

Figure 3.8 shows the variation of the cable steel quantity for the three basic cable systems. It is seen that the harp system shows the smallest quantity and the suspension system the largest. Minimum quantity of cable steel is achieved for

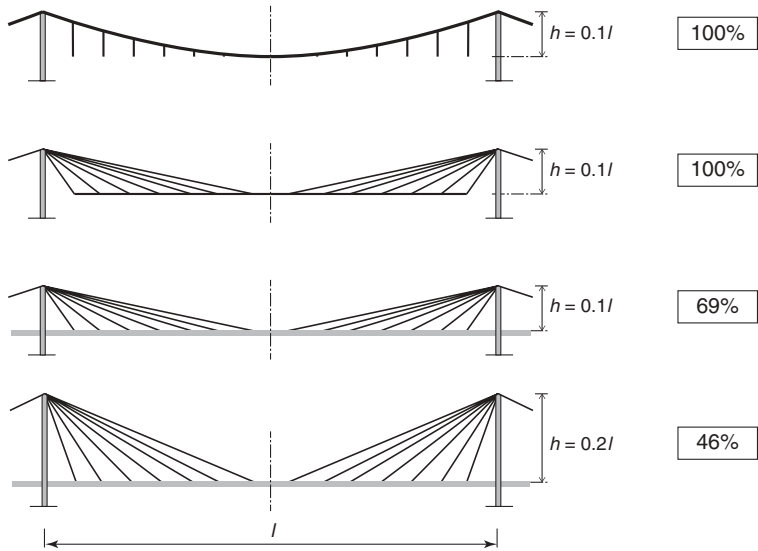
$$\begin{aligned}
 h_S/l &= 0.35 && \text{for the suspension system} \\
 h_F/l &= 0.29 && \text{for the fan system} \\
 h_H/l &= 0.50 \quad (h_H/2l = 0.25) && \text{for the harp system}
 \end{aligned}$$

The  $h/l$  values used in actual structures are smaller than these values as the optimization must take into account the material of the pylon. For the suspension system stiffness requirements furthermore prescribe  $h/l$  values in the interval from 0.08 to 0.12.

In Figure 3.9 the savings to be achieved by the fan system are illustrated for a typical case. If the suspension system is changed to a fan system with the same height and with all elements as cables in tension the cable steel quantity remains the same, as stated in the previous theorem. But by replacing the horizontal cable elements by the deck, the cable steel quantity is reduced to 69%. If finally the pylon height is increased to one-fifth of the span length, then the theoretical cable steel quantity is reduced further to only 46%.

The investigations into the cable steel quantity described above are of a very simplified nature as only one symmetrical span is considered and the consequences on other quantities (in the deck and the pylons) are omitted. Also, the weight of the cable system itself has not been taken explicitly into account.

To give an indication of the influence by taking the pylon material into consideration the very basic systems of Figure 3.10 will be investigated. The system at the top consists of just the stay cable subjected to a vertical force  $P$  acting at the lower end.



**Figure 3.9** Savings in cable steel of the fan system by substituting the horizontal cables by the deck and increasing the pylon height

With the notation of Figure 3.10 the quantity of cable material is expressed by:

$$Q_{cb} = (\gamma_{cb}/f_{cbd})(h + \lambda^2/h)P \tag{3.20}$$

The height  $h_{opt}$  giving minimum quantity of cable steel in the stay cable is found from:

$$\partial Q_{cb}/\partial h = 0$$

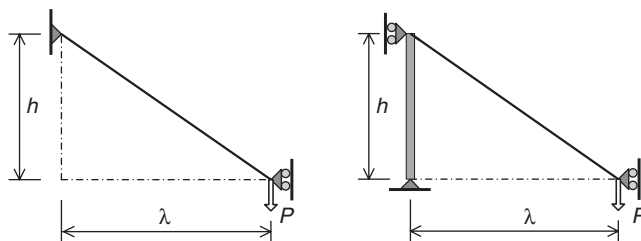
leading to  $h_{opt} = \lambda$ , i.e. a stay cable inclination corresponding to an angle of  $45^\circ$ .

For the system to the left in Figure 3.10 the vertical deflection  $\delta$  at the lower stay cable anchorage can be expressed:

$$\delta = (f_{cbd}/E)(h + \lambda^2/h) \tag{3.21}$$

As this equation contains  $h$  in the same way as (3.20) the minimum deflection is also found for  $h = \lambda$  so also when considering the stiffness the optimum stay cable inclination is found for an angle of  $45^\circ$ .

The system to the right in Figure 3.10 consists of not only the stay cable but also a vertical element that corresponds to the pylon.



**Figure 3.10** Basic systems with cable support: (left) stay cable alone; (right) stay cable + pylon

With a unit price of  $u_{cb}$  for the cable material and  $u_{pl}$  for the pylon material the cost  $C_{cp}$  of the total system becomes:

$$C_{cp} = u_{cb} \frac{\gamma_{cb}}{f_{cbd}} \left( h + \frac{\lambda^2}{h} \right) P + u_{pl} \frac{\gamma_{pl}}{f_{pld}} h \quad (3.22)$$

The minimum cost is found for  $\partial C/\partial h = 0$  which leads to the following expression for  $h_{opt}$ :

$$h_{opt} = \frac{\lambda}{\sqrt{1 + \frac{u_{pl} \gamma_{pl} f_{cbb}}{u_{cb} \gamma_{cb} f_{pld}}}} \quad (3.23)$$

It is seen that for  $u_{pl} = 0$  (ignoring the pylon contribution), (3.23) leads to  $h = \lambda$ , but for any other (positive value) of  $u_{pl}$ ,  $h_{opt}$  from (3.23) will be smaller than  $\lambda$ . This was of course to be expected as the contribution from the pylon will tend to favour a reduced height  $h$ .

With typical values as  $u_{cb} = 2.5u_{pl}$ ;  $\gamma_{pl} = \gamma_{cb}$ ;  $f_{cbd} = 5f_{pld}$ , (3.23) yields  $h_{opt} = \lambda/\sqrt{3}$  so that in this more realistic case the angle of the stay cable should be chosen at  $30^\circ$ , i.e. considerably less than when disregarding the pylon contribution.

For  $h = \lambda/\sqrt{3}$  the deflection  $\delta$  due to the stay cable elongation will be (from (3.21)):  $\delta = 4\lambda f_{cb}/E\sqrt{3}$  – a value which is only 15% larger than the value for  $h = \lambda$ .

### 3.1.3 Stability of the cable system

When studying the stiffness properties of a cable supported bridge under the action of traffic load it is advantageous to evaluate separately the rigidity offered by the cable system. Under this evaluation the definition of the ‘cable system’ should preferably be somewhat widened as shown in the following.

In the traditional earth anchored suspension bridge the cable system can be defined simply as the structural elements made up of cables, i.e. the system, consisting of the main cable and the hangers, as indicated in Figure 3.11.

In a cable stayed bridge a similar definition does not make sense, as the system consisting of only the stay cables will be unable to resist any loading in the vertical direction. The cable system should, therefore, be represented not only by the cables themselves but also by the parts of the deck and pylons resisting axial forces induced by the horizontal or vertical components of the cable forces at the anchor points.

In accordance with this definition the cable system of a cable stayed bridge will be as shown at the bottom of Figure 3.12. By introducing hinges at all cable anchor points and at the intersection between the deck and the pylons, it is ensured that only the axial force resistance of the deck and pylons is included in the ‘cable system’.

With this definition, the cable systems found within cable supported bridges can be divided into the following three groups:

- (1) A cable system stable of the first order. In this system, equilibrium can be achieved without assuming any displacement of the nodes.

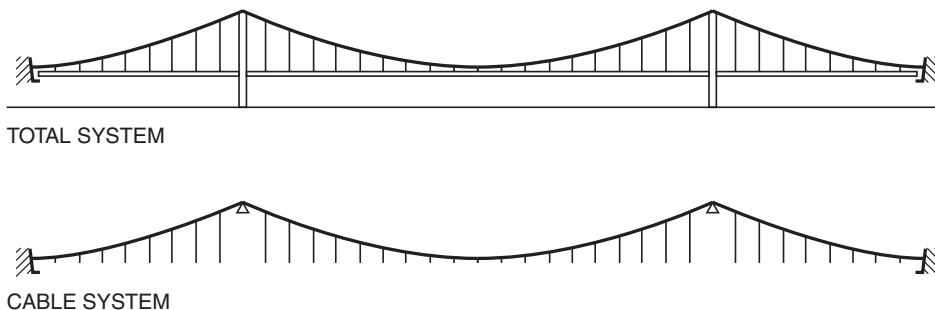
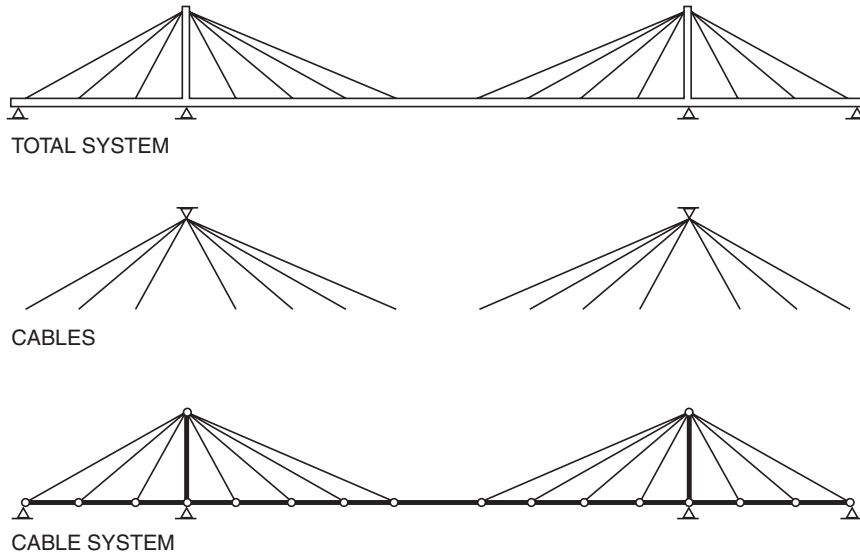


Figure 3.11 Cable system of a suspension bridge (main cable + hangers)



**Figure 3.12** Cable system of a cable stayed bridge (stay cables + parts of the deck and pylons transmitting axial forces)

- (2) A cable system stable of the second order. In this system, equilibrium can only be achieved with nodes displaced under the action of the external load.
- (3) An unstable cable system. In this system, equilibrium cannot be achieved by the cable system itself.

Simple examples of the three types of cable systems are shown in Figure 3.13.

Of the cable systems used in cable supported bridges the fan-shaped system, shown in Figure 3.14, is a typical example of a system stable of the first order. That this is the case can be deduced when considering that any of the partial systems ABCD corresponds to the basic triangulated system with two supporting points (see Figure 3.13 (a)).

Note that the cable A–D forms a part of all the stable partial systems, and this cable is therefore denoted the anchor cable (or backstay), whereas all the other cables are denoted stay cables.

As the stability of the fan-shaped system depends to a large extent on the fixing of all stay cables to the pylon top, so that the horizontal component of the force in any stay cable (e.g. cable C–D of Figure 3.14) can be transferred to the anchor cable. If a set of stays is connected to the pylon by longitudinal movable bearings - as has been the case in some early cable stayed bridges - the system becomes unstable. This will be understood when considering that the partial system EFCB of Figure 3.15 corresponds to the system of Figure 3.13 (c).

Thus, the fan-shaped cable system with an anchor cable will be stable of the first order for traffic load acting in the main span, and for traffic load in the side span up to a certain limiting intensity. For side span loading above this limiting intensity, the fan-shaped cable system will become unstable.

It should be emphasized that the stability of the fan system depends on the fixing of all stay cables to the pylon top, so that the horizontal component of the force in any stay cable (e.g. cable C–D of Figure 3.14) can be transferred to the anchor cable. If a set of stays is connected to the pylon by longitudinal movable bearings - as has been the case in some early cable stayed bridges - the system becomes unstable. This will be understood when considering that the partial system EFCB of Figure 3.15 corresponds to the system of Figure 3.13 (c).

The cable system found in the traditional suspension bridge, shown in Figure 3.16, is a typical example of a system that is stable of the second order. This has already been illustrated in Section 2.4 where the displacement of a single cable under varying loads was treated.

As a downwards, vertical load in any point will increase the tension of the main cable, the suspension system will remain stable of the second order for any loading caused by gravity.

The harp-shaped cable system of Figure 3.17 is an example of an unstable cable system. That this is the case will be understood when considering that the partial system ABCD corresponds to the basic system of Figure 3.13 (c). Only the upper partial system  $A_0BC_0D_0$  will be stable (of the first order) as this system corresponds to the basic system of

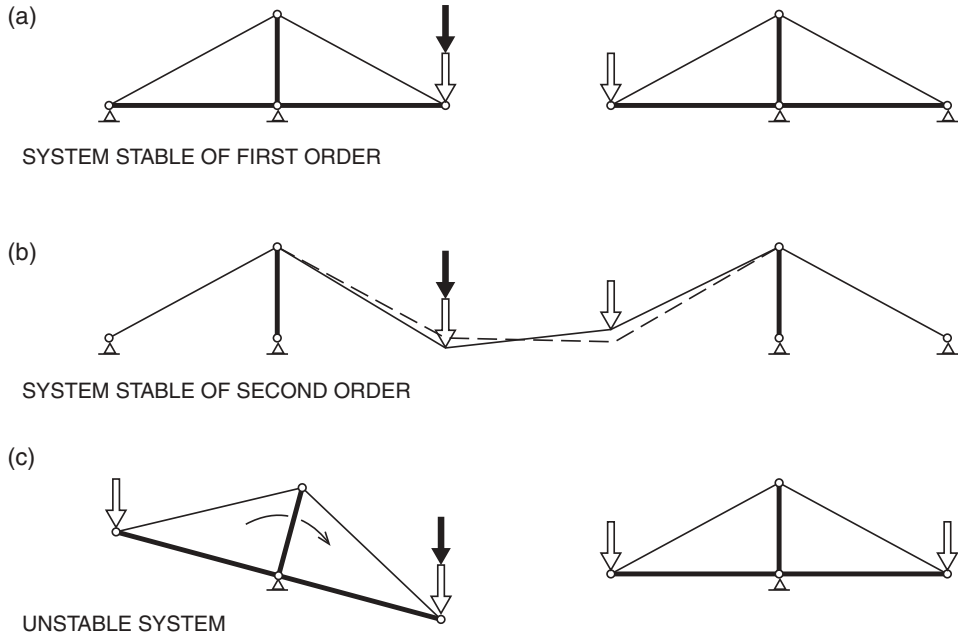


Figure 3.13 Cable systems being stable of the first order, stable of the second order, and unstable

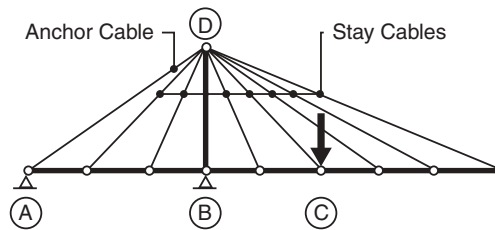


Figure 3.14 Fan system (stable of the first order)

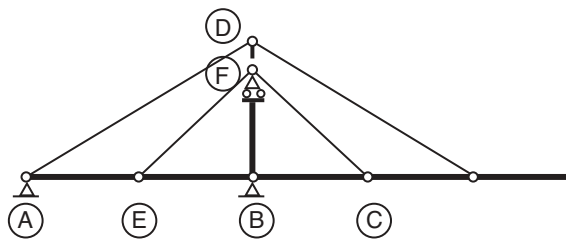


Figure 3.15 Fan system with a movable bearing between a stay set and the pylon

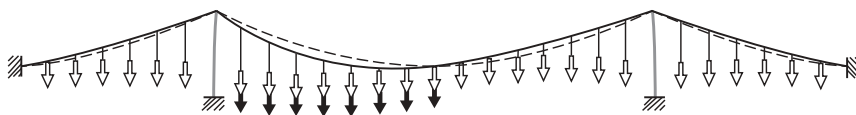


Figure 3.16 Earth anchored suspension system (stable of the second order)

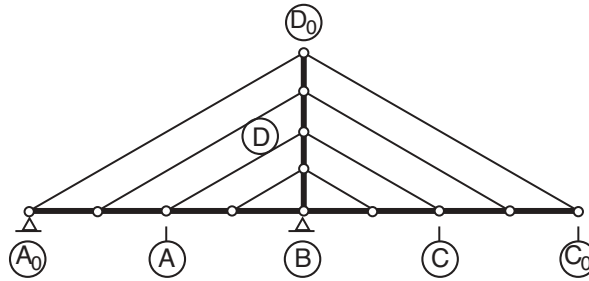


Figure 3.17 Harp system (unstable cable system)

Figure 3.13(a). The fact that the harp system is an unstable cable system does not imply that the total structural system of the bridge is unstable, as the flexural stiffness of the deck and the pylons will add the stability that is lacking in the cable system itself. The instability of the harp system is not astonishing as this system is composed of quadrangles, in contrast to the fan system containing exclusively triangles.

A complete stabilization of the harp system can be obtained if intermediate supports are added in the side spans under the cable anchor points (Figure 3.18). In this case, every partial system ABCD corresponds to the basic system of Figure 3.13 (a), and the total cable system is therefore stable of the first order.

The application of intermediate supports in the side span can be seen in several large bridges with harp-shaped cable systems. Figure 3.19 shows an early and still very prominent example: the Oberkasseler Bridge in Düsseldorf.

From the systems already described it will be seen that self anchored cable stayed bridges might have either cable systems that are stable of the first order, or unstable. Often only smaller changes in the supporting conditions or addition of a few structural elements are required to change the system from unstable to stable of the first order.

To illustrate this, Figure 3.20 shows a number of solutions for a two-span cable stayed bridge with fan-shaped cable systems. All of the bridge systems have a symmetric superstructure with two spans of equal length on either side of the central pylon.

The straightforward solution shown under (a) contains an unstable cable system as is seen clearly from the draft of the cable system. This shows that the application of a triangulated fan system is not in itself sufficient to assure stability of the cable system. The missing link in System (a) is the anchor cable restraining the pylon top from moving horizontally. In the symmetrical two span bridge, two anchor cables are required to arrive at a cable system that is stable of the first order, as shown under (b).

When comparing Systems (a) and (b), it is seen that stability is achieved when the pylon top is supported longitudinally by the anchor cables.

In System (c) the pylon top is restrained longitudinally by application of a free-standing, two-legged A-shaped pylon structure. With movable bearings at the two ends the deck is not directly fixed longitudinally, but it is restrained by the anchor cable that will be in tension.

A full horizontal fixation of the deck is simply achieved by changing one of the end supports from movable to fixed, as indicated under (d). The system is now asymmetric which might give some inconvenience regarding deformations under temperature changes, but for vertical load a stability of first order is achieved.

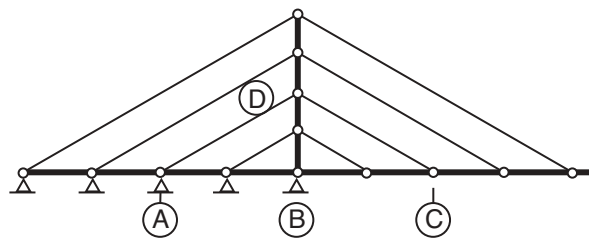


Figure 3.18 Harp system with intermediate supports in the side span



Figure 3.19 Oberkasseler Bridge in Düsseldorf (harp system with intermediate supports in the side span)

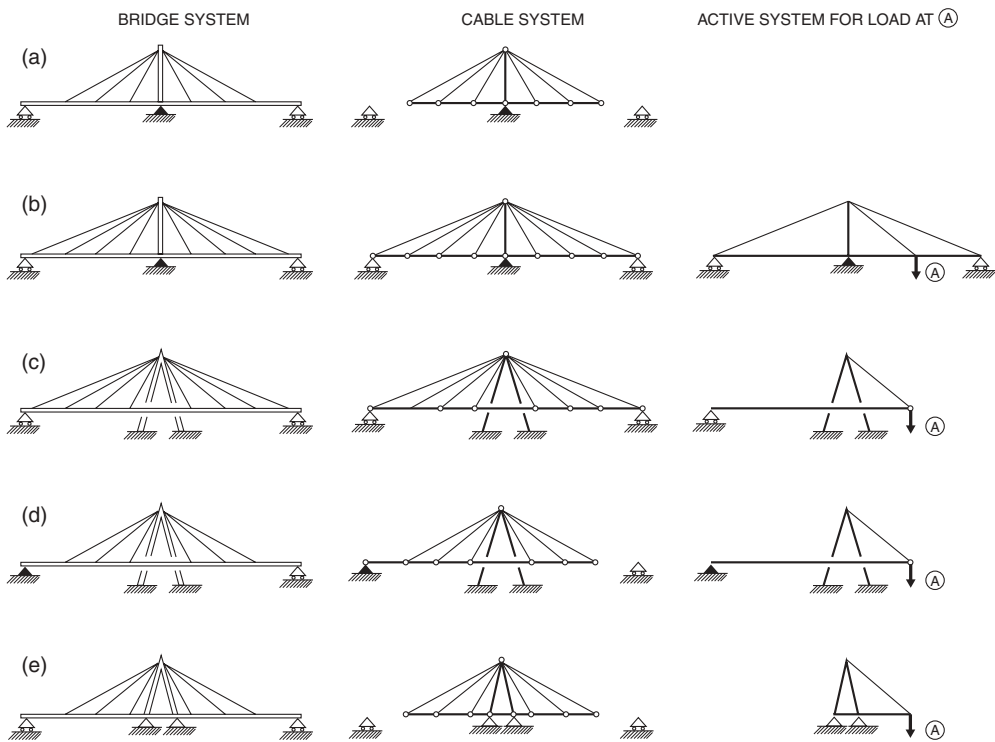


Figure 3.20 Structural systems of a symmetrical two-span cable stayed bridge



In the systems shown under (c) and (d) the pylon structure is assumed to have no direct contact with the deck.

Under (e) is shown a system where the pylon legs are fixed to the deck, which excludes mutual movements of the deck and the pylon top. This implies that the cable system becomes stable of the first order.

When comparing Systems (d) and (e), it should be noted that in (e) vertical load only produces vertical reactions, whereas considerable horizontal reactions will occur in system (d) for asymmetric vertical loading.

From the examples shown in Figure 3.20 it is clear to see that often it requires only small alterations to make the cable system stable of the first order instead of unstable.

In the total structural system of the bridge the cable system only forms one part, and the total system can therefore very well show a satisfactory load-carrying capability, even if the cable system is unstable. However, it will be found that the global stiffness and the load-carrying efficiency of the total system depend to a very large extent on the cable system and especially if the deck is slender and has a modest flexural stiffness.

A comparative investigation of solutions with varying stability of the cable systems will clearly show the advantages of applying systems that are stable of the first order.

The early cable stayed bridge on the elevated highway in Ludwigshafen in Germany (Figure 3.21) had a cable system in the main span corresponding to that of Figure 3.20 (c), but without cables to the end supports.

Figure 3.22 shows a structural system designated System A, which corresponds in principle to the one applied in the Ludwigshafen Bridge, and this system is compared to a system equal to that shown in Figure 3.20 (e), here designated System B. For both systems, dimensions of corresponding structural elements (cables and deck sections) are chosen to have the same values.

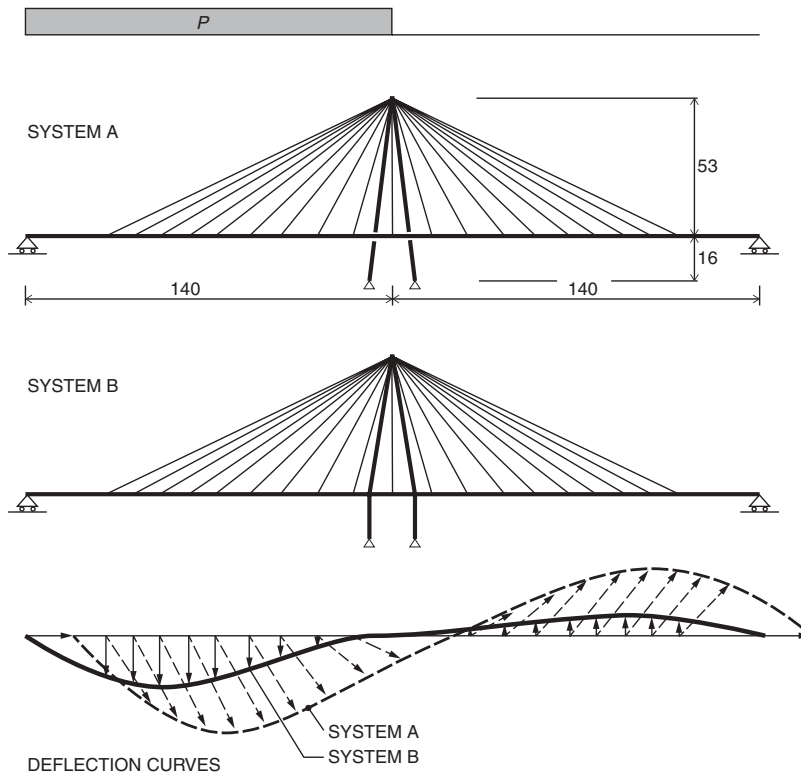
The main difference between the two systems relates to the connection between the deck and the pylon structure. In System A the two elements are connected through the stay cables only and the deck consequently has no direct restraint to move both longitudinally and vertically at the pylon. In System B the pylon legs are fixed to the deck and no mutual displacements can take place. In both systems the deck has longitudinally movable bearings at both ends.

For a load symmetrical about the pylon structure, the two systems will have almost identical deflections, but for asymmetrical loading a significant difference will occur.

In System A the stability of the total system depends decisively on the flexural stiffness of the deck as the cable system itself is unstable. Under asymmetric load the deck moves longitudinally towards the unloaded span and that reduces the



**Figure 3.21** Two-span cable stayed bridge in Ludwigshafen, Germany



**Figure 3.22** Comparison between deflections of two different structural systems

efficiency of all stays as support members. In combination with the limited flexural stiffness of the slender deck, considerable deflections will occur.

In System B the deck is prevented from moving longitudinally in relation to the pylon structure, and this reduces the deflections of the deck to less than half of those occurring in System A. Also, the bending moments in the deck and the stress ranges in the stay cables are smaller in System B than in System A. From this example it is learned that, although stability of the total system is present both with the unstable and the stable cable system, the latter offers considerable advantages with regards to both stiffness and load-carrying capacity.

## 3.2 Suspension System

In the traditional earth anchored suspension bridge each main cable is supported at four points: at the two anchor blocks and on the two pylon tops. The supporting points at the anchor blocks can generally be assumed to be completely fixed both vertically and horizontally, whereas the supporting points at the pylon tops often are represented best by longitudinally movable bearings (due to the horizontal flexibility of the slender pylon legs). Therefore the general arrangement of the suspension bridge cable system will be as shown in Figure 3.23.

### 3.2.1 Dead load geometry

The geometry of the cable system in the dead load condition is generally chosen so that the deck and the pylons are moment-free at mean temperature. To achieve this, the cable curve must coincide with the funicular curve of the total dead load.

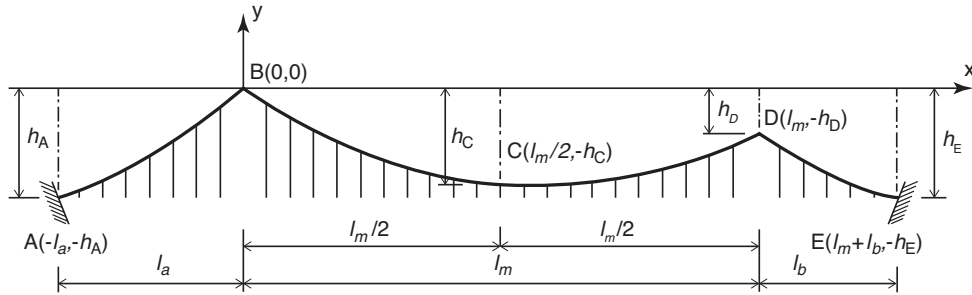


Figure 3.23 Three-span, suspension bridge cable system

The main cable geometry can then be expressed by the following equations, based on (2.4):

$$y = \begin{cases} -\frac{M_a(x)}{H} + \frac{h_A}{l_a}x & -l_a < x < 0 \\ -\frac{M_m(x)}{H} - \frac{h_D}{l_m}x & 0 < x < l_m \\ -\frac{M_b(x)}{H} - \frac{h_D - h_E}{l_b}(x - l_m) - h_D & l_m < x < l_m + l_b \end{cases} \quad (3.24)$$

where  $M_a(x)$ ,  $M_m(x)$ , and  $M_b(x)$  are the moments of simply supported beams with lengths  $l_a$ ,  $l_m$ ,  $l_b$  subjected to the total dead load of main cable, hangers, and deck. To be correct, the dead load should be applied to the main cable as concentrated forces acting at each cable clamp position for the contribution from the dead load of the deck and hangers, whereas the dead load of the main cable itself should be applied as a distributed load. However, in suspension bridges with a large number of closely spaced hangers, all dead load might be assumed to act as a distributed load as a very good approximation.

Besides stipulating the position of the supporting points A, B, D and E, the general geometric conditions of the bridge often lead to a predetermined position of the midspan point C in the main span. The horizontal force  $H$  can then be found from:

$$H = \frac{M_m(l_m/2)}{h_C - h_D/2} \quad (3.25)$$

where  $M_m(l_m/2)$  is the simple moment at the main span centre and  $h_C - h_D/2$  the cable sag at midspan. (3.24) and (3.25) now define the total cable curve when the dead load distribution is known.

In most cases the dead load of the deck is uniformly distributed in the longitudinal direction of the bridge, whereas the dead load per unit length of the cable system shows a moderate variation from its minimum value at the main span centre to its maximum value at the pylon. This is due to the increased length of the hangers and the larger inclination of the main cable near the pylons. However, as the dead load of the deck generally dominates, the total dead load can often be assumed to be uniformly distributed as a good approximation.

### 3.2.2 Preliminary cable dimensions

In the process of designing a suspension bridge it is advantageous to be able to make a quick, preliminary calculation of the cable dimensions [82.2].

A preliminary determination of the maximum hanger force can be based on the assumption that the hanger carries the distributed load acting on a length of the deck equal to the hanger spacing  $\lambda$ , and that concentrated forces can be equalized with a uniformly distributed load of the same magnitude acting on a length of  $30d$ , where  $d$  is the depth of the deck. The latter assumption is of a quite approximate nature, but sufficient for the purpose of getting a first estimate on hanger dimensions.

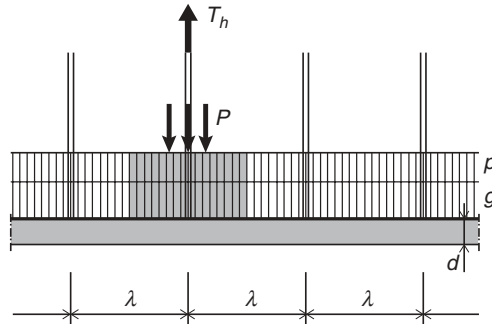


Figure 3.24 Loading case for maximum hanger force

Assuming that  $30d > \lambda$  the maximum hanger force  $T_h$  (Figure 3.24) becomes:

$$T_h = (g + p)\lambda + P \frac{\lambda}{30d} \quad (3.26)$$

and the cross sectional area  $A_h$  of the hanger:

$$A_h = \frac{T_h}{f_{cbd}} = \frac{(g + p + P/(30d))\lambda}{f_{cbd}} \quad (3.27)$$

where  $f_{cbd}$  is the design stress (allowable stress) of the cable steel.

The maximum force  $T_m$  of the main cable in the main span can be determined by assuming the dead load of the deck and the distributed traffic load acting uniformly in the entire main span, and the concentrated forces acting at midspan. In the preliminary investigation the dead load of the hangers might be ignored as this contribution is quite insignificant.

As a further approximation, the dead load of the main cable  $g_{cb}$  (which is unknown until the cable area  $A_m$  has been determined) is assumed to be uniformly distributed horizontally.

The simplifying assumptions regarding the dead load of the cable system are slightly on the unsafe side, but this is to a large extent balanced out by assuming the dead load geometry instead of the deflected geometry.

For a horizontal main cable, as shown in Figure 3.25, the maximum horizontal force  $H_m$  now becomes:

$$H_m = \frac{(g + p)l_m^2}{8k_m} + 2Pl_m + \frac{g_{cb}l_m^2}{8k_m} \quad (3.28)$$

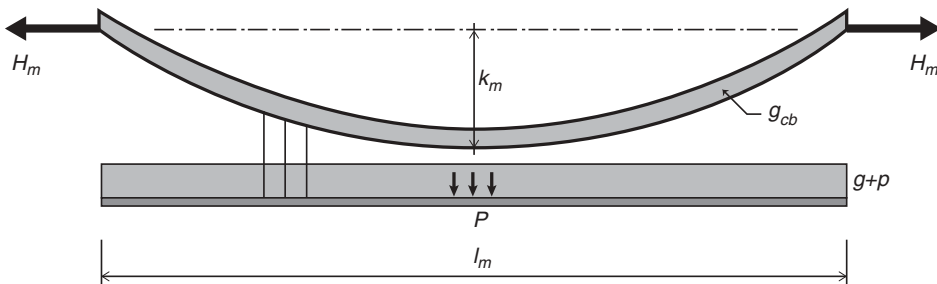
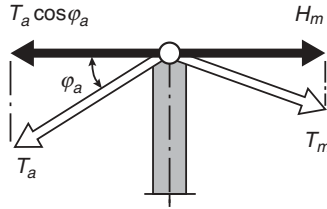


Figure 3.25 Loading case for maximum main cable force



**Figure 3.26** Horizontal equilibrium at the pylon top

and the maximum cable force  $T_m$  (at the pylon):

$$T_m = H_m \frac{\sqrt{(l_m^2 + 16k_m^2)}}{l_m} = [(g + p)l_m + 2P + g_{cb}l_m] \frac{\sqrt{l_m^2 + 16k_m^2}}{8k_m} \quad (3.29)$$

This expression is based on the simplifying assumption that the cable curve is a second order parabola.

The cable area  $A_m$  is now found from (3.29) by replacing for  $T_m$ :  $A_m f_{cbd}$  and for  $g_{cb}$ :  $A_m \gamma_{cb}$ , where  $\gamma_{cb}$  is the (equivalent) density of the cable material:

$$A_m = \frac{[(g + p)l_m + 2P] \sqrt{l_m^2 + 16k_m^2}}{8f_{cbd}k_m - \gamma_{cb}l_m \sqrt{l_m^2 + 16k_m^2}} \quad (3.30)$$

The maximum tension  $T_a$  in the side span main cable is determined by expressing horizontal equilibrium at the pylon top, as indicated in Figure 3.26:

$$T_a = H_m / \cos \phi_a \quad (3.31)$$

where  $H_m$  is the maximum horizontal force from (3.28), with  $g_{cb} = A_m \gamma_{cb}$  found from (3.30).

The preliminary cross sectional area  $A_a$  of the side span cable thus becomes:

$$A_a = \frac{T_a}{f_{cbd}} = \frac{H_m}{f_{cbd} \cos \phi_a} \quad (3.32)$$

### 3.2.3 Quantity of cable steel

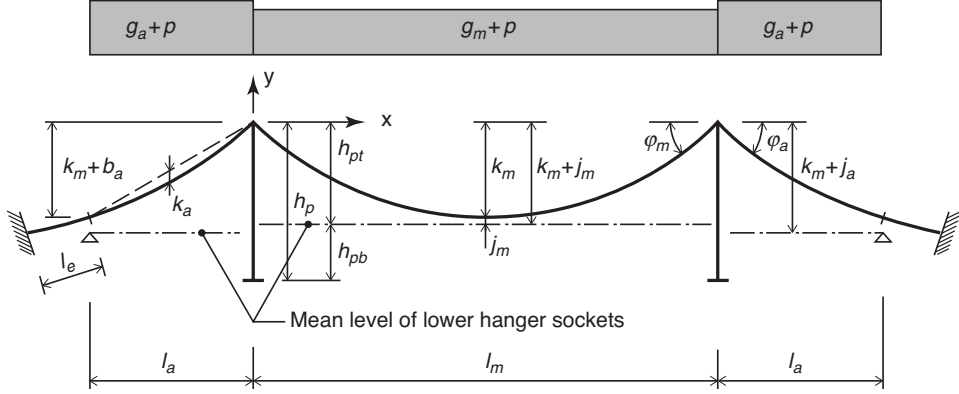
For a symmetrical, three-span suspension bridge subjected to uniform load  $g_m + p_m$  acting on the deck in the main span, and  $g_a + p_a$  in the side span, as indicated in Figure 3.27, expressions for the quantity of cable steel can be derived by the following procedure.

Equation for the main span cable curve:

$$y = 4k_m \frac{x}{l_m} \left( \frac{x}{l_m} - 1 \right) \quad (3.33)$$

Equation for the side span cable curve:

$$y = 4k_a \left( \frac{x}{l_a} \right)^2 + (4k_a + k_m + b_a) \frac{x}{l_a} \quad (3.34)$$



**Figure 3.27** Geometrical parameters of a symmetrical three-span suspension bridge subjected to dead and traffic load in all spans

Cable steel in the main span hangers:

$$Q_{hm} = \frac{\gamma_{cb}}{f_{cbd}} \int_0^{l_m} (g_m + p_m) \left[ k_m + j_m + 4k_m \frac{x}{l_m} \left( \frac{x}{l_m} - 1 \right) \right] dx = \frac{\gamma_{cb}}{f_{cbd}} (g_m + p_m) \left( j_m + \frac{k_m}{3} \right) l_m \quad (3.35)$$

Cable steel in the main span cable (refer to (3.30)):

$$Q_{cm} = \frac{\gamma_{cb}}{f_{cbd}} (g_m + p_m) l_m^2 \frac{\sqrt{1 + 16 \left( \frac{k_m}{l_m} \right)^2}}{8 \frac{k_m}{l_m} - \frac{\gamma_{cb}}{f_{cbd}} l_m \sqrt{1 + 16 \left( \frac{k_m}{l_m} \right)^2}} \left[ 1 + \frac{8}{3} \left( \frac{k_m}{l_m} \right)^2 \right] \quad (3.36)$$

To determine the cable steel in the side spans the horizontal force  $H (= H_m)$  must be known. Assuming a uniform distribution of the cable dead load in the main span implies the following safe expression for the horizontal force  $H$ :

$$H = \frac{(g_m + p_m) l_m^2 + Q_{cm} l_m}{8k_m} \quad (3.37)$$

The sag  $k_a$  of the side span cable then becomes:

$$k_a = \frac{(g_a + p_a) l_a^2 + Q_{ca} l_a}{8H} = \frac{(g_a + p_a) l_a + Q_{ca}}{(g_m + p_m) l_m + Q_{cm}} \frac{l_a}{l_m} k_m$$

As the effect of  $k_a$  on the cable steel quantity generally is small, the following approximate value of  $k_a$  might be used here:

$$k_a \simeq \frac{g_a + p_a}{g_m + p_m} \left( \frac{l_a}{l_m} \right)^2 k_m \quad (3.38)$$

Cable steel in the side span hangers (both spans included):

$$\begin{aligned} Q_{ha} &= 2 \frac{\gamma_{cb}}{f_{cbd}} \int_{-l_a}^0 (g_a + p_a) \left[ k_m + j_a + 4k_a \left( \frac{x}{l_a} \right)^2 + (4k_a + k_m + b_a) \frac{x}{l_a} \right] dx \\ &= \frac{\gamma_{cb}}{f_{cbd}} (g_a + p_a) \left( k_m - \frac{4}{3} k_a + 2j_a - b_a \right) l_a \end{aligned} \quad (3.39)$$

Cable steel in the side span cables (both spans included):

$$Q_{ca} = 2 \frac{\gamma_{cb}}{f_{cbd}} H l_a \sqrt{1 + \left( \frac{k_m}{l_a} + 4 \frac{k_a}{l_a} + \frac{b_a}{l_a} \right)^2} \left[ 1 + \frac{8}{3} \left( \frac{k_a}{l_a} \right)^2 + \frac{1}{2} \left( \frac{k_m + b_a}{l_a} \right)^2 + \frac{l_e}{l_a} \right] \quad (3.40)$$

where  $H$  is found from (3.37) and  $k_a$  from (3.38).

### 3.2.4 Quantity in the pylon

When optimizing the superstructure of a suspension bridge it is essential to take into account the variation in the quantities of the pylons, whereas the quantities (per unit length) of the deck often remain constant and consequently only influence the dead loads  $g_a$  and  $g_m$  to be applied to the cable system.

A correct calculation of the contribution from the pylons to the concrete or steel quantity is of considerable complexity as the required dimensions of the pylons depend not only on the in-plane forces from the cable system but also on wind forces as well as other lateral forces acting on the pylon itself-and on almost every part of the superstructure.

In the following the contribution from the pylons in the optimization process is taken into account by stipulating an effective stress  $f_{pld}$  that can be utilized to carry the vertical force from the cable system to the foundation. To determine the value  $f_{pld}$  it will be necessary to make a preliminary calculation of the stress occurring in the pylon from wind load and other out-of-plane loads and then subtract this stress from the design stress of the material to be used in the pylon. This will generally lead to a  $f_{pld}$  that varies slightly with the pylon height, but in the optimization process it will be sufficient to apply a constant value  $f_{pld}$  corresponding to an average value within the actual interval.

For effectively designed pylon structures the value of  $f_{pld}$  will be between 60% and 80% of the design stress of the material used in the pylon.

For the pylon shown in Figure 3.28, the following equations can be derived:

$$\begin{aligned} N_{pl}(\xi) + dN_{pl}(\xi) &= N_{pl}(\xi) + \frac{\gamma_{pl}}{f_{pld}} N_{pl}(\xi) d\xi \\ N_{pl}(\xi) &= N_{pt} \exp\left(\frac{\gamma_{pl}}{f_{pld}} \xi\right) \\ Q_{pl} = N_{pb} - N_{pt} &= N_{pt} \left[ \exp\left(\frac{\gamma_{pl}}{f_{pld}} h_{pl}\right) - 1 \right] \end{aligned} \quad (3.41)$$

where

$$N_{pt} = H(\tan \phi_a + \tan \phi_m) = \frac{(g_m + p_m)l_m + Q_{cm}}{8} \left( \frac{k_m + 4k_a + b_a l_m}{k_m l_a} + 4 \right)$$

so that the quantity in pylon (weight of pylon legs) becomes:

$$Q_{pl} = \frac{(g_m + p_m)l_m + Q_{cm}}{8} \left( \frac{k_m + 4k_a + b_a l_m}{k_m l_a} + 4 \right) \left[ \exp\left(\frac{\gamma_{pl}}{f_{pld}} h_{pl}\right) - 1 \right] \quad (3.42)$$

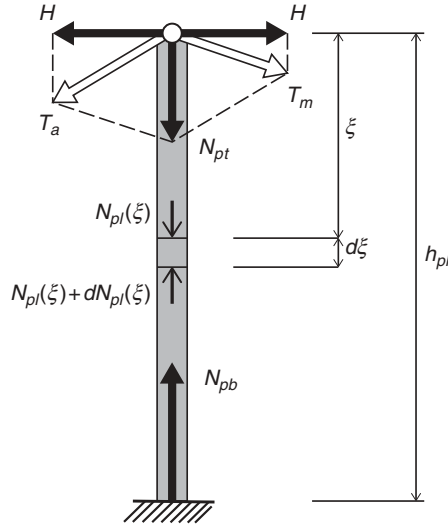


Figure 3.28 Vertical forces acting on a pylon

### 3.2.5 Total cost of cable system and pylon

The total cost  $C_{cp}$  of the cable system plus pylons can now be expressed:

$$C_{cp} = (Q_{cm} + Q_{ca} + Q_{hm} + Q_{ha})u_{cb} + 2Q_{pl}u_{pl} \quad (3.43)$$

where  $u_{cb}$  is the unit price for erected and protected cable steel and  $u_{pl}$  the unit price for the material used in the pylons.

The unit prices  $u_{cb}$  and  $u_{pl}$  will generally vary with the construction methods and the erection procedures. Furthermore, the unit prices might vary from one part of the structure to another, depending on the position of the structural elements to be installed. The unit price for a structural element to be erected at the top of the pylon might easily be higher than for a structural element at the bottom of the pylon. However, in the optimization process, that can generally only be used as guidance for the final choice of main dimensions, each of the unit prices  $u_{cb}$  and  $u_{pl}$  can be stipulated at constant values, corresponding to realistic average values.

Incidentally, it should be noted that in the optimization process only the ratio between the individual unit prices is of significance, so that a detailed knowledge of the absolute values is not required.

For a suspension bridge system with fixed span lengths the main parameter to vary is the sag  $k_m$  of the main span cable.

### 3.2.6 Optimum pylon height

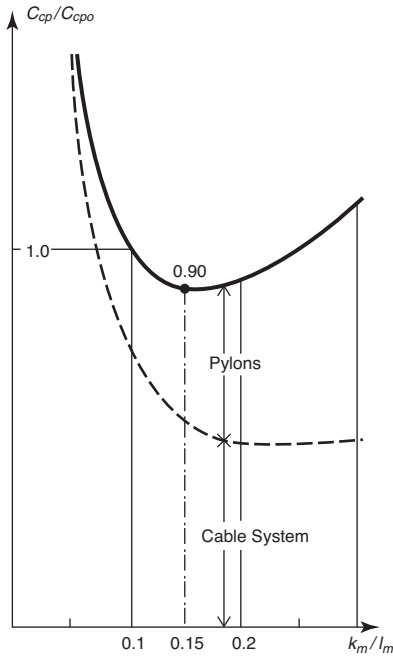
To illustrate the effect of the sag on the quantities, Figure 3.29 shows the relative cost  $C_{cp}/C_{cp0}$  for various ratios  $k_m/l_m$  where  $C_{cp0}$  is the cost of the suspension bridge with the common sag ratio of 1:10.

Note that the optimum occurs for  $k_m/l_m = 0.15$ , where the cost is 10% lower than for the sag ratio of 0.10. If considering only the cable system the optimum occurs for  $k_m/l_m = 0.25$ , and this clearly indicates the necessity of including the pylons in the optimizing process.

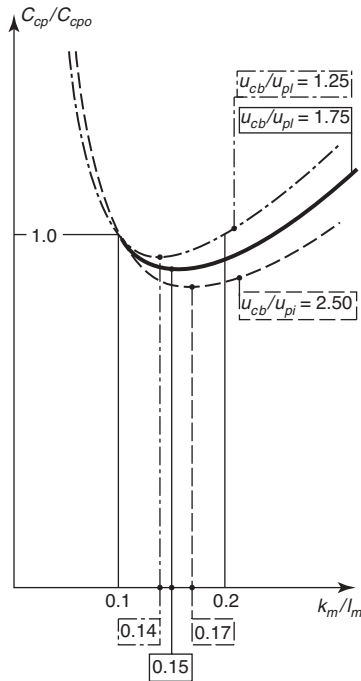
It is interesting to see that the optimum sag ratio is reduced to 60% when taking into account the pylon material – a value close to the  $1/\sqrt{3} \sim 0.58$  found for the basic case in Figure 3.10.

To illustrate that the ratio between the unit prices of the cable and the pylon material only slightly influences the optimization, Figure 3.30 shows the  $C_{cp}/C_{cp0}$  variation for the three ratios  $u_{cb}/u_{pl} = 1.25$ ,  $u_{cb}/u_{pl} = 1.75$  (as in Figure 3.29) and  $u_{cb}/u_{pl} = 2.5$ . When changing from the lower value of 1.25 to the upper value of 2.5 the optimum ratio of  $k_m/l_m$  only changes from 0.17 to 0.14, and within that interval the variation of  $C_{cp}$  is insignificantly small.

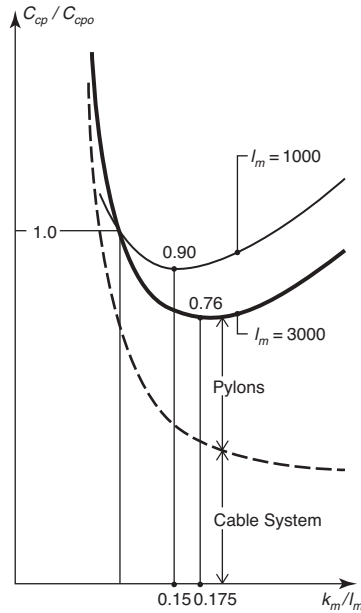




**Figure 3.29** Variation of the relative cost  $C_{cp}/C_{cp0}$  for a three-span suspension bridge with the following parameters (refer to Figure 3.27):  $l_a = 250$  m;  $l_m = 1000$  m;  $l_e = 50$  m;  $b_a = j_a = j_m = 3$  m;  $h_{pb} = 40$  m;  $g_a = g_m = 0.20$  MN/m;  $p_a = p_m = 0.08$  MN/m;  $f_{cbd} = 720$  MPa;  $\gamma_{cb} = 0.08$  MN/m<sup>3</sup>;  $f_{pld} = 160$  MPa;  $\gamma_{pl} = 0.08$  MN/m<sup>3</sup>;  $u_{cb} = 1.75 u_{pl}$



**Figure 3.30** Variation of the relative cost  $C_{cp}/C_{cp0}$  for three different unit price ratios  $u_{cb}/u_{pl}$ . Other parameters as in Figure 3.29



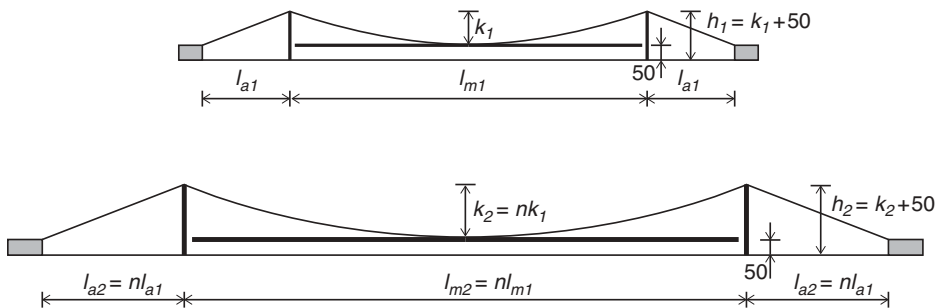
**Figure 3.31** Variation of the relative cost  $C_{cp}/C_{cp0}$  for a three-span suspension bridge with a 3000 m/1000 m main span and the following parameters:  $l_a = 750$  m;  $l_m = 3000$  m;  $l_e = 80$  m;  $b_a = j_a = j_m = 5$  m;  $h_{pb} = 60$  m. Loading and strength parameters as in Figure 3.29

With increasing span length the dead load of the cable becomes more and more dominating and the optimum will therefore move towards the optimum of the cable system itself. This feature is illustrated in Figure 3.31 showing the  $C_{cp}/C_{cp0}$  variation for bridges with main spans of 1000 m and 3000 m. Note that whereas the minimum value of  $C_{cp}$  in the 1000 m case is 10% below the value  $C_{cp0}$  (for  $k_m/l_m = 0.1$ ), then the minimum value in the 3000 m case is 24% below the value for  $k_m/l_m = 0.1$ .

### 3.2.7 Size effect

It is a well-known fact that the quantities to go into a structure of a given type will increase progressively with the span length due to the ever increasing contribution from the self weight of the structural members.

To illustrate the size effect for a suspension bridge, the consequences of increasing the dimensions of the deck, the cable system and the upper pylon part (above the deck) by a factor of  $n$  will be investigated (Figure 3.32).



**Figure 3.32** Suspension bridges with equal proportions but different size

**Table 3.1** Relative quantities of the deck, the cable system and the pylons

| $l_m(m)$ | $Q_{dk}$ | $Q_{cb}$    | $Q_{pl}$    |
|----------|----------|-------------|-------------|
| 500      | 0.5      | 0.23 (0.25) | 0.29 (0.33) |
| 1000     | 1.0      | 1.0         | 1.0         |
| 2000     | 2.0      | 4.8 (4)     | 4.4 (3.3)   |
| 3000     | 3.0      | 15 (9)      | 13 (7)      |
| 4000     | 4.0      | 41 (16)     | 36 (12)     |
| 5000     | 5.0      | 132 (25)    | 119 (18)    |

Notes: \*The relative quantities are calculated with the following values:  $h_{pb}=50\text{ m}$ ;  $g_{gr}=0.16\text{ MN/m}^2$ ;  $p=0.08\text{ MN/m}^2$ ;  $\gamma_{cb}=0.09\text{ MN/m}^3$ ;  $f_{cbd}=720\text{ MPa}$ ;  $\gamma_{pl}=0.08\text{ MN/m}^3$ ;  $f_{pld}=160\text{ MPa}$ .

If it is assumed that the deck cross section is kept constant, i.e.  $A_{d2}=A_{d1}$ , that the traffic load intensity  $p$  is independent of the span length, and that the weight of the cables and the pylons can be ignored, then the following relations will exist:

$$Q_{dk2} = nQ_{dk1}$$

$$Q_{cb2} = n^2Q_{cb1}$$

$$Q_{pl2} = n^2Q_{pl1}$$

$$Q_{ab2} = nQ_{ab1}$$

where the subscript  $dk$  refers to the deck,  $cb$  to the cable system,  $pl$  to the pylon, and  $ab$  to the anchor block.

It is seen that under the given idealized assumptions the quantity of the deck and the anchor blocks will increase proportionally with the span length, whereas the quantities of the cable system and the pylons will increase with the square of the span length.

However, if the quantities of cable steel are calculated from (3.35), (3.36), (3.39) and (3.40), and the quantities of the pylons from (3.42), then the relative quantities will be as given in Table 3.1. In this table the relative quantities of the cable system and the pylons to be found when ignoring the weight of these structural parts are shown in parentheses.

It is seen from Table 3.1 that the progression in quantities of the cable system becomes very significant for large spans. Thus, the quantity for a 4000 m span is increased by a factor of 2.5 (from 16 to 41) when including the cable self weight. For the pylon quantity the progression is even stronger as the relative quantity is increased by a factor of 3 (from 12 to 36) when the weight of both the cable system and the pylons is taken into account.

It must be emphasized that the values in Table 3.1 are based on the somewhat unrealistic assumption that the deck cross section can remain constant as spans are increased. In reality, the deck cross section will also have to be increased with the span and this will lead to a further progression beyond the one illustrated in Table 3.1. However, the relative progression between deck, cable system and pylon will not be influenced by the absolute progression in deck quantities.

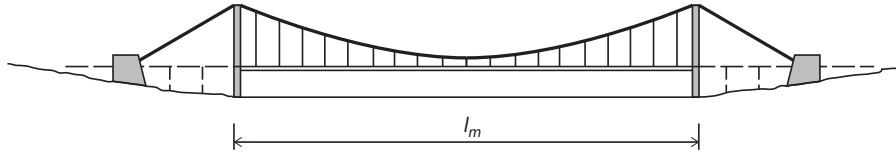
### 3.2.8 Structural systems

After the study of parameters influencing the design of the suspension system, a number of structural systems will be described and discussed.

Figure 3.33 shows a single-span suspension bridge with only the main span supported by the cable system, but with the main cable continued as freely suspended cables (backstays) from the pylon tops to the anchor blocks positioned in some distance from the pylons.

Between the pylons, the bridge system includes a deck supported through hangers to the main cable, whereas the bridge outside the pylons contains approach spans acting independently of the cable system.

The system of Figure 3.33 will generally lead to a structure with favourable deformational characteristics as the pylon tops are efficiently restrained longitudinally by the anchor cables. However, in large bridges with long anchor cables, the sag effect might reduce the efficiency of the horizontal pylon top restraint.



**Figure 3.33** Single span suspension bridge with independent approach spans outside the pylons

As a prominent example of a single-span suspension bridge, Figure 3.34 shows the Fatih Sultan Mehmet Bridge (Second Bosphorus Bridge) in Turkey. Here the bridge site was especially well suited for the application of the single-span solution as the pylons could be positioned at the top of the slopes on either side of the strait. Therefore in this case the approach spans leading to the pylons became superfluous.

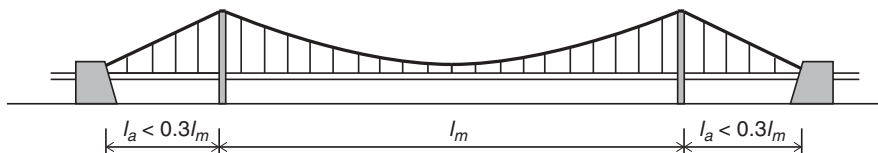
Favourable deformational characteristics are also obtained by the application of relatively short side spans with a length of less than 30% of the main span, as shown in Figure 3.35. With short side spans the sag of the side span cable becomes small and this influences favourably the axial stiffness, as was demonstrated in Figure 2.56.

The George Washington Bridge across the Hudson River (Figure 3.36) is a typical example of a suspension bridge with short side spans, as the ratio between the lengths of the side and main span is as little as 0.17–0.19. Short side spans are often found in bridges with side spans on land above steep slopes (or in shallow water where that clearance requirements do not have to be fulfilled).

In cases where both the main span and the side spans have to be positioned on deep water, long side spans with a length of 40–50% of the main span are found, as illustrated in Figure 3.37. A side-to-main span ratio of 0.5 leads to a pleasing



**Figure 3.34** Fatih Sultan Mehmet Bridge (Second Bosphorus Bridge)



**Figure 3.35** Three-span suspension bridge with short side spans



**Figure 3.36** George Washington Bridge

appearance of the suspension bridge due to the symmetry of the cable system about each pylon. On the other hand, long side spans imply that the cable leading from the anchor block to the pylon top will have a relatively large sag, and that influences unfavourably the horizontal restraint of the pylon top. Long side spans will therefore lead to larger deflections in the main span, as was illustrated in Figure 2.56. So the suspension bridge with long side spans constitutes one among numerous examples of the fact that beauty and structural efficiency do not always go hand in hand.

The 20th April Bridge in Lisbon (Figure 3.38) was constructed with a side-to-main span ratio of 0.48. The reason for choosing such long side spans was a desire to minimize the main span length and at the same time limit the number of river piers to two.

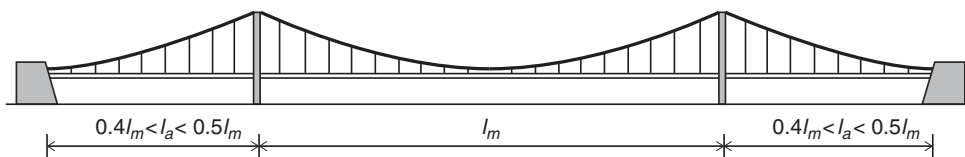
Similar considerations were made for the Akashi Kaikyo Bridge where the same span ratio of 0.48 is found.

Extremely long side spans with a length exceeding half of the main span length will lead to a structure as shown in Figure 3.39. Here the outer portions of the deck in the side spans have to be supported by short columns onto the main cable below. For a conventional suspension bridge system with vertical hangers and slender pylons a system as shown in Figure 3.39 would lead to very unfavourable deformational characteristics.

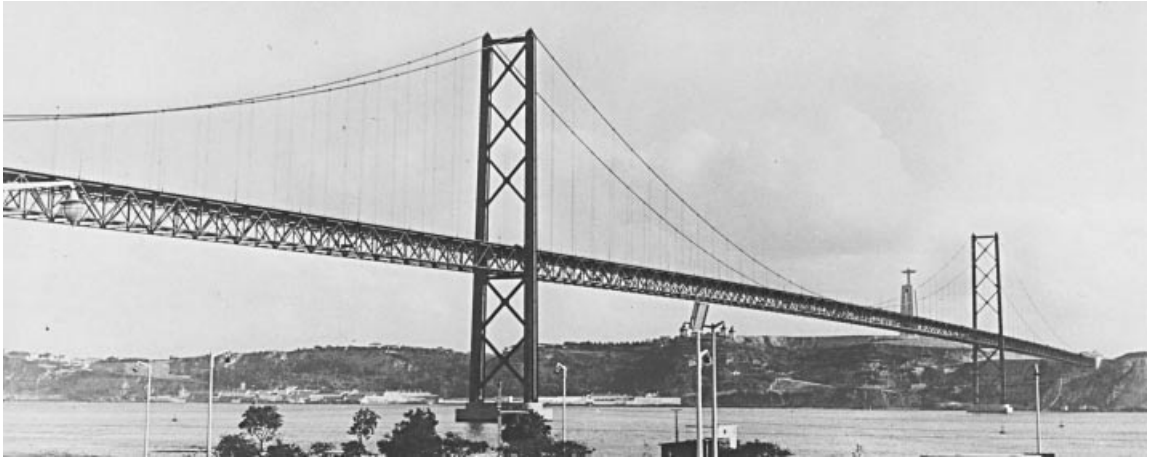
In the Brooklyn Bridge the side-to-main span ratio is as high as 0.59, and short columns were, therefore, added to support the stiffening truss in the outer side span regions, as shown in Figure 3.40. However, the unfavourable deformational characteristics resulting from the application of extremely long side spans were, in the Brooklyn Bridge, counteracted by the use of very heavy pylons with a considerable flexural stiffness and by application of stays to supplement the suspension system.

An even more extreme ratio between the length of a side span and the main span is seen in the London Millennium Bridge (see Figure 1.104) where the southern side span has a length of 75% of the main span.

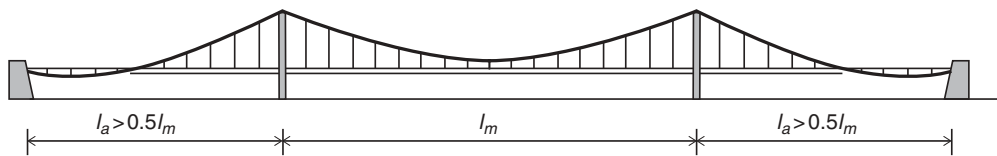
The vast majority of existing suspension bridges are designed to be symmetrical (or very close to symmetrical), i.e. to have side spans of equal length. An exception to this rule is the Humber Bridge with one side span 280 m long and the other 530 m long corresponding to side-to-main span ratios of 0.20 and 0.38, respectively.



**Figure 3.37** Three-span suspension bridge with long side spans



**Figure 3.38** 20th April Bridge



**Figure 3.39** Three-span suspension bridge with extreme side spans



**Figure 3.40** Brooklyn Bridge with the main cable below the stiffening truss adjacent to the anchor blocks



**Figure 3.41** *Tsing Ma Bridge*

For the structural behaviour there is hardly any drawback attached to an asymmetrical configuration and also for the appearance the effect seems to be minor. With the large overall dimensions and the perspective distortions it will be difficult from almost any viewing position to detect the asymmetry.

A more pronounced and easily detectable asymmetry is found in the Tsing Ma Bridge in Hong Kong where one side span is supported through hangers to the main cables whereas the other side span consists of girder spans acting independently of the suspension bridge (Figure 3.41).

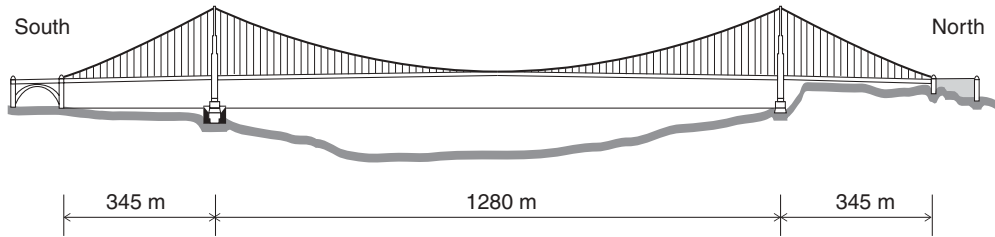
A similar mixture of side spans with and without cable support is found in the Xihoumen Bridge (Figure 3.42), but here the solution was chosen because one of the approach roads had to be horizontally curved all the way to the pylon and that makes the solution logical and fully acceptable.

The mixing of cable supported and pier supported side spans is generally dictated by the local environment on either side of the main span. However, in some cases a symmetrical layout has been used even if the landscape clearly favoured an asymmetry. This is perhaps most clearly illustrated by the Golden Gate Bridge where it was even necessary to excavate a hill on the north side to make the side span clear the ground, as seen on the elevation in Figure 3.43. To go to such an extreme could seem unjustified but the appearance of the bridge has benefitted from the symmetry of the structure.

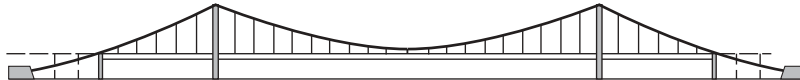
In most three-span suspension bridges the main cables are led directly into the anchor blocks at the ends of the side spans. However, in some cases secondary pylons are positioned at the ends of the suspended side spans and the main cables are then continued to lower anchor blocks closer to the soil, as illustrated in Figure 3.44. Such an arrangement generally leads to



**Figure 3.42** *Xihoumen Bridge*



**Figure 3.43** Elevation of the Golden Gate Bridge



**Figure 3.44** Suspension bridge with secondary pylons and the main cable continued to low anchor blocks

cheaper anchor blocks as the overturning moment from the cable pull is reduced considerably, but at the same time the main cable length is increased. Thus, the quantity of cable steel will go up and the side span cable restraint of the pylon tops will be more flexible. The arrangement of Figure 3.44 becomes less attractive if the bridge structure outside the secondary pylons is above navigable waters so that the main cables below the bridge deck could be accidentally hit by ships.

In the Lillebælt Bridge, shown in Figure 3.45, the application of secondary pylons and low, embedded anchor blocks was chosen to avoid heavy and clumsy anchor blocks on the coastline and to obtain an efficient anchor block structure suitable for the foundation on clay (see Figure 6.89).

In a suspension bridge with asymmetrical traffic load in half of the span, the main cable will deflect in the longitudinal direction at midspan and this will increase the vertical deflections of the two halves of the main span deck (downwards in the half span with traffic load and upwards in the half span without traffic load).

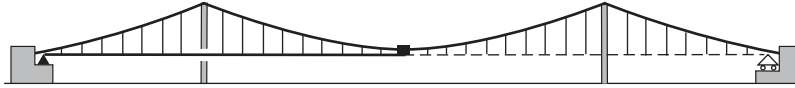
Improved deformational characteristics can be achieved if the main cable is restrained by the deck against longitudinal displacements at midspan.

A suspension bridge system with a central clamp fixing the main cable to the deck at midspan might be arranged as shown in Figure 3.46. Here the continuous deck is supported by a fixed bearing on the left anchor block and by a



**Figure 3.45** Lillebælt Bridge





**Figure 3.46** Three-span suspension bridge with a central clamp and a fixed bearing on one of the anchor blocks

longitudinally movable bearing on the right anchor block. Due to the mutual fixation by the central clamp between the main cable and the deck, axial forces will be induced in the left half of the deck, and in accordance with the definition given earlier, this part of the deck should therefore be regarded as a part of the cable system.

The highest efficiency of the central clamp will exist in systems where the pylon tops are well restrained against longitudinal displacements. A central clamp will, therefore, be especially attractive in suspension bridges with short side spans.

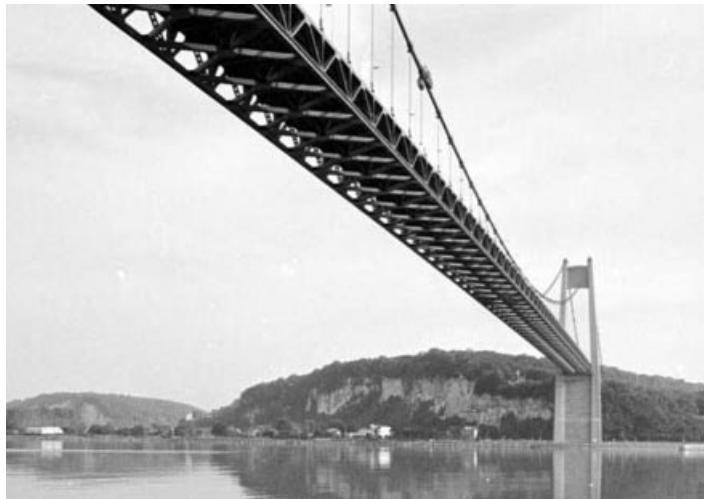
A structural system similar to that shown in Figure 3.46 was used for the first time in the Tancarville Bridge across the River Seine (Figure 3.47). Here the fixed bearing was arranged on the large anchor block on the left bank of the river.

With a structural system as shown in Figure 3.46 the central clamp is efficiently restrained longitudinally under varying traffic load conditions, but longitudinal movements of the central clamp will take place under temperature changes as the deck expands or contracts from the fixed bearing.

The thermal movements are proportional to the length of expansion, so a reduction of the movements will be achieved if the fixed bearing of the deck is positioned on one of the pylons, as shown in Figure 3.48. The feasibility of this solution depends on the intensity of the horizontal forces to be transferred from the deck, as bending will be induced in the pylon legs and the pier below.

Complete elimination of thermal movements at the central clamp can be achieved by using hydraulic devices to centre the deck in the longitudinal direction.

Figure 3.49 shows schematically a hydraulic device described by M. Ellinger and F. Cichocki [64.1]. As indicated in Figure 3.49 the system contains two oil cylinders connected by pressure tubes in such a way that symmetrical movements



**Figure 3.47** Tancarville Bridge



**Figure 3.48** Three-span suspension bridge with a central clamp and a fixed bearing at one of the pylons

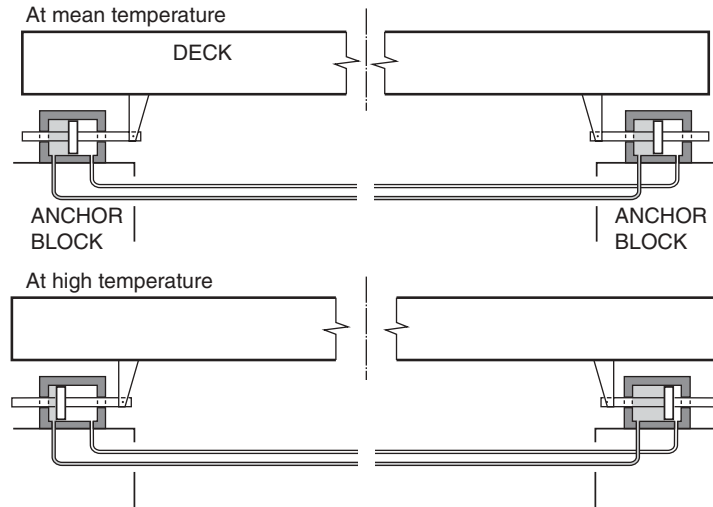


Figure 3.49 Centring device according to Ellinger and Cichocki

of the two girder ends (due to temperature changes) can take place without restraint, whereas asymmetrical movements are resisted by an oil pressure developing in both cylinders.

In the system described by Ellinger and Cichocki, the pressure tubes were placed inside the girder, but the tubes might also lead from one anchor block to the other below the ground or the sea bottom. This arrangement would reduce the temperature change of the oil, and therefore reduce undesirable variations in the oil pressure.

In the Storebælt East Bridge the deck is continuous from one anchor block to the other and the main cable is clamped to the deck at midspan (Figure 3.50). At the same time the deck (with movable bearings at both ends) is connected to the anchor blocks by hydraulic buffers that will allow slow movements, e.g. due to temperature changes, but exclude fast movements due to wind-induced vibrations or moving traffic. Thus for fast movements the system will be as efficient as the system with interconnected oil cylinders, but it does not require longitudinal pressure tubes between the two anchor blocks.

In bridges without a central clamp the main cable is often kept at some distance from the deck so that the connection between the two structural elements can be established by hangers throughout the span, as indicated in Figure 3.51(a).

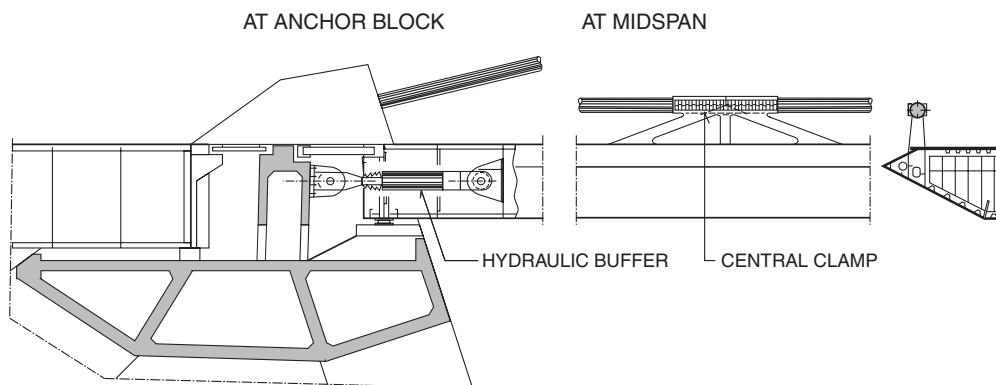
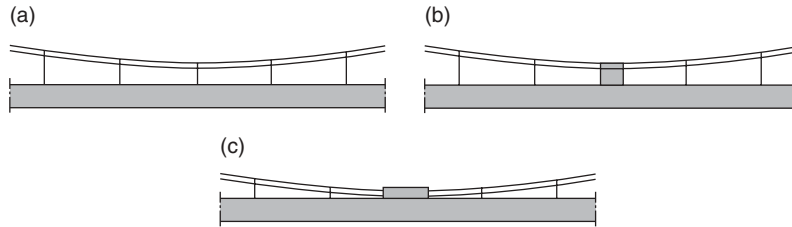


Figure 3.50 Central clamp at midspan and hydraulic buffers at the anchor blocks (Storebælt East Bridge)



**Figure 3.51** Connection between the main cable and the deck at midspan

The same position of the cable might also be used in cases where a central clamp is required and in that case the central hanger is replaced by a vertical bracket, as indicated under (b). This arrangement was used in the Lillebælt Bridge. It should be mentioned that the vertical member of the vertical bracket is superfluous, but nevertheless it has been incorporated in many other bridges with a central clamp.

From the point of view of appearance the Lillebælt Bridge arrangement is not fully satisfactory as the latticed members connecting the central clamp to the deck appear alien elements in poor harmony with the main members, i.e. the main cable and the box girder – as illustrated in Figure 3.52. It will, therefore, be more acceptable if the longitudinal restraint between the deck and the main cables is established through a number of inclined cables, as seen in the Bisan Seto Bridges (Figure 3.53).

There is also the possibility that the main cable might be positioned in such a way that the central clamp can be connected directly to the top flange of the deck (Figure 3.52(c)). This principle can be illustrated by the connection between the main cable and the top chord of the stiffening truss in the 20th April Bridge (Figure 3.54).

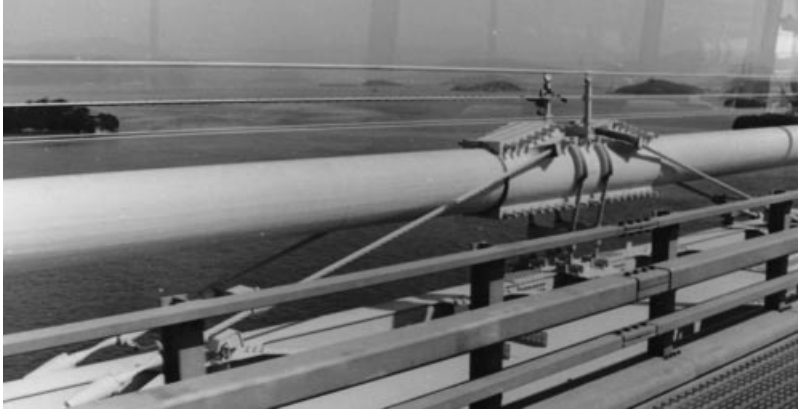
It must be considered that in bridges with a central clamp the vertical distance between the main cable and the deck at midspan will influence the efficiency of this connection.

To investigate the influence of the deck-to-cable distance on the efficiency of the central clamp the deflection curve under symmetric load will be studied. As indicated in Figure 3.55 the centred deck will keep its central point  $C'$  in position but a rotation will take place. When free to move, the central point  $C$  of the cable will tend to move horizontally towards the loaded span under asymmetric load.

It will now be seen that, due to the rotation of the deck at midspan the central clamp will be forced to move horizontally a distance which is proportional to the length of the vertical element between the deck and the cable as shown in Figure 3.56. It will, therefore, be understood that the desired prevention of a longitudinal movement of the central clamp will be less efficient if the distance from the deck to the cable is large.



**Figure 3.52** Central clamp in the Lillebælt Bridge



**Figure 3.53** Inclined tie cables for restraining the main cable in the longitudinal direction at midspan (Bisan Seto Bridges)

However, for realistic values of the vertical distance  $d_{cl}$  from the deck axis to the main cable axis (e.g. within the interval 3–10 m), the central clamp will still be quite effective in preventing mutual longitudinal displacements between the main cable and the deck under asymmetric load. For a 1000 m long free cable the rotation  $\phi$  at midspan typically amounts to  $\phi = 0.03$ , and the horizontal displacement  $\delta_x$  (from (2.32)) to  $\delta_x = 1.0$  m. Consequently, the distance  $d_{cl}$  will have a value of 33 m before  $\phi d_{cl}$  reaches the same value as  $\delta_x$ , and with  $d_{cl}$  in the interval 3–10 m the central clamp will therefore still be 90–75% effective.



**Figure 3.54** Central clamp connecting the main cable to the top chord of the stiffening truss in the 20th April Bridge

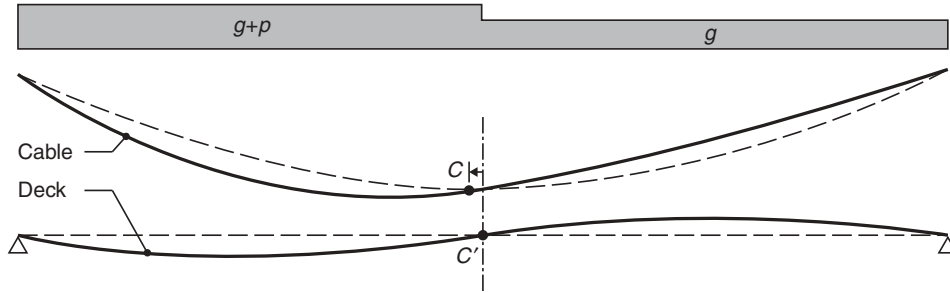


Figure 3.55 Deflection of main cable and deck under asymmetric traffic load

In the conventional suspension system with vertical hangers the cable system does not possess any shear strength so that the shear forces created by the external load must be resisted either by the deck or by a displacement of the main cable (approaching the funicular curve of the applied load).

By arranging inclined hangers, as indicated in Figure 3.57, a truss action can be created so that shear forces can be transferred through the cable system. As shear forces generally induce tension as well as compression in the hangers (acting as truss diagonals) the shear forces from traffic load can only reach a value determined by the condition that the compressive force from traffic load must not exceed the initial tensile force from dead load, as the resulting force in the hangers has to be tension.

The first major suspension bridge to be constructed with inclined hangers was the Severn Bridge in the UK (Figure 3.58). Here the main reason for applying the system was to increase the damping properties of the structure – a damping that was feared to be insufficient due to the all-welded design of the box girder deck.

During wind-excited oscillations the cable will displace longitudinally in relation to the deck and with the inclined hangers a cyclic variation of the hanger forces will be induced. In connection with the hysteresis found in helical cables a damping was expected.

The Severn Bridge was later followed by the First Bosphorus Bridge and the Humber Bridge both built with inclined hangers, but after that the system was abandoned. All bridges based on the streamlined box girder concept that followed such as the Second Bosphorus Bridge, the Ohshima Bridge, the Askøy Bridge, the Storebælt East Bridge, and many more were all designed with vertical hangers.

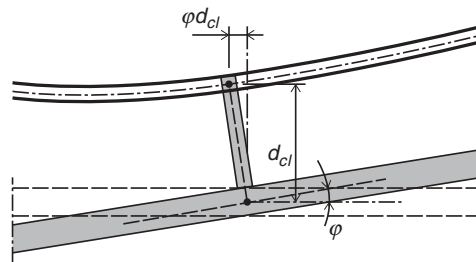


Figure 3.56 Rotation of vertical element connecting the deck to the clamp on the main cable



Figure 3.57 Suspension system with inclined hangers between the main cable and the deck



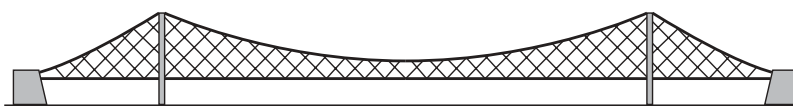
**Figure 3.58** Severn Bridge

The reason for this reversal was that aerodynamic studies proved that the required stability could actually be achieved without the inclined hangers, and also that fatigue problems were experienced in the Severn Bridge hangers due to the stress variations occurring under passing traffic.

Earlier it had also been proposed to make the connection between the deck and the cable as a net of intersecting cables that could more efficiently transfer shear forces between the main cable and the girder (Figure 3.59). With a continuous deck able to transfer axial forces from main to side span this system can to some extent act as a double cantilever truss.

In the mono-cable bridge proposed by F. Leonhardt around 1960, a single main cable was connected to the deck by two inclined hanger nets, as seen in Figure 3.60. Through the application of a triangular cross section consisting of the roadway slab and the two hanger nets a high degree of torsional resistance was achieved, so it would be possible to use a very slender deck without any substantial torsional rigidity. In the proposed system the combination of a single main cable and skew hanger nets made it necessary to keep the cable a certain distance above the roadway at midspan. With a given main cable sag this will require increased pylon heights and steeper side span cables. Furthermore, the system with a hanger net as shown in Figure 3.59 will inevitably complicate the erection procedure compared to systems with vertical hangers only.

All major suspension bridges are built with an earth anchored system where the force of the main cable is transferred to the soil through anchor blocks at the ends of the side spans. However, in some small-to-medium sized suspension bridges the self anchored system, illustrated in Figure 3.61 has been applied. At first glance it might look very promising to get rid



**Figure 3.59** Suspension system with a hanger net between the main cable and the deck



**Figure 3.60** Mono-cable bridge proposed in the early 1960s by F. Leonhardt for the Emmerich Bridge across the Rhine

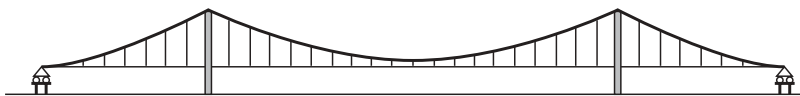
of the large (and often quite clumsy) anchor blocks, but taking into account that the compression in the deck requires a larger cross section (leading to increased deck dead load) and that during erection the main cable cannot carry any load until the deck is in place, this makes the self anchored system less attractive.

The more severe axial compression in the deck of a self anchored suspension bridge compared to a cable stayed bridge is illustrated in Figure 3.62. It is assumed that the two bridges have the same span lengths and the same loading whereas the pylon height above the deck is chosen to the typical values of  $L/10$  for the suspension bridge and  $L/5$  for the cable stayed bridge. With these assumptions it is seen that the compression in the self anchored suspension bridge is twice as large as in the cable stayed bridge and that the compression is constant along the entire length in the suspension bridge whereas the maximum compression in the cable stayed bridge is present only at the pylon location. A measure of the severity of the increased axial compression can be found by calculating  $\int N(x)dx$  for the two systems, and this measure is almost three times larger for the suspension bridge than for the cable stayed bridge.

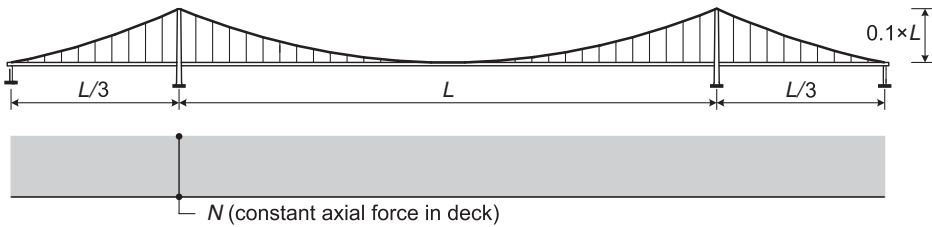
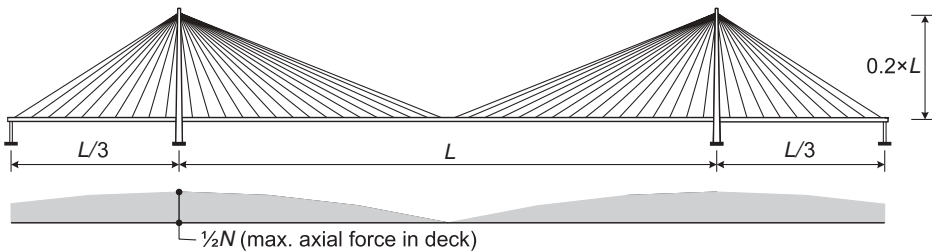
With the dimensions found in the existing self anchored suspension bridges with main spans of around 300 m and wide orthotropic steel decks the transmission of the axial forces has not presented a major problem as the inherent strength reserve in the deck cross section has been sufficient to take care of the axial compression. But with longer main spans the deck of a self anchored suspension bridge will earlier require strengthening than the deck of a cable stayed bridge. When an increased cross section of the deck becomes necessary, then the load will increase and that will make the self anchored suspension bridge even more unattractive in comparison with the self anchored cable stayed bridge.

A number of self anchored suspension bridges were constructed mainly in Europe before World War II but in the post-war period it became evident that with the complications during construction the self anchored suspension system was inferior to both the earth anchored suspension system and the self anchored cable stayed system. The number of self anchored suspension bridges constructed in recent years is therefore small and they have only been chosen in cases where the increased construction cost has been disregarded.

A unique example of a self anchored suspension bridge from the 1980s is the Konohana Bridge in Japan (Figure 3.63). This bridge is not only unusual due to its self anchored suspension system but also by having only one central main cable – as in the original proposal by F. Leonhardt (refer to Figure 3.60). However, Leonhardt introduced the concept primarily to increase the torsional stiffness of long span, earth anchored suspension bridges by connecting the main cable and the deck



**Figure 3.61** Self anchored suspension system

Self Anchored Suspension BridgeSelf Anchored Cable-Stayed Bridge

**Figure 3.62** Magnitude of axial force in the deck of a self anchored suspension bridge and a self anchored cable stayed bridge with a fan system

by two inclined hanger nets attached along the edges of the deck. In the Konohana Bridge the single main cable is connected to the deck through only one vertical hanger plane so the mono-cable arrangement did not result in any torsional support of the deck. However, the 26.5 m wide box girder deck rendered more than sufficient torsional stiffness to the span of 300 m so vertical support by the cable system was sufficient.

The drawbacks of the self anchored suspension system were to some extent demonstrated during construction of the Konohana Bridge as the bridge girder had to be supported by a total of 7 piers (4 permanent and 3 temporary) until the cable



**Figure 3.63** Konohana Bridge in Osaka



system could be erected. In the case of a self anchored cable stayed bridge, the erection could have been carried out without any temporary supports.

Of the few self anchored suspension bridges constructed since 1980 the Konohana Bridge stands out as the most successful, and much more reasonable than the new self anchored San Francisco East Bay Suspension Bridge that marks an extreme in complications during design and construction.

### 3.3 Fan System

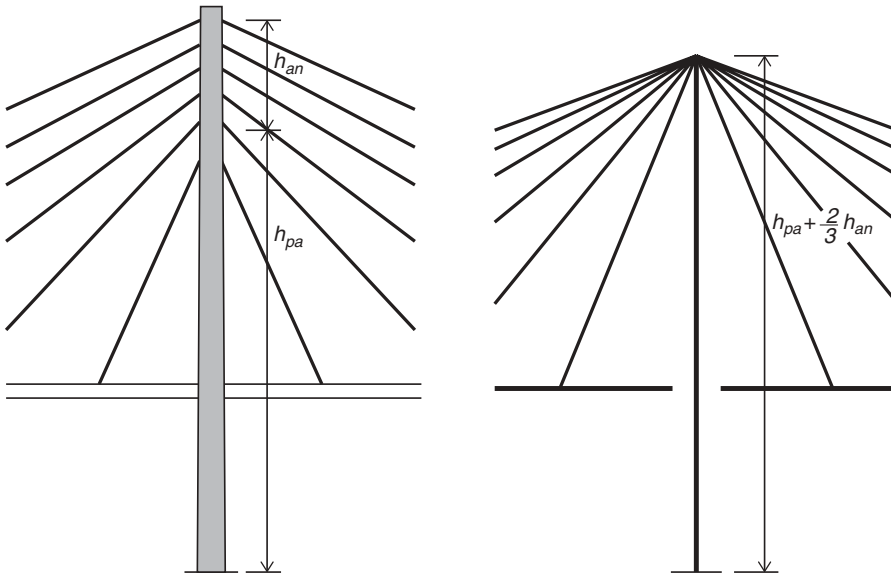
In cable stayed bridges the fan system has become the favourite cable system due to its efficiency and the degree of freedom regarding geometrical adaption.

The fan system is most commonly applied in the form of a semi-fan system where the cable anchor points are spread over a certain height  $h_{an}$  at the pylon top (Figure 3.64 to the left) to give room for an individual anchorage of each stay cable.

In the common cases where the anchor zone at the pylon top is extended over a relatively short distance the behaviour of a bridge with a semi fan system and a pure fan will be very similar. Consequently, the preliminary analyses can be based on an idealized structural system with a pure fan system and the single cable anchor point positioned at the upper third of the actual anchor zone, as indicated in Figure 3.64 to the right.

#### 3.3.1 Anchor cable

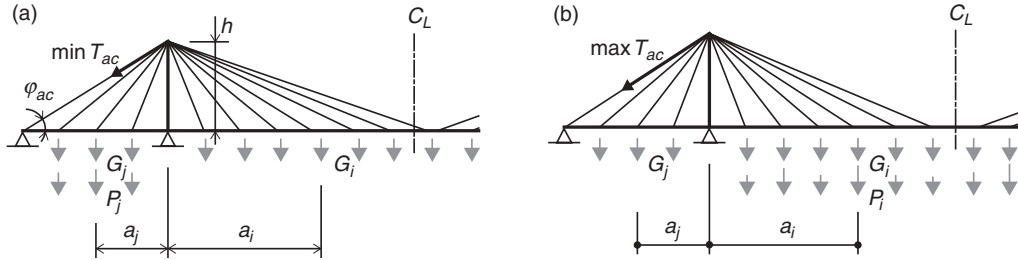
In the fan system, as shown in Figure 3.65, the anchor cable connecting the pylon top to the end support plays a dominant role in the achievement of stability in the cable system, as has already been pointed out. To utilize the anchor cable efficiently, it is required that this cable is in tension for any load combination.



**Figure 3.64** Anchorages of stay cables in a modified fan (left) and an equivalent pure fan (right) to simplify preliminary calculations



**Figure 3.65** Three-span cable stayed bridge with fan systems



**Figure 3.66** Loading cases introducing minimum and maximum tension in the anchor cable

The minimum tension in the anchor cable occurs for traffic load in the side spans only, as indicated in Figure 3.66(a). Ignoring the flexural stiffness of the deck, the following expression for the minimum tension  $\min T_{ac}$  in the anchor cable is derived:

$$\min T_{ac} = \frac{\sum_{i=1}^n G_i a_i - \sum_{j=1}^m (G_j + P_j) a_j}{h \cos \phi_{ac}} \quad (3.44)$$

where  $n$  is the number of loading points in one main span half and  $m$  the number of loading points in the side span.

The maximum tension  $\max T_{ac}$  in the anchor cable occurs for traffic load in the main span only, as indicated in Figure 3.66(b):

$$\max T_{ac} = \frac{\sum_{i=1}^n (G_i + P_i) a_i - \sum_{j=1}^m G_j a_j}{h \cos \phi_{ac}} \quad (3.45)$$

The stress ratio  $\kappa_{ac} = \min \sigma_{ac} / \max \sigma_{ac} = \min T_{ac} / \max T_{ac}$  in the anchor cable is then determined by:

$$\kappa_{ac} = \frac{\min T_{ac}}{\max T_{ac}} = \frac{\sum_{i=1}^n G_i a_i - \sum_{j=1}^m (G_j + P_j) a_j}{\sum_{i=1}^n (G_i + P_i) a_i - \sum_{j=1}^m G_j a_j} \quad (3.46)$$

With a specified value of  $\kappa_{ac}$  and a given main span length this expression can be used to determine the side span length.

For a continuous system with uniform load as shown in Figure 3.67, the expression for  $\kappa_{ac}$  becomes:

$$\kappa_{ac} = \frac{g l_m^2 - 4(g+p) l_a^2}{(g+p) l_m^2 - 4g l_a^2} \quad (3.47)$$

leading to the following expression for the side span length  $l_a$ :

$$l_a = \frac{1}{2} l_m \sqrt{\frac{(1 - \kappa_{ac})g - \kappa_{ac}p}{(1 - \kappa_{ac})g + p}} \quad (3.48)$$

Figure 3.68 shows in diagrammatic form the variation of  $l_a/l_m$  with  $p/g$ , and with  $\kappa_{ac}$  as a curve parameter. Note that the side span length  $l_a$  always will be less than half the main span length  $l_m$  ( $l_a/l_m < 0.5$ ) and that  $l_a$  decreases with increasing values of  $p/g$  as well as with  $\kappa_{ac}$ . For a bridge with  $\kappa_{ac} = 0.4$  and  $p = 0.25g$ , corresponding to a typical road bridge situation,  $l_a/l_m$  becomes 0.38, so that in this case the side span length could amount to almost 40% of the main span length without

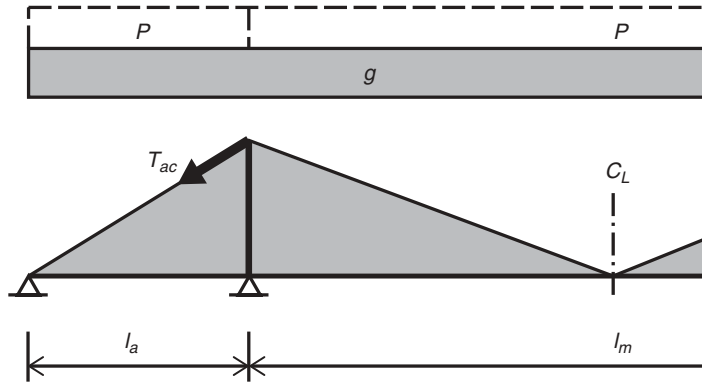


Figure 3.67 Fan system idealized as a continuous system

exceeding the stress ratio of 0.4. With  $\kappa_{ac} = 0.4$  and  $p = g$ , corresponding to a rather extreme railway bridge (or pedestrian bridge) case,  $l_a/l_m$  becomes 0.18, so in this case the side span length should be less than one fifth of the main span length to keep the desired stress ratio. From these examples it can be noted that the relative intensity of the traffic load has a decisive influence on the choice of the main geometry for bridges with a fan system.

It should, however, be emphasized that the expressions (3.46)–(3.48) and Figure 3.68 are based on the assumption that the flexural stiffness of the deck can be ignored. The derived values of  $l_a/l_m$  are therefore somewhat conservative as the flexural stiffness of the deck generally tends to decrease the stress ratio  $\kappa_{ac}$  of the anchor cable.

To illustrate this feature, Figure 3.69 shows the curve for  $\kappa_{ac} = 0.4$  (from Figure 3.68) together with a shaded area indicating the relation between  $l_a/l_m$  and  $p/g$  for  $\kappa_{ac} = 0.4$  in cases where the flexural stiffness is included. The width of the shaded area indicates the interval between cases with a lower and an upper value of the flexural stiffness of the deck.

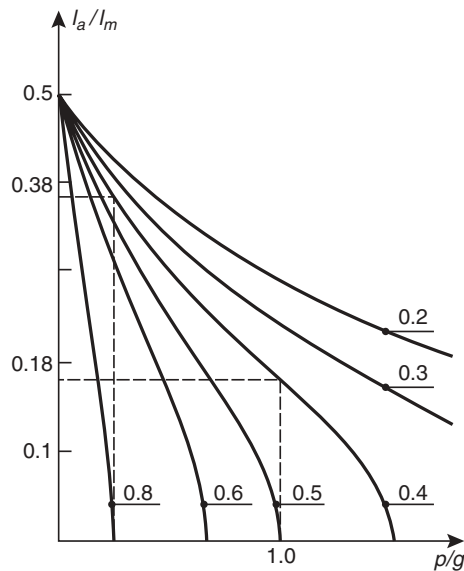
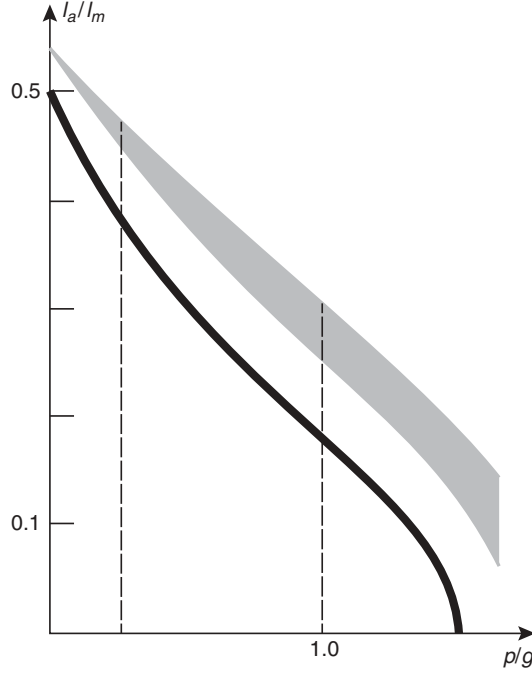


Figure 3.68 Variation of the critical side-to-main span ratio  $l_a/l_m$  with the traffic-to-dead load ratio  $p/g$  and the stress ratio  $\kappa_{ac}$



**Figure 3.69** Influence of the flexural stiffness of the deck on the relation between  $l_a/l_m$  and  $p/g$  (for  $\kappa_{ac} = 0.4$ ). Full line, flexural stiffness neglected; shaded area, flexural stiffness included

It should be noted that the effect of the flexural stiffness is especially pronounced for the higher  $p/g$  values. Thus, for  $p/g = 1.0$  the ratio  $l_a/l_m$  can be increased by 50–70% when taking the flexural stiffness into account, whereas only a 20–25% increase can be allowed for  $p/g = 0.25$ .

### 3.3.2 Preliminary cable dimensions

A preliminary design of stay cables can be based on the same assumptions as those applied for the hangers of the suspension bridge.

Ignoring the influence of the cable sag and with the same distribution length for the concentrated force  $P$  as for the suspension bridge hangers (refer to Figure 3.24), the tension  $T_{sc,i}$  in the  $i$ th stay cable becomes (Figure 3.70):

$$T_{sc,i} \sim \left( g + p + \frac{p}{30d} \right) \frac{\lambda_i + \lambda_{i+1}}{2 \sin \phi_i} + \gamma_{cb} A_{sc,i} \frac{a_i}{\sin \phi_i \cos \phi_i} \quad (3.49)$$

As  $T_{sc,i} = A_{sc,i} f_{cdb}$  the following expression for the cross sectional area of the stay cable can be derived:

$$A_{sc,i} \simeq \frac{(g + p + P/30d)(\lambda_i + \lambda_{i+1}) \cos \phi_i}{2(f_{cbd} \sin \phi_i \cos \phi_i - \gamma_{cb} a_i)} \quad (3.50)$$

The maximum force in the anchor cable will appear for the loading case with the most pronounced unbalance between the two fans, i.e. traffic plus dead load in the main span and dead load only in the side span, as indicated in Figure 3.71. Based on this loading, the cross sectional area  $A_{ac}$  of the anchor cable is first determined by:

$$A_{ac} \simeq \frac{\frac{1}{2}(g_m + p_m) a_m^2 - \frac{1}{2} g_a a_a^2 + 0.8 P a_m + \frac{1}{2} \gamma_{cb} \sum_{i=1}^n (A_{sc,i} a_i^2 / \cos \phi_i)}{h f_{cbd} \cos \phi_{ac}} \quad (3.51)$$

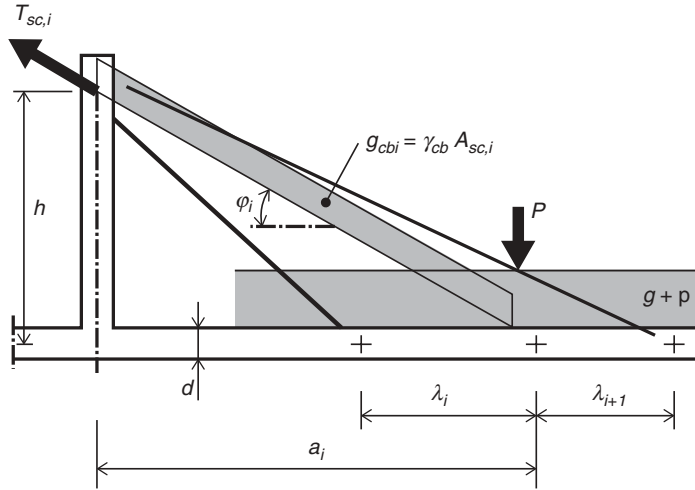


Figure 3.70 Loading case for maximum stay cable force

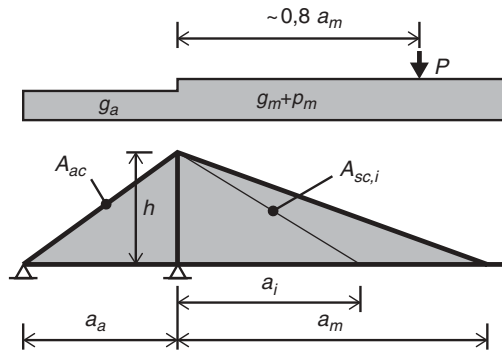


Figure 3.71 Loading case for maximum anchor cable force

where  $A_{sc,i}$  is the cross sectional area of the  $i$ th stay cable (determined by (3.50)) and  $n$  the total number of stay cables in the entire double fan from the end pier to the main span centre.

### 3.3.3 Quantity of cable steel

To arrive at expressions for the quantity of cable steel in a bridge with a fan-shaped cable system, a fan as shown in Figure 3.72 will be considered. The fan is idealized to a continuous system and subjected to uniform load  $g + p$ .

The cable steel quantity  $dQ$  for the cable D-C becomes:

$$dQ \simeq \frac{\gamma_{cb}}{f_{cbd}} \frac{g+p}{h} \left( 1 + \frac{\gamma_{cb}}{f_{cbd}} \frac{x^2 + h^2}{h} \right) (x^2 + h^2) dx \quad (3.52)$$

leading to the following total quantity of cable steel in the fan:

$$Q_F \simeq \frac{\gamma_{cb}}{f_{cbd}} (g+p) \left[ \frac{1}{5} \frac{\gamma_{cb}}{f_{cbd}} a \left( \frac{a}{h} \right)^4 + \frac{1}{3} \left( 1 + 2 \frac{\gamma_{cb}}{f_{cbd}} h \right) \left( \frac{a}{h} \right)^3 + \left( 1 + \frac{\gamma_{cb}}{f_{cbd}} \right) \frac{a}{h} \right] h^2 \quad (3.53)$$

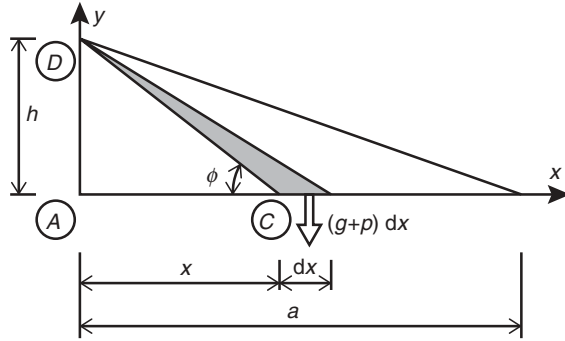


Figure 3.72 Idealized, continuous fan subjected to load  $g + p$

The moment  $M_F$  about A(0,0) from the weight of the fan becomes:

$$M_F \simeq \frac{1}{4} \frac{\gamma_{cb}}{f_{cbd}} (g + p) \left[ \frac{1}{3} \frac{\gamma_{cb}}{f_{cbd}} a \left( \frac{a}{h} \right)^4 + \frac{1}{2} \left( 1 + 2 \frac{\gamma_{cb}}{f_{cbd}} h \right) \left( \frac{a}{h} \right)^3 + \left( 1 + \frac{\gamma_{cb}}{f_{cbd}} \right) \right] \frac{a}{h} h^2 a \quad (3.54)$$

The distance  $e_F$  from the pylon (point A) to the centre of gravity for the fan is determined by:

$$e_F = M_F / Q_F \quad (3.55)$$

For  $a/h$  varying within the interval from 1 to 3, and  $a$  from 100 m to 500 m,  $e_F$  will vary from  $0.28 a$  to  $0.35 a$ . As the weight of the cables generally is of minor importance compared to the load from the deck, it will be sufficient here to fix  $e_F$  at the value  $a/3$ .

For a symmetrical three-span bridge subjected to uniform load  $g_m + p_m$  in main span and  $g_a + p_a$  (or  $g_a$  only) in the side spans, as shown in Figure 3.73, the quantity of cable steel will comprise the following three contributions:

- (a) cable steel in the main span fan
- (b) cable steel in the side span fans
- (c) cable steel in the anchor cables.

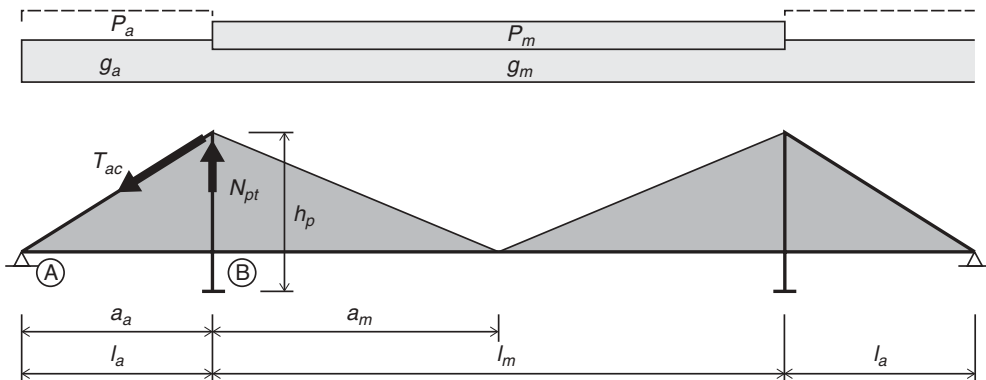


Figure 3.73 Symmetrical three-span bridge with idealized, continuous fans

The contributions from (a) and (b) are found directly from (3.53):

$$Q_{Fm} = \frac{\gamma_{cb}}{f_{cbd}} (g_m + p_m) \left[ \frac{1}{5} \frac{\gamma_{cb}}{f_{cbd}} a_m \left( \frac{a_m}{h} \right)^4 + \frac{1}{3} \left( 1 + 2 \frac{\gamma_{cb}}{f_{cbd}} h \right) \left( \frac{a_m}{h} \right)^3 + \left( 1 + \frac{\gamma_{cb}}{f_{cbd}} h \right) \frac{a_m}{h} \right] h^2 \quad (3.56)$$

$$Q_{Fa} = \frac{\gamma_{cb}}{f_{cbd}} (g_a + p_a) \left[ \frac{1}{5} \frac{\gamma_{cb}}{f_{cbd}} a_a \left( \frac{a_a}{h} \right)^4 + \frac{1}{3} \left( 1 + 2 \frac{\gamma_{cb}}{f_{cbd}} h \right) \left( \frac{a_a}{h} \right)^3 + \left( 1 + \frac{\gamma_{cb}}{f_{cbd}} h \right) \frac{a_a}{h} \right] h^2 \quad (3.57)$$

Note that (3.56) and (3.57) each give the quantity of cable steel in one fan only. Thus, for a symmetrical three-span bridge the total quantity of cable steel in the fans becomes  $2Q_{Fm} + 2Q_{Fa}$ .

The quantity of one anchor cable is determined by:

$$Q_{ac} = \gamma_{cb} A_{ac} a_c / \cos \phi_{ac}$$

where  $A_{ac}$  is to be taken from (3.51).

Replacing the summation  $\frac{1}{2} \gamma_{cb} \sum_{i=1}^n (A_{sc,i} a_i^2 / \cos \phi_i)$  by  $\frac{1}{3} (Q_{Fm} a_m - Q_{Fa} a_a)$  the expression for the anchor cable steel quantity becomes:

$$Q_{ac} = \frac{\gamma_{cb}}{f_{cbd}} \left[ \frac{1}{2} (g_m + p_m) a_m^2 - \frac{1}{2} g_a a_a^2 + \frac{1}{3} Q_{Fm} a_m - \frac{1}{3} Q_{Fa} a_a \right] \left( \frac{a_a}{h} + \frac{h}{a_a} \right) \quad (3.58)$$

### 3.3.4 Quantity in the pylon

The maximum normal force  $N_{pt}$  at the pylon top is determined by taking moments about A ( $-a_a, 0$ ) for a loading case with traffic load throughout the spans:

$$N_{pt} = \frac{1}{2} (g_a + p_a) a_a + \frac{1}{2} (g_m + p_m) \left( 2 + \frac{a_m}{a_a} \right) a_m + \frac{2}{3} Q_{Fa} + Q_{Fm} \left( 1 + \frac{a_m}{3a_a} \right) + \frac{1}{2} Q_a \quad (3.59)$$

The quantity of the pylon is then found from (3.42):

$$Q_{pt} = N_{pt} \left[ \exp \left( \frac{\gamma_{pl}}{f_{pld}} h_{pl} \right) - 1 \right] \quad (3.60)$$

### 3.3.5 Simplified expressions

In bridges with moderate spans the contribution from the cable dead load to the forces in the cables is of minor importance, and the expressions for the cable steel quantity can therefore in these cases be simplified to the following:

$$Q_{Fm} = \frac{\gamma_{cb}}{f_{cbd}} (g_m + p_m) \left( \frac{1}{3} \frac{a_m}{h} + \frac{h}{a_m} \right) a_m^2 \quad (3.61)$$

$$Q_{Fa} = \frac{\gamma_{cb}}{f_{cbd}} (g_a + p_a) \left( \frac{1}{3} \frac{a_a}{h} + \frac{h}{a_a} \right) a_a^2 \quad (3.62)$$

$$Q_{ac} = \frac{1}{2} \frac{\gamma_{cb}}{f_{cbd}} \left[ (g_m + p_m) a_m^2 - g_a a_a^2 \right] \frac{a_a^2 + h^2}{a_a h} \quad (3.63)$$

$$Q_{pl} = \left[ \frac{1}{2}(g_a + p_a)a_a + \frac{1}{2}(g_m + p_m) \left( 2 + \frac{a_m}{a_a} \right) a_m \right] \left[ \exp \left( \frac{\gamma_{pl}}{f_{pld}} h_{pl} \right) - 1 \right]$$

$$N_{pl} = \frac{1}{2}(g_a + p_a)a_a + \frac{1}{2}(g_m + p_m) \left( 2 + \frac{a_m}{a_a} \right) a_m \quad (3.64)$$

### 3.3.6 Total cost of cable systems and pylons

The total cost  $C_{cp}$  of the cable systems and the pylons in the three-span bridge can now be expressed by:

$$C_{cp} = 2(Q_{Fm} + Q_{Fa} + Q_{ac})u_{cb} + 2Q_{pl} u_{pl}$$

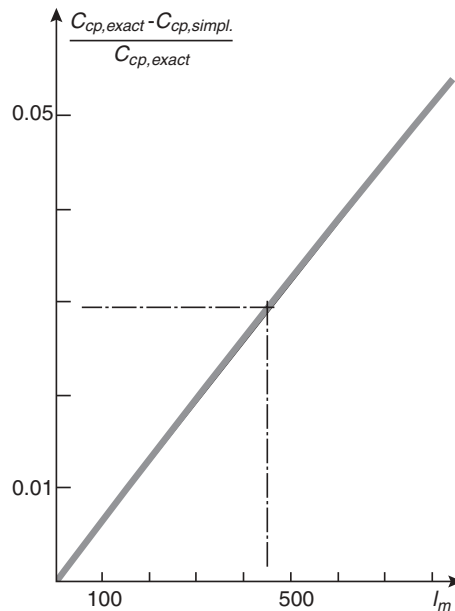
where  $u_{cb}$  is the unit price for erected and protected cable steel and  $u_{pl}$  the unit price for the material in the pylons.

As in the case of the suspension system, the unit prices have to be stipulated at constant values corresponding to realistic average values.

The magnitude of the error introduced by applying the simplified expressions (3.61)–(3.64) is illustrated in Figure 3.74. Here the error, defined as  $1 - C_{cp,simpl}/C_{cp,exact}$  plotted against the main span length  $l_m$ . It is seen that the error remains under 3% for main spans up to 450 m and the approximate approach will therefore be adequate in the preliminary design process for all cable stayed bridges with moderate spans in the 200–400 m main span range.

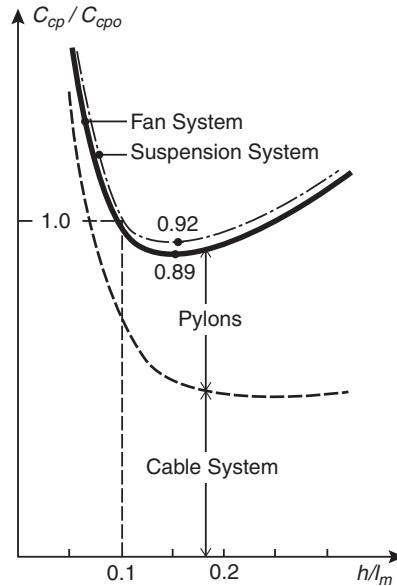
### 3.3.7 Comparison between suspension and fan system

In a comparison between the suspension system and the fan system it can generally be assumed that the unit price for the material to go into the pylon (and the deck) is the same for the two systems. However, for the cable steel there is a difference due to the higher cost of the corrosion protection and the large number of heavy sockets in a cable stayed bridge. Therefore in a comparison the unit price for cable steel in a cable stayed bridge should be stipulated at a value between 1.2 and



**Figure 3.74** Error by application of simplified expressions ignoring the weight of cables. The plot is based on the following parameters:  $a_m = 2a_a$ ;  $h_{pl} = 0.5a_a + 30$ ;  $g_a = g_m = 0.20$  MN/m;  $p_a = p_m = 0.08$  MN/m





**Figure 3.75** Variation of the relative cost  $C_{cp}/C_{cp0}$  for three-span bridges with a fan system or a suspension system. For both systems the following parameters are used:  $l_a = a_a = 125$  m;  $l_m = 2a_m = 500$  m;  $h_{pb} = 30$  m;  $g_a^2 g_m = 0.20$  MN/m;  $p_a = p_m = 0.08$  MN/m

1.8 times the value for cable steel in the suspension bridge main cables. With a value of  $u_{cb}/u_{pl} = 1.75$  for the suspension system with steel pylons, and  $u_{cb}/u_{pl} = 2.5$  for the fan system with steel pylons the variation of the relative cost  $C_{cp}/C_{cp0}$  with the height ratio  $h/l_m$  will be as shown in Figure 3.75. As was the case in Figure 3.29, the cost  $C_{cp0}$  relates to a suspension bridge with the sag ratio 1:10.

It is seen that for equal pylon height the difference between the cost of the cable system plus pylons in a suspension bridge and a cable stayed bridge is marginal when applying the higher unit price for cable steel in stays. However, in a cable stayed bridge a saving can be achieved by choosing the optimum pylon height as stiffness considerations do not lead to a reduced height. Thus, for the example illustrated in Figure 3.75 a saving of 11% can be achieved by choosing a fan system with the optimum pylon height ( $h/l_m \sim 0.17$ ) instead of the suspension system with the traditional sag ratio of 0.10.

It should be mentioned that the optimum height-to-span ratio of the fan system will depend on the dead load of the deck. The value  $h_{opt}/l_m = 0.17$  is found for a relatively light deck of steel so it actually constitutes a lower bound for the optimum height-to-span ratio. For bridges with heavy concrete decks, the optimum pylon height will rather be found for height-to-span ratios around 0.25.

Finally, it must be remembered that a self anchored cable system can lead to substantial savings in the substructure compared to an earth anchored system.

### 3.3.8 Inclined pylons

In elevation the pylons found within cable supported bridges are made in the vast majority of cases with a vertical axis. However, in cable stayed bridges with fan-shaped cable systems, a few examples can be found on bridges with pylons inclined in the longitudinal direction of the bridge. As an example, Figure 3.76 shows the bridge across the Danube River in Bratislava (Slovakia).

The influence of the pylon inclination on the quantities of the system can be studied by a similar procedure as that described for the fan system with a vertical pylon.



**Figure 3.76** The Danube River Bridge in Bratislava

Applying the simplifying assumptions leading to (3.61)–(3.64) results in the following quantities of the fans AOD ( $Q_{Fa}$ ) and DOC ( $Q_{Fm}$ ) indicated in Figure 3.77:

$$Q_{Fa} = \frac{\gamma_{cb}}{f_{cbd}} (g + p) \left( \frac{1}{3} \frac{a_a - e}{h} + \frac{h}{a_a - e} \right) (a_a - e)^2 \quad (3.65)$$

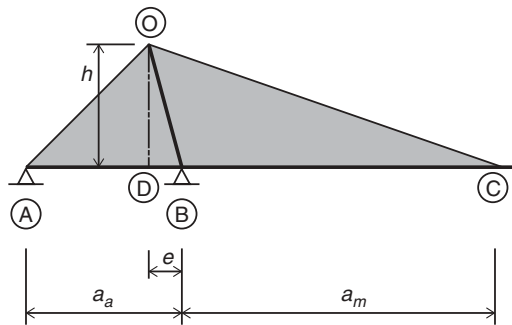
$$Q_{Fm} = \frac{\gamma_{cb}}{f_{cbd}} (g + p) \left( \frac{1}{3} \frac{a_m - e}{h} + \frac{h}{a_m + e} \right) (a_m + e)^2 \quad (3.66)$$

Quantity of the anchor cable A–O ( $Q_{ac}$ ):

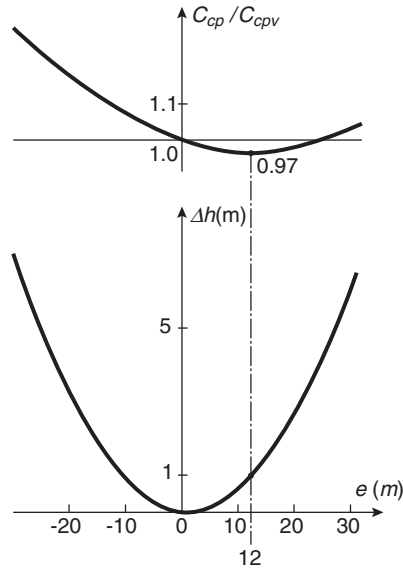
$$Q_{ac} = \frac{\gamma_{cb}}{f_{cbd}} ((g + p)a_m^2 - ga_a^2) \frac{h^2 + (a_a - e)^2}{2ha_a} \quad (3.67)$$

Quantity of the pylon ( $Q_p$ ):

$$Q_{pl} = \frac{\gamma_{pl}}{f_{pld}} (g + p) \frac{(a_a + a_m)^2 (h^2 + e^2)}{2ha_a} \quad (3.68)$$



**Figure 3.77** System with inclined pylon and idealized, continuous fans



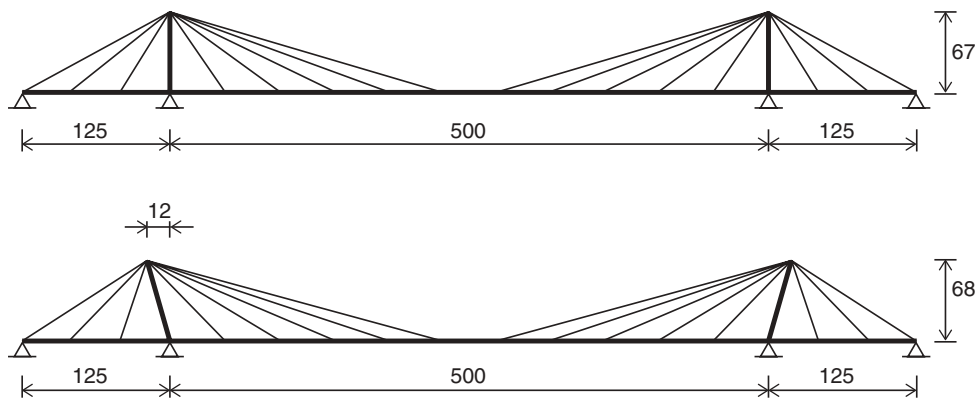
**Figure 3.78** Variation of the relative cost  $C_{cp}/C_{cpV}$  and the additional pylon height  $\Delta h$  with the horizontal pylon projection  $e$

With  $C_{cp}(e, h) = (Q_{Fa} + Q_{Fm} + Q_{ac}) u_{cb} + Q_{pl} u_{pl}$  the optimum pylon height  $h_{opt}$  for a chosen value of  $e$  is determined by the condition  $\partial C_{cp} / \partial C_{cpV} = 0$ , and subsequently the minimum cost by  $C_{cp}(e, h_{opt})$ .

For the geometrical and mechanical values used in connection with Figure 3.75 the increase of the pylon height  $\Delta h = h_{opt, inclined} - h_{opt, vertical}$  and the relative cost  $C_{cp}/C_{cpV}$  will vary as shown in Figure 3.78.

It appears from the example chosen that for the pylon the smallest optimum height is found for an almost vertical pylon whereas minimum cost for the cable system plus pylon is achieved for a pylon with its top displaced 12 m towards the side span, as illustrated at the bottom of Figure 3.79. However, the reduction in the quantity-based cost is only about 3% and this saving might easily be outbalanced by increased erection costs due to the requirement of temporary support to stabilize the partially erected pylon – especially in the case of a concrete pylon.

The investigation shows that the pylon might lean backwards (towards the side span) with an angle in the interval from  $0^\circ$  to  $18^\circ$  without seriously affecting the quantity-based cost, and this indicates a certain freedom in choosing the geometrical configuration.



**Figure 3.79** Comparison between a three-span bridge with vertical pylons and with pylons at optimum inclination

In this connection it should be emphasized that a pylon leaning backwards might lead to a quite pleasing appearance, as it expresses resistance against the pull from the cables carrying the large main span.

**3.3.9 Deformational characteristics**

In cable stayed bridges with slender decks, the deflection of the total system is to a very large extent caused by the elongation of the cables, and the general deflection pattern can therefore be derived by taking into account only the elongation of the cables.

Figure 3.80 shows a fan with the height  $h$  and the length  $a$ . Under the assumption of a fixed supporting point at the pylon top the following variation of the vertical deflection  $\delta_y(x)$  is found:

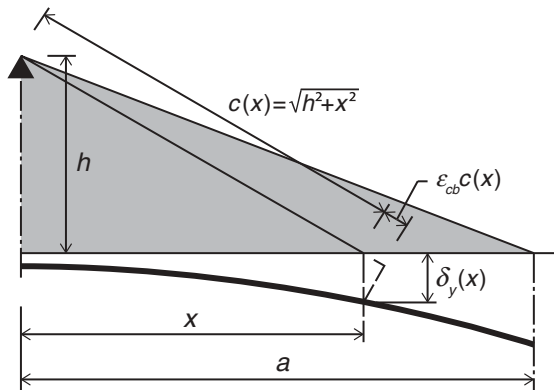
$$\delta_y(x) = h \left( 1 + \frac{x^2}{h^2} \right) \epsilon_c \tag{3.69}$$

For a constant strain  $\epsilon_c$  in all stay cables the deflection curve will be convex, whereas it is concave for the suspension system (refer to Figure 2.59).

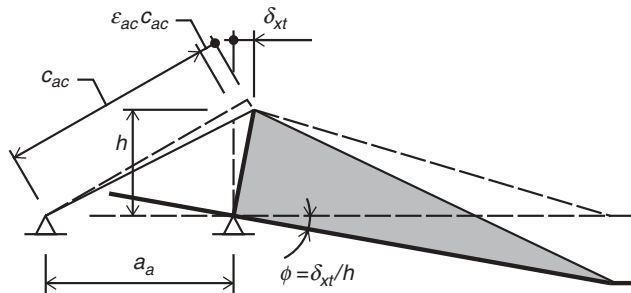
The deflection expressed by (3.69) is due only to the elongation of the stay cables. However, the elongation of the anchor cable will result in a horizontal displacement of the pylon top that also contributes to the vertical deflections of the main span.

As indicated in Figure 3.81, the elongation of the anchor cable implies that the total main span fan rotates. The angle of rotation  $\phi$  is expressed by:

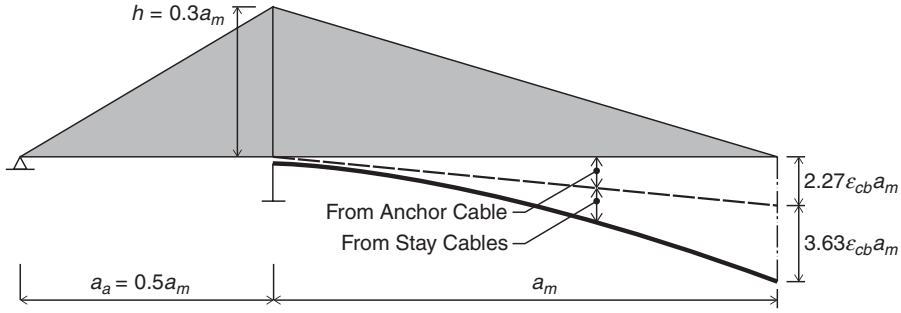
$$\phi = \frac{\delta_{xt}}{h} = \frac{h^2 + a_a^2}{ha_a} \epsilon_{ac} \tag{3.70}$$



**Figure 3.80** Vertical deflection caused by the elongation of the stay cables



**Figure 3.81** Rotation of the cable system caused by elongation of the anchor cable



**Figure 3.82** Deflection of the main span due to elongation of the anchor cable and the stay cables

The total deflection of the deck caused by the cable elongations thus becomes:

$$\delta_y(x) = h \left( 1 + \frac{x^2}{h^2} \right) \varepsilon_{sc} + \frac{h^2 + a_a^2}{ha_a} \varepsilon_{ac} x \quad (3.71)$$

For a fan system with  $a_a = 0.5a_m$ ,  $h = 0.3a_m$  and  $\varepsilon_{sc} = \varepsilon_{ac} = \varepsilon_c$  (= constant) the deflection of the main span will be as shown in Figure 3.82. Note that the elongation of the anchor cable in this case accounts for almost 40% of midspan deflection.

Assuming the same maximum stress  $\sigma_{cb}$  in all cables (= design stress  $f_{cbd}$ ) and ignoring the flexural stiffness of the deck the following cable strains due to traffic are derived:

$$\begin{aligned} \varepsilon_{sc} &= \frac{p}{g+p} \frac{f_{cbd}}{E} \\ \varepsilon_{ac} &= \frac{p}{g[1 - (a_a/a_m)^2] + p} \frac{f_{cbd}}{E} \end{aligned} \quad (3.72)$$

The midspan deflection  $\delta_y(a_m)$  is then found by inserting  $\varepsilon_{sc}$  and  $\varepsilon_{ac}$  from (3.72) into (3.71) with  $x = a_m$ :

$$\delta_y(a_m) = \left\{ \frac{p}{g+p} h \left( 1 + \left( \frac{a_m}{h} \right)^2 \right) + \frac{p}{g[1 - (a_a/a_m)^2] + p} a_m \left( \frac{h}{a_a} + \frac{a_a}{h} \right) \right\} \frac{f_{cbd}}{E} \quad (3.73)$$

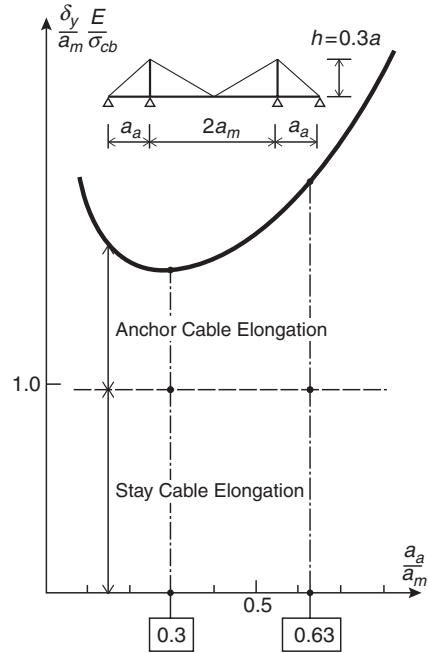
With  $h = 0.3 a_m$ ,  $g = 0.22$  MN/m and  $p = 0.08$  MN/m the midspan deflection  $\delta_y(a_m)$  is plotted against the relative side span length  $a_d/a_m$  in Figure 3.83.

It is seen that, whereas the contribution from the stay cable elongation remains constant, the contribution from the anchor cable elongation will vary with the side span length. Under the given assumptions the minimum deflection occurs for  $a_a \sim 0.3a_m$  corresponding to a  $45^\circ$  inclination of the anchor cable. For  $a_d/a_m$  values above 0.5 the contribution from the anchor cable elongation shows a rapid increase and from  $a_d/a_m \sim 0.63$  the contribution from the anchor cable exceeds the contribution from the stay cable.

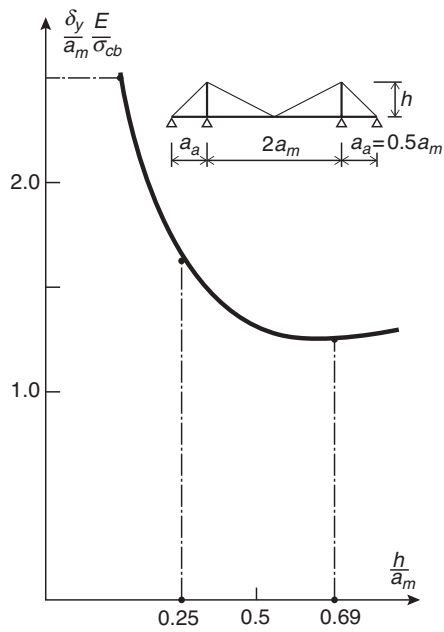
Generally, it can be stated that the side span length has a decisive influence on the deformational characteristics of the fan system, and – as was the case for the suspension system – short side spans are therefore to be preferred when optimum stiffness is desirable.

It should be emphasized that Figure 3.83 does not include the sag effect of the anchor cable. In long span bridges, this effect would tend to further increase the deflections as the side spans grow.

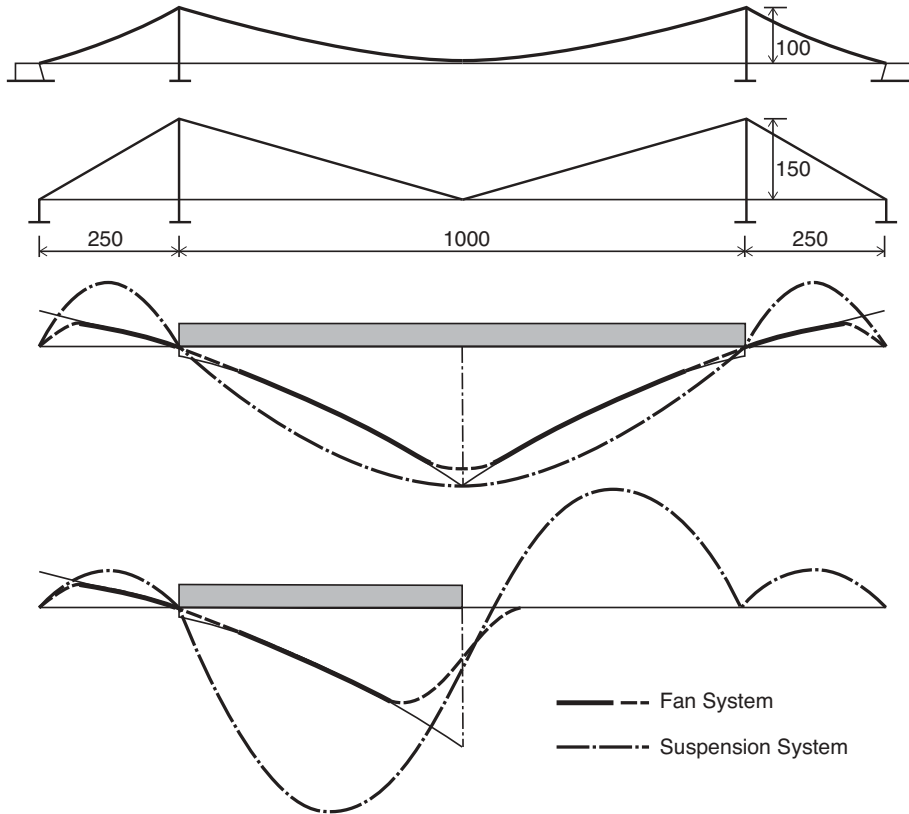
For a system with  $a_a = 0.5a_m$  the variation of the midspan deflection with the relative pylon height  $h/a_m$  is shown in Figure 3.84. Note that the minimum deflection occurs for a pylon height of  $0.69a_m$  which is somewhat higher than used in



**Figure 3.83** Contribution from the stay cable elongation and the anchor cable elongation to the midspan deflection  $\delta_y$



**Figure 3.84** Variation of the midspan deflection  $\delta_y$  with the relative pylon height  $h/a_m$



**Figure 3.85** Comparison between deflections of the fan system and the suspension system

actual construction, where the ratio  $h/a_m$  hardly exceeds the value 0.25. With this value the midspan deflection is approximately 38% larger than for  $h/a_m = 0.69$ .

Some of the basic differences between the deformational characteristics of the fan system and the suspension system are illustrated by the deflection curves in Figure 3.85. These curves are all based on the assumption that the flexural stiffness of the deck and the pylon can be ignored and that all cables are designed to have the same maximum stress (= the design stress  $f_{cbd}$ ).

For traffic load in the entire main span, the midspan deflection is practically the same for the two systems with zero flexural stiffness of the decks. However, in real structures the flexural stiffness of the deck will inevitably round off the deflection curve of the fan system at midspan (as indicated with a dotted line) and this implies that the maximum deflection in this system is somewhat reduced. Note that in the side spans the suspension system shows a considerably larger uplift than the fan system.

For the fan system under asymmetric traffic load in one main span half only, the deflection of the loaded half will be exactly the same as in the symmetrical case when the flexural stiffness of the deck is ignored. For the suspension system under asymmetrical traffic load a pronounced uplift occurs in all unloaded regions.

It is a general trend that the fan system has its deflections concentrated towards the loaded regions, whereas the suspension system also shows considerable deflections (uplift) in the unloaded regions.

With zero flexural deck stiffness the deflections of the fan system will have discontinuities at midspan and end supports. In real structures even a small flexural stiffness of the deck will round off these discontinuities (as shown with dotted lines).

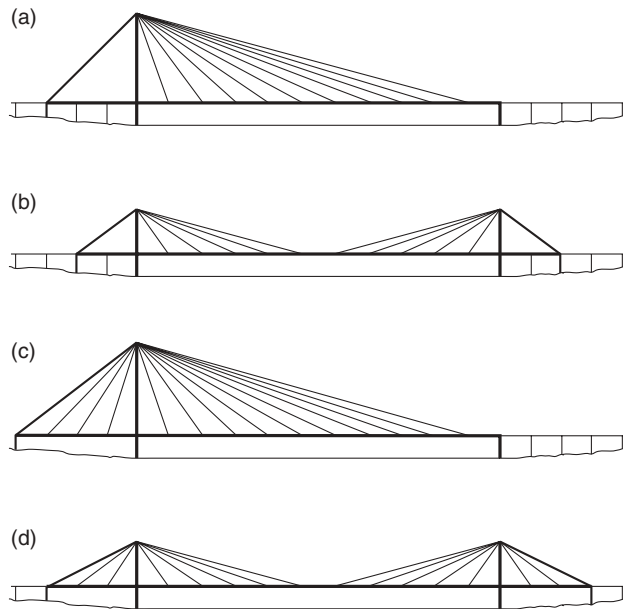
### 3.3.10 Structural systems

In bridges with one main span, a number of different solutions for the configuration of the fan system, exists, as shown in Figure 3.86 and summarized below:

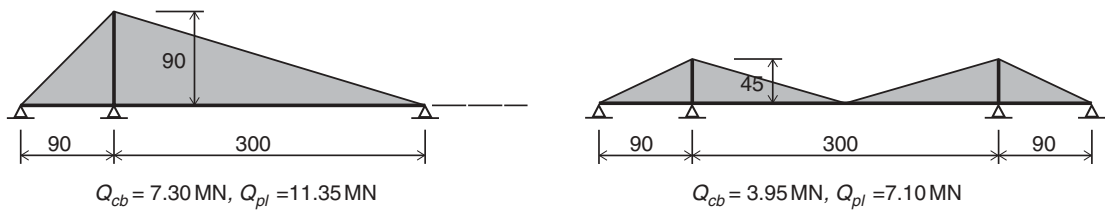
- a single fan with one anchor cable;
- two single fans each with one anchor cable;
- a double fan;
- two double fans.

The solution to be adopted in a given case will often depend on the local conditions at the bridge site. Thus, solutions (a) and (b) require that approach spans with closely spaced piers can be used all the way to the pylons. Solutions (a) and (c) allow curved approach ramps to be added to the main deck immediately outside the right main pier.

Generally, the quantity of cable steel and structural steel (or concrete) in the pylons will be smallest in bridges with two fans, as illustrated by the example shown in Figure 3.87. The quantities given are based on (3.56)–(3.60).



**Figure 3.86** Different arrangements of fan-shaped cable systems to support a large main span



**Figure 3.87** Comparison between quantities of cable steel  $Q_{cb}$  and pylon material  $Q_{pl}$  in a bridge with one double fan and a bridge with two double fans. The comparison is based on the following parameters:  $g = 0.20 \text{ MN/m}$ ;  $p = 0.08 \text{ MN/m}$ ;  $f_{cbd} = 720 \text{ MPa}$ ;  $\gamma_{cb} = 0.08 \text{ MN/m}^3$ ;  $f_{pld} = 160 \text{ MPa}$ ;  $\gamma_{pl} = 0.08 \text{ MN/m}^3$





**Figure 3.88** Early cable stayed bridge with few concentrated stay cables (Strömsund Bridge)

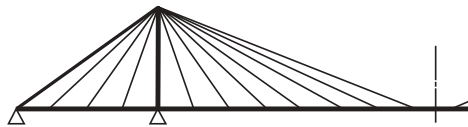
From the given quantities it is seen that the quantity of cable steel is increased by 85% and the quantity of structural steel by 60% when changing from the system with two double fans to the system with only one double fan. The symmetrical system with two pylons is therefore generally to be preferred unless local conditions specifically favour the system with one pylon only.

In early cable stayed bridges with a fan system, only very few concentrated stay cables were used, as illustrated by the Strömsund Bridge, shown in Figure 3.88.

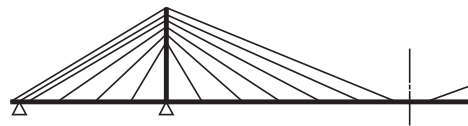
In the bridges with few stay cables the fans could often be arranged symmetrically about the pylon, as the large flexural stiffness of the deck prevented a too large unloading of the anchor cable under traffic load in the side span. Also, with few stay cables the side span length remains with a certain margin below half of the main span length.

In the true cable stayed bridge with a multi-cable system and a slender deck, a symmetrical fan with the side span top cable forming the anchor cable is not feasible, as the required minimum tension in the anchor cable cannot be achieved for all loading cases. Consequently, skew fans, as shown in Figure 3.89, are generally used. In such a system the anchor cable must be made with a considerably larger cross section than the regular stay cables.

In multi-cable fans the cable anchorages are often spread over a certain distance at the pylon top, so that the system actually becomes a semi-fan system. At the same time the anchor cable is often composed of a number of individual strands in parallel, as illustrated in Figure 3.90.



**Figure 3.89** Multi-cable system with a shorter fan in the side span than in the main span



**Figure 3.90** Anchor cable composed of several parallel mono-strand cables



**Figure 3.91** Anchor cable composed of six individual strands (Jindo Bridge)

Such an arrangement is found, e.g., in the Jindo Bridge in Korea (Figure 3.91) where the side-to-main span ratio is 0.2 and the anchor cable is composed of six individual strands.

However, a symmetrical fan might still be applied in a multi-cable system if the end pier is moved in from the side span top cable anchorage towards the pylon, as shown in Figure 3.92. By this arrangement it is obtained that the side span length becomes less than half of the main span length, and also that several of the side span cables attached near the intermediate support will be activated to form the anchor cable. However, this induces a significant local bending in the deck near the intermediate pier – a local bending which does not appear in systems with a concentrated anchor cable connected centrally to the deck above the end pier.

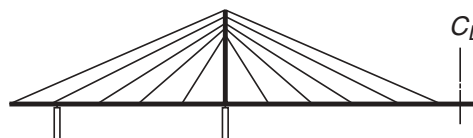
Symmetrical multi-cable fans with intermediate anchor piers were first seen in the Farø Bridge in Denmark (Figure 3.93). Here the intermediate pier is positioned under the anchorage of the second side span stay cable, 16 m from the end of the fan. Thus, the three outer cables of the side span can be regarded as forming the anchor cables.

A symmetrical fan arrangement in combination with an anchor pier positioned at the end of the side span fan has been used in the Tsurumi Tsubasa Bridge in Japan (Figure 3.94). Here the length of the side spans, 255 m, is exactly half of the main span length (510 m). This implies that the cable system itself becomes unstable for traffic load acting in the side spans only, so for this loading case the flexural stiffness of the deck and the pylons has to be activated to achieve stability of the total system.

In a parametric study [93.2], a system as shown in Figure 3.95 was considered. The system comprised a five-span bridge with deck continuity and cable support by two symmetric fans. The outer spans were chosen to have a length of one-fifth of the main span length ( $l_e/l_m = 0.2$ ), whereas the ratio between the side span and the main span was varied between 0.5 and 0.3.

The result of the comparative investigation is summarized in Table 3.2 showing the relative quantities of cable steel, the ratios  $\kappa$  between the minimum and the maximum anchor cable tension, and the relative deflections. The reference system is a three-span system with the same fans and with the anchor pier positioned at the ends of the side span fans.

From Table 3.2 it is seen that, despite the fact that the cable steel quantity only shows a moderate variation, the deformational characteristics are significantly influenced by the side-to-main span ratio. Thus, a reduction of this ratio from



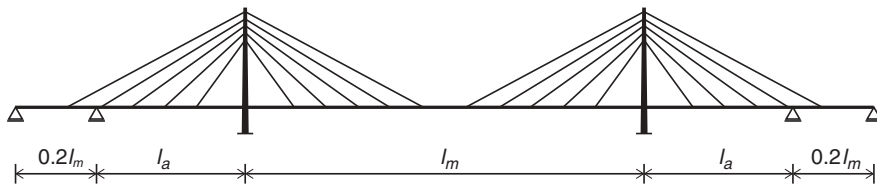
**Figure 3.92** Symmetrical multi-cable fan with the end pier in the side span positioned inside the fan



**Figure 3.93** Cable system of the Farø Bridge in Denmark



**Figure 3.94** The Turumi Tsubasa Bridge in Japan



**Figure 3.95** Five-span bridge system used in a parametric study of the effect of different side-to-main span ratios

0.49 to 0.31 for the five-span bridge will reduce the maximum main span deflection by 30% (from 0.84 to 0.59), the main span uplift by 87% (from 0.31 to 0.04), and the maximum side span deflection by 72% (from 0.36 to 0.10).

It appears that the most pronounced effect of a reduced side-to-main span ratio occurs for the deformations that are influenced by unloading of the anchor cable, i.e. uplift of the main span and deflection of the side span.

From the investigations summarized in Table 3.2 it can be concluded that the side-to-main span ratio has a very strong influence on the stress ratios of the anchor cable and the deformational characteristics. For all performances the smallest side-to-main span ratio results in the most favourable values.

**Table 3.2** Characteristics of cable stayed bridges with different side-to-main span ratios

| $l_a/l_m$ | Relative quantity of cable steel | $\kappa$ for anchor cable | Relative deflections (m) |       |           |       |
|-----------|----------------------------------|---------------------------|--------------------------|-------|-----------|-------|
|           |                                  |                           | Main span                |       | Side span |       |
|           |                                  |                           | max                      | min   | max       | min   |
| Reference | 1.00                             | 0.17                      | 1.00                     | -0.56 | 0.59      | -0.57 |
| 0.49      | 0.97                             | 0.31                      | 0.84                     | -0.31 | 0.36      | -0.35 |
| 0.43      | 0.97                             | 0.46                      | 0.69                     | -0.15 | 0.23      | -0.22 |
| 0.37      | 0.94                             | 0.57                      | 0.61                     | -0.07 | 0.15      | -0.14 |
| 0.31      | 0.92                             | 0.62                      | 0.59                     | -0.04 | 0.10      | -0.09 |

### 3.3.11 Reduction of sag variations

In cable stayed bridges with fan systems and very long spans requiring stay cables with a horizontal projection exceeding 500 m, problems arise due to the sag effect. Consequently, in long span bridges it might prove advantageous to add to the primary cable system secondary cables in the form of cross ties to reduce the sag variations of the main cables, and in Figure 3.96 is shown a solution where a cross tie is added from the deck at the pylon support to the midpoint of the longest stay cable.

The cross tie is clamped to all the stay cables at the intersecting points where it will restrain the stay cables from transverse displacements. The cross tie will be most efficient if clamped to the midpoint of the stay cable and with a straight cross tie that can only be achieved for one of the stays in the fan. However, as the effect of reducing the sag variations is most pronounced for the longest stay cables, the cross tie should lead up to the midpoint of the upper stay cable.

It is important that the cross tie is under tension over the full length for any loading condition. To achieve that the cross tie should during installation be clamped to only a few of the top stays before it is tensioned at the deck level. The cross tie can favourably be composed of two ropes passing on either side of the stay cables in the fan. After having tensioned the cross tie, the clamps on the lower stay cables should be tightened.

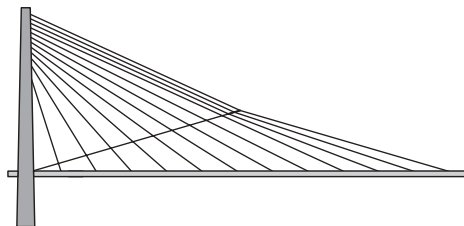
As indicated in Figure 3.96, the initial tensioning of the cross tie will result in a kink in the top stays at the clamps and that will induce a tension by deviation forces. Between the closely spaced clamps on the top stays it will probably be advantageous to let the tie consist of tubular members that can transfer both tension and compression.

To give an idea of the efficiency of cross ties, it can be mentioned that a free stay cable with a 600 m long horizontal projection will change its sag (measured perpendicular to its chord) from 7.0 m to 5.3 m when the stress varies from 540 MN/m<sup>2</sup> to 720 MN/m<sup>2</sup>. For a system with a central cross tie, the sag variation at the midpoint will be limited (by the elastic strain of the tie cables) to around 0.2 m.

In preliminary investigations the stiffness of a long stay cable with support from a cross tie can be determined by the formula:

$$c/E_{eq} = c_1/E_{eq,1} + c_2/E_{eq,2} \quad (3.74)$$

where  $c$  is the total chord length of the stay cable,  $c_1$  the chord length of the stay cable part between the top socket and the cross tie clamp, and  $c_2$  the chord length of the stay cable part between the cross tie clamp and the bottom socket.  $E_{eq}$  is the equivalent modulus of elasticity for the entire stay cable with cross tie, and  $E_{eq,1}$  and  $E_{eq,2}$  the equivalent moduli of elasticity for the two cable lengths on either side of the cross tie clamp, as indicated in Figure 3.97.



**Figure 3.96** Fan system with a cross tie

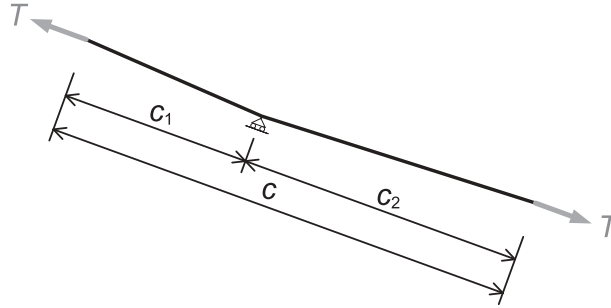


Figure 3.97 Stay cable with an intermediate transverse support

For the top cable where  $c_1 = c_2 = \frac{1}{2} c$  (3.74) yields:  $c/E_{eq} = c/E_{eq,1}$  as  $E_{eq,1} = E_{eq,2}$ . So the equivalent modulus of the cable with a central cross tie will be the same as for a cable with only half the chord length of the entire stay cable.

From the plot in Figure 2.80 it is seen that for a stay cable with a horizontal projection of 800 m the  $E_{eq}/E$  is approximately 0.61 whereas for a stay cable with a horizontal projection of 400 m the  $E_{eq}/E$  is approximately 0.86. So in this example the axial stiffness of the stay cable with a cross tie will be increased by 40%.

In the final calculations the system containing both primary stay cables and cross ties must be treated as a cable net composed of individual cable elements connected at all nodes.

Several cross ties have sometimes been added in an attempt to suppress oscillations of the individual stay cables. However, today dampers positioned at the ends of the stay cables are generally preferred as they are more discreet in appearance. Also, in a number of cases it was experienced that the cross ties broke due to fatigue. The main cause of this was that the cross ties were not correctly installed and tensioned. Thus, in many cases the cross ties were installed and clamped to all stay cables before being stressed from the bottom. But in that case the tension induced will be relieved through the clamps on the lower and shorter stay cables and very little tension will remain at the top cables. Then if the top cables start to oscillate, they will soon completely relieve the small tension in the cross tie and make it slack until full tension returns when the oscillation is reversed.

An argument against cross ties has often been that they will not allow a gantry to move along on the stay cable for inspection and surface repair. The argument is certainly valid if several cross ties are added onto each stay cable but with only one central cross tie, the stay cable can be inspected by one gantry covering the upper half and another the lower half.

### 3.4 Harp System

A harp system as shown in Figure 3.98 with supports positioned at the pylons and at the ends of the cable supported side spans will contain – as pointed out earlier – an unstable cable system, so that the flexural stiffness of the deck and the pylons must be taken into account to achieve equilibrium. To investigate the nature of forces and moments induced in a structure with a harp-shaped cable system a simple example as shown in Figure 3.99 will be considered. The system is supported at the pylon and at the left end, whereas it is considered free at the right end.

In this system the upper stay cable is stabilized by its connection to the end support, and it is therefore the lower stay cable that will be studied to show the problems related to the unstable cable system.

In a loading case as shown in Figure 3.100 with a concentrated force acting at one end of the lower stay, the load can be subdivided into a symmetrical and an antisymmetrical case, as indicated in the figure. In the symmetrical case the lower stay cable will be in equilibrium and consequently the forces can be transmitted to the supports by pure tension in the cable



Figure 3.98 Three-span cable stayed bridge with harp system

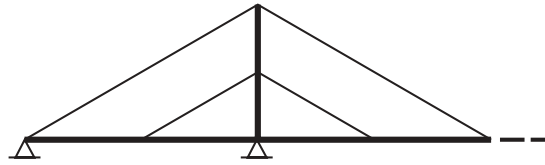


Figure 3.99 Simple harp system with two sets of stay cables

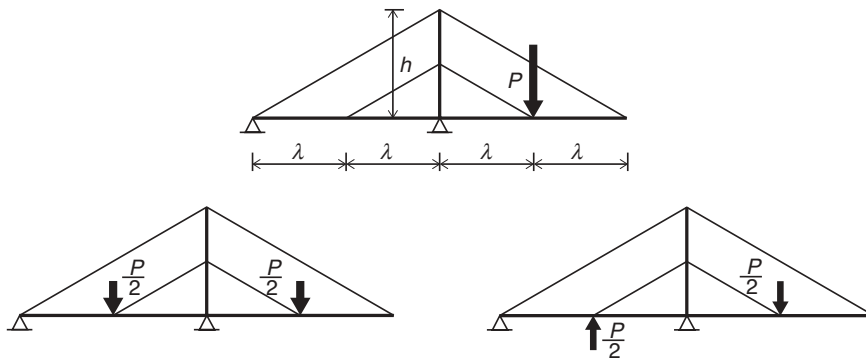


Figure 3.100 Loading case with a single concentrated force subdivided into a symmetrical and an antisymmetrical loading case

and compression in the girder and pylon elements. In the antisymmetrical case the forces will inevitably introduce bending either in the girder or in the pylons or in both.

If the pylon has an insignificant flexural stiffness (or the lower cable is supported by a longitudinally movable bearing at the pylon) the moments will occur entirely in the deck, and the moment curves will be as shown in Figure 3.101(a).

On the other hand if the pylon possesses a considerable flexural stiffness and the deck is slender, then the moments will occur in the pylon, as indicated in Figure 3.101(b).

It is seen from Figure 3.101 that the maximum moment induced in the stiff pylon is twice as large as the maximum moment induced in the stiff girder. However, as the material required is governed primarily by the area of the moment curves, and this area for System (a) is  $0.5P\lambda^2$  and for System (b)  $0.25P\lambda h$  (i.e.  $0.2P\lambda^2$  to  $0.25P\lambda^2$  for  $h$  between  $0.8\lambda$  and  $1.0\lambda$ ), it seems more efficient to apply System (b) than (a). But owing to the fact that the deck often can be made with a more efficient cross section the whole matter requires further investigation to determine the optimum solution in an actual case.

If it is decided to let the pylon transfer the bending, savings can be achieved by applying a modified harp system as shown in Figure 3.102. Here the maximum moment is  $P\lambda(h_t/h)$  and the area of the moment curve  $0.5\lambda h_t$ . For  $h_t = h/4$  the area then becomes only half of that found for the configuration in Figure 3.101(b). Note that for  $h_t \rightarrow 0$  the moment in the pylon vanishes as the harp system transforms into a pure fan system.

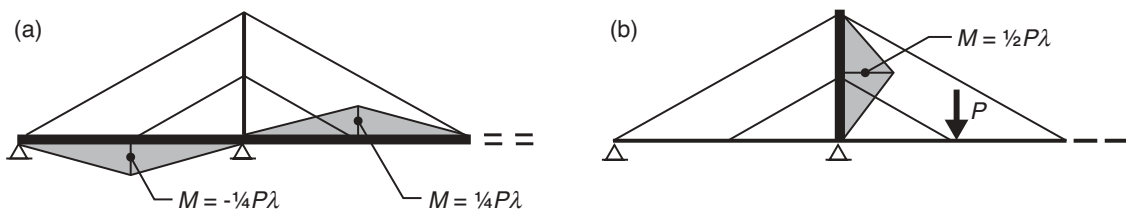
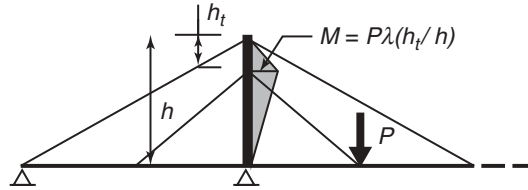


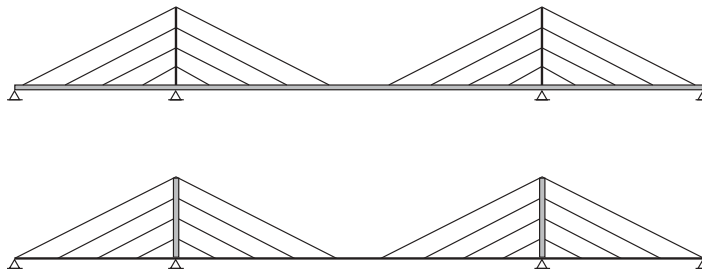
Figure 3.101 Moments induced in the deck or the pylon for the loading shown in Figure 3.91: (a) stiff girder and slender pylon; (b) slender girder and stiff pylon



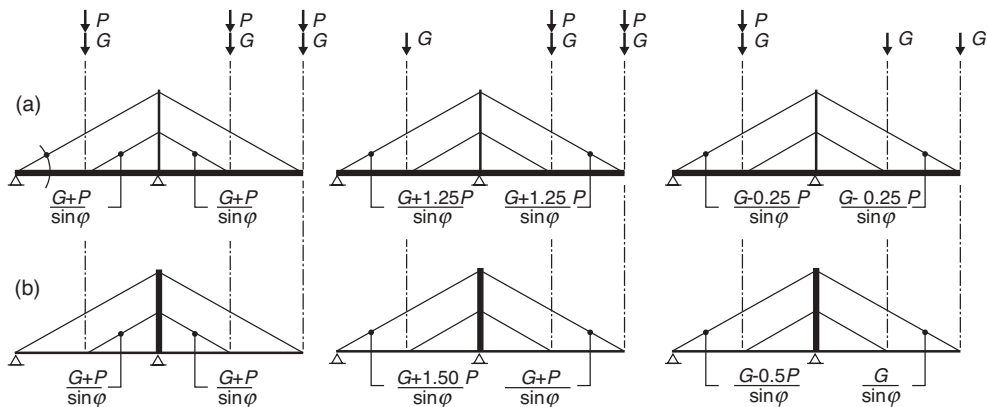
**Figure 3.102** Moments induced in a stiff pylon supporting a semi-harp

As described, the stability of bridges with harp-shaped cable systems can be achieved in principle by two basic structural systems: either by applying a stiff deck and a slender pylon, or by a slender deck and a stiff pylon, as illustrated in Figure 3.103. Between these two extremes, an infinite number of intermediate structural systems exist where the bending moments are distributed between the deck and the pylon. The distribution can be decided largely by the designer through his choice of dimensions, as the largest moments will occur in the elements with the largest flexural stiffness.

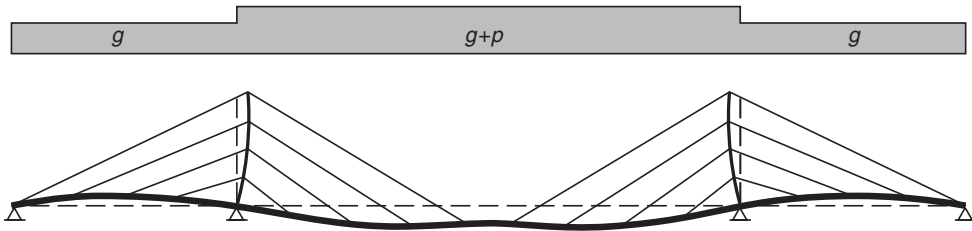
In Figure 3.101 the moment distribution of the two basic structural systems was shown. To illustrate the influence on the cable forces, Figure 3.104 shows the extreme forces for three loading cases, all comprising concentrated forces acting at the cable anchorages at the deck level. The given forces are based on the same simplifying assumptions as applied when calculating the moments in Figure 3.101.



**Figure 3.103** Three-span cable stayed bridges with harp systems: (top) flexural stiffness primarily in the deck; (bottom) flexural stiffness primarily in the pylon



**Figure 3.104** Maximum/minimum cable forces in harp systems subjected to three loading cases: (a) stiff girder and slender pylon; (b) slender girder and stiff pylon



**Figure 3.105** Deformation of a harp system with traffic load in the main span only

From Figure 3.104 it is seen that the maximum design force in the lower stay cable is independent of the chosen structural system, whereas the design force of the upper stay cable is noticeably influenced by the system applied. In system (b) the upper side span cable acts as an anchor cable that stabilises the pylon top against longitudinal movements. As was the case for the anchor cable in bridges with a fan system, the anchor cable in system (b) is also characterized by a larger force variation than the regular stay cables. An investigation similar to that illustrated in Figure 3.68 relating the traffic-to-dead load ratio  $p/g$  to the stress ratio  $\kappa$  might therefore also be required for bridges with harp systems stabilized by stiff pylons.

Due to the bending of the deck and the pylons, the deformation of the harp system under traffic load in only the main span might be characterized by larger deflections near the quarter points than at midspan, as illustrated in Figure 3.105. This is due to the fact that the central part of the main span is supported by the upper stay cable being fixed vertically at the end support, whereas the lower stay cables under one-sided loading will pull the side span girder upwards and thereby give a more flexible support of the main span.

From the simple systems treated above, it is seen that special problems arise in the harp system when subjected to a load unbalanced in relation to the pylon.

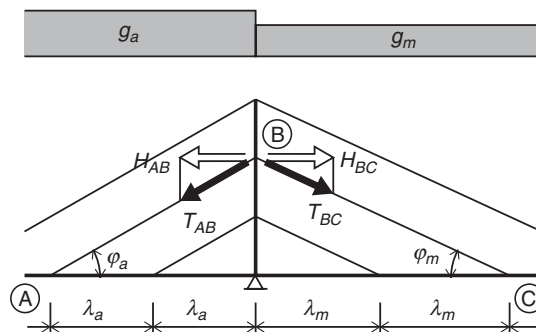
### 3.4.1 Dead load geometry

To avoid unnecessary bending from dead load, the geometry of the harp system is often chosen so that the dead load is balanced completely. For a constant dead load this simply leads to a symmetrical arrangement of the stays in relation to the pylon.

For a difference between the main span dead load  $g_m$  and the side span dead load  $g_a$  as indicated in Figure 3.106 the balance is obtained if the horizontal component  $H_{AB}$  of stay cable AB is equal to the horizontal component  $H_{BC}$  of stay cable BC:

$$g_a \lambda_a \cotan \varphi_a = g_m \lambda_m \cotan \varphi_m$$

$$\lambda_a / \lambda_m = \sqrt{(g_a / g_m)} \quad (3.75)$$



**Figure 3.106** Harp system with different dead load intensity in the main span and in the side span



Consequently, the distance between the cable anchor points shall be inversely proportional to the square root of the dead load intensity to obtain balance.

### 3.4.2 Intermediate supports

The disadvantages of the harp system due to the unstable cable system can be completely eliminated if intermediate supports are added under all cable anchor points in the side spans, as indicated in Figure 3.107. The cable system will then change to a system that is stable of the first order, as was explained in relation to Figure 3.18.

With supported side spans it is unnecessary to balance the dead load as unbalanced dead load can be resisted by the intermediate supports.

For a multi-cable harp system it will not be expedient to have intermediate supports under all cable anchor points in the side span, as this would lead to an overwhelming number of supports. However, already with a few intermediate supports (Figure 3.108) the flexural deformations of the side span deck will be reduced to such an extent that the deformational characteristics will be close to those found in a system with continuous support of the side spans. As a rule of thumb it can be assumed that the side span will be efficiently supported vertically if the distance between the supports is less than twenty times the depth of the deck.

The effect of supporting the side spans is illustrated in Figure 3.109 showing the deflection of three different cable stayed bridge systems, where (F) refers to a fan system, (H1) to a harp system without intermediate supports in the side spans, and (H2) to a harp system with intermediate supports.

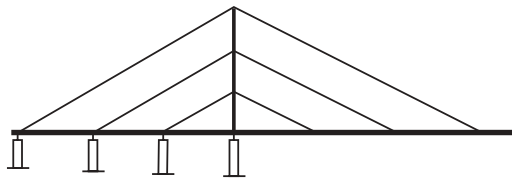


Figure 3.107 Harp system with intermediate supports under the cable anchor points in the side span

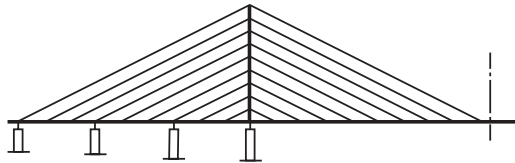


Figure 3.108 Multi-cable harp system with two intermediate supports in the side span

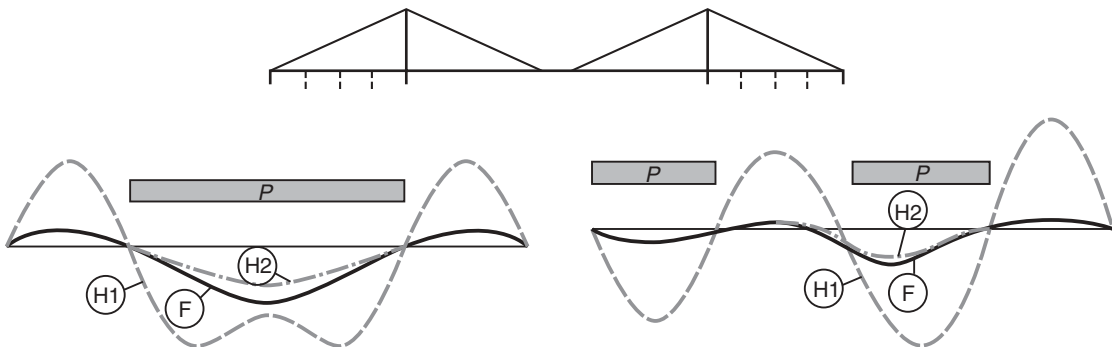


Figure 3.109 Deflections of three-span bridges for two loading cases: F, fan system; H1, harp system with unsupported side spans; H2, harp system with supported side spans

In the symmetrical loading case it will be seen that the difference in midspan deflections between the three systems is not very significant so if this was the only deflection calculated then the three systems might be evaluated as almost equally stiff. However, the harp without intermediate supports will exhibit the largest deflections around the quarter points of the main span and here the deflection is almost twice as large as the maximum deflection of the two other systems (at midspan).

It should be noted that the harp with intermediate supports is the stiffest among the three, so the effect of changing from an unstable to a first order stable cable system is very pronounced.

It is generally seen that the most violent deflections occur in the harp system with unsupported side spans (system H1), whereas the fan system (system F) is characterized by a much smaller uplift in the unloaded regions.

### 3.4.3 Preliminary cable dimensions

In the preliminary design process the cross section of the stay cables can be determined by equations similar to those found for the fan system.

For all stay cables inside the harp (Figure 3.110) the cross section is determined by:

$$A_{sc,i} \simeq \frac{(g + p + P/30d)(\lambda_i + \lambda_{i+1})\cos \phi}{2(f_{cbd} \sin \phi \cos \phi - \gamma_{cb} a_i)} \quad (3.76)$$

which is identical to (3.50).

For the top cable the design forces will depend on the stiffness properties of the deck and the pylon, as was indicated in Figure 3.104 for the simplified structural model.

In a bridge with the primary bending stiffness in the deck (Figure 3.111) the maximum top cable force  $T_{tc}$  can be determined by:

$$T_{tc} \simeq \frac{(g + p)\lambda + \frac{1}{4}pa + P}{\sin \phi} + \gamma_{cb} A_{tc} \frac{a}{\sin \phi \cos \phi} \quad (3.77)$$

where  $A_{tc}$  is the cross section of the top cable.

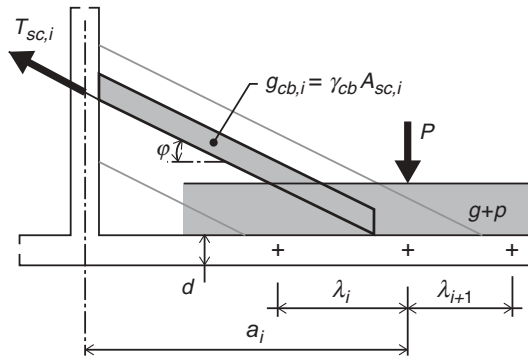


Figure 3.110 Loading cases for maximum force in lower stay cables

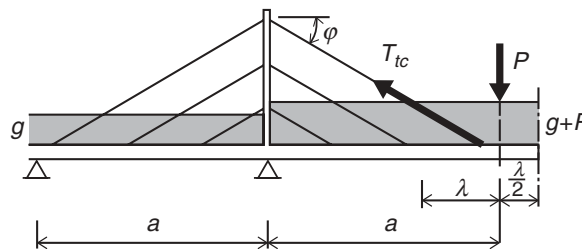


Figure 3.111 Loading case for maximum force in the top cable of a harp system with a stiff girder

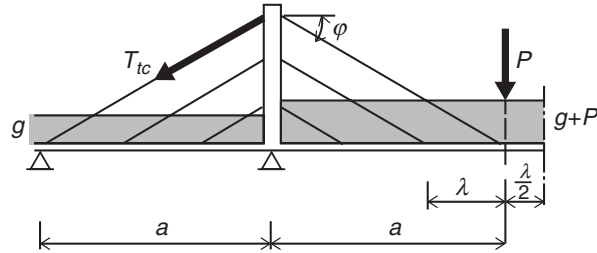


Figure 3.112 Loading case for maximum force in the side span top cable of a harp system with a stiff pylon

With  $T_{tc} = A_{tc} f_{cbd}$ , the following expression for  $A_{tc}$  can be determined:

$$A_{tc} \simeq \frac{(g+p)\lambda + \frac{1}{4}pa + P}{f_{cbd} \sin \phi \cos \phi - \gamma_{cb}a} \cos \phi \quad (3.78)$$

In a bridge with the primary flexural stiffness in the pylon (Figure 3.112), the top cable in the main span might be treated as the regular stay cables, whereas the maximum force  $T_{tc}$  in the side span top cable is found from:

$$T_{tc} \simeq \frac{(g+p)\lambda + \frac{1}{2}pa + P}{\sin \phi} + \gamma_{cb}A_{tc} \frac{a}{\sin \phi \cos \phi} \quad (3.79)$$

leading to the following cross sectional area,  $A_{tc}$ :

$$A_{tc} \simeq \frac{(g+p)\lambda + \frac{1}{2}pa + P}{f_{cbd} \sin \phi \cos \phi - \gamma_{cb}a} \cos \phi \quad (3.80)$$

In bridges with a harp system and supported side spans, all cables of the main span can be treated as regular stay cables and the preliminary cross sections are therefore found from (3.76).

The forces in the stay cables of the side span are found by expressing horizontal equilibrium at the pylon (Figure 3.113):

$$T_{sca,i} \cos \varphi_a = T_{scm,i} \cos \varphi_m$$

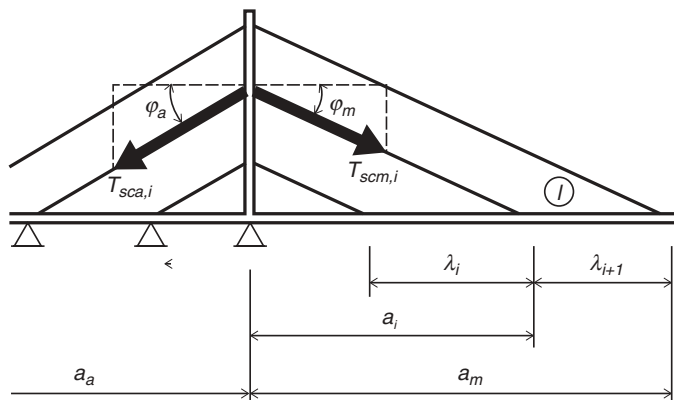


Figure 3.113 Cable forces in a harp system with supported side span

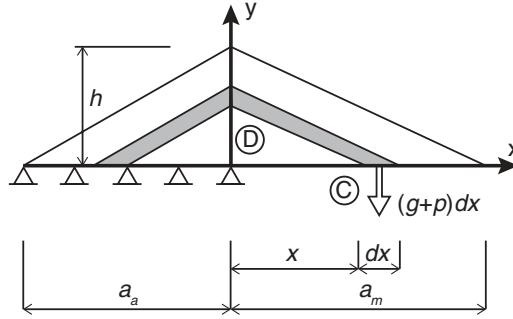


Figure 3.114 Idealized, continuous harp with supported side span and subjected to load  $g+p$  in the main span

For the cross sectional areas  $A_{scm,i}$  and  $A_{sca,i}$  of the two corresponding stays, the following equations are found:

$$A_{scm,i} \simeq \frac{g+p+P/30d}{f_{cbd} \sin \phi_m \cos \phi_m - \gamma_{cb} a_i} \frac{\lambda_i + \lambda_{i+1}}{2} \cos \phi_m \quad (3.81)$$

$$A_{sca,i} \simeq \frac{g+p+P/30d}{f_{cbd} \sin \phi_m \cos \phi_m - \gamma_{cb} a_i} \frac{\lambda_i + \lambda_{i+1}}{2} \frac{\cos^2 \phi_m}{\cos \phi_a}$$

#### 3.4.4 Quantity of cable steel

To arrive at expressions for the quantity of cable steel in a bridge with a harp-shaped cable system and supported side spans, a continuous system as shown in Figure 3.114 will be considered.

The cable steel quantity  $dQ_m$  for the cable C–D is determined by:

$$dQ_m \simeq \frac{\gamma_{cb}}{f_{cbd}} (g+p) \frac{a_m^2 + h^2}{a_m h} \left( x + \frac{\gamma_{cb}}{f_{cbd}} \frac{a_m^2 + h^2}{h a_m} x^2 \right) dx \quad (3.82)$$

and the quantity of the main span harp:

$$Q_{Hm} \simeq \frac{\gamma_{cb}}{f_{cbd}} (g+p) \frac{a_m^2 + h^2}{a_m h} \left( \frac{1}{2} + \frac{\gamma_{cb}}{f_{cbd}} \frac{a_m^2 + h^2}{3h} \right) a_m^2 \quad (3.83)$$

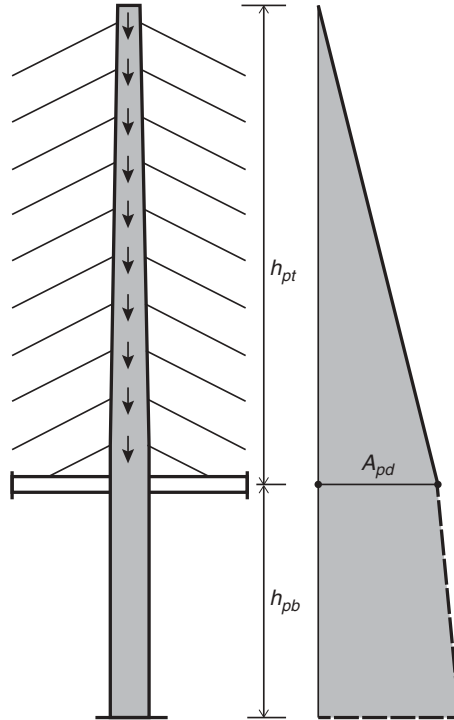
For the side span harp:

$$dQ_a \simeq \frac{\gamma_{cb}}{f_{cbd}} (g+p) \frac{a_a^2 + h^2}{a_a h} \left( x + \frac{\gamma_{cb}}{f_{cbd}} \frac{a_a^2 + h^2}{a_m h} x^2 \right) dx \quad (3.84)$$

$$Q_{Ha} \simeq \frac{\gamma_{cb}}{f_{cbd}} (g+p) \frac{a_a^2 + h^2}{a_a h} \left( \frac{1}{2} + \frac{\gamma_{cb}}{f_{cbd}} \frac{a_a^2 + h^2}{3h} \right) a_a^2 \quad (3.85)$$

#### 3.4.5 Quantity of the pylon

In the harp system the pylon will be subjected to the forces from the cable system evenly distributed along the entire height above the deck – in contrast to the suspension system, and the fan system, where the total force from the cable system is acting only at the pylon top.



**Figure 3.115** Assumed linear variation of the cross sectional area of the pylon above the deck

The pylon of the harp system should therefore be made with a pronounced variation of its cross sectional area if the axial stress is to be kept equal for all sections.

In this investigation it can be assumed with a reasonable degree of accuracy that the cross sectional area of the pylon varies linearly from 0 at the top to the value  $A_{pd}$  at deck level (Figure 3.115). The quantity  $Q_{pd}$  of the pylon above the deck then becomes:

$$Q_{pd} = \frac{1}{2} \gamma_{pl} A_{pd} h_{pt} \quad (3.86)$$

Vertical projection of forces acting on the pylon of a symmetrical harp with  $a_m = a_a$ :

$$N_{pd} = 2(gp)a_m + 2Q_{hm} + Q_{pd} \quad (3.87)$$

With

$$N_{pg} = A_{pg} f_{pld} = 2 \frac{f_{pld}}{\gamma_{pl}} \frac{Q_{pt}}{h_{pt}}$$

the quantity of the pylon above the deck becomes:

$$Q_{pd} = 2 \frac{\gamma_{pl} (g+p)a_m + 2Q_{hm}}{f_{pld} 2 - (\gamma_{pl}/f_{pld})h_{pt}} \quad (3.88)$$

For the pylon part below the deck, the variation of the axial force is due only to the pylon dead load and the quantity  $Q_{pb}$  of this part is therefore found from (3.41) with  $N_{pt} = N_{pd}$  and  $h_p = h_{pb}$ :

$$Q_{pb} = N_{pd} \left[ \exp\left(\frac{\gamma_{pl}}{f_{pld}} h_{pb}\right) - 1 \right] \quad (3.89)$$

The total quantity of the pylon  $Q_p$  now becomes:

$$Q_p = Q_{pd} + Q_{pb} \quad (3.90)$$

### 3.4.6 Simplified expressions

As was the case for the fan system, the contribution from the weight of the cables to the forces in the cable system and in the pylon is of minor importance for moderate spans, so for these the following simplified expressions might be used:

$$Q_{Hm} = \frac{1}{2} \frac{\gamma_{cb}}{f_{cbd}} (g + p) \left( \frac{a_m}{h} + \frac{h}{a_m} \right) a_m^2 \quad (3.91)$$

$$Q_{Ha} = \frac{1}{2} \frac{\gamma_{cb}}{f_{cbd}} (g + p) \left( \frac{a_a}{h} + \frac{h}{a_a} \right) a_a^2 \quad (3.92)$$

$$Q_{pd} = 2 \frac{\gamma_{pl}}{f_{pld}} \frac{(g + p) a_m}{2 - (\gamma_{pl}/f_{pld}) h_{pt}} \quad (3.93)$$

### 3.4.7 Total cost

The total cost  $C_{Hcp}$  of the cable systems and the pylons of a three-span bridge can now be expressed by:

$$C_{Hcp} = 2(Q_{Hm} + Q_{Ha})u_{cb} + 2(Q_{pd} + Q_{pb})u_{pl} \quad (3.94)$$

where  $u_{cb}$  is the unit price of erected and protected stay cable steel and  $u_{pl}$  the unit price of the pylon material.

### 3.4.8 Structural systems

The first cable stayed bridges to be built with the harp system were all characterized by few, concentrated stays arranged symmetrically about the pylon. The deck was flexurally stiff and the pylons slender (Figure 3.116).

A typical bridge from this epoch is the Rhine Bridge at Leverkusen (Figure 3.117). In this bridge, only two sets of stays were arranged from each pylon, so that only four points in the 280 m long main span were cable supported. Therefore, the depth of the deck had to be decided to be 4.2 m, or 1/67 of the main span length.

In bridges with intermediate supports in the side span, as shown in Figure 3.118, the global stability of the structural system is achieved without assistance from the flexural stiffness of the deck or pylon.

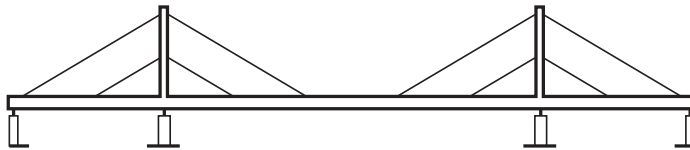


Figure 3.116 Structural system adapted in the early cable stayed bridges with the harp system



**Figure 3.117** Rhine Bridge at Leverkusen

However, in bridges with few and concentrated stays the local bending in the deck due to the transmission of loads to the cable anchor points induced moments of such a magnitude that a drastic reduction of the girder depth is not seen in these cases.

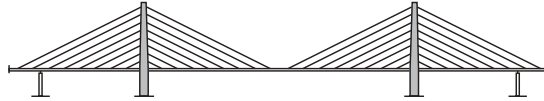
In the Knie Bridge at Düsseldorf (Figure 3.119) the distance between the cable anchor points in the main span was chosen as large as 64 m and this led to a girder depth of 3.2 m, equal to 1/100 of the main span length, or 1/20 of the span between the



**Figure 3.118** Structural system of a bridge with harp systems and intermediate supports in the side spans



**Figure 3.119** Knie Bridge at Düsseldorf



**Figure 3.120** Multi-cable harp system supported by stiff pylons

stay cable supported points. However, another feature associated with the additional support of the side span was fully utilized as the stays were arranged asymmetrically in relation to the pylon, the distance between the cable anchor points in the side span being only  $3/4$  of the distance in the main span.

In modern bridges with a multi-cable harp system, the local bending of the deck becomes insignificant and a very slender deck might therefore be applied if the global stability is achieved without requiring flexural stiffness of the deck. A system as shown in Figure 3.120 with heavy pylons that possess a considerable bending stiffness then becomes attractive. In such a system the stays should be arranged symmetrically with respect to the pylons to keep the dead load in balance. Furthermore, it might prove advantageous to position the end support in some distance from the end of the side span harp to make a number of the upper stays active as anchor cables in the same way as described for the fan system in Figure 3.92.

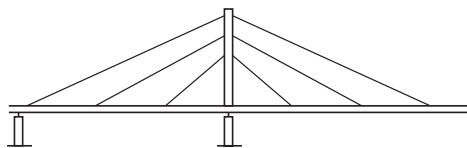
A multi-cable harp system with stiff pylons can be seen in the Napoleon Bonaparte Broward Bridge (Dames Point Bridge) in Florida, as shown in Figure 3.121. Note that in this bridge the end pier is positioned at the extremity of the side span harp to form a transition pier between the approach spans and the cable supported spans.

In the true harp system all cable stays in each harp are parallel, and this feature implies certain advantages regarding the design of the cable anchor points as all stay cables will intersect the deck and the pylon at the same angle.

On the other hand, some savings in the quantities can be achieved by applying a semi-harp as shown in Figure 3.122. Here the inner stay cables will have a more favourable inclination than the corresponding stay cables in a true harp.

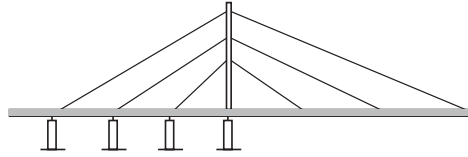


**Figure 3.121** Napoleon Bonaparte Broward Bridge (Dames Point Bridge)



**Figure 3.122** Symmetrical semi-harp system





**Figure 3.123** Asymmetrical semi-harp with a supported side span

In systems with unsupported side spans the semi-harp should be arranged symmetrically about the pylon to balance the dead load, but in bridges with intermediate supports in the side spans an asymmetrical harp can be used (Figure 3.123). This system was applied in the Rhine Bridge at Flehe (Figure 3.124). Here the side span stay cables are arranged in a true harp configuration with parallel cables whereas the main span cables form a semi-harp.

Double-deck bridges are generally characterized by a considerable flexural stiffness of the deck as requirements regarding vertical clearance, light and ventilation prescribe that the deck be made as a deep truss. Therefore, in double-deck bridges the truss contributes significantly to the overall stability so the configuration of the cable system can be chosen more freely.

In the Higashi Kobe Bridge (Figure 3.125) with a main span of 485 m the double-deck truss has a depth of 9 m and an intermediate support is arranged in the 200 m long side span in a distance of 72.7 m from the end support. That ensures a most efficient stabilization of the multi-cable harp system. Also, the presence of the deep truss has allowed a relatively large portion of the deck to be unsupported by the cable system. At midspan the truss is free on a length of 97 m and on either side of the pylons on lengths of 60 m.

The main span of the Øresund Bridge (Figure 3.126) has almost the same length as in the Higashi Kobe Bridge (490 m versus 485 m) but, due to the presence of a double-track railway on the lower deck, the traffic load is considerably larger. At the same time the strict stiffness requirements to allow train passages with speeds of up to 200 km/h made it essential to apply a structural system with the highest degree of efficiency. The cable system is therefore of the harp configuration with relatively steep stays and anchor piers positioned inside the side span harp so that the smallest depth-to-span ratio of the deck in the side spans is  $9.2/160 \sim 1/17$ .

In the Øresund Bridge the anchor points at the top of the truss are positioned 20 m apart inside the harps but on either side of the pylons the truss is free on a length of 45 m and at midspan the distance between the anchor points at the top of the truss is 40 m. However, due to the fact that the pull in the stay cables is transferred through special brackets ('outriggers') outside the trusses to the bottom chord the forces of the two upper stays in the main span are actually transferred to truss nodes at a distance of only 10 m.



**Figure 3.124** Rhine Bridge at Flehe



**Figure 3.125** The Higashi Kobe Bridge in Kobe

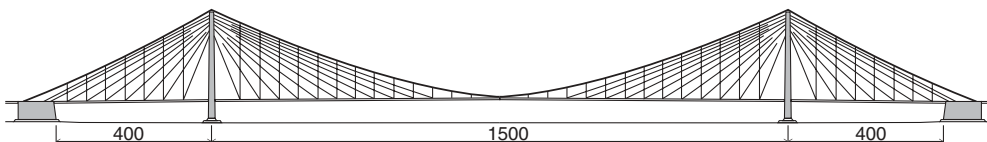


**Figure 3.126** The main span of the Øresund Bridge

### 3.5 Hybrid Suspension and Cable Stayed System

Under the description of the evolution of cable supported bridges it was mentioned that a combination of the suspension and the cable stayed system has occurred at different occasions throughout the history of cable supported bridges, although the system has not been chosen for actual construction of a major bridge since the days of the Brooklyn Bridge.

Although never used in recent years the hybrid systems have been considered on several occasions and as an example, Figure 3.127 shows a preliminary design from 1977 for a combined road and railway bridge with a 1500 m main span across the Storebælt in Denmark.



**Figure 3.127** Design for a bridge with a hybrid cable system investigated for the Storebælt Crossing in 1977

Compared to a pure suspension system the hybrid system should lead to material savings due to the following two features:

- (1) The load carried by the stay cables will require less material than if carried by hangers and parabolic suspension cables.
- (2) A more optimum height of the pylon can be used, as the limitations due to stiffness requirements in the suspension system do not apply to the hybrid system.

It should be remembered in this context that the savings in cable steel quantities must be quite substantial to outweigh the higher unit price for stay cables and the complications to be encountered during erection. However, for bridges with sufficiently long main spans, the reduction in cable steel quantity could turn out to be so large that an overall saving will be achieved.

When choosing the structural system for a bridge with a hybrid, cable system it is important to bear in mind that the deck will have to transfer axial forces of considerable magnitude (in contrast to the pure suspension bridge case). It will in general prove advantageous to introduce compression in the deck adjacent to the pylons and this excludes that expansion joints can be positioned at the pylons (as is the case for most of the traditional suspension bridges).

In the Brooklyn Bridge the stiffening truss was fixed to the pylon on either side whereas the expansion joint in the main span was positioned at midspan. This arrangement has, however, proved to be less advantageous as the largest longitudinal displacements of the truss due to temperature changes occur where the hangers are shortest, i.e. at midspan. It has, therefore, been necessary to replace and redesign a number of the short hangers and their attachments.

Also for the transmission of wind load by lateral bending of the deck it is undesirable to have expansion joints at the centre of the main span, so it seems that the most favourable structural system will be as shown in Figure 3.128 characterized by the following features:

- (1) relatively short side spans with a length of 25–30% of the main span length ( $0.25 < l_a/l_m < 0.30$ )
- (2) continuous deck
- (3) centring devices at the anchor blocks
- (4) central clamp between the top cable and the deck at midspan
- (5) continuous top cable from one anchor block to the other
- (6) all stay cables and the top cable fixed to the pylon top
- (7) no stay cables extending to the outer regions of the side spans (near anchor blocks).

The overall geometry of the combined cable system will be governed by the dead load condition that determines the initial shape of the top cable and the stay cables.

For the main span the dead load condition will be as illustrated in Figure 3.129. For this condition, two parameters, the fan lengths  $a_m$  and the dead load distribution factor  $\alpha = \alpha_{dl}$ , are of special importance. The dead load distribution factor  $\alpha_{dl}$  is equal to the fraction of the total dead load of the deck carried by the suspension system in the regions where both the suspension and the cable stayed system are present.

With given values of  $a_m$  and  $\alpha_{dl}$  the cable curve is determined by (2.4):

$$y = -\frac{k_m}{M_m(l_m/2)} M_m(x) \tag{3.95}$$

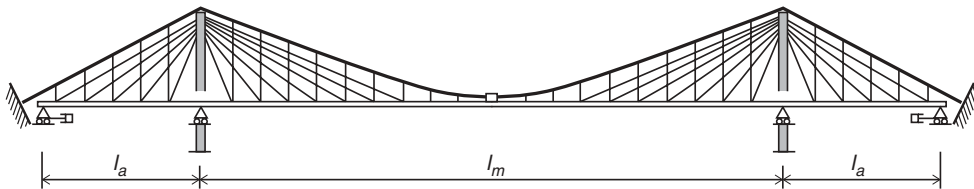


Figure 3.128 Structural system of a bridge with a hybrid cable system

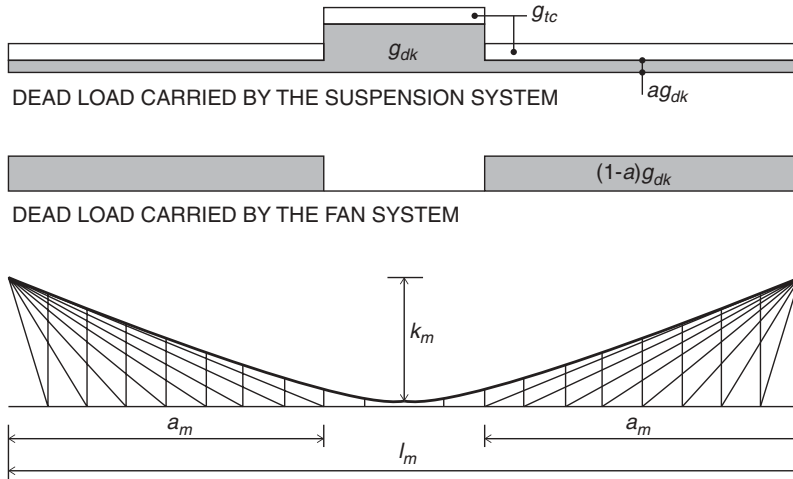


Figure 3.129 Distribution of dead load between the suspension and the fan system

where  $k_m$  is the sag of the main cable and  $M_m(x)$  the moment curve of the dead load acting on the top cable. It should be emphasized that, besides the load  $\alpha_{dl}g_{gr}$  and  $g_{gr}$  from the girder dead load, the weight of the top cable (and the hangers) should also be included when calculating  $M_m(x)$  and  $M_m(l_m/2)$  in (3.90). In the dead load condition the fan of the combined system is treated as an ordinary fan system subjected to the load  $(1 - \alpha_{dl}) g_{gr}$  from the deck.

In relation to the action of live load, one of the advantages to be gained by the combined cable system could be the reduced sag variations in the stay cables due to the connection by clamps to the vertical hangers at all points of intersection. The stay-to-hanger connections will also allow an adjustment of the dead load curve of the stay cables. This is illustrated in Figure 3.130 showing two possible configurations for a stay cable attached to a number of intermediate hangers.

In configuration (a), the dead load curve of the stay cable corresponds to that of the free cable so that all clamps are stress free in the initial condition. However, when traffic load is added the clamps will significantly reduce the change of sag. In configuration (b), the stay cable has all clamps on a straight line as the weight of the cable is carried by the hangers to the main cable above.

In the Brooklyn Bridge, configuration (a) was used as can be seen when looking along a stay cable from the bridge deck (Figure 3.131).

Generally, the quantities required in a bridge with a combined cable system will be between those of a suspension bridge and those of a cable stayed bridge with a fan system. With a decreasing value of the dead load distribution factor  $\alpha_{dl}$  the load

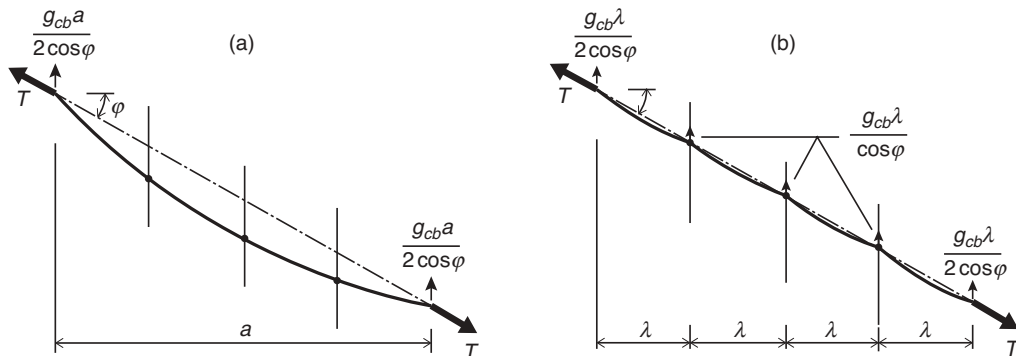


Figure 3.130 Two possible configurations of stay cables connected to vertical hangers



**Figure 3.131** Sagging stays of the Brooklyn Bridge, as seen from the bridge deck

carried by the fan system will dominate and the quantities will approach those of the pure fan system. Consequently, it is advantageous to minimize the value of  $\alpha_{dl}$  and maximize the value of  $a_m$ .

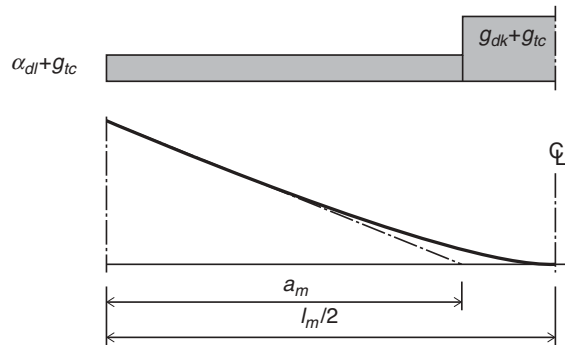
The maximum value of  $a_m$  will be governed by the condition that the upper stay cable must remain under the continuous top cable. Therefore, the limiting value of  $a_m$  will be determined by expressing that the top cable tangent and the upper stay cable tangent shall coincide at the pylon top. Also for this reason, configuration (a) in Figure 3.130 is to be preferred as this leads to a larger inclination of the stay cable tangent at the top than configuration (b).

In a simplified case, as shown in Figure 3.132, where the stay cable sag is ignored, the top cable weight  $g_{tc}$  assumed constant (measured horizontally), and the axis of the deck coinciding with the top cable tangent at midspan, the relation between  $a_m$  and  $\alpha_{dl}$  can be expressed by:

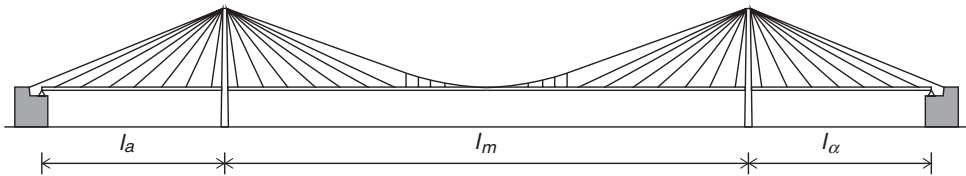
$$a_m = \frac{l_m}{2} \left[ 1 + \sqrt{\frac{\alpha_{dl} g_{gr} + g_{tc}}{g_{gr} + g_{tc}}} \right]^{-1} \quad (3.96)$$

From this expression it is seen that  $\alpha_{dl} = 1$  yields  $a_m = l_m/4$  (corresponding to the pure parabolic suspension case) and that  $\alpha_{dl} \rightarrow 0$  (implying  $g_{tc} \rightarrow 0$  as the top cable vanishes) yields  $a_m = l_m/2$  (the pure fan system case).

In a real structure  $a_m$  could often be chosen somewhat larger than the value found from (3.91) due to the lower position of the deck and the influence of the stay cable sag.



**Figure 3.132** Determination of the fan length  $a_m$  for a hybrid cable system



**Figure 3.133** Cable supported bridge according to the Dischinger system, but with a multi-cable fan in the cable stayed portion

As the material consumption of the fan system is smaller than that of the suspension system,  $\alpha_{dl}$  could be chosen as small as possible, and it could even be advantageous to carry all the load by the cable stayed system in the regions where this system can be applied.

This leads to a system very similar to the one proposed by Dischinger (Figure 1.24), but in accordance with present practice within cable stayed bridges, a more continuous arrangement of stay cables would be preferred today. An updated version of the Dischinger system might therefore look as shown in Figure 3.133.

As will be seen, the system of Figure 3.133 can develop also from the hybrid cable systems of Figure 3.128 by leaving out the hangers in the regions where stay cables are present. This would imply that the load in these regions was taken entirely by the cable stayed system, but, at the same time, other favourable effects of the hangers would be lost. In particular, this relates to the effect of reduced sag variations in the stay cables. Furthermore, for the system with both hangers and stays, the tendency to wind-excited oscillations of the individual cables will be suppressed and probably completely eliminated.

Systems with stay cable support confined to the regions adjacent to the pylons have been investigated at a number of occasions. However, investigations have generally revealed that unfavourable bending moments will occur in the deck at the points where the cable support changes from stay cables to hanger + main cable. So the two systems apparently have a quite big overlap in a transition zone to avoid a sudden jump in stiffness of the cable support.

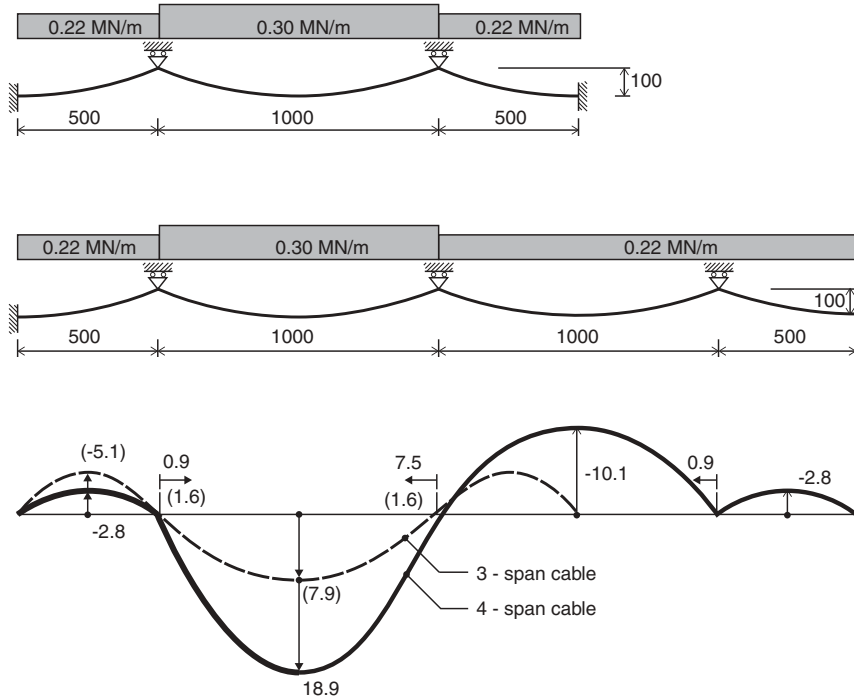
### 3.6 Multi-Span Cable System

The vast majority of cable supported bridges are made with cable support in three, two or one spans, as illustrated by the many examples given on the previous pages.

However, in a number of cases local conditions might favour the construction of cable supported bridges with more than three consecutive spans. In such cases the bridge might simply consist of several three-span bridges placed end to end, as it is the case for the West Bay Crossing of the San Francisco–Oakland Bay Bridge (Figure 3.134), the Bisan Seto Bridges (Figure 1.74) and the Kurushima Kaikyū Bridge (Figure 1.101). Here conventional three-span suspension bridges are present on either side of a central anchor block, that will be subjected to a large horizontal force from unbalanced dead load and traffic load acting in only one of the main spans.



**Figure 3.134** West Bay crossing of the San Francisco–Oakland Bay Bridge comprising two consecutive three-span suspension bridges



**Figure 3.135** Comparison between deflections of a three-span and a four-span cable with traffic load in one main span

In the case of the San Francisco–Oakland Bay Bridge, the side spans have a length of half the main spans so in this case equilibrium could have been achieved without the central anchor pier as the earth anchored cable system is stable of the second order. But the displacements required to achieve equilibrium under traffic load acting in one span only would become so large that it was unacceptable. That this is the case is illustrated by the simple example in Figure 3.135, where a conventional three-span cable is compared to a four-span cable with two equally large main spans.

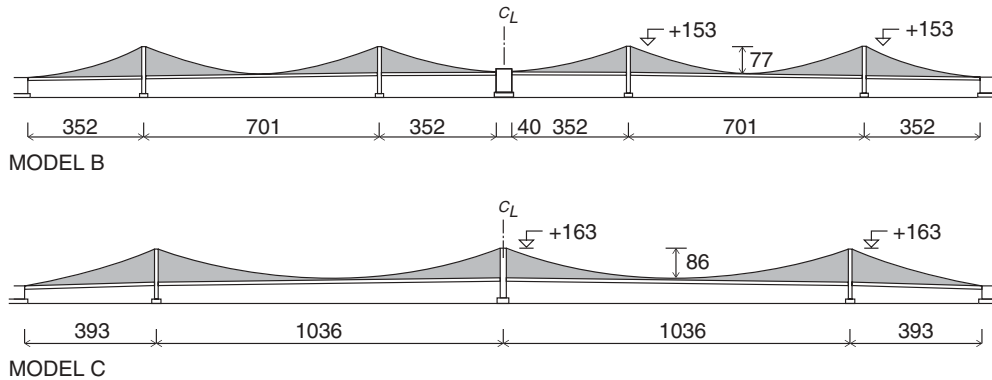
Based on the same values as used for the three-span cable in Figure 2.56 the deflections will be as shown at the bottom of Figure 3.135. It is seen that the maximum deflection of the four-span cable is more than twice as large as that of the three-span cable. The explanation is that substantial displacements are necessary to establish horizontal equilibrium between the two main span cables at the top of the intermediate pylon. This equilibrium requires that the sag of the span with traffic load is increased by 19% and the sag of the span with dead load only is decreased by 10% to arrive at horizontal forces of equal size.

It can be stated clearly that a deflection of 19 m (corresponding to 1/53 of the span length) is absolutely unacceptable. Even the deflection of 7.9 m found in the three-span bridge with long side spans will in many cases be regarded as uncomfortably large and a solution with shorter side spans will consequently be preferred as this results in a significant reduction of the maximum deflection (refer to Figure 2.56).

In the four-span case the large deflections cause a horizontal displacement of the central pylon top equal to 7.5 m, and a reduction of this displacement would therefore lead to more acceptable deformations.

During the preparatory investigations for the Bay Bridge, model tests were conducted to study different structural solutions. Figure 3.136 shows two of the models with indication of some characteristic prototype dimensions.

Model B closely corresponds to the structure that was subsequently built, whereas model C shows a four-span solution with two 1036 m long main spans. With a system corresponding to Model C considerable savings could be achieved in the substructure as two pylon piers and the central anchor pier, all on large foundation depths (71 m, 66 m, and 34 m), could be replaced by one central pylon pier with a foundation depth of 66 m.



**Figure 3.136** Bridge systems investigated (by model testing) for the West Bay crossing of the San Francisco–Oakland Bay Bridge

As it was realized that the solution with two main spans could cause problems in relation to the flexibility, a number of precautions were taken to increase the stiffness of the Model C solution:

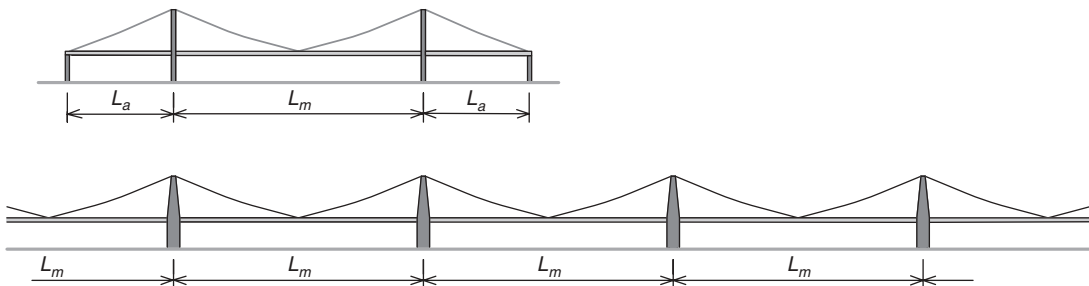
- (1) The sag ratio of the main span was reduced from 1:9 in model B to 1:12 in Model C.
- (2) The flexural stiffness of the truss was increased by a factor of 2.1.
- (3) The stiffening truss was made continuous through the pylons.
- (4) The flexural stiffness of the pylons was increased by a factor of 2.75.
- (5) The side-to-main span ratio was reduced from 0.5 to 0.38.
- (6) The dead load of the deck and the cable system was increased by 54% (due to the larger dimensions resulting from precautions (1) and (2)).

Despite these precautions the deflections of Model C turned out to be more than twice as large as the deflections of Model B. The maximum prototype deflection for traffic load in one of the main spans was 2.9 m for Model B, but 6.1 m for Model C, and the uplift in the unloaded span was 5.2 m. The longitudinal displacement of the central pylon top in model C was 2.2 m compared to 0.7 m for the pylon tops in Model B,

This significant increase in the flexibility in combination with an increase of the quantity of cable steel by a factor of approximately 2.7 resulted in exclusion of the four-span solution.

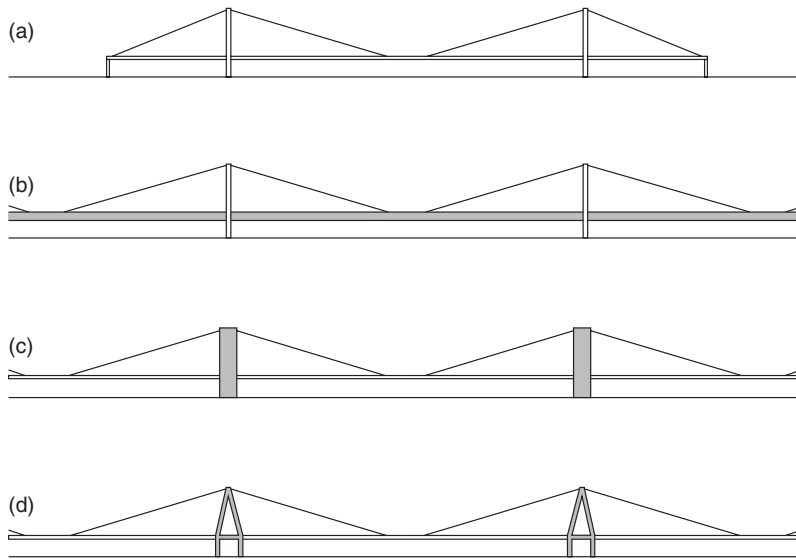
### 3.6.1 True multi-span cable supported bridges

A true multi-span bridge consists of a number of consecutive main spans of equal length and shorter side spans at the extremities only, as illustrated at the bottom of Figure 3.137.



**Figure 3.137** Traditional three-span cable supported bridge (top) and a true multi-span cable supported bridge (bottom)





**Figure 3.138** Multi-span cable stayed bridges with increased flexural stiffness of the deck or the pylons

From a structural viewpoint the problems relate to the lack of longitudinal restraint of the inner pylon tops (without support by an anchor cable) from a point with efficient vertical and longitudinal fixation.

As already indicated in the description of the early studies for the Bay Bridge, the main effort must be to achieve sufficient stiffness as flexible structures can exhibit some side effects that can influence the overall safety. A flexible structure will be more vulnerable to aerodynamic actions and might be characterized by larger stress fluctuations under moving traffic loads, i.e. fatigue might to a larger extent govern the design.

To improve the deformational characteristics of a multi-span cable supported bridge two basic approaches might be followed. One is to increase the flexural stiffness of the deck or the pylons to counteract the inefficiency of the cable system in the same way as the unstable harp system can be stabilized in a three-span bridge. The other approach is to modify the cable system.

For cable stayed systems the effect of increasing the flexural stiffness is illustrated in Figure 3.138 where (a) is the traditional three-span bridge, (b) a multi-span bridge with increased stiffness of the deck, (c) a multi-span bridge with increased stiffness of the pylons, and (d) a variant of (c) where the pylon stiffness is achieved by a triangular configuration above the deck.

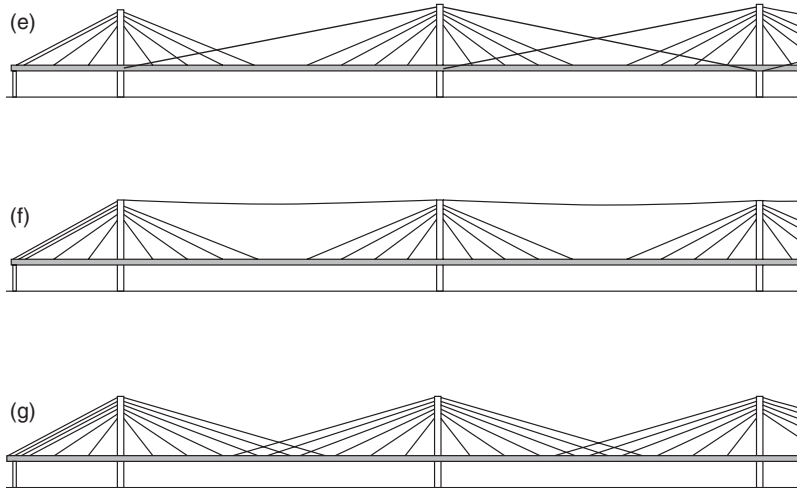
Increased flexural stiffness of the deck will be accompanied by an increased dead load that will influence unfavourably the quantities not only of the deck itself but also of the cable system, the pylons and the substructure. Furthermore, to achieve an adequate flexural stiffness it will be necessary to increase the girder depth to approximately 1/40 of the span length which unfavourably affects the appearance and leads to increased drag on the deck.

Increased flexural stiffness of the pylons will allow the deck and the cable system to be made with dimensions as found in three-span bridges whereas the pylons themselves will be characterized by quite substantial increases of the quantities. Also, the substructures below the pylons will have to be strengthened to allow transmission of large bending moments.

Modifications of the cable system in multi-span cable stayed bridges to stabilize the inner pylons and their adjacent fans can be made as shown in Figure 3.139.

In System (e) the inner pylons are stabilized by long anchor cables leading to the points where the deck intersects the adjacent pylons, i.e. to points with efficient vertical support. This principle was used in the Ting Kau Bridge with four spans (Figure 3.140). Alternatively, the inner pylon tops can be stabilized by a horizontal tie cable connecting all pylons immediately above the anchor zones of the normal stay cables, as shown in System (f).

It is sometimes argued that the application of a horizontal tie cable to stabilize the inner fans of a multi-span bridge is unacceptable, as the breaking of this tie cable will endanger the integrity of the entire structure. A horizontal tie cable should, however, only be regarded as an anchor cable and in most of the traditional three-span cable stayed bridges



**Figure 3.139** Multi-span cable stayed bridges with cable systems modified to stabilize the inner pylons

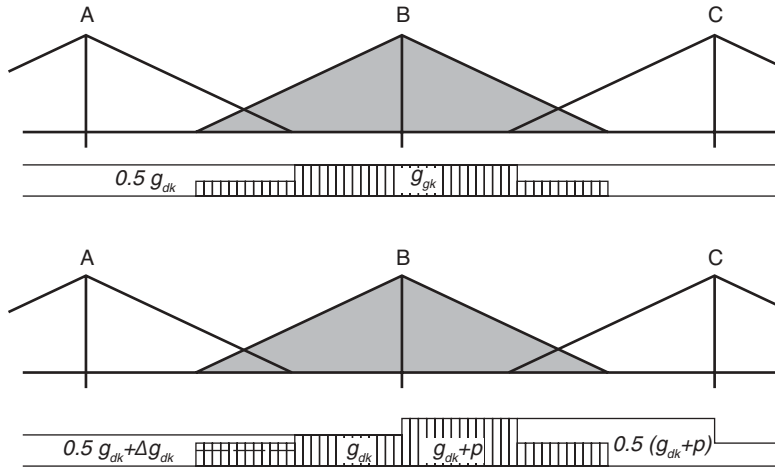
the breaking of an anchor cable will lead to a collapse as the dead load is unbalanced if the anchor cable disappears. In a multi-span bridge the inner fans are in balance for dead load due to their symmetry, so the breaking of the horizontal tie cable will not lead to a total collapse—but probably to relatively large unsymmetrical deflections.

For both Systems (e) and (f) it is disadvantageous if the pylon restraining cables are very long and therefore characterized by a more pronounced sag effect than found in the regular stay cables of the system. Also, the long free length might require special measures to suppress wind-induced oscillations.

System (g) in Figure 3.139 indicates a multi-span cable stayed bridge with overlapping fans in the main spans. This results in a cable system that is stable of the first order (as do Systems (e) and (f)) so that the stability of the total system does not depend on the flexural stiffness of the deck or the pylons. The system with overlapping fans was first presented in [86.1], but has later been further investigated in [95.1]. The first bridge to incorporate overlapping fans is the Third Firth of Forth Bridge shown in Figure 1.115.



**Figure 3.140** The Ting Kau Bridge in Hong Kong



**Figure 3.141** Multi-span cable stayed bridge with overlapping fans subjected to dead load (top), and dead load + traffic load in one span (bottom)

If the pylons are designed with an insignificant flexural stiffness then System (g) will only be applicable in bridges with a limited number of consecutive main spans, but if the pylons are flexurally stiff and moment rigidly fixed to the substructure the system might also be applicable in bridges with a large number of main spans. The required flexural stiffness of the pylons in System (g) will in any case be considerably less than the stiffness required in System (c) of Figure 3.138.

To give a phenomenological understanding of the stabilizing effect achieved by overlapping the fans a system as shown in Figure 3.141 will be considered.

When subjected to dead load only, the fans from each pylon will carry the total deck dead load  $g$  in the regions adjacent to the pylons whereas the dead load in the midspan region with overlapping fans will be distributed between the two fans. The distribution of dead load between the two fans can be adjusted during the installation and tensioning of the relevant stay cables in the construction phase.

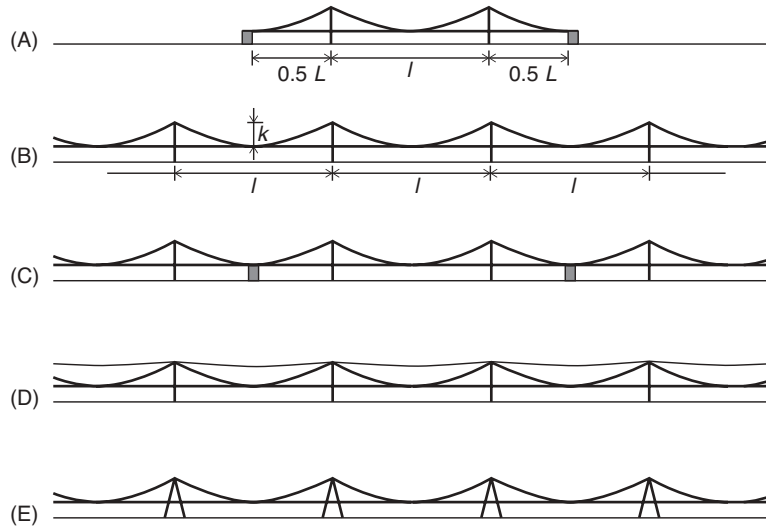
In the dead plus traffic load condition with traffic load only in span B–C the fan from B will show a tendency to rotate clockwise and this will reduce the tension in the overlapping stays leading to Pylon A and increase the tension in the overlapping stays leading to Pylon C. Consequently, the overlapping stays leading to Pylon B will carry a larger part of the dead load in the overlapping region of span A–B. So the destabilizing moment from traffic load in span B–C is counteracted by the stabilizing moment from the additional dead load  $\Delta g_{dk}$  transferred to the fan from B in the overlapping region of span A–B.

In self anchored cable stayed bridges, Systems (e)–(g) can only be used if the deck is continuous from one end to the other as there will be no regions with zero axial force between the end supports.

An earth anchoring of the tie cable in System (e) can be advantageous during construction as it can stabilize the pylon tops longitudinally during the critical free-cantilevering of the deck to midspan. If the systems are entirely self anchored, then the pylon-restraining cables cannot be added until the deck erection has been completed, so in this case the top cable cannot be utilized during deck erection.

In multi-span bridges based on an earth anchored suspension system, the situation is somewhat different from the self anchored systems as earth anchoring will lead to a system that is stable of the second order and therefore able to distort into a configuration that will render equilibrium for any traffic load condition.

However, as already described earlier, a system like System (B) in Figure 3.142 will be characterized by large (and unacceptable) deflections to create equilibrium in a loading case with traffic load in one span only. In a system with a large ( $\sim$  infinite) number of main spans the dead load sag  $k$  will be increased to  $k(p + g)/g$  in the span with traffic load  $p$ . Consequently, the deflection will be  $kp/g$  and with realistic values such as  $p = 0.2g$  and  $k = 100$  m this will result in a vertical displacement of 20 m in the midspan region! With a main span length of 1000 m, this corresponds to one-fiftieth of the span length.

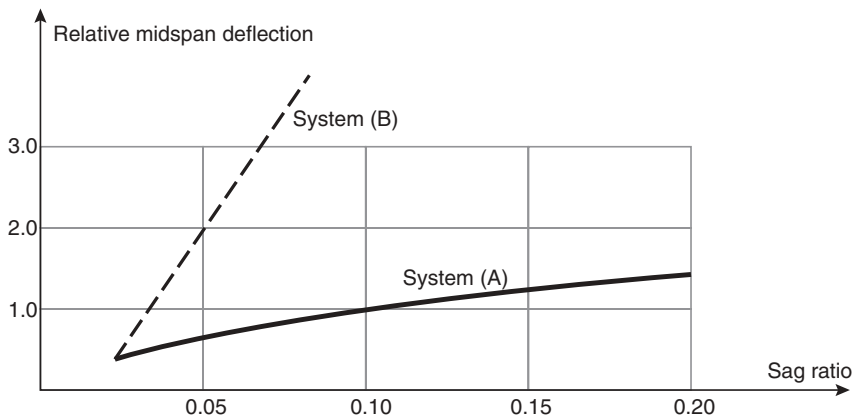


**Figure 3.142** Multi-span suspension bridges with a single parabolic main cable in each cable plane

The extreme flexibility of System (B) compared to the traditional three-span bridge, System (A) in Figure 3.142, is illustrated by the plot in Figure 3.143. It appears that the sag ratio of System (B) should be chosen to be approximately 0.03 or 1/33 to arrive at the same midspan deflection as found for System (A) with the traditional sag ratio of 1/10. However, with a sag ratio of 0.03 instead of the traditional value of 0.1, the quantity of steel to go into the main cable of a 1000 m span will be increased by a factor of  $\sim 4.5$ , and this increment must be regarded as unacceptable due to the severe cost implications.

Considerations along these lines have undoubtedly been decisive for adding intermediate anchor piers, as illustrated in System (C), both in bridges that have actually been constructed and in bridges investigated for future crossings. However, intermediate anchor piers are neither structurally convincing nor aesthetically pleasing.

Elimination of intermediate anchor piers can be achieved – as in the cable stayed case – by connecting all pylon tops by a longitudinal tie cable, as shown under (D) in Figure 3.142. However, this solution will only be applicable in bridges with relatively moderate spans as the horizontal tie cable will be characterized by a too pronounced sag effect if it has to be suspended freely over a long distance.



**Figure 3.143** Comparison between the deflection of a traditional three-span suspension bridge and a multi-span suspension bridge with the same flexural stiffness of the girder and the pylons

In multi-span suspension bridges with a single main cable in each cable plane and very long spans (where the tie cable solution is unattractive), the only solution left appears to be the one shown in Figure 3.142 under (E). Here the pylons are made with two inclined legs so that the necessary longitudinal restraint of the pylon top is achieved by the triangulation of the pylon structure itself. This can lead to deformational characteristics that are even more favourable than found in the traditional three-span bridge (System (A)).

The main disadvantage of applying triangular pylon structures relates to the increase in quantities to go into the pylons themselves. For a maximum unbalanced horizontal force occurring under traffic load in only one of the adjacent main spans the resulting force acting at the pylon top will be directed towards the traffic loaded span. So the pylon leg leaning in the same direction might have to transfer the entire force from the cable system – or even more if the other pylon leg is in tension. The total quantity to go into the triangular pylon structure might for this reason easily be twice of that required for a vertical column-type pylon.

Also, for the substructure increased costs must be anticipated if a triangular pylon structure is used as a considerable moment will have to be transferred to the soil.

**3.6.2 Non-traditional multi-span suspension bridges**

Non-traditional suspension systems with two main cables in each cable plane have been studied for multi-span bridges across straits with large water depths such as the Gibraltar Strait. Here depths of 250–300 m make it very unattractive to apply intermediate anchor piers and also to construct triangular pylon structures.

A system as shown in Figure 3.144 under (J) offers the advantage that the main cable A–B–C can be anchored to the pylon at B. Consequently, the pylon at B will have the double function of giving vertical support to one of the main cables (shown with a dotted line) and at the same time of anchoring the other main cable (shown with a solid line). Immediately this could seem to be killing two birds with one stone but a closer look will reveal that this is not at all the case.

In the dead load condition the cable A–B–C will transfer no force to the pylon at B as the horizontal force is constant and the cable tangent is horizontal on either side of the pylon. This implies that for dead load the cable A–B–C will act as if it were freely suspended between A and C, i.e. a cable with a span that is twice the span of the bridge! At the same time the sag ratio of this cable ( $k/2l$ ) will be only half of the sag ratio  $k/l$  in the traditional System (I). So System (J) will be extremely inefficient in carrying the very decisive dead load.

For traffic load applied after completion of the bridge the main cable can be assumed to be supported both at points A and B but the sag ratio of this cable will be only  $(k/4)l$ , i.e. one quarter of the sag ratio in a traditional bridge. The cable tension due to traffic load will therefore be increased by a factor of almost 4.

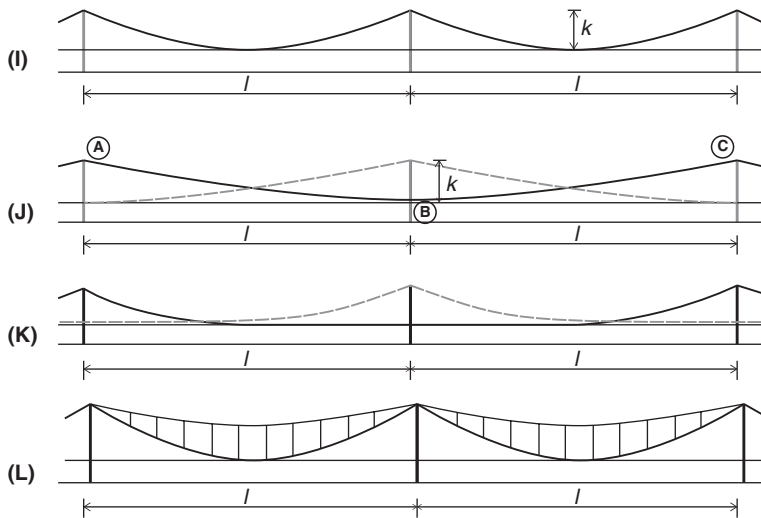


Figure 3.144 Multi-span suspension bridge with two parabolic main cables in each cable plane

For a multi-span bridge with several 1000 m spans, each with a sag of 100 m, the cable stress from the weight of the main cable will amount to almost 50% of the design stress for System (J), so that only half of the total strength will be available for carrying the dead load of the deck and the traffic load. For a traditional system as System (I) the cable stress from the cable weight will be only 12% of the design stress – a much more acceptable value.

Under non-uniform traffic load, System (J) will be characterized by more favourable deformational characteristics than System (I) if constructed with the same pylon height. However, the improvements are primarily due to the reduced sag of the main cable so almost the same performance would be achieved if System (I) was made with a main cable sag ratio of  $1/40$ . This would result in almost equal quantities of cable steel for the two systems, but the quantities to go into the pylons would be significantly smaller for System (I) due to the reduced height.

The inefficiency of System (J) has resulted in the variant shown under (K) in Figure 3.144. Here each main cable is curved in only one half of the main span and straight in the other half. In this case each main cable will have a sag ratio of  $\frac{1}{2}k/l$ , i.e. twice of that found for System (J), but at the same time the weight of the horizontal portion of the main cable will have to be carried through the hangers to the curved main cable above. The stress in the main cable due to the weight of the cable system will be  $\sim 25\%$  of the design stress, which is still about twice of that found in the traditional system.

In System (K) the horizontal part of the main cable will have to be supported by sliding bearings at the deck level to allow strain variations under varying loads without inducing axial stresses in the deck. This complicates both the structural detailing and the erection procedure.

It should be mentioned that the structural benefits attempted by the configuration of System (K) could be achieved in a simpler way by applying the traditional System (I) with a central clamp at midspan and a hydraulic centring of the deck in each main span.

The double-cable system shown under (L) in Figure 3.144 consists of two main cables with different sags but both supported at the top of the pylon. Immediately, the system resembles System (D) in Figure 3.142 as the upper main cable primarily has the function of restraining the pylon top from deflecting longitudinally. However, by interconnecting the two main cables by a number of vertical hanger cables, it is found that System (L) can carry loads of different intensities in one span without affecting the other spans. This is illustrated in Figure 3.145 that shows at the top the system subjected to a dead load  $g$  inducing horizontal forces of  $H_t$  in the top cable and  $H_b$  in the bottom cable, i.e. a total horizontal force of  $H = H_t + H_b$ .

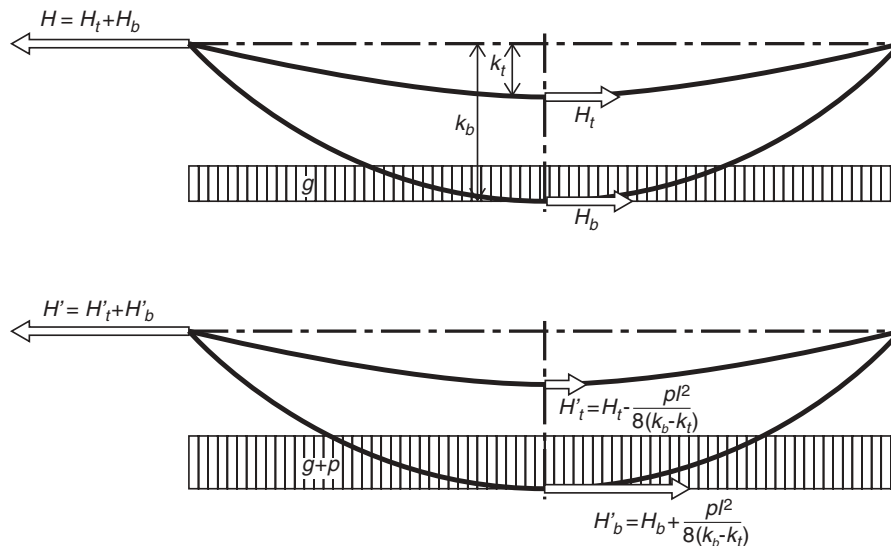


Figure 3.145 Double main cable system subjected to dead load (top) and dead load + traffic load in one span (bottom)

Under the assumption that the bottom cable carries the load  $\alpha_b g$  and the top cable the load  $(1 - \alpha_b)g$  the horizontal force  $H$  can be expressed:

$$H = \frac{\alpha_b g l^2}{8k_b} + \frac{(1 - \alpha_b)g l^2}{8k_t} \quad (3.97)$$

Assuming that under dead plus traffic load in only one span the horizontal forces in the two cables change as shown at the bottom of Figure 3.145, it is seen that the total horizontal force is maintained so that the adjoining spans will be unaffected by the load increase in the span considered.

The total load  $q$  carried by the two cables with the horizontal forces  $H'_t$  and  $H'_b$  will be:

$$q = (H'_t k_t + H'_b k_b) \frac{8}{l^2} = (H_t k_t + H_b k_b) \frac{8}{l^2} + \frac{p k_b - p k_t}{k_b - k_t} = g + p \quad (3.98)$$

So with the changes of horizontal forces indicated at the bottom of Figure 3.145, the double cable system will be able to carry the load  $g + p$ . It is seen that the load  $p$  is actually carried by the two cables acting as a simply supported beam with compression in the upper cable and tension in the lower cable, each corresponding to a numerical force of  $M_p/(k_b - k_t)$  where  $M_p$  is equal to the simple moment  $1/8 p l^2$ .

The assumption that the adjoining spans will be unaffected by the load increase in one span is only valid if the number of spans is very large. In the span with traffic load added, the two adjacent pylon tops will displace longitudinally due to the strain in the upper main cable but if these displacements are distributed over a large (infinite) number of spans on either side, then the distance from pylon top to pylon top will not change in all spans with dead load only. Besides the assumption that the number of spans is very large, it is also an assumption that the vertical pylons can deflect freely in the longitudinal direction.

In a more realistic case where the number of main spans is limited and the pylons possess some resistance to longitudinal displacements at the top, the span with traffic load added will experience an increase of the horizontal force acting on the two main cables at the pylon tops.

It is seen from Figure 3.145 that the minimum tension in the top cable will appear under the load  $p + g$  and, as it is a requirement that the top cable will be in tension under any traffic load condition, the minimum load to be carried by the top cable in the initial dead load condition must be determined by limiting the relaxation of the tension in the top cable.

Assuming that the initial tension can be reduced to half, i.e.  $H'_t = H_t/2$ , the minimum dead load  $(1 - \alpha_b)g$  to be carried by the top cable can be found from the following two equations:

$$H_t - \frac{p l^2}{8(k_b - k_t)} = \frac{1}{2} H_t \quad \text{and} \quad H_t = (1 - \alpha_b) \frac{g l^2}{8k_t} \quad (3.99)$$

leading to:

$$\alpha_b < 1 - 2 \frac{p}{g} \frac{k_t}{k_b - k_t} \quad (3.100)$$

It will generally be advantageous to have the largest portion of the dead load carried by the bottom cable as this cable is characterized by the most efficient sag ratio. Consequently, the value of  $\alpha_b$  should be chosen to be the highest possible value allowed by (3.100).

The fact that System (L) can carry additional traffic load in one span without changing the total horizontal force implies that this system does not require pylons offering a longitudinal restraint so traditional column-type pylons can be used for this multi-span system. On the other hand, the pylons for System (L) will have to be higher than for the traditional three-span bridge to ensure a reasonable sag of the top cable and reasonable difference in sag between the two cables – both features of importance for the quantity of cable steel. For a 1000 m span, a sag of 50 m for the top cable and 150 m for the bottom cable could be a sensible choice.

In a comparative investigation between a conventional three-span suspension bridge with a main span sag of 150 m and spans of 750 m, 1500 m and 750 m, and a multi-span bridge with a cable system as in System (L) with a large (infinite)

number of 1500 m spans, a top cable sag of 75 m and a bottom cable sag of 225 m, it was found that the maximum midspan deflection was very similar for the two systems. The quantity of cable steel per unit length was found to be approximately 20% higher for System (L) than for the three-span bridge.

A comparison between System (E) of Figure 3.142 and System (L) indicates that the quantity of pylon material will be reduced by approximately 15% but the quantity of cable steel increased by approximately 20% when replacing System (E) by System (L). These values indicate that the cost of the substructure has to be taken into account in the comparison due to the substantial savings that might be experienced when only a vertical force will have to be transferred to the soil.

### 3.6.3 Fixing of column-type pylons to piers

As described earlier, a longitudinal restraint of the pylon top can be achieved by fixing the pylon to the substructure, but this will require a substantial increase of the cross sectional dimensions to achieve equally small displacements as those found in a system with an anchor cable [76.2].

In Figure 3.146 two fan systems with one-sided loading are shown. The upper system has a vertical support at the right end and consequently comprises an anchor cable, whereas the lower system is connected to a moment rigid pylon (here assumed to have a constant cross section). For the horizontal displacement of the pylon tops, the following expressions can be derived:

$$\delta_1 = \frac{h_{pt}}{\sin \phi \cos \phi} \frac{\sigma_{ac}}{E_{cb}} \tag{3.101}$$

$$\delta_2 = \frac{2h_{pt}^2 + 6h_{pt}h_{pb} + 3h_{pb}^2}{3d_p} \frac{\sigma_{pb}}{E_{pl}} \tag{3.102}$$

in which  $\sigma_{ac}$  is the tensile stress in the anchor cable;  $E_{cb}$  the modulus of the elasticity for the cable;  $\sigma_{pb}$  the bending stress in the lower part of the pylon; and  $E_{pl}$  the modulus of elasticity for the material used in the pylon.

Equal stiffness under one-sided loading requires  $\delta_2 = \delta_1$ , which leads to:

$$d_p = \frac{2h_{pt}^2 + 6h_{pt}h_{pb} + 3h_{pb}^2}{6h_{pt}} \frac{\sigma_{pb}}{E_{pl}} \frac{E_{cb}}{\sigma_{ac}} \sin 2\phi \tag{3.103}$$

Inserting the following realistic values,  $h_{pb} = h_{pt}/2$ ,  $\phi = 20^\circ$ , and  $E_{cb}\sigma_{pb}/E_{pl}\sigma_{ac} = 0.5$ , into (3.103) yields  $d_p = 0.31 \times h_{pt}$ . For a bridge with 300 m long main spans, the height  $h_{pt}$  of the pylon will be around 50 m, and a moment rigid pylon in this

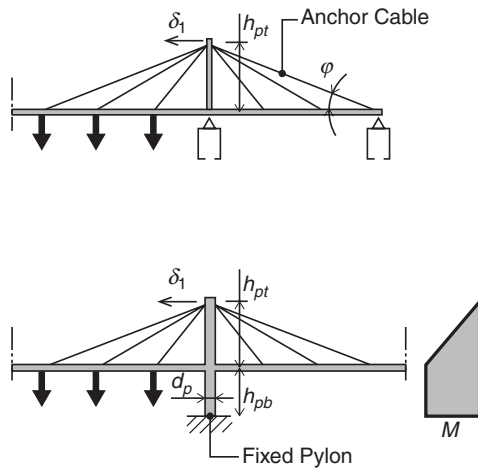


Figure 3.146 Fan-shaped cable systems supported by two piers (top) or by a fixed pylon (bottom)



bridge should therefore have a width of about 15 m to ensure the same stiffness as obtained by the anchor cable. By comparison, note that a 50 m high pylon in a two- or three-span bridge would normally be built with a longitudinal width of 2–3 m. Therefore, to compensate for an anchor cable, it will be necessary to drastically increase the dimensions of the pylons.

For pylons with common cross sectional dimensions and fixation to piers, the horizontal displacement of the pylon tops will be unacceptably large.

### 3.6.4 Triangular pylon structures

The only way to achieve sufficient stiffness in a fixed pylon structure and still get reasonable member dimensions seems to be by using an A-shape, as done, for example, in the Maracaibo Bridge (Figure 3.147).

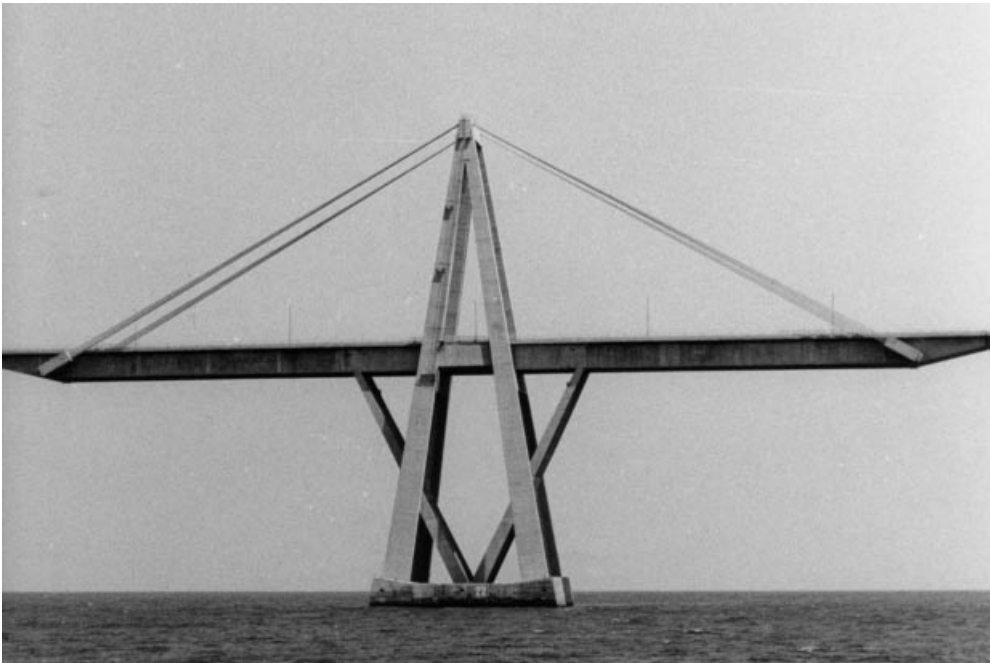
To arrive at the optimum configuration of a pylon structure fixed to the pier, the transmission of forces from the superstructure (cable system and deck) to the substructure must be studied.

If the cable system is earth anchored and the deck longitudinally movable (as in the conventional suspension bridge), then the pylon structure must be able to transmit the unbalanced horizontal force  $H_l - H_r$  all the way to the substructure. The correct form of the pylon structure should consequently comprise two inclined legs meeting at the top, as shown in Figure 3.148.

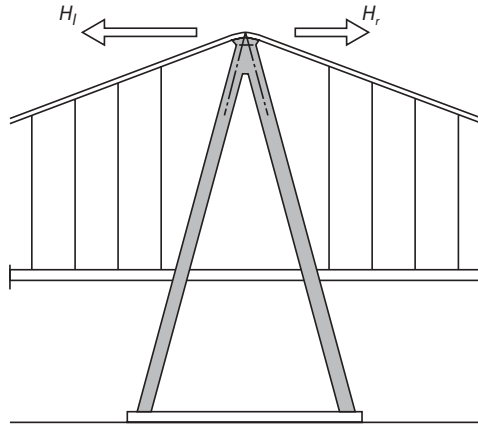
If the cable system is self anchored and the deck fixed to the pylon structure (as found in cable stayed bridges), the situation will be as illustrated in Figure 3.149. For symmetrical loading the horizontal forces in the cables and in the deck will be balanced out and only a vertical force at the pylon top is induced. However, with a one-sided loading both a horizontal and a vertical force will be induced at the pylon top, and another horizontal force in the opposite direction at the deck level.

As the two horizontal forces are of equal size, the moment in the pylon structure will increase from zero at the top to its maximum value at deck level. Below the deck the moment is constant and equal to the maximum value,  $M = Pa$ .

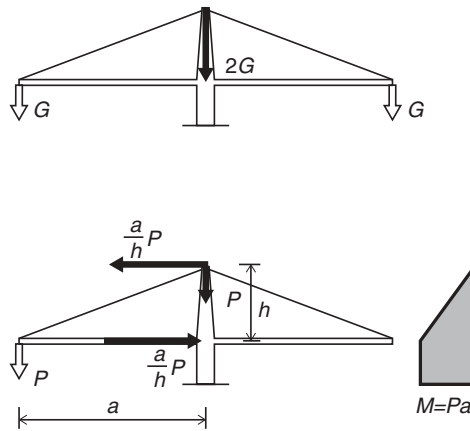
In accordance with the moment induced in the pylon structure of the self anchored system, a configuration as shown in Figure 3.150 seems to be the logical solution. With this configuration the moments acting on the entire pylon structure will induce mainly axial forces in the individual members. At the same time, flexural deformations of the slender vertical members below the roadway level render a certain longitudinal flexibility of the lower part of the pylon structure. This feature might allow the application of a continuous deck over a large bridge length.



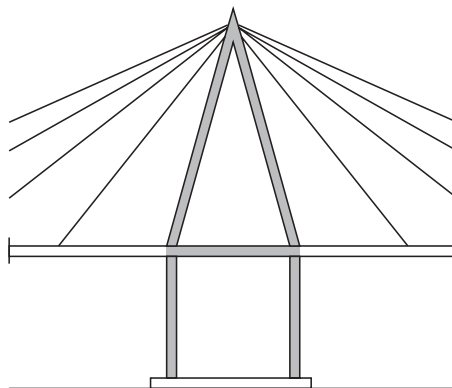
**Figure 3.147** *Pylon structure of the Maracaibo Bridge*



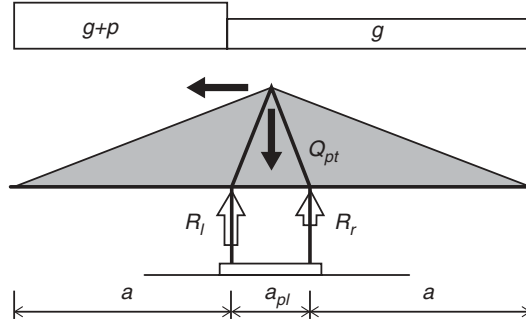
**Figure 3.148** Configuration of a triangular pylon structure in an earth anchored system



**Figure 3.149** Forces acting on a fixed pylon in a self anchored system



**Figure 3.150** Configuration of a triangular pylon structure in a self anchored system



**Figure 3.151** Loading case giving minimum reaction in the right leg of the pylon structure

If large horizontal movements of the deck must be expected, then movable bearings can be arranged between the deck and the vertical legs of the lower pylon structure. These horizontally movable bearings will in no way influence the transmission of the primary forces as long as the upper part of the pylon is horizontally fixed to the deck.

For the design of the connection between the upper and the lower part of the pylon structure it is essential to know whether tensile forces have to be transmitted or not.

Figure 3.151 shows the loading that produces minimum compression in the right leg of the pylon structure. For the reaction  $R_r$  is found:

$$R_r = g \left( a + \frac{a_{pl}}{2} \right) + \frac{1}{2} Q_{pt} - \frac{1}{2} p \frac{a^2}{a_{pl}} \quad (3.104)$$

where  $Q_{pt}$  is the weight of the pylon structure above the deck.

For  $R_r \geq 0$ , compression will always be present in the vertical legs. In combination with (3.104) the condition leads to:

$$a_{pl} \geq \sqrt{\left[ \frac{p}{g} a^2 + \left( a + \frac{Q_{pt}}{2g} \right)^2 \right]} - a - \frac{Q_{pt}}{2g} \quad (3.105)$$

With the values  $a = 250$  m,  $g = 0.20$  MN/m,  $p = 0.08$  MN/m, and  $Q_{pt} = 10$  MN, (3.105) yields:

$$a_{pl} < 42 \text{ m}$$

Whether it will be reasonable to fulfil this condition in a real structure  $a_{pl}$  depends on local condition, e.g. a suitable configuration of the foundation/pier below.

The above values for the dead and traffic loads might be representative for a road bridge with a steel deck, but for a railway bridge the ratio between traffic load and dead load generally will be larger and the following values shall therefore be used to illustrate this case:  $a = 250$  m,  $g = 0.18$  MN/m,  $p = 0.16$  MN/m, and  $Q_{pt} = 12$  MN.

From (3.105) the following condition for  $a_{pl}$  is found:

$$a_{pl} = 85 \text{ m}$$

This is a value that can hardly be achieved in a real structure, so in this case the vertical legs and their connection to the upper part should be designed to transmit tension.

If the triangular pylon above the deck is supported by the pier below in such a way that both compression and tension can be transmitted from the two pylon legs, then the upper part can be shaped in a much more elegant way as was convincingly demonstrated in the Millau Viaduct (Figure 3.152).

The pylon shape with a wide triangular upper part as the one shown in Figure 3.150 is characterized by a high degree of structural efficiency, but from the point of view of appearance it is often regarded as less attractive. This is in contrast to the pylon in Figure 3.148 so in some cases it has been proposed to use that pylon shape also in self anchored systems.

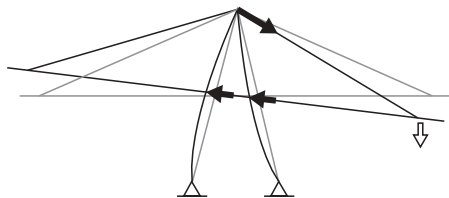
It is, however, not advisable to apply the simple triangular pylon structure of Figure 3.148 in its basic form in self anchored systems. Under one-sided loading the transmission of the horizontal force from the deck will induce a pronounced bending of the pylon legs, as illustrated in Figure 3.153. To avoid this, structural members will have



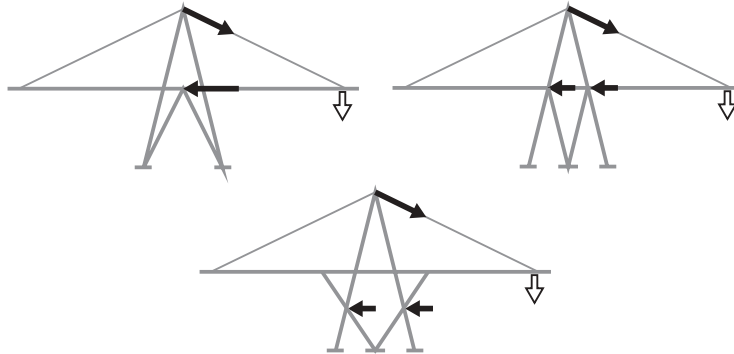
**Figure 3.152** *Triangular pylon above the deck of the Millau Viaduct*

to be added to transmit the horizontal force from the deck to the foundations, and in Figure 3.154 three solutions are outlined.

The two upper solutions are characterized by a genuine triangulation so the transmission of the horizontal force from the deck will produce primarily axial forces in the members of the pylon. The solution at the bottom of Figure 3.154



**Figure 3.153** *Deformation of a simple triangular pylon in a self anchored system under one-sided loading*



**Figure 3.154** Three solutions to supplement the simple triangular pylon by members giving efficient longitudinal support to the girder

corresponds to the configuration found in the Maracaibo Bridge, but here the transmission of the horizontal force from the deck will induce bending in the deck.

The configurations shown in Figure 3.154 will generally lead to larger quantities in the pylon than the configuration in Figure 3.150 – as illustrated in Figure 3.155 for two pylons with typical dimensions and loadings.

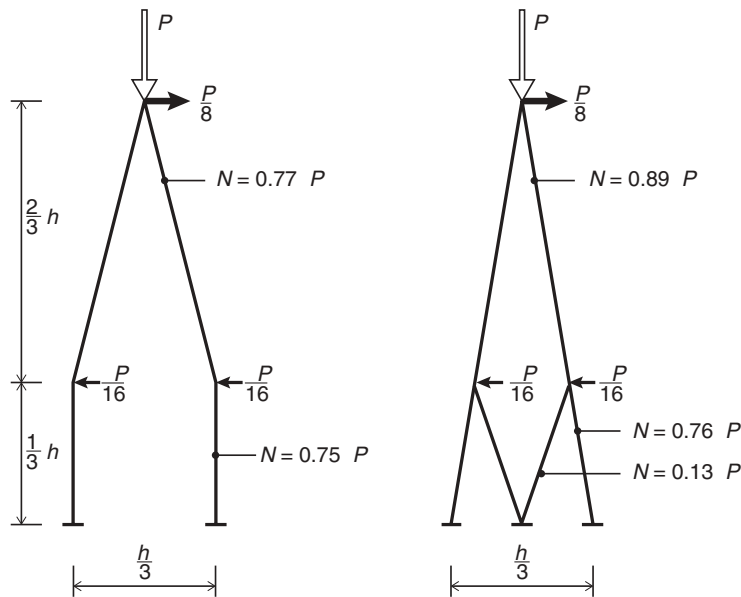
A calculation of the summation of the axial force times the length of the member leads to the following result:

$$\text{Solution I : } \Sigma NI = 1.56Ph$$

$$\text{Solution II : } \Sigma NI = 1.82Ph$$

As the summation  $\Sigma NI$  gives a measure for the quantity of material in the pylon it is seen that under the given assumptions System II will require approximately 17% more material than System I.

To investigate the influence of the geometry on the material consumption of a triangular pylon structure, expressions for the required quantity of a pylon structure as shown in Figure 3.156 will be derived. The pylon structure is here of the shape applicable in earth anchored systems e.g. a pure suspension system.



**Figure 3.155** Axial forces induced in two types of longitudinally rigid pylons

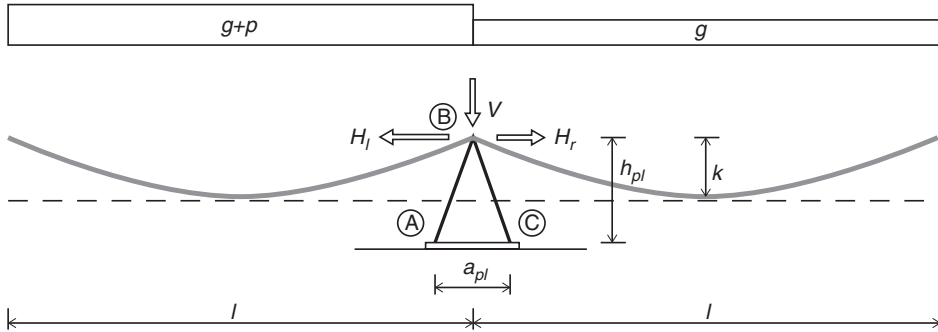


Figure 3.156 Triangular pylon structure in a multi-span suspension bridge

The forces acting at the top are determined by:

$$V = (g + p)l$$

$$\Delta H = H_1 - H_2 = pl^2/8k$$

leading to the following maximum normal force  $N_{\max}$  in the pylon legs:

$$N_{\max} = \frac{V}{2} \frac{\sqrt{h_p^2 + \frac{1}{4}a_{pl}^2}}{h_{pl}} + \Delta H \frac{\sqrt{h_{pl}^2 + \frac{1}{4}a_{pl}^2}}{a_{pl}} \quad (3.106)$$

The total quantity of material in the pylon then becomes:

$$Q_{pl} = \frac{\gamma_{pl}}{\sigma_{pl}} \left[ \left( g + \frac{p}{2} \right) \frac{l}{h_{pl}} + \frac{p}{4} \frac{l^2}{ka_{pl}} \right] (h_{pl}^2 + \frac{1}{4}a_{pl}^2) \quad (3.107)$$

In most cases  $k$  and  $h_{pl}$  will be fixed by considering the cable system (e.g.  $k = l/10$  to achieve sufficient stiffness) and the variable parameter for the pylon design then is the width  $a_{pl}$ .

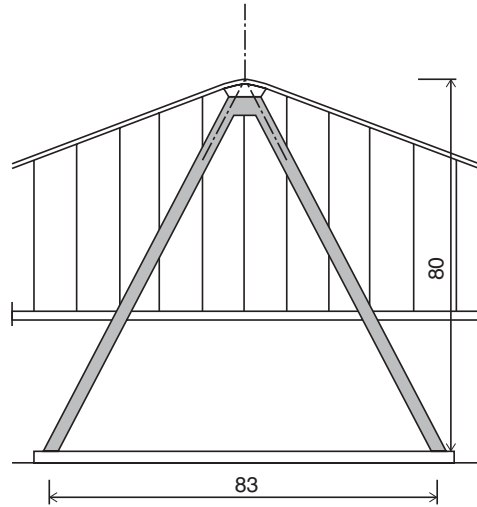
The optimum value of  $a_{pl}$  is determined for  $\partial Q_{pl}/\partial a_{pl} = 0$ , leading to the following cubic equation:

$$\left( g + \frac{p}{2} \right) \frac{l}{h_{pl}} a_{pl}^3 + \frac{pl^2}{8k} a_{pl}^2 - \frac{pl^2}{2k} h_{pl}^2 = 0 \quad (3.108)$$

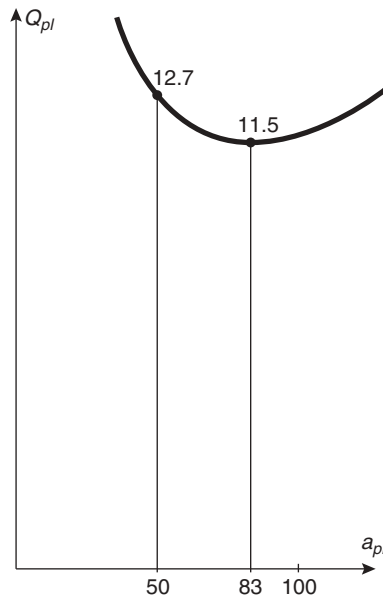
Generally, the optimum value of  $a_{pl}$  determined by (3.109) will lead to a very wide pylon structure. Thus, Figure 3.157 shows an optimized pylon structure with a height of 80 m and a width of 83 m. This is a value that would hardly be used in actual construction due to the excessive width of the pier below the pylon structure. In this connection it should be emphasized that the calculation leading to the value of 83 m is a sub-optimization taking into account only the pylon structure itself and not the substructure.

Based on (3.108) the variation of  $Q_{pl}$  with  $a_{pl}$  is shown in Figure 3.158. As usual, the optimum of  $Q_{pl}$  is rather flat and  $a_{pl}$  can therefore be chosen considerably below the optimum value of 83 m without an unacceptable increase of the quantity required in the pylon. Thus, with  $a_{pl} = 50$  m, the quantity of the pylon is increased by only 11%, an increase that might easily be counteracted by savings in the substructure.

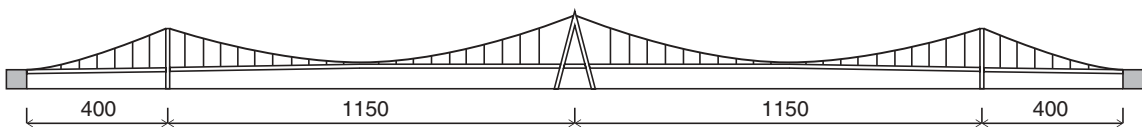
The four-span suspension bridge shown in Figure 3.159 was investigated by T. Fukuda in the mid-1960s [67.1]. It was found that the application of a central triangular pylon gave the system excellent stiffness properties so that the maximum deflection under traffic load in one main span amounted to only 1.79 m, corresponding to 1/670 of the span length. Actually, it was found that the structure could be analyzed as two individual two-span bridges assuming a completely fixed support of the main cables at the top of the central pylon. The large longitudinal stiffness of the triangular pylon was illustrated by the fact that a force of 200 MN would be required to displace its top 1 m longitudinally, whereas the vertical side pylons would have their tops displaced 1 m for a force of only 1 MN.



**Figure 3.157** Optimized configuration of a triangular pylon, structure between two suspension bridge main spans. Parameters:  $l=500\text{ m}$ ,  $k=50\text{ m}$ ,  $h_{pl}=80\text{ m}$ ,  $g=0.22\text{ MN/m}$ ,  $p=0.08\text{ MN/m}$



**Figure 3.158** Variation of the quantity in the pylon structure with the width  $a_p$ . Parameters as for Figure 3.157



**Figure 3.159** Four-span suspension bridge investigated by T. Fukuda



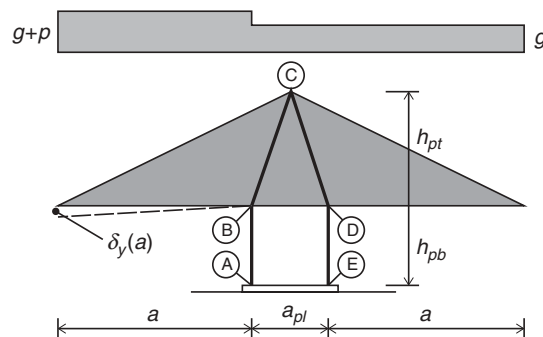
**Figure 3.160** Konaruto Bridge with two consecutive 160 m main spans

It is interesting to compare the results of Fukuda's investigation with those obtained for model C in the Bay Bridge model tests (refer to Figure 3.136) as both bridges have four spans and almost similar loading. Despite the fact that the main span of the bridge with the triangular central pylon is about 16% larger than the main span of the bridge with the vertical central pylon, the maximum deflection for the system in Figure 3.159 is only about 30% of the maximum deflection of the system in Figure 3.136, model C. This clearly indicates the advantages to be gained with a triangular pylon structure in multi-span suspension bridges.

The investigations of Fukuda were probably directed towards the Bisan Seto Bridge project where two main spans of around 1 km were required. However, as shown in Figure 1.74, the bridge was actually built as two three-span suspension bridges with a central anchor block.

On a much smaller scale the principle of a four-span suspension with a central triangular pylon had been realized in the Konaruto Bridge of 1961 (Figure 3.160).

For a self anchored fan system as shown in Figure 3.161 both the height  $h_{pt}$  above the deck and the width  $a_{pl}$  can be regarded as variable parameters for the pylon structure design as stiffness requirements generally do not prescribe a limit to the height of the cable system to the same degree as for a suspension system.



**Figure 3.161** Triangular pylon structure in a multi-span cable stayed bridge with a fan system



With the notation given on Figure 3.161, the following expressions for the quantities of the pylon structure might be derived:

Quantity  $Q_{pt}$  of the top part (BC and CD):

$$Q_{pt} = \frac{\gamma_{pl}}{f_{pld}} \left( g(2a + a_{pl}) + p \frac{(a + p_{pl})^2}{a_{pl}} \right) \frac{h_{pt}^2 + \frac{1}{4}a_{pl}^2}{h_{pt} - \frac{\gamma_{pl}}{f_{pld}} \left( h_{pt}^2 + \frac{1}{4}a_{pl}^2 \right)} \quad (3.109)$$

and the quantity  $Q_{pb}$  of the bottom part (AB and DE):

$$Q_{pb} = \frac{\gamma_{pl}}{f_{pld}} \left( g(2a + a_{pl}) + p \frac{(a + p_{pl})^2}{a_{pl}} \right) \frac{h_{pt} + h_{pb}}{h_{pt} - \frac{\gamma_{pl}}{f_{pld}} \left( h_{pt}^2 + \frac{1}{4}a_{pl}^2 \right)} \quad (3.110)$$

The total quantity  $Q_{pl}$  of the entire pylon structure thus becomes:

$$Q_{pl} = \frac{\gamma_{pl}}{f_{pld}} \left( g(2a + a_{pl}) + p \frac{(a + p_{pl})^2}{a_{pl}} \right) \frac{h_{pt}^2 + h_{pt}h_{pb} + \frac{1}{4}a_{pl}^2}{h_{pt} - \frac{\gamma_{pl}}{f_{pld}} \left( h_{pt}^2 + \frac{1}{4}a_{pl}^2 \right)} \quad (3.111)$$

With the height  $h_{pt}$  as a variable, the quantities of the cable system also have to be included in the optimization proves.

Based on the simplified expression (3.56), the quantity of cable steel becomes:

$$Q_F = \frac{1}{2f_{cbd}} (g + p) \left( \frac{2a + a_{pl}}{6h_{pt}} + \frac{2h_{pt}}{2a + a_{pl}} \right) (2a + a_{pl})^2 \quad (3.112)$$

With a unit price  $u_{cb}$  for the cable steel and  $u_{pl}$  for the pylon material, the total cost  $C_{cp}$  of cable system and pylon structure becomes:

$$C_{cp} = u_{cb} Q_F + u_{pl} Q_{pl} \quad (3.113)$$

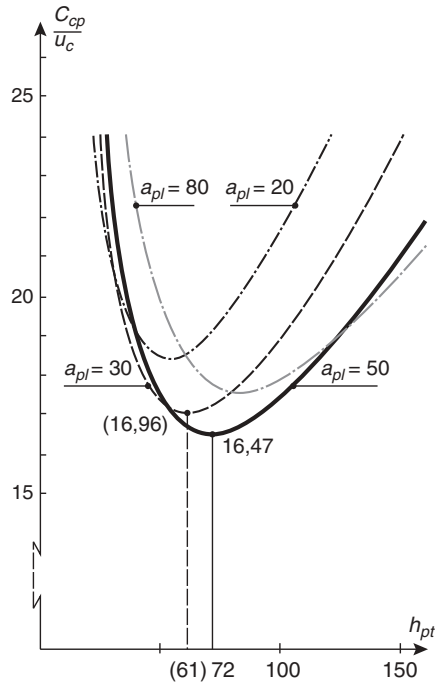
The variation of the quantity  $C_{cp}/u_{cb} = (Q_F + u_{pl}Q_{pl}/u_{cb})$  with the width  $a_{pl}$  and the height  $h_{pt}$  of the upper pylon part is illustrated by the example in Figure 3.162. As indicated, the minimum value of the quantity  $C_{cp}/u_{cb}$  is found for  $a_{pl} = 50$  m. and  $h_{pt} = 72$  m. However, the minimum value for  $a_{pl} = 30$  m ( $h_{pt} = 61$  m) only differs approximately 3% from the absolute minimum value and this indicates that  $a_{pl}$  can be chosen within a certain interval without noticeably influencing the cost of the structure. Consequently, the final choice of the width  $a_{pl}$  must be based on a more elaborate analysis taking into account the substructure, the local boundary conditions (total length of the bridge portion to be cable supported, clearance requirements, etc.), and stiffness considerations.

Generally, the stiffness will improve with increasing values of  $a_{pl}$ , as is illustrated by the plot in Figure 3.163 showing the variation of the midspan deflection  $\delta_y$  with  $a_{pl}$  (for systems with the optimum height  $h_{pt}$ ). As seen, the maximum midspan deflection is reduced by 21% when the pylon width is increased from 30 m to 50 m. However, it should be mentioned that the midspan deflection of an ordinary three-span cable stayed bridge with spans of 125 m, 500 m, and 125 m amounts to 1.89 m (based on the same simplifications as used above). So with this deflection as a limiting value,  $a_{pl}$  could be chosen to have a value as low as 30 m in the present example.

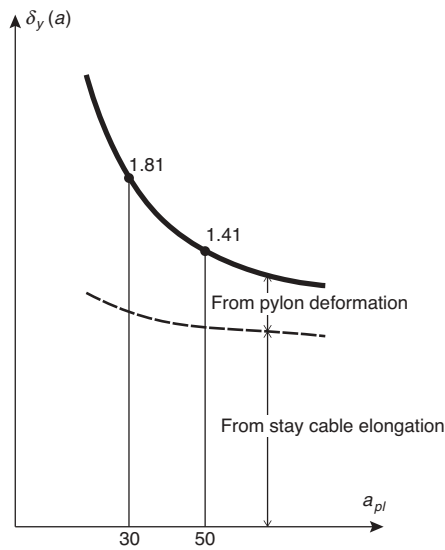
### 3.6.5 Horizontal tie cable between pylon tops

Another way to reduce the longitudinal displacements of intermediate pylon tops is to connect them by a horizontal tie between them, as illustrated in Figure 3.164 for a suspension system and a cable stayed system.

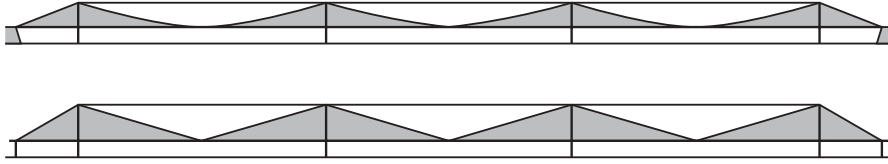
Generally, the horizontal tie cable will be anchored in the same way as the remaining part of the cable system, so that the tie cable of the suspension system becomes earth anchored and the tie cable of the cable stayed system is self anchored.



**Figure 3.162** Variation of the quantity of the pylon structure and the cable system with the width  $a_{pl}$  and the height  $h_{pt}$  (refer to Figure 3.140). Parameters;  $a = 250\text{ m}$ ,  $h_{pb} = 30\text{ m}$ ,  $g = 0.22\text{ MN/m}$ ,  $p = 0.08\text{ MN/m}$ ,  $\sigma_{cb} = 720\text{ MPa}$ ,  $\gamma_{cb} = 0.08\text{ MN/m}^3$ ,  $\sigma_{pl} = 160\text{ MPa}$ ,  $\gamma_{pl} = 0.08\text{ MN/m}^3$



**Figure 3.163** Variation of the midspan deflection  $\delta_y(a)$  with the width  $a_p$  of the pylon structure



**Figure 3.164** Cable supported bridges with a horizontal anchor cable connecting all pylon tops

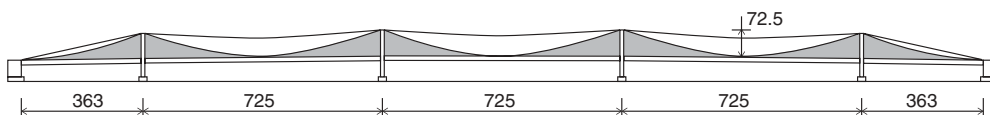
Horizontal tie cables have been used in a number of French suspension bridges built in the nineteenth century (Figure 3.165), and the system was also investigated for the West Bay Crossing of the San Francisco–Oakland Bay Bridge in an attempt to avoid the central anchor pier.

The system investigated for the Bay Bridge is shown in Figure 3.166. It comprised three main spans of equal length (725 m) and two side spans of half length (363 m). Note that the tie cable was continued from the tops of the outer pylons to the anchor blocks to counteract the deformational disadvantages of the long side spans. In the three main spans the suspension cables had a sag ratio of 1:10, whereas the sag of the horizontal tie cables in the dead load condition at mean temperature was 1:50. This resulted in a dead load stress of 360 MPa in the anchor cable.

The investigations showed that the system with the horizontal tie cable gave deflections that were even smaller than those of the system with the central anchor pier (refer to Figure 3.136, Model B). Adding to this that the quantity of cable steel only had to be increased by approximately 15% to cover the tie cable seems to indicate that the system of Figure 3.166 should indeed be very competitive. However, the system was apparently not seriously investigated, probably due to the extremely tight schedule for the construction of the Bay Bridge, which was actually built in  $3\frac{1}{2}$  years. With such a speed it is understandable that a conventional design involving only well-known technology had to be preferred.



**Figure 3.165** Multi-span suspension bridge with a horizontal anchor cable (France, nineteenth century)



**Figure 3.166** Five-span suspension bridge studied for the West Bay crossing of the San Francisco–Oakland Bay Bridge in the early 1930s

One of the special problems in the construction of a bridge with a horizontal tie cable relates to the erection of a long cable with a very small sag ratio requiring an unusually shallow temporary footway (catwalk) during the air-spinning procedure. Also the transfer of large differential cable forces between the saddles of the parabolic main cables and the saddles of the horizontal tie cable would raise special problems.

As the free length of the horizontal tie cable is equal to the main span length, the sag effect will be quite significant in long span bridges. In the case of the horizontal tie studied for the Bay Bridge the equivalent modulus of elasticity (tangent modulus) would be:

$$\frac{1}{E_{\tan}} = \frac{1}{E_{cb}} + \frac{1}{12} \frac{\gamma_{cb}^2 a^2}{\sigma_1^3} = \frac{1}{205 \times 10^3} + \frac{1}{12} \frac{(0.08 \times 725)^2}{360^3}$$

$$E_{\tan} = 92 \text{ GPa}$$

Thus, the sag effect would decrease the axial stiffness of the tie cable to less than half, but, as described earlier, the stiffness of the total system would still be adequate and comparable to that of a conventional three-span bridge.

As the tie cable must be made with the smallest possible sag to get a large axial stiffness and at the same time be anchored at the end piers, temperature effects must be given special attention.

In a self anchored system with the anchor cable attached to the deck, a uniform change of temperature in the entire structure does not induce any additional stresses. Only in the case of a temperature difference between the cable and the deck will stresses occur. As the cross sectional area of the deck is much larger than the area of the tie cable, the necessary strains to assure compatibility will be induced almost entirely in the cable.

In an earth anchored system any change of temperature in the anchor cable will induce stresses as the ends of the tie cable are fixed to the anchor blocks. Thus, the temperature stresses in the anchor cable will be greater in the earth anchored system than in the self anchored system.

The maximum stress  $\sigma_t$  due to temperature change might be expressed by:

$$\sigma_t = E_{eq} \beta \Delta t \quad (3.114)$$

where  $\beta$  is the coefficient of thermal expansion, and  $\Delta t$  the change of temperature in an earth anchored cable or the temperature difference between the tie cable and the deck in a self anchored cable.

With the following values,  $E_{eq} = 92 \text{ GPa}$ ,  $\beta = 12 \times 10^{-6}$  and  $\Delta t = 25^\circ\text{C}$  (representative for the Bay Bridge design), (3.115) yields:

$$\sigma_t = 28 \text{ MPa}$$

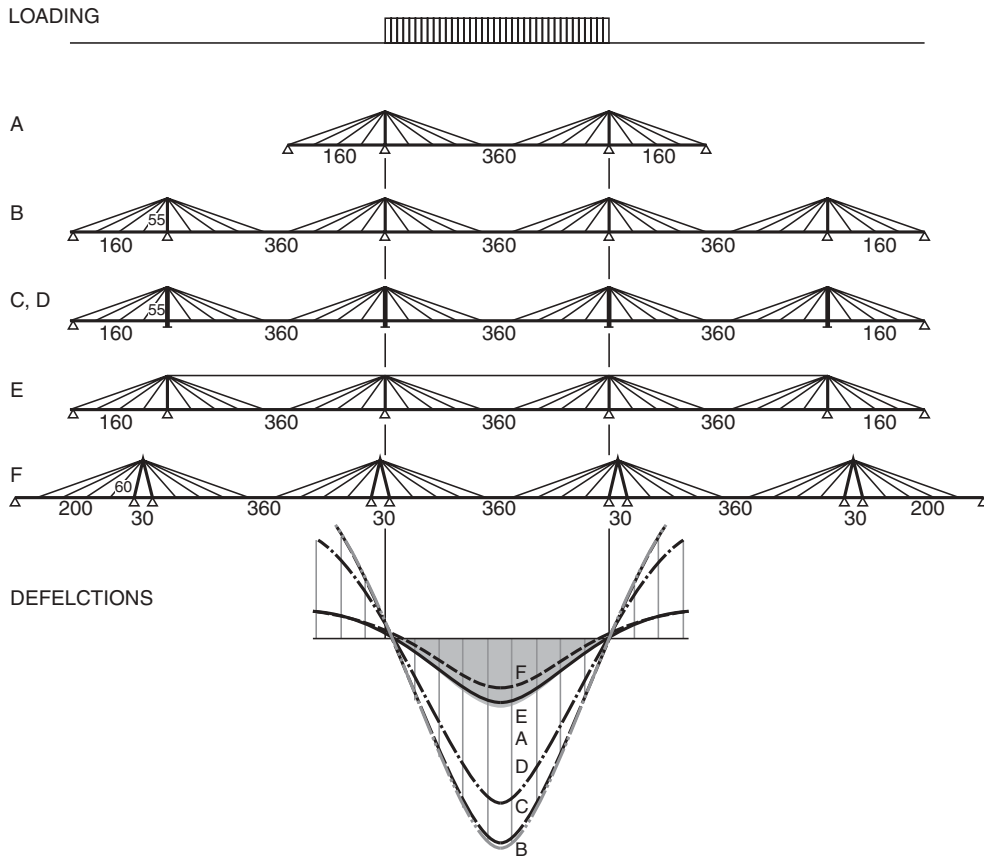
This stress is equal to approximately 4% of the design stress and therefore of little significance.

### 3.6.6 Comparison between deflections of different multi-span cable stayed systems

The results of a comparative investigation into the stiffness properties of different structural systems are shown in Figures 3.167 and 3.168 [76.2].

The principal features of the systems investigated can be summarized as follows: System A is the conventional three-span bridge with a fan-shaped cable system and hinged connections between the superstructure and the substructure. The dimensions and cross sectional properties of the individual members correspond to those required when traditional European loadings were applied. Furthermore, it is assumed that the steel for the deck and the pylon has a yield stress of 350 MPa, whereas the cable wires have an ultimate stress of 1500 MPa.

System B corresponds to System A regarding the size of members and type of connection between superstructure and substructure. Note that equal sectional properties for corresponding members generally are assumed in order to allow for a direct comparison between the stiffness of the systems themselves.



**Figure 3.167** Deflection curves for different cable stayed bridges with loading in the central span only (or 3.67)

Systems C and D have fixed connections between the pylons and the substructure. However, the pylons are of the conventional column-type (in contrast to the pylon structures of system F). In System C, the sectional properties of the pylons are as in Systems A and B, whereas a ten times larger moment of inertia is applied for the pylons of System D.

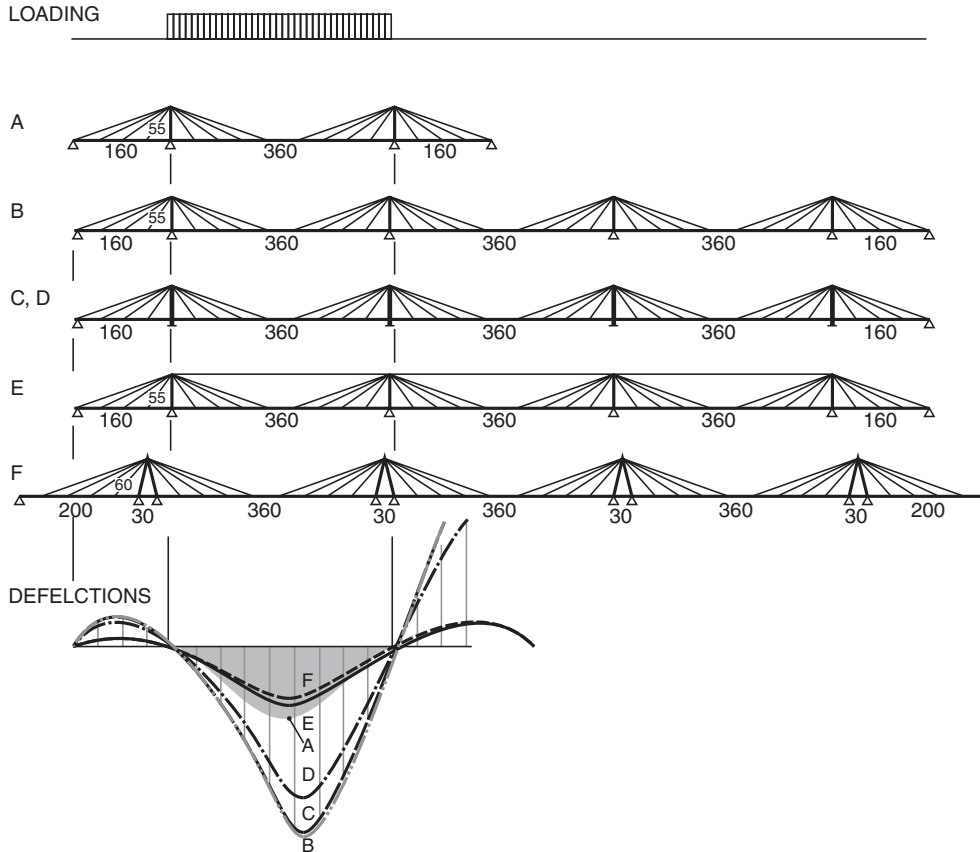
System E contains the earlier described horizontal tie cable between the pylon tops. Apart from this, Systems E and B are identical.

System F contains four triangular pylon structures supported on double bearings. In this way, an effective fixing to the substructure is established.

The deflections of the different systems for uniformly distributed load in one main span are shown at the bottom of Figures 3.167 and 3.168. The deflection of the well-known three-span bridge (System A) is used as a reference and indicated by the shaded area. Note that generally the deflections of the common three-span bridge are regarded as being close to the allowable limit for bridge structures of the actual size.

From the deflection curves, the following characteristics might be deduced:

- (1) The fixing of pylons with common flexural stiffness does not reduce the deflections noticeably (compare Systems B and C).
- (2) Even by fixing and increasing the flexural stiffness of the pylons by a factor of 10, the deflections are not reduced sufficiently (compare Systems B and D).



**Figure 3.168** Deflection curves for different cable stayed bridges with loading in one outer main span only

- (3) A horizontal tie between the pylon tops will reduce the deflections of the multi-span bridge to a permissible limit (System E).
- (4) Triangular pylon structures supported on double bearings also lead to allowable deflections (System F).

As can be seen, the smallest deflections occur in System F. However, the deflection curve for this system is based on the assumption that the two supports under each pylon structure are completely rigid in the vertical direction. In real structures, the pylons will often be connected to pier shafts where axial deformations that result in a rotation of the upper triangular part of the pylon.

When comparing the deflections of the different systems, it is also necessary to take into account the difference in quantities required. In Table 3.3, the relative quantities per unit length for systems A–F are tabulated. It appears that the addition of the horizontal tie cable (system E) increases the quantity of cable steel per unit length by 48% compared to the conventional three-span bridge (system A).

With triangular pylon structures (System F), the amount of cable steel will be reduced by 18%, mainly due to the elimination of the heavy anchor cables. On the other hand, the quantity of structural steel is increased by 14% due to the application of double-legged pylons with larger cross sections.

The last column of Table 3.3 gives the relative equivalent quantity of structural steel for the different systems with System A as reference system (relative quantity = 1.00). To arrive at the equivalent quantity of structural steel, the quantity of cable steel is multiplied by 2.5 and added to the quantity of structural steel. Thus, the last column of Table 3.3 will give

**Table 3.3** Relative quantities per unit length for the systems of Figures 3.167 and 3.168

| System | Structural steel (deck and pylons) | Cable steel (stays) | Equivalent relative quantity of structural steel |
|--------|------------------------------------|---------------------|--|
| A      | 1.00                               | 1.00                | 1.00   |
| B      | 1.00                               | 0.91                | 0.97   |
| C      | 1.00                               | 0.91                | 0.97   |
| D      | 1.03                               | 0.91                | 0.99   |
| E      | 1.00                               | 1.48                | 1.15   |
| F      | 1.14                               | 0.82                | 1.04   |

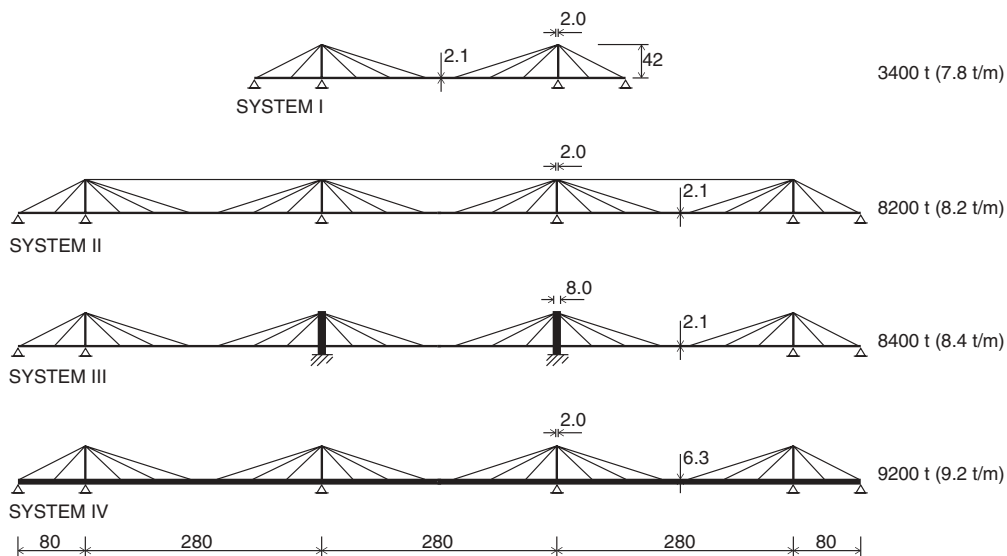
an idea of the relative cost per unit length for the superstructures of the different systems. It is seen that the cost per unit length of System E is considerably higher than the cost of System F, but in this context it must be emphasized that System E could lead to substantial savings in the substructure as mainly vertical forces will have to be transferred to the soil. When evaluating the relative quantities given in Table 3.3, it must be remembered that the average span length of systems E and F (280 m and 295 m) is larger than the average span length of system A (230 m).

In the above investigation the main dimensions of the deck and the cables were kept constant to allow a direct comparison between the flexibility of the cable systems themselves. Another approach could be based on requiring equal deflection of all systems and then compare the corresponding quantities.

In Figure 3.169 the result of such a comparison is summarized. The basic system (System I) is a three-span bridge with a 280 m main span flanked by two 80 m side spans. The other three systems II–IV are designed to get the same maximum deflections under traffic load as found in System I. For the five-span bridge with a horizontal tie cable between all pylon tops (System II) the dimensions of the deck and the pylons can be kept unchanged, as the inner fans are stabilized by the horizontal tie.

Without a horizontal tie cable the inner fans must either be stabilized by fixing the pylons to the piers (System III), or by increasing the flexural stiffness of the deck (System IV). In both cases the relevant structural elements (pylons/deck) must be made with large cross sectional dimensions, which influences the quantities.

Taking into account only the quantities of the superstructure, System II is the most favourable of the five-span structures. However, other factors have to be included in a comparison, such as the forces acting on the substructure and the erection

**Figure 3.169** Four cable stayed bridges designed to have the same maximum deflection under traffic load

procedure. Systems I, II, and IV will transfer only vertical forces to the substructure from vertical load, whereas moments must be carried by the substructure under the two central pylons of System III. On the other hand, System III implies to a higher degree self-stabilization during erection. So all in all, many other factors than just the quantities of structural materials will have to be taken into account when choosing between the different solutions.

### 3.7 Cable Systems under Lateral Loading

So far the characteristics of cable systems have been treated for in-plane vertical loading and immediately it would seem that the cable systems would be able to carry only this type of loading. Actually, the fact that the cable force always coincides with the tangent of the cable curve implies that any combination of cable forces will have its resultant in the cable plane. However, due to second order effects occurring under out-of-plane displacements of the cable system a resistance against loading perpendicular to the initial cable plane can exist in some cases.

The restoring effect that might appear under lateral displacements is often referred to as the pendulum effect and it can be proved that this effect is present only in earth anchored systems although it is sometimes stated that cable stayed bridges of the traditional configuration with self anchoring also will be able to transfer lateral load through cable planes that are initially vertical but appear to incline under lateral deflection of the deck when looking at the cable system along the axis of the bridge.

To explain the lack of pendulum effect in a self anchored cable stayed system, the basic system shown in Figure 3.170 will be considered. The system consists of the inclined cable element A–D and the horizontal girder element B–D.

The system is able to carry a vertical force  $P_v$  at point D by producing tension in the cable element and compression in the girder element. If point D is displaced to a new position at D', then the plane ABD' will still be vertical so in this position the system will also be able to carry a vertical force only.

The lack of pendulum effect can also be explained by the fact that point D will be bound to move around on a horizontal circle in the  $xz$  plane so there will be no change in the potential energy of the vertical force when moving from one position to another.

For an earth anchored cable system the basic system could be illustrated by the system in Figure 3.171. Here a vertical force at point G induces tension in the two cable elements E–G and F–G.

For this system a lateral displacement of the point G to the position G' will result in a rotation of the initially vertical cable plane around the axis E–F. Therefore, the point G will be bound to follow a vertical circle with its centre at point H. So any lateral displacement of point G will lift the vertical force and increase its potential energy. Therefore, the system will be stable only if the plane EFG is vertical, and at any lateral displacement of point G a restoring force will act to let point G return to its original position.

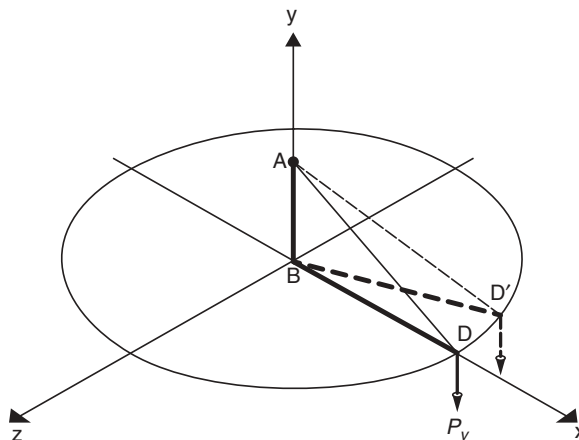
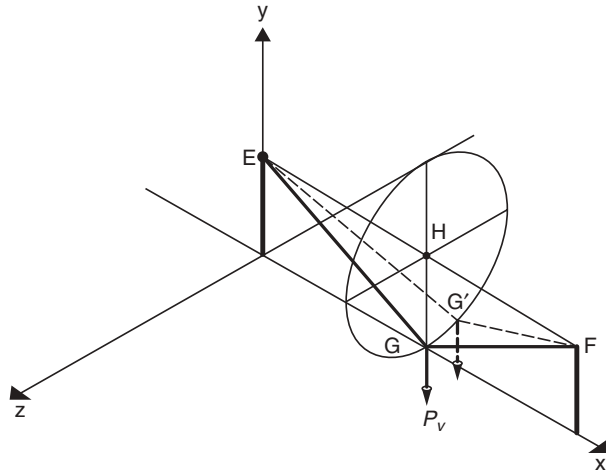


Figure 3.170 Idealized self anchored cable system

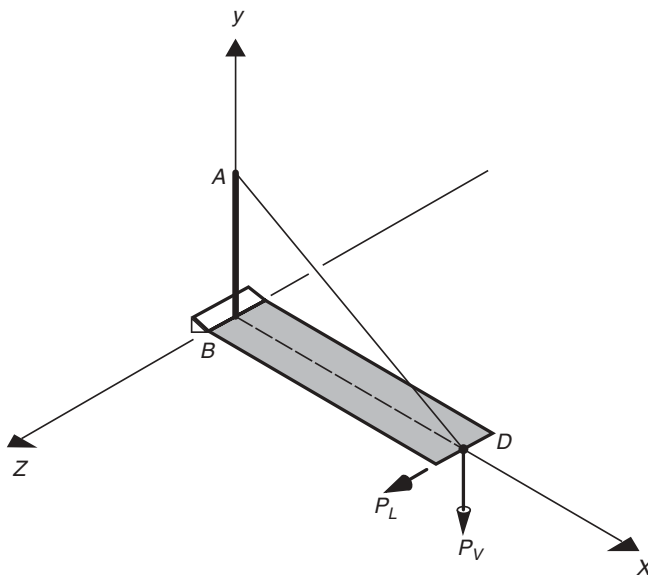




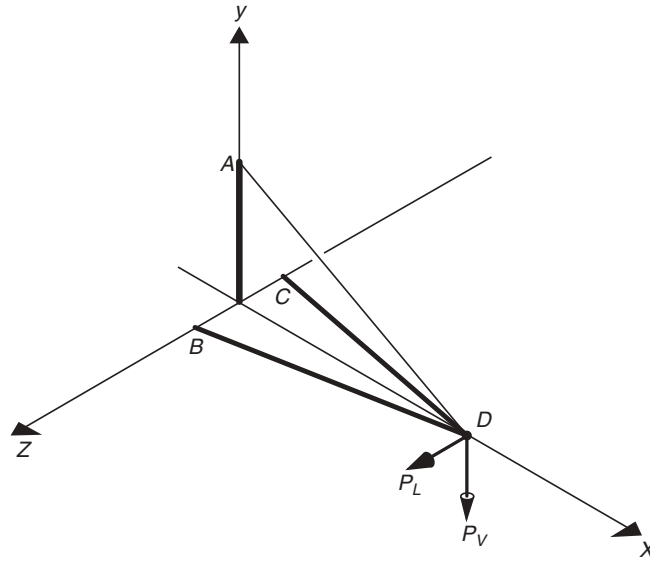
**Figure 3.171** Idealized earth anchored cable system

For systems without a stabilizing pendulum effect the lateral stability has to be ensured by the flexural stiffness of the deck, so that the basic system will be as shown in Figure 3.172. Here the deck is moment rigidly supported along the  $z$  axis so that a moment induced by a lateral load  $P_l$  on the deck can be transferred.

In a further idealization the system with lateral stability established by the flexural stiffness of the deck can be illustrated as shown in Figure 3.173 where the horizontal beam is replaced by two compression members B–D and C–D. This system is clearly able to transmit both a vertical force  $P_v$  and a lateral force  $P_l$  acting at point D.

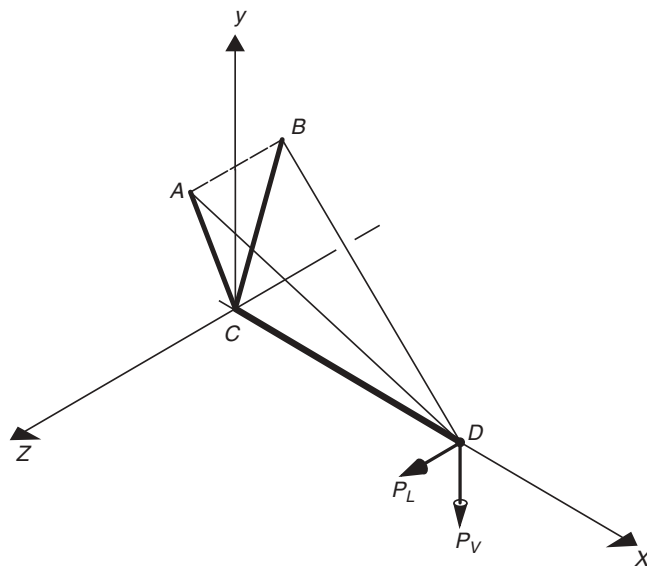


**Figure 3.172** Idealized self anchored system with laterally stable girder

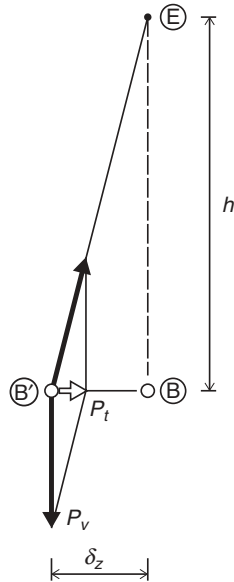


**Figure 3.173** Idealized self anchored system with twin compression members at the deck level

The system shown in Figure 3.173 transmits a load which is mainly vertical by tension in the cable A–D and compression in the two elements B–D and C–D. However the same type of load might also be transmitted by a system as shown in Figure 3.174 with a single compression member C–D and two tension members A–D and B–D. In the latter case the cable system will be a spatial cable system as the three-dimensional stability is achieved by the two stay cables.



**Figure 3.174** Idealized self anchored system with twin stay cables (spatial cable system)



**Figure 3.175** Lateral restoring force  $P_l$  resulting from rotation of an initially vertical cable plane

The application of spatial cable systems will be further described in Section 3.8, so here only systems stabilized by the pendulum effect will be treated.

As indicated in Figure 3.175 the lateral load  $P_l$  resulting from the inclination of the cable plane is determined by:

$$P_l = \frac{\delta_z}{h} P_v \quad (3.115)$$

where  $\delta_z$  is the lateral displacement of point B.

To illustrate the pendulum effect in an earth anchored multi-cable system, as shown in Figure 3.176, the resistance against lateral loading offered by the cable system can be taken into account in the symmetric case by assuming a continuous, lateral, elastic support characterized by a spring constant  $C$  defined by:

$$C = g/h \quad (3.116)$$

where  $g$  is the vertical load per unit length and  $h$  the height of the cable system.

For lateral loading the deck can then be analyzed as a girder on continuous elastic supports throughout the spans, and rigid supports at the pylons and the end piers.

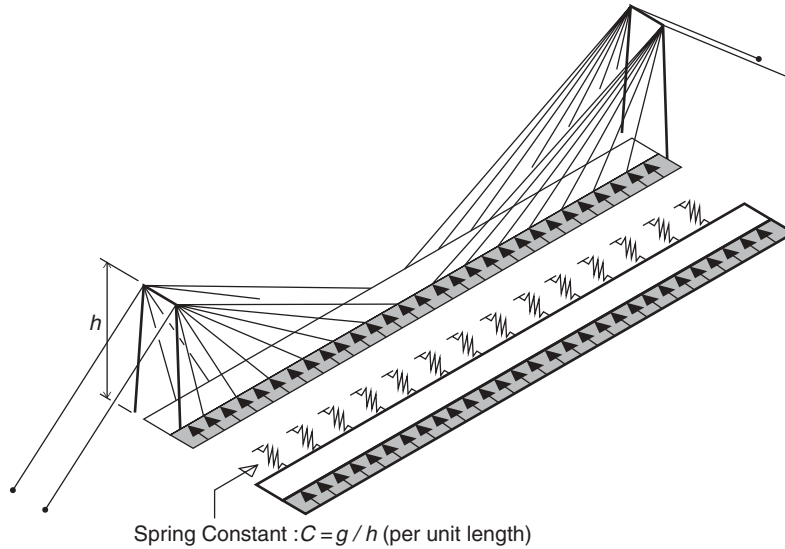
If the flexural stiffness of the deck about the vertical axis is insignificant, then the deck will displace laterally until equilibrium is achieved entirely by the lateral components of the cable forces.

With a lateral load  $u$  per unit length, the required displacement  $\delta_{zc}$  is determined by:

$$\delta_{zc} = uh/g \quad (3.117)$$

Note that the lateral displacement  $\delta_{zc}$  is proportional to the height  $h$ , so that this aspect must be taken into account when making the final choice of the height-to-span ratio of an earth anchored cable system.

The effect of lateral support described for the earth anchored cable stayed system shown in Figure 3.176 will also be found in suspension bridges, and in preliminary calculations the effect can be taken into account simply by assuming a lateral elastic support with the same spring constant as given in (3.117).



**Figure 3.176** Lateral support offered by earth anchored multi-cable fan system replaced by a continuous elastic support

To get an idea of the magnitude of the required displacement  $\delta_{zc}$ , a bridge with a 3 m deep streamlined deck weighing 160 kN/m and with a main span of 1000 m will be considered. With a drag coefficient  $c_{db} = 1.0$  and a dynamic head of wind  $q = 2 \text{ kN/m}^2$  the wind load  $u$  per unit length becomes:

$$u = 1.0 \times 2 \times 3 = 6 \text{ m}$$

Assuming a pylon height of 100 m (above the deck), the displacement  $\delta_{zc}$  becomes:

$$\delta_{zc} = 6 \times 100 / 160 = 3.75 \text{ m}$$

This corresponds to 1/267 of the main span length and a sidesway of this magnitude will generally be acceptable.

In real structures with earth anchored cable systems the lateral wind load will be taken partly by bending in the deck and partly by the cable system.

Assuming that the entire wind load in the above example was taken by bending of the deck about the vertical axis, and assuming a realistic value of the moment of inertia  $I_y$  equal to  $60 \text{ m}^4$ , yields the following lateral deflection  $\delta_{zd}$ :

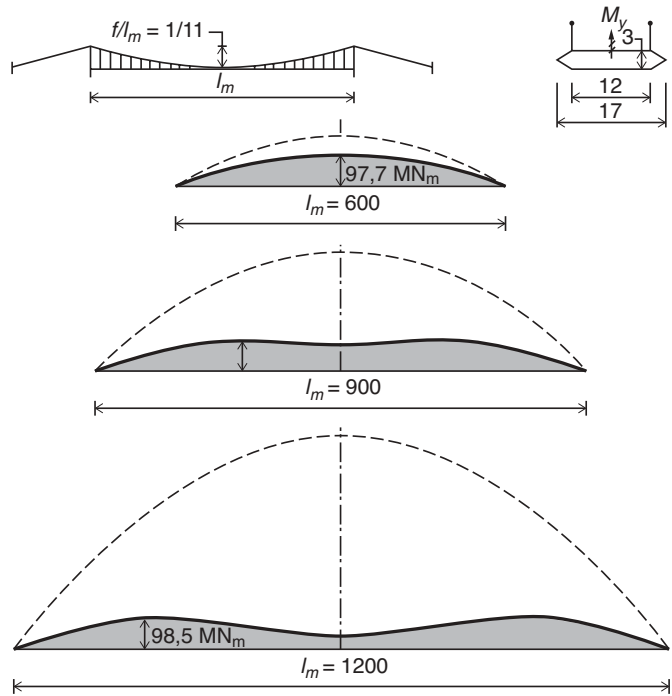
$$\delta_{zd} = 3.7 \text{ m}$$

As  $\delta_{zd}$  has almost the same value as  $\delta_{zc}$  it is indicated that in this case the wind load will be almost equally transferred by lateral bending of the deck and by the pendulum effect of the cable system.

During the model tests for the Bay Bridge it was found that approximately 30% of the wind load was taken by the cable system despite the fact that the width-to-span ratio of the deck was as large as 1:35.

In the final calculations the distribution of the wind load between the cable system and the deck must be based on a three-dimensional non-linear analysis of the entire structure. In this analysis the wind load on cables and pylons should also be included.

In suspension bridges with a small width-to-span ratio of the deck the reduction of the wind-induced bending moments in the deck might be of a very decisive magnitude. This is illustrated in Figure 3.177 showing the moment diagrams for decks with a total width of 17 m and main span lengths of 600 m, 900 m, and 1200 m (from [80.1]).



**Figure 3.177** Moments due to lateral wind load on a suspension bridge with a 17 m wide, streamlined deck and main span lengths 600, 900, and 1200 m

It appears that the reduction of the bending moments becomes more and more pronounced as the span increases (the width-to-span ratio decreases). Thus, for the 600 m span, the maximum moment from lateral wind load is reduced by approximately 40% when including the effect of the cable system, whereas an 85% reduction is found for the 1200 m span. Note that the maximum bending moment in the deck is almost independent of the span due to the increased efficiency of the support offered by the cable system in case of longer spans. Note also that the maximum bending moment only occurs at midspan in the 600 m case, whereas the maximum moment is found closer to the pylons in the 900 m and the 1200 m cases.

For the design of the deck it is a favourable effect that a part of the wind load is carried by the cable system. On the other hand, it must be remembered that the wind load from the main span carried by the cable system will be transferred to the pylon top from where it has to be carried to the pylon foundations.

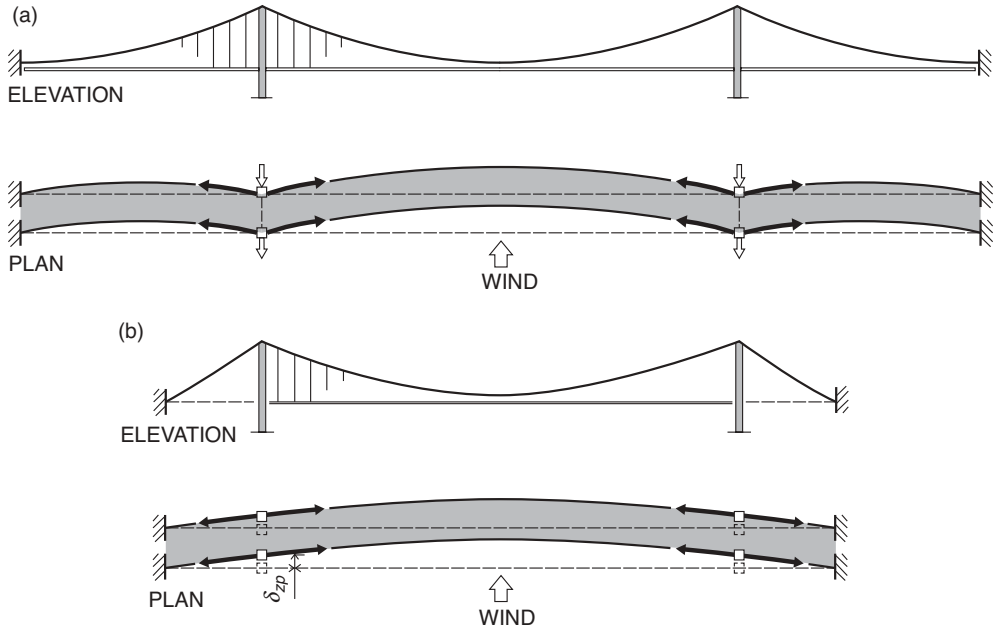
For bridges with long side spans and laterally rigid pylons, the forces from wind load will be transferred to the substructure primarily by the pylon acting as a vertical beam-column. This situation is illustrated in Figure 3.178 (a) where the lateral force at the pylon top is caused by the sidesway of the main span and side span cable.

As another extreme, a bridge with short side spans and laterally flexible pylons will have the wind load from the main span cable transferred primarily by the side span cables being activated by a lateral deflection  $\delta_{zp}$  of the pylon tops, as indicated for a system with straight main cables (backstays) in the side spans as shown in Figure 3.178 (b).

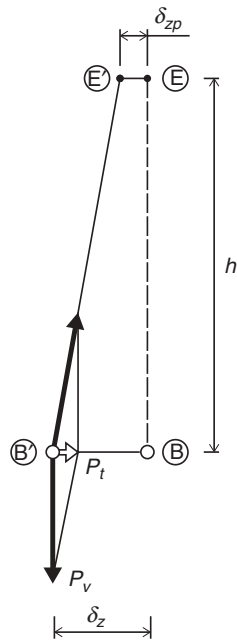
If the lateral deflection  $\delta_{zp}$  of the pylon top is of such a magnitude that it cannot be ignored, (3.109) must be replaced by (refer to Figure 3.179).

$$P_t = \frac{\delta_z - \delta_{zp}}{h} P_v \tag{3.118}$$

It appears that the lateral deflection  $\delta_z$  must be increased by  $\delta_{zp}$  to achieve the same transverse force  $P_t$  and this reduces the efficiency of the lateral support by the cable system.



**Figure 3.178** Equilibrium of lateral forces at the pylon tops: (a) long side spans and laterally rigid pylons; (b) short side spans and laterally flexible pylons



**Figure 3.179** Transversal load  $P_t$  resulting from translation and rotation of an initially vertical cable plane

### 3.8 Spatial Cable Systems

A solution to the problems associated with lateral wind load on cable supported bridges with long and slender spans might be to modify the cable system so that it can resist not only vertical, but also lateral loads, e.g. based on the principle outlined in Figure 3.174.

Spatial cable systems have already in several cases been applied in pipeline bridges where the 'one-dimensional' pipe basically has no lateral strength or stiffness.

Two systems have mainly been used:

- (1) A system where the vertical cable plane is supplemented by two horizontal cable planes on either side.
- (2) A system, with two transversally inclined cable planes.

The two systems are illustrated by the pipeline bridges in Figure 3.180 and Figure 3.181.

Both bridges have cable systems of the suspension type and the Czech bridge in Figure 3.180 has a multi-strand main cable in a vertical plane and two downwards leaning cable planes to give lateral support to the pipe. The downwards leaning suspension systems not only ensure lateral stability but also allow the whole system to be pre-stressed and thereby also stabilize against vertical displacements of the pipe.

The pipeline bridge in Figure 3.181 crosses the Danube at Barbara near Vienna. In this bridge with a main span of 320 m the two suspension type cable planes are transversally inclined to give the very narrow bridge deck (width 1 m) sufficient lateral support.

In bridges with a two-dimensional deck, as found in road or railway bridges, four cable planes are required to give vertical, lateral and torsional support. Therefore, the corresponding arrangement of cable planes will be as shown in Figure 3.182.

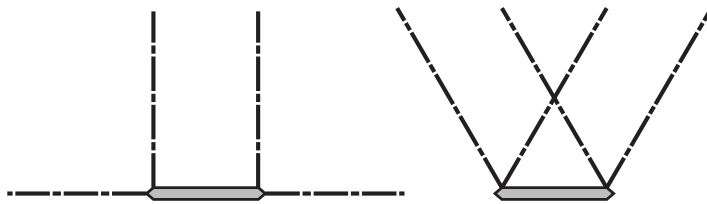
For long span suspension bridges, both arrangements of cable planes will give rise to problems in relation to construction and to some extent also to transmission of dead load.



**Figure 3.180** Pipeline bridge across the Labe River in the Czech Republic



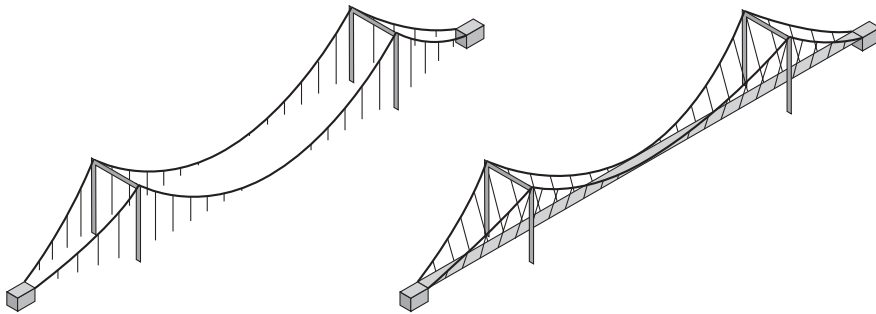
**Figure 3.181** Pipeline bridge across the Danube River at Barbara



**Figure 3.182** Arrangement of four cable planes to give both vertical and lateral support to the deck

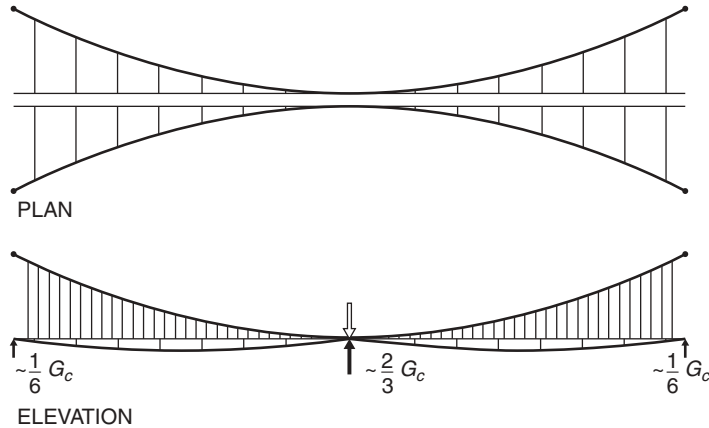
The problems associated with the construction process are related to the fact that the present erection methods for suspension bridge main cables require that the cable planes are vertical during the period when wires or strands are added one by one to build up the entire cable cross section. Therefore, after completion of the main cables it will be necessary to turn the cable planes into an inclined or horizontal cable plane and that will decisively complicate the saddle arrangement (Figure 3.183).

For the system with main cables in a horizontal plane, a vertical force corresponding to approximately  $2/3$  of the total weight of the horizontal cable planes will be required at midspan to keep the cable plane in place (Figure 3.184). So the



**Figure 3.183** Position of main cables during construction (left) and in the final stage (right) for a suspension bridge with inclined cable planes





**Figure 3.184** Vertical forces induced due to the dead load of horizontal suspension cables

vertical cable systems will be subjected to an additional force of considerable magnitude at midspan, i.e. at the most unfavourable position.

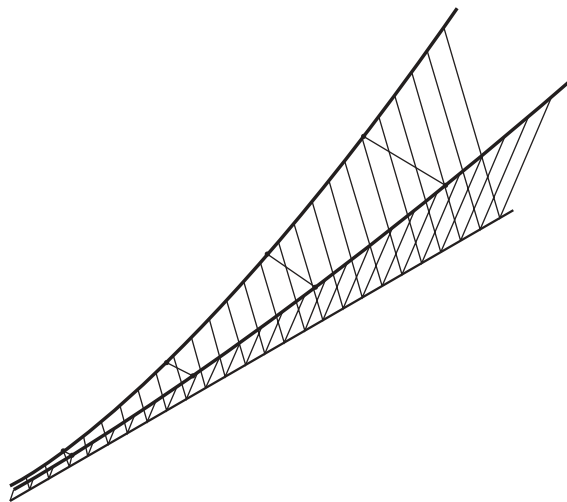
A horizontal suspension cable will also, as indicated in Figure 3.184, be characterized by a vertical, out-of-plane sag of the main cable and this will give a stiffness reducing the sag effect similar to the one known from long cable stays.

With two cable planes inclined in opposite directions, the out-of-plane sags due to the cable dead load can be eliminated by adding a number of light transverse ties as illustrated in Figure 3.185.

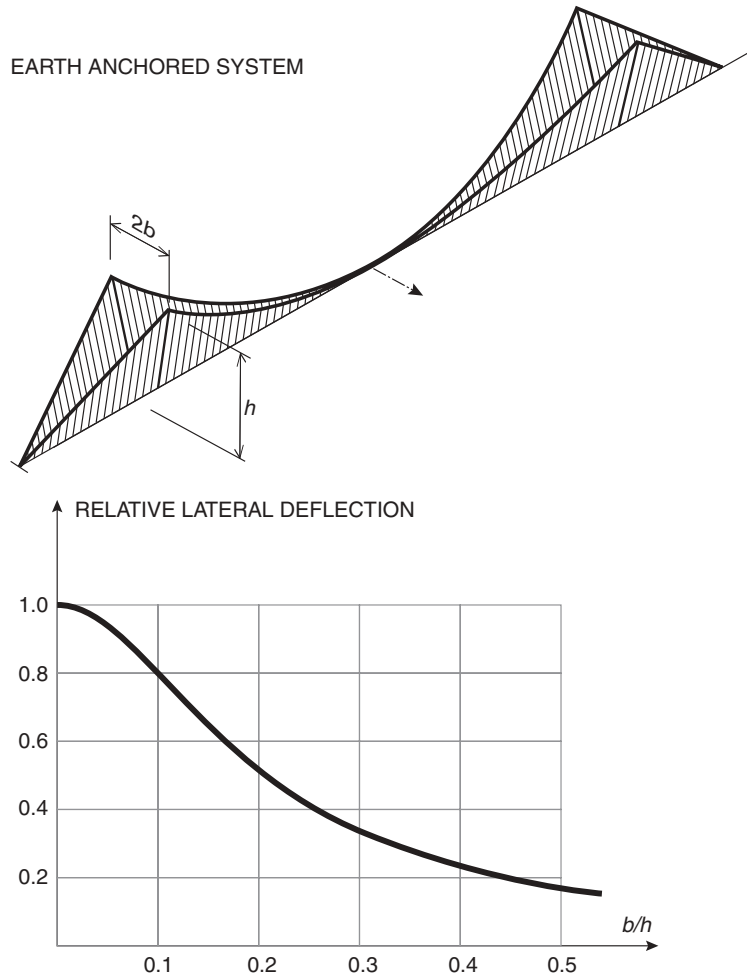
In earth anchored suspension bridges, inclined cable planes can substantially increase the lateral stiffness, as it is indicated in Figure 3.186. It is seen that for a  $b/h$  ratio of 0.4 the sideways will be reduced to one quarter of the value found for a vertical cable plane ( $b/h = 0$ ) where the lateral restraint is due to the pendulum effect alone.

The complications during construction of suspension bridges with inclined cable planes will not apply to the same extent in cable stayed bridges. Here the erection of each stay will be largely independent of whether the total set of cables is in a vertical or an inclined cable plane.

For self anchored cable stayed bridges with vertical cable planes, the maximum achievable span length will be governed by the lateral slenderness of the cantilever arm reaching from the pylons towards midspan during erection. In a number of cases special measures have been necessary to ensure stability during cantilevering, e.g. for the Karnali River Bridge and



**Figure 3.185** Transverse secondary cables to reduce out-of-plane sag due to dead load of main cables



**Figure 3.186** Lateral deflection of a suspension system with inclined cable planes

the Normandy Bridge. However, for these bridges the temporary measures have been relatively simple, and adequate stability in the completed state has been achieved by well-known structural means.

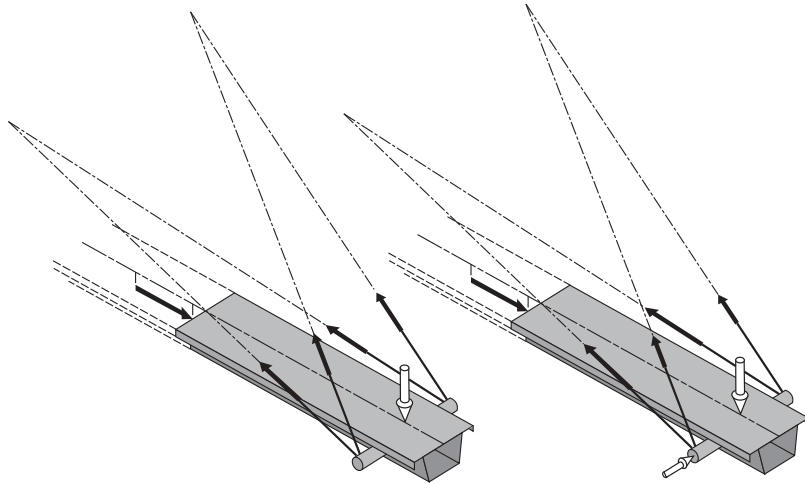
With increased spans and/or a more pronounced lateral slenderness, it might be more problematic to achieve stability both during construction and in the completed state with a traditional cable system that render only vertical and torsional support in these bridges. In such cases a spatial cable system could be the right structural solution.

With a spatial cable stayed system, the transfer of lateral loads (drag on the deck) will take place by an additional tension in the windward stays and a release of the tension in the leeward stays, as illustrated in Figure 3.187.

With spatial cable systems, stayed bridges could be characterized by an exciting appearance as it is illustrated by the model shown in Figure 3.188. In this model the width of the bridge deck is only  $1/120$  of the main span length. This corresponds to a lateral slenderness of one third of that found in the existing cable stayed bridges with the most extreme width-to-span ratios. The four inclined cable planes will have to be attached in pairs to the tips of cantilevered cross beams so that the inward-leaning cables can pass above the clearance diagram of the traffic lanes.

In a spatial cable system with four cable planes the number of individual stays will be twice as large as in the traditional system with two cable planes if all cable planes have stays attached at each anchor point at the deck (Figure 3.189 (a)).

It is, however, possible to distribute the stays from the different cable planes in such a way that the total number remains the same as in the plane system with two cable planes. In the system shown in Figure 3.189 (b), the outward leaning stays are attached at every second anchor point and the inward leaning stays at the intermediate anchor points.

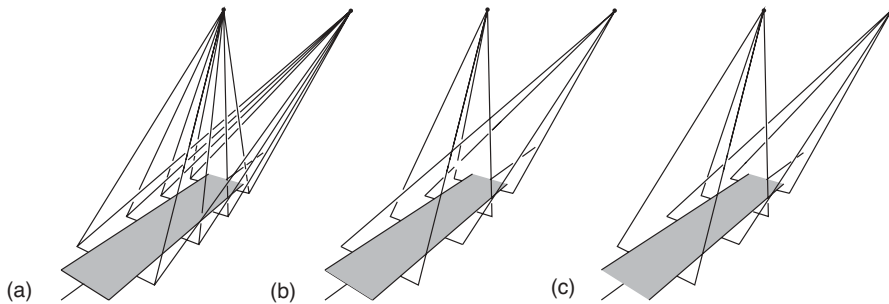


**Figure 3.187** Spatial system with vertical load (left) and vertical + lateral load (right)

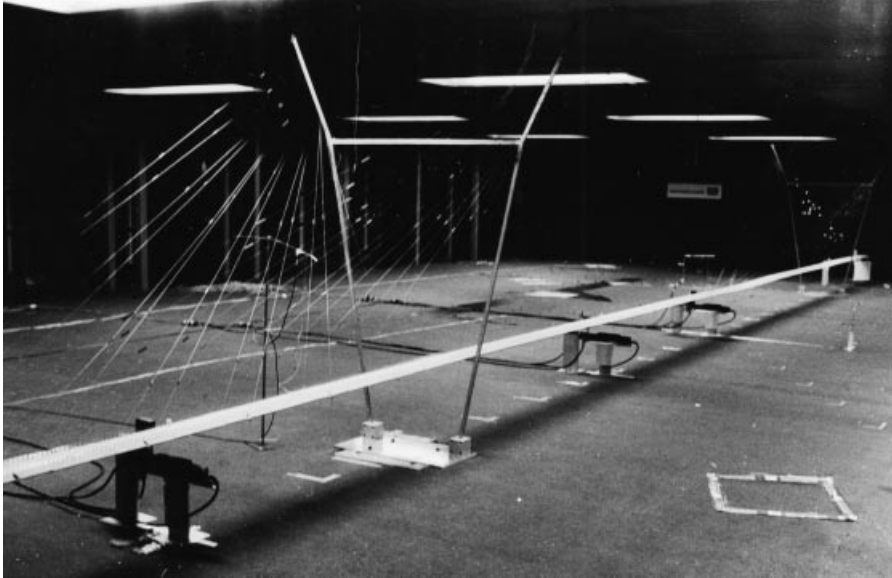


**Figure 3.188** Model of a cable stayed bridge with a spatial cable system

With this arrangement the cable support at each anchor point is symmetrical about a vertical plane through the bridge axis for loads acting vertically and centrally (e.g. dead load). Therefore, for dead and traffic load the deck will be just as efficiently supported as with the traditional vertical cable planes with the same number of stays in two cable planes.



**Figure 3.189** Arrangement of stays in a spatial cable system



**Figure 3.190** Model of a bridge with a spatial cable system in the large wind tunnel at the Danish Maritime Institute

In the system of Figure 3.189 (c) both stays at each anchor point at deck level are connected to one pylon top whereas the neighbouring anchor points have cables connected to the other pylon top. This eliminates the problems related to the intersecting stays of the inward leaning cable planes, but at the same time the transmission of vertical loads will induce lateral bending in the deck. This bending is, however, of a local nature as the lateral force components will change direction from one anchor point to the next. So with realistic ratios between the deck width and the anchor point distance, the stresses originating from the local bending will be small and manageable.

The arrangement shown in Figure 3.189 (c) might be problematic during erection as the tensioning of stays will induce lateral deflections at the tip of the deck each time a new anchor point is reached – in contrast to the arrangement of Figure 3.184 (b) where the tensioning of each set of stays will result in only an axial and a vertical force component.

The properties of the spatial cable system were studied in the mid-1990s in a research project at the Technical University of Denmark and at the Danish Maritime Institute [94.18]. As part of this project, full model wind tunnel tests of 13 m long models were performed (Figure 3.190).

In the full model tests three different bridge types were compared: a conventional three span earth anchored suspension bridge, a self anchored cable stayed bridge with vertical cable planes, and a self anchored cable stayed bridge with four inclined cable planes. All models were built to a scale of 1:100 of a prototype bridge with a main span length of 800 m and a roadway width of 8 m, i.e. with an extreme span-to-width ratio of 1/100.

The tests clearly demonstrated the advantages to be gained by using a spatial cable system, and as an example Figure 3.191 shows the dynamic torsional response at midspan in terms of RMS-values (root-mean-square values) of the suspension bridge and of the spatial cable stayed bridge. It is seen that for torsion the dynamic response is reduced to less than half and similar results were found for the lateral and vertical response (although the reduction of the RMS values for these responses were somewhat smaller – corresponding to a reduction to typically 2/3).

The models of the cable stayed bridges were used to study both the behaviour of the completed bridge and the behaviour of the bridge in the critical erection stage when the girder is cantilevered from the pylon to midspan.

In the erection stage tests the efficiency of the lateral support offered by the spatial cable system was clearly demonstrated, as can be seen from the plots in Figure 3.192. Already for a prototype wind speed of 30 m/s the lateral deflection of the cable stayed bridge with vertical cable planes will exceed 10 m, whereas the spatial bridge with a similar streamlined deck ('spatial 1') will deflect approximately 0.8 m. Even for a bridge with a bluff rectangular box girder deck ('spatial 2') the sidesway at 30 m/s is limited to approximately 1.2 m in the case of a spatial cable system.

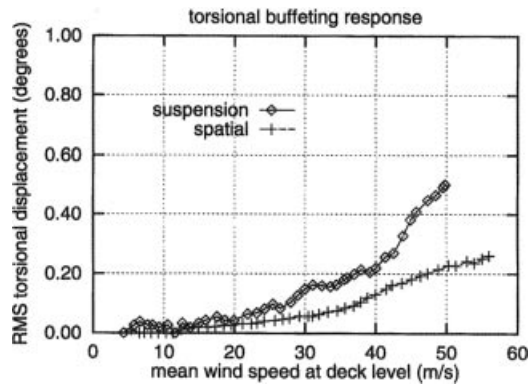


Figure 3.191 Torsional RMS-response at midspan for a suspension system and a spatial cable stayed system

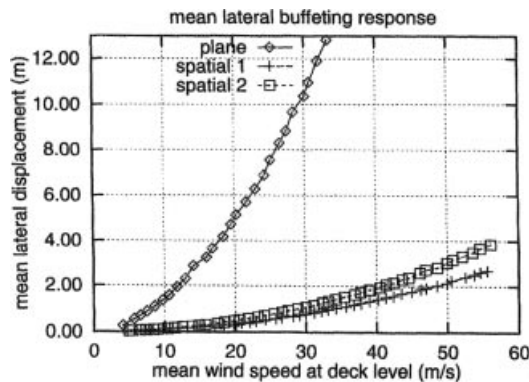


Figure 3.192 Static lateral deflections at midspan in the erection stage for cable stayed bridges with plane and spatial systems

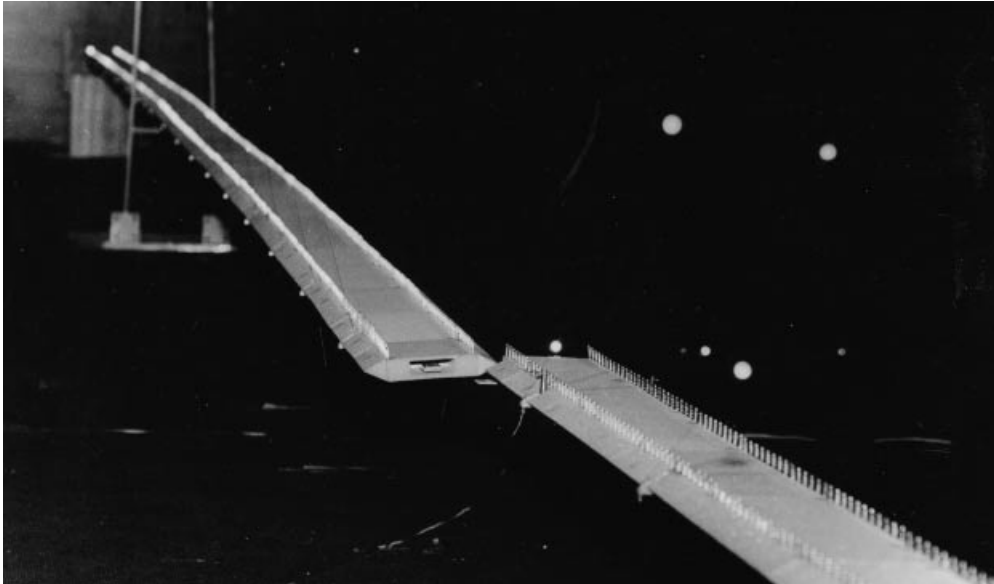
To illustrate very clearly the efficiency of the lateral support offered by the spatial cable system in the erection stage, a special demonstration test was performed by erecting two half models, one with a vertical plane cable system and the other with a spatial cable system. In this test it was seen that when the plane cable system exhibited a sidesway of the tip of the cantilever arm corresponding to the width of the bridge deck then the sidesway of the cable stayed bridge with a spatial cable system was still so small that it could not be detected by the naked eye – as is illustrated in Figure 3.193.

## 3.9 Oscillation of Cable Systems

### 3.9.1 Global oscillations

Global oscillations comprising the entire cable system as well as the deck and the pylons might occur in any type of cable supported bridge. The oscillations are excited primarily by forces acting on the deck, such as forces from wind, moving traffic or earthquake.

The analysis leading to the different modes of oscillation with their corresponding frequencies and displacement forms will today always be performed by a computer program. As only oscillations with relatively small amplitudes are of interest the analysis can be based on a linearization of the force–displacement relation corresponding to the tangent stiffness derived from the dead load condition. For self anchored cable stayed bridges this simply leads to the application of the tangent modulus of elasticity for the stay cables, whereas all other elements of the structure are considered to be linear elastic. For earth anchored systems the geometric non-linearity must be further taken into account when determining the tangent stiffness.



**Figure 3.193** Demonstration test to show the efficiency of a spatial cable system (in the foreground) compared to a plane cable system (in the background)

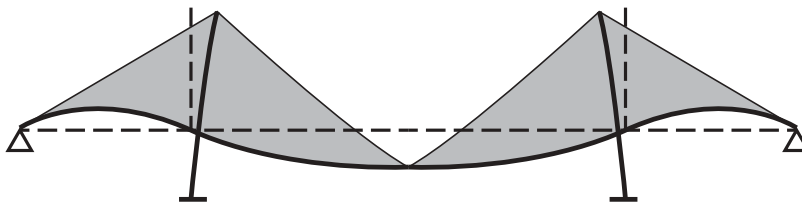
For the common three-span bridge with a symmetrical layout the modes of vibration will be either symmetric or antisymmetric. Whether the first mode, i.e. the mode with the lowest frequency, will be symmetric or antisymmetric depends on the general layout of the cable system (type, side-to-main span ratio, supporting conditions, etc.), as was illustrated in Figures 2.106 and 2.107 for a three-span suspension cable.

In most cases the first symmetric mode will be characterized by having the main span and the side spans oscillating vertically out of phase and the pylons oscillating horizontally, as illustrated by the displacement form in Figure 3.194.

For the main span the first symmetric mode might show different displacement forms, as shown in Figure 3.195. The forms are typically found for the following structures:

- (a) suspension bridge with long side spans;
- (b) suspension bridge with short side spans;
- (c) cable stayed bridge with fan-shaped cable system;
- (d) cable stayed bridge with harp-shaped cable system and supported side spans;
- (e) cable stayed bridge with harp-shaped cable system, unsupported side spans, and slender pylons and girder.

Note how the modes (a), (c), (d), and (e) reflect the basic static deformations of the corresponding systems, as illustrated in Figures 3.85 and 3.109.



**Figure 3.194** Typical displacement form of the first symmetric mode

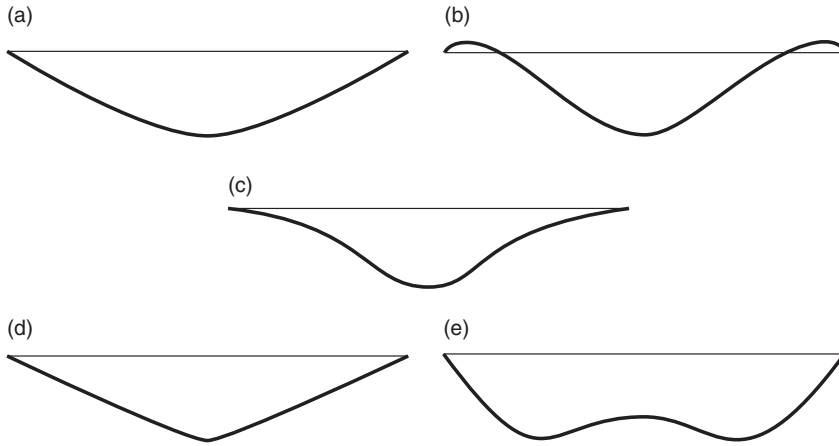


Figure 3.195 Displacement forms of the first symmetric mode in the main span

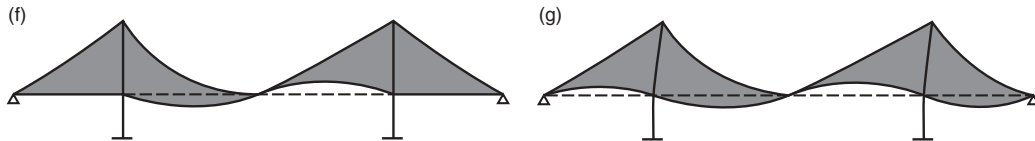


Figure 3.196 Typical displacement forms of the first asymmetric modes

The first antisymmetric mode might be characterized by having the motion confined to the main span, Figure 3.196(f), or by having the side span and the adjoining half of the main span oscillating out of the phase, Figure 3.196(g). Generally, the mode shown under (f) will be found in suspension bridges with short side spans and simple supports of the deck at the pylons, whereas mode (g) will develop in systems with long side spans and continuous deck.

In the very common case where the bridge comprises two cable planes attached to the deck at the edges of the bridge deck, the spatial modes are strongly influenced by the phase of the two cable system's oscillation. Thus, if the two cable systems oscillate in phase, a pure translation (vertical displacement) of the dominating mass in the deck will take place, whereas a pure rotation will result in the case where the two cable systems oscillate out of phase.

For the attainment of aerodynamic stability it has proved important to separate the frequencies of the corresponding vertical and torsional modes. This is due to the fact that the critical oscillation in many cases is a coupled vertical and torsional oscillation occurring when the frequencies-of the two basic modes coincide. As the aerodynamic forces tend to reduce the frequency of the torsional mode the two modes might coincide for small and realistic wind speeds if the difference between the natural frequencies of the vertical and the torsional mode is small.

If the deck and the pylons are without any flexural or torsional stiffness and all masses are concentrated in the cable planes, then the frequencies of the vertical mode and of the torsional mode will be exactly the same.

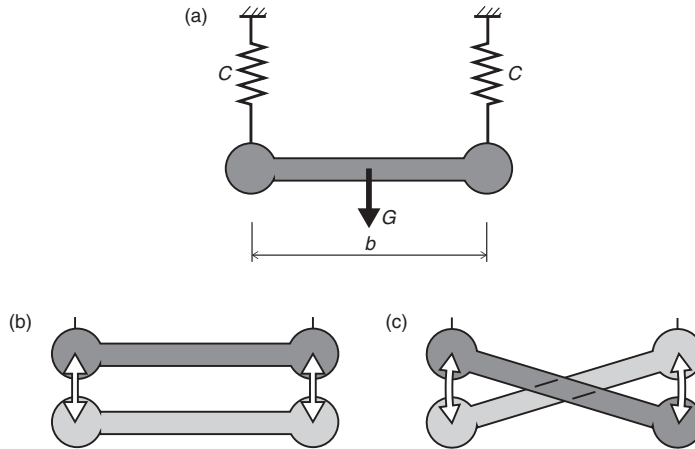
This feature might be illustrated by the simple model of Figure 3.197(a) showing a symmetric mass  $G/g_a$  supported by two springs each with a spring constant  $C$ . For the vertical oscillation (b) the frequency  $n_v$  is determined by:

$$n_v = \sqrt{2 \frac{Cg_a}{G}} \tag{3.119}$$

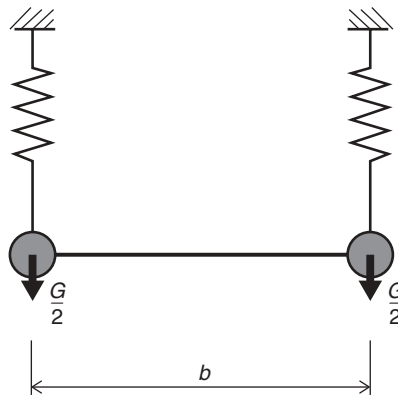
whereas the frequency  $n_t$  of the torsional oscillation (c) becomes:

$$n_t = \sqrt{\frac{C_t}{I_m}} \tag{3.120}$$

where  $C_t = \frac{1}{2}Cb^2$  and  $I_m$  the mass moment of inertia.



**Figure 3.197** Vertical and torsional oscillation of a dynamic model comprising a symmetric mass supported by two springs



**Figure 3.198** Dynamic model with two masses concentrated at the supporting springs

With the mass concentrated in the cable planes, as shown in Figure 3.198, the mass moment of inertia becomes  $I_m = Gb^2/4g_a$ . This leads to a frequency of the torsional mode equal to:

$$n_t = \sqrt{\frac{6Cg_a}{G}}$$

i.e. the same value as for the vertical mode.

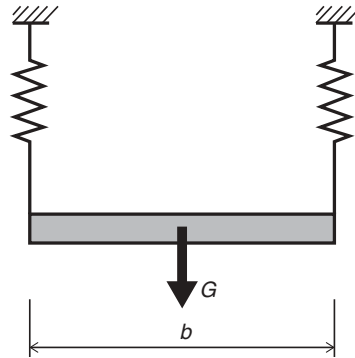
With the mass distributed across the width  $b$ , as indicated in Figure 3.199, the mass moment of inertia becomes  $I_m = Gb^2/12g_a$  and the frequency of the torsional mode:

$$n_t = \sqrt{\frac{6Cg_a}{G}}$$

Thus, in this case the ratio between the torsional and the vertical frequency will be  $n_t/n_v = \sqrt{3}$ .

In real structures the mass distribution will be somewhere between the extremes of Figure 3.198 and Figure 3.199. Thus, the dead load of the cable system and of the main girders or main trusses directly below the cable planes will have its mass distributed according to Figure 3.197, whereas the bridge floor, the cross beams, and the lateral bracing will have a mass distribution according to Figure 3.199. The fact that the mass of the cables has a disadvantageous influence on the frequency ratio will present a serious problem for suspension bridges with very long spans as the mass of the main cables will be more and more dominating as spans grow.





**Figure 3.199** Dynamic model with a symmetric mass uniformly distributed between the two supporting springs

Ignoring the flexural and torsional stiffness of the deck and the pylons should therefore lead to a ratio between the torsional and the vertical frequencies in the interval from 1 to  $\sqrt{3}$ .

Among real structures an assumption of insignificant flexural and torsional stiffness has been best fulfilled by the first antisymmetric mode of the George Washington Bridge in the initial stage with only the upper deck erected. In the antisymmetric mode the motion was concentrated to the main span (refer to Figure 3.196(f)) and, consequently, the pylons with their considerable flexural and torsional stiffness remained immovable during this mode of oscillation.

For the George Washington Bridge in its initial stage the ratio  $n_t/n_v$  was 1.22, i.e. a value within the expected interval.

When taking into account the flexural and torsional stiffness of the deck and the pylons, the natural frequencies will generally increase, but as a general trend the torsional stiffness will have more effect on the torsional frequency than the flexural stiffness will have on the vertical frequency.

For the deck the flexural stiffness will have an insignificant influence on the frequencies if the ratio between the girder depth and node distance (= length of half wave = span of oscillating girder segment) is smaller than approximately 1/50. Thus, for conventional suspension bridges with stiffening trusses having a depth corresponding to 1/100 of the main span length or for the early cable stayed bridges with depth-to-span ratios of 1/60–1/80, the flexural stiffness would influence both the first symmetric mode (due to the restraining effect of the girder on the side span motion) and the first antisymmetric mode with a midspan node.

For the modern cable supported bridges with depth-to-span ratios of 1/200–1/300 the flexural stiffness of the deck will have a small influence on both the first symmetric and the first antisymmetric modes.

For the slender, vertical pylons generally found in three-span cable supported bridges, a very small restraint exists against longitudinal movements of the cable system at the pylon top. This is largely due to the influence of the axial compression in the pylon legs, as will be explained later in more detail (refer to Figures 5.15 and 5.16).

In contrast to the small influence of the flexural stiffness, the torsional stiffness of the deck and the pylons will have a much more pronounced effect. This is mainly due to the fact that, for a given cross section, the flexural restraint is reduced with the third power of the length, whereas the torsional restraint is inversely proportional to the length.

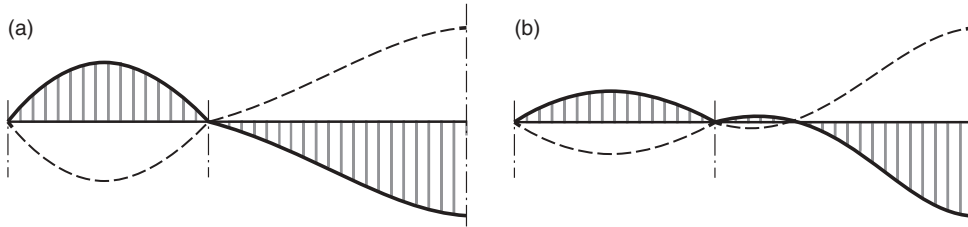
For the George Washington Bridge, initially built without any noticeable flexural or torsional stiffness of the deck, the addition in the 1960s of the lower level introduced a genuine stiffening truss with a depth of 9.12 m and a width of 32.3 m.

Despite the truss depth of more than 9 m the additional flexural stiffness did not increase the frequency of the first antisymmetric vertical mode  $n_v = 0.111$ , whereas the frequency of the first antisymmetric torsional mode was increased from  $n_t = 0.136$  to  $n_t = 0.210$ , i.e. an increase of more than 60%. This resulted in a change of the  $n_t/n_v$  ratio from 1.22 to 1.97.

The torsional stiffness of the pylon legs will generally have a strong influence on all torsional modes associated with longitudinal movements of the pylon tops. Thus, this effect is very pronounced for the first symmetric torsional mode.

This feature is illustrated in Figure 3.200 showing the displacement forms of the first symmetric torsional mode in a case with no torsional stiffness of the pylon legs (a) and in a case with a realistic torsional stiffness of the pylon legs (b) (from [50.1]). Note that the displacement form of the main span changes from having no nodes to having two internal nodes, when taking the torsional stiffness into account. This is a clear indication of the much increased constraining effect of the pylons, which is also illustrated by the change of the frequency from  $n_t = 0.172$  (a) to  $n_t = 0.247$  (b).

For bridges with short side spans, the first antisymmetric mode is characterized by very small or no displacement of the pylon tops and the effect is consequently small of the torsional stiffness of the pylon legs.



**Figure 3.200** Displacement forms of the first symmetric torsional mode of a three-span suspension bridge with no torsional stiffness of the pylon legs (a), and with a realistic torsional stiffness of these elements (b)

For suspension bridges with short side spans the first antisymmetric mode is much more influenced by the type of connection at midspan between the main cables and the deck and by the supporting conditions of the deck. This is due to the fact that the main cable under antisymmetric oscillations will show a tendency to move longitudinally, so that a constraint at midspan strongly influences the mode of vibration.

In Figure 3.201 three different arrangements of the structural system in the main span are shown. Under (a) is shown a system with hangers connecting the deck and the main cable throughout the main span. With this system the cable is free – at least for smaller displacements – to move longitudinally in relation to the deck.

System (b) is characterized by a central clamp connecting the main cable to the deck and by simple, longitudinal movable supports at the ends of the girder. Finally, System (c) has the same central clamp, but here the deck is longitudinally fixed.

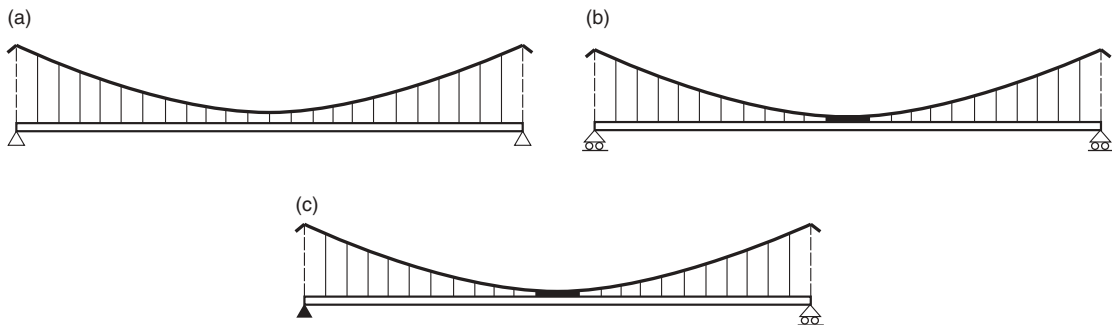
With System (c) both the vertical and torsional antisymmetric modes are greatly influenced by the central clamp as the longitudinal movements of the main cable at midspan will be significantly reduced.

System (b) is characterized by a certain difference between the effect of the clamp on the vertical and the torsional antisymmetric modes. This is due to the fact that in the vertical mode the main cable might move longitudinally at midspan provided the deck with its two movable bearings is moving simultaneously. For the antisymmetric torsional mode the central clamp is bound to remain immovable, as the two cable systems show an opposite tendency to move the deck longitudinally. Thus, for the first antisymmetric, torsional mode no difference will exist between Systems (b) and (c).

This effect was clearly illustrated by the observed oscillations of the first Tacoma Bridge. In this bridge the main span girder had movable bearings at both pylons (as in System (b)), but by the installation of central ties a connection capable of transmitting longitudinal forces between the main cable and the deck was established. Throughout the period where the central ties (giving the same effect as central clamps) were active, only non-catastrophic vertical oscillations were observed, but after a failure of the cables forming the central ties the oscillation changed to the catastrophic torsional mode.

System (b) of Figure 3.201 was applied in the Lillebælt Bridge, as illustrated in Figure 3.202 showing the midspan connection between the main cable and the deck. It is seen that the cable clamp in this case is connected to the girder by a bracing system with a high degree of strength and stiffness.

For suspension bridges the overall form of the most critical modes of oscillation can be determined qualitatively by assuming inextensibility of the main cables. Thus in the first symmetric mode the side spans will be displaced upwards and the pylon tops inwards when the main span is displaced downwards. In a first antisymmetric mode confined to the main



**Figure 3.201** Structural systems for the main span of a suspension bridge



**Figure 3.202** Bracing system between the central clamp and the deck of the Lillebælt Bridge

span, a downwards displacement of the left half is coupled with an upwards displacement of the right half. Consequently, the increased curve length of the main cable from the left pylon to midspan is counteracted by an equal reduction of the curve length from midspan to the right pylon, so that the total curve length remains unaltered.

In reality, some strains will occur in the main cables during the oscillation, but the fact that the modes follow the forms given by assuming inextensibility implies that the modes of oscillation are physically very well defined.

For cable stayed bridges with cable systems that are stable of the first order an assumption of inextensibility will exclude the formation of any global oscillation. Thus, these bridges can only oscillate if the lengths of the individual cables vary. This introduces a change of sag in all stay cables so that the global oscillation will be coupled with a local oscillation of the single cables. However, the fact that the natural frequencies of the single cables generally do not coincide with the natural frequency of the global oscillation makes the mode of oscillation physically very complex. This applies especially to cable stayed bridges with a multi-cable system in which a large number of local oscillations will interact with the global oscillation.

For this reason the oscillation of the multi-cable fan system seems to be characterized by a much more pronounced system damping than found within suspension bridges. Thus, during tests of a dynamic model of the Zarate-Brazo Largo Bridges [79.2] the following observations were made:

- (1) Subjected to pulsating forces the multi-cable fan system would only oscillate with amplitudes of modest magnitude (the maximum amplitudes that were measured corresponded to only 50 mm in the real structure having a 330 m long main spar).
- (2) After discontinuation of the pulsating forces the oscillations were quickly damped. Thus, the average of the measured logarithmic decrements was as high as 0.15.

Consequently, the experiences gained so far seem to indicate that systems with a complex mode of vibration involving interaction between global and local oscillations have more favourable damping characteristics than found in systems with well-defined modes of vibration.

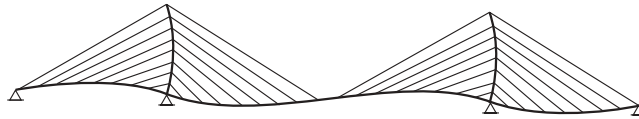
In this connection it should be emphasized that cable stayed bridges with unstable cable systems might have equally well-defined modes of vibration as found in suspension bridges. This is illustrated in Figure 3.203 showing the displacement form of an asymmetric oscillation of a bridge with a multi-cable harp system. As this displacement form is possible under the assumption of inextensibility of the individual stay cables, the mode of vibration is well defined and can develop without interaction between global and local oscillations.

In some cable supported bridges global oscillations might occur without activating the cable system. This is illustrated by the example in Figure 3.204 showing a symmetric mode of a three-span bridge with only one stay cable set from each pylon, and by the example in Figure 3.205 showing a torsional mode of a bridge with only one central cable plane.

The global oscillations described so far have all been characterized by displacements in the cable planes, but lateral oscillations with displacements perpendicular to the cable planes might also occur. Such oscillations might be decisive for bridges with small width-to-span ratios, and for these the lowest of all the natural frequencies might be associated with the first lateral mode.

For an earth anchored suspension bridge the four first transverse modes might have displacement forms as shown in Figure 3.206 (from [80.1]). Note that the first and second modes are characterized by having the deck and the main cables oscillating in phase, whereas the third and fourth modes have the cables oscillating out of phase with the deck.

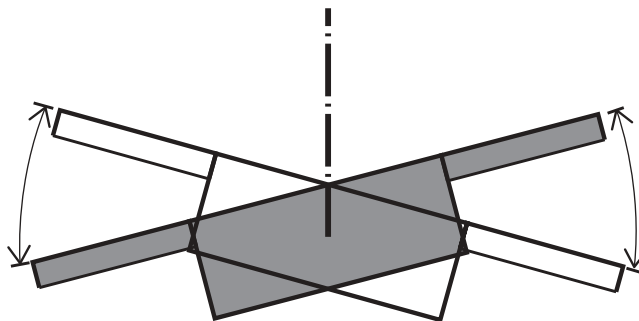
Generally, the transverse oscillations are characterized by a large difference between the natural frequencies of the first and the second modes. Thus, for the system of Figure 3.206, the frequency of the second mode is more than three times as large as the frequency of the first mode. This is in contrast to the vertical oscillation where the frequencies of the first and the second modes in many cases differ by less than 50%.



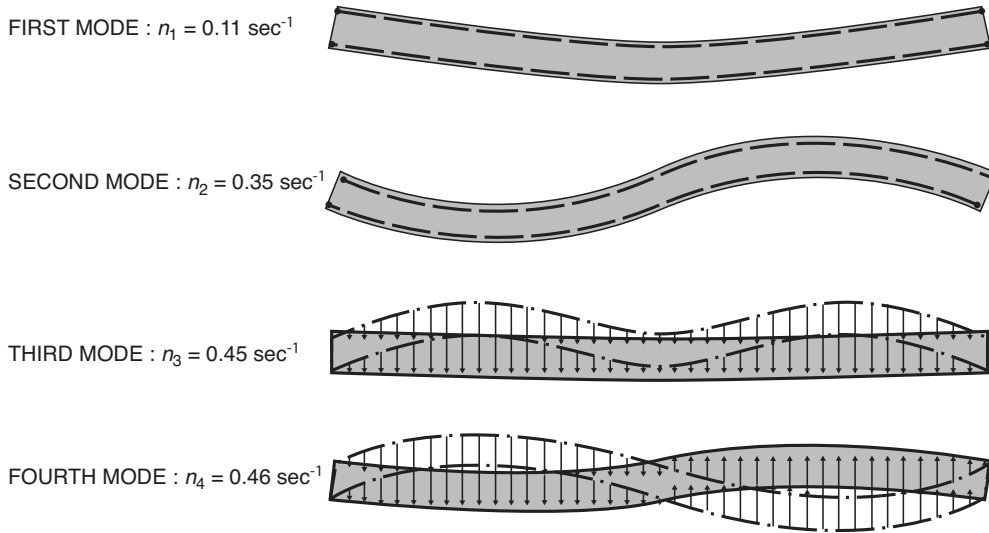
**Figure 3.203** Displacement form of an asymmetric oscillation of a bridge with a multi-cable harp system



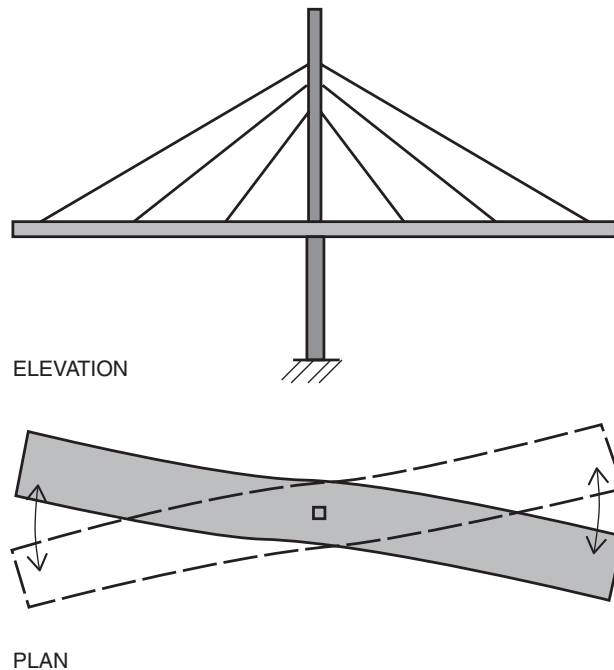
**Figure 3.204** Stiffening girder oscillating independently of the cable system in a bridge with only one set of stays from each pylon



**Figure 3.205** Torsional oscillation of the deck in a system with a central cable plane



**Figure 3.206** First four modes of the transverse oscillations of a suspension bridge main span



**Figure 3.207** Transverse oscillation of a double cantilevered cable stayed bridge

Transverse modes are of interest for the analysis of suspension bridges under wind load and earthquakes. Furthermore, it might prove necessary to investigate transverse modes of cable stayed bridges, in particular during erection when long cantilevers are reaching out from the piers. For cable stayed bridges being erected by double-sided free-cantilevering, it is especially important to take into account the flexibility of the pier shafts being subjected to torsion under transverse oscillation of the deck (Figure 3.207).

# 4

## Deck (Stiffening Girder)

The deck is the structural element subjected to the major part of the external load on a cable supported bridge. This is because the total traffic load is applied directly to the deck, and in most cases both the dead load and the wind area are larger for the deck than for the cable system.

Immediately the deck must be able to transfer the load locally whereas it will receive strong decisive assistance from the cable system in the global transmission of the (vertical) load to the supporting points at the main piers.

This feature is illustrated in Figure 4.1, showing at the top a typical dead load moment diagram for a continuous three-span girder bridge, and at the bottom a possible dead load moment diagram for a three-span cable stayed bridge. It is seen that, even in the case of only four cable supported points in the main span (as illustrated in Figure 4.1), the dead load moments are substantially reduced.

For the traditional cable supported bridges with vertical cable planes, the support by the cable system is most efficient for the dead load, less efficient for the traffic load and least efficient (or even non-existent) for the horizontal loads.

### 4.1 Action of the Deck

#### 4.1.1 Axial stiffness

In the traditional suspension bridge with vertical hangers the load acting on the deck will be transferred to the parabolic main cable without inducing axial forces. This is in contrast to cable stayed bridges where the deck has to transfer the horizontal cable components by axial compression (or tension) – as explained in connection with Figure 3.12.

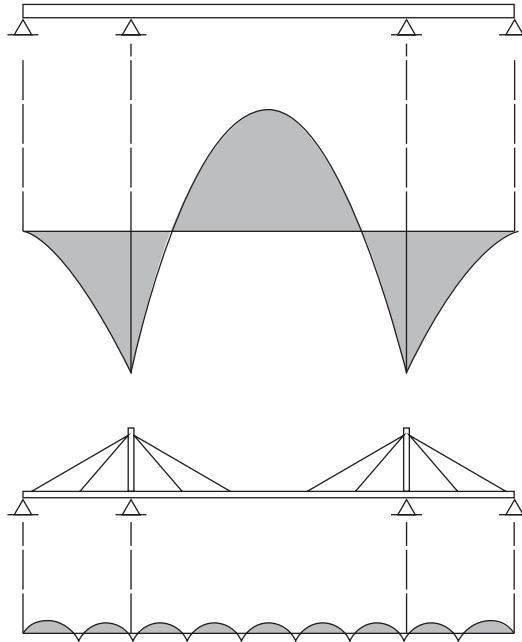
In a self anchored cable stayed bridge the axial compression in the deck will reach its maximum value at the pylon.

In a bridge with the deck made of concrete the axial compression can be beneficial as it reduces the tensile stresses from the bending moments due to the local transfer of the deck load to the cable anchor points. But in bridges with a steel deck the axial compression might make it necessary to add more stiffeners to the steel panels to avoid buckling.

#### 4.1.2 Flexural stiffness in the vertical direction

The participation of the deck in the transfer of vertical loads depends on the general arrangement of the total structural system. In principle, the action of the deck can be divided into:

- Action 1: to carry the load locally between cable anchor points.
- Action 2: to assist the cable system in carrying the load globally.
- Action 3: to distribute concentrated forces.



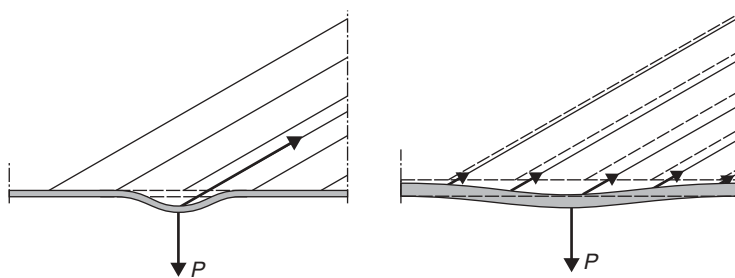
**Figure 4.1** Comparison between the dead load moments in a three-span continuous girder and in the girder of a cable stayed bridge

As the deck is subjected directly to the traffic load and its own weight, but only supported by the cable system at the cable anchor points, the deck must as a minimum be able to span between these points. Action 1 of the deck therefore corresponds to the action of stringers in a truss bridge where the load on the bridge floor has to be carried to the cross beams at the nodes of the main trusses.

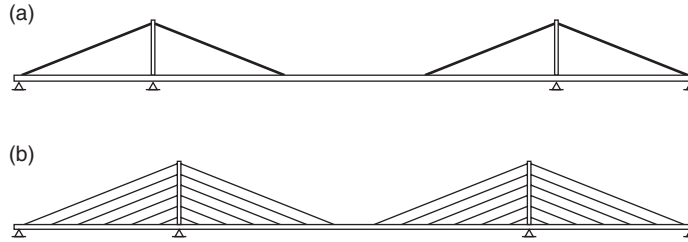
Action 2 of the deck is found in bridges with unstable systems, as has been described, e.g. for the harp system. Here the deck must be able to carry a part of the traffic load not only between adjacent cable anchor points but also between the main supports of the bridge.

The deck's ability to distribute concentrated forces (Action 3) will be utilized primarily in bridges with a large number of cable supported points as found in both the suspension bridges and cable stayed bridges at the multi-cable system.

Distributing a concentrated force between a number of cables, as indicated in Figure 4.2, will reduce the maximum design force in the cables and give a more even curvature of the bridge deck at the concentrated force.



**Figure 4.2** Distribution of a concentrated force by the deck



**Figure 4.3** Two structural systems for a three-span cable stayed bridge

The distribution of a concentrated force is also found in multi-cable systems with the end support displaced inwards from the top cable attachment, as illustrated in Figure 3.92. Here the concentrated force is the reaction from the end pier (acting downwards) and by the distribution it is obtained that a number of the adjacent stay cables are activated as anchor cables.

The way in which Actions 1–3 are utilized in an actual cable supported bridge depends on the chosen structural system. To illustrate this, Figure 4.3 shows two cable stayed bridges:

- (a) System with only one set of stay cables from each pylon
- (b) System with a multi-cable harp system.

In System (a), Action 1 of the deck becomes very important as the deck will have to carry the load to the cable anchor points over a distance corresponding to one-third of the main span length. Actions 2 and 3 will be of minor importance as the cable system is stable of the first order and as it will be inefficient to distribute concentrated forces longitudinally due to the long distance between the cable anchor points.

In System (b), Action 1 is of minor importance due to the short distance between cable supported points. On the other hand, Action 2 is essential as the cable system is unstable, and also Action 3 can be fully utilized to distribute concentrated traffic load (and end pier reaction) over several stay cables or hangers.

#### 4.1.3 Flexural stiffness in the transverse direction

The transmission of lateral forces from wind (or an earthquake) acting on the deck and on the cable system induces bending about a vertical axis. If the cable system is self anchored, the entire lateral load acting on the deck must be transferred by lateral bending, whereas an interaction between the deck and the cable system is found in earth anchored systems, as described in Section 3.7.

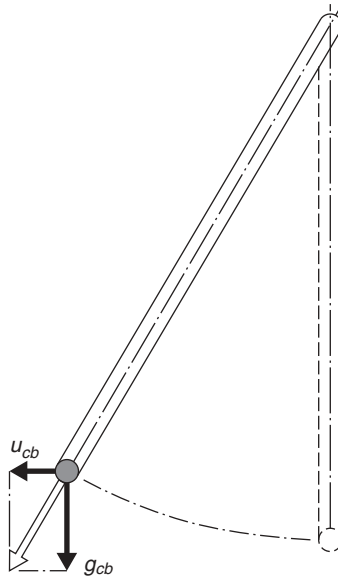
It should be noted that the wind load acting on the deck is due not only to the load on the deck itself but also to some of the load on the cable system. Under lateral wind load the stay cables will swing sideways to make the plane of the catenary coincide with the direction of the resultant force from the cable dead load  $g_{cb}$  and the wind load  $u_{cb}$ , as illustrated in Figure 4.4. Consequently, the wind load will be transferred to the cable anchor points in the same way as the dead load. Therefore, lateral forces equal to half the total wind force  $^{1/2}u_{cb,c}$  will be induced at the deck and the other half at the pylon (Figure 4.5).

For the transmission of lateral forces it will generally be advantageous to make the deck continuous, so that the total moment in the main span can be distributed between a positive moment at midspan and negative moments at the pylons.

This feature is illustrated in Figure 4.6 showing three structural systems for the deck under lateral load. In System (a) the deck is composed of three simply supported spans, and consequently the lateral load in the main span will induce positive moments throughout the span. In System (b) the deck has a hinged connection at the main span centre and the moments will therefore be negative throughout the main span. Finally, in System (c) the deck is continuous, so the moments in the main span vary from positive at midspan to negative at the pylons. As seen, this leads to a noticeable reduction of the maximum design moment in System (c) compared to Systems (a) and (b).

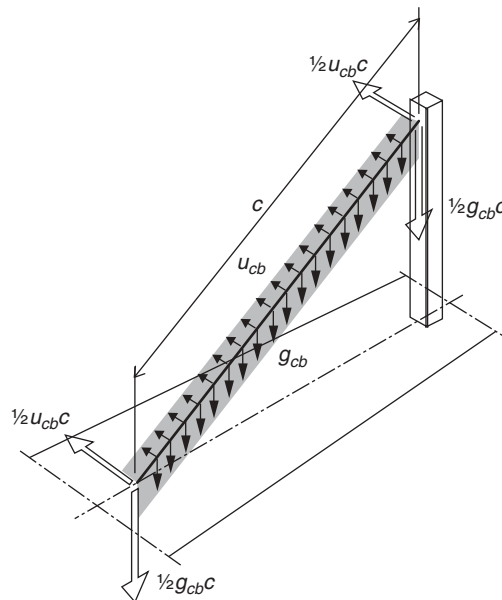
The moment diagrams of Figure 4.6 are those found in self anchored systems with vertical cable planes where the total lateral force is transferred by horizontal bending of the deck. In earth anchored systems, the interaction between the deck





**Figure 4.4** Side sway of stay cable subjected to its own weight  $g_{cb}$  and a wind pressure  $u_{cb}$

and the cable system (due to the pendulum effect) will be influenced by the supporting conditions of the deck. Increased flexibility of the deck in the transverse direction implies that a larger portion of the lateral load will be carried by the cable system. As change from simply supported spans to continuous spans significantly decreases the lateral deflection of the deck, the load carried by the cable system will be reduced.



**Figure 4.5** Vertical and horizontal (lateral) forces induced at the cable anchor points due to weight  $g_{cb}$  and wind pressure  $u_{cb}$

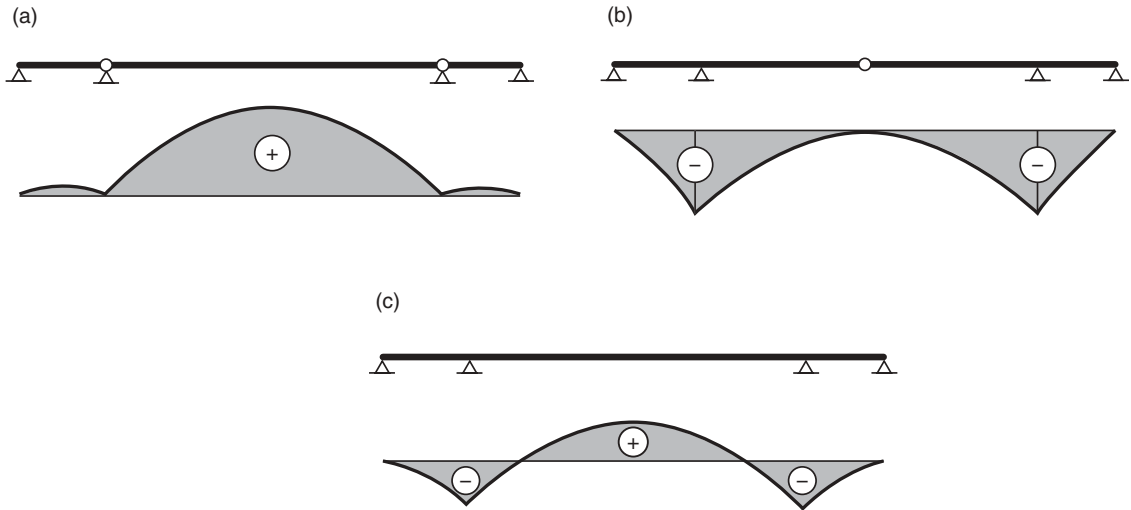


Figure 4.6 Three structural systems for the deck in the lateral direction

#### 4.1.4 Torsional stiffness

The torsional stiffness (and strength) required in the deck depend to a large degree on the amount of torsional support offered by the cable system. Thus, in a bridge with only one central cable plane, the stability of the total system under eccentric traffic load is totally dependent on the torsional stiffness of the deck. In bridges with two cable planes along the edges of the bridge floor, a torsional stiffness of the deck is not essential but it might lead to a favourable distribution of forces between the two cable planes.

This is illustrated in Figure 4.7 showing under (d) a system with a central cable plane and a torsionally rigid deck, under (e) a system with two cable planes and a deck without torsional rigidity, and under (f) a system with two cable planes as well as a torsionally stiff deck.

In System (d) the total torsion  $Pe$  must be transferred through the deck. Therefore, a box girder will generally be required, and often the main dimensions will be governed by the required torsional stiffness.

In System (e) the eccentric force  $P$  can be distributed to the two cable planes according to the lever arm principle, and in that case no torsional moments will be induced in the deck.

In System (f) the torsional moment  $Pe$  is taken partly by the deck and partly by the cable system. As indicated, this reduces the difference between the two forces acting on the cable systems (compared to System (e)). Therefore, the torsional stiffness of the deck results in a more even force distribution between the two cable systems, and in a reduction of the twist angle.

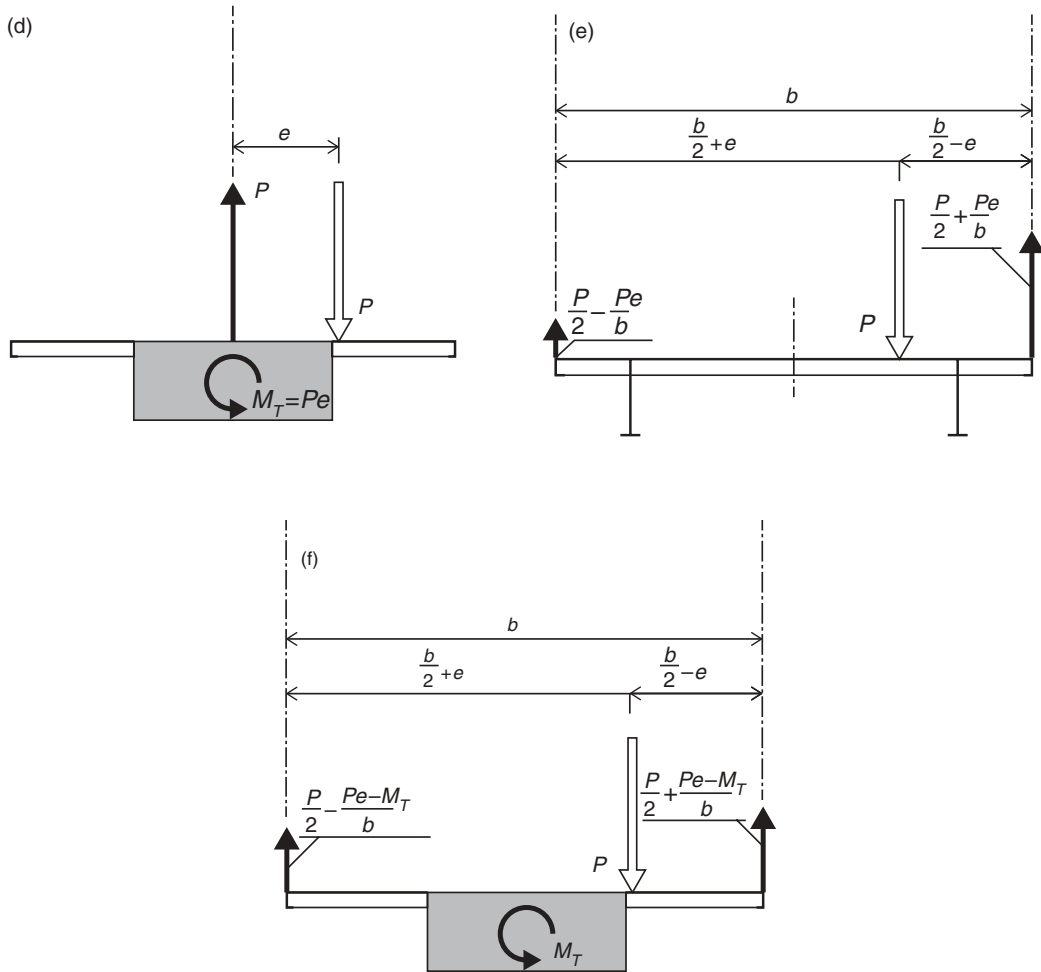
## 4.2 Supporting Conditions

The interaction between the deck, the cable system and the pylons in the transmission of vertical and horizontal loads is decisively influenced by the choice of the supporting conditions for the deck.

In the conventional three-span suspension bridge the deck often consists of three individual girders with simple supports at the pylons and the end piers (anchor blocks), as indicated in Figure 4.8. Generally, the end pier supports will be longitudinally fixed whereas all other supports are made longitudinally movable, so that all expansion will take place in the two joints at the pylons.

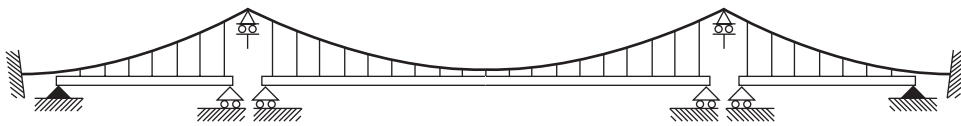
The supporting conditions shown in Figure 4.8 are especially favourable for the deformations under temperature change as the largest longitudinal displacements of the deck will occur in the regions with the longest hangers. The change of inclination of the hangers will therefore be modest.

In the dead load condition the bearings under the deck will be subjected to small forces as almost all dead load is carried by the cable system. However, under traffic load the bearings might be subjected to tension as well as compression depending on the loading condition.



**Figure 4.7** Transmission of an eccentric force  $P$  in three systems with different positions of the cable planes and varying torsional stiffness of the deck

In the traditional suspension bridge the bearings at the pylons are often made as relatively long end links pinned at one end to the deck and at the other to brackets on the pylon, as shown in Figure 4.9. The end links have in most cases been positioned above the bridge deck which makes them very visible. In the Akashi Kaikyo Bridge the end links were positioned below the bridge deck and next to the end verticals of the truss (Figure 4.10). This arrangement results in a much more discreet appearance of the links.



**Figure 4.8** Supporting conditions of the conventional three-span suspension bridge



**Figure 4.9** End links to transfer vertical forces from the deck to the pylon (Kurushima Bridge)

The end links will be designed to transfer vertical forces only, and a supplementary lateral support in the form of a wind bearing is therefore required to transfer the lateral forces. The wind bearing can be made as brackets with double-sided sliding surfaces protruding from the deck and supported on the cross beam of the pylon (Figure 4.11) or by vertically sliding bearings between the edges of the bridge deck and the inner faces of the pylon legs, as illustrated later in Figure 4.19.

With movable bearings at both ends, the deck of the main span will be supported longitudinally only by the cable system. Therefore, in conventional suspension bridges with vertical hangers throughout the main span a longitudinal displacement of the deck is required to ensure the transmission of a longitudinal force by inclination of the shorter hangers, as illustrated in Figure 4.12.

In bridges with moderate longitudinal forces, e.g. braking forces on road bridges, the required longitudinal displacement will be small, and the solution is therefore very well feasible. On the other hand, in bridges with large longitudinal forces a further restraint of the main span deck might be desirable. Such a restraint could be accomplished in the following ways:

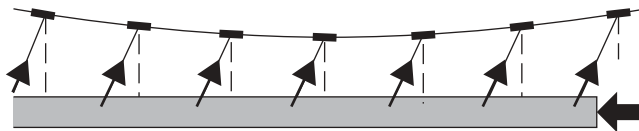
- (1) By applying a fixed support at one of the pylons.
- (2) By connecting the deck and the main cable through a central clamp at midspan.
- (3) By centring the main span deck by a device, as shown in Figure 3.49.



**Figure 4.10** End links at the pylons of the Akashi Kaikyo Bridge



**Figure 4.11** Wind bearings between the deck and the pylon cross beam (Lillebælt Bridge)



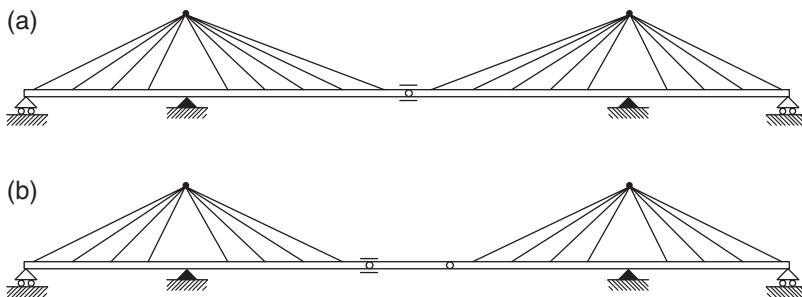
**Figure 4.12** Inclination of the short hangers at midspan to transfer a longitudinal force from the deck to the main cable

- (4) By installing shock absorbers at the pylons, allowing slow thermal movements but excluding movements from short-term loading such as braking forces.

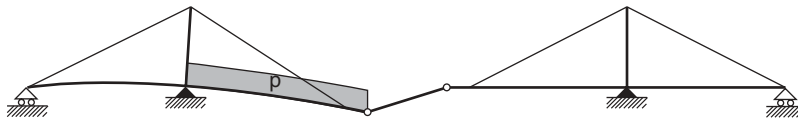
In self anchored cable stayed bridges the maximum axial forces in the deck occur at the pylons, and it is therefore not possible to make the deck discontinuous at these points. Only at midspan in the region between the two top cable anchor points will it be possible to arrange an expansion joint, as the axial force is zero at that location.

Figure 4.13 shows two structural systems with expansion joints at the centre of the main span. In both systems the deck is supported by fixed bearings at the pylons and by longitudinally movable bearings at the end piers. In System (a) the expansion joint is positioned exactly at midspan, whereas System (b) contains a drop-in span with an expansion joint at one end.

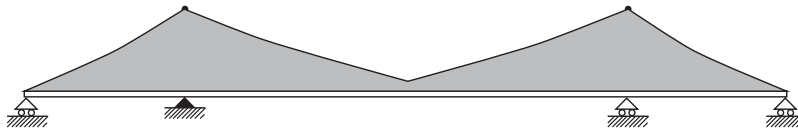
In bridges with a multi-cable system the solution with only one central expansion joint is to be preferred as it allows a close spacing of the cable anchor points all the way to midspan. In System (b) it is necessary to give the drop-in span a certain length to avoid an undesirable inclination under traffic load on one cantilever arm only, as illustrated in Figure 4.14. In general, System (b) of Figure 4.13 is somewhat dubious in cable stayed bridges as they are characterized by relatively large



**Figure 4.13** Two structural systems for cable stayed bridges with expansion joint at midspan



**Figure 4.14** Deflection under asymmetric load of a cable stayed bridge with a central drop-in span



**Figure 4.15** Cable supported bridge with a continuous deck

vertical deflections (in contrast to truss bridges where a similar structural system has been widely used). So, System (b) has only been applied in a few cable stayed bridges with a heavy concrete deck where deflections under traffic load were modest.

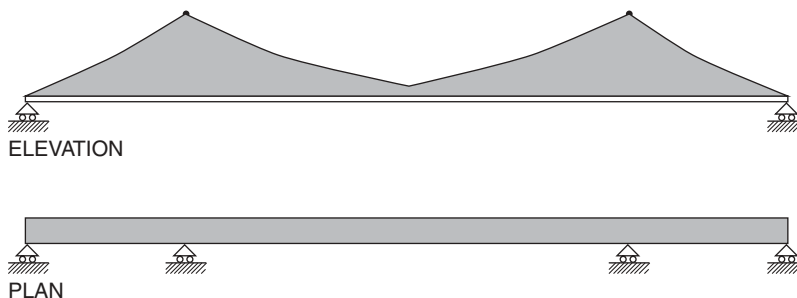
The most commonly used system in cable stayed bridges is that shown in Figure 4.15 with a deck continuous from one end to the other. In this system the deck will have one fixed and three longitudinally movable bearings, or fixed bearings at both pylons and longitudinally movable bearings at both ends, or four movable bearings. In the latter case the longitudinal restraint must be established through the cable system and by the pylons acting as cantilevered beam-columns fixed to the main piers – unless special centring devices are introduced. In the system with fixed bearings at both pylons it is required that the lower pylon parts or the pier structures below deck level possess a certain flexibility in the longitudinal direction so that the deck can expand and contract under temperature variations without inducing an unacceptable bending.

A continuous deck can also be applied in an earth anchored suspension bridge. Here the main advantage to be gained is that the large angular changes occurring at the pylons under certain traffic load conditions will be eliminated. This might be of special importance in bridges carrying a train load.

On the other hand, a suspension bridge with a continuous deck will have large negative moments induced in the deck at the supports on the pylons. This might result in stresses of such a magnitude that high tensile steels will be required for the deck sections near the pylons. Furthermore, special attention must be paid to the inclination of the short hangers near the ends of the side span, where the largest longitudinal displacements due to temperature change and asymmetric traffic load will occur.

In suspension bridges and cable stayed bridges with multi-cable systems where the deck is almost continuously supported by the cable system from one end to the other, it might be possible to omit the vertical supports of the deck at the pylons, as shown in Figure 4.16. This will lead to a noticeable reduction of the bending moments in the deck at the pylons.

For a major suspension bridge the system illustrated in Figure 4.16 was used for the first time in the Storebælt East Bridge. Here the lack of vertical deck support at the pylons is clearly indicated by omitting the traditional cross beam between the pylon legs beneath the deck (Figure 4.17).



**Figure 4.16** Cable supported bridge with the deck supported vertically on the end piers only, but laterally at the pylons as well as on the end piers



**Figure 4.17** Pylon of the Storebælt East Bridge without a cross beam below the deck

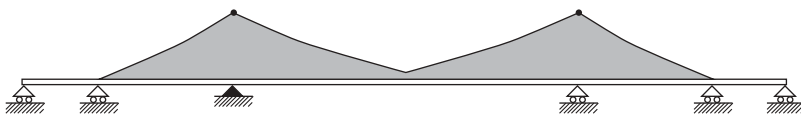
In the lateral direction it will often be required to have bearings both at the end piers and at the pylons, as indicated on the plan of Figure 4.16. This is due to the fact that the cable system in many cases does not render a very efficient lateral support to the deck.

In the system with a continuous deck the largest angular changes will occur at the end supports. To reduce the angular changes, a system with the deck continued into short beam spans as shown in Figure 4.18 might prove efficient.

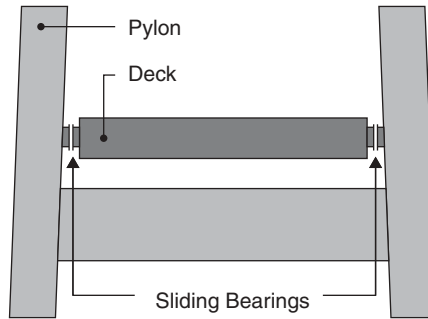
The lateral support of the deck at the pylons can be accomplished by applying vertical sliding bearings between the deck and the inner faces of the pylon legs, as shown in Figure 4.19. This system was used in the Storebælt East Bridge.

In bridges where the cable system, does not render an efficient torsional support of the deck, as in cable stayed bridges with only one central cable plane, it might furthermore be required to give the deck torsional support at the pylons. To still allow vertical displacements a solution as shown in Figure 4.20 can be used. Here vertical movements are possible but lateral movements and twisting rotations are prevented. A torsional support without vertical restraint might also be established by a hydraulic device similar to the one shown in Figure 3.49. Such a system was applied in the Farø Bridge in Denmark (Figure 4.21).

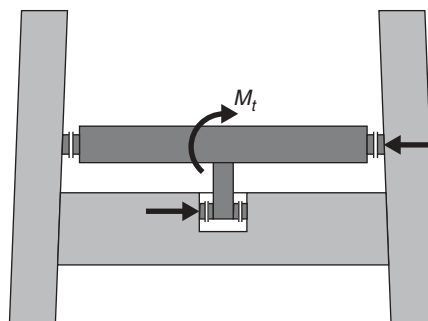
As it will be understood by examining the solutions of Figures 4.20 and 4.21, torsional support without vertical support leads to some complications in the detailing of the connection between the deck and the pylon. Therefore, in each case it should be thoroughly investigated, whether the achieved reduction of the bending moments due to vertical load justifies the complications introduced in the deck-to-pylon connection.



**Figure 4.18** Cable supported bridge with the deck continued into short beam spans

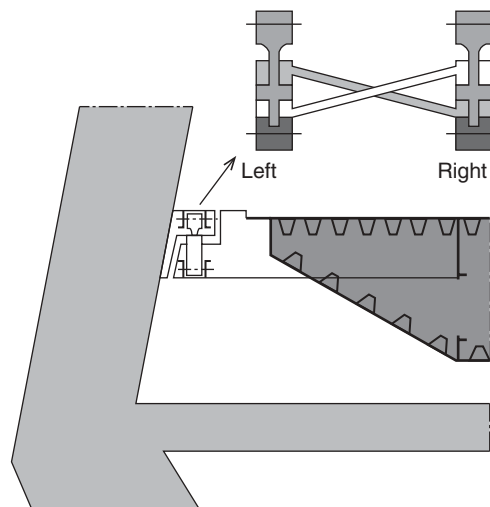


**Figure 4.19** Connection between the deck and the pylon through vertical sliding bearings for transmission of lateral forces



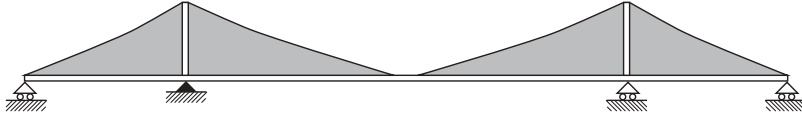
**Figure 4.20** Connection between the deck and the pylons capable of transmitting lateral forces and torsional moments

In the previous examples on supporting conditions for the deck it has been assumed that the deck and the pylon pass each other without a direct connection. However, in cable stayed bridges a system as shown in Figure 4.22 has been used – especially in some of the early cable stayed bridges. Here the pylons were moment rigidly fixed to the deck, and bearings were positioned between the deck and the pier below. With this system at least one of the bearings must be fixed

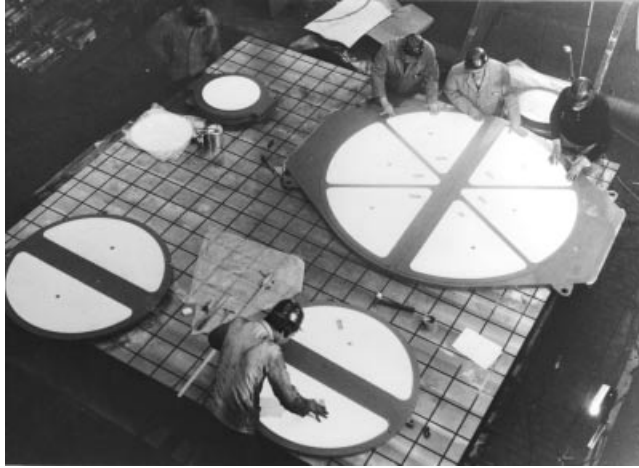


**Figure 4.21** Torsional support through a hydraulic device with coupled oil cylinders (Farø Bridge, Denmark)





**Figure 4.22** Structural system with pylons fixed to the deck



**Figure 4.23** Neopot-Teflon bearing in the Oberkasseler Bridge

longitudinally, and often it was chosen to have one of the pylon bearings fixed and the other longitudinally movable, as indicated in Figure 4.22.

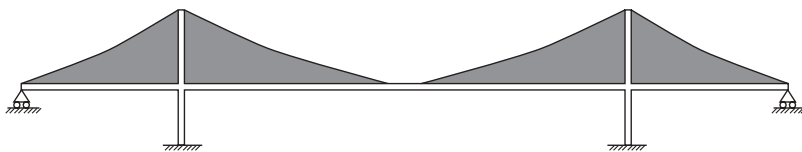
The bearings under the pylons were generally subjected to vertical forces of a considerable magnitude. In modern cable stayed bridges a compact Neopot bearing (or a spherical) bearing is often used. For a movable bearing the Neopot bearing will be supplemented by a sliding Teflon bearing, as shown in Figure 4.23.

In bridges with the deck high above the foundation below, a structural system as shown in Figure 4.24 might be possible. With high and slender pylon shafts under the deck, the necessary flexibility to allow thermal movements might be obtained, without requiring bearings to be installed. This system has been used in the Normandy Bridge where the deck, cross beam and pylon legs were monolithically joined (Figure 4.25).

For the Normandy Bridge the problems related to displacements caused by temperature variations of the deck were to some extent relaxed by the deck's pronounced convex curvature and an associated change of camber.

At the end piers the deck of a cable stayed bridge will generally have to be supported by longitudinally movable bearings capable of transmitting tension to counteract the pull of the anchor cable (Figure 4.26).

In some cases this requirement has been met by connecting the deck and the pier by an end link, as shown in Figure 4.27. If the side spans are small compared to the main span, the end support might be subjected exclusively to tension under any loading condition, and the link can then be made of simple eye bars. However, if the end support can be subjected to compression also, the end link must be designed as a column, e.g. with a box-shaped cross section. In cable stayed bridges with adjoining approach spans, the tension at the end support can be significantly reduced if the connection is designed so



**Figure 4.24** Structural system with pylons rigidly connected to the deck and continued to a lower pier



**Figure 4.25** Monolithic joint between the deck and the pylon in the Normandy Bridge

that the reaction from the nearest approach span counteracts the uplift from the anchor cable. This was done in the Köhlbrand Bridge by supporting a heavy concrete approach span on a bracket at the end of the deck in the cable stayed bridge (Figure 4.28). The uplift from the anchor cable pull was then fully reduced by the reaction from the approach span. As a result, only a modest vertical anchoring was required.

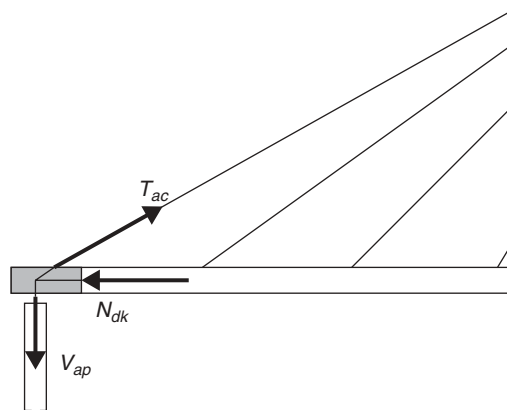
In a system with the deck continued into the adjacent beam spans, as was illustrated in Figure 4.18, the reaction from the approach span will be directly activated to reduce the vertical anchor force without any special precautions.

The transmission of tension from the deck to the anchor pier can also be established by supplementing a regular sliding bearing by vertical, post-tensioned cables inside the pier shaft (Figure 4.29). This is the preferred solution in modern cable stayed bridges.

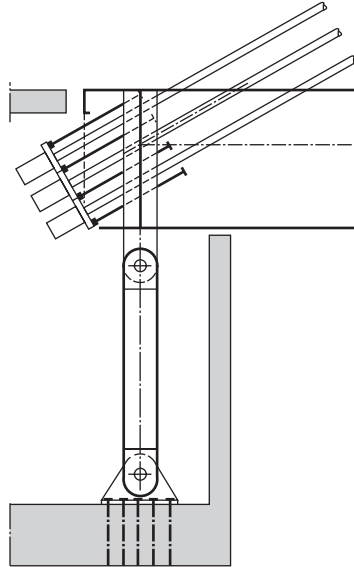
In a number of cable stayed bridges the problems related to uplift at the side span supports have been completely eliminated by application of a much heavier deck in the side span than in the main span, e.g. a steel deck in the main span and concrete deck in the side span.

### 4.3 Distribution of Dead Load Moments

In the design process for traditional structures such as beams, trusses and arches it is quite common to apply both dead load and live load to the structural system with the geometry of the final structure, i.e. assume that the unloaded (stress-free)



**Figure 4.26** Anchoring of the deck end to transmit the vertical component of the anchor cable force



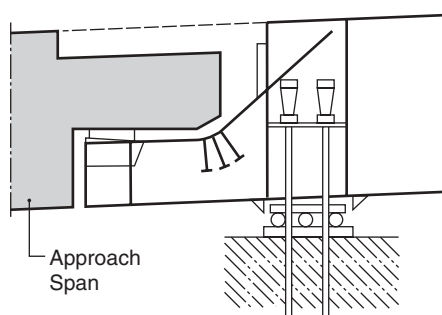
**Figure 4.27** Anchorage of the deck end at the anchor cable attachment through end links inside the abutment

condition has the final configuration. However, for a cable supported bridge this might lead to quite erroneous results as the geometry of the final system is present when the structure is subjected to its dead load and not in an imaginary stress-free state.

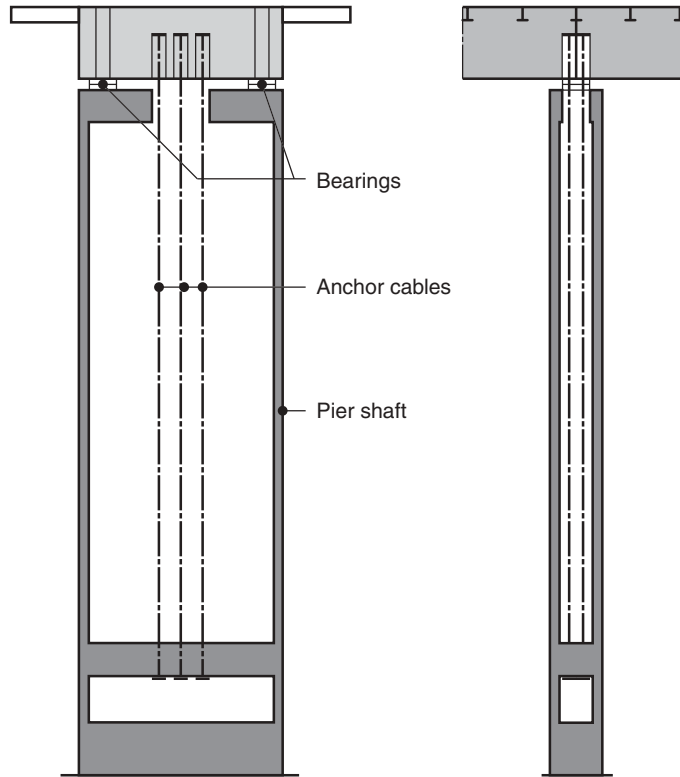
An almost stress-free condition could be achieved for a cable stayed bridge in the initial stage if the contractor throughout the construction period supported the structure by temporary supports under all the cable anchor points in the deck, as indicated in Figure 4.30 at the top.

Now, if the contractor had cautiously assembled the bridge so that it had its final geometry in the stress-free condition then he would find that the structure would deflect under the influence of the dead load when he removed the temporary supports. This would lead to a substantial change of geometry, as indicated in the bottom of Figure 4.30. A structure where the specified geometry is not present under permanent dead load is obviously not acceptable to the owner of the bridge.

To return to the initial geometry, the contractor could then tension the stay cables further so that the cable anchor points were lifted up to the positions they had when supported by the temporary supports. Then the deck would return to its original shape so the bending moments would be the same as found for the girder when resting on the rigid temporary support.

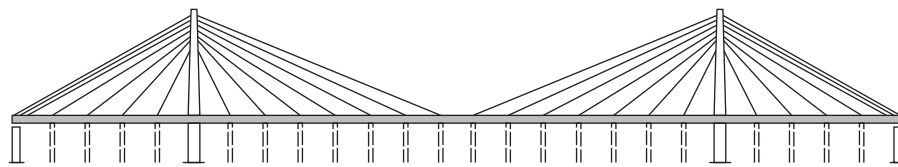


**Figure 4.28** Approach span supported on brackets at the end of the main bridge deck (Köhlbrand Bridge)

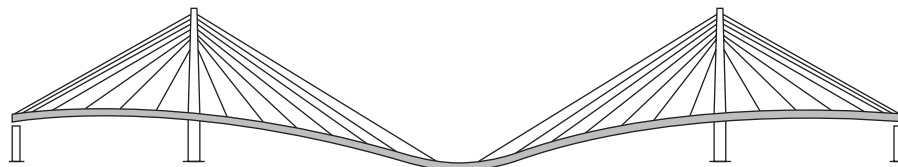


**Figure 4.29** Anchoring of the deck by vertical cables inside the shaft of an anchor pier

It will be understood that for dead load the flexibility of the cable supported points can be eliminated by stressing the cables so that the points will end up in the same position as they had before the structure was subjected to dead load. In other words, the elastic strains in the cables when subjected to tension from dead load can be counteracted by the shortening of the cables (by moving the sockets at the anchorages).



Stress-free erection on temporary supports



**Figure 4.30** (Top) Cable stayed bridge erected 'stress-free' on temporary supports with the desired final geometry; (bottom) Deflected shape after removal of the temporary supports

If the procedure outlined above was followed, then the dead load moments in the deck would be the same as found for a continuous girder on fixed supports.

In the real world it is not common practice to erect the entire deck on temporary supports but to gradually add deck elements and tension stay cables. In that case it will be possible to end up with virtually any (statically permissible) distribution of the dead load moments so the distribution does not necessarily have to coincide with that of a continuous girder on rigid supports.

**4.3.1 The dead load condition**

The distribution of the dead load moments will be fully described by the moments  $M_{g,i}$  at the cable anchor points (and at the pylons) together with the intensity  $g_{i,i+1}$  of the deck dead load between each anchor point, as illustrated in Figure 4.31.

With a given distribution of the dead load moments, the total dead load condition of the entire structure will be uniquely determined. Thus, with the notation of Figure 4.32 the cable force  $T_i$  is found from:

$$T_i = \left( \frac{1}{2}(g_{i-1,i}\lambda_{i-1,i} + g_{i,i+1}\lambda_{i,i+1}) + \frac{M_{i-1} - M_i}{\lambda_{i-1,i}} + \frac{M_{i+1} - M_i}{\lambda_{i,i+1}} \right) \frac{1}{\sin \phi_i} \tag{4.1}$$

Conversely, if the cable forces  $T_i$  are known, then the moment distribution in the deck can be calculated uniquely.

In suspension bridges it is generally attempted to minimize the bending of the deck in the dead load condition. This leads to a moment distribution as shown in Figure 4.33, with small (often insignificant) local moments varying between  $-g\lambda^2/16$  and  $+g\lambda^2/16$ .

In cable stayed bridges a similar minimization of the dead load moments will, in most cases, not lead to an optimum solution. This is due to the fact that the ratio between positive and negative moments induced by traffic load varies along the span, and that the deck sections in many cases will possess a varying ability to transmit positive and negative moments (due to the influence of the axial force as well as asymmetry of the deck section). Thus, it might prove advantageous to

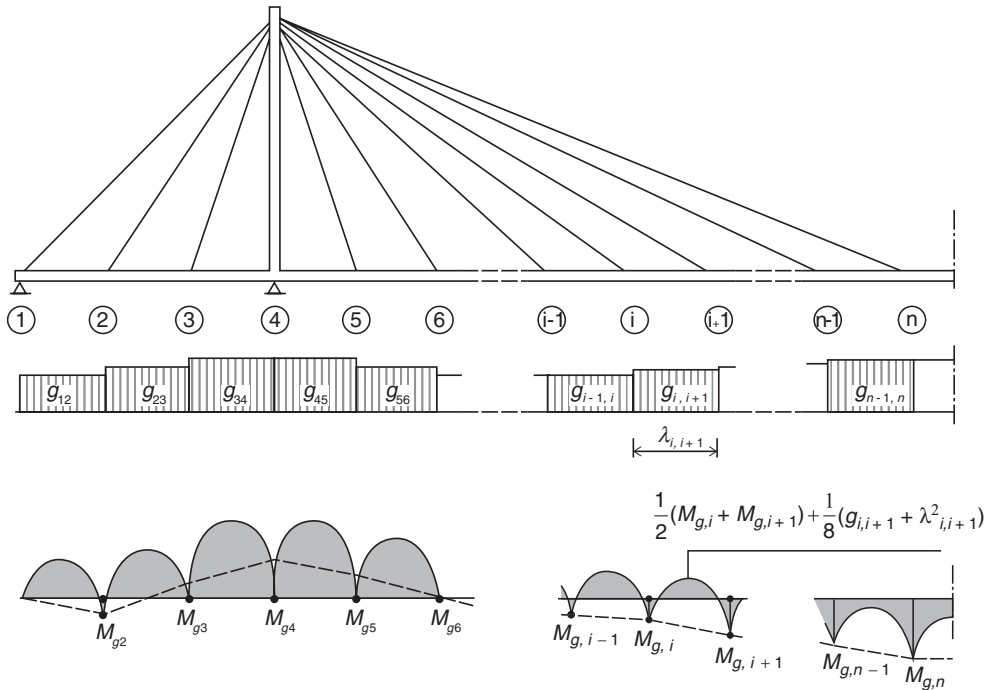
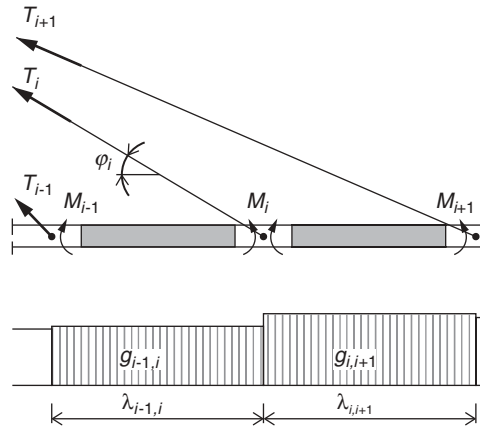


Figure 4.31 Dead load moment distribution

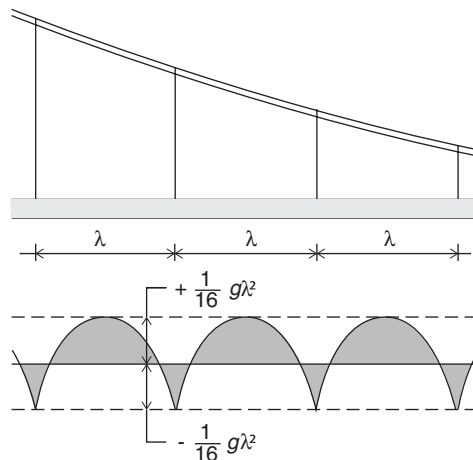


**Figure 4.32** Determination of cable force corresponding to a specified distribution of dead load moments

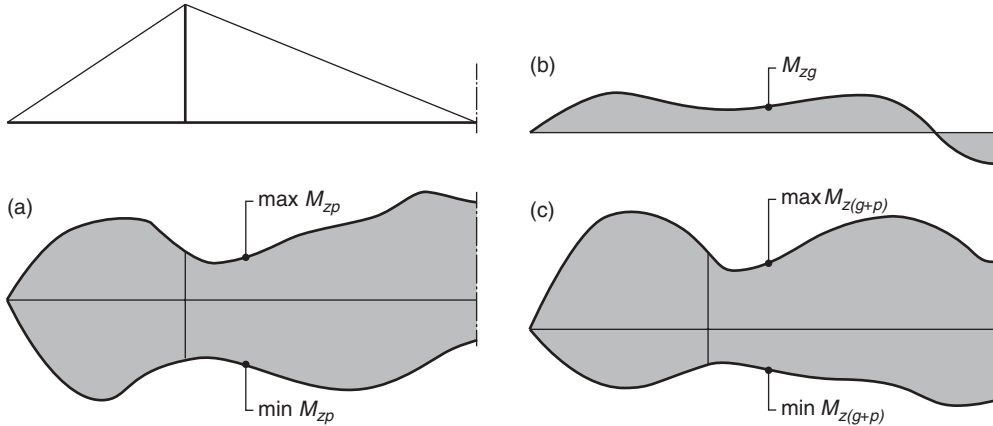
adjust the ratio between positive (sagging) and negative (hogging) moments by choosing a distribution of dead load moments different from that of Figure 4.33.

Figure 4.34 shows under (a) a typical distribution of maximum and minimum moments due to traffic load for a three-span cable stayed bridge with a multi-cable system. Note that the ratio between the positive and negative moments varies along the spans. The moment distribution under (a) is characterized by numerically larger negative moments than positive moments in most regions, except at midspan. However, in many cases it is advantageous to have larger positive than negative moments in regions with compression of some magnitude, and positive and negative moments of equal size in regions with small or no axial force. Therefore, a more favourable moment distribution can be achieved by adding a dead load moment distribution as shown under (b), so that the final distribution of positive and negative design moments will be as indicated under (c).

As mentioned, the deck will show different moment capacities for positive and negative moments due to the action of the axial force and to asymmetry of the cross section.



**Figure 4.33** Typical distribution of dead load moments in the deck of a suspension bridge



**Figure 4.34** Distribution of traffic load moments, dead load moments, and final design moments in a multi-cable stayed bridge

For a cross section as shown in Figure 4.35 subjected to a moment  $M_z$  and an axial force  $N$ , the following conditions must be fulfilled:

$$\begin{aligned}
 f_{tf,cd} &\leq \frac{N}{A} - \frac{M_z}{Z_{tf}} \leq f_{tf,td} \\
 f_{bf,cd} &\leq \frac{N}{A} + \frac{M_z}{Z_{bf}} \leq f_{bf,td}
 \end{aligned}
 \tag{4.2}$$

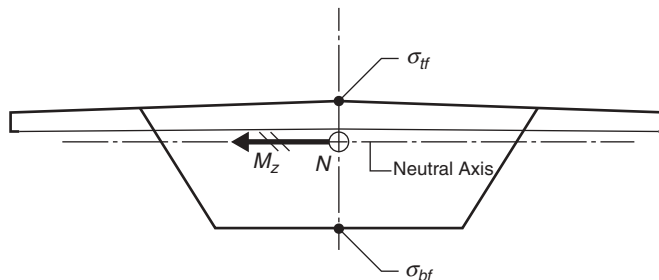
where  $f_{tf,cd}$  is the limiting compressive stress and  $f_{tf,td}$  the limiting tensile stress in the top flange (floor plate), whereas  $f_{bf,cd}$  and  $f_{bf,td}$  are the corresponding limiting stresses in the bottom flange.  $A$  is the cross sectional area of the deck, and  $Z_{tf}$  and  $Z_{bf}$  the section moduli for the top and the bottom flange, respectively.

Note that the numerical values of the limiting stresses  $f_{tf,cd}$ ,  $f_{tf,td}$ ,  $f_{bf,cd}$  and  $f_{bf,td}$  in most cases will be different due to local action of wheel load on the deck plate, to differences in material properties (e.g. in a composite girder), and to buckling phenomena in the compressed panels.

Based on (4.3), an  $N-M_z$  diagram as shown in Figure 4.36 can be drawn for the actual cross section. From this diagram the largest positive moment  $M_z^+(N)$  and the smallest negative moment  $M_z^-(N)$  to be allowed for a given value of the axial force  $N$  can be determined.

A procedure to be followed when seeking the most favourable distribution of dead load moments could be as indicated below:

**Step 1** The general layout of the deck is chosen. Based on minimum thickness of all plates the sectional properties and dead loads are determined for this minimum section.



**Figure 4.35** Typical asymmetrical cross section of the deck

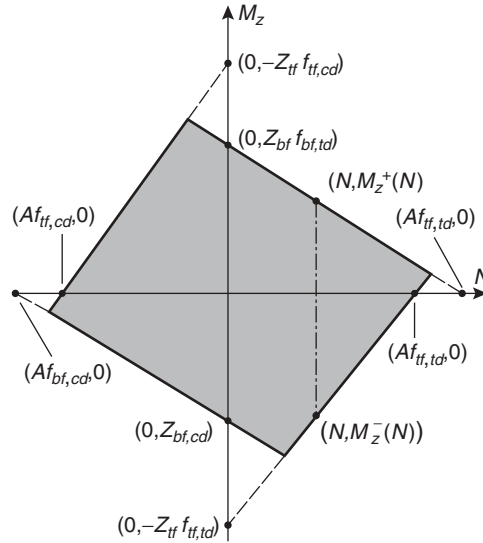


Figure 4.36  $N-M_z$  diagram for a cross section as shown in Figure 4.35

- Step 2* Based on the minimum section, the cable system is preliminarily designed and the total structural system is analysed to give the maximum and minimum moment envelope. In this step a preliminary distribution of dead load moments must be chosen, e.g. the distribution with minimum dead load moments ( $-g\lambda^2/16 \leq M_g \leq +g\lambda^2/16$ ) at the cable supported points. For multi-cable bridges where  $\lambda$  is a small fraction of the span length, the dead load moments will be so small that they can be ignored ( $M_g \sim 0$ ).
- Step 3* With the normal forces determined during the analysis of step 2, the positive and negative moments  $M_z^+$  and  $M_z^-$  to be carried by the minimum cross section are found from the  $N - M_z$  diagram.
- Step 4* The maximum and minimum moment curves determined during step 2 can now be compared with curves showing the variation of  $M_z^+$  and  $M_z^-$  as determined during step 3.

A typical plot of these moment curves might look as shown in Figure 4.37. Here three regions are indicated:

Region A, characterized by:  $\max M_z \leq M_z^+$  and  $\min M_z \geq M_z^-$

Region B, characterized by:  $\max M_z - M_z \leq M_z^+ - M_z^-$

Region C, characterized by:  $\max M_z - \min M_z > M_z^+ - M_z^-$

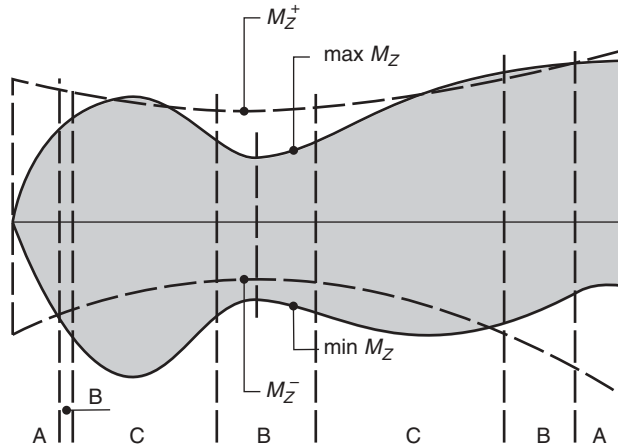
In Region A the chosen distribution of dead load moments leads to total moments within the moment capacity of the minimum section so a redistribution of dead load moments is not required.

In Region B the chosen distribution of dead load moments leads to  $\max M_z > M_z^+$  or  $\min M_z < M_z^-$  but as  $\max M_z - \min M_z \leq M_z^+ - M_z^-$  it will be possible to fulfil both of the conditions,  $\max M_z \leq M_z^+$  and  $\min M_z \geq M_z^-$  by redistribution of the dead load moments. Consequently, the minimum deck section is adequate if a more favourable distribution of the dead load moments is chosen.

In Region C the range between  $\max M_z$  and  $\min M_z$  exceeds the interval between the moment capacities  $M_z^+$  and  $M_z^-$ , so a redistribution of the dead load moments (which leaves the moment interval unchanged) cannot lead to a dead load moment distribution where the minimum cross section is adequate.

- Step 5* A new distribution of the dead load moments is now chosen, so that the minimum section can be applied both in Regions A and B. For Region C, deck sections with increased plate thickness (or higher material strength) are chosen to give the required moment capacities.





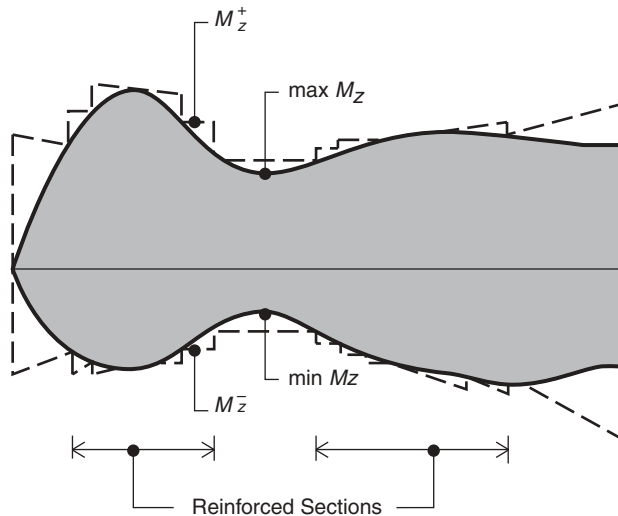
**Figure 4.37** Distribution of maximum design moments before adjusting the dead load moment distribution

After these adjustments the moment curves of Figure 4.37 will be changed to those shown in Figure 4.38.

Subsequently, the procedure described has to be repeated, as the changes made in Step 5 will lead to a revision of the dead load and the cross sectional properties. This implies a redesign of the cable system and a new analysis to give revised maximum and minimum moment envelopes. The iteration has to be continued until sufficient agreement is obtained between the cross sectional properties used during the analysis in Step 2 and the cross sectional properties resulting from the dimensioning in Step 5.

After the final dead load condition has been determined by the above procedure, the problem remains to achieve this condition with the chosen erection procedure.

The final dead load condition will mainly be influenced during the initial cable tensioning. However, the cables must initially be tensioned to forces quite different from those of the final dead load condition, due to the fact that the initial cable forces will change drastically as the erection proceeds. In general it will not be feasible to adjust the forces in the individual cables throughout the erection period as this will lead to an overwhelming amount of work, especially in a



**Figure 4.38** Distribution of design moments after adjusting the dead load moments and reinforcing the deck sections

| ERECTION STAGE | OPERATION | CALCULATION STEP | STRUCTURAL SYSTEM   |
|----------------|-----------|------------------|---------------------|
| (n-1),g        |           | 4,g              | n-1                 |
| (n-1),c        |           |                  |                     |
| n, g           |           | 3,g              | n                   |
| n, c           |           |                  |                     |
| (n+1),g        |           | 2,g              | n+1                 |
| (n+1),c        |           |                  |                     |
| n+2            |           | 1                | n+2<br>FINAL SYSTEM |

Figure 4.39 Illustration of the opposite direction of the sequence of analysis and the sequence of erection

multi-cable system. The ideal situation is to tension each cable only once immediately after its installation. To achieve this and still arrive at the desired dead load moment distribution, the correct initial force for each cable must be calculated beforehand.

The procedure to be followed is illustrated in Figure 4.39 showing a possible erection sequence. Here the last six erection stages leading to the final condition are shown.

In Stage  $(n-1),g$  the deck is cantilevered from D to C. During this process the partially erected structure will be subjected to the dead load of the added deck segment.

In Stage  $(n-1),c$  the cable  $(n-1)$  is installed and tensioned to the initial force  $Y_{n-1}$ .

Stage  $n, g$  corresponds to Stage  $(n-1),g$  as this stage involves the erection of a deck segment (from C to B).

In the same way, Stage  $n, c$  corresponds to Stage  $(n-1),c$  involving the installation and tensioning of a new cable (cable  $n$ ).

In Stage  $(n+1),g$  the deck is cantilevered to the centre of the main span (Point A) where it meets the other cantilever arm.

In Stage  $(n+1),c$  a moment  $Y_{n+1}$  is assumed to be introduced at the centre before closing the joint between the two deck parts (this stage will be required to get a specific dead load moment at midspan in the final condition).

In Stage  $(n + 2)$  the superimposed dead load from wearing surfaces, railings, light posts, etc., is added to the completed structure, and the final dead load condition is then reached.

As specific moments and forces are desired in the final dead load condition, this will be the well-defined condition whereas the initial cable forces  $Y_1, Y_2, \dots, Y_n$  and the initial moment  $Y_{n+1}$  are unknowns.

The trick is now to let the sequence of analysis be opposite to the sequence of erection, as this allows the calculations to start out from the well-defined final condition. So, instead of analyzing the erection procedure, a 'demolishing' procedure involving the same steps but in the opposite sequence is analyzed. In the final condition the governing cable forces and the midspan moment  $M_{n+1}$  in the deck are designated  $(T_{1,0}, T_{2,0}, \dots, T_{n,0})$  and  $M_{n+1,0}$ .

The first calculation step (no. 1) implies the removal of the superimposed dead load  $g_s$ . The analysis is performed by subjecting the final structural system to the load  $-g_s$  ( $g_s$  acting upwards). Designating the calculated cable forces and the midspan moment due to the load  $-g_s$  by  $\Delta T_{1,1}, \Delta T_{2,1} \dots \Delta T_{n,1}, \Delta M_{n+1,1}$ , the resulting cable forces and the moment after calculation step 1 become

$$(T_{1,1}, T_{2,1} \dots T_{n,1}, M_{n+1,1}) = (T_{1,0} + \Delta T_{1,1}, T_{2,0} + \Delta T_{2,1}, \dots, T_{n,0} + \Delta T_{n,1}, M_{n+1,0} + \Delta M_{n+1,1}) \quad (4.3)$$

equal to the cable forces present after erection stage  $(n+1),c$ .

The moment  $Y_{n+1}$  to be introduced at midspan before closing the joint is equal to the moment  $M_{n+1,0} + \Delta M_{n+1,1}$  found at midspan after calculation step 1.

In calculation step no.2,c the structural system comprising one bridge half is subjected to a moment equal to  $-Y_n = -M_{n+1,0} + \Delta M_{n+1,1}$  acting on the free end of the deck at the main span centre.

In calculation step 2,g the same structural system as used in step 2,c is subjected to the load  $-g_{gdkr}$  acting on the deck segment from A to B. During calculation steps 2,c and 2,g the cable forces have changed by:  $\Delta T_{1,2}, \Delta T_{2,2} \dots \Delta T_{n,2}$  so now the cable forces have the following values:

$$(T_{1,2}, T_{2,2} \dots T_{n,2}) = (T_{1,0} + \Delta T_{1,1} + \Delta T_{1,2}, T_{2,0} + \Delta T_{2,1} + \Delta T_{2,2}, \dots, T_{n,0} + \Delta T_{n,1} + \Delta T_{n,2}) \quad (4.4)$$

equal to the cable forces present after erection stage  $(n+2),c$ .

The cable force  $Y_n$  to be introduced in cable  $n$  during the initial tensioning is then equal to the force  $T_{n,2} = T_{n,0} + \Delta T_{n,1} + \Delta T_{n,2}$  found after calculation step 2,g.

In calculation step no. 3,c the partial structural system, without the central segment of the deck and cable no.  $n$ , is subjected to the force  $-Y_n = -T_{n,2}$  acting at the anchor points of cable  $n$ .

The same structural system is subjected to the load  $-g_{dlk}$  acting on the deck segment from B to C. During calculation steps 3,c and 3,g the cable forces have changed by  $\Delta T_{1,3}, \Delta T_{2,3} \dots \Delta T_{n,3}$  so now the cable forces have the following values:

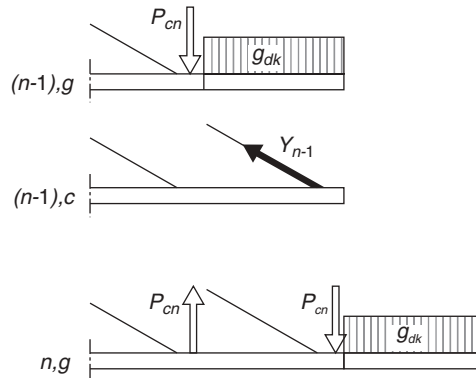
$$(T_{1,3}, T_{2,3} \dots T_{n,3}) = (T_{1,0} + \Delta T_{1,1} + \Delta T_{1,2} + \Delta T_{1,3}, T_{2,0} + \Delta T_{2,1} + \Delta T_{2,2} + \Delta T_{2,3}, \dots, T_{n-1,0} + \Delta T_{n-1,1} + \Delta T_{n-1,2} + \Delta T_{n-1,3}) \quad (4.5)$$

The cable force  $T_{n-1,3}$  in cable  $n-1$  is now equal to the initial force  $Y_{n-1}$ .

The procedure can then be continued until the entire structure has been 'demolished'. The general principle will be that, after each calculation step prior to the removal of a cable, the initial force in that particular cable will be determined. Then the structural system is changed by removing the cable and subjecting the remaining structure to the cable force with opposite sign.

The accomplished analysis results in a complete set of initial cable forces to be applied at the time of each cable installation, and with these initial forces the prescribed final dead load condition will be reached.

However, it should be remembered that the cable forces also change with temperature, which can easily vary throughout the erection period. Therefore, it is required to measure the temperature in the structure prior to each cable installation and adjust the structural calculations accordingly. In bridges with decks of concrete it is furthermore necessary to take into account the changes of forces due to creep and shrinkage. When analyzing the erection procedure



**Figure 4.40** Imitation of a moving crane load  $P_{cn}$  during analysis of the erection procedure

backwards, as described above, it must be remembered to insert the strains due to creep and shrinkage with opposite sign in the calculations.

For erection equipment, like a derrick crane, that will be moved forward as the erection proceeds, a special procedure must be followed, as illustrated in Figure 4.40, showing erection stages between  $(n - 1),g$  and  $n,g$  from Figure 4.39 but with the crane weight  $P_{cn}$  added.

In erection stage  $(n - 1),g$  the crane weight  $P_{cn}$  is applied at the location where it will be positioned when lifting the actual segment. The weight of the crane should therefore be included in the external load together with the deck weight  $g_{gr}$ .

In erection stage  $n,g$  the crane weight is then applied at the new location for lifting the relevant segment but at the same time a force  $-P_{cn}$  is applied at the position where  $P_{cn}$  acted in erection stage  $(n - 1),g$ . In this way the moving of the crane along the deck is imitated in the analysis.

Besides giving the initial cable forces, the described erection procedure also makes it possible to check stresses in the entire structure throughout the erection procedure, as the governing forces and moments can be determined in each calculation step.

If the stress check leads to the conclusion that stresses are kept within the design stress interval, then the prescribed erection procedure is feasible, as the final condition can be reached by the assumed procedure without further adjustments.

If an overstressing occurs during one or more erection stages, changes have to be introduced either in the erection procedure or in the structural design.

Changes in the erection procedure could involve:

- (1) Modification of the final dead load condition.
- (2) Repositioning of the joints between deck segments.
- (3) Tensioning of cables in more steps.
- (4) Use of temporary stay cables.

Changes in the structural design could involve:

- (5) Strengthening of overstressed structural elements.
- (6) Increasing the number of cables (to reduce the distance between cable anchor points).
- (7) Redesign of the deck cross section.
- (8) Addition of intermediate supports (e.g. in the side spans).
- (9) Change of structural material

In an actual case where overstressing occurs, the first measures to be taken should be those involving modest adjustments such as (1), (2), (3), and (5) above.

## 4.4 Cross Section

In the process of designing a cable supported bridge the choice of deck cross section marks an important step. This is due to the fact that the general layout of the deck not only determines its participation in the total structural system but also decisively influences the size of the vertical dead load and the lateral wind load (drag). Furthermore, the shape of the deck might be of importance for achieving aerodynamic stability.

### 4.4.1 Bridge floor

In modern cable supported bridges, the bridge floor, whether in steel (orthotropic) or concrete, will always be incorporated in the deck to increase both stiffness and strength.

In road bridges a concrete floor will generally consist of a slab with a thickness between 200 mm and 300 mm requiring linear support by stringers or cross beams in distances of 3000–5000 mm. However, a larger distance between the supporting beams can be used if the concrete slab is designed with haunches and is pre-stressed.

A concrete slab will always be used if the remaining part of the bridge deck is of concrete; but it is also common to use a concrete slab as part of a composite deck where all other parts of the deck cross section are in steel.

The main advantage to be gained by a concrete bridge floor is the low cost of the slab itself. On the other hand, the weight of the concrete slab increases the total dead load, and that leads to larger cross sections of cables, pylons, and piers. The choice between concrete and steel in the bridge floor should therefore not be based solely on a comparison between the cost of the bridge floor itself but also by considering the consequences of increased dead load of the floor on all other structural parts.

Furthermore, the construction process has to be considered as a heavier concrete deck can lead to an overstressing of the cable system (and of the deck segments already in place) when cantilevering from one cable anchor point to the next. As a consequence, it might be necessary to take costly measures such as additional support by temporary stay cables or to apply a special post tensioning of the deck.

The popularity of a composite deck in cable stayed bridges is mainly linked to the advantages to be gained during erection as a cantilever from one anchor point to the next can be made initially by the relatively light steel structure allowing the following stay cable to be installed before the heavy concrete slab is to be added. Also, the smaller overall dead load of a composite deck in comparison with a concrete deck will result in savings in cables, pylons and foundations.

The use of concrete in the entire (or in a part of) the deck will mainly be confined to self anchored cable stayed bridges where the ability of the concrete to transfer compression can efficiently be utilized.

A steel floor will be considerably more expensive per unit floor area than a concrete floor, but due to its lower weight that amounts to only around one quarter of that of a concrete slab, decisive savings can often be achieved in the remaining part of the structure.

A steel floor generally consists of a relatively thin steel plate (typically 14 mm thick) stiffened by longitudinal trapezoidal ribs rendering linear support at a distance of approximately 20–25 times the plate thickness (typically 300 mm). The longitudinal ribs are in turn supported by cross beams or diaphragms positioned 3000–5000 mm apart.

### 4.4.2 Cross section of the deck

An important aspect of the deck design is the degree of torsional stiffness to be achieved, as will be described for the four basic cross sections shown in Figure 4.41.

In cross section (a) the deck consists of the floor slab and two vertical plate girders. As the section is open, the torsional stiffness is insignificant so it is essential that the cable system renders efficient torsional support. Thus, two cable planes attached along the edges of the deck are required.

In (b) the deck itself is box-shaped and therefore with a considerable torsional stiffness. Therefore, this section will be found in structures where the cable system does not give any torsional support, i.e. in a deck with support from only one central cable plane. A torsionally stiff section might, however, also be used in connection with cable systems rendering torsional support if the largest possible torsional stiffness of the total system is desirable.

Cross section (c) corresponds to (a) with the exception that the vertical girders are substituted by trusses. This change does not noticeably influence the torsional properties and Section (c) must therefore also be regarded as being without torsional stiffness.

A cross section corresponding to (c) has been used in suspension bridges with vertical cable planes positioned directly above the trusses. This was the case for the Golden Gate Bridge as it was built initially in the 1930s. However, it was later

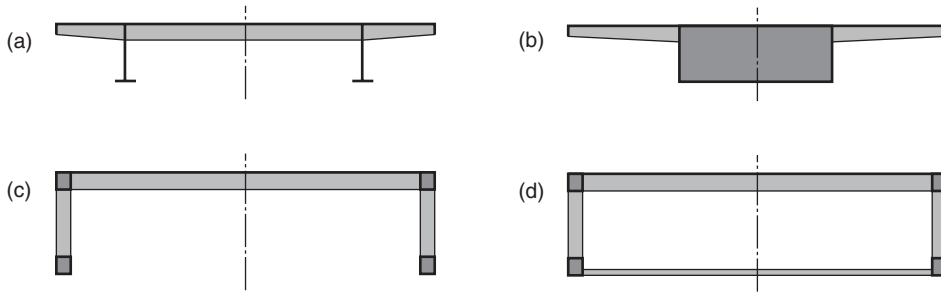


Figure 4.41 Four basic cross sections of the deck/truss

discovered that the lack of torsional stiffness led to an inadequate aerodynamic stability of the total structure. Therefore, the original cross section (c) was later changed to a cross section corresponding to (d) by adding a lower wind bracing between the bottom chords.

Cross section (d) with the bridge floor and three trusses, two vertical and one horizontal, corresponds in its torsional properties to the box girder (b). This type of cross section is used in all modern suspension bridges with a stiffening truss.

Figure 4.42 shows three basic cross sections to be found in cable stayed bridges with double cable planes rendering both vertical and torsional support to the deck. The deck of Figure 4.42 (e) consists of an orthotropic steel floor and two plate girders. The cable planes are positioned outside the edges of the deck, so that the transmission of forces from the deck to the cables must take place through relatively heavy transverse girders at the cable anchor points.

An important geometrical parameter for the cross section of Figure 4.42 (e) is the distance  $b_e$  from the plate girder web to the edge of the bridge deck. When considering the support of the cross beams, the most favourable value of  $b_e$  is approximately  $0.2b$ , but for the moments in the transverse girders at the cable anchorages it is favourable to have the main girders as close to the edge as possible. Thus, in a given case, the optimum value of  $b_e$  must be determined by comparing different solutions where  $b_e$  is varied between zero and  $0.2b$ .

In bridges with a wide bridge deck, the span of the cross beams becomes considerable and a special load-distributing stringer along the centre line of the floor (as indicated in Figure 4.42) might therefore be favourable to reduce the moments from concentrated wheel loads. However, even without a special stringer, a favourable load distribution will be established by the concrete slab or the continuous ribs of an orthotropic floor.

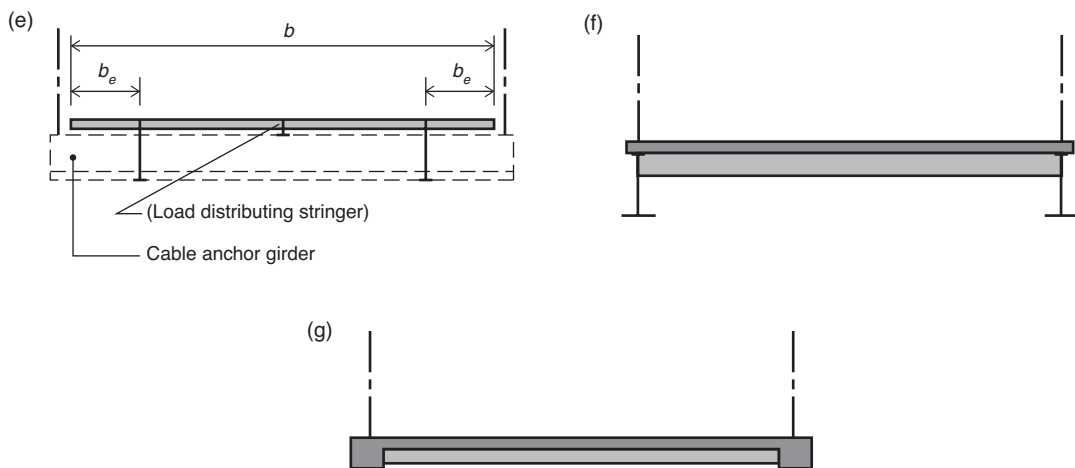


Figure 4.42 Three types of decks for bridges with cable systems rendering efficient vertical and torsional support

The open cross section shown in Figure 4.42(f) is based on the principle of composite action between the floor slab and the underlying plate girders, two in the longitudinal direction and numerous in the transverse direction. The main girders are here shown directly below the cable planes which will make the design of the cable anchorages relatively simple, but it will result in long spans for the cross beams. However, with the given arrangement the cross beams will be subjected to positive (sagging) moments over their entire length, which is favourable for a composite beam. The cross beams will have to be spaced at a distance of 3–5 m to limit the span of the concrete slab in the longitudinal direction of the bridge.

In Figure 4.42(g) is shown a basic cross section used in several cable stayed bridges with concrete decks. Here the heavy edge beams that are positioned directly under the cable planes constitute a considerable part of the total cross section.

With this arrangement the anchorage of the stay cables can be made in a very simple way, as the cables can be anchored by sockets at the bottom of anchor tubes embedded in the edge beams. Also the fact that a large portion of the cross section is present in the edge beams right at the cable anchorages ensures a most efficient transmission of the horizontal cable components to the deck.

To support the concrete slab between the edge beams, cross beams have to be positioned at a distance of 3–4 m. These cross beams might either be made as thin concrete ribs or as steel plate girders in composite action with the bridge slab. With steel cross beams, a reduced dead load is achieved.

A cross section similar to the one shown in Figure 4.42(e) was used in the Knie Bridge at Düsseldorf, as will be seen from Figure 4.43. The total width of the orthotropic steel floor is 29.3 m and the cantilevered parts are 3.9 m, i.e. a  $b_e/b$  ratio of 0.133. The two plate girders are each 3.2 m deep (1/100 of the main span length of 320 m) and the widths of the bottom flanges are 1 m.

The cable anchor girders are made as inclined box girders with the webs parallel to the cable axis, as seen in Figure 4.44. However, the webs of the anchor girders are only present in the cantilevered parts, so that the section between the two main girders only consists of the bottom flange and at the top a participating part of the orthotropic floor.

In the Knie Bridge the distance between the cable anchor points in the main span is as large as 64 m. This limits the number of anchor girders, but on the other hand it implies that each anchor girder will be subjected to large forces at each stay anchorage.

In multi-cable bridges the number of anchor girders will be large and this could make it advantageous to reduce the size of these girders by positioning the main girders closer to the edge of the bridge deck.

As explained earlier the arrangement with the longitudinal main girders positioned directly under the cable planes is often used in bridges with a composite deck. As an example, Figure 4.45 shows the cross section of the deck in the Alex Fraser Bridge in Vancouver.

In this bridge the distance between the two 2 m deep main girders is 28 m, and cross beams are positioned every 4.5 m. The bridge deck was made of pre-cast concrete slabs with a thickness of only 220 mm and each comprising half of the total deck width. Efficient joints between the pre-cast slabs and the steel girders were established by casting wide *in situ* joints with overlapping reinforcing bars positioned above the top flanges of the cross beams. The joints were subsequently subjected to a favourable compression as the compressive force in the deck gradually increased during the following steps of the deck erection.

A deck with two longitudinal main girders and closely spaced cross beams is often referred to as a “ladder deck”. With a ladder deck a very simple layout of the deck structure can be achieved, as seen in Figure 4.46. All cross beams have the

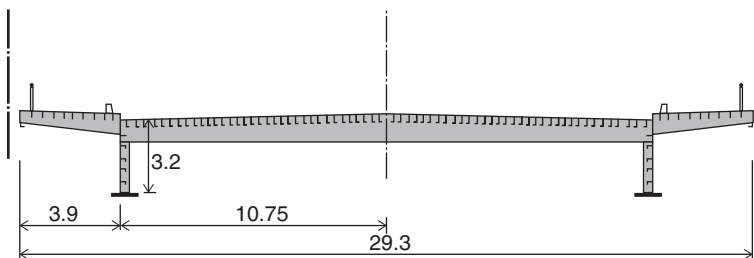
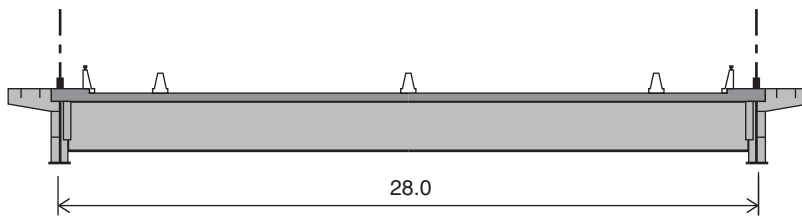


Figure 4.43 Cross section of the deck in the Knie Bridge at Düsseldorf



**Figure 4.44** Inclined anchor girders of the Knie Bridge



**Figure 4.45** Cross-section of the deck in the Alex Fraser Bridge in Vancouver



**Figure 4.46** Ladder deck seen from below (Yangpu Bridge)





**Figure 4.47** The deck of the Second Severn Bridge as seen from below

same dimensions and are equidistantly spaced. Also, they are only attached to the main girders on one side by a joint that shall primarily transfer a shear force

In the main span of the Second Severn Bridge the deck comprises two plate girders acting compositely with the concrete floor slab but here the main girders are positioned 4 m inwards from the cable planes requiring triangular brackets to be arranged for all cable anchorages at deck level (Figure 4.47). Another deviation is the application of transverse trusses instead of solid web cross beams.

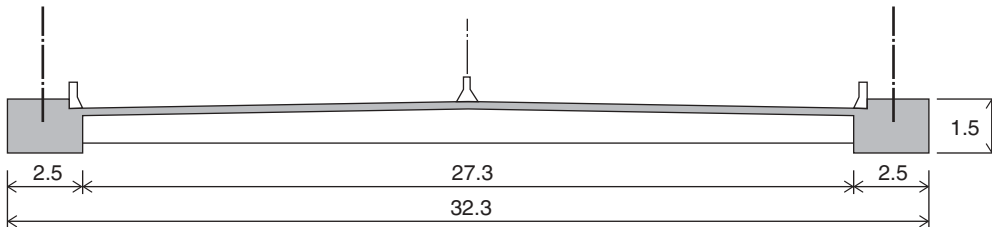
The cross section of the Napoleon Bonaparte Broward Bridge is shown in Figure 4.48. In this cross section two solid concrete main girders are positioned directly under each cable plane. The cross beams are designed as relatively thin concrete ribs with almost the same depth as the main girders.

Many cable stayed bridges carrying divided highways have been built with only one cable plane positioned above the central reserve of the roadway. In these bridges it is essential that the deck possesses a considerable torsional strength and stiffness, so it is indispensable to use a closed box section.

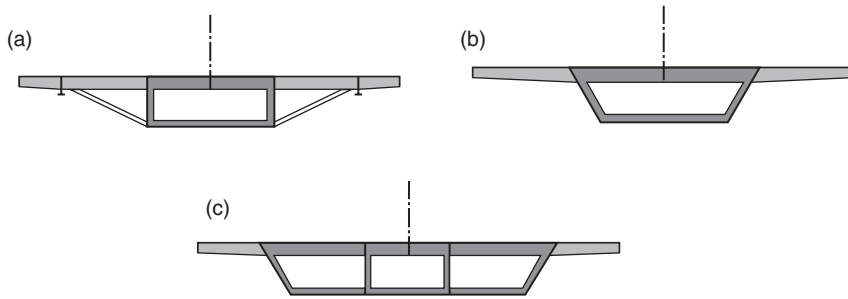
Figure 4.49 shows three basic cross sections to be found in cable stayed bridges with a central cable plane.

Figure 4.49 (a) shows the application of a narrow rectangular box girder with wide deck overhangs supported by inclined struts from the widely cantilevered cross beams to the bottom of the main box. At the points where the struts join the cross beams, a secondary longitudinal girder has often been added. If all cross beams are supported by struts, then the only function of the secondary, longitudinal girder is to distribute concentrated wheel loads, but if only some of the cross beams are supported by struts then the longitudinal girder will also have to fulfil the function of supporting the intermediate floor beams. The design of Figure 4.49(a) was widely used in German cable stayed bridges built in the 1960s, but the design is no longer being implemented due to the rather complicated structural composition.

Figure 4.49(b) shows the application of a wider trapezoidal box girder supporting the cross beams more efficiently so that the inclined struts can be omitted. This will simplify the structure by reducing the number of structural elements and



**Figure 4.48** Cross section of the Napoleon Bonaparte Broward Bridge



**Figure 4.49** Basic cross sections for a deck supported by a central cable plane

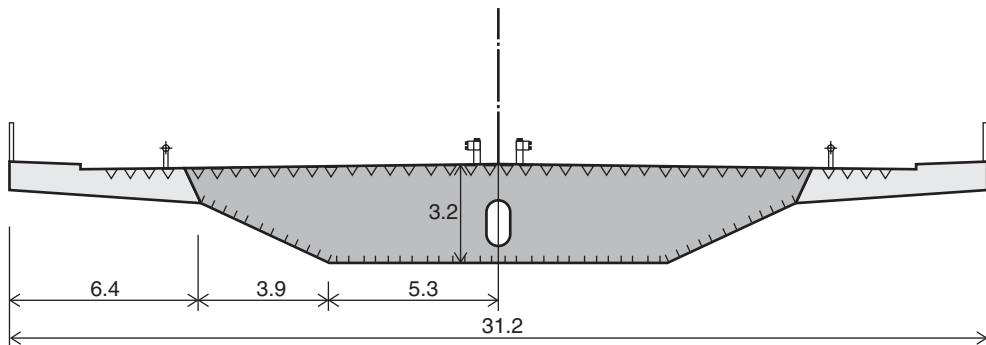
joints. In bridges with a considerable width, it might be advantageous to substitute the single-cell box by a multi-cellular box, as shown in Figure 4.49 (c), so that the cross beams become continuous with supports on several main girder webs.

The system with a central box and cantilevered floor areas supported by inclined struts and cross beams was used in the Friedrich Ebert Bridge at Bonn. Here inclined struts were positioned at every cross beam, as can be seen in Figure 4.50.

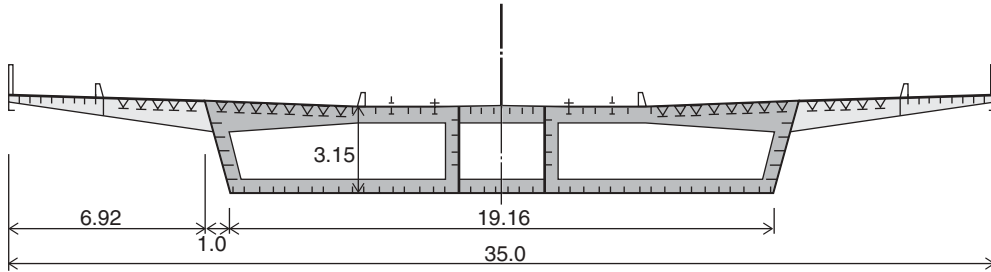
In the Erskine Bridge in Scotland the deck was made with a hexagonal shape, as shown in Figure 4.51. This shape was chosen to give a low drag coefficient ( $\sim 0.7$ ) and to reduce the cantilevered length of the cross beams. Inside the box girder, the cross beams are replaced by full diaphragms.



**Figure 4.50** Deck of the Friedrich Ebert Bridge with all floor beams supported by inclined struts



**Figure 4.51** Cross section of the deck in the Erskine Bridge



**Figure 4.52** Cross section of the deck in the Oberkasseler Bridge in Düsseldorf

The depth of the deck is 3.2 m corresponding to  $1/93$  of the main span length (305 m). This is a remarkable slenderness, taking into account that the Erskine Bridge only has one set of cable stays radiating from each pylon, so that the deck must span more than 100 m without any support from the cable system (see Figure 1.48).

The deck of the Oberkasseler Bridge in Düsseldorf (Figure 4.52) was designed as a tri-cellular box with a 35 m wide orthotropic floor. The width of the bottom plate is 19.2 m, and the outer webs are slightly inclined to give the box a trapezoidal contour. The depth of the box girder is 3.2 m corresponding to  $1/80$  of the main span length.

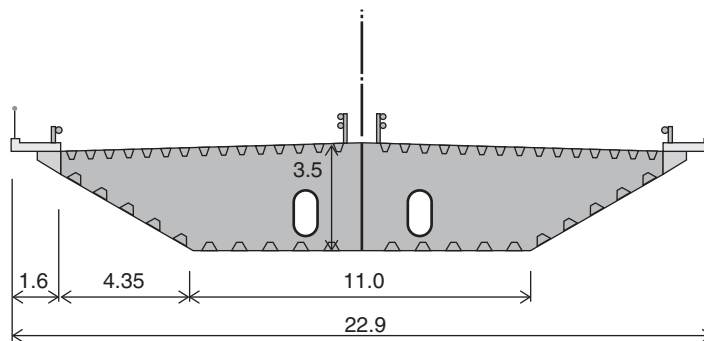
The tri-cellular box is characterized by a narrow central cell with a width of only 3.1 m. As this width corresponds to the width of the pylon at the roadway level, a moment rigid connection between the deck and the centrally positioned pylon is efficiently achieved. Furthermore, the narrow central cell makes it easier to arrange the cable anchorages inside the main box girder.

The deck of the Farø Bridge in Denmark consists of a bi-cellular box with a trapezoidal cross section as shown in Figure 4.53. In contrast to the boxes of the Erskine Bridge and the Oberkasseler Bridge, both with a considerable deck overhang, the Farø Bridge has its entire orthotropic floor slab above the box. The main reason for this arrangement is to get all stiffeners and diaphragms inside the box where corrosion protection can be established efficiently by dehumidifying the air. Therefore, painting only has to be carried out on the outside of the webs and the bottom plates, i.e. on very clean surfaces without the many intersecting plates found inside the box.

The width of the steel deck in the Farø Bridge is 19.7 m and it is designed with an orthotropic floor consisting of a 12 mm steel plate stiffened by trapezoidal stiffeners spanning 4 m between interior diaphragms made of 8 mm thick stiffened panels (Figure 4.54).

The combination of a central cable plane and a box-shaped deck is also found in cable stayed bridges of concrete, as is illustrated by the cross section of the Brotonne Bridge in France (Figure 4.55). Here the deck consists of a single cell trapezoidal box with a depth of 3.80 m corresponding to  $1/84$  of the main span length (320 m).

In bridges with two cable planes, box girders might also be used in the deck, although a torsional stiffness is not essential in this case due to the torsional support offered by the cable system. Figure 4.56 shows three basic

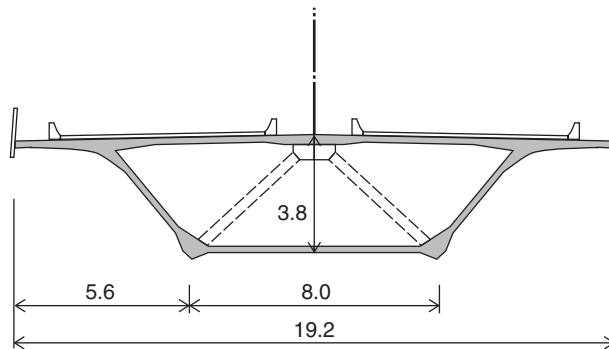


**Figure 4.53** Cross section of the deck in the Farø Bridge (Denmark)

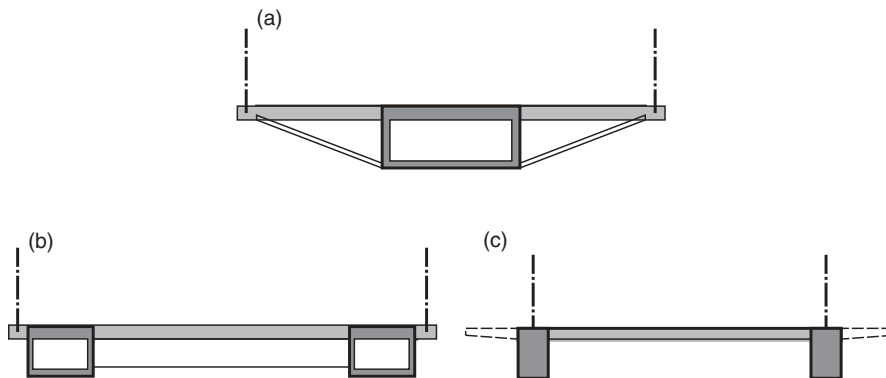


**Figure 4.54** Deck element for the Farø Bridge

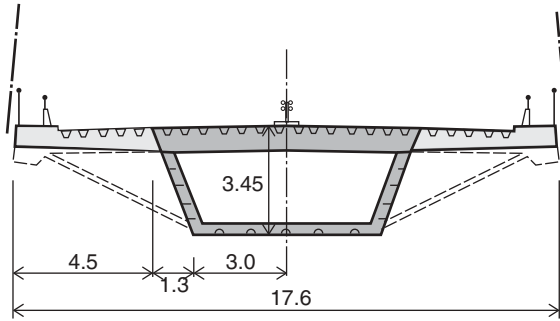
cross sections of decks with box-shaped main girders supported at both edges by the cable system. In (a) a relatively narrow box girder is positioned centrally whereas the cables are anchored to brackets outside the roadway area. As the load has to be transferred from the box girder webs to the cable system, cross beams with increased strength have to be positioned at the anchor points. Figure 4.55 indicates a solution where the additional strength is achieved by adding inclined ties from the bottom of the box to the anchor brackets at the points of cable attachment. Note the similarity between the cross section of Figure 4.49(a) and Figure 4.56(a), both with a narrow box girder and inclined members connecting the box girder bottom flange to the cross beams. Despite this similarity, the action of the inclined members is quite different, as those in Figure 4.49(a) are in compression and those in Figure 4.56(a) in tension.



**Figure 4.55** Cross section of the deck in the Brotonne Bridge



**Figure 4.56** Basic cross sections for torsionally rigid decks in bridges with double cable planes



**Figure 4.57** Cross section of the deck in the Köhlbrand Bridge

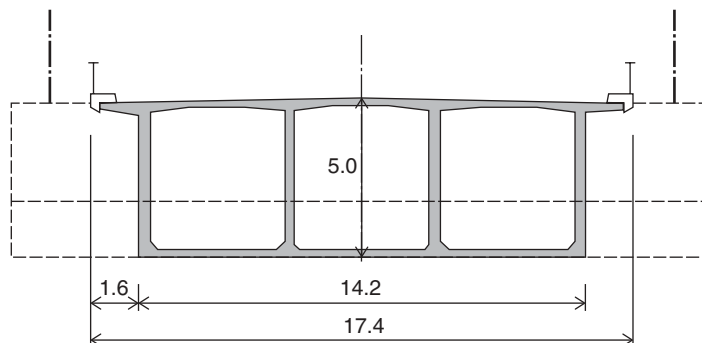
The cross section in Figure 4.56(b) contains two box girders positioned at the edges of the bridge deck. This implies that the main girders will be in more direct contact with the cable system as the cables can be attached almost directly to the outer box girder webs. However, to assure the transmission of forces from the inner webs to the cable system, heavy cross girders are still required at the anchor points.

Under (c) is shown a cross section with two box girders, but here each box is centred under the cable plane. Therefore, the transmission of forces from the main girder webs to the cable anchorages only requires diaphragms inside each box girder at the anchor points.

In bridges carrying a single continuous roadway the arrangement under (c) leads to an unnecessarily large area of the bridge floor as the areas outside the cable planes cannot be utilized to carry traffic. But in cases with separated lanes of traffic, e.g. a central roadway flanked by secondary lanes for pedestrians and bicycles, the area between the cable planes can be used for the roadway whereas the secondary lanes can be positioned outside the cable planes partly on cantilevered bridge floors, as indicated by dotted lines.

The cross section of the deck in the Köhlbrand Bridge, shown in Figure 4.57, corresponds in principle to the basic cross section of Figure 4.56(a). However, in the Köhlbrand Bridge the box girder is trapezoidal which improves the aerodynamic properties and results in a more efficient support of the cross beams (the width of the box at the top corresponds to half the width of the bridge deck whereas the width at the bottom only corresponds to a third of the deck width). The depth of the box girder is 3.45 m corresponding to  $1/94$  of the main span length (325 m).

The deck of the Maracaibo Bridge is made as a tri-cellular box of concrete (Figure 4.58). The width of the deck is 17.4 m whereas the box is 14.2 m wide. The depth of the girder is 5 m corresponding to  $1/47$  of the span (235 m). The large girder depth is due to the required moment capacity as each main span is supported by the cable system at two points only (Figure 4.59). The four webs of the box girder are each 250 mm thick, which is quite modest in relation to the girder depth of 5 m. The anchor girder is made with a solid cross section  $2 \times 5$  m and is heavily pre-stressed in the transverse direction.



**Figure 4.58** Cross section of the deck in the Maracaibo Bridge

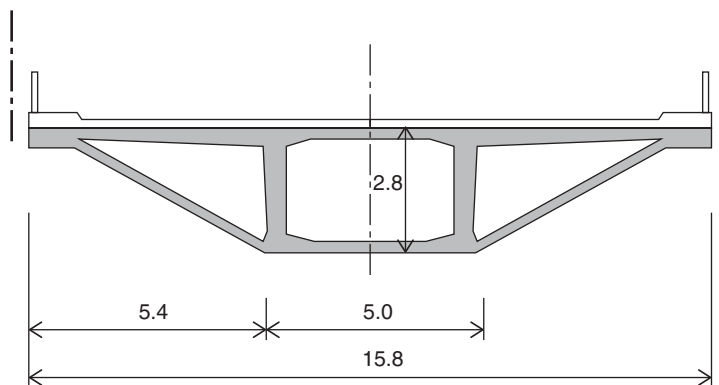


**Figure 4.59** Stays anchored to an inclined anchor girder (Maracaibo Bridge)

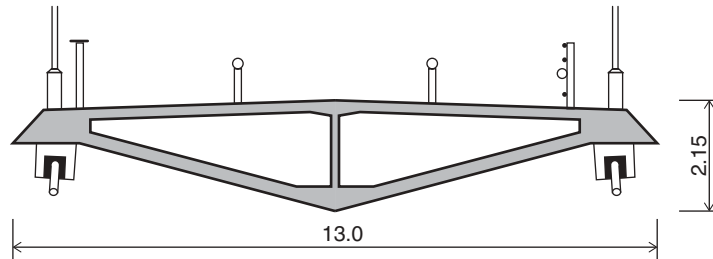
In the cable stayed bridge across the Donaukanal in Vienna (Figure 4.60), the deck is also made as a tri-cellular box but here with a trapezoidal cross section. The inner main webs are 500 mm thick whereas the outer inclined webs are made of prefabricated slabs with a thickness of only 150 mm. The depth of the girder is 2.8 m, corresponding to 1/42 of the main span length (119 m). Heavy transverse anchor girders are positioned at the cable anchor points and the stay cables are anchored to small steel brackets.

The Kvarnsund Bridge from 1991 has still the longest cable stayed concrete bridge span of 530 m. The deck has a triangular cross section with a total width of only 13 m (1/41 of the span) and a depth of 2.15 m (1/247 of the span). The deck (Figure 4.61) has a top slab with a thickness of 230 mm whereas the inclined bottom slabs are 150–180 mm thick. At the edges the deck has solid portions used for anchoring the stay cables. The shape of the deck in the Kvarnsund Bridge proved to be very favourable from the point of view of aerodynamic performance.

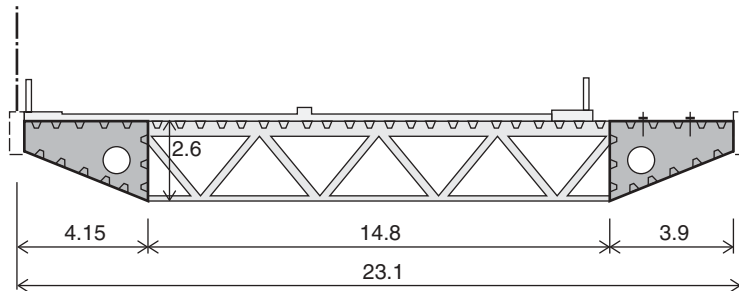
The Zarate-Brazo Largo bridges across the Parana River in Argentina show the application of a deck with two 3.9 m wide box girders at the edges (Figure 4.62). The box girders are here made with inclined bottom flanges claimed to improve the aerodynamic properties. The depth of the box girders (2.6 m) corresponds to 1/127 of the main span length (330 m). The bridge carries a four-lane roadway and a single railway track positioned asymmetrically, above one of the edge girders. The bridge floor is made as a composite slab consisting of an orthotropic steel plate with a concrete slab on top. In the railway area the tracks are laid directly with wooden sleepers on the steel floor. To support the bridge floor between the



**Figure 4.60** Cross section of the deck in the bridge across the Donaukanal in Vienna



**Figure 4.61** Cross section of the deck in the Kvarnsund Bridge



**Figure 4.62** Cross section of the deck in the Zarate-Brazo Largo Bridges (Argentina)

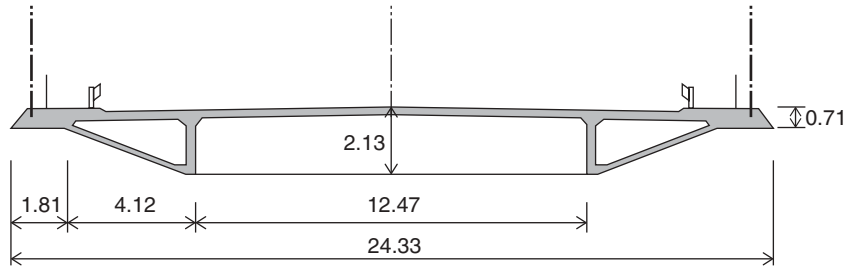
box girders, latticed cross beams are located at a distance of 3.14 m except at the cable anchor points where the cross beams are made as plate girders with solid webs.

Due to the eccentric load from the railway a lateral bracing is added between the two box girders at the bottom (Figure 4.63). This considerably increases the torsional stiffness of the entire deck.

Two box-shaped edge girders were also applied in the Pasco–Kennewick Bridge in the USA (Figure 4.64). However, here the edge girders are of triangular shape and the entire deck is made of concrete. The deck is 2.13 m deep, corresponding to 1/140 of the main span length (299 m). The floor slab with a thickness of 200 mm is supported



**Figure 4.63** Lower lateral bracing in the Zarate-Brazo Largo Bridge to increase torsional stiffness of the deck



**Figure 4.64** Cross section of the deck in the Pasco-Kennewick Bridge (USA)

by cross beams 2.74 m apart. Outside the edge girders the thickness of the floor slab is increased to 710 mm to allow the anchoring of the stay cables.

The Yangpu Bridge in Shanghai has a deck with two box-shaped main girders acting compositely with the concrete slab forming the bridge floor (Figure 4.65). The total width of the deck is 32.5 m including the fairings outside the railings. The stay cables are anchored inside the main girders positioned so that it has been possible to have 2.6 m wide pedestrian lanes outside the cable planes. Between the two main girders a large number of cross beams designed as composite girders are positioned to support the concrete floor.

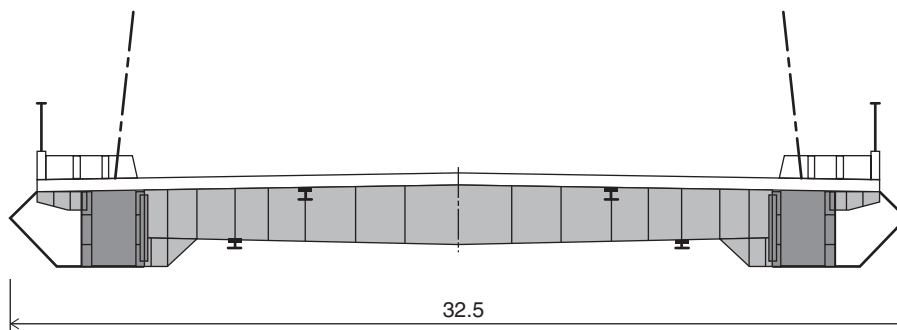
In the previous description of the deck cross sections it has been pointed out in some cases that the shape was chosen to improve the aerodynamic properties. To further emphasize this aspect of the design, Figure 4.66 shows a number of solutions arranged in order of streamlining. The bluff cross sections are characterized by an orthogonal geometry composed of vertical and horizontal planes. This leads to a rather high drag coefficient around 1.5 for the deck itself (railings and crash barriers will further increase the drag coefficient).

In the semi-streamlined cross sections the flow of the wind around the deck is improved by inclining the web plates. Even with moderate modifications of a bluff cross section, it is possible to reduce the drag coefficient to below 1.0.

The true streamlined cross sections are characterized by fairings with sharp leading edges to divide the air flow, and by web plates with a modest inclination in relation to the direction of the wind. This further decreases the drag coefficient to about 0.5 and at the same time the tendency to vortex-shedding can be reduced. The application of streamlined cross sections has therefore proved to be an efficient way to reduce the tendency to develop wind-excited oscillations.

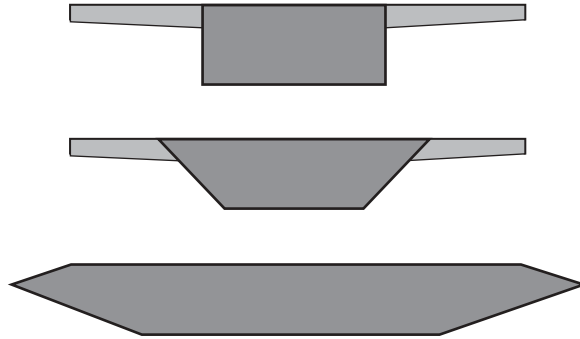
The principle of streamlining the cross section was first applied in the Severn Bridge built in the mid-1960s. The box has a hexagonal shape with cantilevered floors for the pedestrian lanes protruding from the sharp edges of the box girder, as seen in Figure 4.67. The depth of the box was 3.05 m corresponding to only 1/324 of the main span length (988 m).

A similar cross section was later used in the two Bosphorus Bridges and the Humber Bridge. However, in the Humber Bridge the depth was increased to 4.5 m and the width of the bottom flange was somewhat reduced (Figure 4.68). In the bridges with cantilevered floors under pedestrian lanes, the hangers were generally attached at the sharp edges of the box.

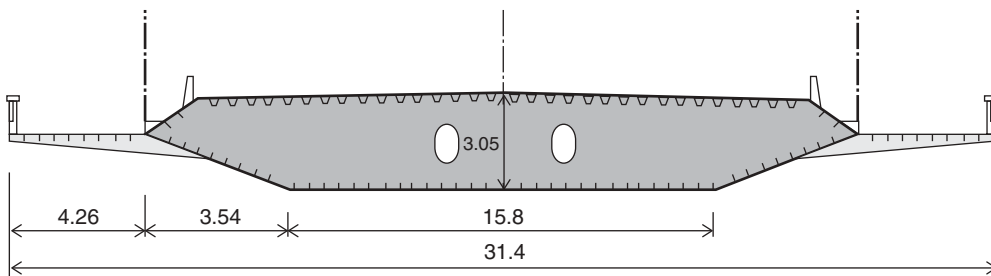


**Figure 4.65** Cross section of the deck in the Yangpu Bridge in Shanghai





**Figure 4.66** Box-shaped decks arranged in order of streamlining



**Figure 4.67** Cross section of the deck of the Severn Bridge

The increased depth of the box girder in the Humber Bridge was probably introduced to avoid too large a deviation from the slenderness ratio of the decks in the Severn and the Bosphorus Bridges. However, the increase was probably not necessary as a 3m deep box girder has later proved to be sufficient for the Runyang Suspension Bridge with a span of 1490 m (Figure 4.69).

In the Lillebælt Bridge where no pedestrian lanes were required, the deck cross section is of a slightly different shape (Figure 4.70). Other differences relate to the curved (and costly) transitions between flange plates and the inclined, as well as to the position of the cable planes at the edges of the roadway rather than at the outer sharp edges of the box.

The first suspension bridge in Japan to be built with a wide box forming the deck was the Ohshima Bridge in the western route of the Honshu–Shikoku bridge links. The box of the Ohshima Bridge has an overall width of 20 m and a depth of only



**Figure 4.68** Erection unit for the Humber Bridge

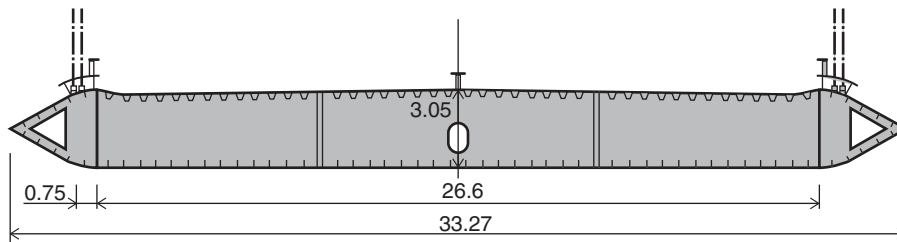


**Figure 4.69** Runyang Bridge

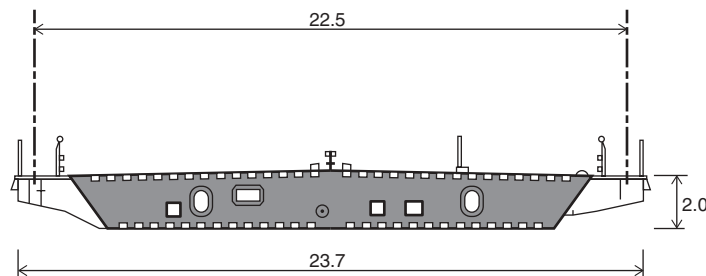
2.0 m (Figure 4.71). The hangers are attached along the edges of the bridge deck to brackets positioned in continuation of the main diaphragms inside the box.

It is interesting to compare the cross section of the decks in the Lillebælt Bridge and the Ohshima Bridge as they differ both in relation to ease of fabrication and in degree of streamlining. The Ohshima box is clearly simpler in fabrication as it is composed of plane panels and also the box is narrower than the total floor width. The box is of a 'traditional' trapezoidal shape with no 'wind nose' but with the limited span of 560 m (Lillebælt Bridge: 600 m) there proved to be no problems in achieving the required aerodynamic stability with the simple box girder layout.

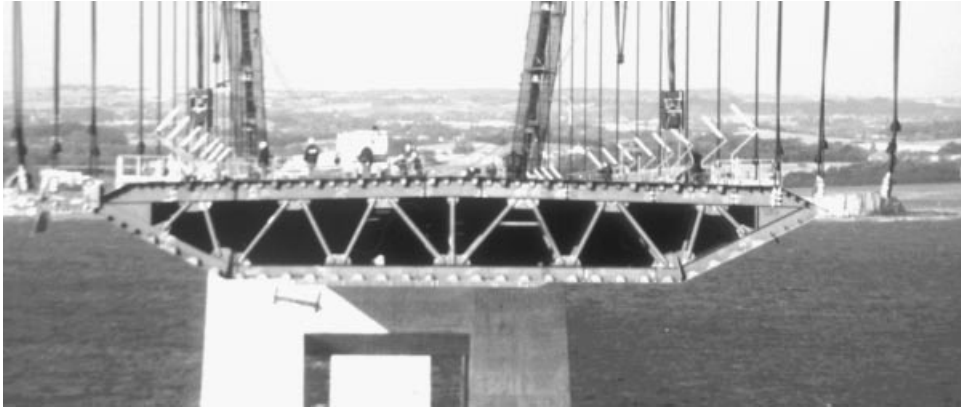
The deck of the Storebælt East Bridge has an overall width of 31 m and a depth of 4.4 m (Figure 4.72), corresponding to a depth-to-span ratio of close to 1/400. The East Bridge box is composed entirely of plane-stiffened panels with plate thickness 12 mm under the roadway area and 10 mm elsewhere. Generally the longitudinal stiffeners have a trapezoidal cross section and they are supported by diaphragms every 4 m.



**Figure 4.70** Cross section of the deck in the Lillebælt Bridge



**Figure 4.71** Cross section of the Ohshima Bridge



**Figure 4.72** The deck of the Storebælt East Bridge

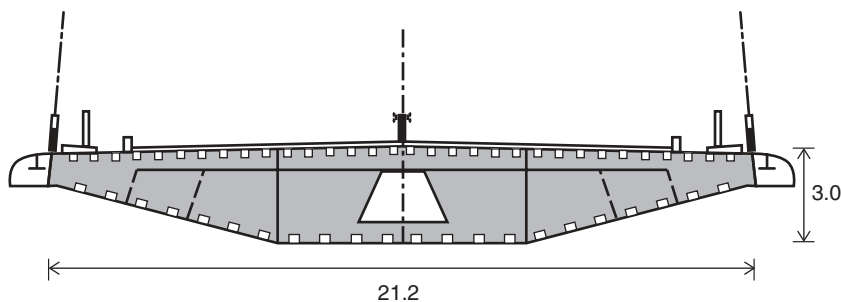
In medium span cable stayed bridges it has often proved unnecessary to streamline the deck as it has been possible to achieve aerodynamic stability with more bluff sections. However, when moving into the long span range, streamlining has also become a necessity for cable stayed bridges to reduce the drag coefficient and improve the aerodynamic performance. Note that in cable stayed bridges with long spans and small width-to-span ratios, the transmission of the lateral load by transverse bending becomes a problem, as described in Section 3.7.

The Normandy Bridge with its main span of 856 m has a deck made of steel in the central 624 m of the main span and of concrete in the remaining part of the main span and in the side spans. The depth of the Normandy Bridge box is 3 m (1/285 of the span) and the structural width 21.2 m. However, outside the structural part of the deck, curved fairings are added to improve the aerostatic and aerodynamic behaviour (Figure 4.73). The outer contour of the deck is the same for the steel and for the concrete parts so the transition from one structural material to another can only be detected when looking closely at the surface of the material (Figure 4.74).

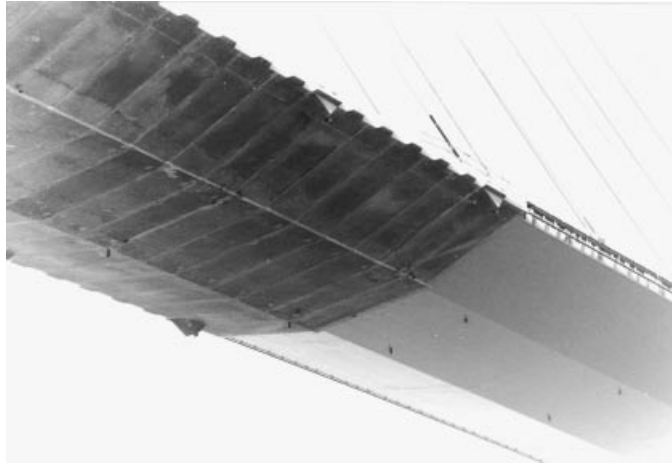
In the Tataru Bridge with its main span of 890 m, the major part of the deck is made of steel both in the main span and the side spans. Only in the outer regions of the side spans is the structural material changed to concrete to increase the weight and thereby reduce the need for a vertical anchoring. The box of the Tataru Bridge has an overall width of 25 m and a depth of 2.8 m and it is made in a streamlined shape (Figure 4.75).

The principle of shaping the deck of a cable supported bridge in such a way that a sufficiently high critical wind speed is achieved without an excessive increase of cross sectional dimensions was carried to a climax during the very elaborate investigations at the end of the 1980s for a bridge across the Messina Strait between Sicily and continental Italy.

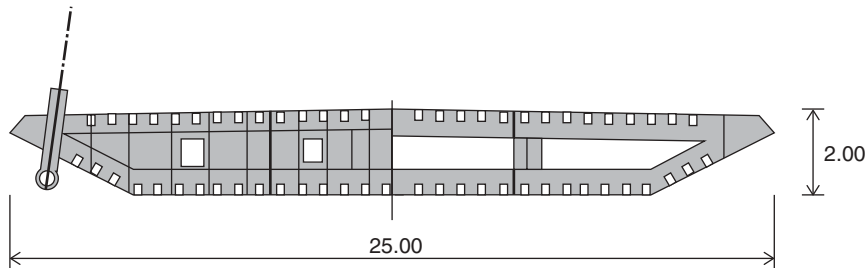
In cross section the Messina Bridge deck was composed of three shallow boxes characterized by a very high degree of streamlining through application of gently curved bottom plates (Figure 4.76). The longitudinal boxes were designed to be supported on the hanger cables by box-shaped transverse-girders at 30 m distance. The cross girders had a depth in the central portion of 4.7 m – about twice the depth of the longitudinal boxes.



**Figure 4.73** Cross section of the steel deck in the Normandy Bridge



**Figure 4.74** Transition between the concrete deck and the steel deck in the Normandy Bridge

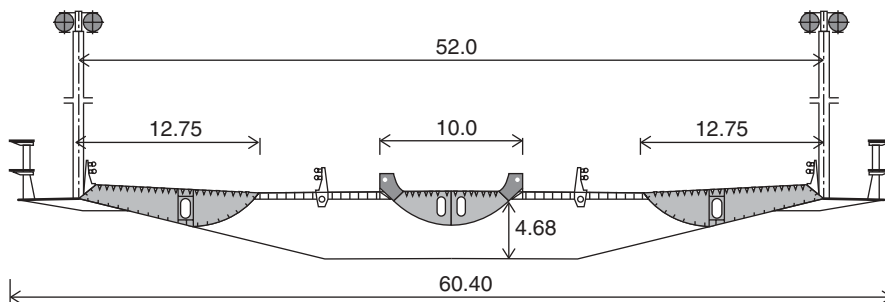


**Figure 4.75** Cross section of the deck in the Tataru Bridge

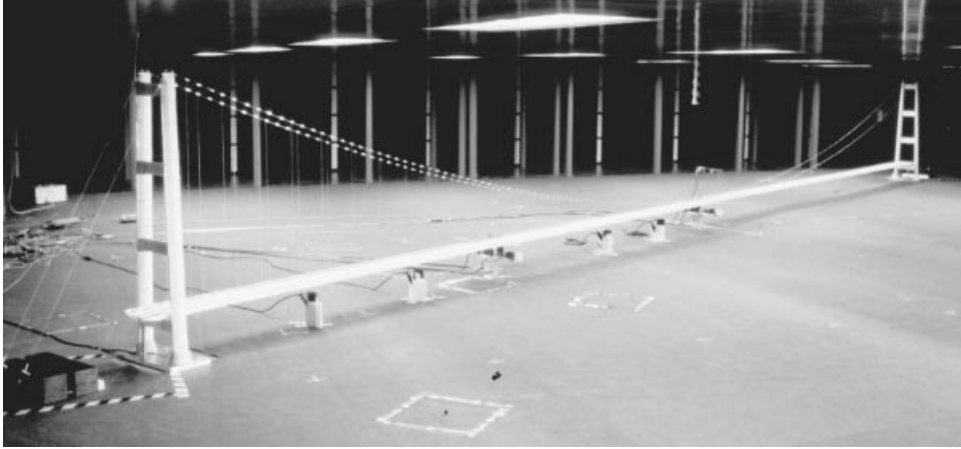
The Messina Strait Bridge is planned to carry a twin-track railway (on the central box) and two traffic lanes plus an emergency lane on each of the outer boxes. The Messina Strait Bridge design had an extreme deck width of 60.4 m and the distance between the two cable planes was as large as 52 m.

With a main span of 3300 m it was realized from the beginning of the investigation period that the issue of aerodynamic stability would be of paramount importance for the Messina Strait Bridge. The design of the deck was therefore gradually refined as the investigations on aerodynamic behaviour went on to reach the final level of perfection.

Numerous wind tunnel tests were carried out, and among these a full model test on a scale of 1:250 in the large wind tunnel at the Danish Maritime Institute. The aero-elastic model comprised only the main span with a length of 13.2 m in the model scale (Figure 4.77).



**Figure 4.76** Cross section of the deck in the Messina Strait Bridge as developed for the 'Progetto definitivo' in 1992



**Figure 4.77** Full bridge model of the Messina Strait Bridge in the large wind tunnel at the Danish Maritime Institute

A number of long span bridges with dual box decks (vented decks) have recently been constructed and more have been designed.

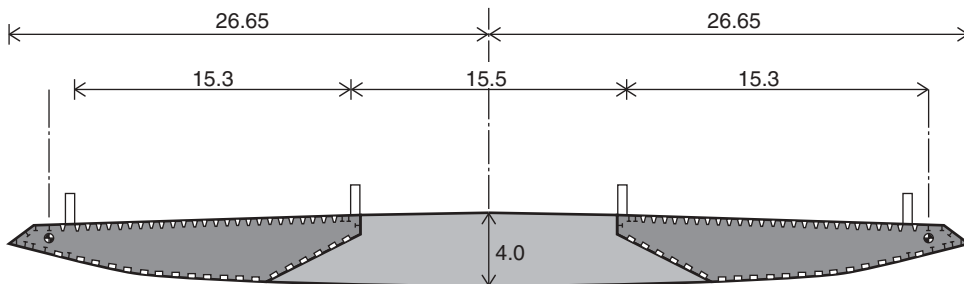
In the design competition in 2000 for the Stonecutters Bridge in Hong Kong SAR, the winning design was based on a dual box deck. Here the choice of a dual box configuration was actually driven by the design of the two 300 m high pylons each made as a simple vertical column of conical shape. The width of the gap between the two deck boxes, 14 m, was dictated by the pylon diameter at the level of the deck.

The dual box configuration gave a clear improvement of the aerodynamic behaviour, but it was actually found that the cable stayed Stonecutters Bridge with its span of 1018 m could have been designed with a mono-box deck if a different pylon configuration had been chosen.

In the original competition design for the Stonecutters Bridge, each of the two boxes had a continuously curved soffit but during detailed design the box shape was changed so that only the outer parts of the boxes were curved whereas the inner parts were plane (Figure 4.78). This design change simplified the joint between the longitudinal boxes and the cross beams, as well as improving the aerodynamic behaviour.

Coinciding with the design of the Stonecutters Bridge another major cable supported bridge was under design in Hong Kong SAR: the Tsing Lung Bridge (Figure 4.79). With a span of 1450 m that bridge would have had the third longest span of any suspension bridge at the time.

Due to its location in the vicinity of the International Airport in Hong Kong there was a height restriction for the pylons and as a consequence the main cable sag would have had to be limited to 1/15 of the span length – a smaller value than found in any other major suspension bridge.



**Figure 4.78** Cross section of the Stonecutters Bridge deck



**Figure 4.79** Design from 2002 for the Tsing Lung Bridge in Hong Kong. (Courtesy of Highways Department of HKSAR)

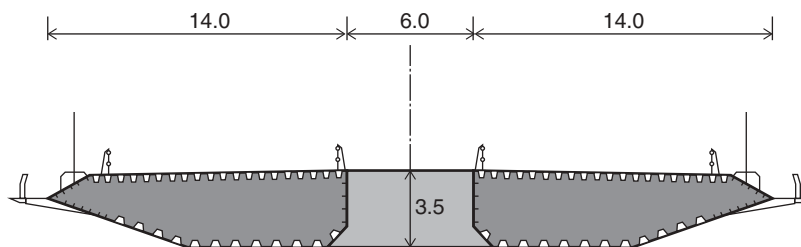
To achieve a satisfactory aerodynamic behaviour, the bridge deck had to be vented, i.e. composed of two individual boxes separated by a 10 m wide gap. The shape of the two boxes was chosen to be almost identical to the two outer roadway boxes in the Messina Bridge Design. The main reason for that undoubtedly was the fact that Dr William C. Brown, who had been a main contributor to the development of the Messina Bridge Design in the late 1980s, also had a very active role during the conceptual design of the Tsing Lung Bridge.

Unfortunately the Tsing Lung Bridge did not reach the construction stage after completion of the detailed design and it is uncertain when (and if) the project will be revived.

The largest Chinese suspension bridges, the Xihoumen Bridge, with its main span of 1650 m, has a deck composed of two box girders separated by a gap of 6 m and interconnected by cross beams at the hanger positions. This design proved to fulfil the requirement of a critical wind speed of more than 80 m/sec whereas the tests on a single box deck had failed to give adequate aerodynamic stability. This was actually expected because it was known that the critical wind speed of the Storebælt East Bridge had been determined to be 72 m/sec, sufficient to keep the specified critical wind speed for that bridge above 60 m/sec.

Each of the two box girders forming the deck of the Xihoumen Bridge are composed of plane stiffened steel panels to simplify fabrication (Figure 4.80).

The new East Bay suspension bridge at San Francisco is due to be completed in 2012. The design was driven primarily by the desire to create a visually impressive structure – and cost was apparently not an issue. This resulted in an unusual design, with one centrally located pylon and a self anchored suspension system (Figure 4.81). What appears as a pair of cables is actually one continuous cable that loops around the west end of the deck and has both ends anchored at the east end.



**Figure 4.80** The twin box deck of the Xihoumen Bridge



**Figure 4.81** The self anchored suspension bridge of the new East Bay Crossing at San Francisco (Image © Caltrans)

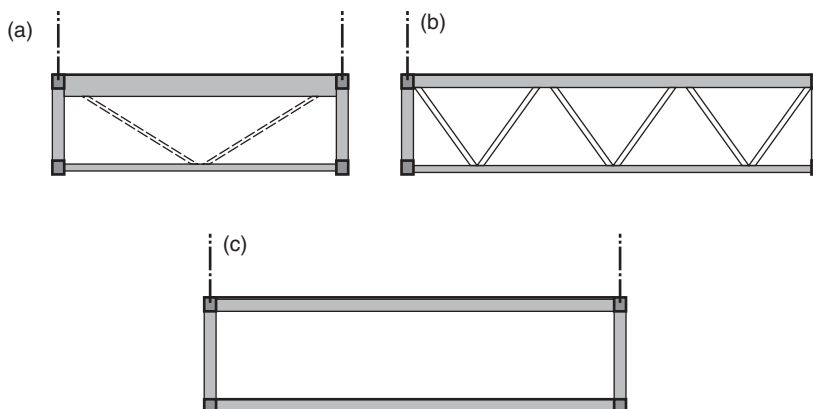
The bridge is asymmetric with a main span of 385 m and a single side span of 180 m. With such short spans and such a stiff structural system, the aerodynamic stability is of little concern. As for the Stonecutters Bridge, the central pylon forced the design to be two boxes with a gap of about 14 m between them. The girders are connected by 10 m wide transverse cross beams spaced at 30 m. There is a pedestrian/bicycle path cantilevered from the eastbound girder, balanced by a counterweight in the outer edge of the westbound girder.

#### 4.4.3 Cross section of stiffening trusses

The decks treated so far have all been made up of solid plates or slabs, but in the history of cable supported bridges, for a long time trusses were the preferred solution to achieve the required flexural and torsional stiffness of the deck structure, and even today the application of stiffening trusses will sometimes be preferred, e.g. in bridges carrying traffic at two levels.

In modern practice, the stiffening truss will be made as a space truss comprising four chords connected by four diagonal bracings: two vertical and two horizontal. However, the horizontal bracing at the roadway level will often be substituted by the bridge floor acting as a horizontal web between the top chords of the space truss.

If traffic is to be carried at one level only, nowadays the roadway will be positioned at the top, and a typical cross section for a bridge with a moderate deck width might therefore look as shown in Figure 4.82(a). Here the bridge deck is supported



**Figure 4.82** Basic cross sections for stiffening trusses

by cross beams spanning between the top chords of the vertical trusses, and the orthotropic floor is incorporated in the top chord.

To ensure the transmission of torsional moments, sway bracings must be arranged at a number of points throughout the spans. In general it will be adequate if these sway bracings (indicated by dotted lines) are at a distance of 50–100 m.

In bridges with a large deck width, the span of the cross beams will be considerable and it might therefore prove advantageous to make the cross section as shown in Figure 4.82(b). Here the cross beams are substituted by transverse trusses with a depth corresponding to the depth of the vertical main trusses. Besides carrying the vertical load on the bridge floor to the main trusses the transverse trusses double as sway bracings. Also in cross section (b) the floor should preferably be incorporated in the top chord.

In bridges with traffic at two levels, bridge floors will have to be positioned both at the top and at the bottom of the stiffening truss, as illustrated in Figure 4.82(c). The truss now comprises two vertical main trusses and two floors acting as chords and substituting the horizontal bracings.

In the two-level solution, sway bracings cannot be positioned inside the truss due to the clearance requirements above the lower floor. Consequently, the sway bracing must be replaced by a closed frame comprising the two cross beams and the intermediate verticals (or diagonals) of the main trusses.

In general, the distance between the nodes of the stiffening truss will exceed the optimum longitudinal span of the floor slab and consequently it will not be sufficient just to have the cross beams (or transverse trusses) supported at the nodes of the main trusses.

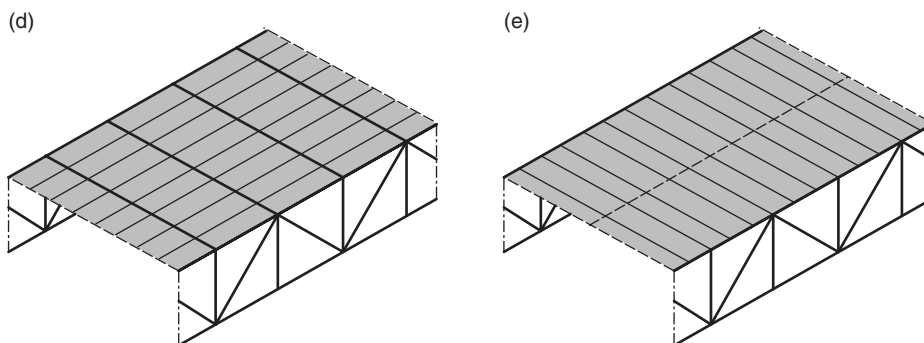
Figure 4.83 now shows two solutions to achieve the necessary support for the floor slab. In Solution (d) the cross beams at the nodes are supplemented by stringers spaced to give the slab adequate support in the transverse direction. This arrangement was preferred in earlier days when the bridge floor acted independently of the truss and it might still be a favourable solution if the floor consists of a concrete slab acting compositely with the stringers, the cross beams, and the top chords of the main trusses. But in bridges with the floor made of stiffened steel panels, Solution (d) would require that the ribs were oriented in the transverse direction, and this is generally less desirable.

In Solution (e), the cross beams are positioned not only at the nodes but also in between, so that the distance corresponds to the adequate span for the deck slab in the longitudinal direction. Thus, a stiffened steel plate would have its ribs oriented longitudinally.

With cross beams connected to the top chord between the nodes of the vertical trusses, the top chord must be designed for bending, thus requiring increased dimensions. In bridges with a large roadway width, it might be advantageous to add a load-distributing stringer at the centre line of the bridge floor (as indicated with a dotted line) to reduce the moments in the cross beams from concentrated wheel loads.

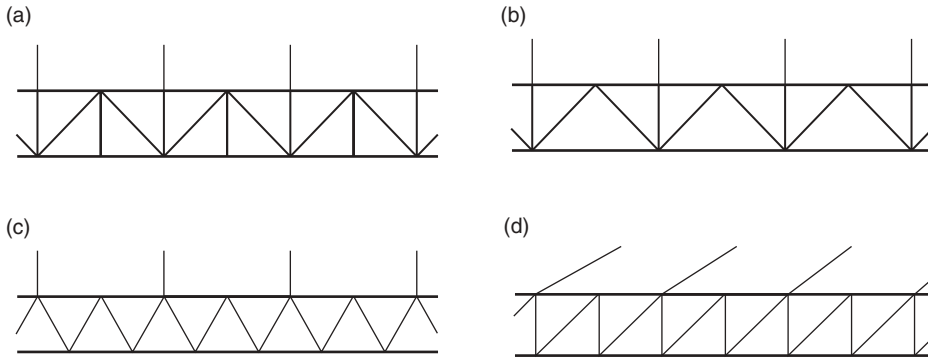
Note that Solution (e) cannot be combined with the cross section of Figure 4.82(b), as transverse trusses can only be positioned at the verticals of the main trusses. With a deck structure according to (e), cross sections of type (a) or (c) should consequently be used.

The bracing systems used in stiffening trusses are generally the same as found in other trusses with constant depth. In Figure 4.84 a number of relevant bracing systems for the vertical main trusses are shown.



**Figure 4.83** Two solutions for the arrangement of floor beams and stringers under the bridge floor





**Figure 4.84** Relevant bracing systems for the main trusses

The Warren truss with verticals at all nodes (a) has been widely used in suspension bridges as simple connections between the hangers and the truss can be made at the nodes where only a vertical intersects the top chord. At the same time transverse trusses as shown in cross section (b) of Figure 4.82 can be positioned at all nodes.

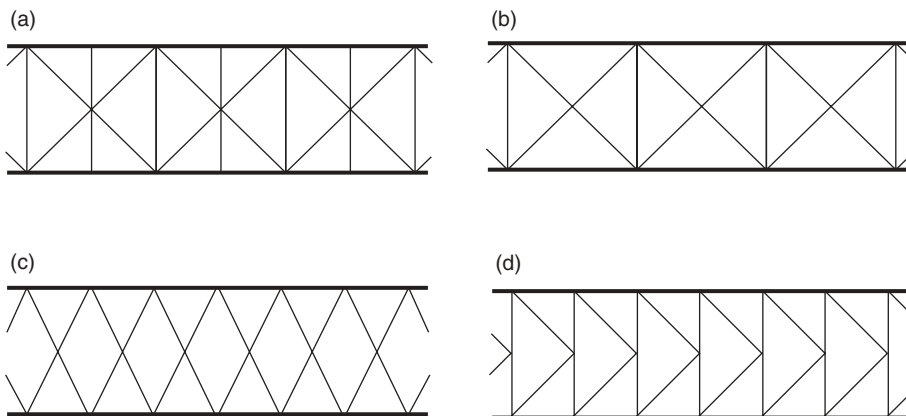
With the bridge floor at the top as shown in Figure 4.82(a), every second vertical can be omitted and the bracing system can then be simplified to the one shown in Figure 4.84(b).

The pure Warren truss without verticals (Figure 4.84(c)) offers advantages in relation to fabrication of the trusses, as simple nodes with a uniform geometry and only four members to be connected at each node can be used throughout the structure. On the other hand, complications might arise if sway bracing has to be arranged, due to the lack of verticals in the main truss. This bracing system is consequently most relevant in cases where the sway bracing is substituted by a cross frame, as indicated in Figure 4.82(c). The fact that the cross frame will not be positioned in a vertical plane is of less importance as the required frame action can easily be established through the inclined diagonals of the main trusses.

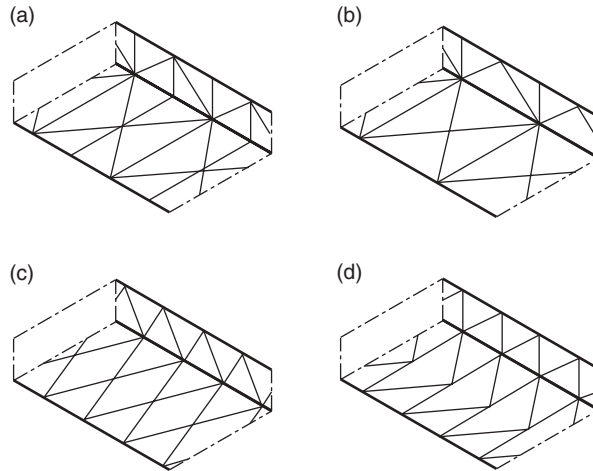
An equally simple uniform geometry of the nodes can be achieved by using a Pratt truss, as shown in Figure 4.84(d). As this has verticals, the arrangement of transverse bracings will be equally simple as in the Warren truss with verticals.

For the horizontal lateral bracing a symmetrical configuration will generally be applied. Figure 4.85 shows four solutions based on the application of X-bracing, diamond bracing or K-bracing. The number and position of 'verticals' in these bracings will be determined by the requirements of the transverse trusses, the sway bracing or the cross frames.

As the vertical main trusses and the horizontal bracing at the bottom can be viewed from the same position (below the bridge), it is advantageous to make the two bracing systems match. Thus, in Figure 4.86 is illustrated how the bracing systems of Figure 4.85 can match the vertical trusses of Figure 4.84.



**Figure 4.85** Systems for the lateral bracing between the main trusses



**Figure 4.86** Lateral bracing systems matching the bracing systems of the main trusses

To illustrate the application of the different bracing systems in actual structures, the following pictures show a number of stiffening trusses as used in cable supported bridges built in the past.

The two-level San Francisco–Oakland Bay Bridge (Figure 4.87) can be chosen as one of the many examples of the application of the Warren truss with verticals in the main trusses. As seen in Figure 4.87, the cross beams are arranged between the main truss nodes only, so that the concrete bridge slab must receive its main support from closely spaced stringers. Thus, the deck arrangement corresponds to that shown in Figure 4.83(e). In cross section the Bay Bridge corresponds to Figure 4.82(c) but in accordance with the practice of the 1930s, the bridge slabs did not participate in the truss, and horizontal K-bracing systems were therefore arranged between both the top chords and the bottom chords of the main trusses.

In the single deck Tancarville Bridge, the bracing system of Figure 4.84(b) was used, as seen in Figure 4.88. Here the verticals extend upwards from the lower nodes of the main trusses, and the hanger attachments are arranged at the simple nodes at the top of the verticals.



**Figure 4.87** Truss of the San Francisco–Oakland Bay Bridge

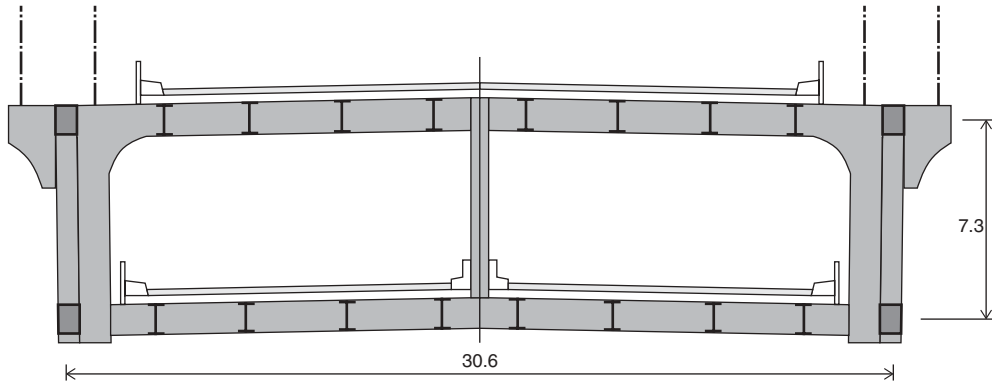


**Figure 4.88** Truss of the Tancarville Bridge

In the Verrazano Narrows Bridge, the main trusses are made as Warren trusses with verticals from the top chord nodes only, as seen in Figure 4.89. However, the verticals are primarily added to form the vertical elements of the heavy cross frames positioned at every hanger connection. The transverse elements of these cross frames constitute the cross beams, supporting the stringers under the concrete floor slabs (Figure 4.90). At the centre of the cross section the transverse girders of the cross frame are connected by a vertical member allowing a distribution of concentrated forces acting on one of the two floors. However, under full traffic load on both floors, the vertical deflections of the two transverse girders will be of equal size and the vertical member is then inactive. For the transmission of vertical loads to the main trusses it is, therefore, not important to connect the two transverse girders at their centres, but there might be a more pronounced effect on the diagonal stiffness of the cross frame.



**Figure 4.89** Truss of the Verrazano Narrows Bridge



**Figure 4.90** Cross section of the Verrazano Narrows Bridge

In the vertical Warren trusses of the Verrazano Narrows Bridge, the verticals were positioned so that they connect to the upper nodes of the diagonal bracing where also the hangers are anchored. All complicated joints between diagonals, verticals, top chords, transverse girders and cable anchor brackets are, therefore, concentrated in the same nodes.

In the Emmerich Bridge (Figure 4.91), a pure Warren truss was for the first time applied in a major suspension bridge, and it illustrates the pleasing appearance achieved by the simple truss geometry.

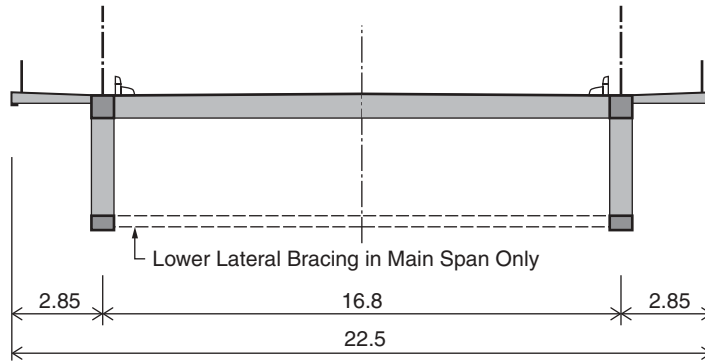
From the cross sections in Figure 4.92 it is seen that the bridge floor in the Emmerich Bridge is made as an orthotropic steel slab forming the top chord of the stiffening truss. In the main span a horizontal bracing is arranged between the two bottom chords to give the necessary torsional stiffness, but in the relatively short side spans with lengths of 151.5 m, the lower horizontal bracing is omitted as the torsional support from the cable system was adequate to give the desired strength and stiffness.

In the first double-level cable stayed bridge, the Rokko Bridge in Kobe (see Figure 1.54), the deck consists of two vertical trusses with participating orthotropic steel floors. The stiffened floor plates contain cross beams at a distance of 2.45 m – one-fifth of the bay length of the main trusses. At the bottom level the cross beams are cantilevered on either side of the trusses to support floors under the pedestrian and bicycle lanes (Figure 4.93).

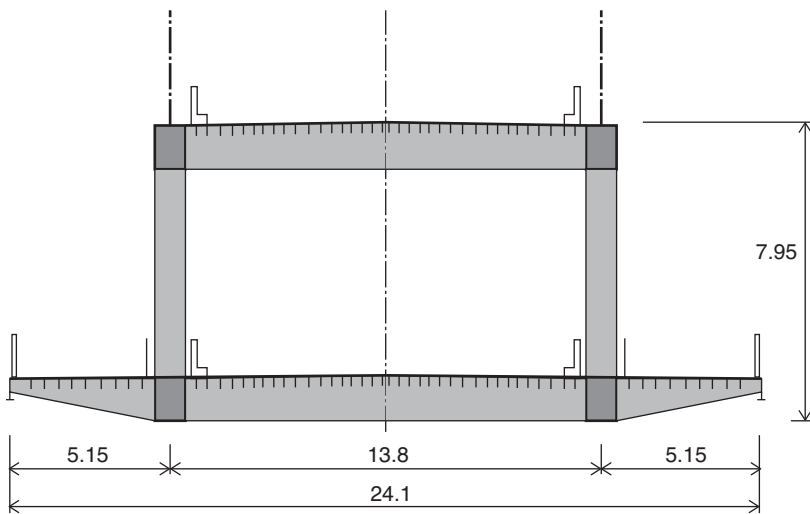
Another example of the application of the pure Warren truss is illustrated in Figure 4.94, showing the truss of the Higashi Kobe Bridge. In this bridge the cross section corresponds to the one shown in Figure 4.82(c) with both floors made as orthotropic steel slabs forming the top and the bottom chords of the stiffening truss (Figure 4.95). In this context it should be



**Figure 4.91** Stiffening truss of the Emmerich Bridge



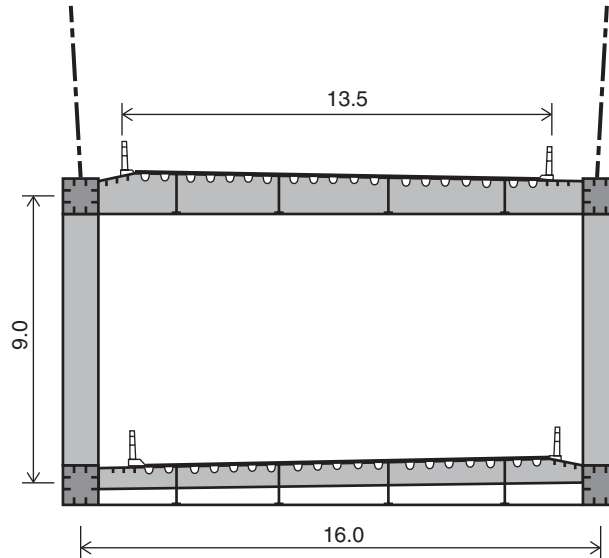
**Figure 4.92** Cross section of the Emmerich Bridge deck



**Figure 4.93** Cross section of the Rokko Bridge



**Figure 4.94** The stiffening truss of the Higashi Kobe Bridge as seen from below



**Figure 4.95** Cross section of the Higashi Kobe Bridge

emphasized that in a cable stayed bridge with axial forces induced into the deck, the participation of the floor slabs is especially advantageous.

In the Higashi Kobe Bridge the deck structures incorporate both of the systems of Figure 4.83 as the orthotropic slab is supported by four intermediate stringers at 3.4 m distance as well as by secondary cross beams at a distance of approximately 3 m.

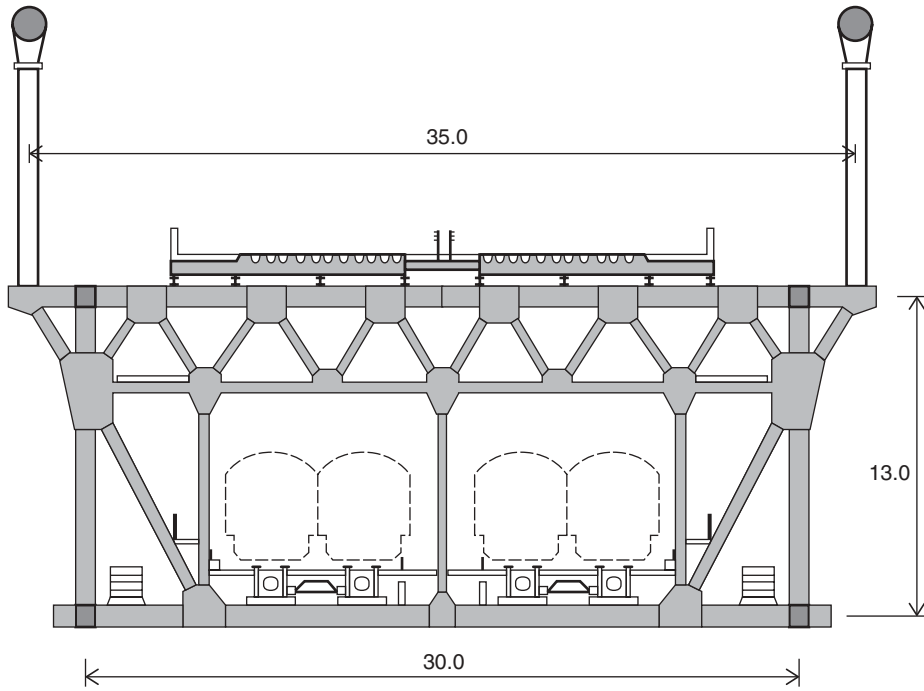
In road bridges with two levels, the widths of the two floors are generally the same, as the total number of lanes is divided equally at the two levels. But in combined road and railway bridges, where a two-level solution with the railway at the lower level functionally is very advantageous, the widths of the two floors often differ significantly. This is clearly illustrated by the cross section of the stiffening truss in the Bisan Seto Bridges in Japan (Figure 4.96). However, for these bridges a future addition of two separate tracks for the high-speed trains, the Shinkansen, has been anticipated so at that time the difference in deck widths will be less significant.

In most cases the railway floor will have to accommodate only two tracks, corresponding to a required width of 10–12 m, whereas the road floor will be 25–30 m wide to carry a dual two- or dual three-lane expressway.

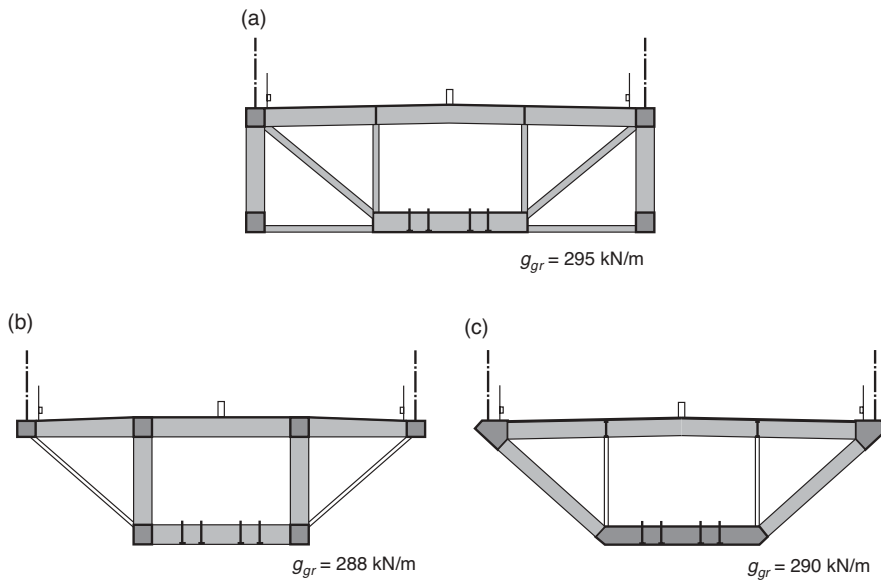
The special problems arising in such cases were studied in 1977–78 for a proposed bridge carrying both a motorway and a railway across the eastern channel of the Storebælt. In the bridge studies it was assumed that a 29 m wide dual three-lane motorway should be positioned at the upper level and an 11 m wide floor for a double-track railway at the lower level. Three different cross sections as shown in Figure 4.97 were investigated and, as seen from the calculated weights per unit length, only minor differences in quantities were found.

The cross section in Figure 4.97(a) corresponds to the layout generally used in road bridges with one or two floors, as the main trusses here are vertical and positioned directly under the cable planes. However, as the railway tracks have to be positioned at the centre to exclude excessive torsion from trains passing on one track, a quite heavy cross bracing must be added on both sides of the railway area to efficiently ensure the transmission of the heavy train load to the main trusses and the cable systems.

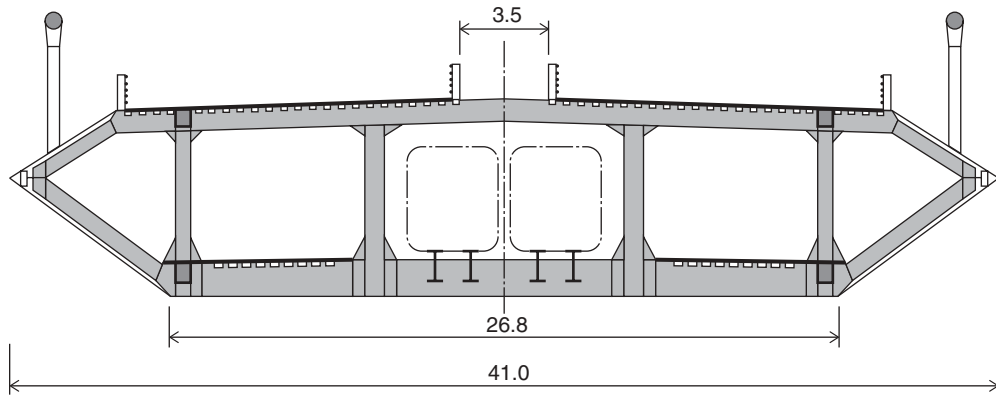
Cross section (b) is characterized by main trusses positioned immediately outside the railway area, which eases the transmission of the heavy train load to the trusses. With this arrangement the direct contact between the main trusses and the cable system is repealed and supplementary members would have to be added to ensure the transmission of forces from the main trusses to the edge beams at the roadway level where the hangers/stays have to be attached. As seen in Figure 4.97, inclined ties were proposed to connect the bottom of the main trusses to the edge girders.



**Figure 4.96** Cross section of the truss in the Bisan Seto Bridges



**Figure 4.97** Three cross sections studied for the Storebælt Bridge in 1977-78



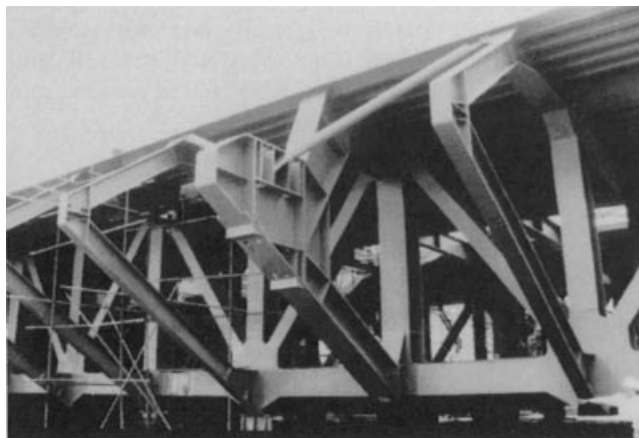
**Figure 4.98** Cross section of the deck structure in the Tsing Ma Bridge

In cross section (c) the main trusses were inclined transversally so that the entire cross section would be trapezoidal. This made it possible to maintain the direct contact between the main trusses and the cable systems and yet limit the width of the railway floor. Furthermore, by application of secondary vertical columns extending upwards from the edges of the railway floor, efficient support of the cross beams below the roadway floor could be achieved.

The studies for a combined road and railway bridge across the eastern channel of the Storebælt later became superfluous as it was decided by the politicians that the crossing should have separate road and railway links with the railway in a tunnel and the road on a bridge.

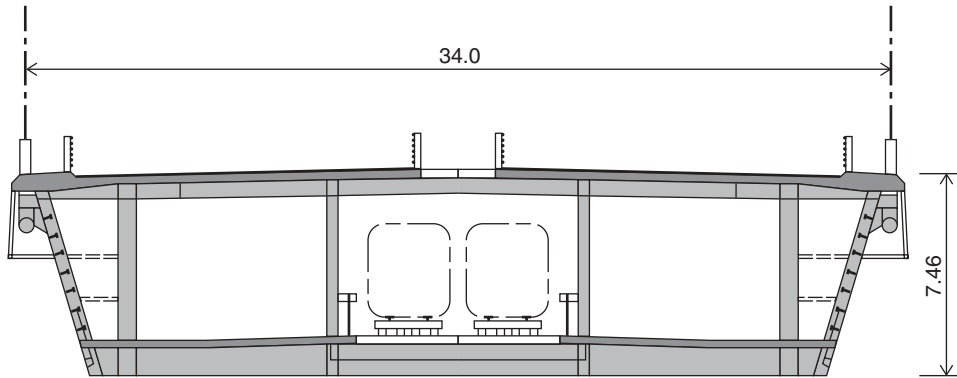
An unusual application of stiffening trusses is found in the Tsing Ma Bridge in Hong Kong. Here the difference in width between the upper roadway deck and the lower railway deck is utilized to add two typhoon-protected emergency lanes on either side of the railway tracks at the lower level (Figure 4.98). In the Tsing Ma Bridge the main trusses are positioned slightly inwards from the vertical cable planes and this has required the hanger cables to be anchored to triangular brackets with quite a complicated geometry and large eccentricities of the axial forces in the inclined members (Figure 4.99). Outside the main trusses the deck structure is, in the final stage, covered by non-participating fairings of corrugated 1.5 mm. thick stainless steel plates. These fairings improve the aerodynamic properties and protect the traffic lanes on the lower deck from side wind. Another measure to improve the behaviour under typhoon wind conditions relates to the arrangement of a 3.5 m wide gap between the two carriageways at the upper level.

With the solid fairings on both sides of the deck structure it could appear unnecessary to apply trusses between the two decks, as trusses are in most cases chosen primarily to give daylight and fresh air at the lower level. In the Tsing Ma Bridge



**Figure 4.99** Truss element with bracket for hanger attachment in the Tsing Ma Bridge



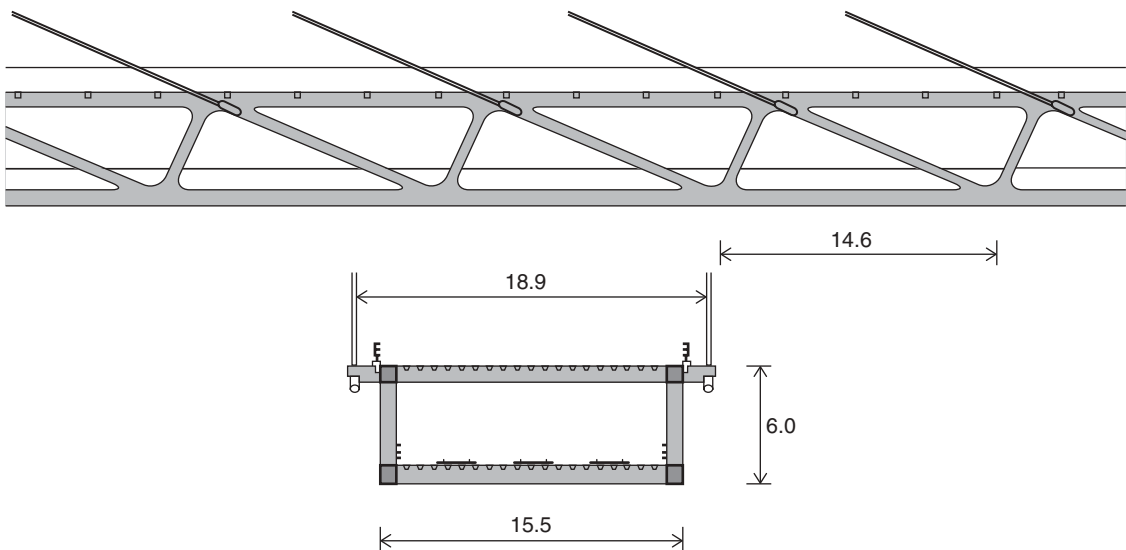


**Figure 4.100** Cross section of the deck structure in the main span of the Kap Shui Mun Bridge

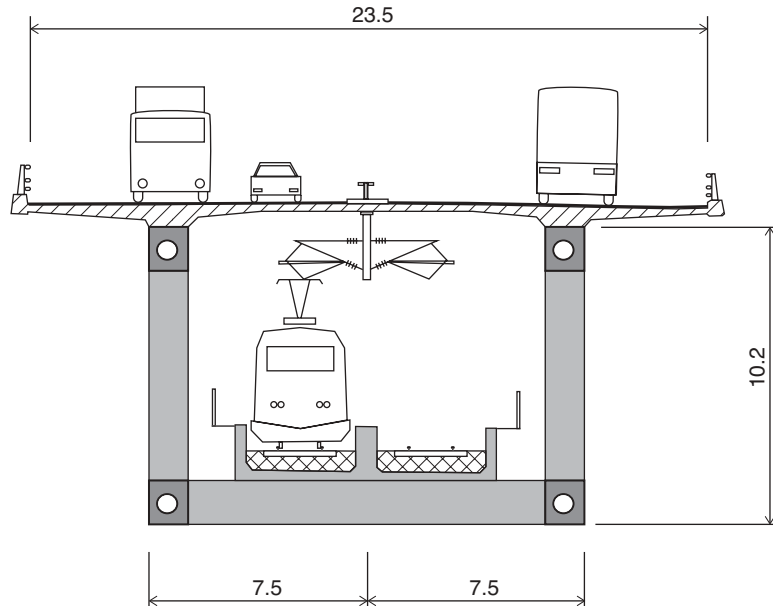
the traffic at the lower level would have had no disadvantage if the vertical trusses had been replaced by vertical or slightly inclined stiffened plates.

In the cable stayed Kap Shui Mun Bridge, located in almost direct continuation of the Tsing Ma Bridge, the connection between the upper and the lower decks is actually established by webs of stiffened steel plates (Figure 4.100). The deck of the Kap Shui Mun Bridge differs from that of the Tsing Ma Bridge not only by its clearer and simpler layout but also by having concrete floors acting compositely with a grid of longitudinal and transversal steel beams.

In Figure 4.84 a number of traditional bracing systems for the main trusses were shown. These were characterized by diagonals inclined  $45^\circ$  in the systems with verticals whereas the angle was  $60^\circ$  in the systems with diagonals only (the pure Warren truss). In a competition design in 1988 for a proposed replacement of the Williamsburg Bridge in New York, a new concept was presented for the bracing system of a truss in a double-deck cable stayed bridge (Figure 4.101). Here the truss geometry was harmonized with the geometry of the harp-shaped cable system by a design of the pure Warren truss with long diagonals in the direction of the stay cables and short diagonals in between. This resulted in a most pleasing and logic appearance of the truss and it also eased the detailing of the cable anchorages that could be positioned on small brackets outside the main trusses in the direction of the long diagonals.



**Figure 4.101** Truss geometry as proposed in a design for a replacement of the Williamsburg Bridge in the 1988 competition



**Figure 4.102** Cross section of the approach spans in the Øresund Bridge

The bracing system proposed for the Williamsburg Bridge replacement was apparently not appreciated at that occasion, but it was later reused during the design of the main span for the Øresund Bridge – at the time the longest of all cable stayed bridges carrying both road and railway traffic. The Øresund Bridge between Denmark and Sweden has a total length of 7.8 km and, of this length, the cable stayed portion at the navigation channel constitutes approximately 1 km, or only 13%. It was, therefore, obvious that the cross section of the two-level truss had to be chosen with due regard to the very long approach bridges to be constructed as continuous trusses with spans of 140 m.

This consideration led to a configuration with two vertical main trusses positioned immediately outside the clearance profile of the railway tracks at the lower level (Figure 4.102). With this layout it was not only ensured that the heavy train load should be carried a minimum distance transversally to the main trusses but also that the upper roadway slab could be efficiently supported with a reasonable ratio between the intermediate span above the railway tracks and the overhangs outside the main trusses. This made it possible to design the roadway floor with its total width of 23.5 m as a haunched and pre-stressed concrete slab supported only on the top chords of the main trusses.

To allow basically the same configuration in the cable stayed portion, it was decided to anchor the stay cables to triangular ‘outriggers’ so that the vertical cable planes could be positioned 3.5 m from the edges of the roadway deck (Figure 4.103).

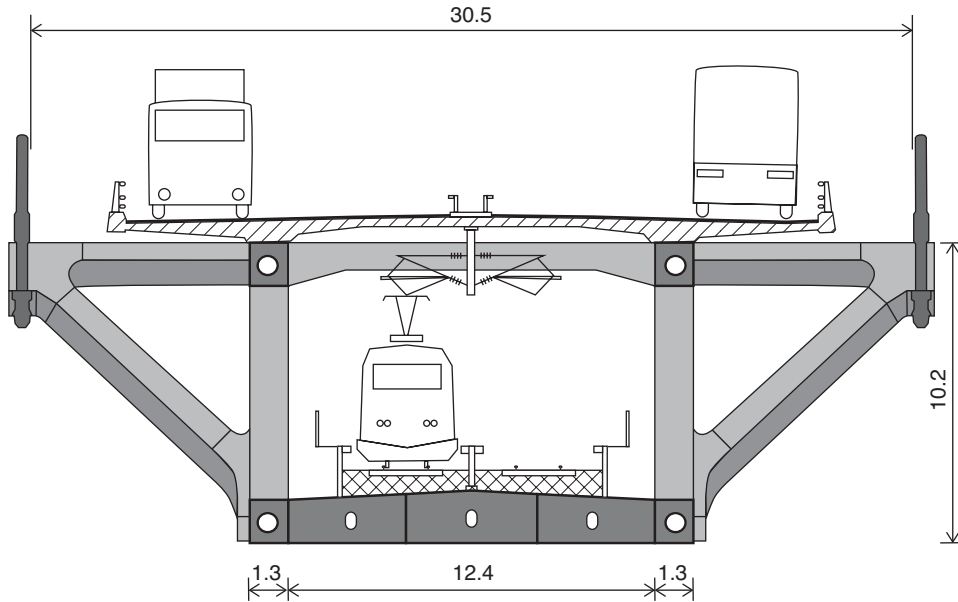
In the cable stayed portion of the Øresund Bridge the cross section of the deck consists of the upper concrete slab, the two vertical trusses and a shallow steel box beneath the lower railway deck.

In the approach spans, the main trusses are formed as pure Warren trusses without verticals and with diagonals at an angle of approximate  $45^\circ$  with the chords. This configuration is changed in the cable stayed bridge where the truss geometry is harmonized with the harp-shaped cable system so that long diagonals follow the stay cable inclination and short diagonals are oriented so that the node distance is the same as in the approach spans (Figure 4.104).

## 4.5 Partial Earth Anchoring

Figure 4.105 shows three ways to establish horizontal equilibrium of one girder half subjected to the pull of the stay cables.

- System A: Earth anchored system with tension throughout the deck.
- System B: Self anchored system with compression in the deck.
- System C: Partially earth anchored system with compression in the deck at the pylons and tension at midspan.

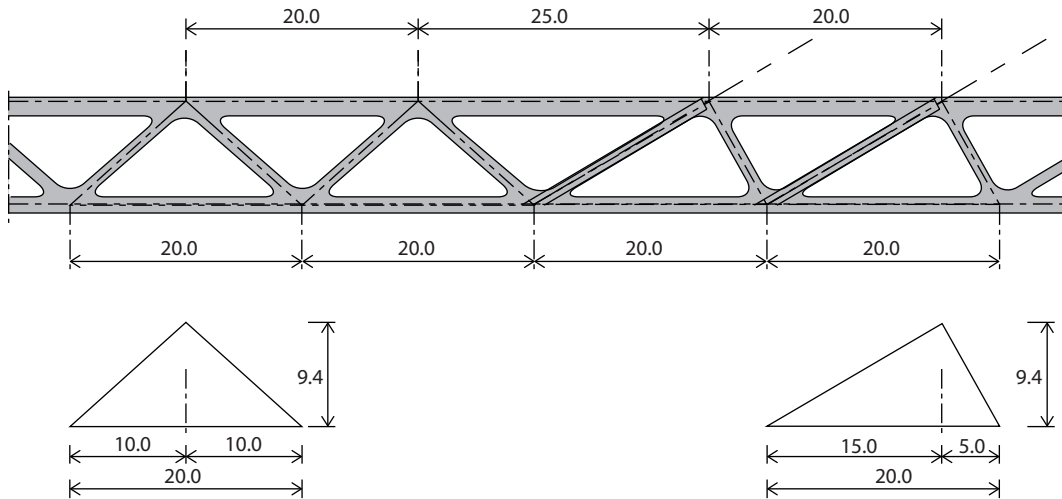


**Figure 4.103** Cross section of the deck structure in the cable stayed portion of the Øresund Bridge

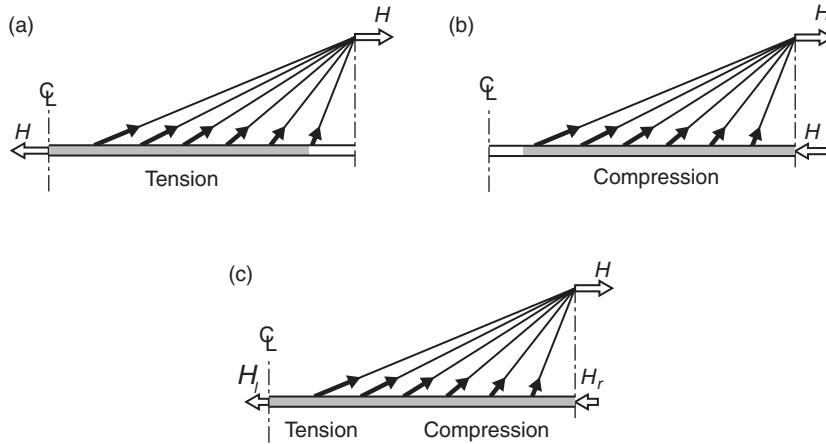
The three systems of equilibrium, shown in Figure 4.105, can be established by the choice of the supporting conditions for the deck and the attachment of the anchor cable at the ends of the side spans, as illustrated in Figure 4.106.

In System A the deck has expansion joints at the pylons and fixed bearings at the ends. This leads to an earth anchored system with zero axial force at the pylons and tension throughout the length of the deck.

In System B the deck is continuous from one end to the other and supported by movable bearings on both end piers and on one of the pylon piers. As the anchor cable furthermore is attached directly to the deck, the system becomes self anchored with compression in the deck.



**Figure 4.104** Truss configuration in the transition zone between approach spans and cable supported spans of the Øresund Bridge

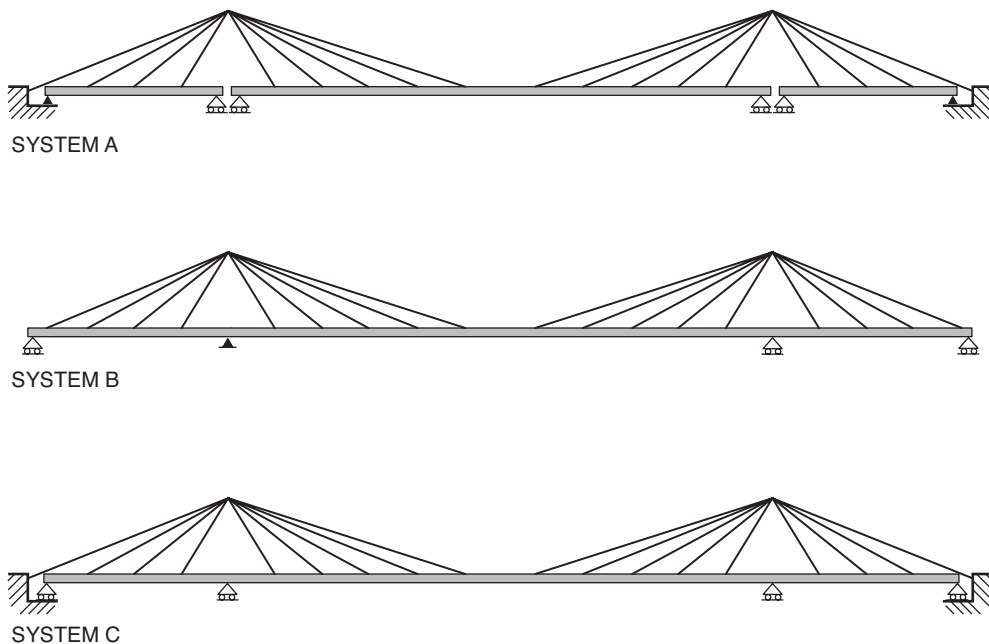


**Figure 4.105** Three possibilities of horizontal deck equilibrium

In System C the deck is also continuous and exclusively on movable bearings, but here the anchor cable is attached to the end pier (anchor block). This implies that tension will be induced at the centre of the main span whereas the side spans and the outer parts of the main span will be in compression.

In the following some characteristics of the three systems will be revealed by investigating systems that are idealized to be continuous and subjected to a uniform load  $q$  along the entire length of the deck.

The axial force in the deck can be determined by integrating  $dN = q(x/h) dx$ , where  $dN$  is the axial force produced by the load  $q dx$  in the distance  $x$  from the pylon, as indicated in Figure 4.107.



**Figure 4.106** Three structural systems for bridges with fan-shaped cable systems

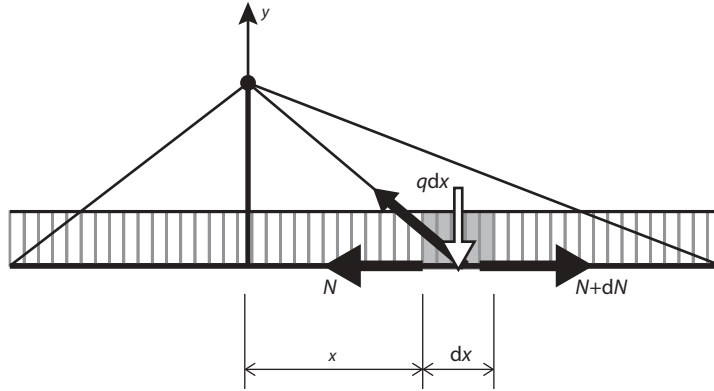


Figure 4.107 Transmission of load  $qdx$  acting on a length  $dx$  of the deck

For the three systems of Figure 4.106 the boundary conditions that determine the axial force diagrams will be:

- System A:  $N = 0$  at the pylons
- System B:  $N = 0$  at the main span centre
- System C:  $N = 0$  at the ends of the side spans.

With these conditions the axial force variation is determined by:

$$N(x) \begin{cases} \int_0^x dN = \frac{1}{2} \frac{q}{h} x^2 & \text{System A} \\ - \int_x^{l_m/2} dN = \frac{1}{2} \frac{q}{h} \left( x^2 - \frac{l_m^2}{4} \right) & \text{System B} \\ - \int_x^{l_a} dN = \frac{q}{h} (x^2 - l_a^2) & \text{System C} \end{cases} \quad (4.6)$$

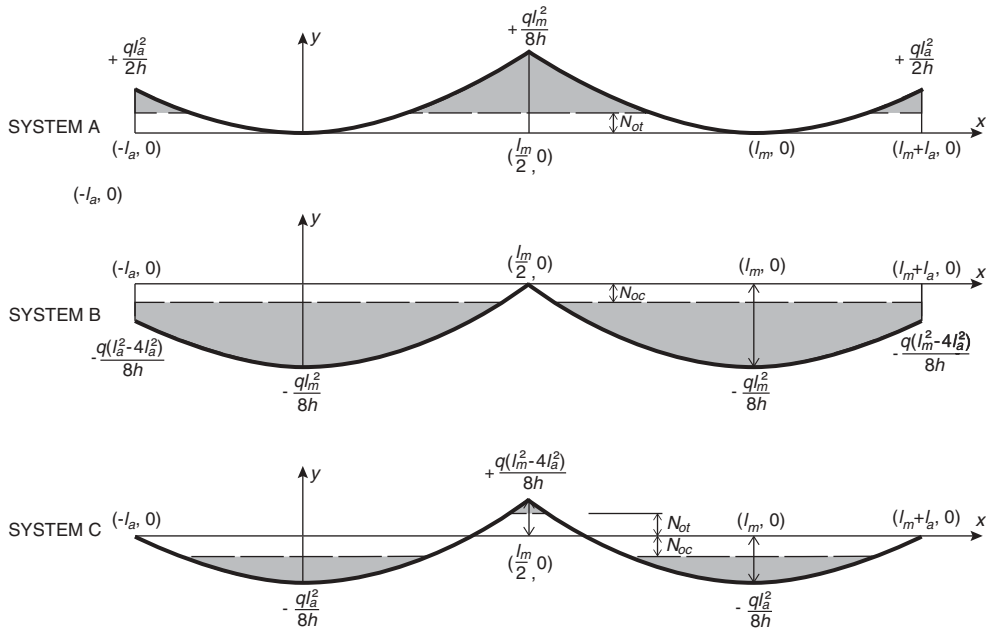
The corresponding axial force diagrams are shown in Figure 4.108.

As will be seen, the axial forces of the three systems differ significantly both in sign and size. Thus, the quantities required to enable the deck to transmit the axial forces will vary from system to system.

An approximate estimate of the quantity of additional steel or concrete required in the deck to transmit the normal forces can be based on determining the area  $A_N$  under the normal force curve:  $A_N = \int N(x) dx$ . However, as the deck always possesses a capability of transmitting axial forces up to certain values  $N_{0c}$  (compression) and  $N_{0t}$  (tension), without requiring strengthening, only areas of the axial force curve outside these values should be included in  $A_N$ , i.e. the shaded areas in Figure 4.108.

For a bridge with a side-to-main span ratio of 0.25 and  $N_{0c} = N_{0t} = N_0$ , the variation of  $A_N$  with the relative main span length  $l/l_0$  is shown in Figure 4.109. Here  $l_0$  is defined as the maximum main span length that can be allowed without requiring strengthening of the deck sections in Systems A and B.

From Figure 4.109, it will be seen that System B consumes considerably more material than the other systems for span lengths exceeding the value  $l_0$ . For example, with  $l = 4l_0$  the additional material required for the deck of System B will be eight times larger than for System C. However, the fact that System B is self anchored will lead to savings in the substructure subjected to vertical forces only, and these savings might very well balance out the additional cost of the deck. This will be especially true for moderate spans such as those found within present cable stayed bridges with relative span lengths  $l/l_0$  typically in the interval from 1 to 2.



**Figure 4.108** Axial force diagrams for the deck of the structural systems in Figure 4.106 (idealized to have continuous fans)

With increasing span lengths, the savings in the superstructure of System C will be more dominating, and therefore eventually make this system more competitive.

#### 4.5.1 Limit of span length for self anchored cable stayed bridges

The increase from the 180 m span of the Strömsund Bridge (1955) to the 1088 m span of the Sutong Bridge (2008) has been possible without deviating from the self anchored concept. A further span increase with the self anchored concept up to around 1500 m appears to be realistic but above that the situation is not so clear.

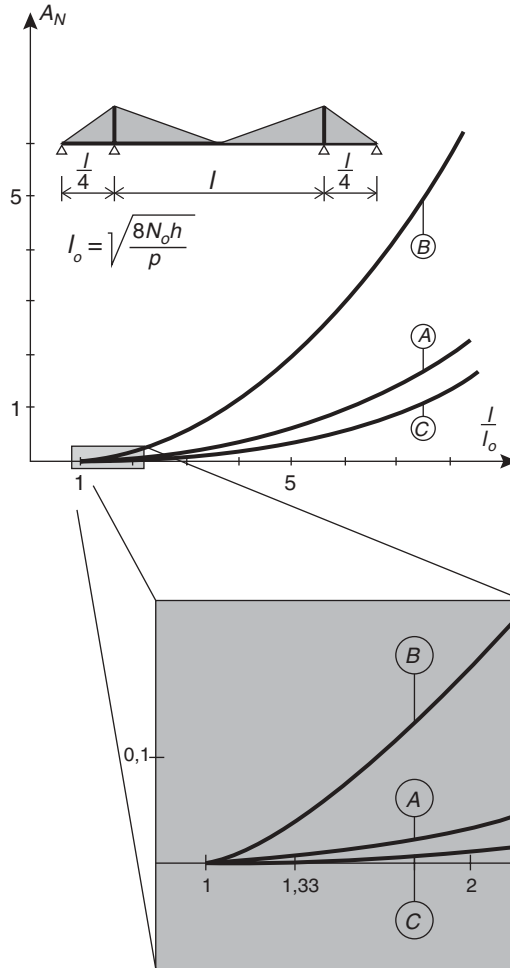
A cable stayed bridge with a span beyond the present maximum will of course always be evaluated against the earth anchored suspension bridge that for more than 70 years has had total dominance within spans of more than 1100 m.

It is obvious that the self anchored cable stayed bridge will be more sensitive to further span increases than the earth anchored suspension bridge in a number of respects.

The more important issues are as follows:

- (1) The axial compression in the deck of a cable stayed bridge will increase with the span and eventually require a substantial strengthening followed by a weight increase. In a suspension bridge the deck will be subjected to only minor axial compression – if any.
- (2) During a free-cantilever erection of a cable stayed main span, the lateral stability will depend entirely on the flexural strength and stiffness of the deck in the transverse direction. In a suspension bridge the lateral stability is safeguarded by the pendulum effect so the deck does not have to be cantilevered from the pylons.
- (3) The free length of the longest stay cables will be several times that of the longest hanger cables in a suspension bridge. Problems related to individual cable vibration will therefore be more severe in cable stayed bridges.

For the reasons outlined above it is clear that it will be more problematic to increase the span of self anchored cable stayed bridges beyond the present limits than to expand the span range of suspension bridges upwards.



**Figure 4.109** Variation of the area  $A_N$  under the axial force curves of Figure 4.108, indicating the amount of structural material required to make the deck able to transmit the normal forces

**4.5.2 Axial compression in the deck of the self anchored cable stayed bridge**

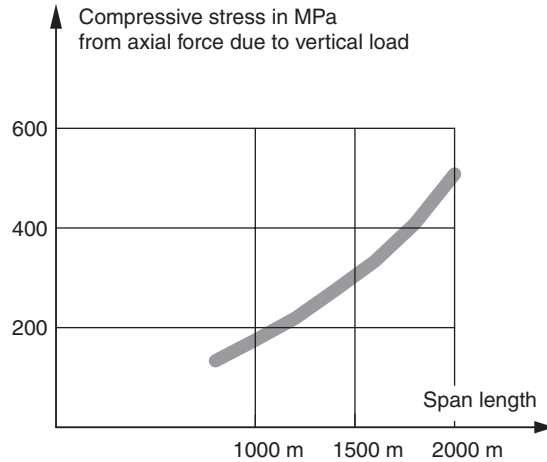
In a self anchored cable stayed bridge with a fan shaped cable system the axial compression  $N_{max}$  at the pylon can be expressed:

$$N_{max} = M_{cantilever}/h$$

where  $M_{cantilever}$  is the cantilever moment at the pylon from the vertical load on the adjacent half span and  $h$  the vertical distance from the deck to the centre of the cable anchorages at the pylon top.

As the cantilever moment increases with the span squared and the height generally increases proportional to the span, it is easily deduced that the axial compression will increase in proportion to the span – if the vertical load is constant per unit length. This is, however, not the case as the dead load will increase by at least the span squared for the cable system, as well as by a possible strengthening of the deck cross section.

The increase in axial compression can to a certain extent be counteracted by the use of higher strength steels. However, if the span is increased towards 2000 m, then the axial compression will be so large that switching to higher strength steels in itself will not be sufficient.



**Figure 4.110** Maximum compressive stress in the deck cross section due to the axial force induced by the horizontal components of the stay cable forces.

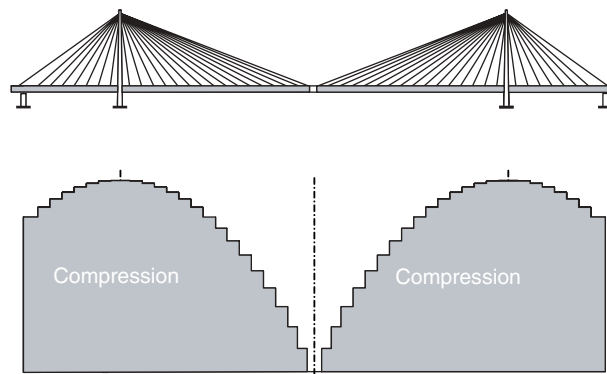
This is illustrated in Figure 4.110 showing the variation of the compressive stress from the axial force for spans up to 2000 m. The plot is based on the assumption that the deck cross section is kept constant (i.e. no increase of the cross-sectional area) as well as on realistic values for the ratio between dead load, superimposed dead load and traffic load.

It appears that the compression due to the axial force will move up from approx. 160 MPa to 500 MPa if the span is increased from 1000 m to 2000 m.

When evaluating the result of Figure 4.110, it must be remembered that apart from the axial compression due to the horizontal components of the stay cable forces, axial stresses in the deck cross section are also induced by other actions. Thus compressive stresses will be induced from local bending in the orthotropic deck slab, from global, vertical bending of the entire deck and from lateral bending due to e.g. wind load. Therefore, the available design stress of the actual steel grade will have to be reduced by these bending stresses before determining the compressive stress that will be available for the axial force in the deck cross section. Also, local and global buckling might reduce the design stress.

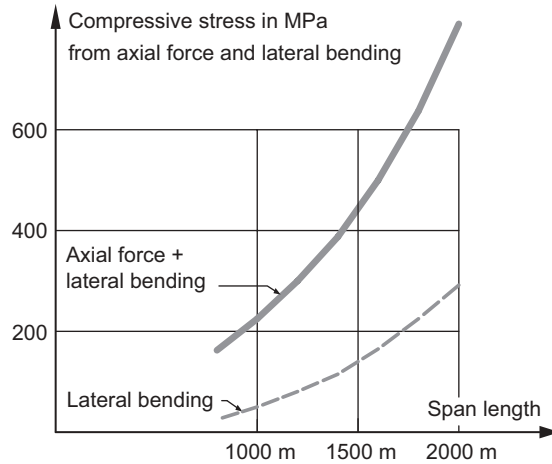
If the accumulated compressive stress exceeds the design stress, the solution is of course to strengthen the cross section either by use of stronger steels or by an increase of the cross sectional area. In the latter case the dead load of the deck will increase and thereby influence the design of the cables and the pylons.

As the maximum compressive stress from the axial force is present at the pylons, it is in these regions the demand for strengthening first appear. However, as it is seen from the axial force diagram in Figure 4.111 the compression in the



**Figure 4.111** Variation of the axial force in the deck due to the horizontal components of the cable pull





**Figure 4.112** Maximum compressive stress in the deck cross section due to axial force and lateral bending

deck only decreases with small steps near the pylon so the demand for strengthening will rapidly spread out over a relatively long length.

#### 4.5.3 Lateral bending of the deck

In a self anchored bridge with vertical (or quasi-vertical) cable planes the lateral loads (e.g. from drag forces on the deck and on the lower half of the stay cables) will have to be transmitted to the main supports by lateral bending of the deck.

Based on a number of realistic assumptions for the dimensions of the deck, e.g. a depth of 3 m and a width of 30 m, the maximum compressive stress in the deck cross section will be as shown in Figure 4.112.

It is seen that up to a span of approximately 1500 m the compressive stress will still be manageable with high strength steel and moderate strengthening in the critical regions near the pylons. So with the structural materials available today the limiting span of the self anchored cable stayed bridge appears to be around 1500 m.

The declining competitiveness of the self anchored cable stayed bridge against the earth anchored suspension bridge is illustrated in Figure 4.113, showing the results of a comparative investigation (where only the transmission of vertical load was considered). It is seen that the quantity of structural steel in the deck and pylons increases much more for the cable stayed bridge than the suspension bridge when moving up from a 1000 m span to a 2000 m span. If including the transmission of lateral load the trend would be even more pronounced.

When evaluating the results outlined in Figure 4.113 it should be considered that the unit price of cable steel is higher for stay cables than for suspension bridge main cables. On the other hand, the substructure cost will be higher for suspension bridges due to the demand for anchor blocks.

#### 4.5.4 Partial earth anchoring of a cable stayed bridge

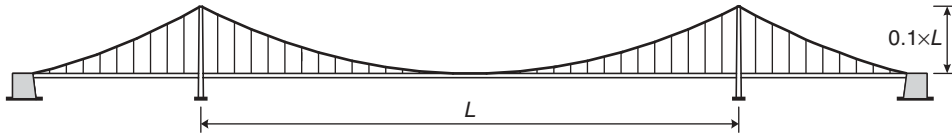
From the previous section it is evident that the transmission of the horizontal components of the stay cable forces will be one of the decisive factors for the competitiveness of cable stayed bridges if considering spans beyond the present limits. It is, therefore, interesting to consider whether modifications of the structural system could reduce the critical compression in the deck of a cable stayed bridge.

As already pointed out, a partial earth anchoring of the cable stayed system will be efficient in reducing the maximum axial force to be transmitted by the deck.

The basic difference between a self anchored and a partially earth anchored system is illustrated in Figure 4.114 and again it is the anchoring of the back stay that will determine the type of system to be found in an actual case.

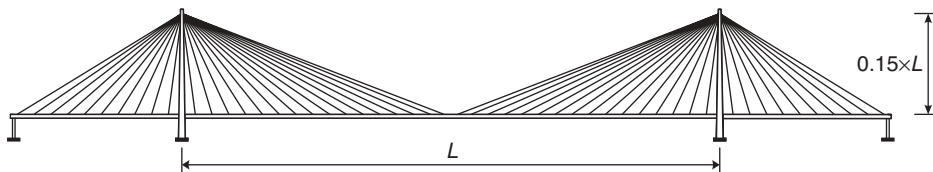
For the partially earth anchored system it should be pointed out that the ratio between tension and compression will be determined by the side-to-main span ratio.

## Earth Anchored Suspension Bridge



|               |                      |   |
|---------------|----------------------|---|
| $L = 1000$ m: | Cable steel: 7500 t  | Structural steel (deck + pylons): 23000 t |
| $L = 2000$ m: | Cable steel: 36000 t | Structural steel (deck + pylons): 55000 t |

## Self Anchored Cable-Stayed Bridge



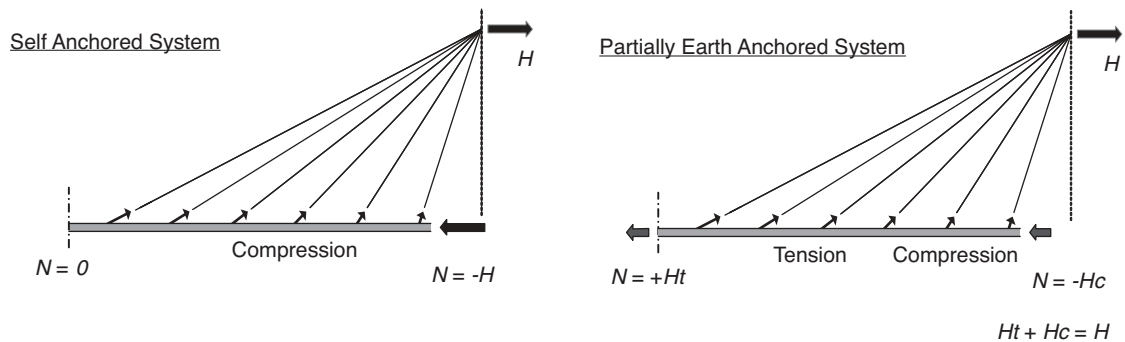
|               |                      |  |
|---------------|----------------------|--|
| $L = 1000$ m: | Cable steel: 3900 t  | Structural steel (deck + pylons): 25000 t        |
| $L = 2000$ m: | Cable steel: 21000 t | Structural steel (deck + pylons): <b>97000 t</b> |

**Figure 4.113** Comparison between quantities of a suspension bridge and a cable stayed bridge with spans of 1000 m and 2000 m, respectively

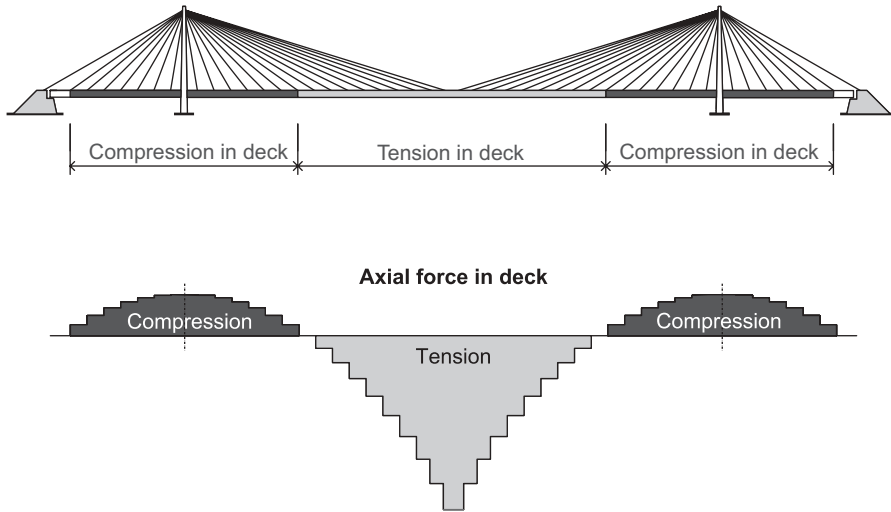
For a side span length of approximately one-third of the main span length, the maximum axial force in the deck will be approximately halved.

With side spans shorter than one third of the main span the tension at midspan will be greater than the compression at the pylons, as illustrated in Figure 4.115. It should be noted that the maximum tension at midspan rapidly decreases when moving away from midspan, so a strengthening will only be required in a relatively short region. However, if the strengthening is followed by a weight increase, it will have more consequences to strengthen at midspan than closer to the supports.

If an increased tensile capacity of the deck is made by applying thicker plates in the deck cross section, then the weight will go up by almost the same amount as if the compressive capacity were to be increased. However, a higher tensile



**Figure 4.114** Horizontal equilibrium of the deck in a self anchored and a partially earth anchored cable stayed system



**Figure 4.115** Axial force diagram for the deck of a partially earth anchored cable stayed bridge

capacity might be achieved by adding horizontal cables inside the deck. As the design stress of cable steel is 2–3 times higher than that of high strength structural steel, the weight increase associated with an increased tensile capacity will be more than halved.

To further reduce the weight increase, it could be attractive to apply cables with a higher strength-to-density ratio than that of steel cables. With cables of carbon fibre material the weight per force unit can be reduced to about one quarter compared to steel cables and to around one-tenth compared to high strength structural steel.

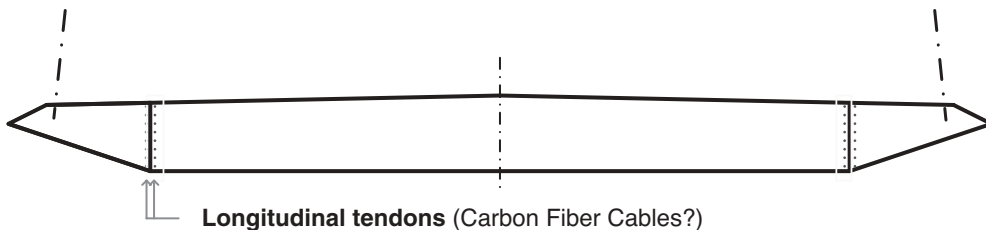
In very long spans it could be relevant to use carbon fibre cables as longitudinal tendons not only to reduce the weight increase but also because longitudinal cables inside the deck box will be well protected and easy to inspect and replace (Figure 4.116).

For a cable stayed bridge with a main span beyond that of a self anchored system, the concept could be based on choosing a main-to-side span ratio so that the basic deck cross section (with moderate strengthening) will be sufficient to transmit the compression at the pylons. Then the remaining horizontal force to establish equilibrium within each main span half must be provided by a tensile force at midspan. In bridges with a considerable length of the main span this could lead to a larger tensile force in the central region than the compressive force at the supports, as illustrated in Figure 4.117.

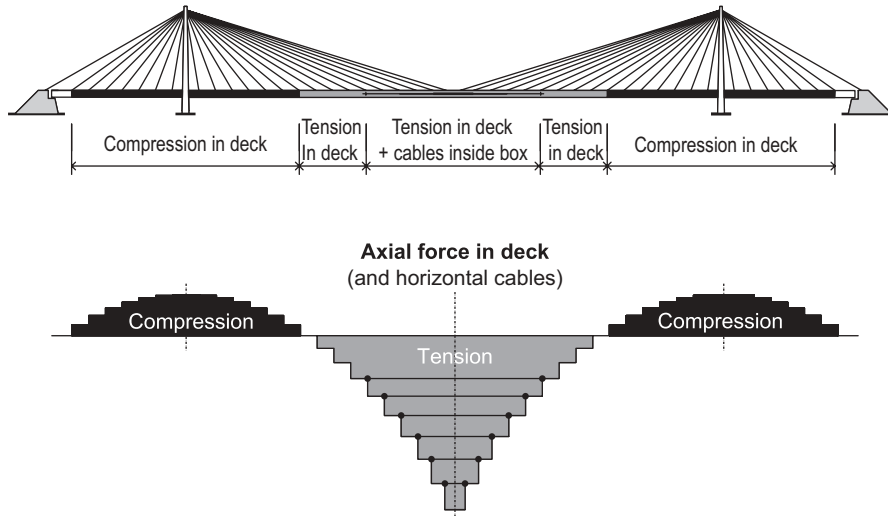
Compared to an earth anchored suspension bridge, a partially earth anchored cable stayed bridge could lead to considerable savings in the quantity of cable steel and to a reduction of the horizontal force to be transmitted to the soil at the anchor blocks. On the other hand, the quantity of pylon material will go up as the optimum pylon is 1.5–2 times higher in a cable stayed bridge than in a suspension bridge.

#### 4.5.5 Improving the lateral stability

In a cable stayed bridge with axial tension in the central main span region, a pendulum effect will be present so that the transmission of the lateral loads will not take place exclusively by transverse bending of the deck. However, as the pylon is higher than in a suspension bridge, the pendulum effect will be less pronounced.



**Figure 4.116** Steel box with longitudinal tendons to increase tensile capacity



**Figure 4.117** Cable stayed bridge with horizontal cables inside the deck to increase the tensile capacity in the central region of the main span

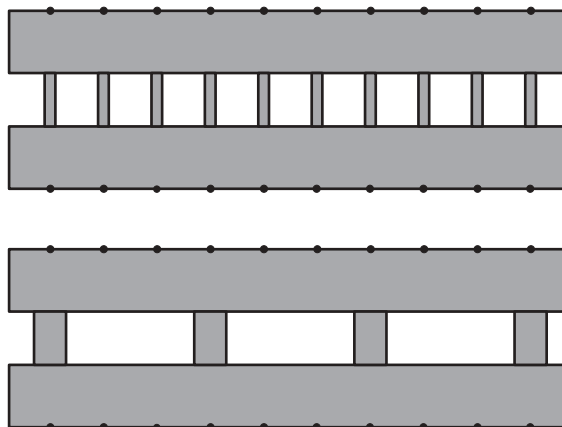
The flexural strength and stiffness of the deck in the lateral direction can be efficiently improved by a twin box configuration where each of the two carriageways is separated by a relatively wide gap. The two longitudinal boxes together with the cross beam will then form a Vierendeel girder.

If the two boxes are interconnected by narrow cross beams positioned at each point of stay cable anchorage, then the Vierendeel action might be rather weak. So in cases where an efficient lateral stiffness is essential, it might be preferable to reduce the number of cross beams and make them wider, as illustrated in Figure 4.118.

A system with fewer but wider cross beams in distances longer than the distance between the stay cable anchorages will generally be permissible due to the substantial torsional stiffness of the longitudinal deck boxes.

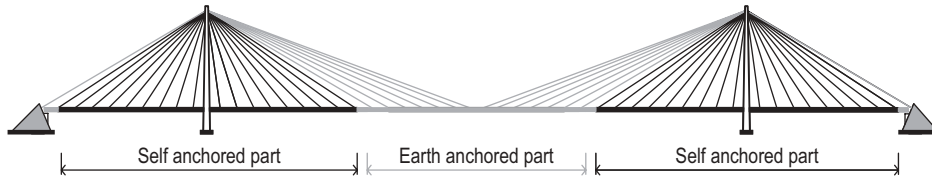
#### 4.5.6 Construction procedure for partially earth anchored cable stayed bridges

The preferred erection method for long span cable stayed bridges is the free-cantilever method where the deck is cantilevered from each pylon towards the centre of the main span. This method is in good harmony with the self anchored system as all stay cables will induce compression in the deck – as in the final system.

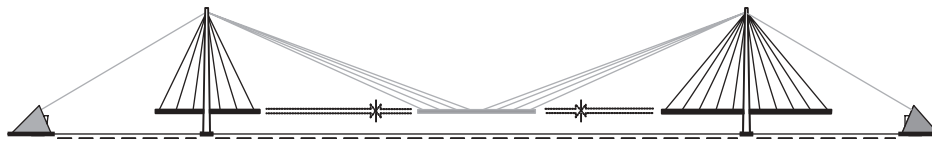


**Figure 4.118** Plan of twin box deck: (top) narrow cross beams at every stay cable anchorage position; (bottom) wide cross beams at every third stay cable anchorage position

Partially Earth Anchored Cable Stayed Bridge



Erection Procedure



**Figure 4.119** Erection procedure for partially anchored cable stayed bridge to induce tension in the central part of the deck in the main span

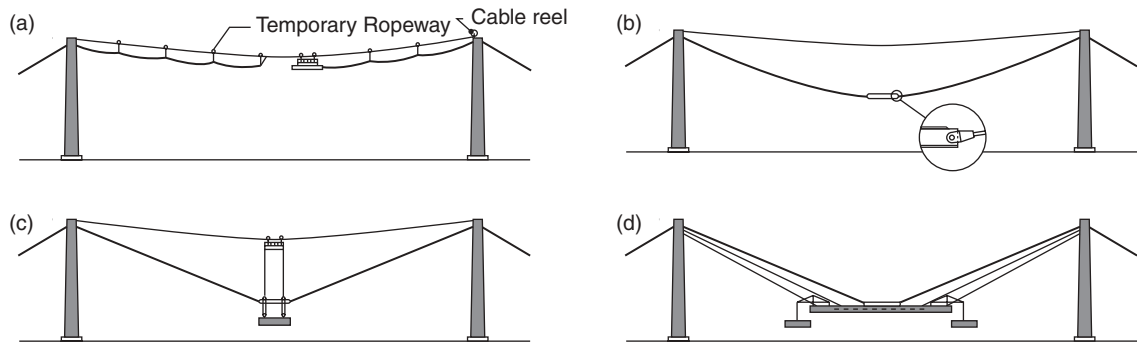
The method might also be applicable in a partially earth anchored system if the region with tension in the deck at midspan is relatively modest. In that case, self anchoring can be used until the closure at midspan if the expansion joints at the anchor blocks are temporarily locked. After completion of the central deck joint, a release of the expansion joints will transform the system from self anchored to partially earth anchored.

In a case where the final system is characterized by a considerable tension at midspan (as illustrated in Figure 4.117), the free-cantilever method will not be possible. Therefore, the central part of the main span must be erected as an earth anchored system (Figure 4.119).

Deck erection from midspan to the pylons is a well-known procedure for earth anchored suspension bridges where it is made possible by completing the erection of the main suspension cables prior to deck erection (Figure 4.120).



**Figure 4.120** Deck erection of the Storebælt East Bridge from midspan towards the pylons



**Figure 4.121** Erection procedure for the central part of the deck in a partially earth anchored cable stayed bridge: (a) top stay cable pulled along and supported by a temporary ropeway; (b) top cable with hinged connection to a short tension member at midspan; (c) first deck segment lifted to the top cable; (d) double-sided erection of deck segments and installation of stay cables

Similarly, in a partially earth anchored cable stayed system a continuous top cable must be erected initially from anchor block to anchor block via the pylon tops, e.g. by pulling across a prefabricated strand supported by a temporary ropeway (Figure 4.121). When in place the top cable can be used to support the central deck segment. Then the erection of the earth anchored part can proceed by lifting new segments and erecting stay cables in sequence.

# 5

## Pylons

### 5.1 Introduction

In principle, the pylon is a tower structure, but in contrast to a free-standing tower, where the moment induced by the horizontal loading (drag) from wind dominates the design, the most decisive load on a regular pylon will be the axial force originating from the vertical components of the forces in the cables attached to the pylon.

In Chapter 3, the pylon has already been treated as a part of the cable system, and in (3.41) the relation between the quantity  $Q_{pl}$  of the pylon legs and the pylon height  $h_{pl}$  was given. Based on this expression, Figure 5.1 shows the relation between the pylon height and the ratio  $Q_{pl}/N_{pl}$  for different values of  $f_{pl}/\gamma_{pl}$  (dimension: metre).

It should be noted that the stress  $f_{pl}$  is the stress available for carrying the axial compression in the pylon cross sections. Consequently,  $f_{pl}$  is smaller than the design stress  $f_d$  of the actual structural material. This is due to the fact that a certain portion of the design stress has to be reserved to cover stresses from other loads, primarily lateral wind load.

For pylons of steel the ratio  $f_{pl}/\gamma_{pl}$  might typically be found within the interval from 1000 m to 2000 m. With values in this interval the weight of the pylon legs increases almost linearly with the pylon height (for a constant top force  $N_{pl}$ ) and it is seen that, even for larger heights, the pylon weight is well below the top force. Thus, with  $h_{pl} = 300$  m, the increase of the normal force from the pylon top to the base due to the weight of the pylon legs is only 17–35%.

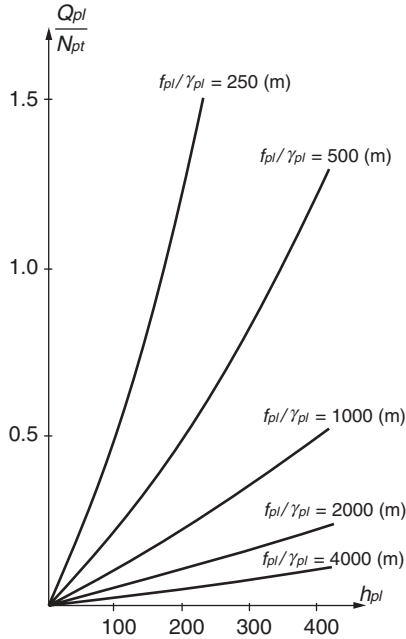
For pylons of concrete, the ratio of  $f_{pl}/\gamma_{pl}$  will be between 500 m and 250 m, giving a much more progressive increase of the pylon weight with the height. With  $f_{pl}/\gamma_{pl} = 250$  m the weight of the pylon legs will be equal to the top force already for a height of 175 m, and for  $h_{pl} = 300$  m the pylon weight will correspond to 2.3 times the top force.

Despite their considerable weight, concrete pylons have proved to be competitive for heights up to 300 m and, depending on local conditions, they might even be competitive beyond that. However, very many factors will influence the choice of the material for the pylons, such as soil conditions, speed of erection, stability in the construction phase, etc. Consequently, the choice of pylon material should not be based solely on a quantity based cost estimate.

### 5.2 Structural Behaviour of the Pylon

The force  $N_{pl}$  acting at the pylon top will be the resultant of all vertical components of the cable forces at the supporting point. In a simple case, as shown in Figure 5.2, with only two (weightless) stay cables radiating from the pylon top, and with horizontal equilibrium between the two chord forces  $\underline{T}_A$  and  $\underline{T}_C$ , the axial force  $\underline{R}_T$  acting on the pylon will be the resultant of these two forces:

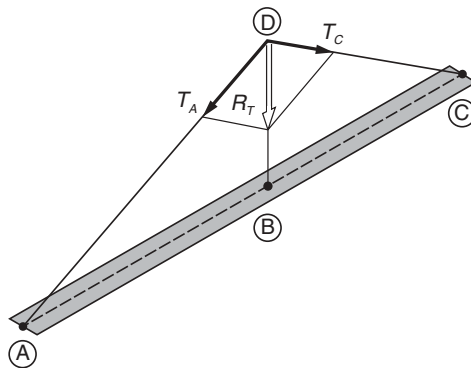
$$\underline{T}_A + \underline{T}_C = \underline{R}_T \quad (5.1)$$



**Figure 5.1** Relation between the relative pylon weight  $Q_{pl}/N_{pt}$  and the pylon height  $h_{pl}$  for different stress-to-density ratios

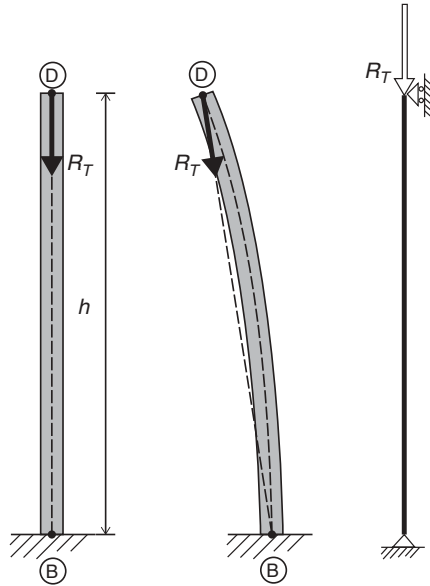
As the cable plane is defined by the pylon top and the anchor points A and C at the deck, the top force  $R_T$  acting on the pylon must be located in this plane. When considering the buckling of the pylon in the case of vertical loading only, the top force  $R_T$  will remain directed towards the point B where the pylon axis and the deck axis intersect (Figure 5.3). This implies that the effective column length of the pylon is equal to the height  $h$  and not  $2h$  as would be the case if the force  $R_T$  remained vertical under the lateral deflection of the column.

Under lateral loading the deck might bend in the horizontal plane so that the anchor points A and C and the pylon base B will no longer be on a straight line, as is indicated in Figure 5.4 with the deflected deck in the position A'BC.



**Figure 5.2** Resultant  $R_T$  of cable forces  $T_A$  and  $T_C$  acting at the pylon top



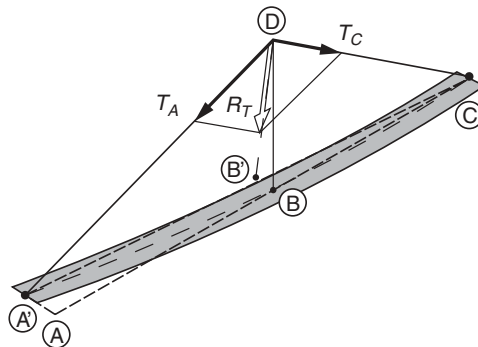


**Figure 5.3** Resultant  $R_T$  pointing towards the pylon base B under lateral displacement of the pylon top

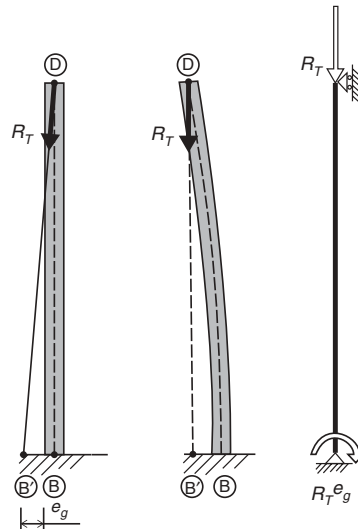
The cable plane is now determined by the pylon top D and the straight line from A' to C, and the resultant  $\underline{R}_T$  of the cable forces  $\underline{T}_A$  and  $\underline{T}_C$  will consequently point towards point B' on the straight line from A' to C. This is also the case for the deflected column as illustrated in Figure 5.5, so the proper mathematical model for the pylon will be a simply supported column with an axial force  $R_T$  and a moment  $R_T e_g$  at the bottom.

So far the pylon has only been studied under the action of the resultant from the cable chord forces  $\underline{T}_A$  and  $\underline{T}_B$ , but this only constitutes a part, albeit a very important part, of the total system of forces acting on this structural element. Other forces to be taken into account include: reactions from cable dead load  $\underline{R}_{gcb}$  and wind load  $\underline{R}_{ucb}$  as well as dead load  $g_{pl}$  and wind load  $u_{pl}$  on the pylon itself.

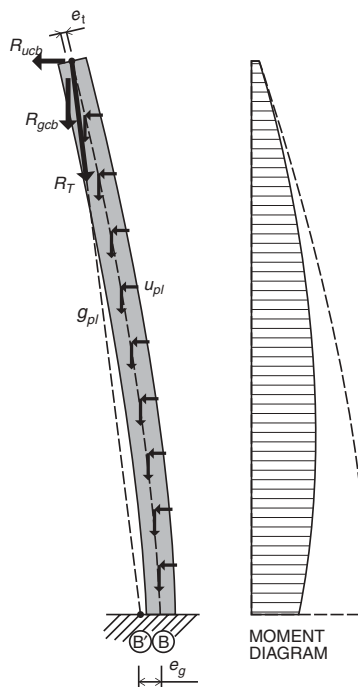
Figure 5.6 shows the total set of loads to be applied when investigating buckling in the transverse direction. Note that, whereas the resultant  $\underline{R}_T$  of the cable chord forces is directed towards the point B', then the resultant of the cable dead load reactions  $\underline{R}_{gcb}$  ( $= \sum \frac{1}{2} g_{cb} c$ ) and the dead load of the pylon itself remains vertical.



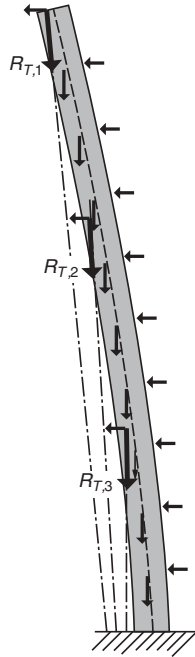
**Figure 5.4** Direction of the pylon force  $R_T$  when the deck deflects laterally



**Figure 5.5** Resultant  $R_T$  pointing towards a fixed point ( $B'$ ) during buckling of the pylon



**Figure 5.6** Forces acting on a free-standing pylon with corresponding moment diagram (fan or suspension system)



**Figure 5.7** Forces acting on a free-standing pylon supporting a harp system

As indicated in Figure 5.6, a certain eccentricity  $e_r$  of the forces from the cables will often be assumed, to cover inaccuracies during construction. Typically  $e_r$  is chosen at a value of 100 mm.

The fact that the primary force  $R_T$  points towards B' implies that the maximum moment of the deflected pylon occurs near mid-height, as indicated by the moment diagram. In the case where the force  $R_T$  remained vertical, the moment diagram would be as shown by a dotted line, and the maximum moment would appear at the bottom.

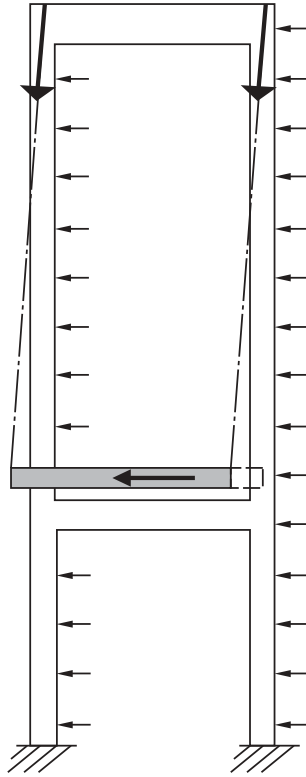
The forces indicated in Figure 5.6 are those to be found in a pylon supporting a fan-shaped (or a suspension) cable system. If a harp-shaped cable system is being supported, the forces from the cable system will be applied at different levels, as indicated in Figure 5.7 for a pylon supporting three sets of stay cables.

For free-standing column-type pylons, as shown in the previous examples, the common requirement to keep the width at the deck level as small as possible means that buckling becomes a decisive factor in the design, and consequently it is essential to use a nonlinear analytical method taking large displacements into account (second order analysis).

In other types of pylons, such as the portal type shown in Figure 5.8, a much larger lateral rigidity is achieved and consequently nonlinear geometrical effects will be of less importance. This is especially true if the pylon forms a part of an earth anchored system supporting the deck laterally (refer to Figure 3.178). In this case it is essential to have considerable rigidity in the transverse direction and consequently a linear analysis will often be adequate, although the validity of this analysis should always be checked by calculating the deflected geometry and evaluating the resulting change of moments.

If a linear analysis is performed, then the distinction between forces directed towards a fixed point or remaining vertical becomes unimportant and the forces from each cable system can then be represented by a single force equal to the resultant of all tangential cable forces.

In the longitudinal direction of the bridge, the design of the pylon will be strongly influenced by the supporting conditions not only for the pylon itself but also for the structure as a whole.



**Figure 5.8** Portal-type pylon supporting an earth anchored cable system

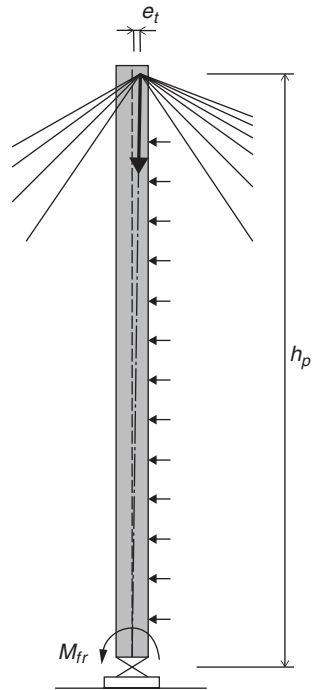
The simplest conditions will be found if the pylon is pivoted at the base and the cable system supported at the top (Figure 5.9). In this case the primary force from the cables will be acting in the axial direction assuming a small eccentricity  $e_{tx}$  at the top. Additional moments will occur from wind blowing longitudinally and also a moment  $M_{fr}$  from friction in the base bearing should be taken into account.

With the pivoted base the column length of the pylon is well defined as being equal to the height  $h_{pt}$ . The application of pivoted pylons is, however, restricted to structures with moderate reactions from the cable system, as the cost of the bearings prohibits this system to be used for larger pylons. Also during construction a pivoted pylon requires special measures to achieve the necessary stability in the temporary stages prior to installation of the cables.

Pivoted pylons of the portal type were used in the Strömsund Bridge, as shown in Figure 5.10. Pivoting was chosen in this bridge to allow relatively large longitudinal displacements of the pylon top during installation and tensioning of the stay cables. During erection the 28 m high pylon was temporarily stabilized by a strut from the initially erected side span girder.

For a pylon fixed at the base, four cases, as outlined in Figure 5.11, will be discussed in the following. The characteristics of the four cases are:

- (1) The pylons are fixed to the piers below and supporting a self anchored cable system with all bearings under the deck longitudinally movable.
- (2) The pylons are fixed to the piers below and supporting a self anchored cable system with a longitudinal deck support through one fixed end bearing.



**Figure 5.9** Pylon pivoted at the base



**Figure 5.10** Pylon of the Strömsund Bridge

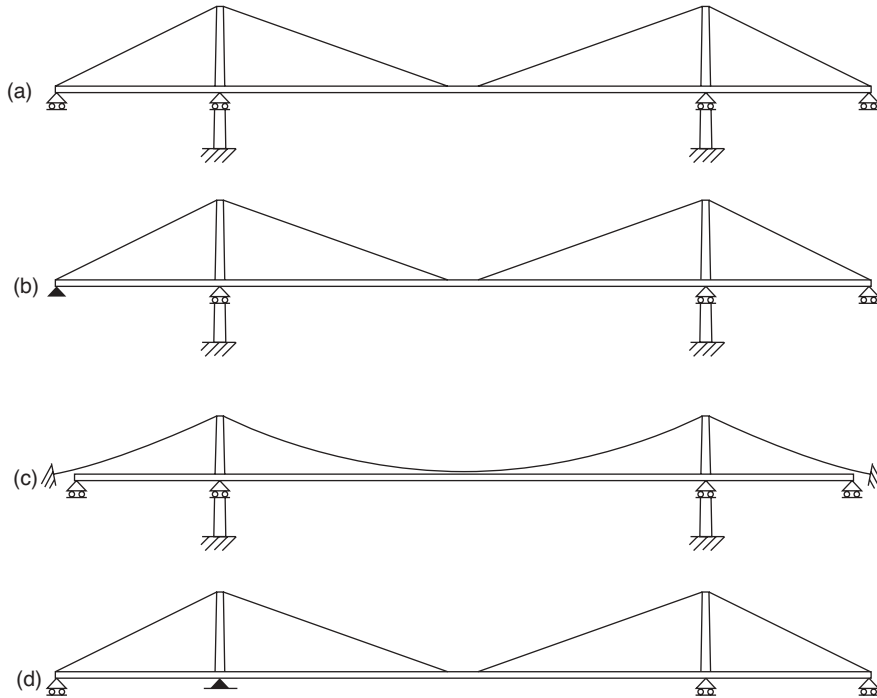


Figure 5.11 Four structural systems comprising pylons fixed at the base

- (3) The pylons are fixed to the piers below and supporting an earth anchored cable system with all bearings under the deck longitudinally movable.
- (4) The pylons are fixed to the deck and supporting a self anchored cable system.

In Case (a), the critical deflection will be characterized by a longitudinal displacement of both pylon tops in the same direction, as indicated in Figure 5.12. During this deflection the primary force  $N_{pt}$  from the cable system due to the vertical load on the deck will remain vertical, as all reactions from the deck will be vertical. Thus, the effective column length of the pylon for buckling in the longitudinal direction will be twice the height ( $l_c = 2h_{pt}$ ). Adding to this, that all longitudinal forces on the bridge (e.g. from braking forces and longitudinal wind load) will be applied to the pylon at the top, makes it evident that a considerable flexural stiffness of the pylon will be required in the longitudinal direction.

In Case (b), all longitudinal forces acting on the deck will be transferred through the fixed end bearing and at the same time a longitudinal restraint of the pylon tops is achieved by the anchor cables. These two features significantly reduce the required flexural stiffness and consequently more slender pylons can be used.

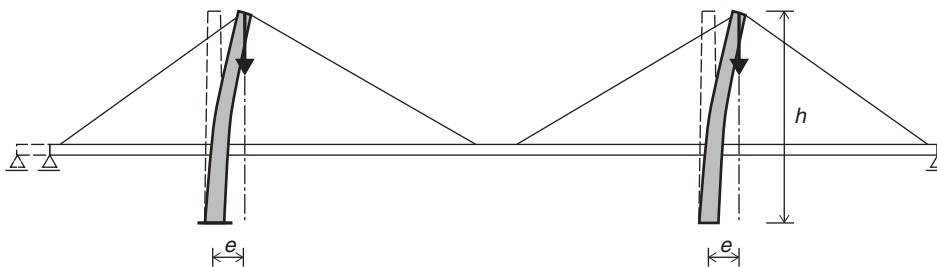
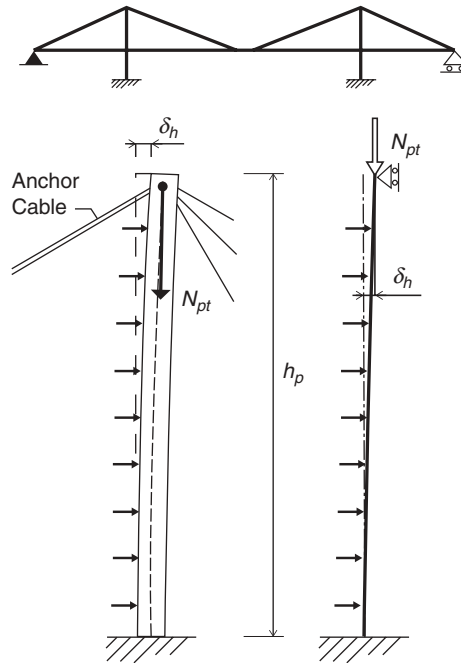


Figure 5.12 Simultaneous buckling of the two pylons in a system with no longitudinal restraint of the deck



**Figure 5.13** Limited longitudinal displacement of the pylon top in a system with a fixed bearing under the deck

As the pylon is fixed at the base and longitudinally supported at the top by the anchor cable, the effective column length will be approximately  $0.7h_p$ , almost one-third of the effective column length in Case (a). However, due to elongations of the anchor cable (and the deck) from traffic load or temperature change, a limited longitudinal displacement  $\delta_h$  of the pylon top will occur. Conversely, the horizontal restraint offered by the anchor cable implies that the force  $N_{pt}$  from the cable system does not have to stay vertical but might turn into an inclined direction, as illustrated in Figure 5.13. Under longitudinal wind load the anchor cable renders support to the pylon.

When investigating buckling of the pylon it can generally be assumed that the anchor cable constitutes a fixed support in the longitudinal direction. Thus, the analysis should be based on investigating a column fixed at the base and simply supported at the top, and subjected to an axial force  $N_{pt}$ , a top displacement  $\delta_h$ , and a longitudinal wind load.

In Case (c) the earth anchored side span main cable will give the pylon top a similar longitudinal support as described for the anchor cable in Case (b). However, the longitudinal displacements of the pylon top under traffic load might be larger, especially if the suspension bridge has cable suspended side spans.

In Case (d) the pylon is equally well supported by the anchor cable at the top as in Case (b), but due to the rigid connection to the deck, moments will be induced at the bottom. Thus, when investigating the buckling of the pylon a simple support at the top and a fixed base might be assumed, provided the column is subjected to the axial load  $N_{pt}$ , the relevant angular change  $\Delta\phi$  at the bottom, as well as the longitudinal wind load (Figure 5.14).

The resistance of the pylon top against horizontal displacements due to elongation of the anchor cable depends on the ratio between the axial force  $N_{pt}$  and the critical force  $N_{cr}$  of the free-standing column.

Remembering that an elastic column subjected to an axial force equal to the critical force will be in equilibrium, in any deflected state leads – with reference to Figure 5.15 – to the following conclusions regarding the horizontal resistance of the pylon top.

If the axial force  $N_{pt}$  is smaller than the critical force  $N_{cr}$  of the column with a free end at the top, the pylon will tend to return to its vertical position and the cable system must consequently subject the pylon top to a horizontal force  $\Delta H$  away from the neutral position to keep the pylon in the deflected state. Conversely this means that the pylon appears to resist the longitudinal displacement  $\delta_h$  by the force  $\Delta H$ .

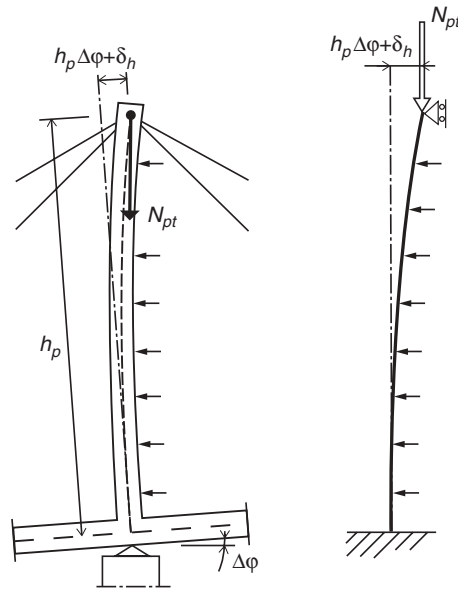


Figure 5.14 Deflection of pylon fixed to the deck

If the axial force  $N_{pt}$  is equal to the critical force  $N_{cr}$  then no horizontal force is required to keep the pylon in the deflected state, and the pylon will consequently show no resistance against longitudinal displacements of the pylon top. Thus, the support offered by the pylon to the cable system corresponds to that of a friction-free longitudinally movable bearing.

Finally, if the axial force  $N_{pt}$  is larger than the critical force  $N_{cr}$  of the free-standing column, the pylon tends to further increase its deflection and a horizontal force  $\Delta H$  acting against the displacement is consequently required to keep the pylon in place.

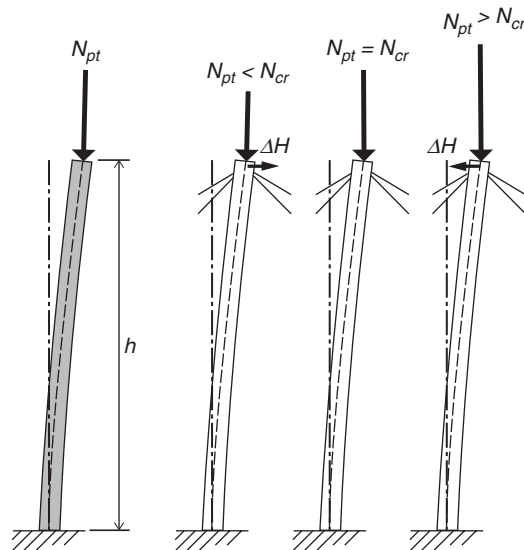
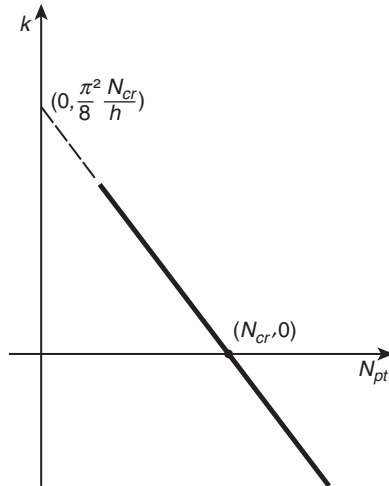


Figure 5.15 Direction of horizontal force  $\Delta H$  from cable system depending on the size of the normal force in relation to the critical force of the free-standing column





**Figure 5.16** Variation of the spring constant  $C$  for the longitudinal support of the pylon top with the normal force  $N_{pt}$

The resistance of the pylon against horizontal displacement of the top might be expressed by a spring constant  $C$  defined by:

$$C = \Delta H / \delta_h \quad (5.2)$$

For a pylon with a constant cross section, the spring constant  $C$  will vary with the axial force  $N_{pt}$  as shown in Figure 5.16 (assuming a sinusoidal deflection curve). It is seen that the spring constant is positive for  $N_{pt} < N_{cr}$  and negative for  $N_{pt} > N_{cr}$ . For  $N_{pt} = 0$  the spring constant will be:

$$C = \frac{\pi^2}{8h} N_{cr} = \frac{\pi^4 EI}{32 h^3} \sim 3.04 \frac{E}{h^3}$$

whereas the correct value (with the correct deflection curve for this case) is  $3EI/h^3$ . These values are based on the assumption of a constant cross section, but in principle the relation between the normal force  $N_{pt}$  and the spring coefficient  $C$  will be as shown in Figure 5.16 also for a pylon with variable cross section [42.1].

The moment at the base of a pylon with constant cross section is determined by:

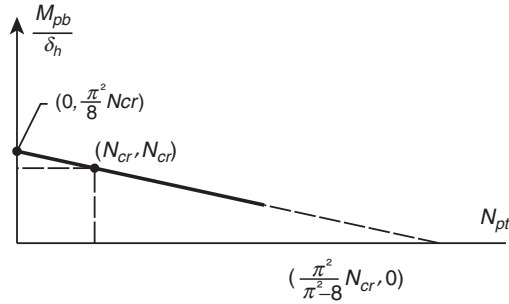
$$M_{pb} = N_{pt} \delta_h + \Delta H h = (N_{pt} + Ch) \delta_h = \left[ \frac{\pi^2}{8} N_{cr} + \left( 1 - \frac{\pi^2}{8} \right) N_{pt} \right] \delta_h \quad (5.3)$$

From the plot in Figure 5.17 is seen that the moment  $M_{pb}$  decreases with  $N_{pt}$  and that

$$M_{pb} = 0 \quad \text{for} \quad N_{pt} = \frac{\pi^2}{\pi^2 - 8} N_{cr} \sim 5.28 N_{cr}$$

It will often be attempted to construct the pylon with a slenderness so that  $\max N_{pt} \sim N_{cr}$  but other factors such as stability during the construction period (when the pylon must be able to withstand lateral load without support from the anchor cable) might have a decisive influence on the choice of dimensions.

In major suspension bridges the compromise between longitudinal flexibility in the final stage and stability in the construction phase has generally resulted in pylon legs with an average width in the longitudinal direction of 1/20–1/25 of

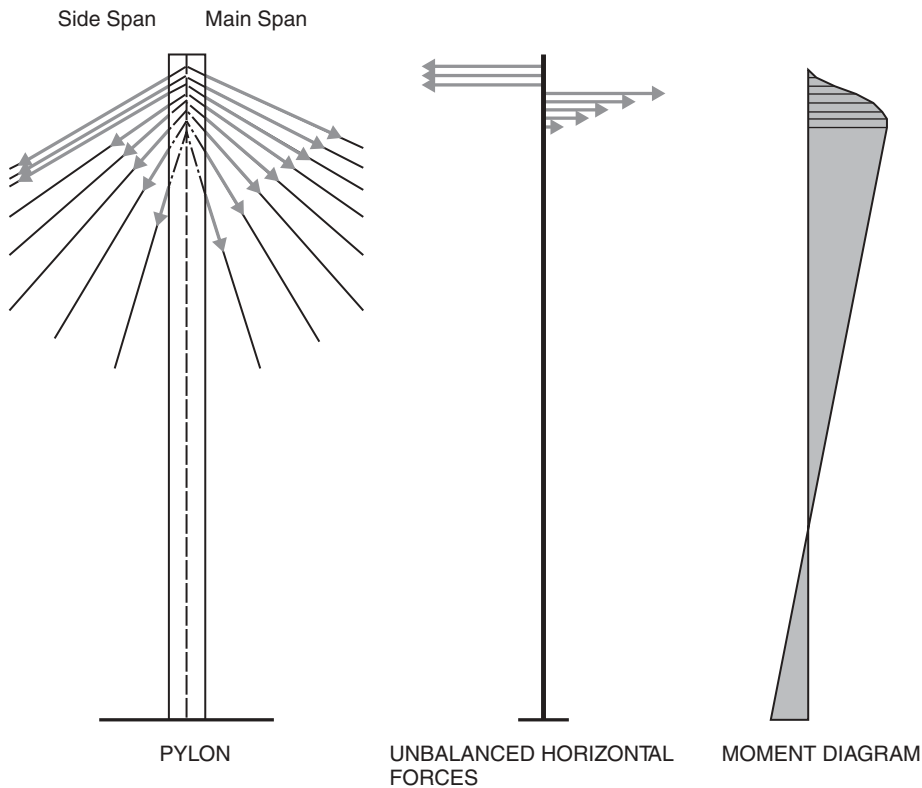


**Figure 5.17** Variation of the moment  $M_{pb}$  at the pylon base with the normal force  $N_{pt}$

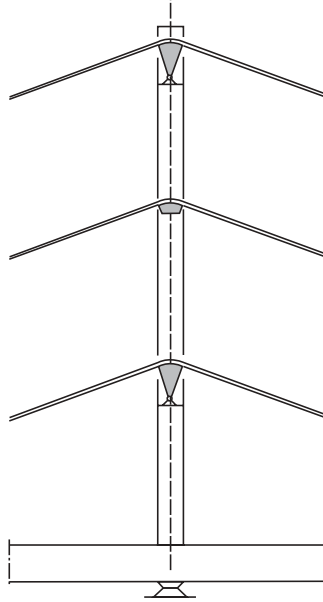
the pylon height. In many cases the pylon legs are slightly tapered so that the horizontal dimensions at the top is 0.6–0.9 times the corresponding dimensions at the bottom.

For the pylons shown in Figures 5.6–5.17 it has been assumed that the total force from the cable system is acting in a single point at the pylon top, corresponding to cable systems of either the suspension type or the pure fan type.

Due to the practical problems of anchoring all stay cables in a concentrated zone at the pylon top, the pure fan system is rarely used, but has been replaced by the modified fan system where the cable anchorages are spread over the upper part of the pylon, as indicated in Figure 5.18. In this case the pylon will be subjected to bending as



**Figure 5.18** Moment diagram for pylon supporting a semi fan system



**Figure 5.19** Harp system with the upper and lower stay cables supported through rocker bearings on the pylon

differential horizontal forces have to be transferred between cables anchored at different levels. In Figure 5.18, a case is indicated with the side span subjected to dead load only and the main span to dead plus traffic load. This implies that a difference will exist between the horizontal forces of corresponding cables on either side of the pylon, and consequently the unbalanced horizontal components must be transferred (primarily) to the anchor cable introducing moments, as shown in Figure 5.18. Note that the maximum moment for this loading might occur at the top rather than at the bottom.

As the induced moments are proportional to the distance between the cable anchor points, it is desirable to make the anchor zone as concentrated as possible. This effect was also described in connection with Figure 3.102.

If the cable system to be supported by the pylon is of the harp configuration, the cable anchorages will be distributed along the entire pylon above the deck. This might lead to bending moments of considerable magnitude when unbalanced horizontal cable components are transferred between the different cable anchorages. However, the intensity of unbalanced forces at the pylon is influenced by the ratio between the flexural stiffness of the pylon and the deck, as explained in connection with Figure 3.101.

If the flexural stiffness of the pylon supporting a harp system is insignificant compared to the stiffness of the deck, the pylon will give only a modest contribution to the global stability of the structural system. In such a case an attempt has been made to further decrease the bending of the pylon by applying longitudinally movable bearings under some of the stay cables, thus entirely excluding the transmission of horizontal forces (except frictional forces) from the stay cables to the pylon.

In one of the very early cable stayed bridges, the Theodor Heuss Bridge in Düsseldorf, the stay cables were connected to the pylon as shown in Figure 5.19, where the upper and the lower stay cables are supported by movable rocker bearings.

The longitudinally movable bearings were also seen in other of the early cable stayed bridges, but today they are rarely used, and certainly not in multi-cable harp systems. This is also due to the fact that the introduction of movable bearings actually reduces the efficiency of the total structural system.

Pylons subjected primarily to a resulting vertical force from the cable system are generally made with a vertical axis in the elevation of the bridge. However, other configurations are also seen. As an example, Figure 5.20 shows a V-shaped pylon with two inclined legs and a harp-shaped cable system with four sets of stay cables.

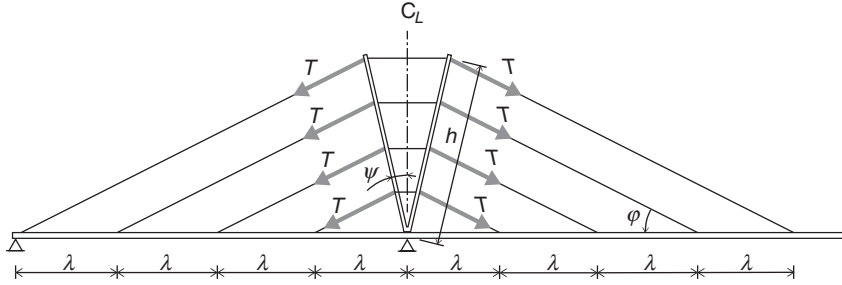


Figure 5.20 Harp system supported by a V-shaped pylon

Considering only the action of the primary axial forces and ignoring the dead load of the pylon leads to the following expression for the pylon quantity:

$$Q_{pl} = 20 \frac{\gamma_{pl}}{f_{pl}} T \lambda \frac{\sin^2 \phi}{\cos \psi \cos(\phi - \psi)} \tag{5.4}$$

By determination of  $\partial Q_{pl} / \partial \psi$  the optimum inclination of the pylon legs can be found:

$$\frac{\partial Q_{pl}}{\partial \psi} = 20 \frac{\gamma_{pl}}{f_{pld}} T \lambda \sin^2 \phi \left( \frac{\sin \psi}{\cos^2 \phi} - \frac{\sin(\phi - \psi)}{\cos^2(\phi - \psi)} \right) = 0$$

leading to  $\psi = \phi/2$ . Thus, the pylon legs should have the direction of the angle bisector between the inclined and the horizontal cable direction. Note that this direction of the pylon legs also ensures a constant force  $T$  in the stay cables.

With  $\psi = \phi/2$  (5.4) becomes:

$$Q_{pv} = 20 \frac{\gamma_{pl}}{f_{pld}} T \lambda \frac{2 \sin^2 \phi}{1 + \cos \phi} \tag{5.5}$$

The quantity  $Q_{pc}$  of a vertical pylon is determined by inserting  $\psi = 0$  in (5.4):

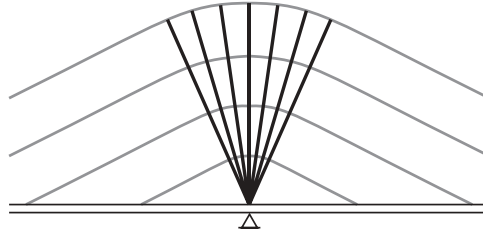
$$Q_{pc} = 20 \frac{\gamma_{pl}}{f_{pld}} T \lambda \frac{\sin^2 \phi}{\cos \phi} \tag{5.6}$$

The ratio between the theoretical quantity of the V-pylon and the vertical column now becomes:

$$\frac{Q_{pv}}{Q_{pc}} = \frac{2 \cos \phi}{1 + \cos \phi} \tag{5.7}$$

With  $\phi = 26.^\circ 6$  corresponding to an inclination of 1:2 of the inclined stay cables, the ratio  $Q_{pv}/Q_{pc}$  becomes 0.94. Thus, in this case the theoretical savings in the pylon quantity by application of a V-shape amount to 6%. At the same time there will be a modest saving of about 2% in the theoretical quantity of cable steel. However, it should be remembered that only the primary action has been considered and a more elaborate analysis would therefore be required to give a precise answer on the real savings to be achieved.

As a curiosity it should be mentioned that the theoretical optimum for a pylon to support a harp system would look as shown in Figure 5.21 where a large (infinite) number of legs radiates from the supporting point at deck level. With such a pylon, the theoretical quantity  $Q_{p0}$  becomes  $20(\gamma_{pl}/f_{pld})T\lambda \sin \phi$ . Inserting  $\phi = 26.^\circ 6$  yields  $Q_{p0} = 0.93Q_{pc}$  and the further (theoretical) savings by proceeding from the V-shape to the theoretical optimum



**Figure 5.21** Theoretical configuration of the optimum pylon structure to support a harp system

configuration therefore only amount to approximately 1%. Consequently, the V-shape is indeed very close to the theoretical optimum solution.

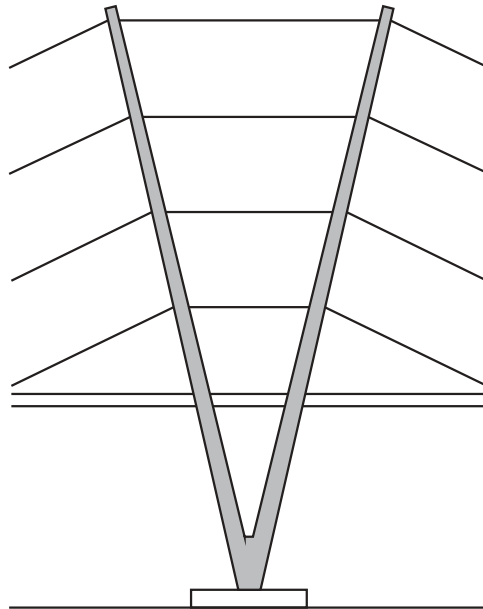
The description of the V-shaped pylon will be concluded by pointing out that further (theoretical) savings might be achieved if the supporting point is situated below the deck level as indicated in Figure 5.22.

### 5.3 Pylons Subjected Primarily to Vertical Forces from the Cable System

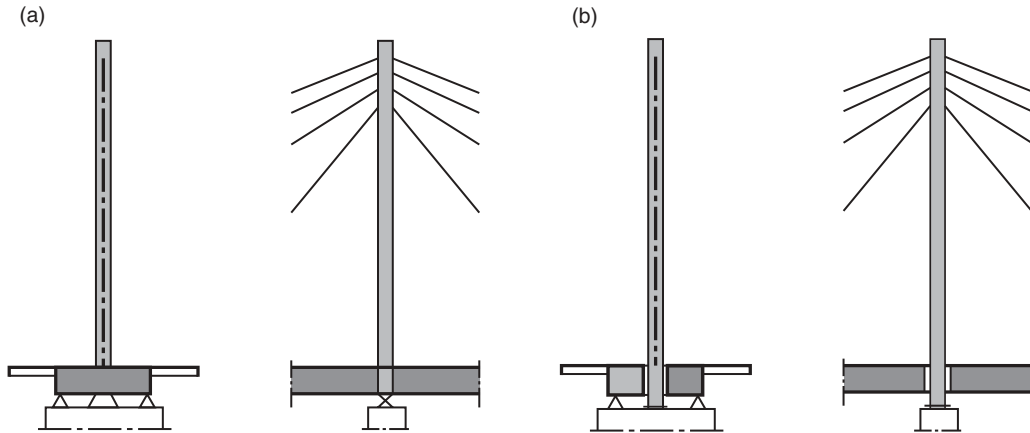
When selecting the form of the pylon it must be remembered that the most important task for the pylon is to transmit the reactions from the cable system to the substructure. To achieve the best economy it is essential that the vertical force primarily induces axial forces in the pylon sections.

For bridges with a single central cable plane the immediate solution, as shown in Figure 5.23, is to design the pylon as a mono-pole with its axis in the cable plane. In this case the pylon can either be connected moment rigidly to the deck (a) or pass through an opening in the deck to be fixed to the top of the pier (b).

In Solution (a) a large bearing must be positioned below the deck directly under the pylon, and lateral stability must be ensured by a moment-rigid connection to a transverse girder (diaphragm) inside the deck. At the ends of this transverse girder two more bearings are required to transmit torsional moments from the deck and bending moments from lateral load on the pylon.



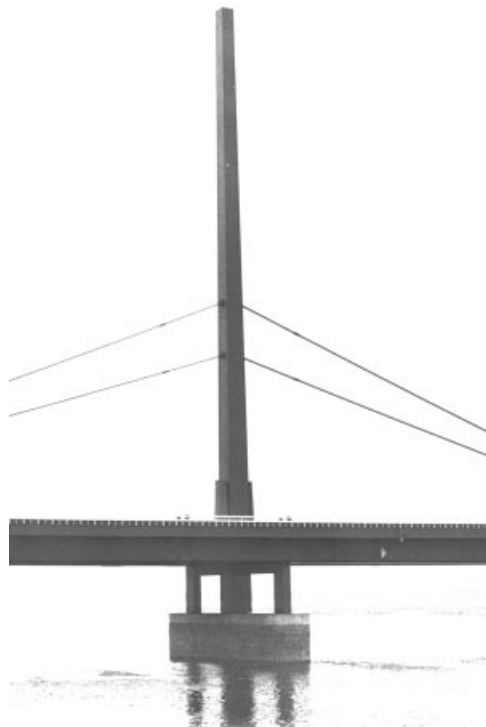
**Figure 5.22** V-shaped pylon with inclined legs spreading out from a low pier top



**Figure 5.23** Two structural systems for a free-standing pylon supporting a central cable system

Solution (a) was first applied in the Norderelbe Bridge in Hamburg, as shown in Figure 5.24. Here the bearings were positioned at some distance below the deck with short columns introduced between the girder bottom and the pier top.

In Solution (b) of Figure 5.23 the lateral stability of the pylon is ensured directly by a moment rigid connection between the pylon base and the pier (foundation), so that the two edge bearings only have to transmit forces and moments from the deck.



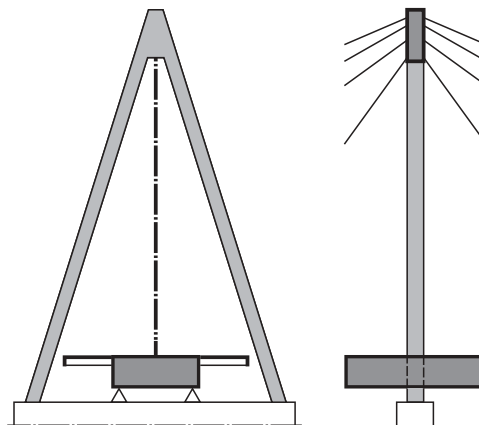
**Figure 5.24** Pylon of the original Norderelbe Bridge



**Figure 5.25** Pylon of the Stonecutters Bridge

In the Stonecutters Bridge the pylon is positioned in the gap between the two boxes forming the deck, as seen in Figure 5.25. To give the deck lateral support, vertically and longitudinally sliding bearings are positioned between the inner faces of the two boxes and the pylon. Furthermore, large hydraulic buffers are added between the pylon and the nearest transverse girders of the deck.

A central cable plane might also be supported by an A-shaped pylon with two inclined legs straddling over the deck, as shown in Figure 5.26. Due to the more indirect transmission of the primary vertical force, this form inevitably leads to increased costs of the pylon. However, the solution makes it possible to reduce the width of the deck, as the space required to let the stay cables pass between the traffic lanes is considerably less than that required for a mono-pole pylon. Thus, the



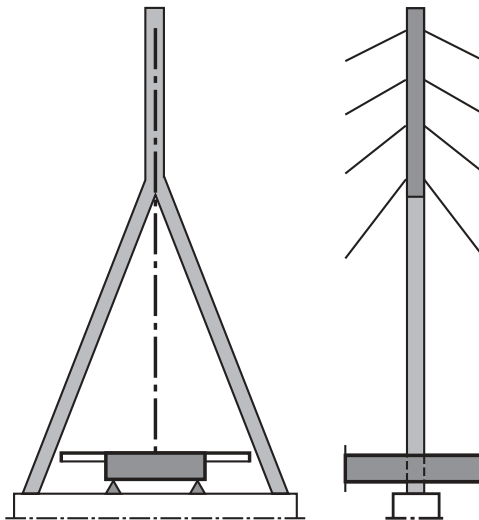
**Figure 5.26** A-shaped pylon supporting a central fan system



*Figure 5.27 Pylon of the Rhine Bridge at Speyer*

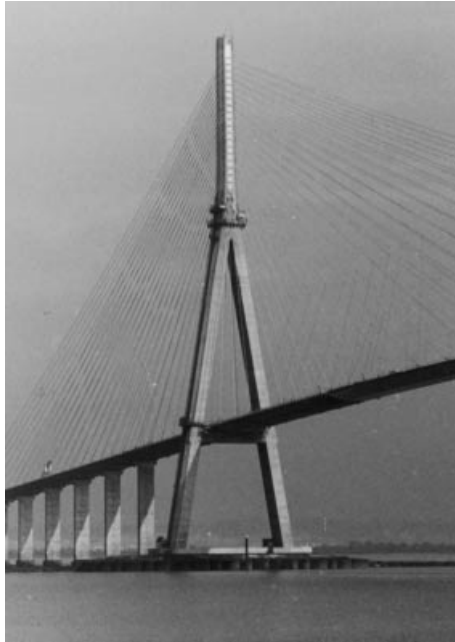
increased cost of the A-shaped pylon might be counteracted by a reduction of the deck area. The combination of a central cable plane and an A-shaped pylon was used in the cable stayed bridge across the Rhine at Speyer (Figure 5.27). Here the pylon legs were supported by Neopot bearings onto the pier, so that the pylon structure actually was pivoted in the longitudinal direction.

It should be noted that, whereas the mono-pole pylons of Figure 5.23 can support a fan system as well as a harp system, the A-shaped pylon of Figure 5.26 can only be used for a fan system with all stay cables radiating from the pylon top. However, with a form as shown in Figure 5.28, where the inclined legs are topped by a vertical pylon part ( $\lambda$ -shape), modified harp systems and multi-cable, modified fan systems might also be supported by this type of pylon.



*Figure 5.28  $\lambda$ -shaped pylon supporting a modified harp system*

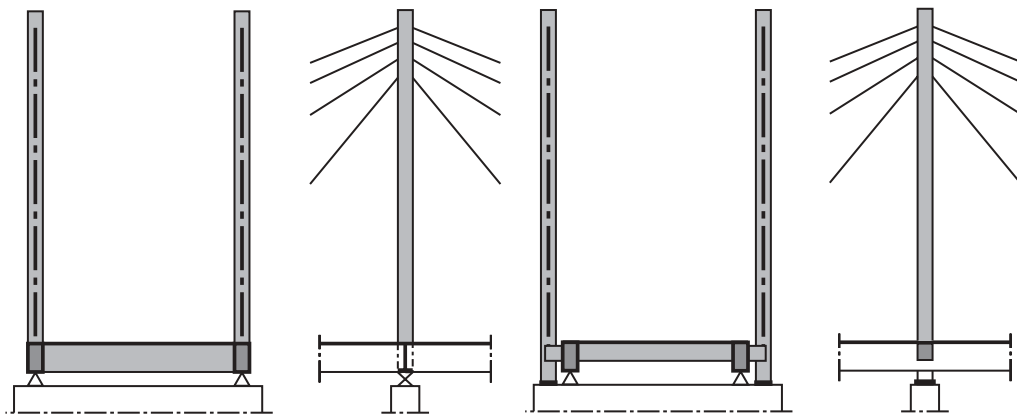




**Figure 5.29** Pylon of the Normandy Bridge

The 214 m high concrete pylons of the Normandy Bridge have an elegant  $\lambda$ -shape as seen in Figure 5.29.

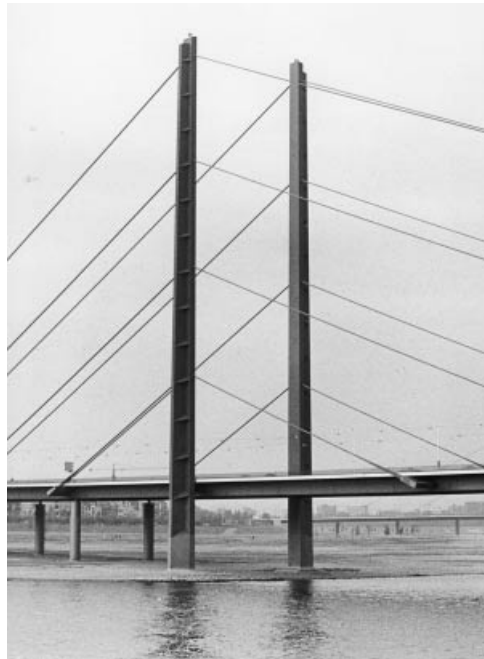
In bridges with two vertical cable planes the pylon might be composed of two free-standing columns, as shown in Figure 5.30. The two solutions in Figure 5.30 correspond closely to those of Figure 5.23, as (a) comprises a moment rigid connection between the pylons and the deck, and (b) a direct fixity of the pylons at the pier. It should be emphasized that in solution (b) it is important that the pylon axis coincides with the cable plane to avoid unnecessary bending moments in the pylon legs. This will require that the anchorages of the stay cables are positioned outside the deck on small brackets.



**Figure 5.30** Two structural systems for pylons comprising two free-standing columns



**Figure 5.31** Pylon of the Theodor Heuss Bridge



**Figure 5.32** Pylon of the Knie Bridge

The system of Figure 5.30(a) was applied in the Theodor Heuss Bridge in Düsseldorf (Figure 5.31) and the system of Figure 5.30(b) for the 114 m high steel pylons of the Knie Bridge, also in Düsseldorf (Figure 5.32). As can be seen, the pylon legs in the Knie Bridge are continued to a lower pier top and the deck is therefore supported through a transverse girder to brackets on the inner faces of the pylon legs.

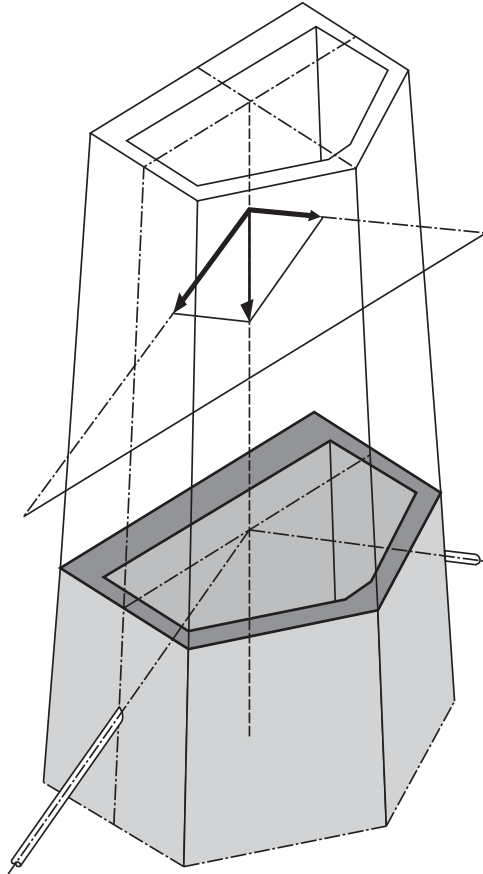
In the Øresund Bridge the 203.5 m high concrete pylons consist of free-standing columns above the deck (Figure 5.33). Below the double-deck truss the two pylon legs are connected by a cross beam with its top at a level of + 54 m so the free-standing upper part of the pylon legs is almost 150 m high. With this height and the choice of concrete as structural material it was important to avoid an eccentricity of vertical forces from all dead load. This was achieved by arranging the vertical cable planes in such a way that they coincided with the vertical centroid of the pylon legs as indicated in Figure 5.34.

Each pylon leg in the Øresund Bridge has a pentagonal cross section composed of four relatively thin walls and a wide and relatively thick wall facing the bridge deck. With this cross section it can be seen that the vertical axis of the pylon leg is in the cable plane. The pylon legs of the Øresund Bridge are constantly tapered from the bottom to the top and as the axis of each leg is vertical, the inner face of the pylon legs will be slightly inclined, which actually had the favourable visual effect that the legs do not appear to be leaning towards each other.

During the design of the Øresund Bridge it was investigated whether savings could be achieved by adding cross beams or other forms of transverse bracing between the two legs but it was found that the achievable reduction in quantities of the pylon legs would be counteracted by the quantities in the cross beam itself – and in the complications of the construction due to the heavy formwork required to cast a cross beam at a high altitude. This conclusion is, however, only valid when eccentricities are completely avoided in the pylon legs – as in the case of the Øresund Bridge



**Figure 5.33** Pylon of the Øresund Bridge



**Figure 5.34** Pylon with the cable plane and the pylon axis in the same vertical plane (Øresund Bridge)

design. With their height of more than 200 m, the Øresund pylons are unique by their unbraced pylon legs above the bridge deck.

The importance of having the axes of the free-standing pylons coincide with the cable planes is illustrated by the example in Figure 5.35. Here a system as shown at the top is considered. In this system the cable planes are inclined so that the stays can be attached along the edges of the deck without requiring the brackets indicated in Figure 5.30.

In this case the axial force in the pylon will have a resultant acting slightly outside the cross section of the pylon, but even if the resultant was acting at the edge of a square pylon section the results would be as indicated under (ii) and (iii) in Figure 5.33.

- (i) shows for comparison the cross section required if the axial force was acting without eccentricity. In this case the cross sectional area will be  $A_0 = 4bt_0$ .
- (ii) shows the cross section required if all of the side plates have the same thickness  $t_s$ . In this case all plate thicknesses will have to be  $2.5t_0$  so the cross sectional area will be increased by a factor of 2.5.
- (iii) shows the cross section required if the eccentricity of the axial force is counteracted by an asymmetrical cross section with the largest plate thickness in the plate coinciding with the resultant of the axial force. It is here assumed that this plate reasonably can be given a plate thickness of three times the thickness of the other three side plates.

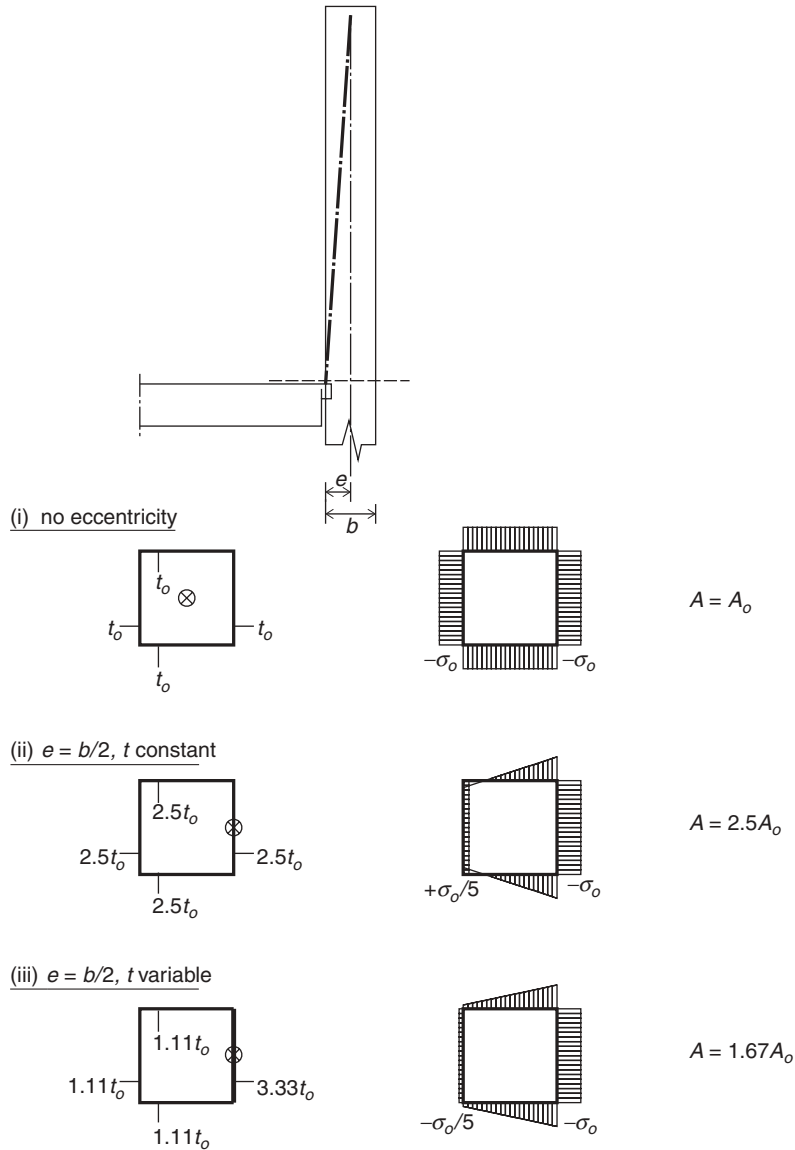
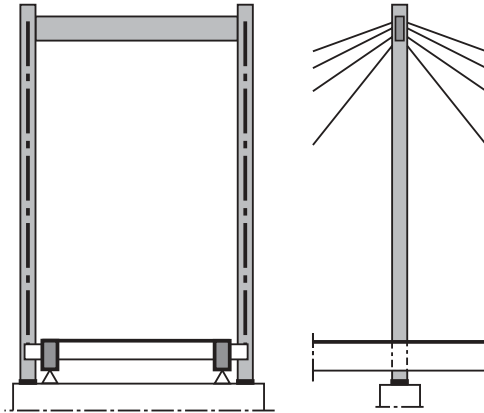


Figure 5.35 Comparison between pylons with pure compression and with eccentric normal force

For (iii) the cross sectional area has to be increased by a factor of 1.67 which is more reasonable but still a substantial increase to cope with the eccentricity.

From the plots of the stress distributions across the cross sections it is seen that for a constant plate thicknesses and eccentric load (ii), the sign of the normal force will change across the section, i.e. tension will occur in the side plate opposite the force resultant. For the asymmetrical cross section compression will exist over the entire section but in the side plate away from the force resultant the stress will be only one-fifth of the maximum stress.



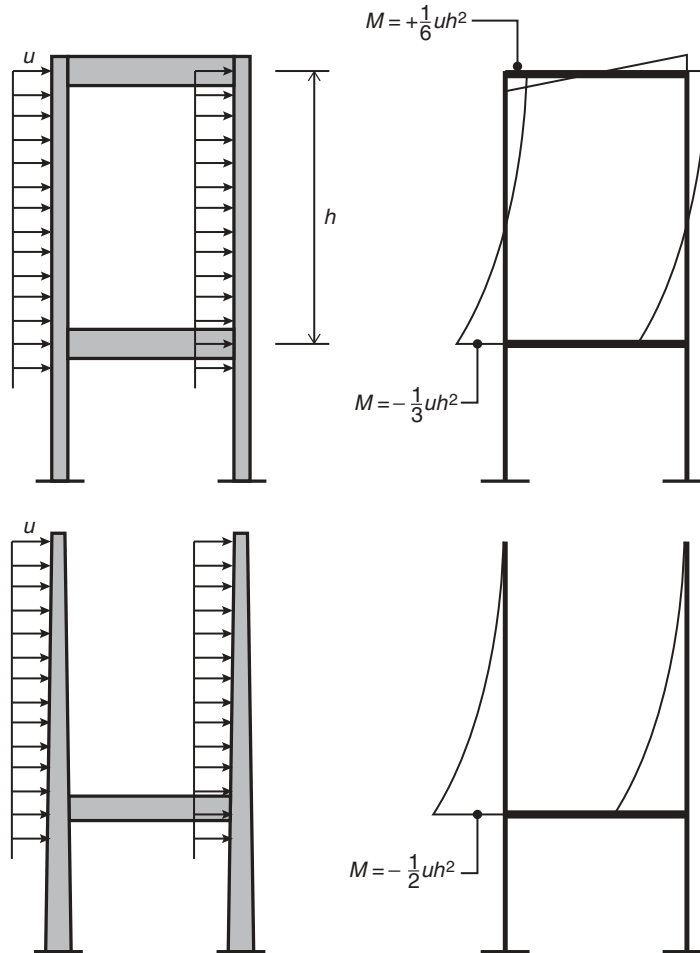
**Figure 5.36** Simple portal-type pylon with two legs connected by an upper strut

In the vast majority of bridges with more than 100 m high pylons and two legs a horizontal cross beam is added above the deck as shown in Figure 5.36. In bridges with a deck width exceeding the distance between the two cable planes and continuity of the deck (requiring that the pylon legs pass outside the edges of the deck), it will be equally beneficial to connect the two pylon legs by a horizontal strut at the top. As an example on a bridge with a pure fan system and a portal type pylon, Figure 5.37 shows the concrete pylon of the Pasco–Kennewick Bridge.

The effect of adding a cross beam between the top of the two pylon legs in relation to transmission of lateral (wind) load is not as pronounced as might be immediately expected. As seen in Figure 5.38, the bending moment due to wind load on the



**Figure 5.37** Pylon of the Pasco–Kennewick Bridge

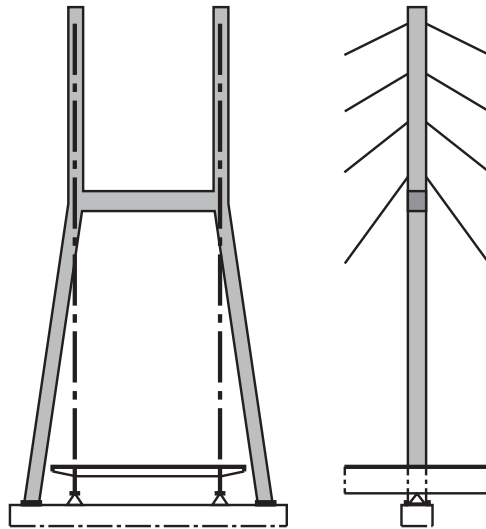


**Figure 5.38** Comparison between the bending moments due to lateral wind load in a pylon with a stiff cross beam at the top and a pylon with free-standing legs above the deck.

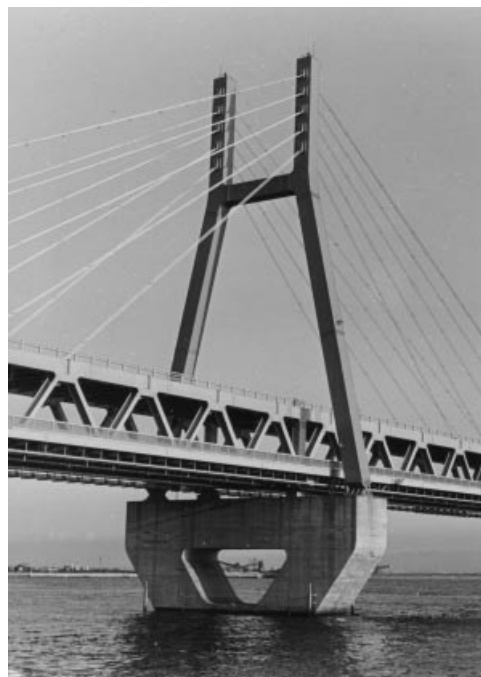
pylon structure is only reduced to 2/3 if a pylon with free-standing legs is replaced by one with a stiff cross beam added at the top. The reduction of quantities in the pylon legs might, therefore, not outweigh the quantity required in the cross beam, especially not if there is a wide gap between the two pylon legs.

In bridges with a modified fan or harp system it will not be convenient to have the pylon legs leaning in the regions where the cables are to be attached, so the horizontal strut should not be positioned at the top. The pylon legs should be vertical at the top where cables are attached, and the cross beam should be positioned below the anchor region. Below the strut, the legs can be leaning as illustrated in Figure 5.39. This pylon configuration was used for the first time in the Rokko Bridge in Kobe (Figure 5.40).

In bridges with high-level decks the pylon legs are often continued below the deck to a lower pier rather than have pier shafts projecting to the deck level. In such cases the pylon legs have traditionally been joined by a cross beam not only at the top but also immediately below the deck, as shown in Figure 5.41. With increasing pylon height it might prove advantageous to further increase the number of cross beams, as illustrated by the 180 m high concrete pylons of the Humber Bridge (Figure 5.42). Here the modestly tapered pylon legs have their inner faces in vertical planes whereas the outer faces are slightly inclined.

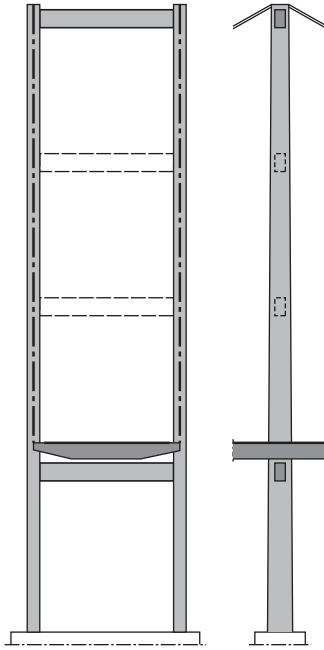


**Figure 5.39** Pylon supporting two semi-harp systems positioned some distance from the deck edges



**Figure 5.40** Pylon of the Rokko Bridge

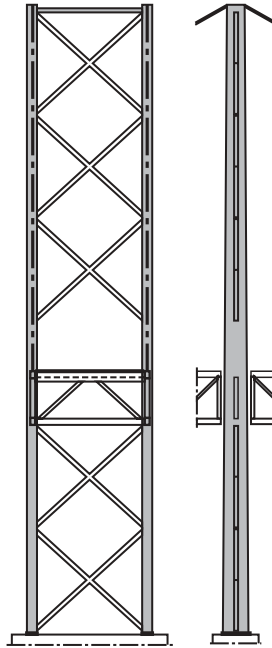




**Figure 5.41** Portal-type pylon with two legs connected by cross beams



**Figure 5.42** Pylon of the Humber Bridge



**Figure 5.43** Pylon with diagonal bracing between the two legs

A pylon with two legs connected by cross beams is in principle a vertical, cantilevered Vierendeel truss transferring the lateral load by shear and bending in the legs and in the cross beams. Consequently, the pylon legs must be designed as beam-columns.

The highest degree of lateral rigidity is obtained by connecting the pylon legs by diagonal bracing, so that the pylon is acting as a vertical, cantilevered truss (Figure 5.43). However, due to the requirements of clearance above the bridge deck the diagonal bracing must be omitted immediately above the bridge deck, and consequently the lateral forces have to be transferred locally by shear and bending in the pylon legs at the level of the deck.

Diagonal bracing has been used in the pylons of several major suspension bridges such as the San Francisco–Oakland Bay Bridge, the Firth of Forth Road Bridge, the Tagus River Bridge, the Kanmon Bridge, the Bisan Seto Bridges – and most prominently in the Akashi Kaikyo Bridge (Figure 5.44).

The pylon configurations shown in Figures 5.41 and 5.43 have been widely used in major suspension bridges. To position the cable system and the axis of the pylon leg in the same vertical plane, the deck has typically been arranged as shown in Figure 5.45.

In Solution (a) each vertical truss is positioned in the same plane as the axis of the pylon leg so that the cable plane can be arranged as shown in Figure 5.41. The edges of the roadway area are situated at some distance inwards from the vertical trusses to allow the full roadway width to pass between the pylon legs. However, the area between the curbs of the roadway and the cable system might be used for pedestrian lanes if they are passing outside the pylon legs on cantilevered decks, as shown for the Golden Gate Bridge in Figure 5.46.

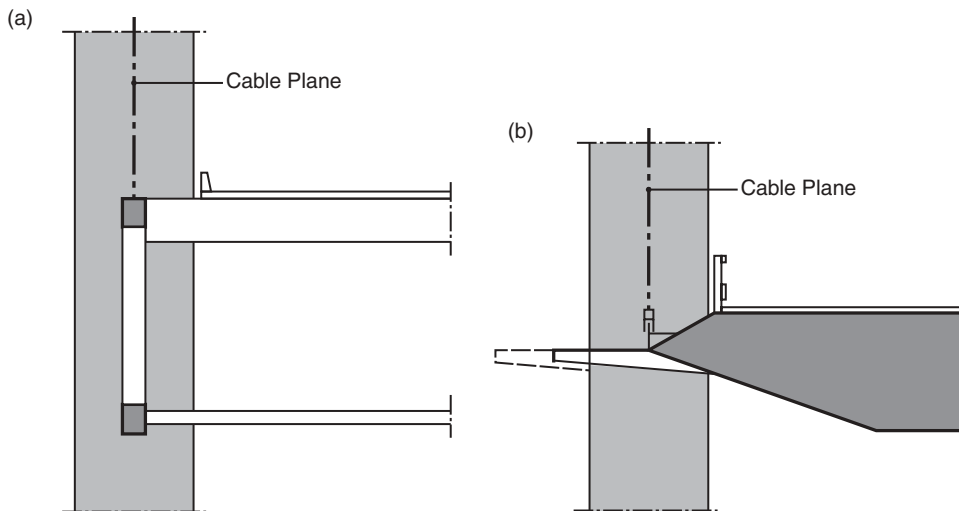
In Solution (b) of Figure 5.45 the deck is formed as a streamlined box with the hanger attached at the sharp edge of the box. As the roadway has to be positioned on the horizontal deck plate of the box, the required distance between the roadway edge and the cable system is dictated by the inclined portion of the top plate. Again with this solution, the pedestrian lanes must go around the pylon legs on the outside.

The cross sections in Figure 5.45 are generally found in bridges with simple supports and expansion joints at the pylons. Here the trusses or girders are discontinued on both sides of the pylons so that no intersection problems arise.



**Figure 5.44** Pylon of the Akashi Kaikyo Bridge

In bridges with a continuous deck it is preferable to let the entire cross section pass the pylon, and this leads to a different layout of the pylon. With the portal-type pylon the free passage of the deck can be achieved by a slight inclination of the pylon legs, as shown in Figure 5.47. Due to the cross beam at the top, the vertical forces from the cable system will be turned into the direction of the legs, so that an eccentricity of the axial forces can be avoided.



**Figure 5.45** Arrangements of the deck to make the cable plane coincide with the axis of the pylon leg



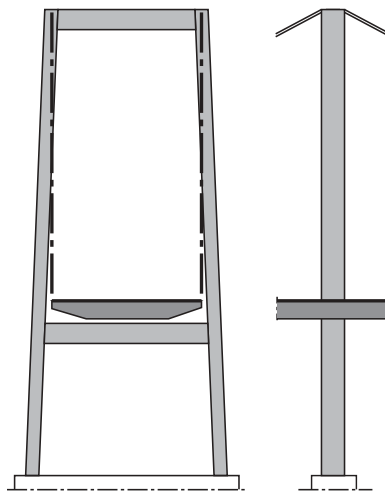
**Figure 5.46** Cantilevered deck attached to the pylon for passing of pedestrian lane outside the pylon leg (Golden Gate Bridge)

Another possibility is shown in Figure 5.48. Here the pylon legs are still vertical but positioned outside the deck, whereas the cable saddles are positioned on top of the cross beam. With this arrangement a considerable bending is induced in the cross beam, requiring a larger depth than for the solution of Figure 5.47.

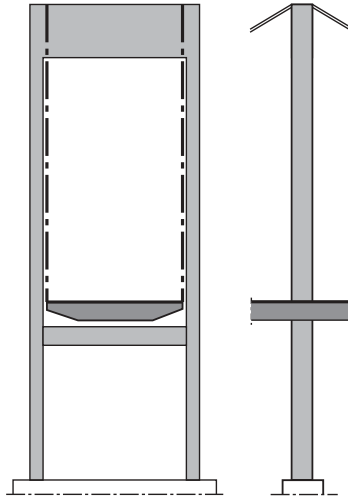
A configuration corresponding to that of Figure 5.47 was chosen e.g. for the concrete pylons of the Lillebælt Bridge, as illustrated in Figure 5.49. Here the configuration was selected to allow the hangers to be attached close to the roadway area (and not to allow continuity of the deck).

A continuous deck was used in the Storebælt East Bridge so here the pylon solution with leaning legs was the natural choice. However, due to the much larger distance from the bridge deck up to the top of the pylon than down to the water surface, the intermediate strut was positioned above the bridge deck approximately at mid-height.

The omission of the cross beam immediately below the deck has a favourable influence on the appearance of the bridge as it very clearly emphasizes the fact that the deck is actually suspended from the cables (Figure 5.50). At the same time no special structural problems existed at the intersection due to the continuity of the deck at the pylons. However, without the



**Figure 5.47** Portal-type pylon with inclined legs passing outside the deck



**Figure 5.48** Portal-type pylon with vertical legs and the cable system supported on the upper strut

lower cross beam, an efficient closed frame action was not at hand for transmission of the quite large lateral force from wind load on the deck. It was therefore necessary to increase the taper of the pylon legs below the deck, but this feature also turned out to have a favourable aesthetic impact as a monolithic transition could be established between the pylon legs and the pier below.



**Figure 5.49** Pylon of the Lillebælt Bridge



**Figure 5.50** Pylon of the Storebælt East Bridge

The 206 m high concrete pylons of the Tsing Ma Bridge resemble in their main arrangement the Humber Bridge pylons as the legs are interconnected by several cross beams (Figure 5.51). In the Tsing Ma Bridge each pylon leg has a constant width laterally but they have a slight inclination towards each other, at a slope of 1 in 100. The quite modest transverse slope implies that the cable planes must be positioned at some distance from the edges of the upper roadway area and this made it necessary to anchor the hanger cables to heavy brackets outside the main trusses (see Figure 4.99). With a more pronounced inclination of the pylon legs, the hanger cables could have been attached to the main trusses more directly.

In cable stayed bridges with semi-fan systems and a deck high above ground the upper part of the pylon should have a configuration as shown in Figure 5.39, whereas different options exist for the pylon part below the deck as shown in Figure 5.52.

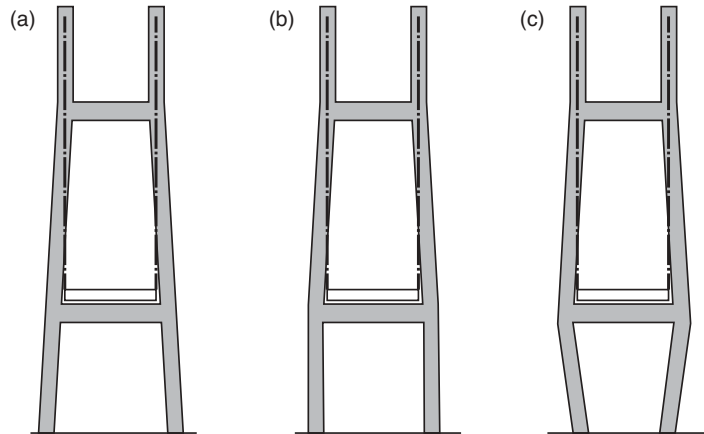
In the Alex Fraser Bridge the system of Figure 5.52(b) was used, as is seen in Figure 5.53. From a purely structural point of view this pylon configuration can be justified, but the double change of direction of the legs makes the pylon less convincing from an aesthetic viewpoint.



**Figure 5.51** Pylon of the Tsing Ma Bridge

A much more pleasing appearance is found in the pylons of the Yokohama Bay Bridge where the inclination of the pylon legs is kept constant from top to bottom (Figure 5.54). The simple geometry of these pylons implies that the upper, cantilevered parts of the legs with the stay cable anchorages are leaning, which result in some eccentricity moments. However, these moments remain small and they are balanced out for the lower part of the pylon by the cross beam.

In bridges with true harp-shaped cable systems the pylon legs have to be vertical and preferably coincide with the cable planes. The Higashi Kobe Bridge constitutes a prominent example on a major cable stayed bridge with pure harp systems and pylons with vertical legs. However, in the Higashi Kobe Bridge the cable planes are not strictly vertical as the stay cables are attached to the top chords of the stiffening truss positioned to pass inside the pylon legs. So in this bridge the pylon legs also had to be designed for some eccentricity moments. The pylons of the Higashi Kobe Bridge are distinctly characterized by the shape of the cross beams and also by the position of the upper cross beam that leaves a large upper part of the pylon as high free-standing columns (Figure 5.55).



**Figure 5.52** Configuration of a pylon with vertical legs in the upper anchor zone and different configurations below

In major suspension bridges the two cable planes are traditionally kept vertical primarily due to the advantages that can be gained during construction. For cable-stayed bridges with two cable planes a similar concern does not apply, and the cable planes might consequently be made with any inclination.

In bridges with two inclined cable planes meeting at the top, a pylon with an A-shaped upper part will generally be used, but in principle two cable systems might also be supported by a single vertical pylon as shown in



**Figure 5.53** Pylon of the Alex Fraser Bridge

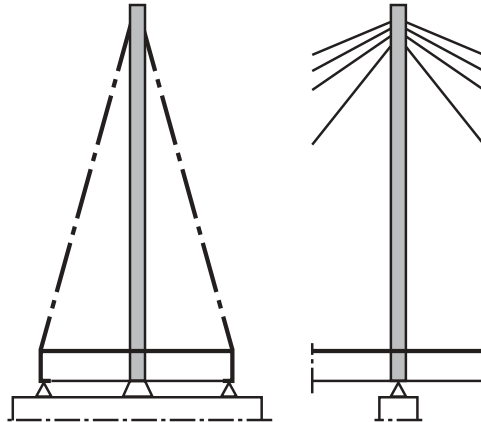




**Figure 5.54** Pylon of the Yokohama Bay Bridge



**Figure 5.55** Pylon of the Higashi Kobe Bridge



**Figure 5.56** Two inclined cable systems supported by a central pylon

Figure 5.56. Most prominently this principle has been used for the Stonecutters Bridge with its 300 m high pylons (Figure 5.57).

Inclined cable planes are seldom seen in suspension bridges but in Figure 5.58 is shown the Jiandong Bridge with two inclined suspension systems supported by a central pylon. A similar arrangement is seen in the main span of the new East Bay Bridge at San Francisco.

In cable stayed bridges with two inclined cable planes, the central pylon will to a large extent be supported laterally by the anchor cables so that stability does not entirely depend on the moment-rigid connection at the base. Consequently, the transverse dimensions of the pylon at the roadway might be chosen smaller than in the case where the pylon supports a single central cable plane.



**Figure 5.57** Pylon of the Stonecutters Bridge

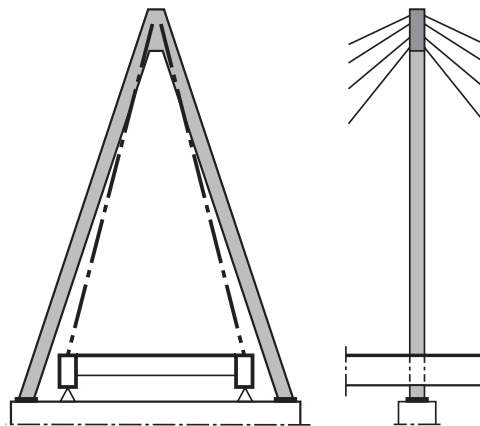


**Figure 5.58** Pylon of the Jiandong Bridge

With the A-shaped pylon, shown in Figure 5.59, the bridge deck is kept free of any structural elements so a large degree of freedom exist in the layout of traffic lanes. The A-shaped pylon was first applied in the Severins Bridge where the pylon legs were continued to a lower pier top, whereas the deck was supported onto the pylon legs through brackets outside the two main girders (Figure 5.60).

For the transmission of the primary vertical force from the top, where the cable system is attached to the base, an inclination of the pylon legs will inevitably lead to increased quantities as both the axial force and the length will be larger for an inclined than for a vertical pylon leg.

This effect is illustrated in Figure 5.61 showing how the relative quantity  $Q_{pl}/Q_{pv}$  ( $Q_{pv}$  is the quantity of the vertical pylon) varies with the width-to-height ratio  $b_{pl}/h_{pl}$ . It appears that for  $b_{pl}/h_{pl} = 0.5$ , corresponding to a leg inclination



**Figure 5.59** A-shaped pylon supporting two inclined cable planes



Figure 5.60 Pylon of the Severins Bridge

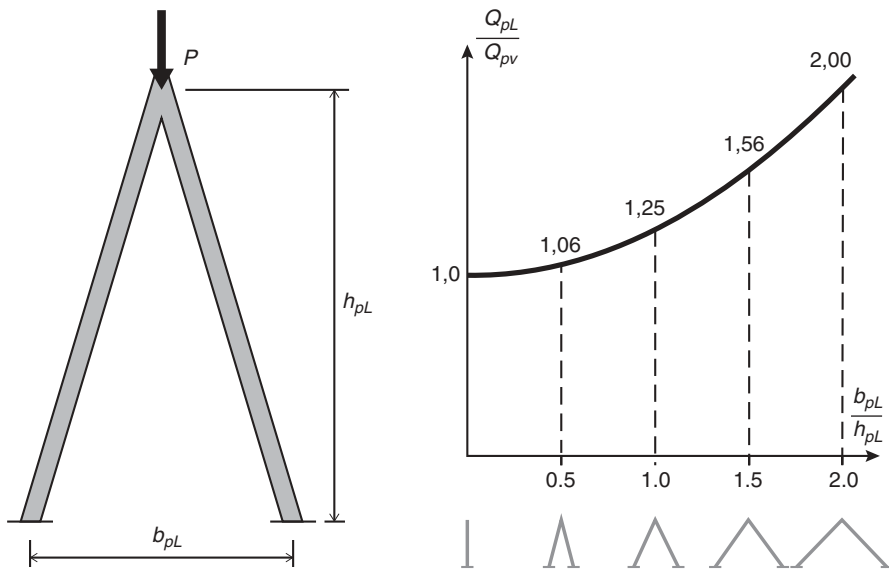
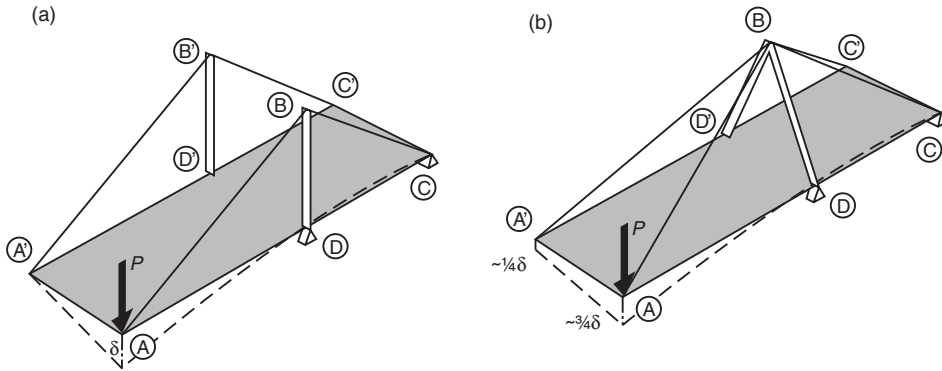


Figure 5.61 Variation of the ratio between the quantity of an A-shaped pylon  $Q_p$  and the quantity of a vertical pylon  $Q_{pv}$  with the width-to-height ratio  $b_p / h_p$



**Figure 5.62** Comparison between deflections of a system with two vertical cable planes supported by free-standing pylons and a system with two inclined cable planes supported by an A-shaped pylon

of 4:1, the quantity will only be increased by approximately 6%, whereas a 100% increase will result if the leg inclination was 1:1. Thus, A-shaped pylons are most appropriate if the width-to-height ratio is reasonably small – and this ratio is governed by the width of the bridge deck and the height (sag) of the cable system.

It should, however, be emphasized that only the material required to transmit the vertical force  $P$  is included in the plot of Figure 5.61, and that the advantages to be gained by the increased lateral stability of the A-shaped pylon consequently have been ignored.

The combination of an A-shaped pylon and two inclined cable planes will give a special deformational effect under eccentric traffic load, as illustrated in Figure 5.62.

For System (a) with two free-standing pylons and vertical cable planes, the deflection  $\delta_y$  under the vertical force at A will be due mainly to the elongation of the cables AB and BC. If the deck has an insignificant torsional stiffness, no deflection will occur in the unloaded cable plane, so that the total deformations will be as indicated by the dotted line.

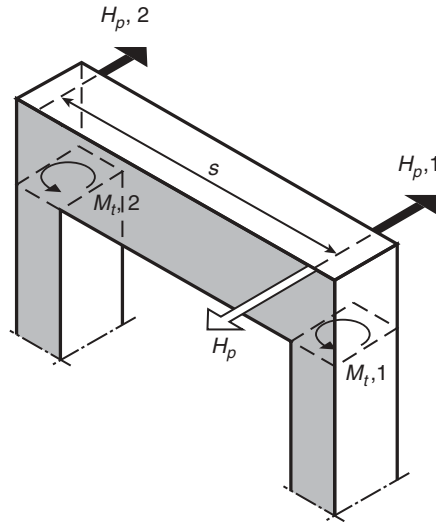
For System (b) with an A-shaped pylon and two inclined cable planes, the pylon top B will be restrained by both the anchor cable BC and BC', and consequently the longitudinal displacement of point B will only be about half of that found in system (a). Thus, the deflection under the force at A is reduced to approximately  $3/4 \delta_y$ , but at the same time the unloaded point A' will deflect approximately  $1/4 \delta_y$  due to the longitudinal displacement of the pylon top. Comparing the deformation of the two systems it appears that the twist angle is reduced to about half when changing from System (a) to System (b).

A similar effect will be found in portal type pylons with torsionally rigid legs topped by a flexurally and torsionally rigid cross beam. Here a horizontal force  $H_p$  acting at one of the cable planes can be distributed partially to the other cable plane inducing torsional moments  $M_{t,1} = M_{t,2} = 1/2 H_p s$  in the pylon legs as indicated in Figure 5.63. Actually, these torsional moments might easily be of such an intensity that they must be taken into account in the design of the pylon legs especially if they are made of concrete.

The reduction of the torsional deformations associated with an A-shaped pylon or a torsionally rigid portal pylon will generally have a favourable influence on the aerodynamic stability, as it suppresses the twisting movements.

In bridges with high level decks a pure A-shaped pylon will look as shown in Figure 5.64. Here the inclined pylon legs are continued to the pier below and a cross beam is positioned directly under the deck. This type of pylon was used e.g. for the 122 m high pylons of the Meiko Nishi Bridge in Japan (Figure 5.65).

In some cases it might be disadvantageous for the substructure to have the legs of the A-shaped pylon spread as widely as indicated in Figure 5.64. This has led to the diamond-shaped pylon shown in Figure 5.66 where the direction of the pylon legs is changed at the deck level, thus reducing considerably the width of the pylon at the bottom. However, this configuration requires a considerable flexural stiffness in the lower part, as the legs below the deck are inclined in the 'wrong' direction for the transmission of lateral forces from the upper part. This feature is illustrated in Figure 5.67 showing three different pylon configurations all with a triangular upper part. Subjected to a lateral force  $P_z$  acting at the level of the cross beam (e.g. a wind force from the deck), the moments in the three pylons



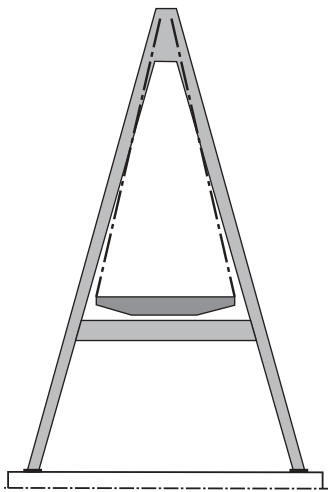
**Figure 5.63** Distribution of horizontal force  $H_p$  between two cable systems by activating the torsional stiffness of the pylon legs

will be as indicated at the top of the figure. It is seen that the moment at the base is 56% larger in System (c) than in System (a).

However, the difference in lateral deflections is much larger, as shown at the bottom of Figure 5.67. With the pure A-shape (System (a)) a deflection  $\delta_z$  occurs at the cross beam due to bending of the pylon legs but at the top (where the cable system is attached), the lateral deflection will be insignificantly small.

The pylon with vertical legs in the lower part (System (b)) is characterized by a somewhat larger lateral deflection equal to  $1.32 \delta_z$  at the cross beam as well as at the top.

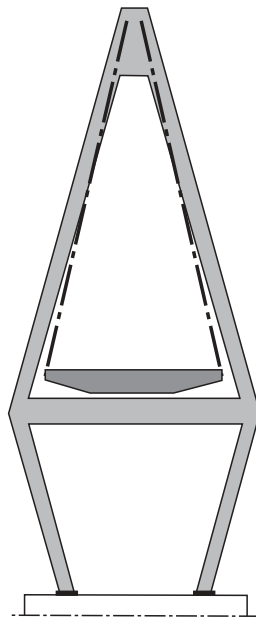
In the diamond-shaped pylon the lower part (System (c)) the lateral deflection of the cross beam amounts to  $1.8 \delta_z$  and this deflection is amplified by the geometric configuration to twice as much at the top.



**Figure 5.64** A-shaped pylon, with the legs continued to a lower pier



**Figure 5.65** Pylon of the Meiko Nishi Bridge



**Figure 5.66** A-shaped pylon with inward-leaning legs below the bridge deck (diamond shape)

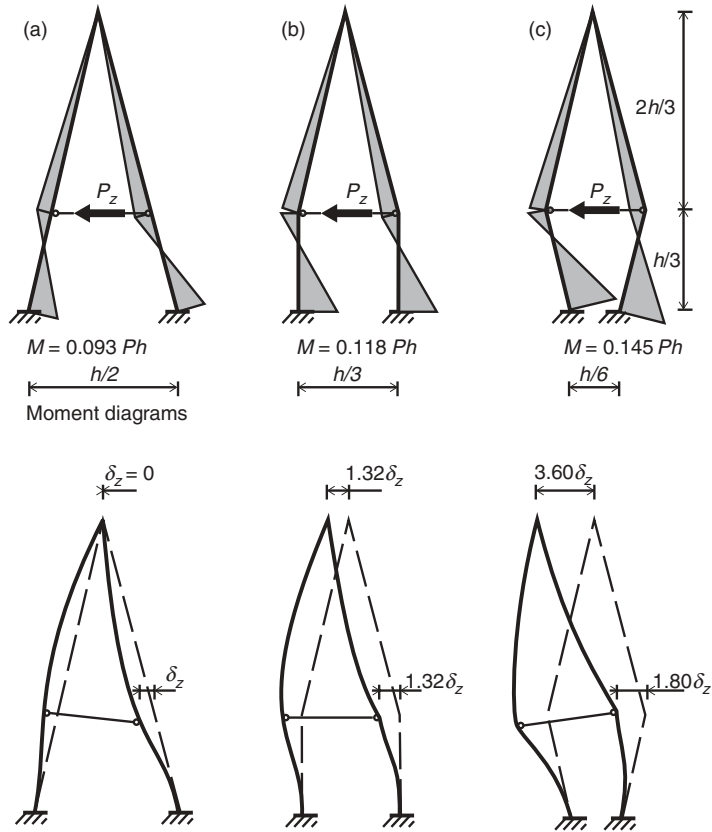


Figure 5.67 Moments and deformations of three types of pylons with a triangular upper part

The immediate feeling of less stability in the system with inward leaning legs is therefore easily demonstrated by a simple analysis such as the one illustrated in Figure 5.67.

The deformational drawbacks of System (c) has not prevented the diamond shape from being widely used, but it must be remembered that the inexpediency of the form will have to be compensated for by increased flexural stiffness of the legs. Thus, to reduce the lateral deflection of the pylon top in System (c) to the same value as found at the level of the strut in System (a), the moment of inertia for the legs must be increased by a factor of 3.6.

The configuration of Figure 5.66 was chosen for the Farø Bridge pylons that support a single-plane semi fan system. It was here essential to keep the pylon dimensions small at water level as the pylon had to be standing on a conical caisson with a relatively small diameter at the top.

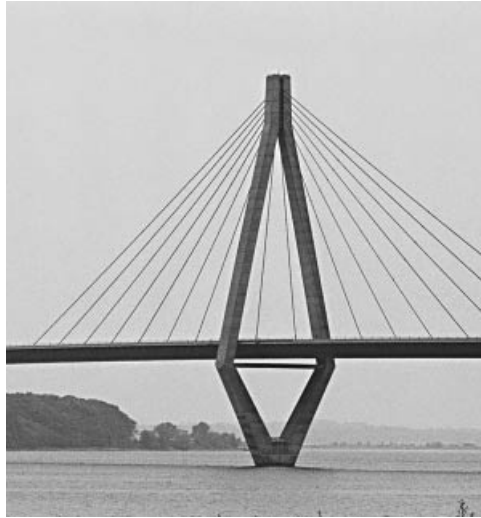
In the pylons of the Farø Bridge the additional flexural stiffness required in the lower part of the pylon is clearly reflected in the shape of the pylon legs with taper from the bottom to the deck (Figure 5.68).

An improved lateral rigidity of the pylon with inward-leaning legs can be achieved by bracing the lower part as shown in Figure 5.69. The vertical K-brace will ensure an efficient lateral support of the cross beam, and with small deflections at the roadway level the deflections at the pylon top will also be small – although somewhat amplified.

The principle of bracing the lower pylon part is seen in the Tempozan Bridge in Japan, as shown in Figure 5.70. Here the lower part of the pylon contains a double bay K-brace that significantly increases the lateral stiffness.

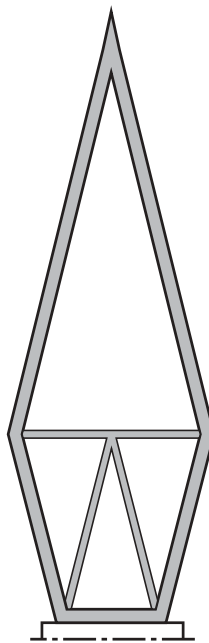
Besides being braced below the deck level, the pylons of the Tempozan Bridge are also unique by having all stay cable anchorages in the pylon positioned in the inclined parts of the pylon legs below the top part. In most other bridges with a λ-shaped upper part all cable anchorages are arranged in the vertical top part where the two legs are merged.





**Figure 5.68** Pylon of the Farø Bridge

In the Fred Hartman Bridge across the Houston Ship Canal, the pylons are made in a double-diamond configuration, as can be seen in Figure 1.88. This implies that the lower part is efficiently braced by the perfect triangulation. So both vertical and lateral forces acting at the top and the deck level can be transferred as axial forces in the members of the pylon. It has therefore not been necessary to widen the legs in the lower part of the pylon structure.



**Figure 5.69** A-shaped pylons with inward-leaning legs braced below the deck



**Figure 5.70** Pylon of the Tempozan Bridge

The principle of legs leaning inwards below the deck was also applied in the Köhlbrand Bridge (Figure 5.71). However, here the lengths of the elements in the lower part of the steel pylon are so small that the bending deformations in this part are of limited significance.

A variant of the pylon configuration used in the Köhlbrand Bridge is seen in the Tsurumi Fairway Bridge – the world’s longest single plane cable stayed bridge (main span 510 m). Here the upper  $\lambda$ -shaped pylon part in steel is supported on a concrete pier shaft by a heavy cross beam in steel immediately below the bridge deck (Figure 5.72).

Pylons of the  $\lambda$ -shape have become the preferred solution for many of the largest cable stayed bridges, e.g. the Normandy Bridge and the Sutong Bridge. Here the vertical top part typically constitutes approximately 25% of the total height, but there is quite a variation of the overall geometrical shape to be seen from one bridge to another.

The pylon of the Rama VIII Bridge in Bangkok is characterized by an unusual high vertical top part that gives support to a semi-harp cable system (Figure 5.73). As can be seen, the top part constitutes approximately half of the total height of the 160 m high concrete pylon.

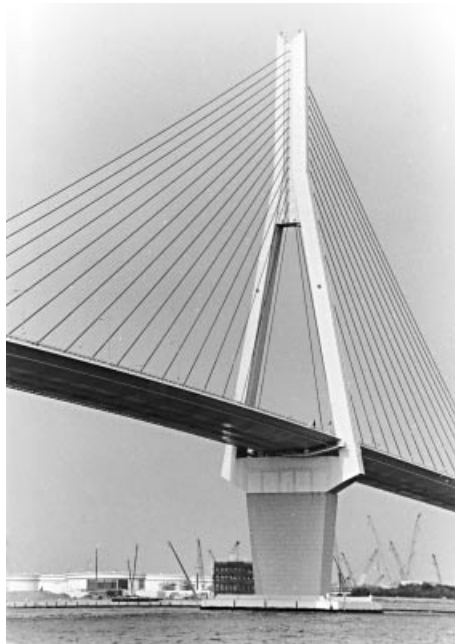
One consequence of the high top part is that each of the two straddling legs will have a more pronounced inclination. In the final condition this might not present a major problem but during construction when the two legs will have to be cast independently it must be taken into account that gravity will induce additional bending from the dead load of every new casting.

This is illustrated in Figure 5.74 where a comparison between a vertical pylon leg and an inclined is shown. It is seen that in a vertical leg a new casting actually stabilizes the pylon by increasing the uniform compression (and thereby improves the ability to resist bending from wind drag or other lateral loads). In an inclined leg on the other hand, the new casting will increase the bending and in the given example tensile stresses will occur already for the weight of a leg segment with a length of three times the width of the leg. The leg will, therefore, be sensitive to wind blowing from left to right.

To counteract the bending induced by gravity, the two inclined pylon legs can be stabilized against each other by temporary horizontal struts that are not required in case of vertical legs.



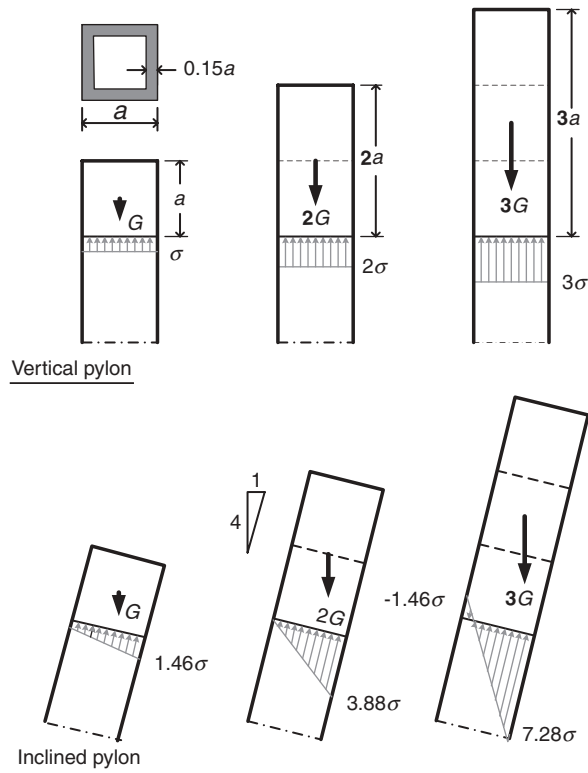
**Figure 5.71** Pylon of the Köhlbrand Bridge



**Figure 5.72** Pylon of the Tsurumi Fairway Bridge



**Figure 5.73** Pylon of the Rama VIII Bridge in Bangkok



**Figure 5.74** Dead load stresses in a vertical and an inclined pylon leg during construction

## 5.4 Pylons Subjected to Longitudinal Forces from the Cable System

Pylons with slender legs positioned in a vertical plane perpendicular to the bridge axis are characterized by a large flexibility of the pylon top in the longitudinal direction. These pylons are therefore primarily used in bridges where longitudinal displacements of the pylon top are restrained by the cable system, e.g. by an anchor cable.

In multi-span bridges a considerable stiffness of the pylon top in the longitudinal direction might be required, as explained in the section on the multi-span cable system. There it was also explained that the required stiffness could be achieved by a triangular pylon structure that gives both vertical and longitudinal support to the cable system at the top.

For an earth anchored cable system such as the suspension system, the triangular pylon structure should comprise straight, inclined legs all the way from the top to the pier.

Figure 5.75 shows such a pylon structure with four legs connected by a cross beam at the top. Furthermore, the legs are connected by transverse beams below the deck so that a lateral and a torsional support of the deck can be established. A vertical support of the deck at the cross beams might not be advantageous in most cases as it would result in a too strong fixity.

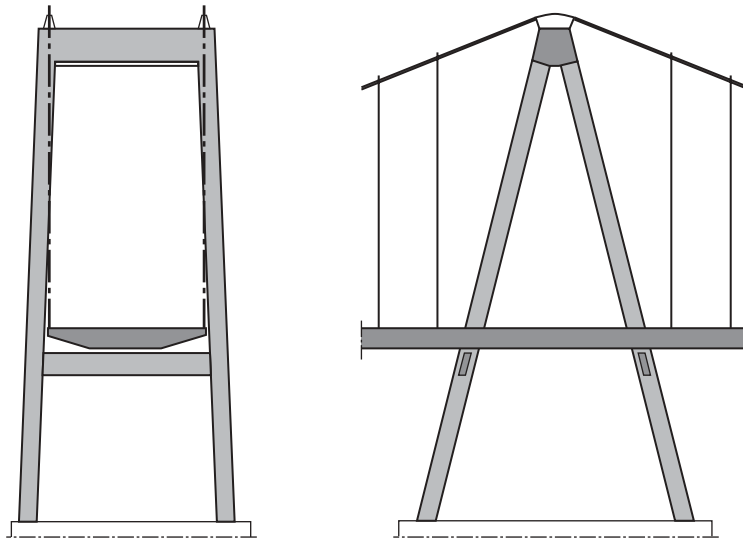
Note that the axes of the pylon legs and the main cable tangents should intersect at the same point of the elevation to avoid bending of the legs from the horizontal force.

With self anchored cable systems only the upper part of the pylon structure (above deck level) should be triangular, and at the same time an intimate connection between this part and the deck is essential, as a considerable horizontal force has to be transferred between the two elements. This leads to a design where the triangular part of the pylon is fixed to the deck, and preferably also made of the same structural material.

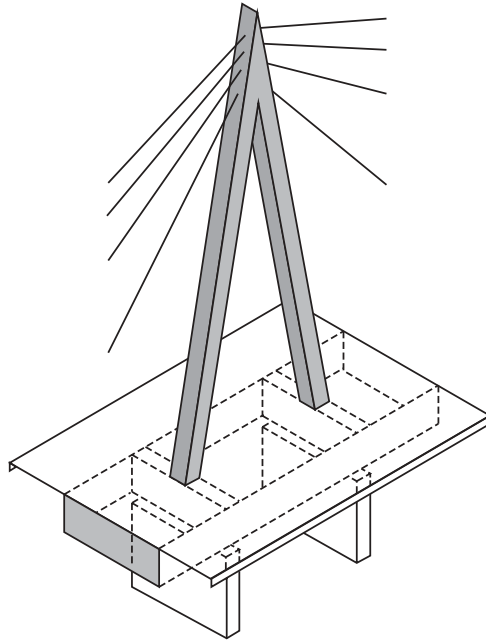
In bridges with a central cable plane, the triangular pylon must be positioned in the median strip (Figure 5.76). In this case the pylon legs should be moment-rigidly connected to the deck through interior diaphragms in the box. Bearings must be placed directly under each pylon leg to transmit the vertical forces to the substructure. These bearings often have to be anchored to allow transmission of tensile forces.

The principle of Figure 5.76 was applied in the two-span cable stayed bridge across the Rhine at Neuwied, as illustrated in Figure 5.77. In this bridge where the structural system is as shown in Figure 3.20(e), the pylon supports a multi-cable modified fan system.

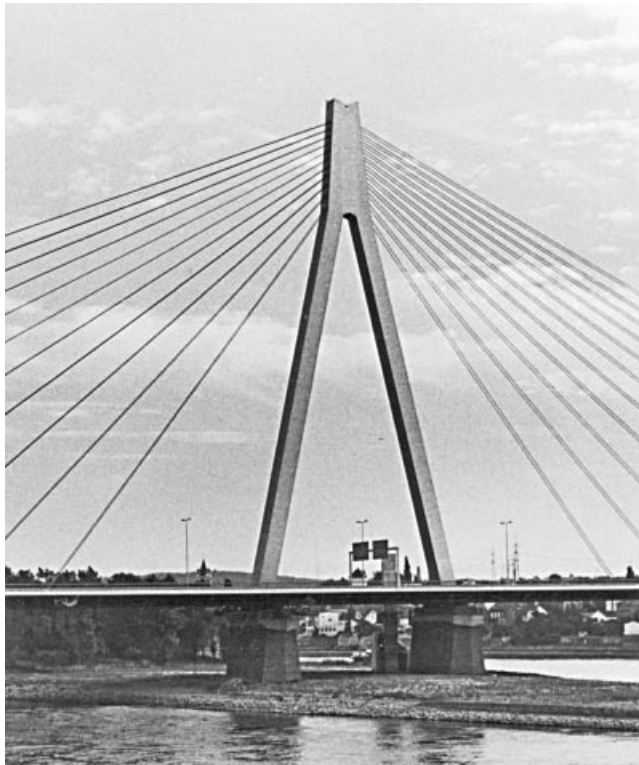
More recently the system of Figure 5.76 has been used in the Millau Viaduct as illustrated in Figure 5.78. The pylons are made of steel (as the deck) whereas the V-shaped or Y-shaped pier shafts below are in concrete with a height of up to 245 m.



**Figure 5.75** Triangular portal-type pylon rendering vertical and longitudinal support to the main cable



**Figure 5.76** Triangular pylon positioned centrally in the median strip and fixed to the deck



**Figure 5.77** Pylon of the Rhine Bridge at Neuwied

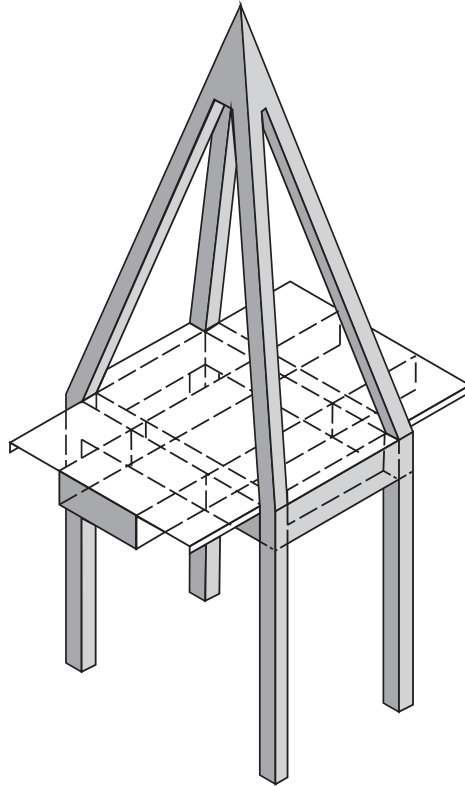


**Figure 5.78** Pylon of the Millau Viaduct

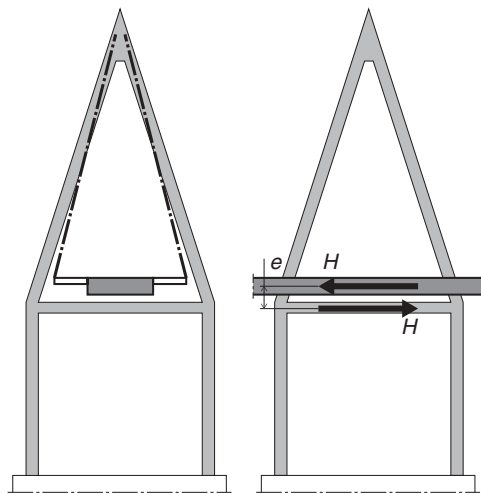
With two inclined cable planes the upper pylon part becomes pyramidal, as shown in Figure 5.79. Furthermore, in this figure is indicated a different design of the lower pylon part with four vertical legs in continuation of the inclined legs of the upper part. The transition from the inclined legs to the vertical legs takes place at the roadway level so that the entire deck can act as a tie both longitudinally and transversally. To ensure efficient transmission of horizontal forces from the deck to the pier, a frame action in the lower part is advantageous and the legs should therefore be interconnected by box girders in two directions below the bridge floor, as indicated in the figure.

It is important to notice that, whereas the triangular pylon structure supporting an earth anchored cable system (refer to Figure 5.75) to a large degree is separated from the deck, then the triangular pylon structure of a self anchored cable system should be in very close contact with the deck. Therefore in the earth anchored system the structural material of the deck and the pylon can be chosen more independently than for the self anchored system.

In a self anchored bridge with moderate pylon height an overall estimate might indicate that the entire pylon structure should be made of concrete even though the deck was made of steel. In such a case one could be tempted to design a pylon structure as shown in Figure 5.80, but this arrangement will result in structural problems related to the transmission of the large horizontal force from the deck to the pylon structure. First of all, bearings capable of transferring much larger horizontal than vertical forces must be inserted between the deck and the pylon, and at the

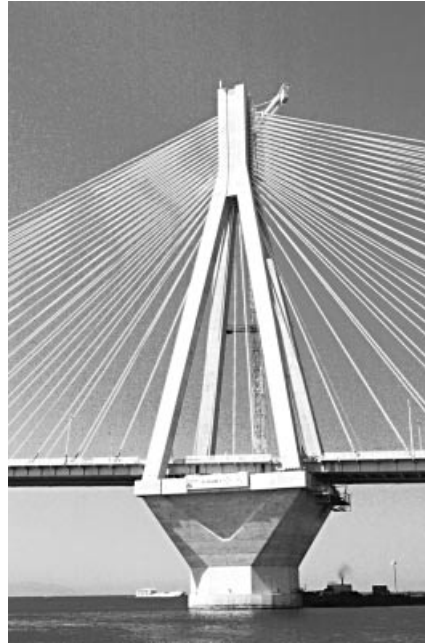


**Figure 5.79** Pylon structure with a pyramidal upper part



**Figure 5.80** Pyramidal concrete pylon with structural elements kept free of the deck in steel





**Figure 5.81** Pylon of the Rion-Antirion Bridge (Photo credit: Francis Vigouroux/Photothèques Vinci et filiales)

same time a moment  $M = He$  from the eccentricity between the horizontal force in the deck and in the pylon structure will have to be taken either by the deck or by the pylon. Due to the large intensity of the horizontal force to be transferred, this moment will be of a considerable magnitude. It is therefore very doubtful whether a structure as shown in Figure 5.80 will be superior to that of Figure 5.79 although a sub-optimization should indicate that the pylon treated separately should be made of concrete.

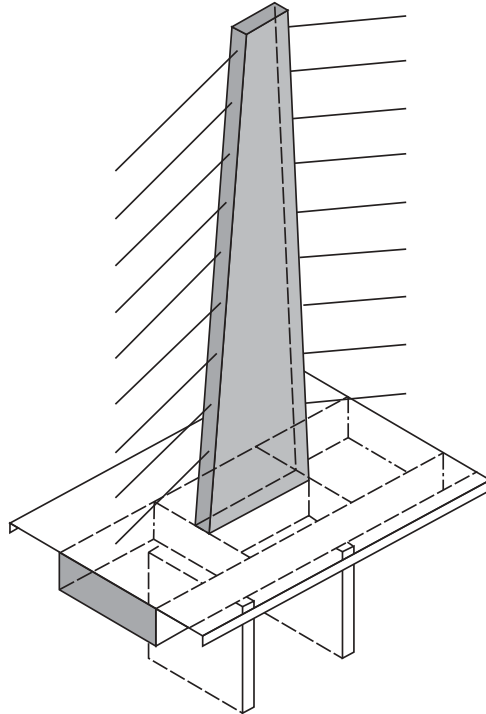
A better solution in the case of a concrete pylon and a steel deck seems to be to make the entire structure above the pier (both the pylon structure and the deck between the pylon legs) of concrete with a configuration as shown in Figure 5.79, and then change the material of the deck to steel immediately outside the pylon. This requires a transition from steel to concrete in the deck but such transitions have already been made in several two-span and three-span bridges with a steel deck in the main span and a concrete deck in the side span(s), e.g. in the Normandy Bridge (Figure 4.74).

In the Rion-Antirion Bridge the four pylon structures with their pyramidal configuration above the deck was made of concrete (Figure 5.81). In the early design process it had been assumed that the deck should be longitudinally fixed to the pylon piers (as in Figure 5.80) but due to the severe seismic conditions at the site it was chosen to let the deck ‘float’ in the longitudinal direction. That also allowed the entire deck of the cable stayed bridge be made continuous.

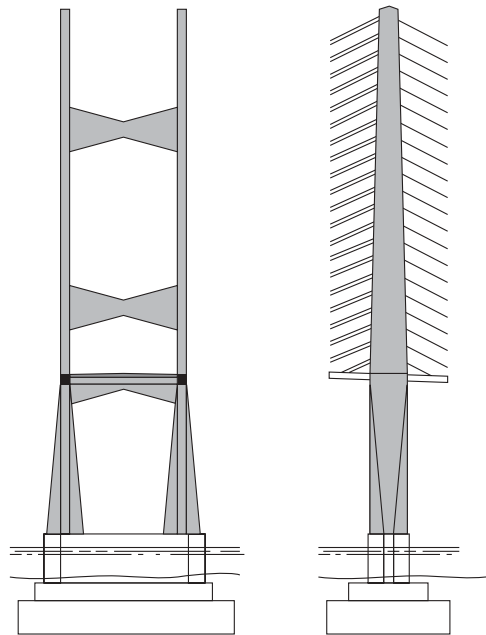
Generally, triangular pylon structures only render an efficient longitudinal support to cable systems attached in one point, viz. the point where the axes of the inclined legs intersect. This feature makes triangular pylons well suited for supporting suspension and (pure) fan systems, but unsuited in case of harp systems.

To give longitudinal support to a harp system, the pylon should be designed as a cantilevered beam-column with a considerable flexural stiffness in the longitudinal direction of the bridge. This leads – as illustrated in Figure 5.82 – to a pylon with a pronounced rectangular cross section being tapered above the bridge deck in the longitudinal direction of the bridge. To give the desired effect the pylon should be fixed to the deck and supported by the substructure in such a way that moments can be transmitted, e.g. by application of two bearings in a certain distance.

A pylon with a considerable flexural stiffness in the longitudinal direction is found in the three-span Napoleon Bonaparte Broward Bridge (Figure 5.83). Here the 136 m high pylon is fixed to the substructure to improve very efficiently the deformational characteristics of the multi-cable harp system.



**Figure 5.82** Pylon with large bending stiffness to give longitudinal support to a harp-shaped cable system



**Figure 5.83** Pylon of the Napoleon Bonaparte Broward Bridge

## 5.5 Cross Section

When designing the cross section of a pylon, the task is generally well defined, as all major forces and the functional requirements are known. As the axial force produced by the cable system in most cases is the dominant action, an effective column section is essential.

Steel pylons of moderate size are generally made with a quasi-square box shape, as this constitutes an effective column section. Due to the common desire of keeping the cross sectional dimensions small, relatively thick side plates with thicknesses from 25 mm and up to 100 mm are often required.

Pylons with moderate cross sectional dimensions, as found in cable stayed bridges, are often fabricated in segments, each comprising the full cross section so that only transverse erection joints have to be made on site.

Due to the large compressive stresses in the pylon it is necessary to efficiently stiffen the individual plates against buckling. However, as the longitudinal stiffeners themselves form a part of the cross section available for transmission of axial compression the consequences of applying stiffeners with ample dimensions are very slight. Thus, the typical cross section of a pylon with moderate cross sectional dimensions will be as shown in Figure 5.84 with efficient, longitudinal stiffeners spaced at a distance of 30 to 40 times the plate thickness. To support the longitudinal stiffeners, bulkheads are placed inside the box. As very little torsion is applied to the pylon leg sections on the free lengths, the number and spacing of bulkheads can generally be decided by considering the buckling aspects only.

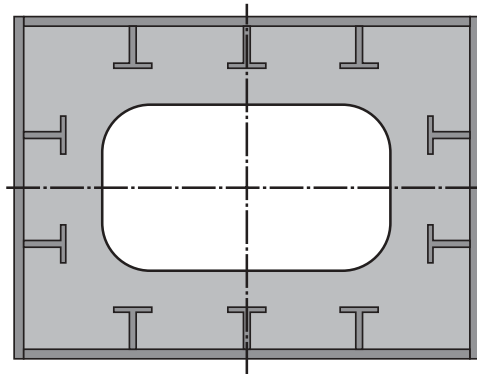
Steel pylons with large cross sectional dimensions, as found in major suspension bridges, cannot be fabricated in segments comprising the full cross section due to limitations during transportation and erection.

The subdivision of the cross section into smaller units can be made by using a multi-cellular layout as shown in Figure 5.85. Here each cell constitutes a prefabricated unit with dimensions chosen to satisfy requirements due to transportation and erection.

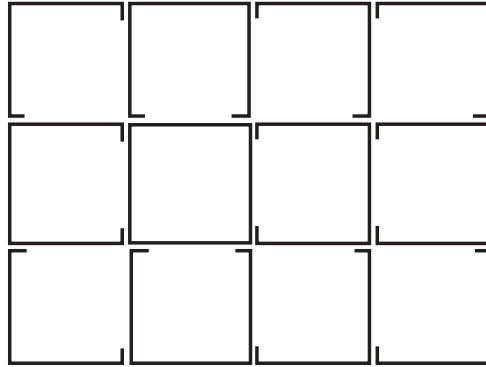
The multi-cellular concept has been used for the majority of the American suspension bridges built up to the mid 1960s. Thus, this concept was used for the 192 m high pylons of the Verrazano Narrows Bridge (Figure 5.86). As illustrated in Figure 5.87 each pylon leg consisted of 68 cells. Due to the relatively small cross sectional dimension of each cell (approximately 1.1 m  $\times$  1.1 m) the shop-riveted erection units comprised 4, 6 or 8 cells. For the field splices, high strength bolts were used, as might be seen from Figure 5.88 showing the inner face of the pylon at the roadway level.

Generally, the multi-cellular concept does not give an optimum cross section to carry compressive forces and bending moments, as a considerable amount of the material is positioned close to the centroid. This feature is illustrated in Figure 5.89 by the moment of inertia for a square multi-cellular box section (with equal plate thicknesses throughout) and for a square mono-cellular box, both having the same area. It is seen that the moment of inertia of the mono-cellular box is twice as large as that of the multi-cellular box.

This has led to a pylon design where the cross section is composed of four panels, each constituting one side of the total box section. In modern construction, it is often preferable to use shop welding for each panel made as a stiffened plate, whereas it is sometimes preferred to use bolts in the field splices. With a design as shown in Figure 5.90 it is possible to avoid loose splice plates in the vertical joints and with horizontal end plate joints that transfer compression by contact all bolts can be inside the box.



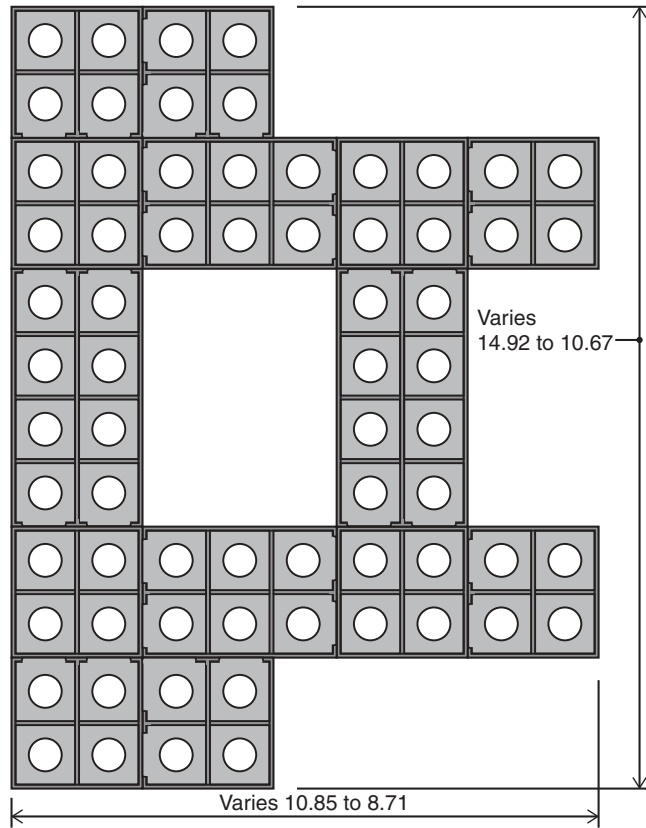
**Figure 5.84** Cross section of a welded pylon with moderate dimensions



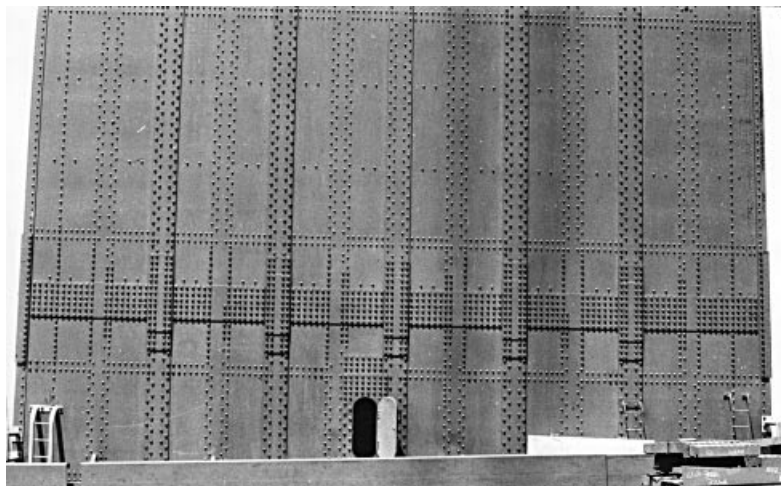
**Figure 5.85** Multi-cellular layout of a pylon cross section



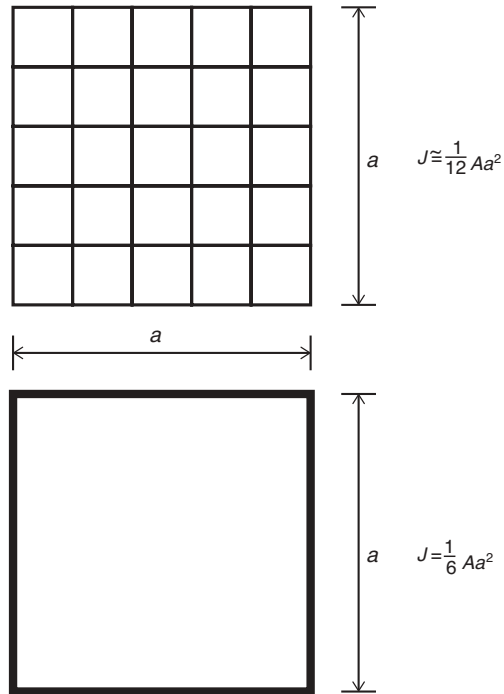
**Figure 5.86** Pylon of the Verrazano Narrows Bridge



**Figure 5.87** Cross section of the Verrazano Narrows Bridge pylon



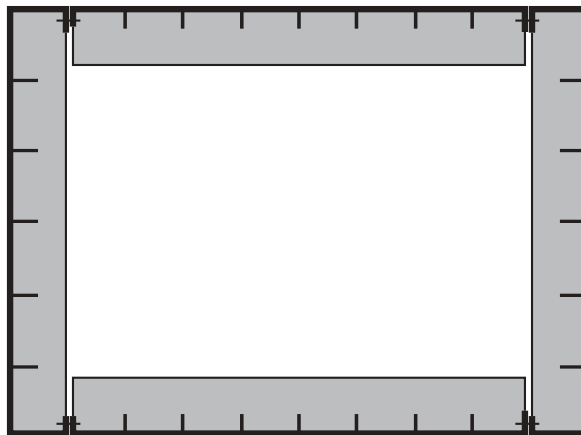
**Figure 5.88** Pylon of the Verrazano Narrows Bridge at the roadway level



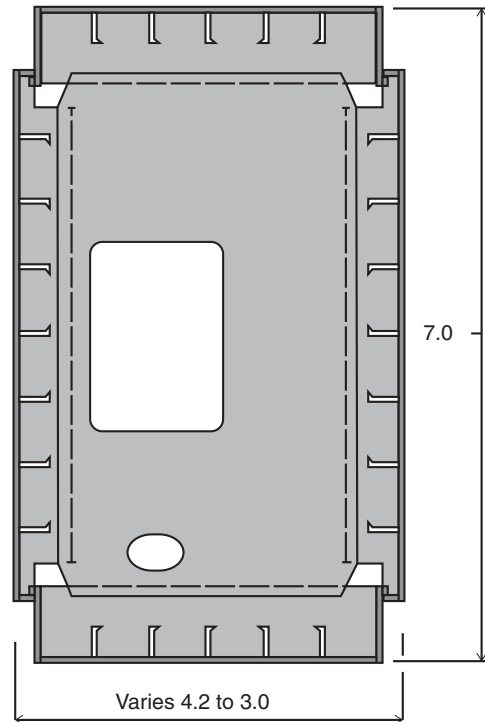
**Figure 5.89** Comparison between the moment of inertia for a multi-cellular box and a mono-cellular box

The principle of a mono-cellular box composed of four stiffened panels was first applied in the Severn Bridge, and later the same principle was used in the First Bosphorus Bridge with a pylon leg cross section as shown in Figure 5.91. Here the side plates have thicknesses varying between 20 and 22 mm, and the vertical stiffeners are made of bulb flats. The horizontal diaphragms consist of a stiffened panel bolted to the transverse stiffeners of the side plates.

Concrete pylons will, in most cases, have a hollow cross section but due to the intensity of the axial force large wall thicknesses are often required. In the final structure the dominating axial force from the cable system ensures compression across the main part of the cross section, but during construction when the pylon acts as a cantilever with a moderate



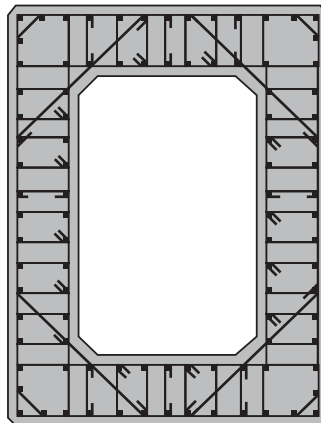
**Figure 5.90** Mono-cellular pylon composed of four stiffened panels



**Figure 5.91** Cross section of the Bosphorus Bridge pylon

axial force from its own weight, the horizontal wind load can give tension in a considerable part of the cross section. Also in cases where the pylon stabilizes a partially erected superstructure the unavoidable lack of balance during lifting of deck units induces moments in the pylon legs. Thus, the vertical reinforcement is often determined by the temporary conditions during construction.

In the pylon legs the vertical reinforcing is generally made of ribbed bars that should be efficiently supported by stirrups, as indicated in Figure 5.92. Post-tensioned reinforcing might be found locally in struts and cable anchor zones, whereas it



**Figure 5.92** Cross section of a concrete pylon

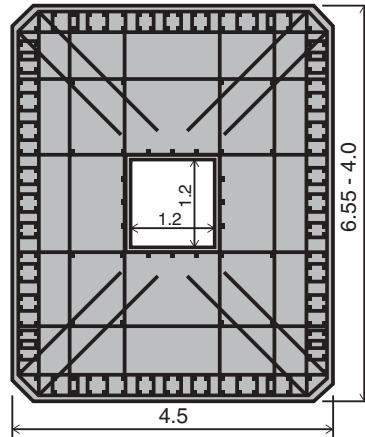


Figure 5.93 Cross section of the Lillebælt Bridge pylon

will only be considered for the pylon legs if the final condition is characterized by a considerable bending, e.g. in a case where the pylon stabilizes a harp system.

The concrete pylons of the Lillebælt Bridge (Figure 5.49) have legs with a rather massive cross section as only a shaft of modest dimensions is found inside these elements, as shown in Figure 5.93. The massive section implied that the outer dimensions could be kept small and this gave the pylon the required flexibility to follow the longitudinal displacements of the top imposed by elongations in the side span cables. On the other hand, the flexibility made it necessary to arrange a temporary longitudinal cable support of the pylon during construction (see Figure 7.11).

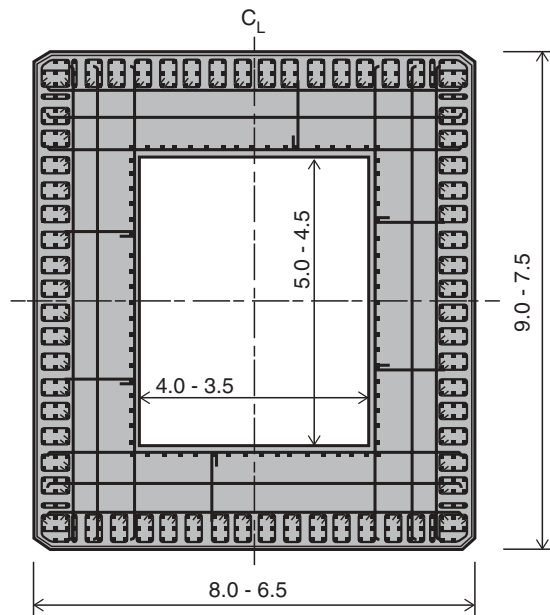
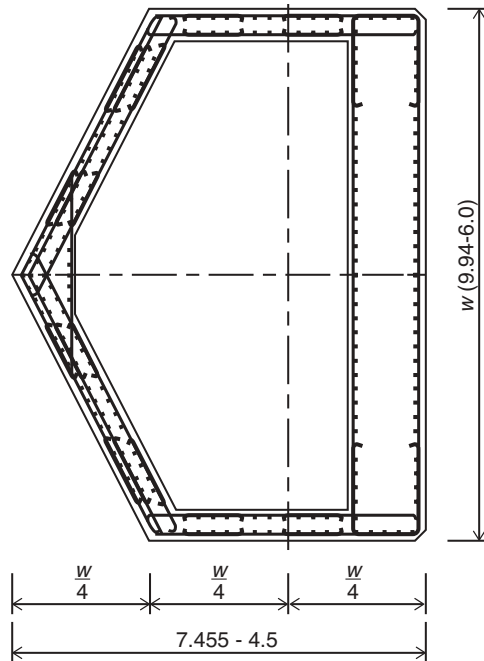


Figure 5.94 Cross section of the legs in East Bridge pylon above the deck level





**Figure 5.95** Cross section of the pylon leg above the deck level in the Øresund Bridge

In the Storebælt East Bridge the concrete pylons are more than twice as high as in the Lillebælt Bridge and this has naturally resulted in much larger cross sectional dimensions. Thus, from the level of the bridge deck to the top of the pylon the outer dimensions of the rectangular box section varies from  $9000 \times 8000$  mm to  $7500 \times 6500$  mm.

The pylons of the East Bridge are designed with less massive cross sections than those of the Lillebælt Bridge – as seen from the cross section in Figure 5.94.

The 203.5 m high concrete pylons of the Øresund Bridge are designed with a pentagonal cross section and a relatively large wall thickness in the side facing the bridge deck (Figure 5.95). All dimensions are varied affine above the bridge deck in such a way that the centroids in all cross sections are positioned on a vertical axis. In this way it is achieved that the vertical components of all cable forces subject the pylon legs to pure, axial compression.

# 6

## Cable Anchorage and Connection

In cable supported bridges the structural connections between elements of the deck and the pylon, as well as connections between the superstructure and the substructure, can be designed by principles generally known from other types of structures. Only when it comes to the structural connections where the elements of the cable system are attached to the deck, the pylons, and the substructure do special details have to be worked out. At the same time, an efficient design of these details is extremely important, as the cables constitute the main load-carrying elements of the structure.

### 6.1 Anchoring of the Single Strand

The anchoring of the single strands is strongly influenced by the following features:

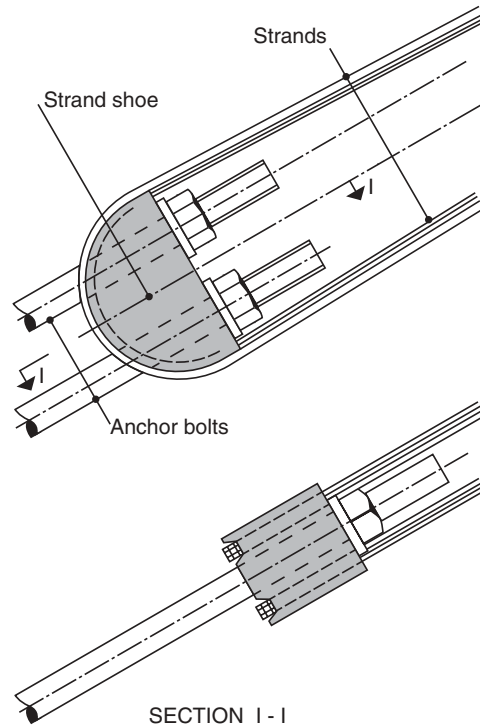
- (1) The force in the strand is concentrated on a small cross sectional area due to the high stresses.
- (2) Welding or bolting used to join other parts of steel structures cannot be used to connect steel wires to other structural parts.

For *in situ* cables built up from individual wires at the site, e.g. parallel-wire cables erected by the air-spinning method, the anchoring is generally established by looping the wires around a strand shoe, as shown in Figures 6.1 and 6.2. Here the axial forces in the wires are transferred by side pressure on the semi-circular face of contact, and further from the strand shoe through threaded rods to a base plate fixed to the massive concrete part of the anchor block.

In earlier times the forces from the strands were transmitted through eye-bars acting as tiers partly embedded in the concrete of the anchor block. In such a case the strand shoes could simply consist of grooved circular discs placed in pairs with one on either side of the eye-bar (Figure 6.3).

For prefabricated strands the most common way of anchoring is by socketing the ends of the strands. In its simplest form a socket for a helical strand consists of a steel cylinder with a conical cavity (Figure 6.4) in which the broomed end of the strand is inserted. Subsequently the conical cavity is filled with a metallic alloy having a relatively low melting temperature. When the cable subsequently is subjected to tension, a wedge action will develop and a tri-axial state of stress in the cast material inside the cone will then efficiently promote the force transmission from the wires.

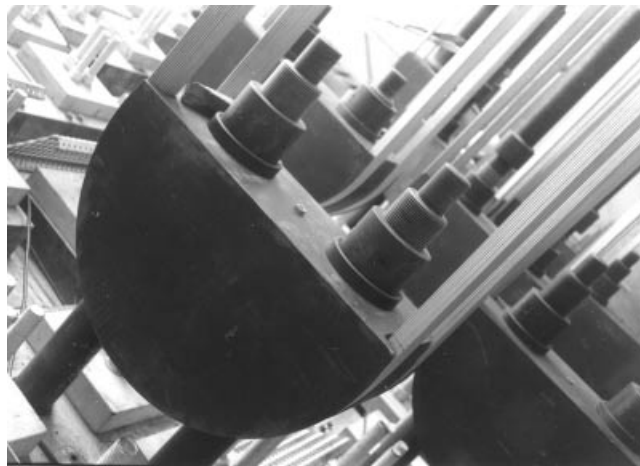
The fact that the high strength of the wire is achieved during the cold drawing process implies that a strength reduction might appear if the metallic alloy requires a high pouring temperature. This feature is illustrated in Figure 6.5 showing the result of breaking tests with wires subjected to pouring temperatures of 350 °C, 400 °C, and 450 °C at varying time intervals. It appears that the reduction of strength will be more than 10% if a pouring temperature of 450 °C is maintained for more than 4 minutes. The pouring metal consists of alloys made of zinc, lead, copper or aluminium. With lead alloys it is possible to keep the pouring temperature as low as 350 °C, but due to unfavourable creep properties and serious health implications, these alloys have been rejected in recent times. Instead, alloys based mainly on zinc are used,



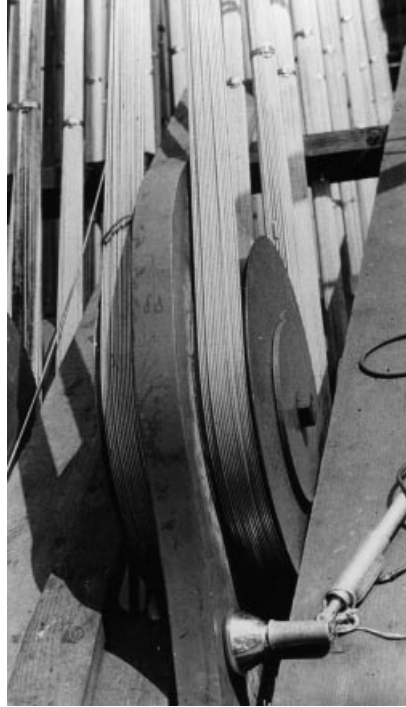
**Figure 6.1** Strand shoe for anchoring strands erected by the air-spinning method

requiring a pouring temperature of 400–420 °C. A very good resistance against creep seems to be achieved by a Zn-Cu alloy with 2% Cu.

It should be mentioned that with galvanized wires the strength reduction described above is of less significance as the wires have already been subjected to elevated temperatures during the galvanizing process.



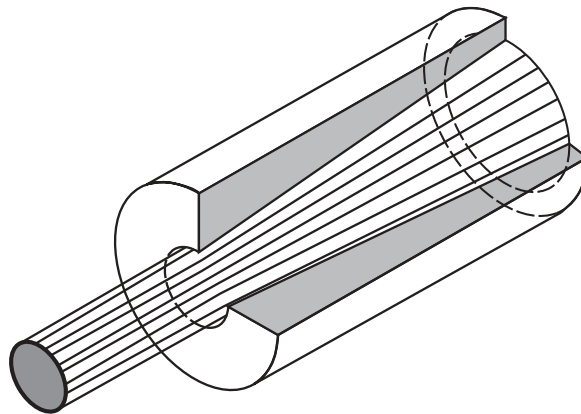
**Figure 6.2** Strand shoe of the Storebælt East Bridge



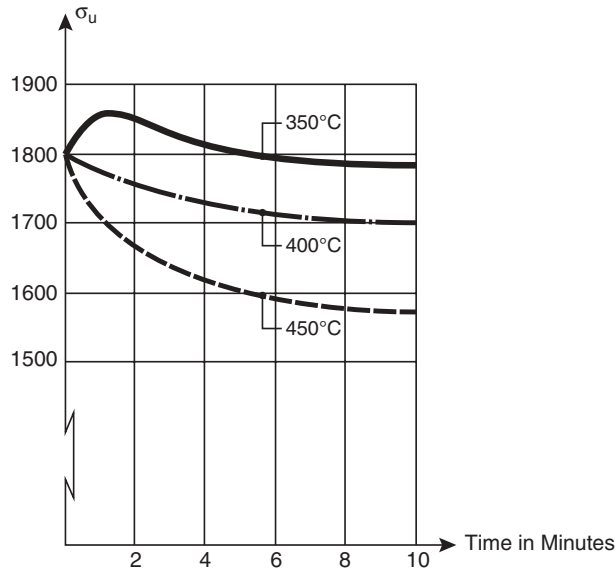
**Figure 6.3** Strand shoe consisting of two circular discs pin connected to an intermediate eye-bar (Verrazano Narrows Bridge)

For the anchoring of parallel-wire strands a special socket, as shown in Figure 6.6, was developed in the 1970s. Here the wires were led through holes in a locking plate at the far end of the socket and provided with button heads to increase the resistance against the slipping of individual wires. The conical cavity inside the socket can be filled with a hot casting material (e.g. the metallic alloys described above) but to improve the fatigue resistance of the anchorage it was preferred to use a cold casting material composed of epoxy resin, zinc dust, and small hardened steel balls (diameter 1–2 mm) [69.1].

Figure 6.7 shows a typical socket based on the application of a cold casting material. To indicate the higher fatigue resistance of this socket it was called a ‘HiAm’ socket, where HiAm stands for high amplitude.



**Figure 6.4** Cable socket

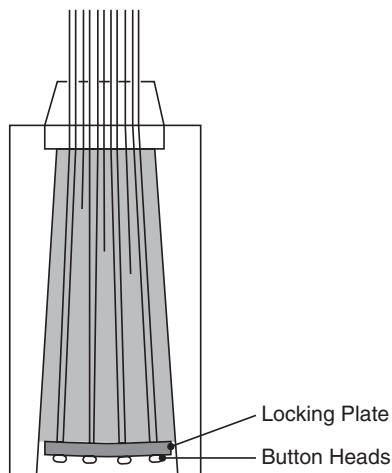


**Figure 6.5** Influence of pouring temperature on the ultimate strength  $\sigma_u$  of wires

For the Storebælt East Bridge hangers, a cold socketing material composed of polyester resin with silica powder as filler material was used with a good result.

For the simple bearing socket shown in Figure 6.8, the dimensions will typically be in the intervals indicated, provided the anchor socket is made of steel with a yield stress of 250–300 MPa. Generally, the slope  $\beta$  of the inner cone will be smallest for sockets with epoxy resin and largest for sockets with metallic alloys.

The diameter  $d_i$  of the bearing surface must be chosen so that the compressive stress is below the limiting value for the actual steel material. When calculating the compressive stress, it must be remembered that the bearing area does not always cover the entire area of the socket end. Thus, with shim plates shaped as shown in Figure 6.9, the effective bearing area



**Figure 6.6** Socket for parallel wire strand

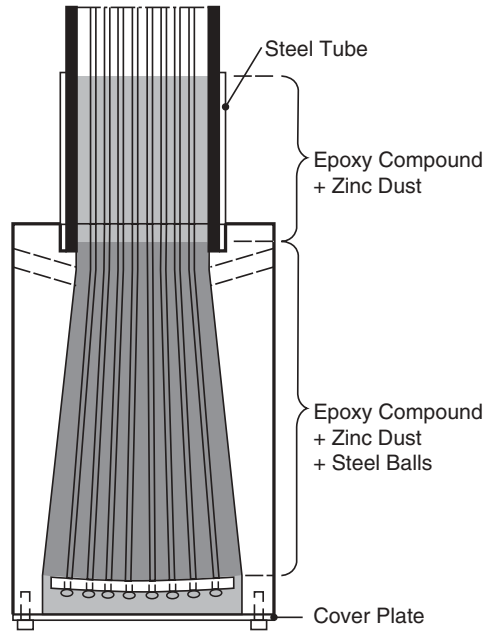


Figure 6.7 HiAm socket

should only be assumed to include the shaded areas. If an increased bearing area is required, a socket with a collar, as shown in Figure 6.10, might be used.

Besides the dimensioning of the socket end to ensure the transmission of the cable force as compression, a check of the wall thickness is also required as the side pressure from the casting material induces a ring tension in the socket walls. The determination of the wall thickness is often based on the following approximate method that seems to lead to safe dimensions in the sense that the ultimate strength of the cable anchor will not be governed by the socket itself [49.2].

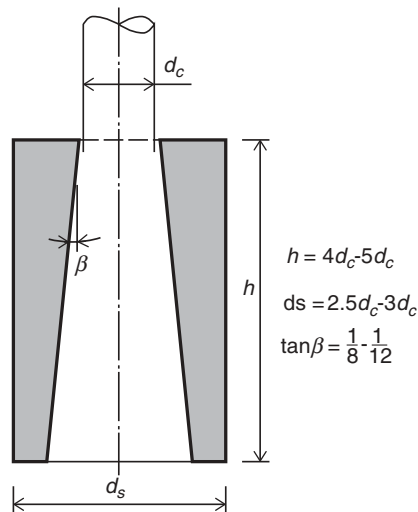
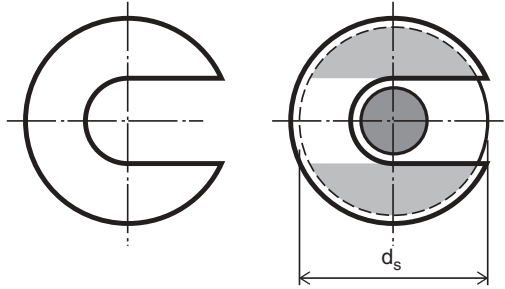


Figure 6.8 Typical dimensions for bearing sockets



**Figure 6.9** Effective bearing area (shaded) for socket in contact with a shim plate shaped as shown to the left

As indicated in Figure 6.11, the effective length of the socket is assumed to be  $2/3$  of the total length, as complete filling of all cavities between the individual wires cannot be expected in the region where the compact cable enters the socket. Furthermore, it is assumed that the pressure from the casting material acts under an angle  $\phi$  with the inner face of the socket wall, corresponding to a coefficient of friction  $\mu = \tan \phi$ . For metallic casting materials  $\tan \phi$  will often be chosen to a value of 0.2, whereas the epoxy-based casting materials used in HiAm anchors will allow a value of  $\tan \phi$  equal to 0.45. The total ring tension  $P_r$  can now be determined by:

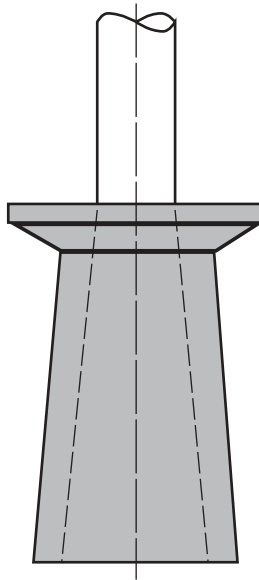
$$P_r = \frac{T}{2\pi \tan(\phi + \beta)} \quad (6.1)$$

where  $T$  is the cable force and  $\beta$  the angle between the generator and the axis of the inner cone.

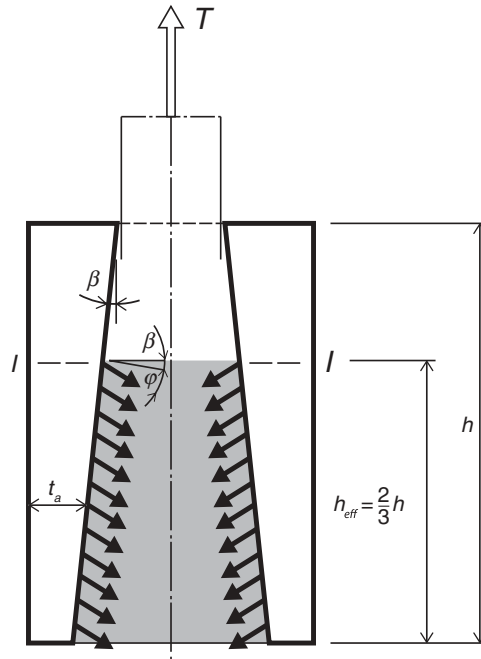
Assuming that the ring tension is taken by the effective part of the socket with a height of  $h_{eff} = \frac{2}{3} h$  leads to the following stress:

$$\sigma = \frac{3 P_r}{2 h t_a} = \frac{3 T}{4\pi \tan(\phi + \beta)} \quad (6.2)$$

where  $t_a$  is the average thickness of the socket wall in the effective part.



**Figure 6.10** Socket with collar to increase bearing area



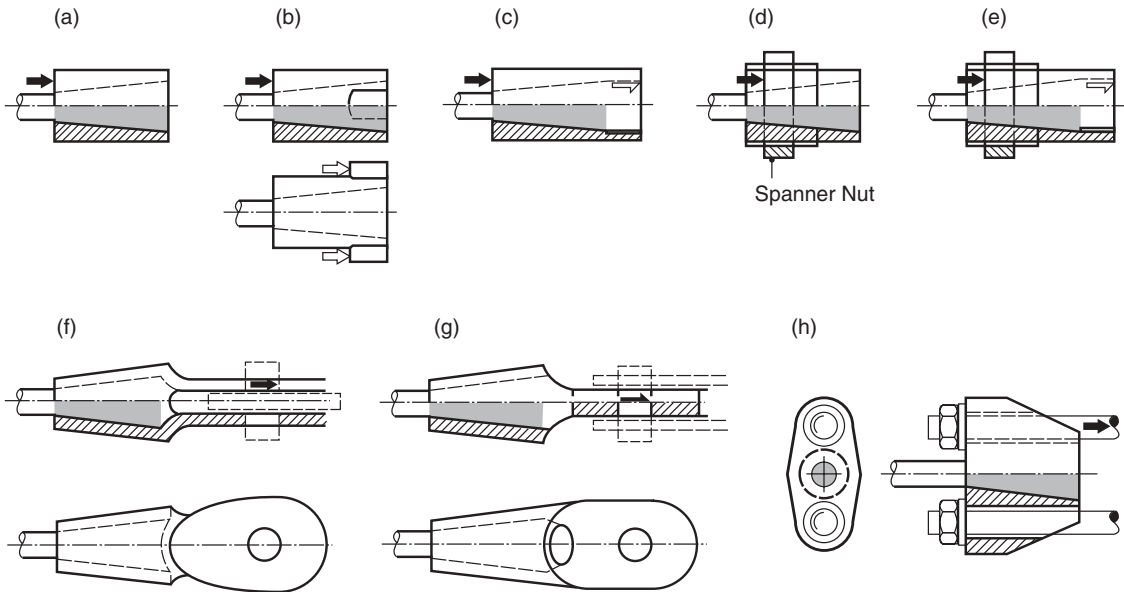
**Figure 6.11** Idealized force transmission from the socket to the casting material inside the cone

It should be mentioned that the axial stress in Section I-I in Figure 6.11 should also be checked, as the total cable force  $T$  must be transferred through this section.

Besides the simple bearing socket described above other more complicated forms of sockets are also found. Such sockets are designed to give advantages in relation to tensioning, length adjustments, and load transfer. Figure 6.12 shows a number of sockets that might be found within cable supported bridges.

- (a) the simple bearing socket mainly used as a dead-end anchor where jacking equipment does not have to be attached.
- (b) a slightly modified version of the socket with two integrated brackets ('ears') allowing the attachment of jacking equipment for the initial tensioning of the strand.
- (c) a socket with an internal thread allowing a rod to be screwed into the socket. In most cases the threaded rod will be used only temporarily during the initial tensioning whereas the final load transfer will take place by bearing, but in a few cases the rod has also been used as part of the final anchoring system.
- (d) a socket with an exterior thread and a spanner nut allowing continuous adjustments of the cable length. In the final condition the load will be transferred by bearing on the spanner nut, as indicated.
- (e) a socket with both external and internal threads, so that a threaded rod can be inserted during tensioning, whereas the final load transfer takes place through the spanner nut. This type of socket is especially well suited in cases where a later adjustment of the cable length is required.
- (f) a fork socket allowing a pin-connection to the adjoining structural parts. With this socket large angular changes can take place between the cable and the structure during installation, but in the final stage the friction around the pin will probably exclude mutual rotations. The open socket does not in itself allow any adjustments of the cable length so it is not well suited to be used at the live end where the cable shall be tensioned.
- (g) a tongue socket with a similar function and the same characteristics as that of the fork socket (f).
- (h) a socket allowing the cable force to be transferred to two rods or bolts. This type of socket is mainly used at the ends of prefabricated parallel-wire strands in suspension bridges, where it will allow a similar connection to threaded rods (anchor bolts), as shown for the strand shoe in Figure 6.1.



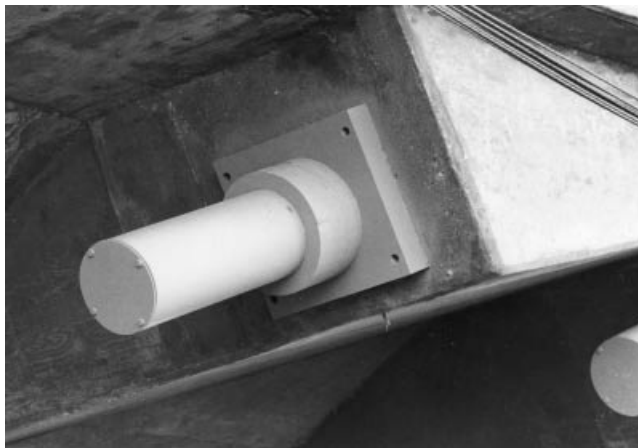


**Figure 6.12** Different types of sockets

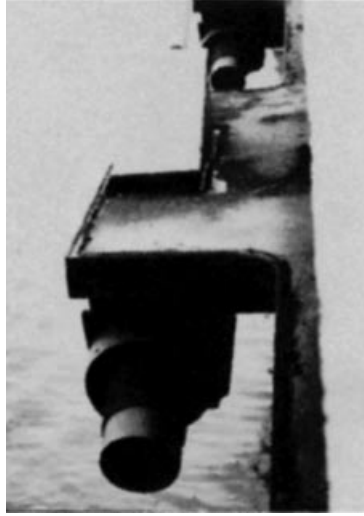
A socket corresponding to type (c) with an internal thread was used in the HiAm anchors shown in Figure 6.13. In the final condition the socket acts as a bearing socket with the cable force being transmitted through shim plates to a base plate. As seen in Figure 6.13, a thin cover plate is bolted to the end of the socket to protect the thread and the epoxy compound against deterioration. A Type (e) socket with interior as well as exterior threads is shown in Figure 6.14.

Fork sockets with pin-connections have been used for attachment of both hangers and stay cables. As an example, Figure 6.15 shows the connection between the hangers and the stiffening truss in the Akashi Kaikyo Bridge.

In parallel-strand cables the individual seven-wire strands are commonly anchored through a three-piece jaw (wedge) claimed to be designed for high fatigue strength. For a stay cable with an upper stress of 800 MPa the mean stress range at  $2 \times 10^6$  cycles has been determined by fatigue testing to be  $\Delta\sigma = 210$  MPa. The allowable stress range at  $2 \times 10^6$  cycles for a parallel-strand cable will be, according to Table 2.3, 130 MPa, so the 'safety factor' will in this case be  $210/130 = 1.6$ .



**Figure 6.13** HiAm socket with interior thread protected by cover plate



**Figure 6.14** Socket used on a locked-coil mono-strand cable

In the Freyssinet anchor (Figure 6.16) developed in the late 1980s, the strand bundle is passed through a deviator and spread out towards the anchor which it enters through a so-called guide-stuffing box assembly at the end of the anchorage steel tube. Inside this tube the strands are corrosion-protected by a wax compound, and in this region the transition from sheathed to unsheathed strands takes place. The individual seven-wire strands are anchored through the three-piece jaws at the far end of the anchorage, where the strand forces are transferred to the anchorage block and further by contact pressure to the bearing surface of the adjoining structure (Figure 6.17). Outside the anchor zone an injection cap is finally added to allow a corrosion protection of the strand ends by the same wax compound as used inside the anchorage tube. With an anchor as shown in Figure 6.16, it is possible to tension each seven-wire strand individually by the so-called isotension method.

For anchors or bearing sockets (refer to Figure 6.12 (a)–(c)), the force transmission to the adjoining structure generally takes place through a bearing block to diaphragms in rigid connection with the structure, as shown in Figure 6.18. As the



**Figure 6.15** Fork sockets on the hangers of the Akashi Kaikyo Bridge

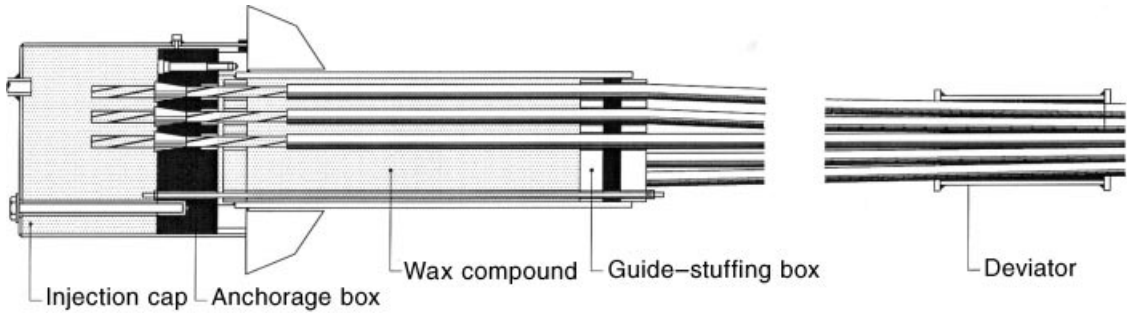


Figure 6.16 Freyssinet anchor as developed in the late 1980s



Figure 6.17 Anchorage block with partially installed seven-wire strands in a Freyssinet anchor (Normandy Bridge)

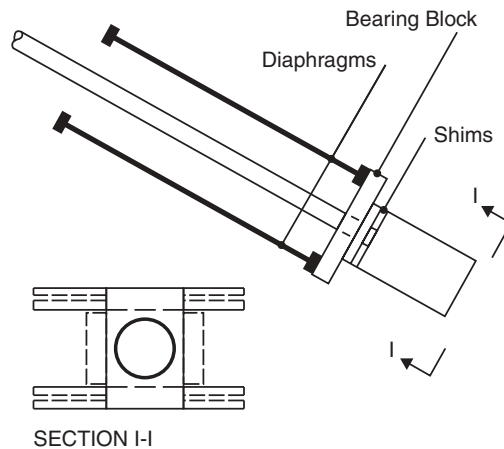
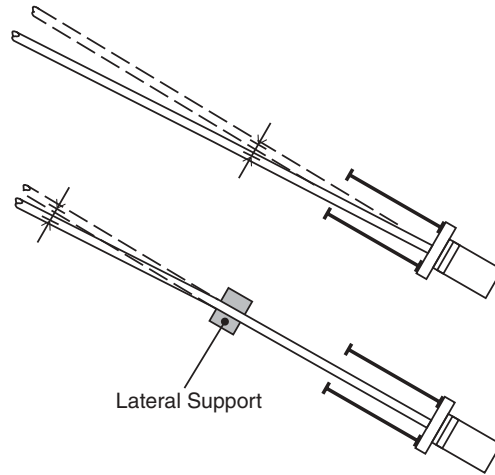


Figure 6.18 Rectangular bearing block for transmission of the cable force from the socket to diaphragms

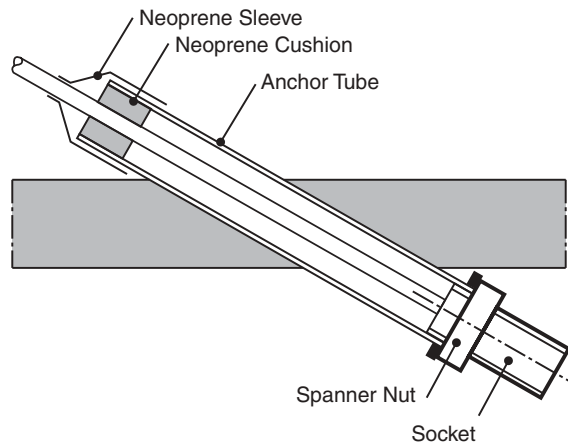


**Figure 6.19** Elimination of angular changes at the socket through lateral support of the cable some distance from the anchorage

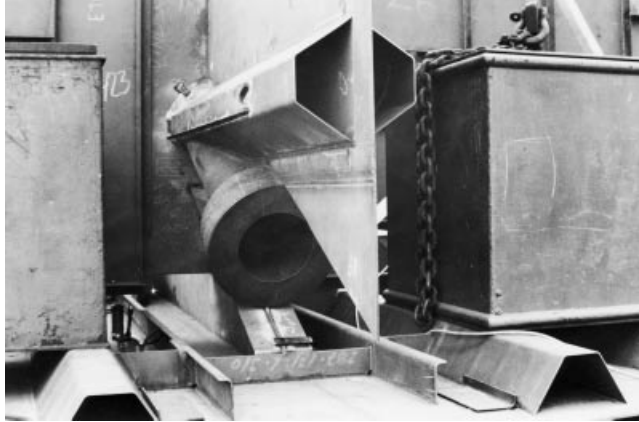
hole in the bearing block will have a diameter that is only slightly larger than the strand diameter, the bearing block must be positioned on the strand before it is socketed. To allow the strand to pass between the diaphragms during erection, the bearing block has a rectangular shape.

For mono-strand cables, it is important to avoid cable bending concentrated at the cable entrance to the socket. A cable anchorage as shown in Figure 6.18 should, therefore, be supplemented by a lateral support of the cable in some distance from the socket, as shown at the bottom of Figure 6.19.

Figure 6.20 shows an anchorage detail often found in bridges with mono-strand cables of the parallel-wire type. Here the strand contains a socket of the type (e) from Figure 6.12 with the spanner nut bearing on an anchor tube in rigid connection with the deck structure. Note that the diameter of the anchor tube is chosen to be large enough that the socket can be pulled through during installation. At the upper end a Neoprene cushion is inserted to give the stand the lateral support described above. A less satisfactory feature of the anchor tube connection is the fact that the cable is inaccessible for inspection in the critical zone just outside the socket. Also, the tube is vulnerable to water intrusion if the upper Neoprene sleeve is not absolutely watertight. Note that if the interior of the anchor tube is in the dehumidified space of the deck structure, the lack of access for inspection is less critical.



**Figure 6.20** Anchorage and lateral support of stay cable in an anchor tube



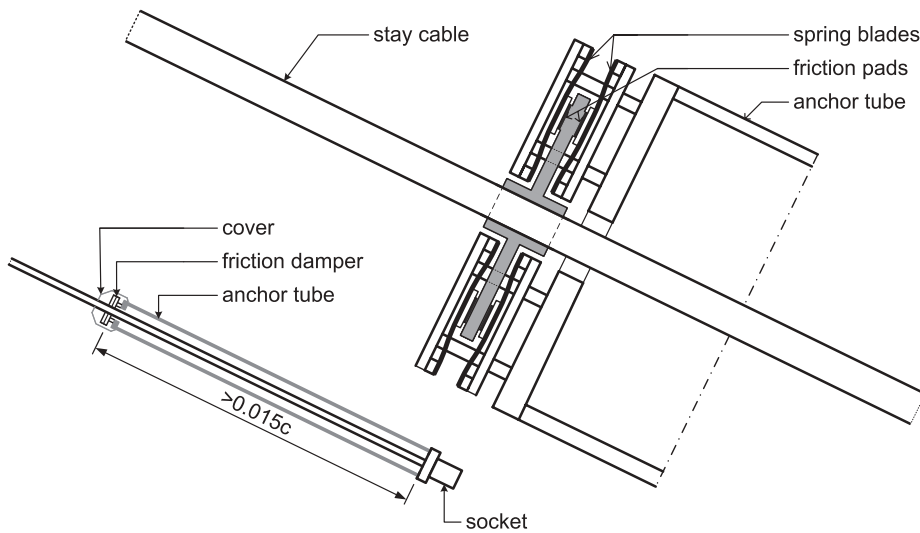
**Figure 6.21** Anchor tube welded to the central web in the box girder of the Farø Bridge

The anchor tube detail has been used in several bridges with parallel-wire strands and with decks in both steel and concrete.

In the photograph in Figure 6.21, taken during assembly of the box girder for the Farø Bridge, it is seen that the anchor tube is welded to the central, vertical web and provided with a heavy bearing ring at the bottom. During tensioning of the PWS cables, the box had a suitable hole in the bottom plate, but this hole was subsequently closed by a welded fill-in plate.

The anchor tube with a Neoprene sleeve as shown in Figure 6.20 can be used for stay cables of short to medium length where wind-induced vibration of the single stay does not present a problem. However, for long stay cables it will often be necessary to install dampers at the end anchorages to suppress vibrations of the single cable.

The preferred damper seems to be a friction damper installed at the upper end of the anchor tube in the deck. To be efficient the friction damper must be located at a distance of at least 0.015 times the stay cable chord length (from end socket to end socket), as illustrated in Figure 6.22. This implies that for a stay cable with a length of 500 m, the anchor tube must be at least 7.5 m long.



**Figure 6.22** Anchor tube with friction damper



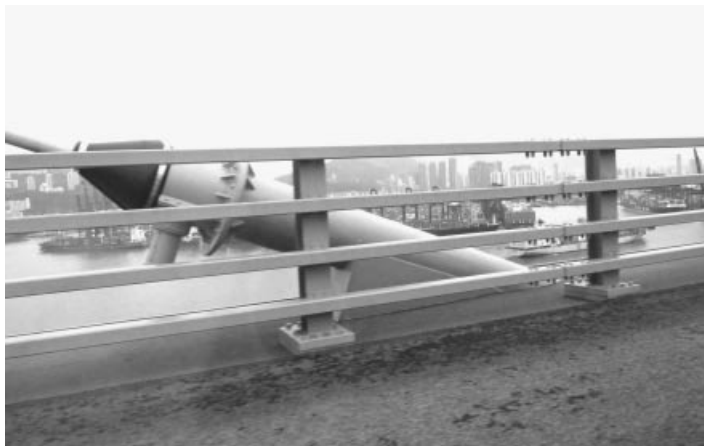
**Figure 6.23** The deck of the Stonecutters Bridge as viewed from below

In cases where the deck is designed as a shallow box girder, it will often be required to let the anchor tube protrude through both the floor plate and the soffit plate, as illustrated in Figures 6.23 and 6.24. When viewed from the roadway, the anchor tube might look quite clumsy and it is, therefore, preferable if the top of the anchor tube can be kept below the top of the railing.

In a number of bridges the dampers have had to be positioned high above the roadway level and supported by additional structural members. This will often give a rather unpleasant visual impact when seen from the bridge floor (Figure 6.25).

As an example of an application of anchor tubes in bridges with a concrete deck, Figure 6.26 shows the anchorage of a backstay composed of four individual PWS cables. Here the anchor tubes are embedded in the solid edge portions of a concrete girder. The tubes are furthermore extended upwards from the bridge deck to give a suitable distance between the socket and the upper Neoprene cushion.

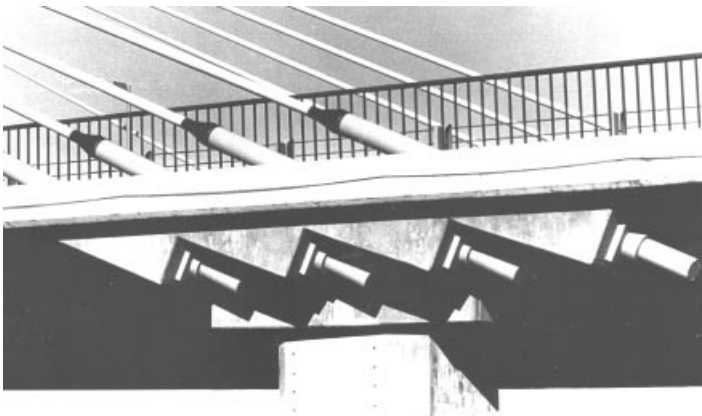
The open socket shown in Figure 6.12(f) cannot in its integrated form be used in combination with parallel-strand cables, so for these it will be necessary to make a fork-like transition piece of cast steel, as was done in the Normandy Bridge (Figure 6.27).



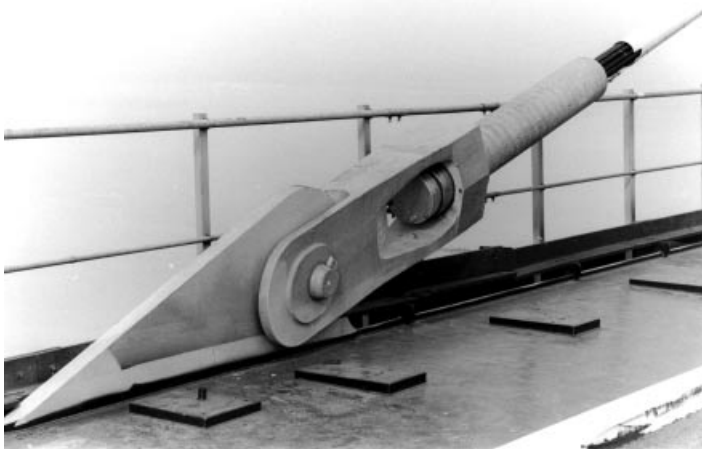
**Figure 6.24** The anchor tube of the Stonecutters Bridge as seen from the roadway



**Figure 6.25** Stay cable damper positioned high above the roadway



**Figure 6.26** Anchorage of a four strand anchor cable to a concrete girder



**Figure 6.27** Anchorage of a parallel-strand cable via a cast steel transition piece (Normandy Bridge)

## 6.2 Connection between Cable and Deck

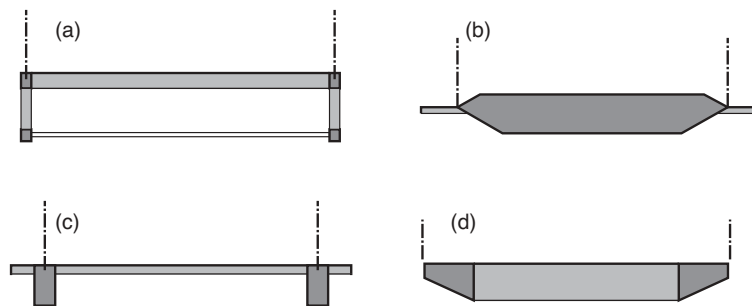
In the design of a cable supported bridge, it is very important to follow thoroughly the transmission of forces from the cables into the deck to ensure an efficient design of these important details.

In some cases the deck will have a cross sectional layout that allows direct connection to the cables, as indicated in Figure 6.28(a)–(d). With these cross sections it will only be necessary to add the anchor tubes, small diaphragms or modest brackets to transfer the forces from the cables to the main elements of the deck.

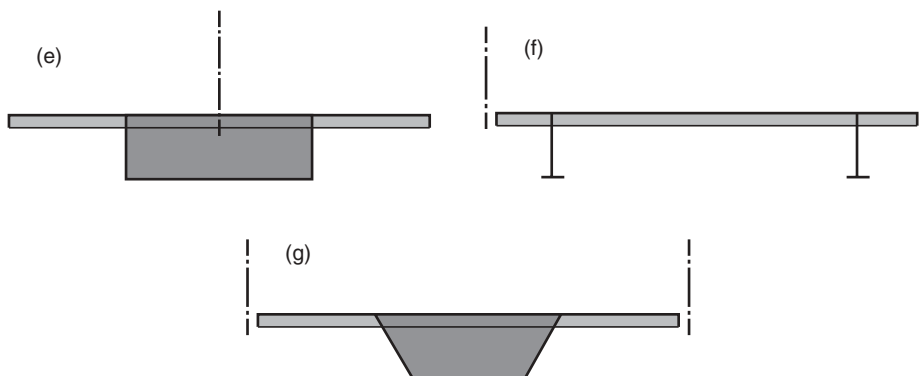
In other cases the main load-carrying elements of the deck will be situated at such distances from the cable planes that larger structural elements have to be added at the cable anchor points to ensure the transmission of the cable forces. Thus, with the cross sections of Figure 6.29(e), (f), and (g) the cables will only come into immediate contact with secondary structural elements such as the cross beams or the edge girders.

Figure 6.30 shows the principal layout of the connection between a stay cable and a wide, single-cell box girder. As seen, two transversal and two longitudinal diaphragms are required at the cable anchor point. The force is initially transferred from the cable through sockets (anchors), bearing blocks, and small radial diaphragms to the longitudinal diaphragms. From these the horizontal cable force component is transferred by shear to the top and the bottom flanges of the box girder, whereas the vertical component is transferred from the longitudinal diaphragms to the transverse diaphragms and further by shear to the girder webs.

The layout shown in Figure 6.30 will be used in cases where the cable force to be transmitted is of considerable magnitude, i.e. in bridges with multi-strand or very large mono-strand stay cables. In bridges with a multi-cable system, only a relatively modest force has to be transferred at each anchorage and it is therefore unnecessary to arrange full-depth diaphragms at these points. Instead a layout as shown in Figure 6.31 can be used. Here the stay cables are anchored to a continuous, longitudinal anchor girder under the floor plate from where the vertical force component is transferred

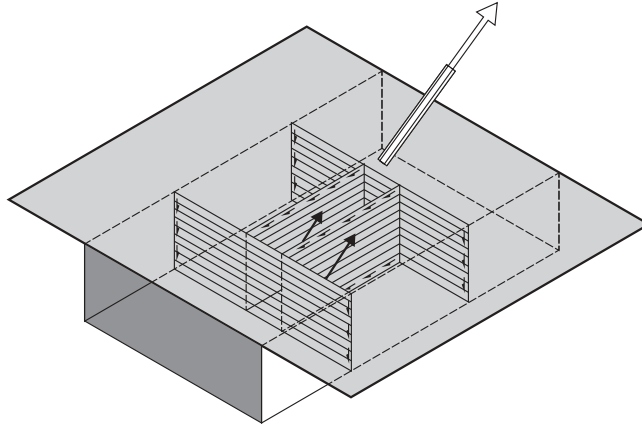


**Figure 6.28** Types of stiffening truss or girder sections allowing a direct connection to the cables

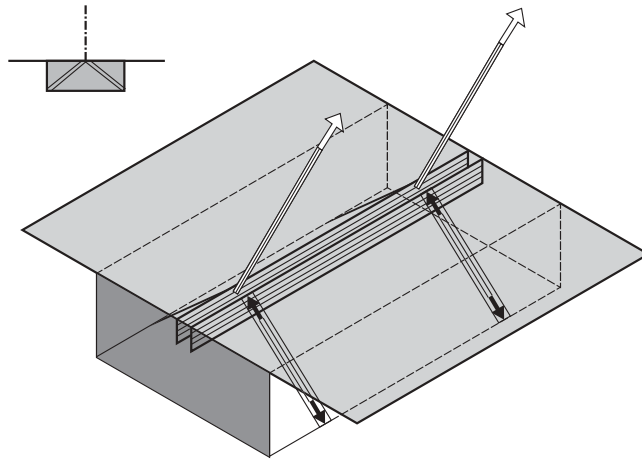


**Figure 6.29** Types of decks giving indirect connection to the cables





**Figure 6.30** Connection between a large multi-strand stay cable and a wide mono-cellular deck



**Figure 6.31** Connection between mono-strand stay cables and a wide mono-cellular deck

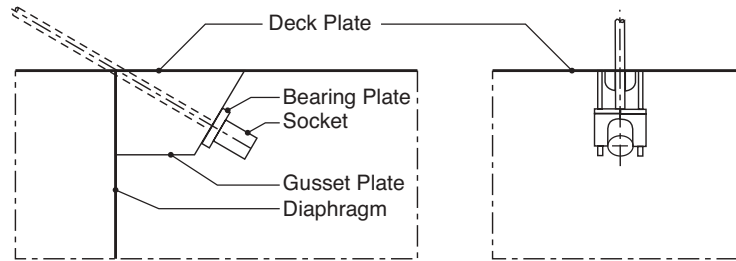
by two inclined ties leading to the bottom of the box at the intersection with the outer webs. This principle was illustrated for the Brotonne Bridge in Figure 4.55, but it has been applied in many other bridges both in steel and concrete.

Another solution to the problem of anchoring a mono-strand with a relatively small force to a box girder is shown in Figure 6.32. Here the cable force is transferred from the socket through a bearing plate onto two gusset plates welded to the top flange and to a plated diaphragm. Thus, the horizontal component of the cable force is transferred to the floor plate by shear in the longitudinal weld and the vertical component to the diaphragm by shear in the vertical weld. It should be emphasized that, with the detail shown in Figure 6.32, the floor plate and the diaphragm must intersect exactly at the cable axis to exclude the occurrence of an unfavourable eccentricity moment.

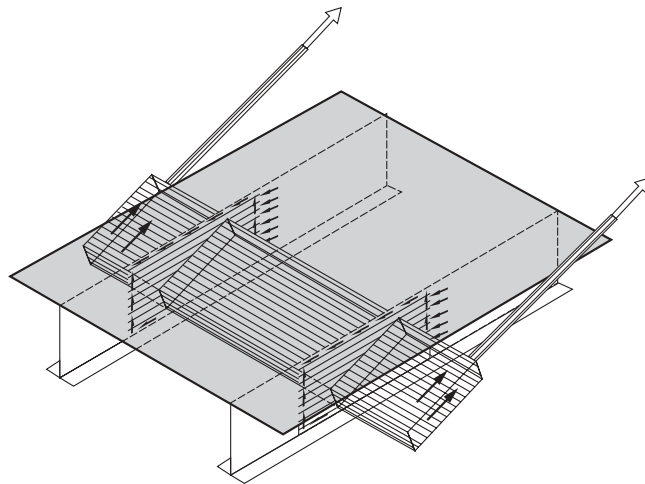
In cases where an eccentricity cannot be avoided, the gusset plates shown in Figure 6.32 will have to be connected to a longitudinal beam with an adequate flexural strength (as in Figure 6.31) or to a torsionally stiff cross beam.

For a deck with two plate girders positioned at some distance from the edges, the layout of the anchor point could be as shown in Figure 6.33. Here the stay cables, positioned outside the roadway area, are anchored to an inclined box-shaped anchor girder that transfers the cable forces by bending and shear to the plate girder webs.

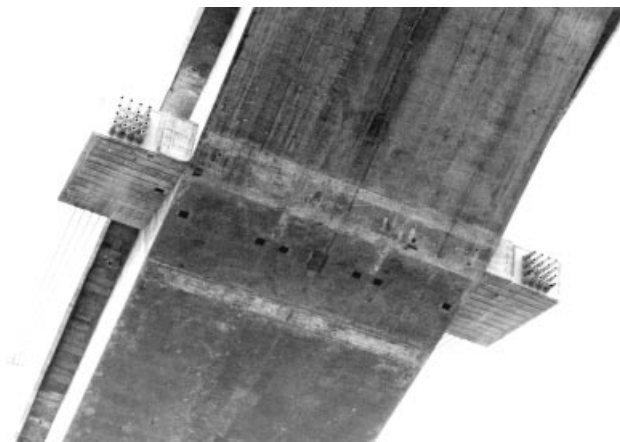
The application of inclined anchor girders is not restricted to bridges with two plate girders (as in Figure 6.33) but it can also be used in bridges with more plate girders or with box girders. As a classical example, Figure 6.34 shows the anchor girder in the Maracaibo Bridge where the deck is a tri-cellular box.



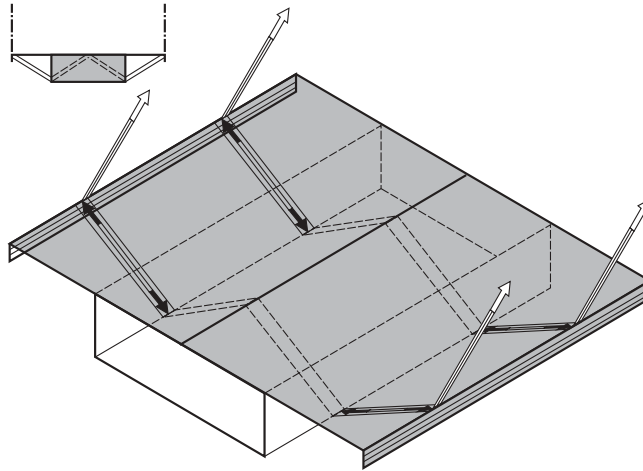
**Figure 6.32** Simple connection between a mono-strand cable and a girder with a plated diaphragm



**Figure 6.33** Inclined anchor girder to transfer forces from the webs of the deck to the stay cables



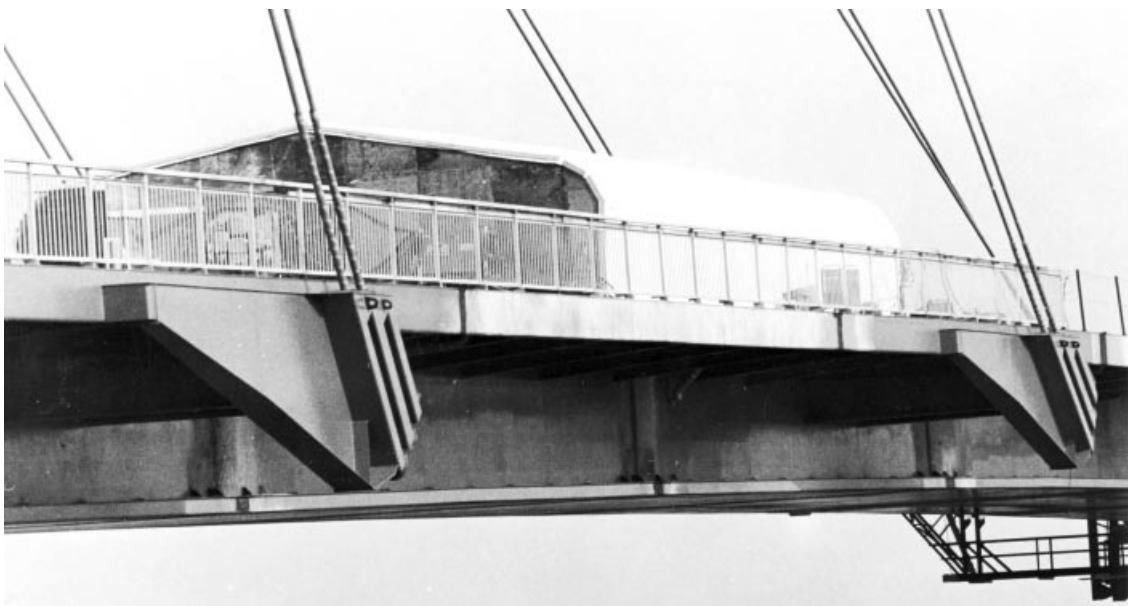
**Figure 6.34** Inclined anchor girder in the Maracaibo Bridge



**Figure 6.35** Connection between a central box girder and mono-strand stay cables attached at the edges of the deck

Inclined anchor girders will be used at points where large cable forces have to be transmitted, whereas a more simple layout, such as the one shown in Figure 6.35, will be used in bridges with a multi-cable system. Here the edge girder acts as a continuous, longitudinal anchor girder connected by inclined ties to the box girder bottom flange at the anchor points.

The fact that the vertical force component to be transferred at each cable anchorage is of limited magnitude in a multi-cable system also makes it possible to apply ordinary vertical transverse girders. This was done in the Tjörn Bridge, as illustrated in Figure 6.36. As seen, the transverse girder at the anchor point is only slightly deeper than the ordinary cross beams and this clearly indicates the limited magnitude of the vertical force to be transmitted.



**Figure 6.36** Vertical cable component transferred through a transverse girder from edge anchorages to a central box girder (Tjörn Bridge)



**Figure 6.37** Stay cable anchored to a triangular outrigger outside the main trusses in the Øresund Bridge

The concept of transmitting the stay cable force to the girder through an inclined anchor girder is applied in the Øresund Bridge. Here the anchor girder is designed as a triangular ‘outrigger’ positioned in an inclined plane that also contains the stay cables and the long diagonals of the main trusses (Figure 6.37). With this arrangement the cable force is transferred to the lower nodes of the main trusses, i.e. where the dominating traffic load from the railway is applied.

In cable stayed bridges, the horizontal component of the cable force will induce normal stresses in the deck. However, as the horizontal component generally will be applied to a concentrated part of the deck, the normal stresses will not be distributed uniformly near the cable anchorage. This feature is illustrated in Figure 6.38 that shows the distribution of axial stresses across a plate subjected to a concentrated line load  $\Delta N$  and supported at the upper edge. This situation corresponds to that found in a top or bottom flange where the horizontal cable component is transferred by shear from a local longitudinal web (in the chosen example with a length of 0.2 times the plate width  $b$ ).

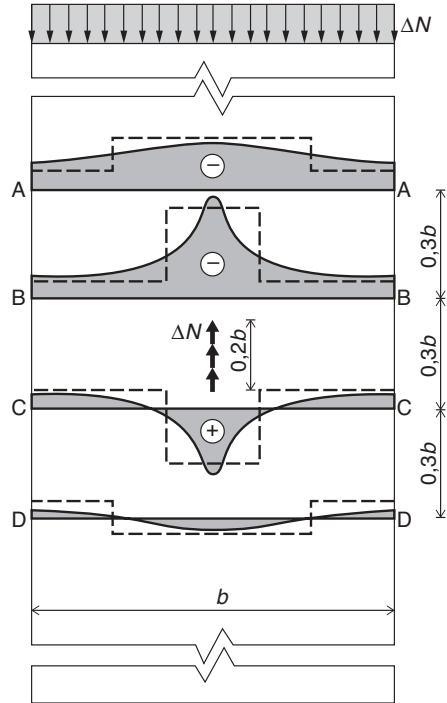
It is seen that the stress distribution near the point of force application is very uneven with a significant concentration of stress near the force. Thus, in section B–B the ratio between maximum and minimum compressive stress is approximately 5. However, the concentration of stress vanishes rapidly when moving away from the point of force application. Already in section A–A, situated less than half the plate width from the force centre, the ratio between maximum and minimum stress is only approximately 1.5. Furthermore, it should be noted that, despite the fact that the force globally will be transferred as compression, a considerable tension occurs locally behind the force in section C=C. This is especially important to consider if the floor slab is made of concrete.

In the final design the distribution of the axial stresses will always be based on a finite element analysis, but for the preliminary investigations carried out to check whether a local strengthening of the plates at the anchor point is required or not, a simplified approach as described below might be used.

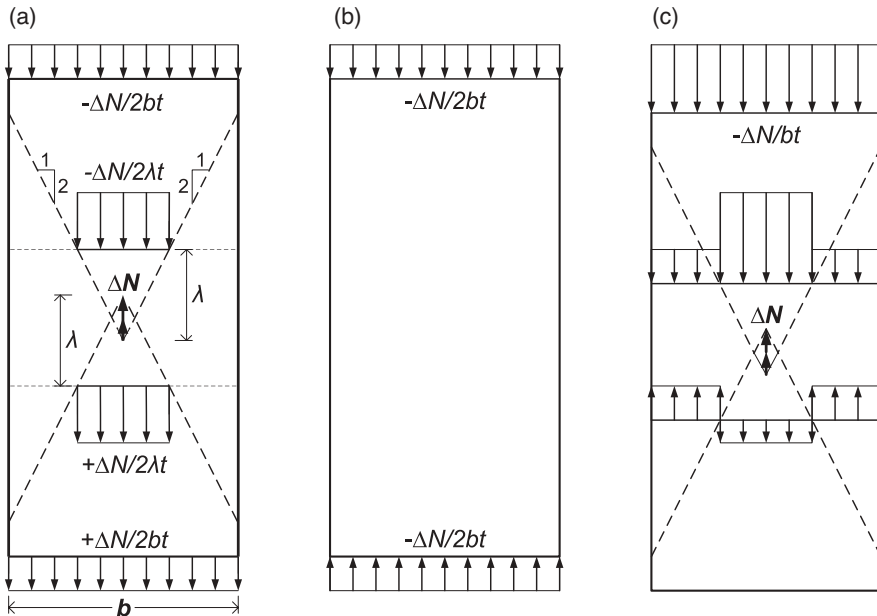
In a floor slab where the line load  $\Delta N$  was distributed equally as compression  $\frac{1}{2} \Delta N$  on one side and tension  $\frac{1}{2} \Delta N$  on the other, a complete antisymmetry would exist, as seen from Figure 6.39(a). Assuming a distribution under 1:2, as indicated in Figure 6.39, the axial stress will be inversely proportional to the distance from the actual section to the far end of the line load.

Superposing the stresses under (a) with a constant compressive stress  $\sigma = -\Delta N/2bt$  as shown under (b), leads to a total stress distribution as shown under (c). In contrast to the real stress distribution the simplified stress distribution is characterized by a discontinuous variation across the plate width but, as seen from Figure 6.38, where the results of the simplified approach are shown with a dotted line, there is a reasonably good agreement between the maximum stresses.

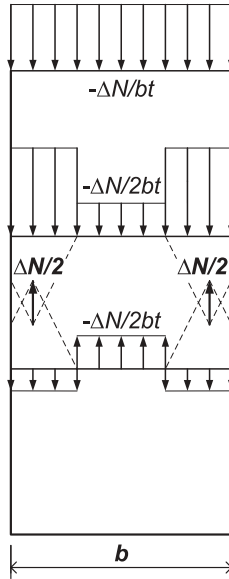
The simplified approach assuming a distribution of the force under 1:2 can also be applied if the horizontal cable components are transferred closer to the edges of the slab, as indicated in Figure 6.40.



**Figure 6.38** Stress distribution in a plate subjected to a concentrated force  $\Delta N$  at the centre



**Figure 6.39** Variation of axial stresses assuming two-way force distribution under 1:2



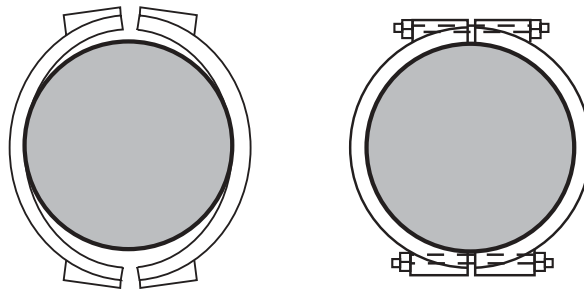
**Figure 6.40** Idealized variation of axial stresses in a plate subjected to two concentrated forces  $\Delta N/2$  near the edges

As a general rule, the problems of distributing the horizontal component of the stay cable forces across the deck cross section are much easier to overcome in bridges with multi-cable systems as the force to be transferred at each cable anchor point is relatively small.

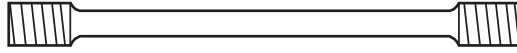
### 6.3 Connection between Main Cable and Hanger

In suspension bridges the connection between the main cable and the hangers is made by means of a cable clamp shaped to allow attachment of the hangers. The cable clamp will generally consist of two semi-cylindrical halves connected by high-tensile steel bolts to activate the necessary friction. As the clamps must conform with the cable shape after bolt tightening, a relatively thin wall thickness and good ductility are required.

In Figure 6.41 the situation before and after tightening of the clamping bolts is shown with some exaggeration. During tightening the cable clamps will be subjected to bending that will reduce the diameter until contact is established around the cable. After tightening, a small gap must still exist between the two halves to avoid the bolt tension being transferred



**Figure 6.41** Cable clamp before and after bolt tightening



**Figure 6.42** Waisted bolt

directly from one half to the other by contact pressure. Also, the gap should be sufficient to allow re-tightening of the bolts at a later date.

The bolts are generally highly stressed during tightening of the nuts, and to reduce the risk of breakage it might be advantageous to make a waisting of the bolts so that the highest tensile stresses occur on the smooth central part of the bolt (Figure 6.42). With such a waisting, it has even been suggested stressing the bolts into the plastic range to provide a maximum margin against having the tension relaxed.

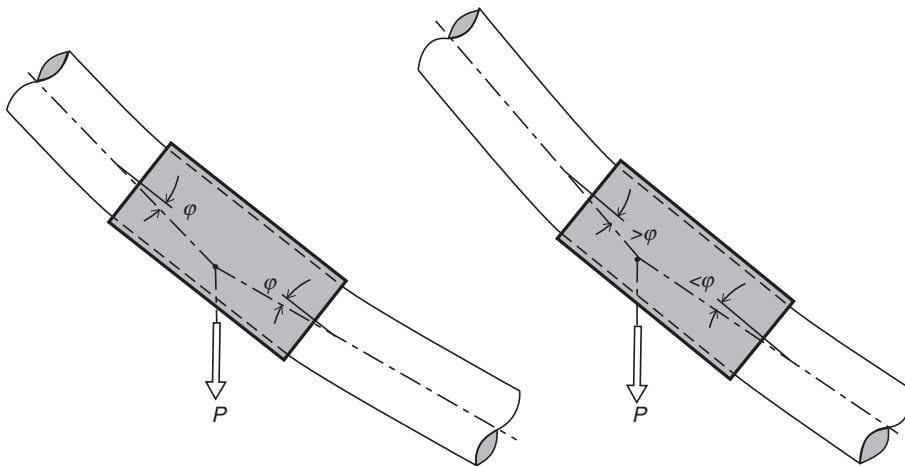
The required friction at the cable clamp depends on the inclination of the cable, and the largest friction is consequently required near the pylons. For this reason the number of bolts in each cable clamp is often increased from midspan towards the pylons. An exception to this rule might be the cable clamps at the ends of a continuous deck, as these clamps also will be subjected to quite large axial shear due to their pronounced inclination under asymmetrical load and temperature change.

At the cable clamp the main cable will be subjected to a concentrated vertical force which will introduce an angular change of the cable axis, as illustrated in the top of Figure 6.43. This angular change will, however, be distributed between two angular changes at the ends of the clamp due to its stiffness.

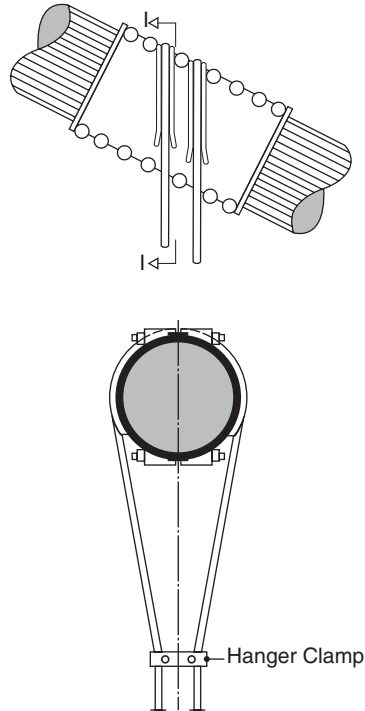
To make the angular changes as small as possible it will be favourable to give the clamp a geometry as shown at the top, where the total angular change is equally distributed between the two angular changes at the ends of the clamp. With an eccentric attachment of the hanger to the cable clamp, as shown at the bottom of Figure 6.43 the angular change at the near end will be larger than at the far end.

To give support for the hangers, the cable clamps traditionally have been made with grooves on the upper surface so that the hangers can simply be looped around the clamp, as shown in Figure 6.44. Here is also indicated the application of a hanger clamp below the cable clamp to reduce the distance between the hanger ropes. Whether such a hanger clamp has to be used depends on the requirements of transverse hanger rope spacing at the deck.

Hanger clamps to reduce the distance between hanger ropes have been used in many large suspension bridges (e.g. the Golden Gate Bridge, as shown in Figure 6.45). However, the hanger clamps will introduce vulnerable spots with regards to corrosion.



**Figure 6.43** Angular changes of the cable axis at the ends of a cable clamp. Top: Hanger axis at centre of the cable clamp; bottom: Eccentric hanger attachment



**Figure 6.44** Grooved main cable clamp with a double hanger rope clamp below

In a few suspension bridges the individual hanger ropes are separated sufficiently at the deck level to avoid the double hanger clamps below the main cable clamps (Figure 6.46). This appears to be a simple way to avoid the points being vulnerable to corrosion.

As the inclination of the main cable varies along the span, and as the grooves have to be arranged in a vertical plane, a large number of moulds with few re-uses have to be applied. This leads to a rather high cost of fabricating this type of cable clamp. On the other hand, savings are achieved as no special fittings are required at the top of the hanger ropes themselves.



**Figure 6.45** Hanger clamps below the main cable clamp to reduce hanger rope spacing (Golden Gate Bridge)





**Figure 6.46** Hanger ropes of the 20th April Bridge spaced to avoid hanger clamps below the cable clamps

Grooved cable clamps were used in all the American and in the majority of the Japanese suspension bridges built in the twentieth century. As an example, Figure 6.47 shows the cable clamps of the Verrazano Narrows Bridge before installation, and Figure 6.48 a mock-up of the cable clamps of the Bisan Seto Bridges. In these cable clamps the bolts are horizontal so that the band consists of a left and a right part when viewed in the direction of the main cable axis.

A recent example on the use of grooved cable clamps is found in the Xihoumen Bridge of 2009, as seen in Figure 6.49.

In the major European suspension bridges the looping of the hanger cables around the clamp has been replaced by a pinned connection between the cable clamp and a fork socket at the top of the hanger cable (Figure 6.50). In this case, the lower part of each cable clamp will be shaped as a vertical ‘gusset’ plate with the relevant pin holes. One important reason for choosing the socket solution is the fact that grooved cable clamps can only be used if the hanger ropes consist of helical strands as only these can be curved with a very small radius.

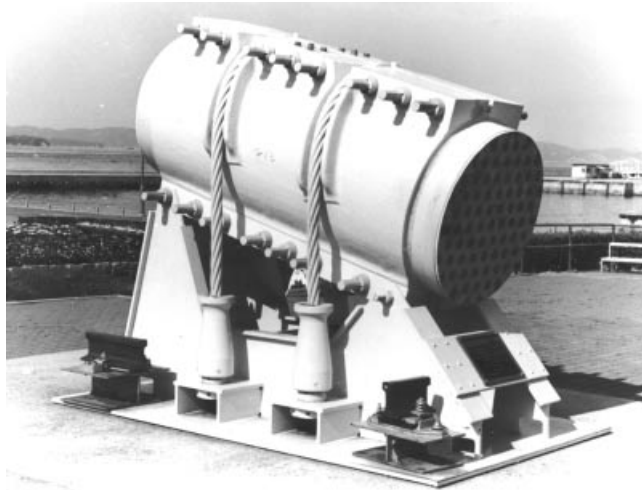
With the arrangement of Figure 6.50 a larger number of cable clamps can be made identical as eccentricities can be avoided by drilling the pin holes after casting of the lower part of the clamp (Figure 6.51). However, because the number of clamping bolts has to be increased with the slope of the main cable, a number of different cable clamp sizes will still be required.

As an example on the application of cable clamps with pin holes, Figure 6.52 shows the clamps used in the Runyang Bridge.

Cable clamps with socketed hanger cables were also used in the bridges with inclined hangers, as illustrated by the cable clamp in Figure 6.53 (Severn Bridge). Here the clamps were divided into an upper and a lower part so that that the tightening bolts were positioned in vertical planes.



**Figure 6.47** Grooved cable clamps for the Verrazano Narrows Bridge



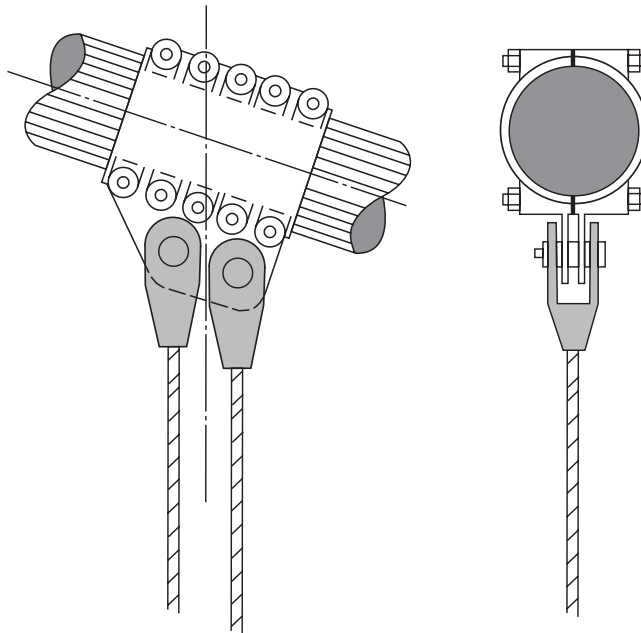
**Figure 6.48** Mock-up of a cable clamp in the Bisan Seto Bridge



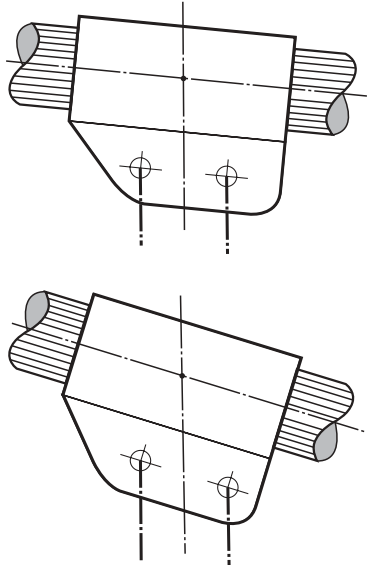
**Figure 6.49** Grooved main cable clamp with helical hanger ropes in the Xihoumen Bridge from 2009

A similar configuration but with vertical hanger cables was used for the Storebælt East Bridge (Figure 6.54). Note that the lower clamp half is thickened towards the vertical gusset plate below to cope with the out-of-plane bending of the cylinder wall.

In the Akashi Kaikyo Bridge, the traditional looping of the hangers around the cable clamp has been replaced by the European system with fork sockets on the hangers. The vertical gusset plates are wider apart so that the twin hangers



**Figure 6.50** Hangers connected with fork sockets to cable clamps



**Figure 6.51** Elimination of eccentricities by adjusting the position of pin holes in accordance with the cable band inclination

are positioned side by side rather than one after the other (Figure 6.55). The position of the gusset plates closer to the vertical tangent plane of the clamp cylinder has a favourable effect in reducing the out-of-plane bending of the cylinder wall.

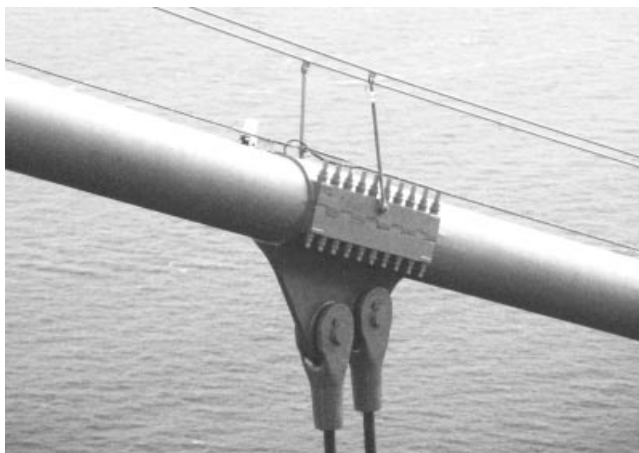
As a curiosity the description of the cable clamps concludes by the connection between the hangers and the cable clamps used originally in the Tancarville Bridge (Figure 6.56). Here the hanger rope is connected to the cable clamp through a socket corresponding to the type shown in Figure 6.12(h) and a large stirrup-shaped rod. This allowed an adjustment of the



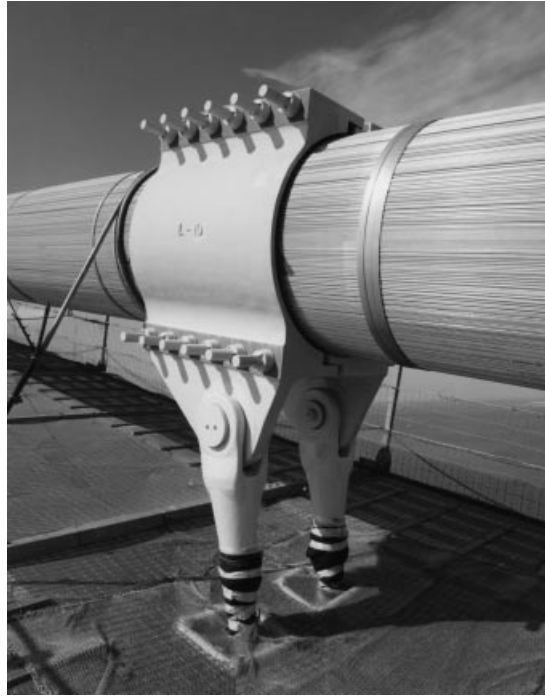
**Figure 6.52** Cable clamps for the Runyang Bridge



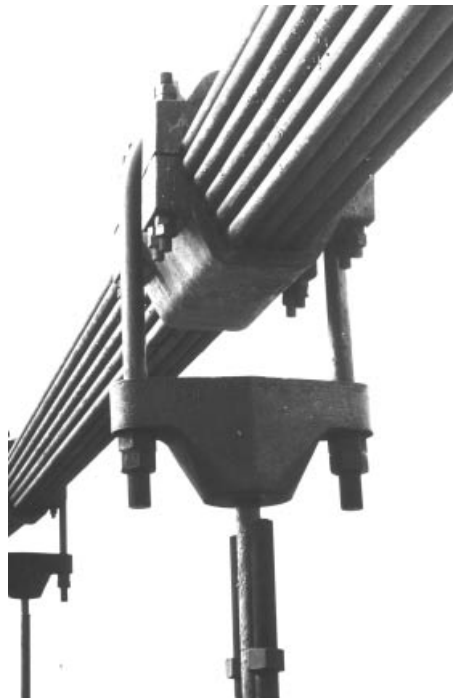
**Figure 6.53** Cable clamp in the Severn Bridge



**Figure 6.54** Cable clamp for the Storebælt East Bridge



**Figure 6.55** Cable clamp in the Akashi Kaikyo Bridge



**Figure 6.56** Cable clamp in the Tancarville Bridge

hanger length at the main cable level by tightening or loosening the nuts on the threads of the stirrup rod. Clearly the hanger attachment at the deck level also allowed length adjustments.

## 6.4 Connection between Cable and Pylon

The connection between cables and pylon can be made either through saddles or by anchoring the cables to the pylon. In Figure 6.57 three possibilities are shown for the connection between a cable set and the pylon.

In Solution (a) the cable is curved continuously over a saddle fixed to the pylon. This is the type of connection preferred in all major suspension bridges, and the solution was also found in early cable-stayed bridges with multi-strand stay cables.

In Solution (b) a saddle is also used, but here a longitudinal movement is made possible by applying rollers under the saddle. This principle has in a number of cases been used in suspension bridges during erection when mutual adjustments are required to avoid an undesirable bending of the pylon legs in the final condition. However, when the erection is completed, the saddle will generally be fixed longitudinally to the pylon as in Solution (a).

Solution (b) has also been applied in some early cable stayed bridges to reduce the bending of the pylons, but as at the same time the total structural efficiency is reduced, it is doubtful whether overall savings were achieved.

In Solution (c) the cable (of the mono-strand type) is discontinued at the pylon and both ends of the cable set are anchored. This principle is preferred in modern multi-cable stayed bridges as it implies a large degree of freedom in selecting the number and size of the stay cables as well as their inclination. Also, during transportation and erection, advantages can be gained when each prefabricated stay can be made with a length corresponding to the distance from the anchor point in the pylon and in the deck.

Due to the large number of stay cables in a multi-cable system, it is required to have the cable anchorage zone extended over a certain height of the pylon. Therefore, the typical cable system will be a semi fan with the cable anchors arranged as indicated in Figure 6.58. Here the sockets are positioned at minimum distances considering installation and maintenance, so that the system is as close to the pure fan as possible, and still have the anchors in a vertical plane.

In the Pasco–Kennewick Bridge a considerable concentration of the cable anchorages was achieved by composing the pylon head of three segments, allowing the cable anchorages to be distributed not only vertically but also horizontally (Figure 6.59). However, the advantages to be gained by the reduced eccentricities to get close to the pure fan system were to

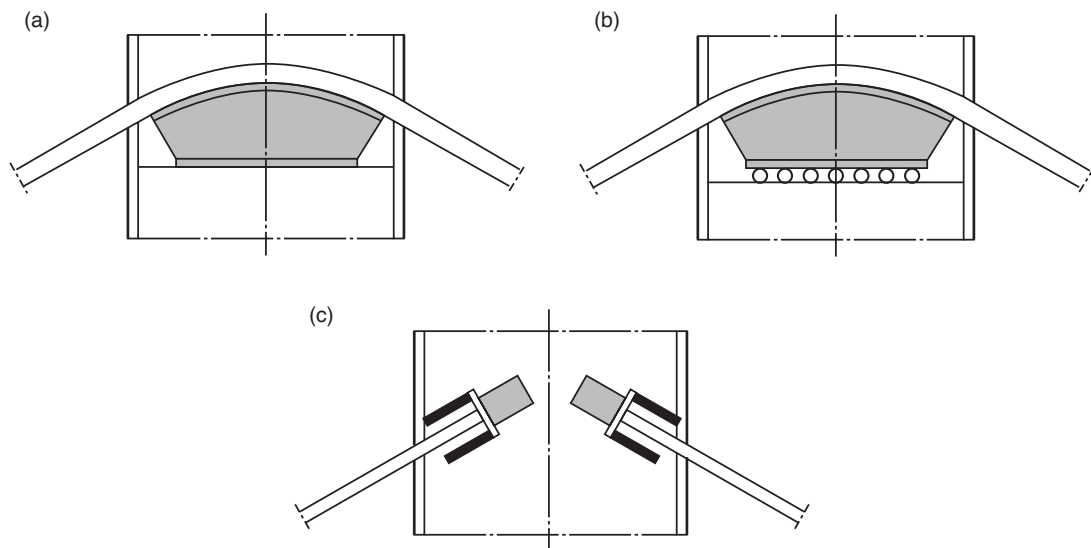
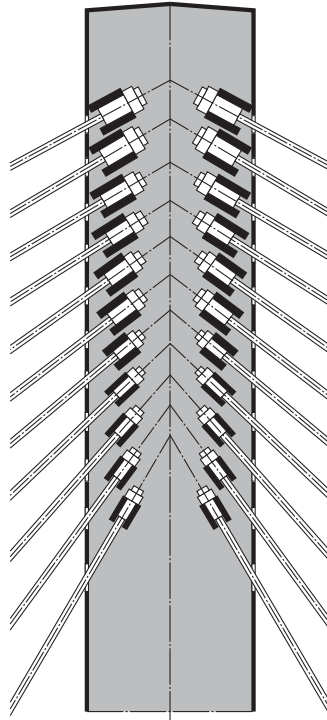


Figure 6.57 Three basic types of connection between cables and pylon



**Figure 6.58** Arrangement of cable anchors in a modified multi-cable fan system



**Figure 6.59** Pylon head with a lateral displacement of stay cables to allow the anchorages to be positioned side by side at the pylon head (Pasco-Kennewick Bridge)



some extent paid for by aesthetic drawbacks due to the varying lateral displacement and the visually crossing stays, as illustrated in Figure 6.59.

The solution shown in Figure 6.58 for the anchorage of a multi-cable system to the pylon is only immediately applicable if the pylon is made of steel (at least locally) since the horizontal cable force components have to be transferred as tension through the longitudinal walls of the pylon.

For a pure concrete pylon the anchoring of a multi-cable system might be accomplished as shown in Figure 6.60.

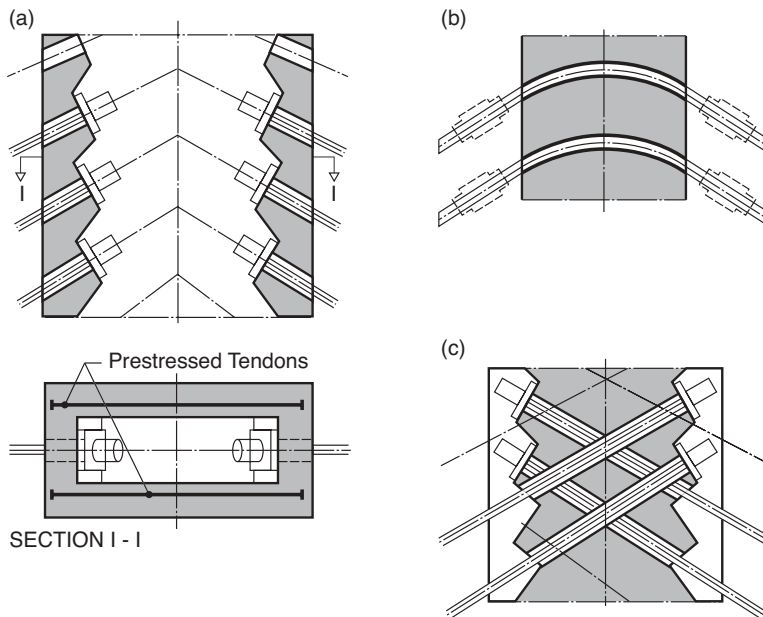
Solution (a) corresponds in its general arrangement to the solution of Figure 6.58, as the stay cables are anchored inside the hollow pylon on either side of the axis. As described above, this requires that the horizontal cable force components can be transferred horizontally from the left to the right face of the pylon. That can be accomplished by adding horizontal tendons in the longitudinal pylon walls at the anchor zone.

In Solution (b) the stay cables are led continuously through the pylons in curved tubes. By this arrangement the horizontal cable force components are directly transferred without affecting the pylon, but the solution is only applicable in connection with special erection procedures for the stay cables. The system has mainly been used in cases where the stay cables are made of iso-tensioned seven-wire strands.

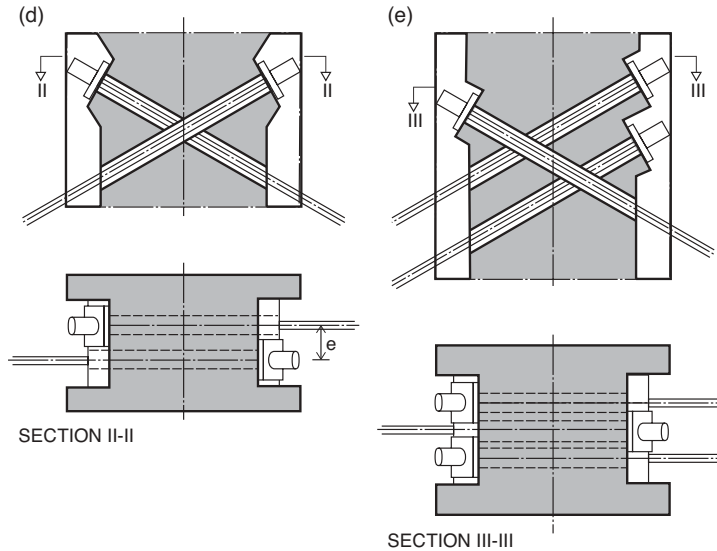
With prefabricated stay cables comprising the full cross section and socketed ends, the solution of Figure 6.60(b) is not directly applicable, but it might still be used if couplings (as indicated by dotted lines) are arranged immediately outside the pylon. In this case the prefabricated stay cables will be straight so that no special problems arise. The couplings might be established by using threaded sockets (as shown in Figure 6.12(c), (d), and (e)) connected by exterior sleeves or interior rods.

Finally, a multi-cable system anchorage could be designed as shown in Figure 6.60(c). Here the stay cables are led through anchor tubes in the pylon and anchored on the opposite side so that an overlapping is established. By this is obtained that the horizontal cable force components induce compression in the pylon and that the sockets can be made as regular bearing sockets.

Due to the required intersection of the stay cables inside the pylon a lateral eccentricity is unavoidable if each stay cable consists of a single strand, as illustrated in Figure 6.61(d). The eccentricities will induce torsion of the pylon leg which is less attractive due to the limited shear resistance of concrete. The eccentricity can be completely avoided if each stay cable



**Figure 6.60** Three solutions for the anchoring of mono-strand cables to a concrete pylon



**Figure 6.61** Overlapping of stay cable anchorages in a concrete pylon (left, with eccentricity; right, without eccentricity)

is made of two strands arranged as shown in Figure 6.61(e). As can be seen the two strands are placed one on top of the other in the left span and side by side (horizontally) in the right span.

In the Øresund Bridge with hollow concrete pylon legs the stay cables were anchored to short steel members designed to transfer the horizontal component of the cable pull so that only the vertical components (and under certain loading conditions a differential horizontal component) had to be transferred to the concrete (Figure 6.62).

A more radical application of steel in the anchor zones of concrete pylons is seen in e.g. the Farø Bridge and the Normandy Bridge (Figure 6.63). In these bridges a special anchor box of steel with all the necessary supporting diaphragms has been positioned inside the upper, vertical part of the concrete pylon. With this arrangement only the resulting force from all stay cable pulls will have to be transferred to the concrete, e.g. through shear connectors in the vertical interfaces.

In cases where the cable is passing continuously over a saddle in the pylon, two design features must be carefully considered:

- (1) radius  $R$  of the saddle
- (2) transmission of the differential cable force  $T_l - T_r$  (Figure 6.64).

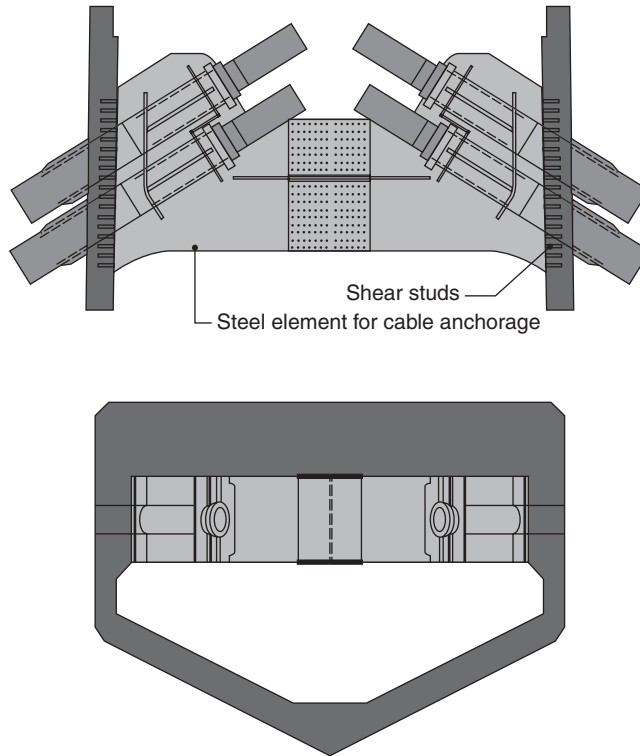
The radius of the saddle is determined by the allowable side pressure on each strand. This side pressure has to be limited to avoid a reduction of the axial cable strength, especially the fatigue strength.

According to the early German specifications, the allowable side pressure for locked-coil strands was limited to 1 kN/mm if the strand was in direct contact with steel, whereas the side pressure could be increased to 2.5 kN/mm if sheaths of soft metal with a minimum thickness of 1 mm were inserted between the strand and the steel saddle. For parallel-wire strands the corresponding values for the side pressure were set at 0.7 kN/mm and 1.8 kN/mm, respectively.

The soft metal sheaths were typically made of lead, copper or aluminium with a thickness of 2 mm. Alternatively, the sheaths could be substituted by a thick galvanizing ( $>1$  mm) of the relevant part of the saddle surface.

For a cable passing over a simple saddle without a cover (Figure 6.64), the maximum force,  $\max T_l$ , in the left cable is determined by Eytelwein's equation:

$$\max T_l = T_r \exp [\mu (\varphi_l + \varphi_r)] \quad (6.3)$$



**Figure 6.62** Stay cable anchorage in the pylon of the Øresund Bridge

where  $T_r$  is the cable force in the right cable,  $\mu$  the coefficient of friction, and  $\varphi_l + \varphi_r$  the angle between the two cable axes. The coefficient of friction  $\mu$  is generally stipulated to be 0.1 – the same value as in the case of a cable clamp. As  $\mu(\varphi_l + \varphi_r)$  is small compared to 1, (6.3) might be simplified to:

$$\max T_l \simeq [1 + \mu(\varphi_l + \varphi_r)] T_r \quad (6.4)$$

The available friction in a simple saddle will generally be quite small so the two cable forces can only deviate modestly. With  $\mu = 0.1$  and  $\varphi_l = \varphi_r = \pi/6$ , (6.4) yields  $\max T_l = 1.105T_r$ , so in this case the two cable forces can only differ by approximately 10% if sliding is to be avoided.

For a saddle as shown in Figure 6.65, where a cover is pressed with  $m$  pre-tensioned bolts against the cable, (6.4) will be modified to:

$$\max T_l \simeq [1 + \mu(\varphi_l + \varphi_r)] T_r + 2 \mu m P_b \quad (6.5)$$

where  $P_b$  is the axial tension in each bolt.

It is now theoretically possible to achieve any value of  $\max T_l$  by choosing a sufficiently large value of the total clamping force  $mP_b$ . However, as the side pressure per unit length is limited, large values of  $\max T_l$  will require a large length of the saddle.

The connection between the cable saddle and the walls of the pylon might be established by supporting the saddle on a short longitudinal beam inside the pylon (Figure 6.66). With this arrangement the vertical component of the cable forces is transferred only to the transverse walls and a local reinforcing of these plates might therefore be required.

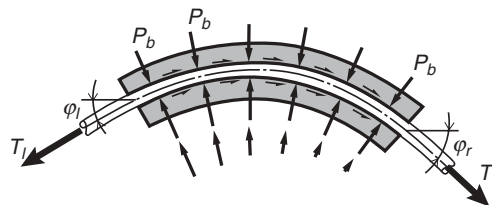
The cable saddles found in suspension bridges were for many years made as one large steel casting and as a typical example Figures 6.67 and 6.68 show the saddle of the Little Belt Bridge. This saddle was initially erected in a longitudinally displaced position (Figure 6.67) and supported on rollers to allow the saddle to be moved by jacking as



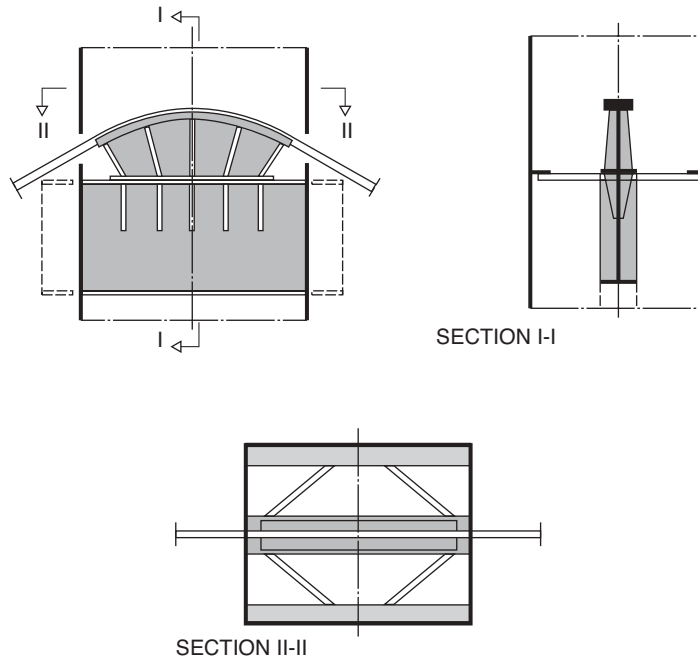
**Figure 6.63** Anchor box at the top of the pylon in the Normandy Bridge



**Figure 6.64** Frictional forces acting on a saddle without cover



**Figure 6.65** Frictional forces acting on a saddle with a cover clamped onto the curved cable

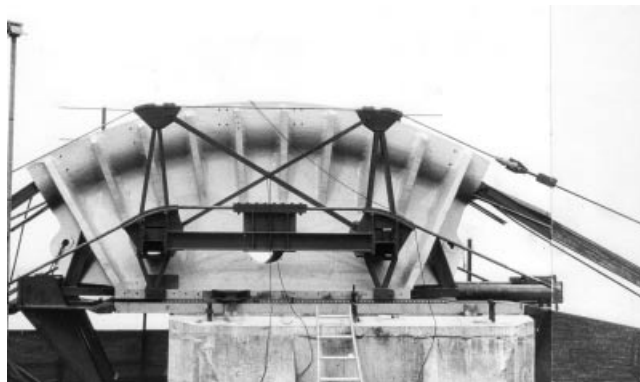


**Figure 6.66** Saddle supported by a longitudinal girder inside a steel pylon

the side span cable elongates during erection of the deck. In the final stage the saddle was centred and fixed to the pylon (Figure 6.68).

In more recent suspension bridges the major part of the saddle is assembled from plates welded together, as shown in Figure 6.69. Here only the saddle groove is made of cast steel, whereas the lower part that transfers the vertical force to the base plate is made as a grid of longitudinal and radial plates welded together. After casting, the cable groove is machined on a rotary planing machine to suit the strand arrangement of the main cable. The radius of the saddle groove is typically chosen to be 12 times the main cable diameter.

The pylon saddles of the Storebælt East Bridge were based on the principle illustrated in Figure 6.69. However, the entire grid of longitudinal and radial plates was covered by steel plates (Figure 6.70) to allow the interior to be protected against



**Figure 6.67** Cable saddle of the Lillebælt Bridge during erection



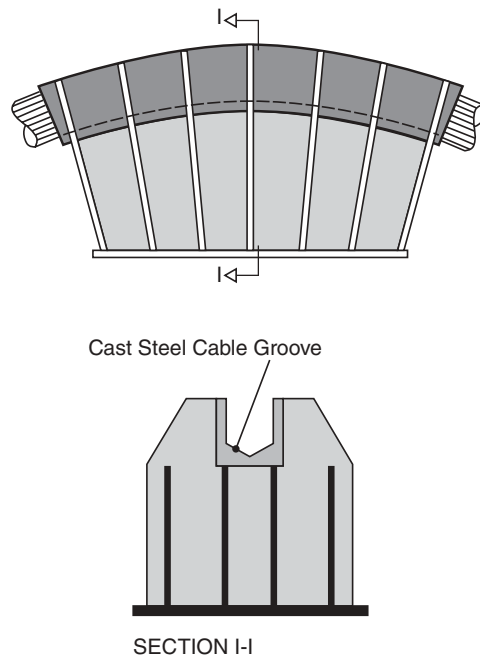
**Figure 6.68** Cable saddle of the Lillebælt Bridge in the final condition

corrosion by dehumidification. The dehumidification in the completed stage also comprises the main cable above the saddle, as a cover plate is bolted to the top of the saddle groove to form an enclosure around the cable.

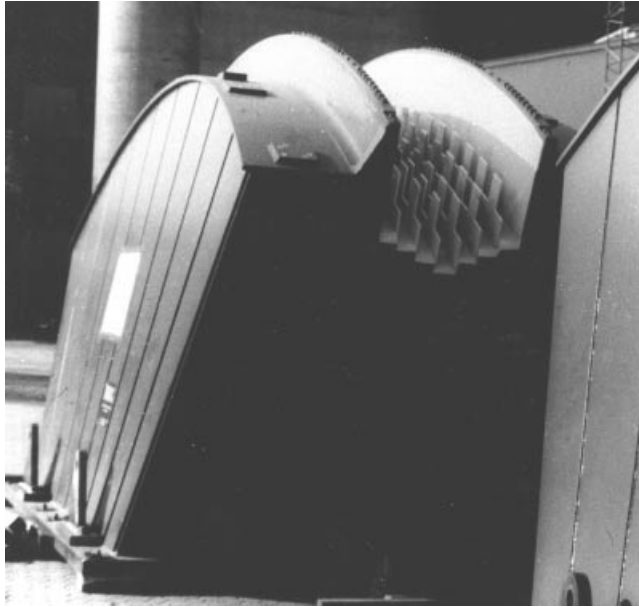
In the Høga Kusten Bridge the principle of welding the saddles was carried even further as also the groove was assembled by welding so that steel castings were entirely avoided (Figure 6.71).

In suspension bridges with short side spans, the maximum cable force in the main span and the side span will differ to such an extent that it will prove advantageous to increase the number of strands in the side span cable. In this case the additional strands in the side spans are positioned on top of the continuous main span strands, and the connection to the saddle is made by strand shoes or sockets, as indicated in Figure 6.72.

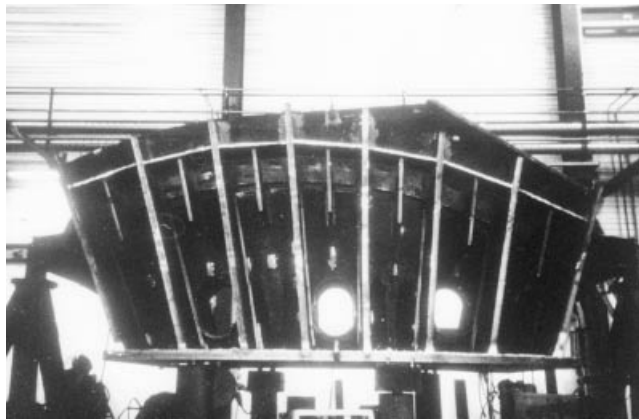
The present design of cable saddles is to a large extent based on the principles used in the period when pylons of major suspension bridges were of steel. However, today concrete has become the favoured material for pylons and in that case it



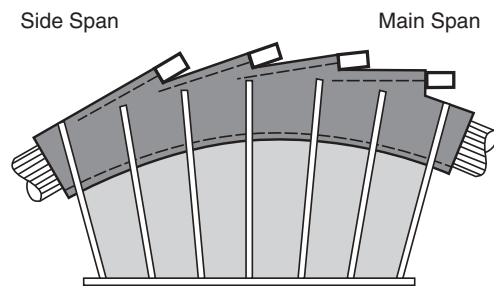
**Figure 6.69** Cable saddle with a cast steel saddle groove and a welded bottom part



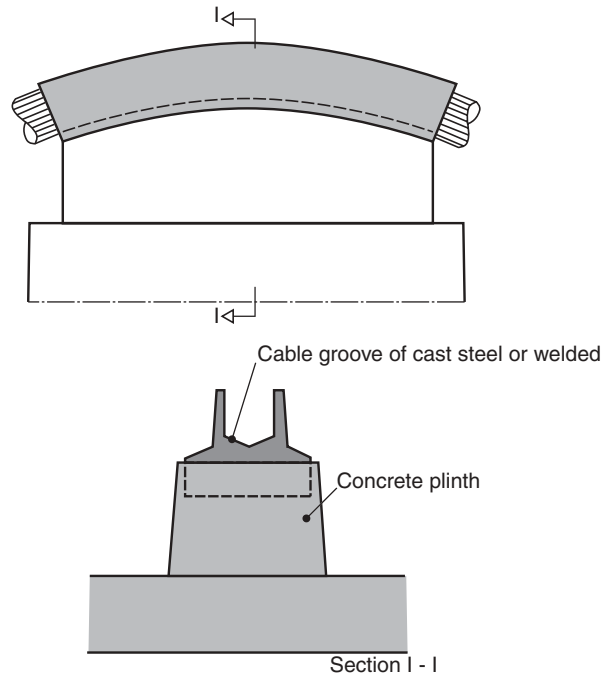
**Figure 6.70** Cable saddle for the Storebælt East Bridge



**Figure 6.71** Cable saddle for the Høga Kusten Bridge



**Figure 6.72** Suspension bridge cable saddle with additional strands of the side span cable anchored to the saddle above the continuous strands



**Figure 6.73** Cable saddle with a saddle groove supported directly onto concrete

would seem natural to replace the heavy grid of longitudinal and radial plates below the main cable groove with concrete as illustrated in Figure 6.73.

In most of the European suspension bridges the cable in the saddle groove is protected by a cover plate bolted onto the top of the saddle, as described for the Storebælt East Bridge. A different way of protecting the cable in the saddle region is seen in many of the major American and Japanese suspension bridges, where the pylon legs are extended up above the cable saddles to enclose both the cable and the saddle, as illustrated in Figure 6.74.



**Figure 6.74** Pylon top of the Bisan Seto Bridges



## 6.5 Connection between Cable and Anchor Block

In bridges with earth-anchored cable systems the total force of the main cables has to be transferred through the anchor block to the soil. The force transmission from cable to anchor block is established by anchoring the individual strands to the concrete of the block. Therefore, the cable is split into individual strands as they pass over a splay saddle, as illustrated in Figure 6.75. Note that in the vertical plane the strands are flared only downwards from the main cable tangent as this will allow the strands to be added layer by layer during cable erection.

The splay saddles will have to be supported on the anchor block in such a way that axial displacements of the cable can take place as it elongates or contracts due to varying stress or temperature.

In many cases the longitudinal movement is made possible by forming the splay saddle as a large pendulum – illustrated in Figure 6.76 by the splay saddle for the Storebælt East Bridge. Here, as in other splay saddles, the cable groove is made with a double curvature to allow a flaring of the strands both vertically and laterally.

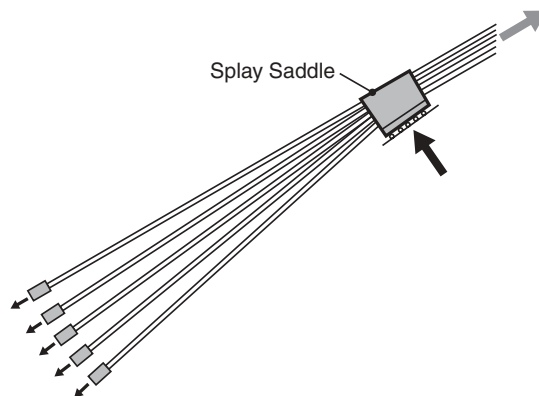
Flaring of the strands takes place inside a splay chamber in the anchor block, and at the bottom of this chamber the strands are anchored by strand shoes or sockets. From here the strand forces are transferred to the anchor block by steel rods, eye-bars or tendons embedded in the concrete.

Figure 6.77 shows a number of solutions for transmission of the strand forces into the concrete of the anchor block. Under (a) is shown the solution that was used in major American suspension bridges built in the first half of the twentieth century. Here the strand forces were transferred from the strand shoe through a chain of eye-bars to an anchor girder at the rear end of the anchor block. The length of each eye-bar, and the number of tiers in the chain, was determined by the size of the steel plates from which the eye-bars were cut or by restrictions due to transportation and erection. In connection with the application of eye-bars for force transmission, strand shoes as shown in Figure 6.3 were generally used. As these strand shoes did not allow any length adjustments, some of the eye-bars had elongated holes to permit shimming, as shown in Figure 6.78.

Instead of eye-bars the strand forces might also be transferred through rods threaded at the upper end. With this arrangement, indicated in Figure 6.77(b), the length adjustment takes place between the strand shoe and the threaded rods. The limiting factor for the application of Solution (b) is the length of the rods, because long and heavy rods are difficult to handle during construction.

After introduction of the pre-stressing technique it has proved advantageous to use tendons or cables to transmit the strand forces further into the concrete of the anchor block. Thus Figure 6.77(c) shows a solution with the strand shoes or sockets connected to relatively short rods embedded in the concrete over a length just sufficient to assure force transmission by bond. Further transmission of the forces into the concrete is then established by post-tensioned bars.

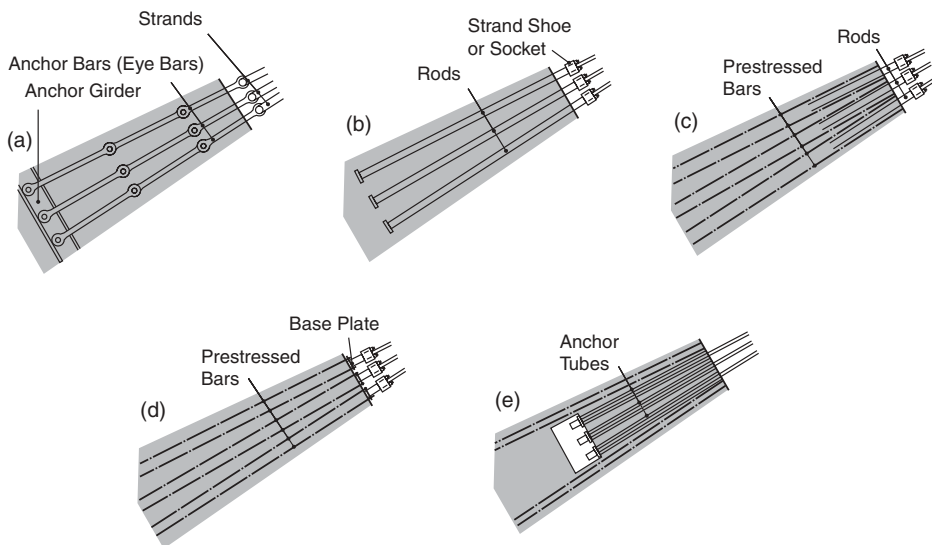
Alternatively, the transmission of the strand force to the post-tensioned bars could take place at the outer face of the concrete by connecting the threaded rods through base plates to the tendons, as indicated in Figure 6.76(d). This solution was adopted for the first time in the Severn Bridge (Figure 6.79).



**Figure 6.75** One-sided flaring of strands downwards from splay saddle



**Figure 6.76** Splay saddle at the anchor block of the Storebælt East Bridge



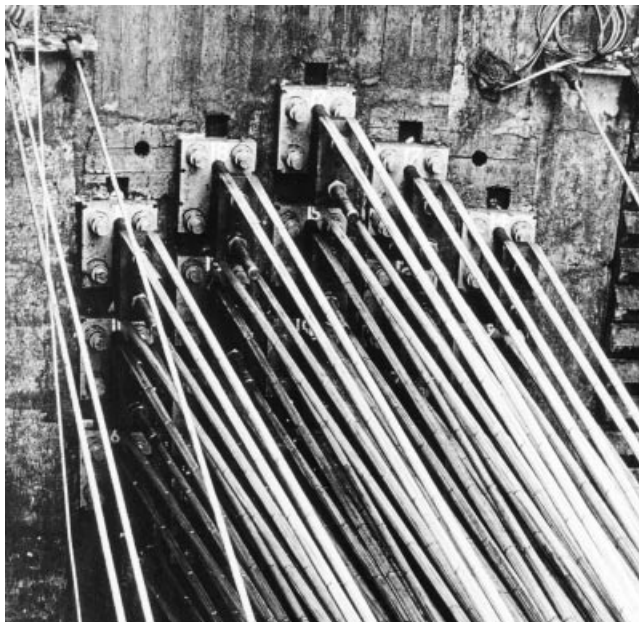
**Figure 6.77** Five solutions for the transmission of strand forces to the anchor block



**Figure 6.78** Eye-bar chains with elongated holes to allow adjustments by shimming (Verrazano Narrows Bridge)

In bridges with main cables erected by the parallel-wire strand method, the solution of Figure 6.77(e) has been applied. Here the strands have conventional bearing sockets that are pulled through anchorage tubes and anchored inside the concrete. Again, in this case, further transmission of the cable force is established by tendons.

After the cable force has been transferred to the anchor block as described above, the further transmission to the soil is much influenced by the local conditions.



**Figure 6.79** Strand shoes connected through threaded rods and base plates to post-tensioned bars (Severn Bridge)

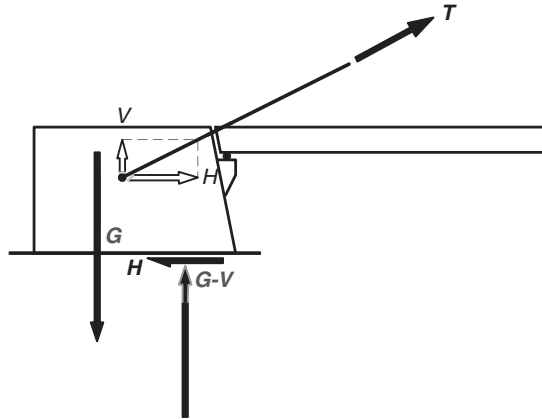


Figure 6.80 Gravity type anchor block

The most common type of anchor block is probably the gravity type shown in Figure 6.80. With this type of anchor block a very large dead load is required to counteract the vertical component of the cable force and give sufficient pressure at the foundation level to assure the transmission of the horizontal cable force component.

With the notation of Figure 6.80 and  $\mu$  as the friction coefficient in the foundation area, the following condition can be set up by expressing horizontal equilibrium:

$$R_H \leq \mu R_V \Rightarrow H \leq \mu (G - V)$$

From this the following expression for the weight  $G$  of the anchor block is derived:

$$G \geq V + H/\mu \quad (6.6)$$

As  $\mu$  always has a value below one, it will be seen that the weight  $G$  of the anchor block will have to be considerably larger than the horizontal force of the cable. With the following typical values:  $H = 2V$  and  $\mu = 1/3$ , (6.6) will imply that  $G \geq 3.5H$ .

From Figure 6.80 it appears that the overturning moment from the cable pull will move the resultant of the vertical earth pressure  $R_V$  towards the tip A of the anchor block. There is, however, a limit to how close to the tip the resultant can act without inducing unacceptably large vertical stresses in the contact area. Also, it must be considered that with a resultant close to the tip there will be no contact pressure at the rear end of the anchor block.

For all normal loading cases it will be in accordance with good engineering practice to choose the overall dimensions and the weight of the anchor block so that there will be a contact pressure over the entire foundation area. Assuming a linear (elastic) stress variation as indicated in Figure 6.80, this leads to the condition that  $e_R \geq \lambda/3$ .

Expressing moment equilibrium around the tip A leads to:

$$(G - V) e_R + H e_H + V e_V = G e_G$$

Combining this expression with the condition regarding  $e_R$  results in the following supplementary condition regarding the weight  $G$  of the anchor block:

$$G \geq [3He_H - V(3e_V + \lambda)]/(3e_G - \lambda) \quad (6.7)$$

It will be seen from (6.7) that it will be favourable to have as large a value of  $e_G$  as possible, i.e. to concentrate the weight of the anchor block at the rear end.

Equations (6.6) and (6.7) will allow an early determination of the overall dimensions of the anchor block, but the result will, of course, have to be checked in the detailed design phase by a much more elaborate analysis of the structure/soil interaction, e.g. based on a three-dimensional finite element model.



**Figure 6.81** Anchor block of the Benjamin Franklin Bridge

In major suspension bridges the gravity type anchor block will be characterized by very large dimensions, and efforts are consequently made to improve the appearance by an architectural treatment. In the old days the architectural treatment resulted in all kinds of ornamentation as illustrated by the anchor block of the Benjamin Franklin Bridge built in the 1920s (Figure 6.81). The ornamentation could, however, not hide the fact that the anchor block is a very dominating and massive structure.

Later attempts were made to give the anchor blocks a more pleasing appearance by an interesting geometrical configuration, as illustrated by the anchor block of the Bronx–Whitestone Bridge from the late 1930s (Figure 6.82).



**Figure 6.82** Anchor block of the Bronx Whitestone Bridge



**Figure 6.83** Anchor block of the Verrazano Narrows Bridge

However, here it can be argued that the curved top contradicts the function as the top strands of the flared cable are straight from the splay saddle to the anchorages at the lower end of the splay chamber.

The anchor block of the Verrazano Narrows Bridge, as shown in Figure 6.83, exhibits a more logical shape as the top slab above the splay chamber follows the top strand. The anchor block has a length of 105 m, a width of 49 m (at ground level), and a visible height of approximately 50 m. The resulting pull from the cables is 1120 MN.

In the large Japanese suspension bridges from the 1980s the anchor blocks were made in a very basic quadrilateral form, as shown in Figure 6.84 showing one of the anchor blocks in the Bisan Seto Bridges. It is seen that an attempt has been made to break the monotony of the large surfaces by a profiling of the walls but this has hardly concealed the fact that it is indeed an enormous lump of concrete.

The Storebælt East Bridge has its anchor blocks situated in the middle of the sea, several kilometres from shore. For this reason they cannot be combined with terrain formations, vegetation or surrounding buildings to divert attention from their massiveness. It was, therefore, decided to split the anchor blocks into discrete elements with the largest possible openings in between (Figure 6.85).

The East Bridge anchor block comprises an underwater caisson with a length of 120 m and a width of 55 m founded at a water depth of 12 m on two wedge-shaped, compacted stone beds. On top of the caisson two triangular trestles are added. The inclined rear leg houses the splay chamber as clearly reflected in the outer wedge shape. The front leg constitutes a



**Figure 6.84** Anchor block of the Bisan Seto Bridges



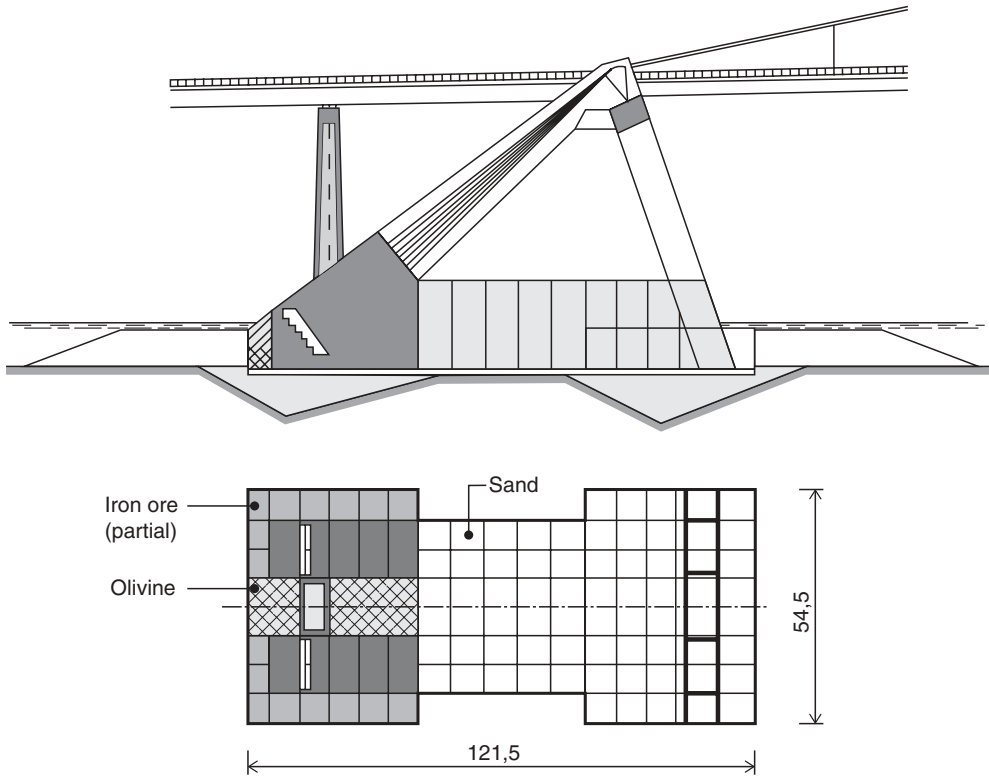
**Figure 6.85** *The Storebælt East Bridge anchor block*

column to transfer the deviation force from the splay saddle to the front of the caisson. At the rear end of the caisson a vertical pier shaft is added between the two splay chambers to give support to the approach span girder. To keep the outer dimensions small it has been necessary to use heavy filling materials such as iron ore or olivine to ballast the anchor block, especially at the rear end (Figure 6.86).

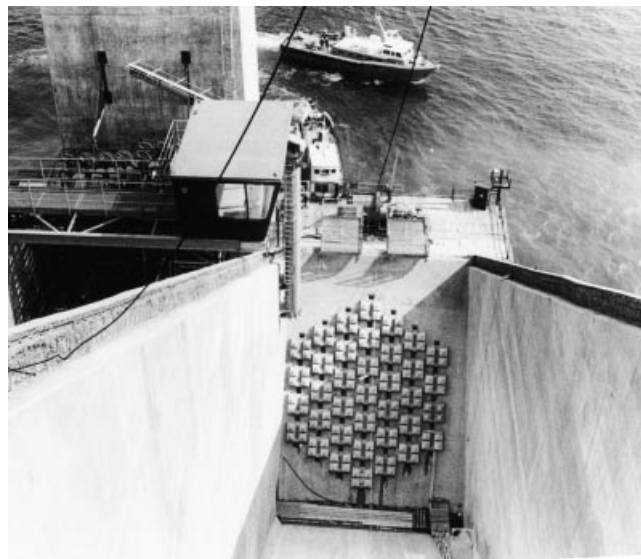
During cable erection the splay chambers were kept open (Figure 6.87), but after completion they were closed by casting a top slab. Subsequently the interior is kept dry by installation of a dehumidification plant.

In cases where sound rock is present at the location of the anchorage it will often be advantageous to embed the anchorages in the rock rather than use gravity anchorages above ground level. As illustrated in Figure 6.88, showing the southern anchorage of the Firth of Forth Road Bridge, the anchorage is made as a concrete block filling a conical tunnel driven into the rock. Note that the strand forces are transmitted to the concrete block by longitudinal tendons according to the system of Figure 6.77(d). The total cable force to be transmitted through the anchorage is 276 MN. The main dimensions of the concrete block depend on the size of the cable forces, the shear strength of the rock, the friction between the concrete and the rock, and the quantity of overburden above the rock.

In the Little Belt Bridge the anchor blocks were subjected to a somewhat smaller total force of 168 MN, but on the other hand the foundation had to be constructed on glacial tills. As huge and dominating anchor blocks were undesirable above the ground for aesthetic reasons, an anchor block as shown in Figure 6.89 was constructed [70.3]. This anchor block is almost entirely buried below the surface, and by sloping the underside of the block approximately  $10^\circ$ , it was possible to achieve the resulting force between concrete and soil acting almost perpendicular to the interface.

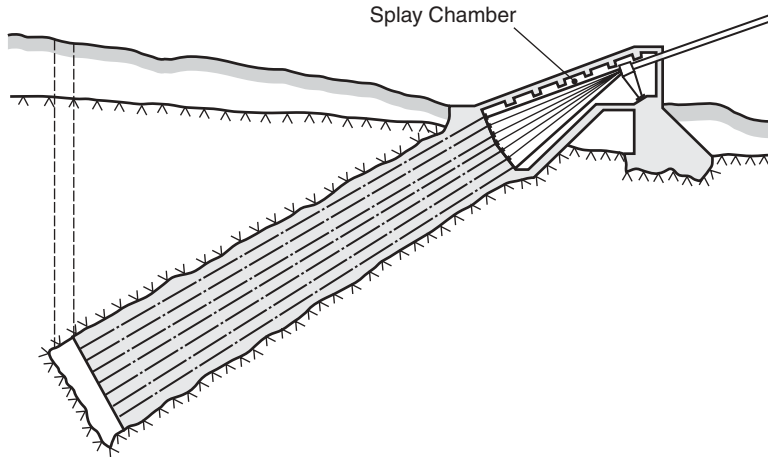


**Figure 6.86** Position of ballast in the Storebælt East Bridge anchor block

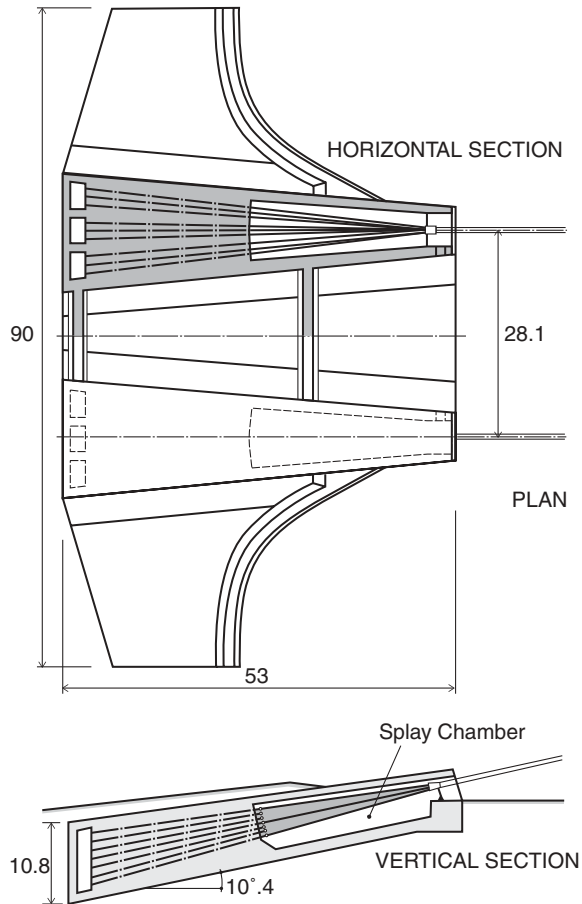


**Figure 6.87** Splay chamber in the anchor block of the Storebælt East Bridge prior to cable erection

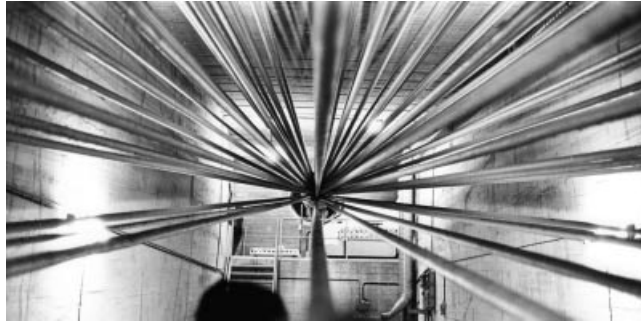




**Figure 6.88** Main cable anchorage in rock (Firth of Forth Suspension Bridge)



**Figure 6.89** Anchor block of the Lillebælt Bridge



**Figure 6.90** Splay chamber inside the Lillebælt Bridge anchor block

As seen Figure 6.89, the anchor block is shaped like a snow plough, and it consists of a continuous bottom slab, 1.5 m thick, with two anchor housings on top. Outside these housings the bottom slab is provided with a 4 m high front edge that can develop a considerable passive earth pressure if the anchor block should start to slide. However, the calculated safety against sliding is about 2, even in the worst case.

Inside the anchor housings the strands of the cable are flared in the splay chamber (Figure 6.90) and connected through sockets to threaded rods. As it is generally difficult to establish an efficient corrosion protection of the individual strands near the splay collar, a dehumidification of the entire splay chamber was used for the very first time in the anchor blocks of the Little Belt Bridge. Later dehumidification plants have been installed in the splay chambers of several other suspension bridges – also as a retrofit, e.g. in the Humber Bridge.

# 7

## Erection

### 7.1 Introduction

For the concept and design of cable supported bridges, aspects related to the construction have a very strong influence, as is the case for any structure of considerable size. Thus, the choice of structural system and material as well as the design of details must be made with due respect to the construction process, as emphasized several times in the previous chapters.

The erection procedure to be used depends to a large degree on the external anchoring of the cable system, as this will determine the sequence in the construction of the pylons, the cable system and the deck. With a fully earth anchored cable system, as found in all major suspension bridges, the different main components will have to be added one after the other: first, the pylons and the anchor blocks, then the main cables and the hangers, and finally the deck.

In self anchored systems such as those found in the traditional cable stayed bridges the different main components will have to be erected in turns. During a cantilever erection of the deck from the pylon towards midspan the stay cables will have to be installed and tensioned every time an anchor point in the deck is reached. In some cases even the construction of the pylons can go along in parallel with the erection of the deck and the stay cables. This might be the case if the cable system is of the harp configuration where only the lower part of the pylon has to be completed before it is possible to install the lower stay cables to give support to the deck adjacent to the pylons.

The strict order in which an earth anchored suspension bridges has to be constructed makes the whole process vulnerable to delays as the following activities cannot start before the previous activity is completed. Therefore both pylons and both anchor blocks will have to be in place in their entirety before any cable work can be carried out.

In cable stayed bridges the deck and cable erection can start as soon as the first pylon has reached the anchor points for the lower stay cables, and the erection from one pylon can proceed independently of the erection from the other pylon.

For the reasons above it is often claimed that cable stayed bridges can be erected faster than suspension bridges because it is possible to work on several fronts simultaneously. However, this might not always be true as the lower pylons of suspension bridges and the easier deck erection by vertical lifts save time compared to cable stayed bridges.

### 7.2 Construction of Pylons

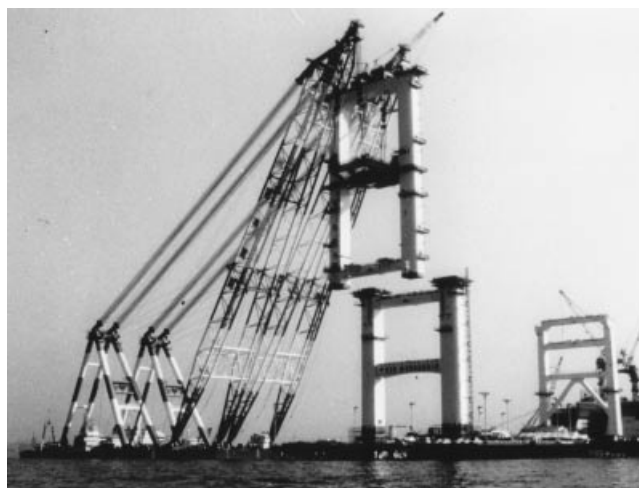
The methods used during the construction of pylons are generally the same as found in other high, slender structures. For smaller steel pylons such as found in cable stayed bridges of moderate size the erection might be carried out by mobile cranes with high booms or floating cranes.

Erection by land or sea-based cranes might also be used for at least the lower parts of high pylons, as illustrated in Figure 7.1 that shows the initial erection of the Verrazano Narrows Bridge pylon by a floating derrick crane on a lattice tower.

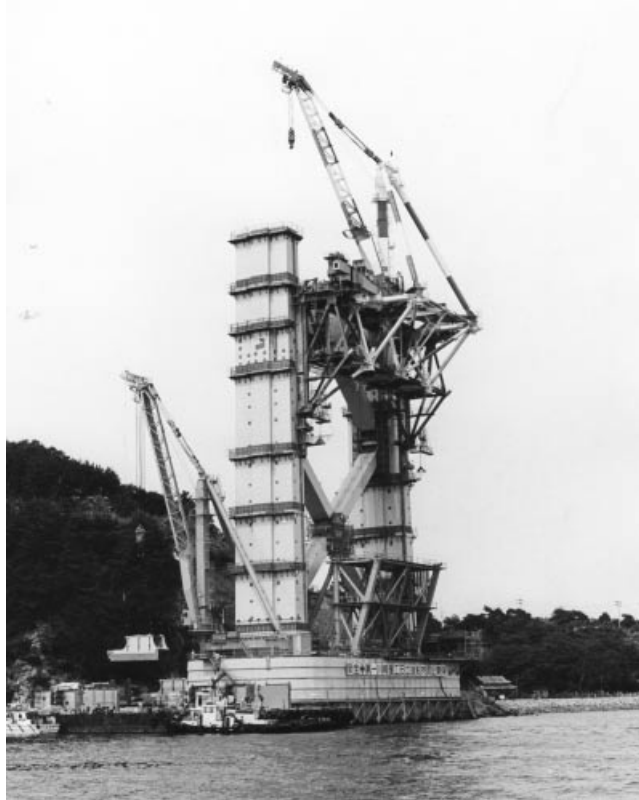
With the evolution in size of floating cranes experienced since the 1970s it has become possible to erect the entire pylon in one or two pieces, as illustrated in Figure 7.2 showing the erection of the steel pylon for the Rainbow Bridge in Tokyo. Here the entire 126 m high pylon was erected in just two pieces (weights of 1850 and 3400 tonnes, respectively).



**Figure 7.1** Erection of the lower part of the Verrazano Narrows Bridge pylon by a floating derrick crane



**Figure 7.2** Erection of the Rainbow Bridge pylon by a floating crane



**Figure 7.3** The pylon of the Bisan Seto Bridge during erection

For very high pylons it is necessary to erect at least the upper part by the traditional procedure where a climbing crane follows the pylon as it grows. The crane applied to hoist the prefabricated pylon units into place generally consists of a derrick crane on a latticed cross beam attached to both pylon legs, as illustrated by the erection of the pylons for the Bisan Seto Bridge in Figure 7.3.

For the steel pylons of the First Bosphorus Bridge a different procedure was applied, as seen in Figure 7.4. Here the basic equipment consisted of two special tower cranes operated by winches at ground level. With this arrangement a substantial reduction of the weight to be climbed was achieved, and at the same time a much smaller operating radius was required for each crane [76.1].

For the erection of the Akashi Kaikyo Bridge pylons just one centrally positioned climbing tower crane was used. This crane was supported by a tubular column stabilized against buckling by struts leading to the two permanent pylon legs (Figure 7.5).

For concrete pylons either slip forms or jump forms can be used during casting of the pylon legs. Slip forms will lead to the shortest construction period due to the continuous casting but will be logistically demanding as this requires a continuous delivery of ready-mixed concrete. Consequently, slip forms will be best suited if the pylons are to be built on land or can be reached from temporary access bridges leading out from the coast. These conditions were found at the sites of the Humber Bridge (Figure 7.6) and the Tsing Ma Bridge.

In the case of the Storebælt East Bridge the pylons had to be cast 2–3 km from the coast so all concrete had to be brought in by sea and this was one of the main reasons for using jump forms. The decision was also influenced by the less favourable experiences from the use of slip forms during construction of the caissons for the Storebælt West Bridge where the same type of dense concrete was specified.



**Figure 7.4** Erection of the Bosphorus Bridge pylon by twin tower cranes

The pylons of the East Bridge were cast in lifts of 4 m so with a mean return period of about one week and a total height of 254 m, the construction time for the pylons exceeded one year.

To allow the reinforcement to be positioned and the concrete to be cast under severe weather conditions, a four-level platform was attached to the jump forms on each pylon leg (Figure 7.7).

Independent of the method used to cast the vertical pylon legs, special procedures have to be applied when casting the horizontal cross beams between the two legs. Here it will be necessary to erect a temporary transverse girder between the pylon legs and use this girder to support the formwork (and the wet concrete) until the concrete has hardened and been post-tensioned (Figure 7.8).

Pylons for suspension bridges generally have almost vertical legs which makes it easy to use either slip forms or jump forms. In cable stayed bridges with A- or diamond-shaped pylons the legs will be inclined so that the dead load will induce considerable bending as the legs are extended. It is, therefore, necessary to add temporary struts between the two legs during construction, as illustrated in Figure 7.9 (Farø Bridge).

Traditionally, pylons are designed with a pronounced slenderness in the longitudinal direction of the bridge to allow the pylon to follow the longitudinal displacements of the cable system. However, during construction of the pylons, the cable system is not in place so the pylons must possess the necessary resistance against horizontal wind load by themselves. Often the most critical phase in the construction of the pylon occurs in the period from when the pylon is at full height until the first



**Figure 7.5** The Akashi Kaikyo Bridge pylon during erection

stay cables or the catwalks are erected. In this period wind-induced oscillations of the pylon in the longitudinal direction of the bridge might be experienced.

From a description of the erection of the Firth of Forth Suspension Bridge [65.2], the following quotation should illustrate the problem:

In a South-west wind of about 20 miles/h (32 km/h) the tower began to oscillate considerably, the movement at the top being estimated at several feet. The butt joints were opening and closing at the north and south faces, the opening of the lowest joint amounting to 0.05 in. (~1 mm) . . . with the tower at its full height and the climbing structure at the top, the sway culminated in a measured double amplitude of 7 ft 6 in. (2.3 m).

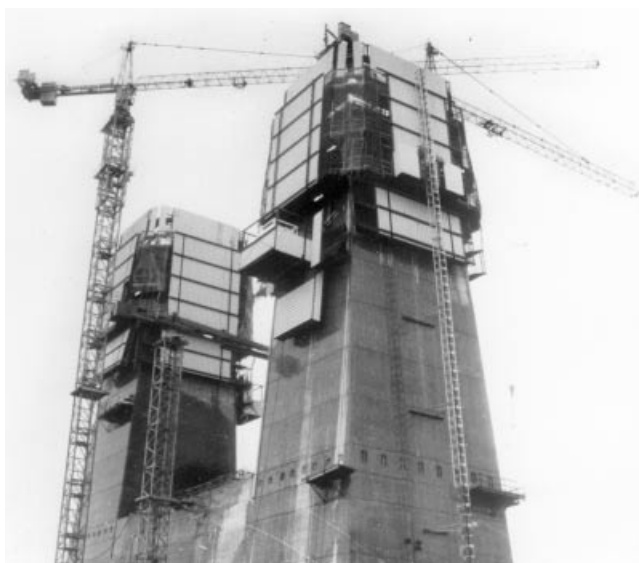
The longitudinal oscillations are generally caused by the slenderness of the pylon in this direction, combined with the large wind areas at the top from the cross beam and the climbing crane.



**Figure 7.6** Slip forming of the Humber Bridge pylon

The problems related to wind-induced oscillations of the free-standing pylons will generally be more pronounced for steel pylons than for concrete pylons due to the steel structure's smaller mass, larger flexibility, and lower damping. In a number of cases it has therefore been necessary to take special measures to achieve aerodynamic stability in the critical construction phases. In Japan, larger pylons often have had tuned-mass dampers installed temporarily once a certain height has been reached and until a supplementary support is provided by the cable system.

For major cable supported bridges it has become common to perform wind tunnel tests to check the stability of the free-standing pylon and to determine in which phases it will be necessary to take precautionary measures. As an example, Figure 7.10 shows a dynamic model of the Øresund Bridge pylon in the boundary layer wind tunnel at the Danish Maritime Institute.



**Figure 7.7** Pylon of the Storebælt East Bridge during the early construction phase





**Figure 7.8** The East Bridge pylon after installation of the scaffolding beam for the lower cross beam

The Øresund pylons are made of concrete but due to their extreme height (slightly over 200 m) and the long free-cantilevered legs above the lower cross beam it was found necessary to perform wind tunnel tests. The tests were initially made in smooth wind on a model with a very small damping, and in this idealized condition vortex-shedding oscillations did occur, but after having switched to a model with more realistic damping characteristics and in a turbulent wind, it could be concluded that the pylon would be stable throughout the construction phase – and this assumption was also confirmed during the actual construction that followed.

The 254 m high concrete pylons of the Storebælt East Bridge were completed in the summer of 1995 and in the following autumn they were entirely free-standing. In this period a number of measurements were taken and during a storm, vortex-induced oscillations with amplitudes of up to 200 mm were recorded at a mean wind speed of 17 m/s (measured at a height of 70 m). The amplitudes of 200 mm, however, were so modest (less than one-thousandth of the height) that they did not lead to any unacceptable stresses or cracking in the concrete.

As explained earlier, the pylon must be flexible to follow the displacement of the cable system, and as the displacement of the pylon top increases significantly with the side span length, the problems of fulfilling the requirements of stability during construction and flexibility in the final stage will be more severe in bridges with large side-to-main span ratios. If both requirements cannot be fulfilled, a temporary support of the pylon in the longitudinal direction might become a necessity.



**Figure 7.9** Pylon of the Farø Bridge during construction

Such a temporary support was established during the construction of the Lillebælt Bridge in Denmark. As illustrated in Figure 7.11, the temporary support consisted of bracing cables leading from one end pier to the pylon (at a height of 85 m), across the main span to the other pylon, and further down to the other end pier. The bracing cables were added as soon as the pylons reached the relevant height and consequently they were fully effective when the pylon top and the upper cross beam were cast. To allow an adjustment of the tension in the bracing cables, tie-down ropes were arranged at both pylons and at the end piers.

In the case of the Lillebælt Bridge, the pylons were made of concrete which might accentuate the cantilever problem as a relatively modest amount of vertical reinforcing is required in the completed structure due to the effective pre-stressing from the vertical compression induced by the cable system. Therefore, when designed only for the final stage, a pylon can show an insufficient flexural strength during construction.

To reduce the oscillations of the free-standing pylon it might not be required to install a continuous bracing cable leading from one anchor block to the other via the main span, as in the case of the Lillebælt Bridge. For each of the 254 m high

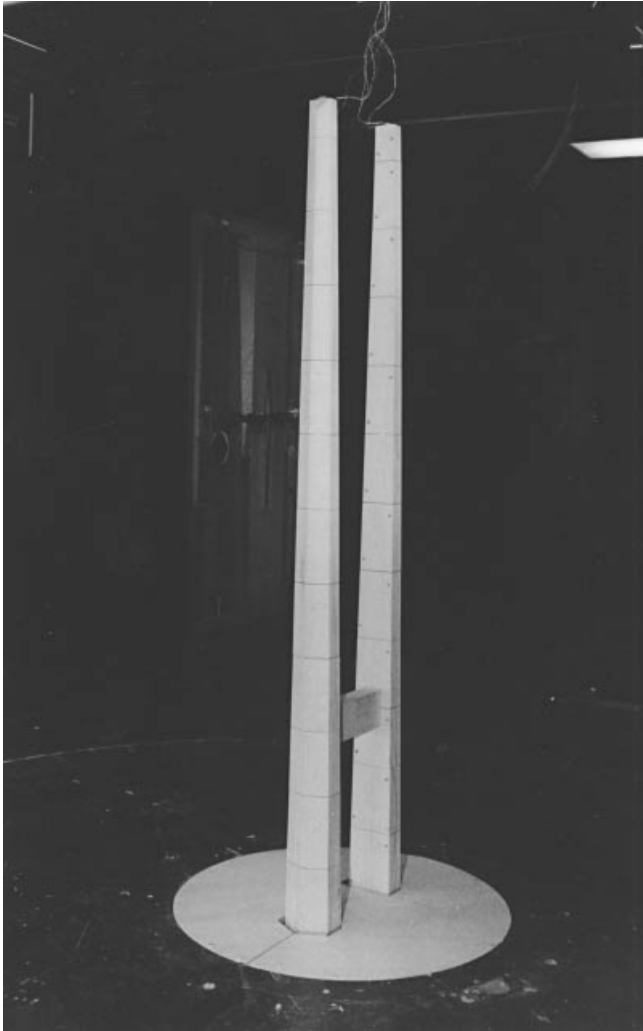


Figure 7.10 Model of the free-standing Øresund pylon in the wind tunnel at the Danish Maritime Institute

concrete pylons of the Storebælt East Bridge a stabilization was achieved by a single set of tie-back cable leading to the nearest anchor block, as seen in Figure 7.12. The tie-back cables were primarily added to allow the pylon tops to be displaced approximately 1.2 m away from midspan to counteract the displacements caused by the strains of the side span main cable during the subsequent erection of the deck. The aim was to arrive at a vertical pylon with zero bending in the final dead load condition.

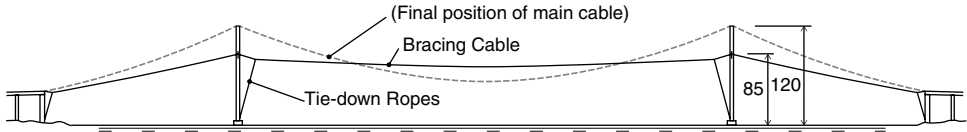
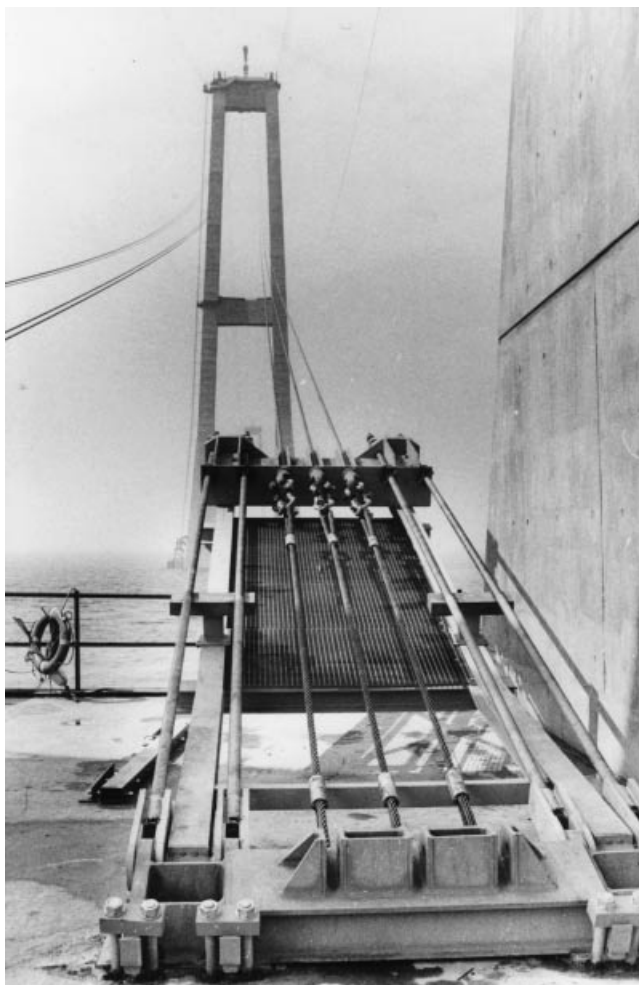


Figure 7.11 Bracing cables installed to stabilize the concrete pylons of the Lillebælt Bridge



*Figure 7.12 Tie-back cables from the anchor block to the pylon in the Storebælt East Bridge*

### **7.3 Erection of Suspension Bridge Main Cables**

The erection of main cables in major suspension bridges is generally initiated by erecting a temporary footbridge, or, as it is often called, a catwalk. The catwalk allows access to any spot along the main cables during cable erection as well as in the following operations of compaction, wrapping, cable clamp erection and hanger installation (Figure 7.13).

The catwalk is supported by a number of temporary helical strands (catwalk ropes) positioned under the walk area. The catwalk ropes are pulled across the spans after installation of a pilot rope leading from one anchor block via the pylons to the other anchor block. The pilot rope will generally have a smaller cross section and therefore be lighter than the catwalk strands.

The pilot rope is in most cases pulled across by a tug boat from one anchor block to the other via the pylon piers. Subsequently, the rope is lifted from the sea bottom to the top of the pylons by a light crane. However, such a procedure requires that the navigation under the bridge can be closed for a few hours during the lifting of the pilot rope installation. This was the case for the Storebælt East Bridge where it proved possible to get permission to interrupt the international ship traffic from the North Sea to the Baltic Sea for a period of three hours.

When such a disruption is not possible, the pilot rope has in some cases, e.g. at the cable erection of the Akashi Kaikyo Bridge, been accomplished by carrying a rope across by helicopter. This requires that the weight of the rope itself is very modest, and in the case of the Akashi Kaikyo Bridge, where the distance from anchor block to anchor block is close to 4 km,



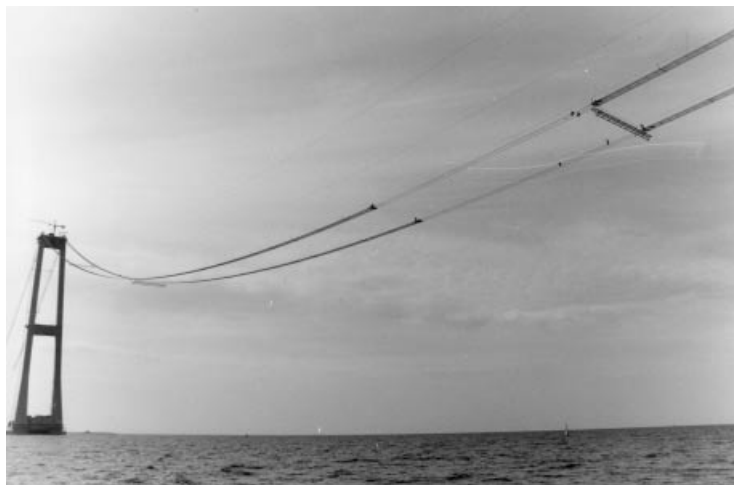
**Figure 7.13** Suspension bridge with catwalks as installed during cable erection (Tsing Ma Bridge)

the rope was made of Kevlar fibres to keep the weight down. The first light Kevlar rope was then utilized to carry a stronger steel rope across and this rope was then used to pull the heavier catwalk strands across.

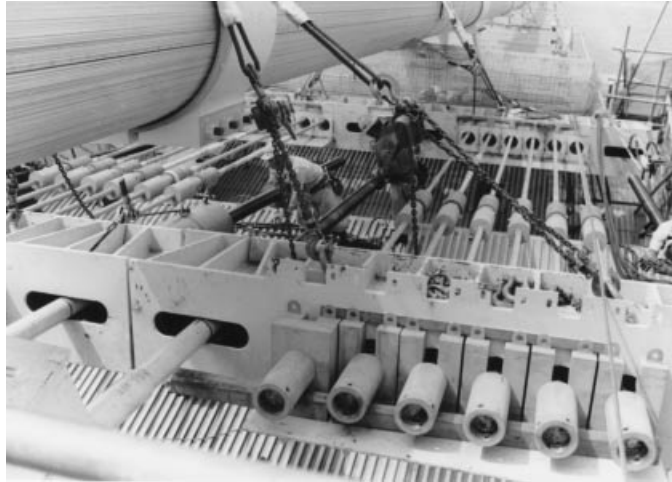
A transfer by helicopter of the first catwalk rope was also used during the construction of the Askøy Bridge in Norway. However, in this case, the main reason for using a helicopter was the fact that the water depth is up to 300 m under the bridge, so that a catwalk rope of the requisite length could not be brought to a temporary rest on the sea bottom prior to the lift into place.

When all catwalk strands have been positioned, the floor mesh is unreeled from large reels at the pylon top and slid down to the anchor blocks and to the main span centre (Figure 7.14). The catwalk floor is pre-fabricated with wooden cross beams and an intermediate wire mesh. Subsequently, hand ropes and wire meshes are added at the sides of the catwalk to transform it into a safe work area. The hand ropes are connected to the catwalk ropes at certain intervals by open, U-shaped steel frames.

The catwalk ropes are fixed to the anchor blocks as well as to the saddles on the pylon tops. To ensure that the catwalk is positioned at a reasonable distance below the main cables it will be required to adjust the catwalk ropes as the erection



**Figure 7.14** Catwalk wire mesh in the process of being pulled across on top of the catwalk ropes (Storebælt East Bridge)

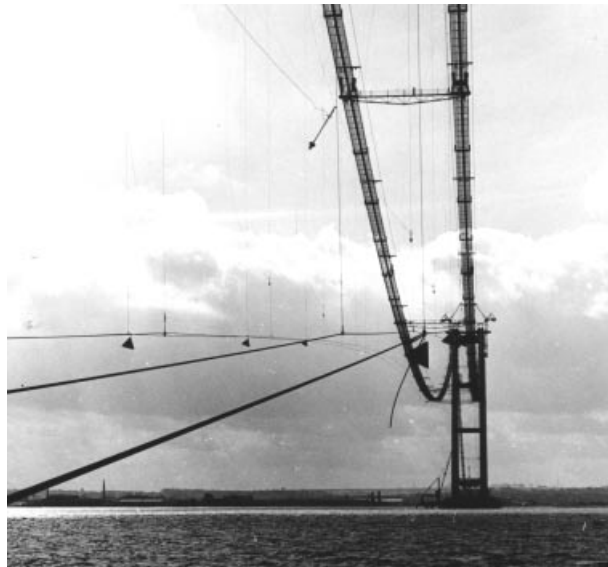


**Figure 7.15** Anchoring of catwalk strands at the pylon top (Akashi Kaikyo Bridge)

proceeds (Figure 7.15). Thus, during lifting of the deck segments the main cables will elongate and increase their sag so the catwalk will have to be lowered. This is achieved by a slight release of the tension in the catwalk ropes while the catwalk is tied to the main cable at a number of points along the span.

The catwalk constitutes a very flexible structure stabilized only by gravity as no flexural stiffness is provided. This might make the catwalk too vulnerable to wind actions and to counteract this vulnerability a so-called storm system is in most cases added to the catwalk structure. This storm system consists of a convex cable connected by vertical or inclined hanger cables to the catwalk strands (Figure 7.16).

It is not always possible to add a storm system as the convex cable can come in conflict with clearance requirements due to navigation during the construction period. This was the case for the Akashi Kaikyo Bridge so here it was chosen to stabilize the catwalk by increasing its weight.



**Figure 7.16** Storm system to stabilize the catwalk during cable erection (Humber Bridge)

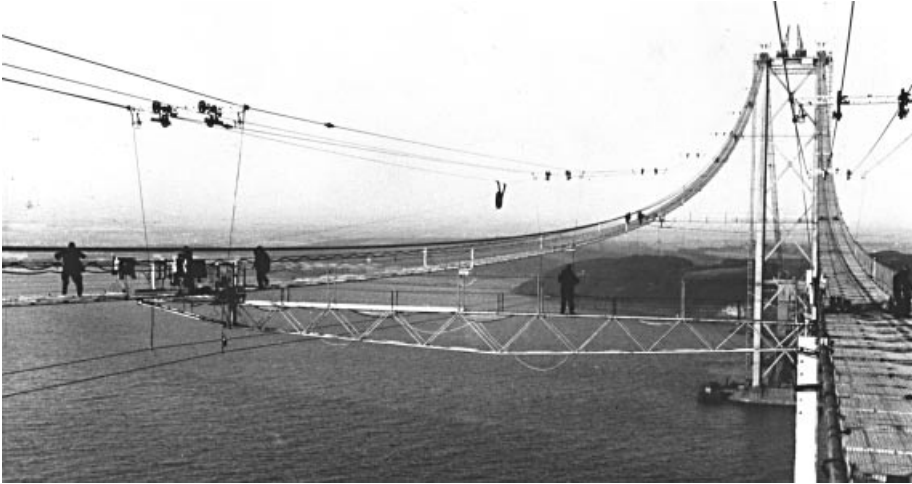


Figure 7.17 Cross bridge connecting the two catwalks (Firth of Forth Road Bridge)

In the traditional suspension bridge with two main cables a catwalk will naturally have to be erected under each cable and between these two catwalks a number of cross bridges will be added to allow access from one catwalk to the other at a number of locations along the span (Figure 7.17).

In major suspension bridges the main cables will be composed of so many wires that it is impossible to fabricate and erect the entire cable in one piece. Consequently, the main cables will have to be built up either on site from the single wires (the air-spinning or AS method) or from pre-fabricated strands (the pre-fabricated parallel-wire strand method or PPWS method).

The traditional method for suspension bridge main cable erection has been the AS method (Figure 7.18) that has now been in use for more than 120 years. This method is an *in situ* method because the cable is actually built up from the

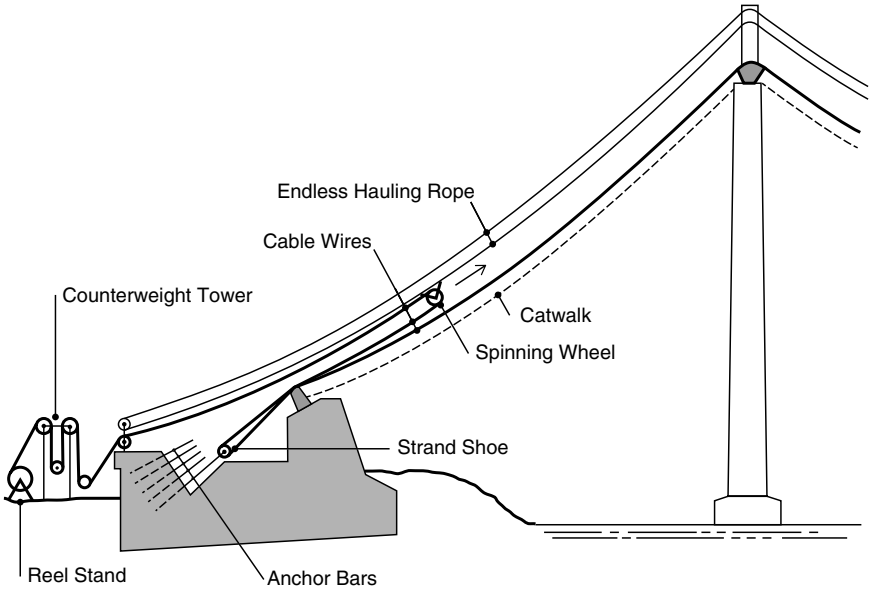


Figure 7.18 The air-spinning method (Verrazano Narrows Bridge)



**Figure 7.19** Wire coils transported by truck to the site of the Storebælt East Bridge

single wires delivered to the site in coils (Figure 7.19). The coils generally have a weight of around 1 tonne, corresponding to a wire length of up to 5000 m. This length is, however, too short to allow for a sufficiently continuous cable spinning so the coils are transported by forklifts to loading swifts (Figure 7.20) from where they are wound onto wire drum units, each containing a total wire length corresponding to 10–20 times the distance from one anchor block to the other. The drum units are in most cases positioned at one of the anchor blocks from where the wires are to be unreeled. For each wire two drums are at disposal to allow one of the drums to be wound with new wires while the other is unreeled as cable spinning proceeds (Figure 7.21).

As the content on each drum corresponds to that of several coils a splicing is required between wires and this splicing is generally made by a compression fitting pressed onto the two wire ends (Figure 7.22). The major part of the splices are completed as the coils are unreeled by application of a stationary trolley-mounted press. However, a portable press must



**Figure 7.20** Loading swift at the Storebælt Bridge site





**Figure 7.21** Wire drums on the reel stand at the Storebælt Bridge site

also be available to perform in situ splicing in case of wire breaks or to replace splices that would land in the ‘forbidden zones’ above the saddles or on the strand shoes.

From the relevant drums the wires are taken through the counterweight tower (Figure 7.23) to ensure a constant, predetermined stress in the wires. This is achieved by leading the wires over sheaves at the top of the tower and down around a sheave carrying a well-defined mass. During spinning the sheave with its mass is hanging in the wires and kept positioned freely suspended around mid-height of the tower.

From the counterweight tower the wires are curved around the spinning wheel and back to the anchorage. The spinning wheels will be provided with two or four grooves, allowing two or four loops of wire to be carried across in each run (Figure 7.24). As the lower wires are connected to the anchorage at one end, these stationary wires are designated ‘dead wires’, whereas the ‘live wires’ going from the spinning wheel to the reels move forward at twice the speed of the spinning wheel.



**Figure 7.22** Splice in a wire of a suspension bridge main cable



**Figure 7.23** Counterweight tower at the anchor block of the Humber Bridge



**Figure 7.24** Spinning wheel



**Figure 7.25** Sag adjustment of individual wires during spinning operations at the Tsing Ma Bridge

The spinning wheels are carried across by an endless tramway rope connected to the catwalk by closed support frames. Each tramway rope will generally have two spinning wheels attached in such a way that they move in opposite direction and meet halfway between the anchor blocks, i.e. at midspan in case of a symmetric suspension bridge.

During passage of the spinning wheel it was traditionally attempted to maintain a stress equal to the stress of a freely hanging wire subjected to its own weight. In that case the wires would get the same sag as that of the completed cable and the wires would, therefore, carry their own weight also during the spinning process. This method is now referred to as the high-tension method, whereas a more recent method where the wires are pulled across with a lower stress that requires a wire support by the catwalk (or the completed part of the cable) is denoted the low-tension method or the controlled-tension method.

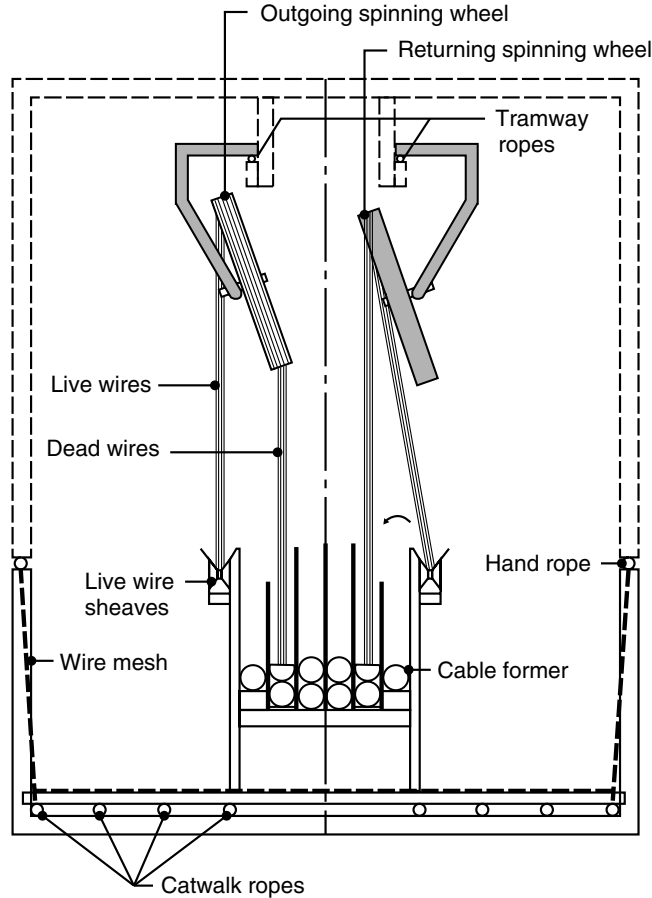
For the high-tension method equal stress in all wires is assured by a sag adjustment of every wire immediately after each run of the spinning wheel (Figure 7.25). The sag adjustment has to be done subsequently for each span so it is a labour-consuming process and it is also the main cause of the weather sensitivity associated with this method. Therefore, the adjustments can only take place at wind speeds below approximately 15 m/s.

Depending on whether drum units and counterweight towers are available at both anchor blocks or only at one, the spinning wheel will then return either with a new set of wires, or empty.

When a reasonable number of wires (300–500) have been pulled across by the spinning wheel, they are bundled by aluminium bands into a stand. The reason for the bundling into strands is to stabilize the partially erected cable and avoid a tangling of the individual wires as well as to allow an accurate sag adjustment of each of these *in situ* strands. So even though the wires have been individually sag adjusted in the case of the high-tension method, the completed strand will still have to be accurately sag adjusted. To achieve a sufficient accuracy in the adjustment of the sag it is generally necessary to work at night when a uniform temperature can be expected.

It should be mentioned that very accurate sag adjustments are not really required to ensure a reasonable constant dead load stress over the cross section of the completed cable. Thus, due to the fact that the stress from the weight of the cable is inversely proportional to the sag, a difference in sag of 1% (corresponding to 1 m for a main span cable with a span of 1000 m and a sag of 100 m) between two strands would only result in a difference in stress between these two strands of 1%. This difference is, however, only the difference due to the weight of the cable, and as this will probably only account for approximately one-fifth of the total dead load stress, the difference would ultimately be only 0.2%, and such a deviation would of course be fully acceptable under all circumstances.

So the main reasons for performing the sag adjustments with what seems to be an unnecessary accuracy are considerations regarding the integrity of the partially erected main cable. Thus, if there was a difference of 1 m



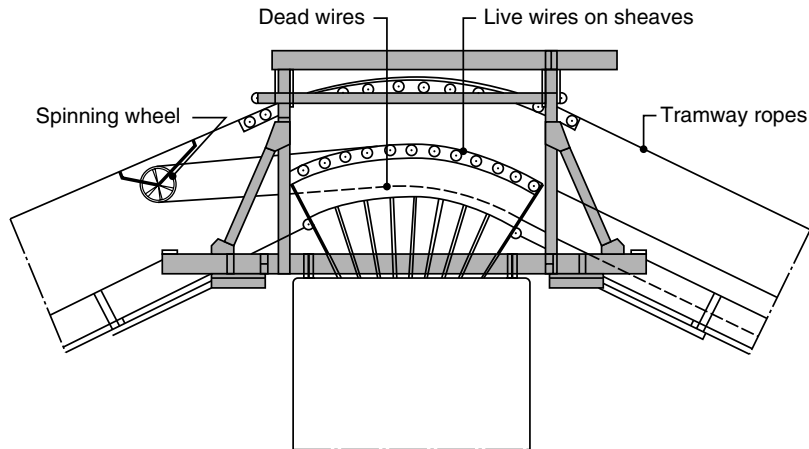
**Figure 7.26** Cross section of a catwalk with tilted spinning wheels in outgoing and return positions (low-tension method)

or more between the sag of the different strands it could be quite complicated to form a single cable after all strands were erected.

The more recent low-tension method has primarily been developed to reduce the work required during the cable erection and especially during sag adjustments. With the low-tension method the spinning wheel is tilted during its trip across the span so that the dead wire will fall gently down on the completed cable whereas the live wire will be laid down on a number of sheaves positioned on the catwalk on one side of the cable. On its way back the spinning wheel then picks up the former live wire and transfers it from the sheaves onto the main cable (Figure 7.26).

At the saddles the sheaves have to be positioned tighter together above and next to the cable groove to allow the live wires to be supported more continuously at the locations where there is a change of direction over a short length (Figure 7.27).

Throughout the build-up of the *in situ* strand the wires will rest on the completed part of the main cable and there will be no individual wire sag adjustment. However, after completion of each *in situ* strand the sag adjustment will have to be carried out, but now for 300–500 wires at a time. This sag adjustment is performed by pulling the strand at the pylon saddles as well as at the splay saddles, and finally making the necessary length adjustments at the strand shoe. The length adjustments will generally be larger with the low-tension method as strains corresponding to maybe 50% of the self weight



**Figure 7.27** Support of dead and live wires at pylon saddle during cable spinning

stress will have to be compensated for, whereas the stress in the *in situ* strand erected by the high-tension method will be very close to the final self weight stress due to the individual wire sag adjustment.

With the low-tension method the partial support of the wires by the catwalk during the spinning operation implies that the catwalk strands will be subjected to a varying dead load as wires are added to form the *in situ* strand. Then as the strand is sag adjusted, the catwalk will be relieved of the wire load until additional wires are added to form the subsequent strand.

During spinning of the first strands the wire load will result in substantial deflections of the catwalk strands and it is therefore necessary to compensate for these deflections by increasing the tension in special Sag Control Strands (SCS) positioned along the catwalk floor. So at pre-determined intervals the SCS will be tensioned to bring the catwalk back to its initial profile.

As the number of *in situ* strands is increased, the varying wire load during strand spinning becomes less and less significant as the completed strands will participate in carrying the wire dead load. Consequently, the compensation by SCS will only be required early in the spinning process and it is often decided to stop the sag control adjustments after erection of six to eight *in situ* strands.

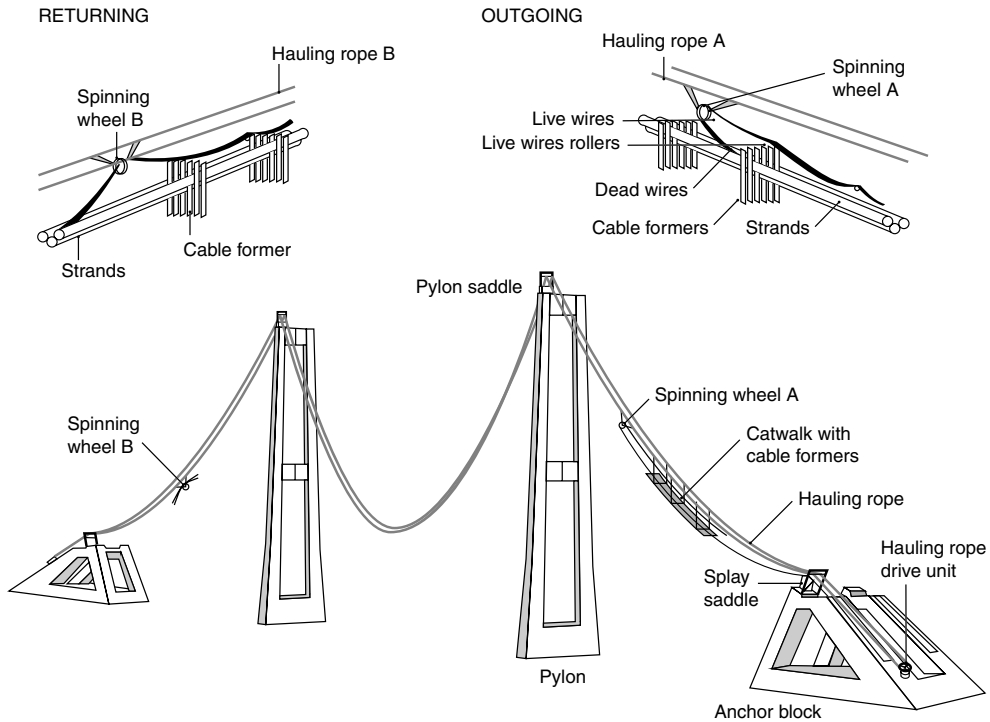
It should be emphasized that with the high-tension method it will not be necessary to use sag control strands as the wires will be practically self supporting due to the imposed stress close to that of a freely hanging wire.

The low-tension method was originally developed for erection of the main cables of the Shimotsui Seto Bridge in Japan performed in the mid 1980s. Later the method was further developed for the erection of the main cables for the Second Bosphorus Bridge.

For the cable erection of the Storebælt East Bridge the low-tension method was applied in a slightly modified form called the controlled-tension method (Figure 7.28) where the wires were initially stressed to approximately 80% of the self weight stress. This implied that the adjusting displacements at saddles and strand shoes could be reduced compared to the low-tension method, as only 20% of the self weight strains had to be compensated for - instead of 50%.

The PPWS method involves the erection of an entire prefabricated strand containing more than one hundred 5 mm wires in the full length of the main cable between anchor blocks.

The parallel-wire strand with sockets at both ends is delivered to the site on large reels weighing up to 85 tonnes (Akashi Kaikyo Bridge). After positioning of the reels in an unreeling machine (Figure 7.29) at one of the anchor blocks, the parallel-wire strand is pulled across to the other anchor block by means of a hauling rope. As the strand moves along, it is supported by rollers positioned on the catwalk besides the final position of the main cable (Figure 7.30). The first strand erected is used as a standard strand for the sag adjustment of all the following strands. Consequently, the adjustment of the first strand is being made with great care.



**Figure 7.28** Controlled-tension method for erection of the main cables of the Storebælt East Bridge

During the build-up of the cable, the strands are arranged in a hexagonal pattern, either vertical (with the apex at top and bottom) or horizontal (with the horizontal sides top and bottom), as shown in Figure 7.31. Both patterns have been used for very large main cables. For example, the horizontal arrangement was used in the George Washington Bridge, the Verrazano Narrows Bridge, and the 20th April Bridge, and the vertical arrangement in the Golden Gate Bridge, the Forth Road Bridge,



**Figure 7.29** Unreeling machine for the PPWS of the Akashi Kaikyo Bridge

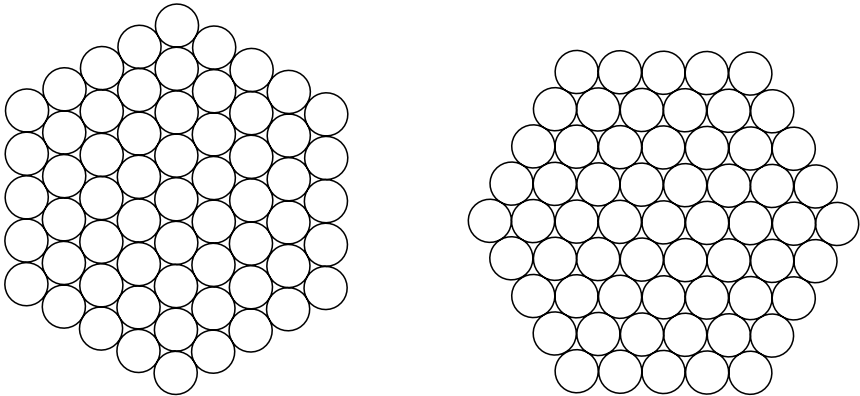


**Figure 7.30** PPWS in the process of being pulled across on the catwalk

and the Humber Bridge. The trend seems to be moving towards preferring the vertical arrangement, as this allows the installation of vertical spacers between each row of strands. With such spacers the correct position of the strands is achieved efficiently. On the free length of the cable the spacers (cable formers) are only used temporarily, whereas they might be permanent in the saddles to prevent the strands from interfering in these regions characterized by a considerable side pressure (Figure 7.32).

For these reasons the vertical hexagonal arrangement has been chosen for all the major Japanese suspension bridges using the PPWS method and it has also been preferred for the cables erected by the low-tension AS method.

For parallel-wire cables erected by either the AS or PPWS method, compaction of the cable is required when all the strands are in place. The compaction is made by a compacting machine squeezing the wires together by means of hydraulic jacks (Figure 7.33). During compaction the shape of the cable is changed from a hexagonal to an almost circular configuration. The efficiency of the compaction is generally measured by the percentage of voids in the cable. The



VERTICAL HEXAGONAL ARRANGEMENT

HORIZONTAL HEXAGONAL ARRANGEMENT

**Figure 7.31** Vertical hexagonal arrangement and horizontal hexagonal arrangement of strands in suspension bridge main cables



**Figure 7.32** Cable saddle with spacer plates

theoretical minimum percentage of voids in a perfectly compacted cable would be 9.3%, but practical experience shows that the percentage of voids after compaction will remain, within 17–23%. This is mainly due to the fact that true parallelism of all wires cannot be achieved.

As compaction proceeds the cables are tightly bound with temporary steel straps at a distance of typically 750 mm (Figure 7.34).

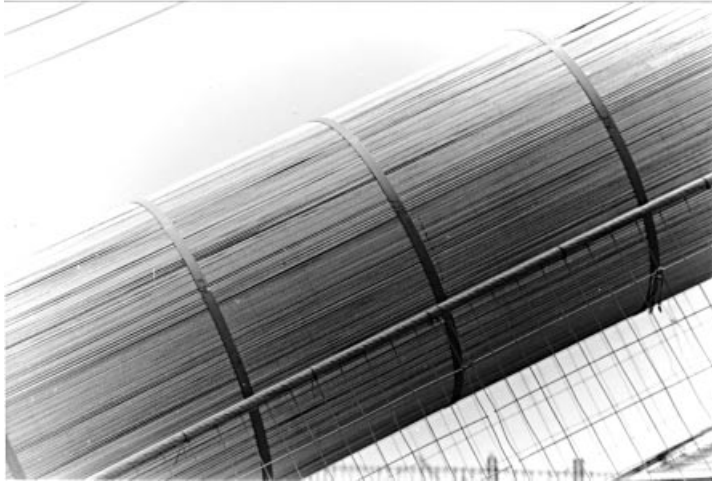
After the compaction has been completed, the cable clamps are erected and tightened together by means of high-tensile steel bolts. Due to the fact that the percentage of voids inside the compacted cable is approximately twice the theoretical minimum, mutual displacements between the wires might take place as time goes by and it is therefore necessary to re-tighten the clamping bolts at subsequent occasions. This re-tightening is also required during the erection of the deck, as the Poisson effect tends to reduce the cable diameter when axial tension is increased.

Subsequently, the cable is wrapped between the cable clamps. In all major bridges the wrapping has traditionally been done by a soft annealed galvanized wire, typically with a 3.5 mm diameter. More recently the round wrapping wire has been



**Figure 7.33** Compaction of the main cable in the Innoshima Bridge



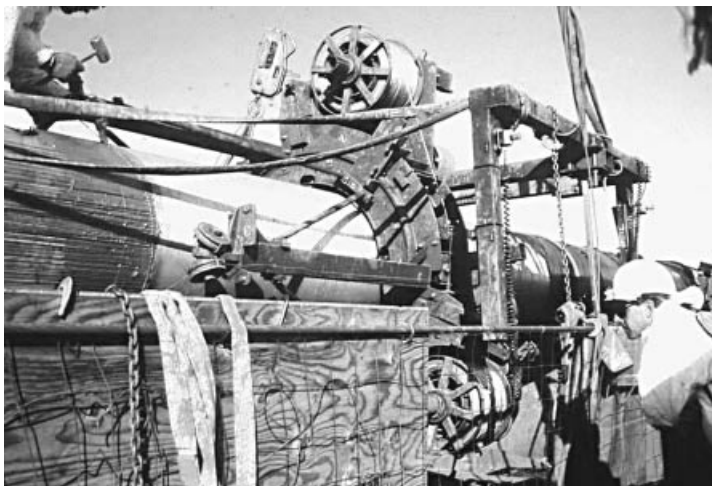


**Figure 7.34** Compacted cable with temporary steel straps

replaced by a special Z-shaped wire (see Figure 2.27). The wire is wrapped under a tension corresponding to a stress of approximately  $150\text{ N/mm}^2$  by means of a wrapping machine moving along the cable (Figure 7.35).

In the Tancarville Bridge the main cables were made of prefabricated helical strands (refer to Figure 2.17) pulled across the spans while supported by a guide rope. As no compaction or wrapping of the main cables was to be performed for the Tancarville Bridge, cable erection could take place without a catwalk. This constitutes the only example of a major suspension bridge where the main cables have been erected without a catwalk.

After installation of the cable clamps the cable system of the suspension bridge is completed by adding the hangers. In most cases the hangers are lifted vertically to their final positions after transportation to the site on a barge. However, in cases where the main cable is assembled from parallel-wire strands pulled across on the catwalk, the equipment used during installation of the main cable strands might also be used to transport the hangers along the catwalk and erect them from top to bottom.



**Figure 7.35** Cable wrapping (Storebælt East Bridge)

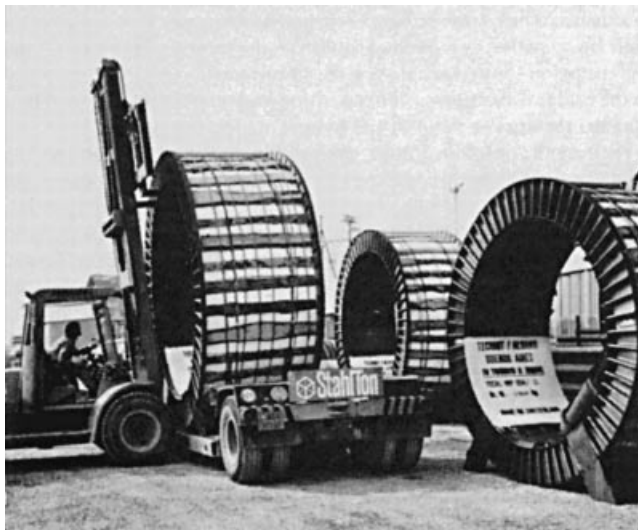
## 7.4 Erection of Stay Cables

Turning to the other main type of cable supported bridge – the cable stayed bridge – it is characteristic that here the cross section and the length of each cable are much smaller than for the suspension bridge main cables, and this naturally leads to different erection procedures.

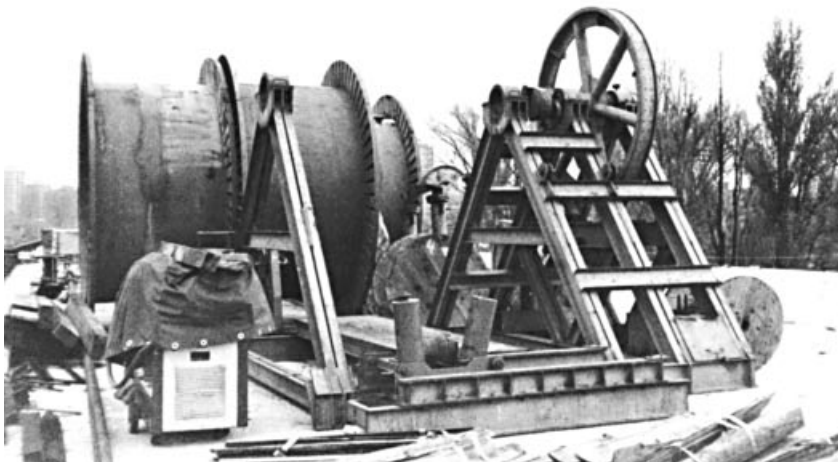
In modern cable stayed bridges the stays are either of the mono-strand type (or composed of a few mono-strands) or composed of seven-wire strands erected and tensioned individually (by the isotension method).

The mono-strand stays are fabricated in full size at the shop and reeled for transportation, as illustrated in Figure 7.36.

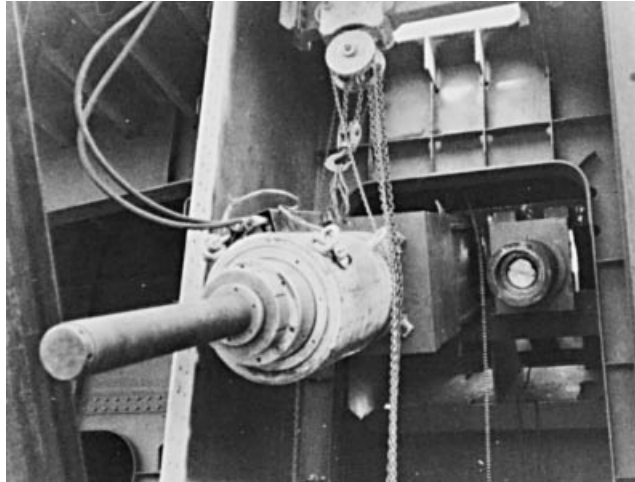
After arrival at the bridge site the cable reels are mounted in a reel stand (Figure 7.37) that might be situated on the bridge deck, at the abutments or below the bridge. From here the strand is directly unreeled as it is pulled by a hauling rope from the far end of the final strand (e.g. the pylon top). Alternately, the strand might initially be stretched on the bridge floor below its final position and then lifted to the anchor point at the pylon.



**Figure 7.36** Parallel-wire cable reel being loaded onto a truck



**Figure 7.37** Reel stand on the deck of the Danube River Bridge at Novi Sad (Serbia)



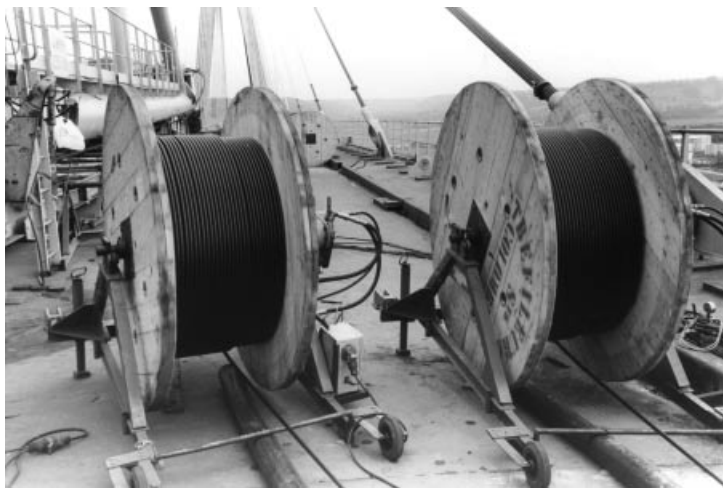
**Figure 7.38** Jack with a threaded rod for tensioning of a mono-strand cable

With both procedures the cable will be characterized by a large sag immediately after it is connected to the deck and the pylon due to the fact that the pulling equipment only allows a modest tensile force in the cable. The final tensioning by jacks will, therefore, require large movements between the socket and the adjacent structure.

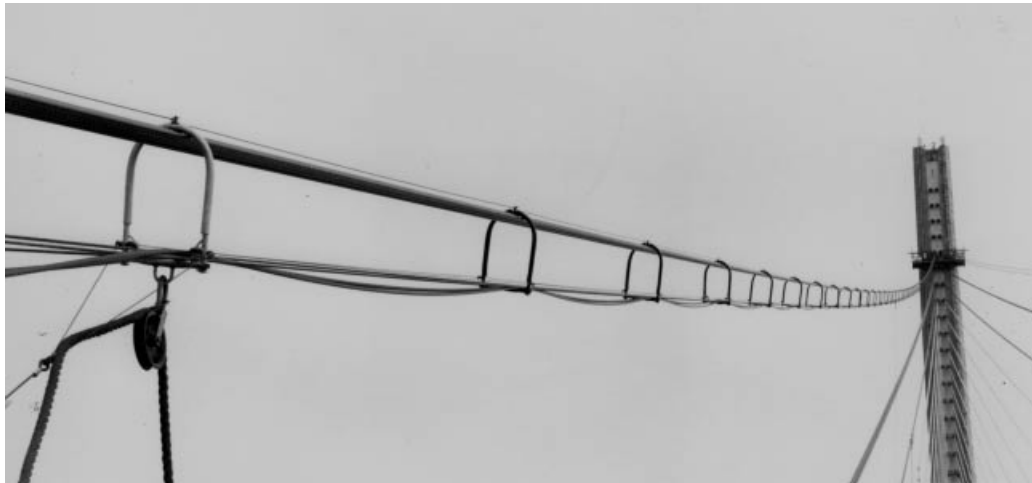
The final tension in a prefabricated mono-strand will be achieved by jacking the socket at one end. In the past the jacking operations have taken place both at the deck level and in the pylon. The decision on where to carry out this operation will often be based on an evaluation of the access facilities and the space available. In many bridges of moderate size the space available in the pylons is so limited that the jacking operations can only take place at the deck level.

To tension pre-fabricated strands a special jack containing a central threaded rod (as shown in Figure 7.38) is often used. With this equipment the jacking is made stepwise to allow for very large displacements, the only limiting factor being the length of the threaded rod.

For parallel-strand cables composed of seven-wire strands in HDPE sheaths the erection of the entire cable can be made by the so-called isotension method where each seven-wire strand is installed and tensioned individually. In this case the seven-wire strands are delivered on reels as seen in Figure 7.39. The first strand of the cable is pulled from the bridge deck to



**Figure 7.39** Seven-wire strands delivered on reels at the Normandy Bridge



**Figure 7.40** Seven-wire strand supported by stirrups during installation of the isotensioned stay cables in the Normandy Bridge

the pylon top using a simple winch and it is then cut to length, tensioned to a predetermined force and temporarily anchored. During construction of the Normandy Bridge the following strands were subsequently pulled along and supported by stirrups attached to the strands that had already been tensioned (Figure 7.40).

In a number of more recent bridges the first seven-wire strand is used to support the permanent protective PE-tube and the following seven-wire strands are then pulled through the PE-tube to give support instead of the stirrups (Figure 7.41).

As each strand reaches the top, it is tensioned using a small mono-strand jack with a load cell. The reading on this load cell is compared to a reading on a load cell at the anchor of the initially erected strand and when the two readings coincide, the tension operation is stopped. In this way it is ensured that all strands will be subjected to the same force at the end of each tension session.



**Figure 7.41** The permanent PE-tube erected to support seven-wire strands during erection (Øresund Bridge)

### 7.5 Deck Erection - Earth Anchored Suspension Bridges

A possible erection procedure for an earth anchored suspension bridge is outlined in Figure 7.42, where six stages are indicated:

- Stage 1 Construction of the main piers, pylons, and anchor blocks.
- Stage 2 Erection of the main cables.
- Stage 3 Start of erection of the deck from the centre of the main span. When the weight of the deck is added stepwise to the main cable, large displacements and changes of curvature occur, and the joints between the segments of the deck are therefore initially left open to avoid excessive bending of the girder sections.
- Stage 4 Erection of the deck in the side spans to reduce the horizontal displacements of the pylon tops.
- Stage 5 Erection of the closing pieces in the deck at the pylons.
- Stage 6 Closing of all deck joints. Actually, the closing of these joints will often start already during stages 4 and 5, as soon as adjoining segments become lined up.

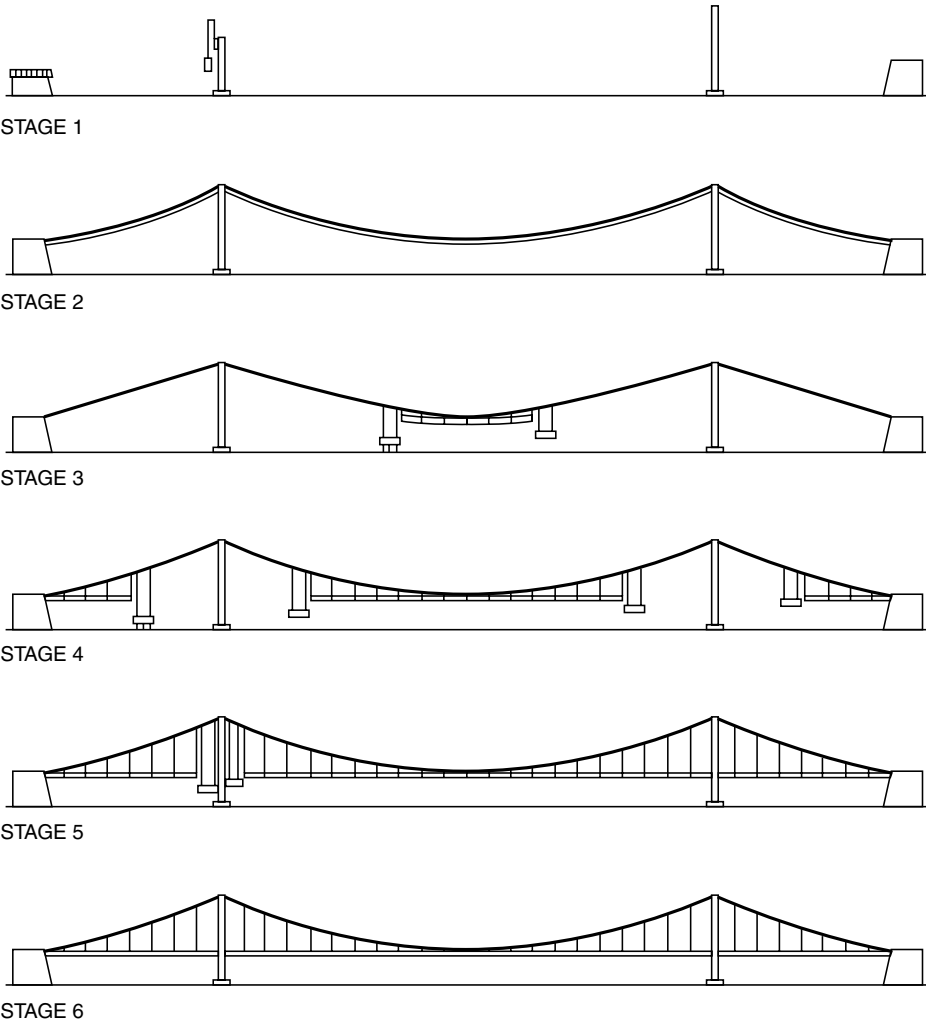


Figure 7.42 Earth anchored suspension bridge with the deck erected from midspan towards the pylons



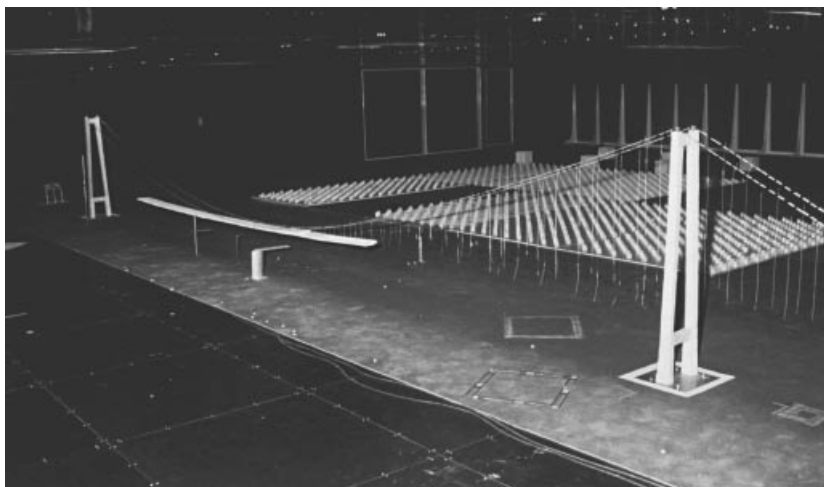
**Figure 7.43** The Tsing Ma Bridge during erection

The erection procedure outlined has the advantage that the deck segments adjacent to the pylons are erected when the main cable is reaching its final configuration. This makes it possible to reduce the secondary bending stresses in the main cable as the final tightening of the cable bands near the pylons can be postponed to a stage when only insignificant permanent angular changes of the main cable at the pylon top remain.

The erection procedure of Figure 7.42 has been widely used during the construction of many suspension bridges, among these for the Tsing Ma Bridge, as shown in Figure 7.43.

In cases where the deck is erected from midspan towards the pylons, the lifting of the deck segments has generally been performed symmetrically so that an asymmetry has only appeared for a short period between lifting a segment on one side and the subsequent adding of the symmetrical counterpart.

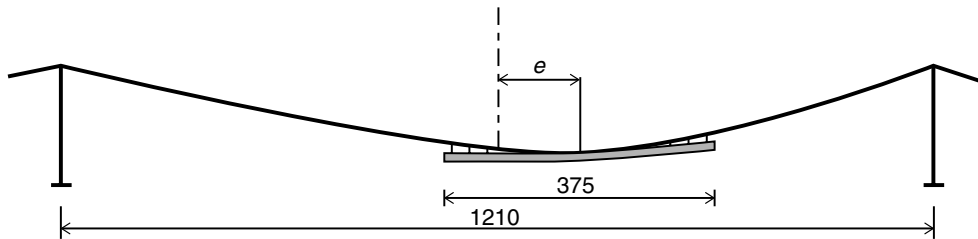
During the wind tunnel tests for the construction stages of the Høga Kusten Bridge (Figure 7.44), it was revealed that an asymmetric erection of the deck would lead to an increased stability in the critical phases when approximately one-third of the deck was in place. The tests indicated that an asymmetric suspension with an eccentricity of approximately one-tenth of the main span length (Figure 7.45) could lead to an increase of the flutter speed by almost 15%, as shown in Table 7.1.



**Figure 7.44** Model of the Høga Kusten Bridge in the large wind tunnel at the Danish Maritime Institute. The model is prepared for testing a construction phase where the girder is partially erected and asymmetrically suspended

**Table 7.1** Relation between the eccentricity of the suspension and the critical flutter speed as determined during the wind tunnel tests for the construction stages of the Høga Kusten Bridge

| Eccentricity $e$ | Flutter speed |
|------------------|---------------|
| 0                | 57 m/s        |
| 40 m             | 58 m/s        |
| 80 m             | 64 m/s        |
| 120 m            | 65 m/s        |



**Figure 7.45** Partially erected girder with length 375 m suspended asymmetrically in the 1210 m main span of the Høga Kusten Bridge

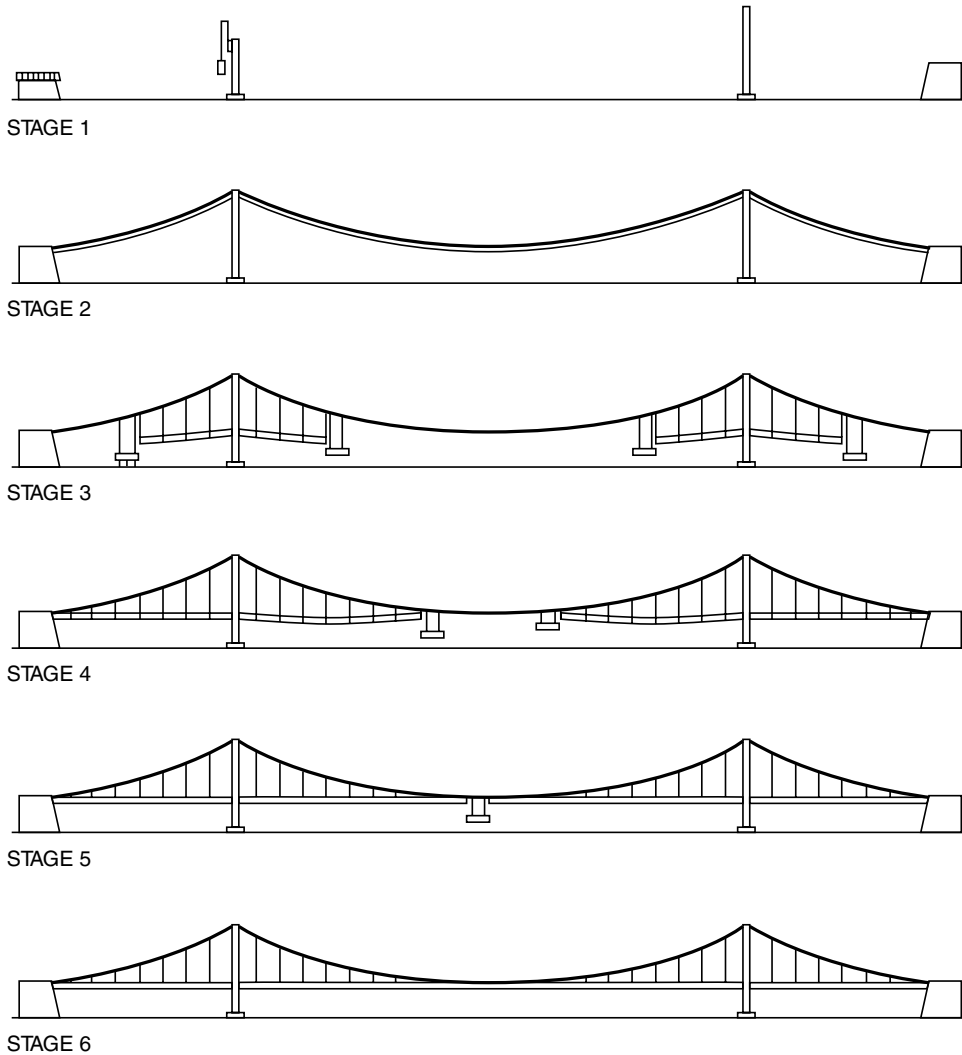
The results summarized in Table 7.1 are based on the assumption that the deck segments are joined in such a way that they are free to rotate in the vertical plane but are excluded from twisting mutually (see Figure 7.61).

In relation to the results obtained during the wind tunnel tests for the Høga Kusten Bridge, it should be emphasized that the increased flutter speed can be achieved at practically no extra cost as the number of operations during erection will remain unaltered if lifting is performed asymmetrically instead of symmetrically.

For the Storebælt East Bridge it was initially anticipated that the erection of the deck should take place by alternating lifts in the main span and the side spans. However, during his detailed planning of the erection procedure the contractor found out that it would be possible to erect the entire main span deck prior to lifting deck segments in the side spans (Figure 7.46).



**Figure 7.46** The Storebælt East Bridge after erection of the main span deck



**Figure 7.47** Earth anchored suspension bridge with the deck erected from the pylons towards midspan

The advantage of doing so was that it would only be necessary to move the four gantry cranes operating on the main cables once from the main span to the side spans.

As described earlier, the East Bridge pylons were pulled 1.2 m towards the side spans by temporary tie-back cables (see Figure 7.12) before erection of the main cables. As the cable spinning progressed, the tie-back cables were gradually released and at the end of the main cable erection the pylons had returned to the vertical position. Then as the main span deck segments were lifted into position, the pylon tops deflected 1.2 m towards midspan finally to return to the vertical position after erection of the decks in the side spans.

Another erection procedure to be found within suspension bridges is illustrated in Figure 7.47. As seen here, the sequence of adding the deck segments is the opposite of that shown in Figure 7.42.

The erection procedure of Figure 7.47 offers the advantage that the erection crew can easily reach the bridge deck from the pylon piers, and also easily move from the main span to the side span. With the procedure of Figure 7.42, the erection crew have to use the catwalk to get to the partially erected deck in the main span (during stages 3 and 4).





**Figure 7.48** *The Akashi Kaikyo Bridge during erection*

It should also be mentioned that working out from the pylons will imply that the torsional stiffness of the deck can be activated right from the start of erection if the necessary connection to the pylon is established initially. This is in contrast to the erection procedure of Figure 7.42 where the partially erected deck is stabilized against twisting only by the ‘gravity’ action of the main cables.

The procedure of Figure 7.47 has been used during the erection of many major suspension bridges and among these the Akashi Kaikyo Bridge, as shown in Figure 7.48.

It will also be possible to combine both of the procedures shown in Figure 7.42 and 7.47 as it might prove advantageous to initially erect a few deck segments at midspan to tighten up the main cables before proceeding with the erection by moving out from the pylons.

In some cases the erection of stiffening trusses in suspension bridges has been done by a traditional truss erection where each chord and diagonal member is lifted into place by a crane based on the completed part of the bridge deck. This procedure was used for the Firth of Forth Road Bridge, as illustrated in Figure 7.49, where the derrick cranes at the tips of the stiffening trusses are clearly seen.



**Figure 7.49** *Firth of Forth Road Bridge during erection. Note the derrick cranes at the tips of the stiffening truss*



**Figure 7.50** Temporary work site at the pylon pier (Akashi Kaikyo Bridge)

The same procedure, although with larger erection units, was used during construction in the 1980s and 1990s for major Japanese suspension bridges as these bridges were built across straits that had such an intensity of navigation that no direct lifting of large deck segments from the water surface could be allowed. Instead pre-fabricated segments of the vertical trusses were transported to temporary work sites at the pylon piers (Figure 7.50) and lifted to the bridge deck outside the navigation channel. For the Akashi Kaikyo Bridge the different elements of the stiffening truss were fabricated in large elements, one comprising a vertical truss segment with a length corresponding to the distance between hangers, and another the transverse sway bracing between the two vertical trusses.

After arrival at the deck (Figure 7.51) the truss elements were moved to the tip of the erected truss by a multi-wheel trailer with a supporting frame (Figure 7.52). From here a derrick crane picked up the truss elements and swung them into position (Figure 7.53).



**Figure 7.51** Prefabricated truss elements for the sway bracings and the vertical main trusses of the Akashi Kaikyo Bridge after being lifted onto the bridge deck at the pylons



**Figure 7.52** Multi-wheel trailer for transport of prefabricated truss elements along the deck of the Akashi Kaikyo Bridge

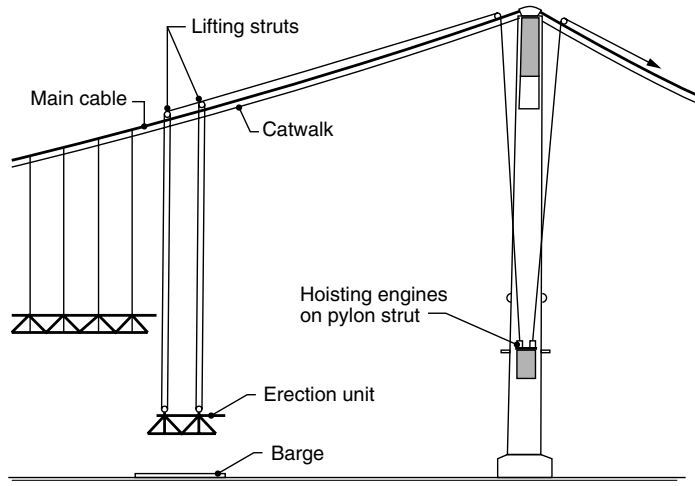
Following the erection of the vertical main trusses and their intermediate sway bracings, the members of the upper and lower lateral bracings had to be added and finally the orthotropic steel floor was added on top of the new part of the truss.

As will be understood, the erection procedure used in the major Japanese suspension bridges requires a considerable amount of assembly work to be performed on site. Consequently, this procedure will only be chosen if a vertical lift of large deck segments is excluded – as it was the case for the Akashi Kaikyo Bridge and other major Japanese suspension bridges.

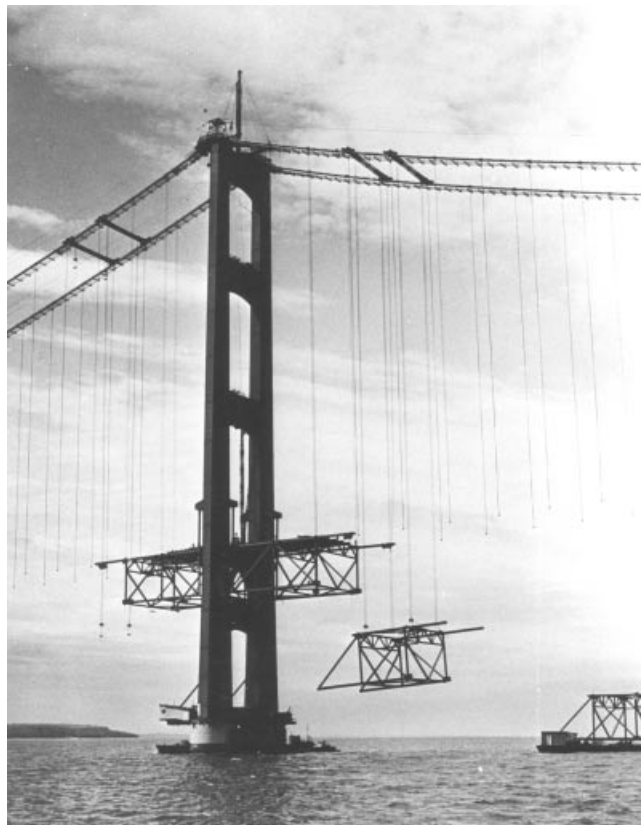
The full benefit of the earth anchored cable system with its large load-carrying capacity throughout the construction phase will only be achieved if very large erection units can be hoisted vertically into position by lifting struts or gantry cranes positioned on the main cable, as illustrated in Figures 7.54 and 7.55. The lifting struts were provided with wheels to



**Figure 7.53** Derrick crane at the tip of the stiffening truss of the Akashi Kaikyo Bridge. The crane is about to pick up a sway bracing element and move it into position between the previously erected main truss extensions



**Figure 7.54** Position of hauling engines during lift of truss segments (Verrazano Narrows Bridge)



**Figure 7.55** Lifting of truss unit during erection of the Mackinac Bridge



**Figure 7.56** Gantry cranes on the Storebælt Bridge main cables

allow change of position along the main cable. However, during the lifting operations the struts were lowered onto the main cable and locked to avoid longitudinal displacements caused by the pull of the lifting ropes.

The hoisting engines were traditionally positioned at the pylon piers, as shown in Figure 7.54, and this allowed the application of very powerful engines so that a large lifting capacity could be achieved. It was possible to lift full width erection units with a weight of up to 500 tonnes and a length up to 50 m. The disadvantage of hoisting engines positioned at the pylon piers was that the hoisting ropes became very long and therefore were characterized by an unfavourable elastic flexibility. This drawback became more and more pronounced as span lengths increased.

For the erection of the Tsing Ma Bridge, where each lift comprised a 36 m long truss segment with a weight of 1000 tonnes, it was therefore decided to use gantry cranes with strand-jacking equipment instead of lifting struts. This eliminated the long elastic hoisting ropes but at the same time an additional weight had to be taken into account as the gantry cranes were considerably heavier than the lifting struts.

The idea of doubling the length of the truss segments to 72 m to reduce the number of site joints had been considered, and it was found that a lift of 2000 tonnes would actually be possible with the strand-jacking method. However, lifting segments to be attached to three sets of hanger cables will introduce many additional problems related to cable distortions and adjustments of hanger forces as the erection proceeds, so such a step is probably not advisable, and it was also finally abandoned in the case of the Tsing Ma Bridge.

Self-propelled gantry cranes were also used to lift the 48 m long deck segments of the Storebælt Bridge (Figure 7.56).

In modern suspension bridges with a streamlined box girder deck, the erection units will always have the full width and a length of 20–50 m. Figure 7.57 shows a 30 m wide and 12 m long segment for the Lillebælt Bridge in the fabrication yard. At the work site area close to the bridge location two of these segments were joined to a 24 m long erection unit weighing 280 tonnes.

The erection units are generally transported to the bridge on barges. However, during the construction of the Severn Bridge the pre-fabricated box segments were fabricated with watertight bulkheads, so that the unit could float by itself and it was therefore possible to avoid transport by barges (Figure 7.58). Although this seemed to be a quite ingenious solution, it did give some problems during the subsequent field welding of the box girder joints due to impurities in the grooves. Therefore, in suspension bridges with streamlined box girders following the Severn Bridge, transportation on barges was again preferred.

At the Severn Bridge erection, only a single lifting strut was used, as shown in Figure 7.59. This gave a simple but somewhat unstable support of the erection unit so that the primary lifting ropes had to be supplemented by inclined ropes to achieve aerodynamic stability and allow adjustments of the longitudinal slope [67.2]. With two lifting struts the erection



**Figure 7.57** Fabrication unit for the deck of the Lillebælt Bridge

unit will be supported by four hoisting ropes which introduces a static indeterminateness. However, by a special arrangement of the lifting ropes, it is possible to ensure an equal pull in all ropes.

As an example Figure 7.60 shows the arrangement applied during the deck erection of the Lillebælt Bridge [70.1]. Here the lifting strut had a central clamp to lock the lifting rope to the strut. With the clamp left open, an equal force in the lifting ropes on both sides was ensured, but with a locked clamp the forces in the lifting ropes could differ. During the lifting operation one of the two struts had its clamp left open and the other the clamp locked. After completion of the lifting operation, the permanent hangers were connected to the unit, and the lifting struts moved to a new position.

To ensure that the deck is moment-free in the dead load condition, the segments are generally suspended from the main cable without closing the joints as long as the erection proceeds. However, it might be necessary to make temporary joints

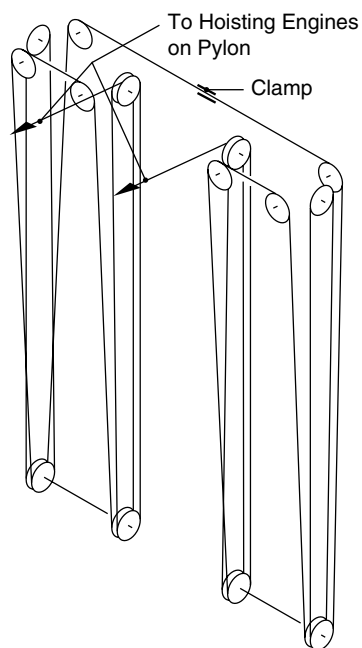


**Figure 7.58** Self-floating erection unit for the deck of the Severn Bridge

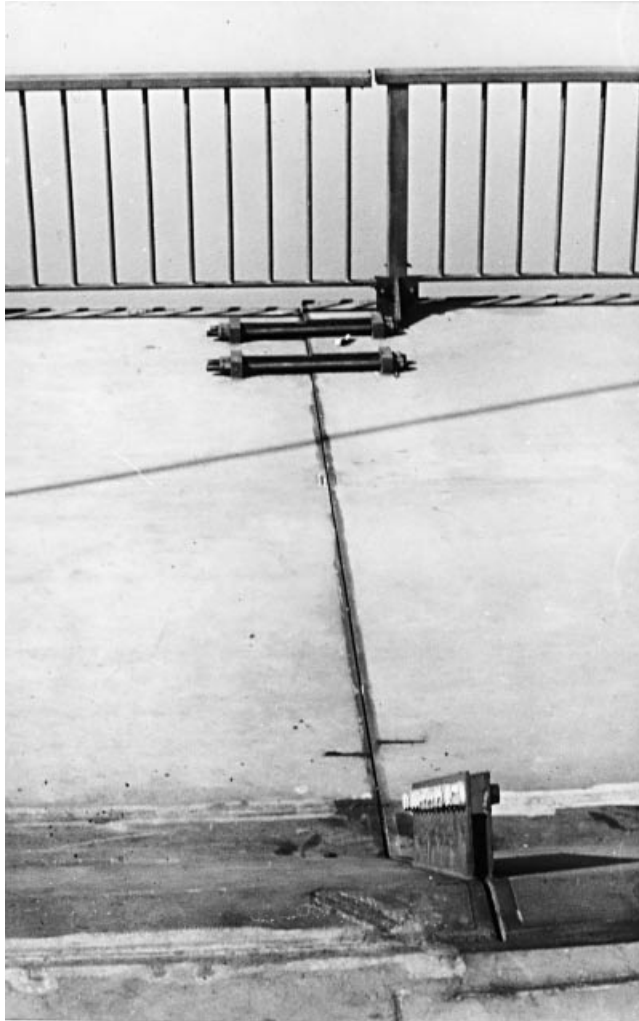


**Figure 7.59** Erection unit of the Severn Bridge box girder lifted by a single lifting strut

between the units to achieve aerodynamic stability of the partially erected deck. This was the case e.g. for the Severn Bridge where temporary joints, as shown in Figure 7.61, were used to connect the box girder top flange. As the joints were made only in the top flange and the deck had a concave curvature during erection, no flexural stiffness in the vertical direction was present so a moment-free dead load condition was achieved.



**Figure 7.60** Schematic drawing of the lifting rope arrangement for the Lillebælt Bridge



**Figure 7.61** Temporary erection joint in the box girder top flange during erection of the Severn Bridge

The application of lifting struts or strand-jacking gantries is restricted to bridges with earth anchored cable systems, but equally large, or even larger, lifting capacities can be achieved by the use of floating cranes and they can be used both in earth anchored and self anchored systems.

A most efficient use of a floating crane was seen at the deck erection of the Askøy Bridge in Norway (Figure 7.62). Here the erection of the 850 m long main span was accomplished in just five working days! To achieve this it was necessary to have the floating crane moored at the location of the bridge and to transport a number of the box girder segments to the site on a large barge. It was also necessary to design a special coupling device between the deck units so that the crane could be removed immediately after completion of the attachment to the neighbouring deck segment. In the Askøy Bridge the length of the erection unit was chosen to be 36 m, corresponding to three times the distance between the hangers. Consequently, each box segment weighing 180 tonnes had to be attached to three sets of hangers.





Figure 7.62 Erection of deck segments in the Askøy Bridge by a floating crane

### 7.6 Deck Erection - Self Anchored Cable Stayed Bridges

In bridges with self anchored cable systems, the load-carrying capacity of the single cable depends on the transfer of the horizontal component of the cable force through the deck. Therefore, a given cable cannot be installed before the adjoining part of the deck has been erected. Then a straightforward solution is to erect the entire deck on temporary supports before adding the cables, as illustrated in Figure 7.63 for a cable stayed bridge with a self anchored fan system.

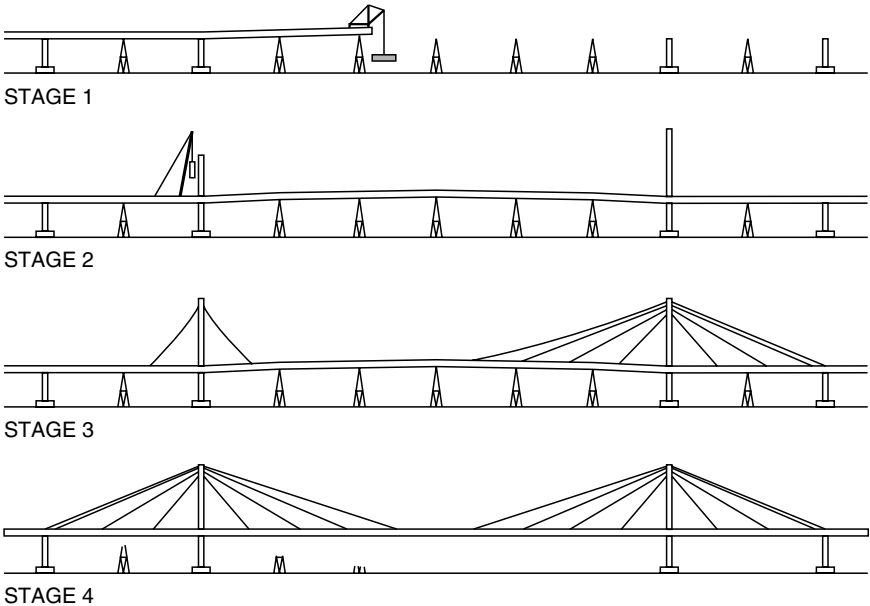


Figure 7.63 Self anchored cable stayed bridge erected on temporary supports

In the four stages indicated, the following main operations are performed:

- Stage 1* Erection of the deck on the permanent piers and the temporary supports. In this stage the erection is actually a normal girder erection and any of the procedures used for the construction of girder bridges can consequently be applied.
- Stage 2* Erection of the pylons from the deck of the completed deck.
- Stage 3* Installation of the stay cables. In this stage the cables only need to be tensioned moderately as the final cable tension will be induced in the following stage.
- Stage 4* After installation of all stay cables, the temporary supports are removed and the load transferred to the cable system. During this process the deck will deflect downwards and it is therefore necessary to initially erect the deck in an elevated position to arrive at the desired final geometry when the total dead load of the deck has been transferred to the stay cables.

With the deck erected on temporary supports and subsequently lowered, a permanent bending will be induced in the deck sections. However, with slender decks the bending moments might well be within acceptable limits, but with a stiffer deck the procedure might have to be modified to eliminate this permanent bending. In that case the deck must initially be erected with its final elevation on the temporary supports and then be jacked up before the stay cables are attached and partly stressed.

The erection procedure illustrated in Figure 7.63 offers the advantage that the deck can be erected continuously from one end to the other and thereby allow transportation of men, equipment, and material on the completed part of the deck. Also, the procedure leads to an efficient control of the geometry and the cable tension.

The disadvantage of the procedure is related to the temporary supports that are required. In many cases a clearance profile will have to be respected also during the construction period so that temporary supports cannot be allowed. Even if the clearance requirements are not prohibitive, the cost of erecting the temporary supports, e.g. on large water depths in the main span, might be of such a magnitude that the procedure will not be feasible.

The erection procedure based on temporary support of the deck prior to erection of the cable system is indispensable in the case of a self anchored suspension bridge, as the main cable tension here is transferred through the deck from one end to the other. For the self anchored suspension bridge the requirement of temporary support has had the consequence that this type of bridge has been abandoned in all cases where construction cost matters.

For a cable stayed bridge the erection procedure of Figure 7.63 was used during the construction of the Rokko Bridge in Japan, as shown in Figure 7.64. Here the large flexural stiffness of the two-level truss made it possible to apply only two temporary supports in the main span, and at the same time very large units could be lifted into place by floating cranes. Furthermore, the fact that the bridge was built in the port of Kobe at a reclamation site (without any ship traffic during the construction period) facilitated the use of temporary supports.



**Figure 7.64** *The Rokko Bridge under construction*



**Figure 7.65** Erection of the stiffening truss of the Øresund Bridge by application of temporary piers in the main span

For the 490 m long main span of the Øresund Bridge the principle of deck erection prior to stay cable installation could be used due to the moderate water depths (< 8 m) and the fact that the navigation channel was to be relocated after completion of the main span erection. Therefore, during erection of the cable stayed bridge temporary piers could be positioned freely in the future navigation span.

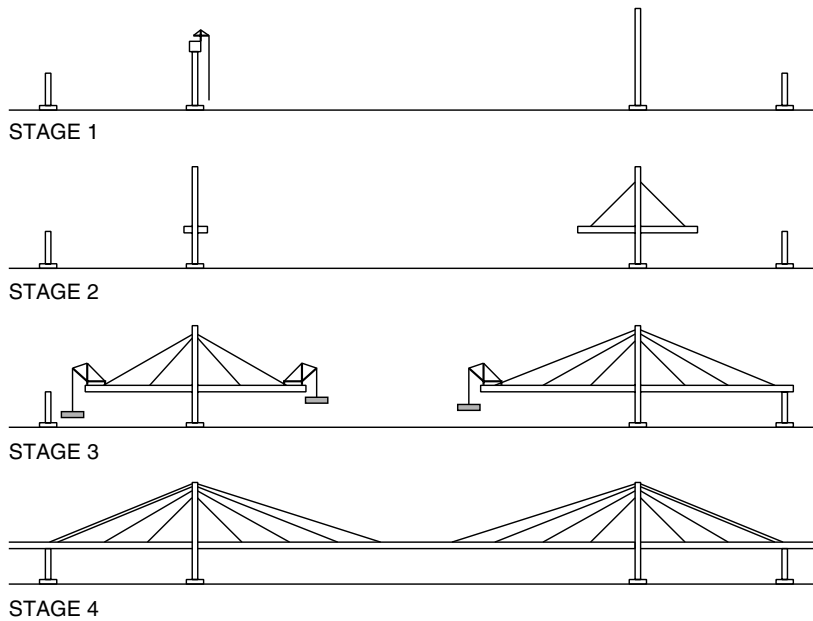
The first truss element with a length of 140 m was moved into place between the pylon legs and lowered onto the pylon cross beam and a temporary pier in the main span in such a way that a 20 m cantilever extended into the side span. Then a 140 m long truss element was erected in the first side span to reach from the 20 m cantilever to the nearest permanent side span pier before erection of the following 141 m truss in the second side span.

After erection of the truss in both side spans and in the temporarily supported 120 m span in the main span, the lower stay cables were added prior to erecting a 125 m long truss element reaching from the outer temporary pier to a central temporary pier (Figure 7.65). Then the remaining stay cables of the relevant bridge half were installed and the outer temporary pier was dismantled and moved to the other bridge half where the procedure was repeated. With the chosen procedure the entire main bridge with a length of 1092 m could be erected by lifting only eight truss elements into place and by applying only two temporary piers. The composite truss elements with their upper concrete slab had a weight of up to 6000 tonnes.

Temporary supports can be completely avoided if a self anchored bridge is erected by the free-cantilever method, as illustrated in Figure 7.66. Here the procedure involves the following stages:

- Stage 1* The pylons (and the deck units above the main piers) are erected and fixed to the piers.
- Stage 2* A balanced free cantilever is initiated using derrick cranes operating on the deck to lift deck segments transported to the site on barges.
- Stage 3* As the cantilevers grow, the stay cables are installed and tensioned initially to relieve the bending moments in the deck. Often the cantilever process is completed for one bridge half, before moving the cranes to the other half.
- Stage 4* The deck is joined at midspan and additional loading from wearing surface, railings, etc., is applied.

With this procedure it is essential to have a very efficient fixity of the superstructure to the pylon piers throughout the construction period, as the entire stability depends on this fixity until the end pier is reached. Also, the lateral flexural stiffness of the deck must be sufficient to ensure the stability of the cantilever arm that will eventually reach a length corresponding to half the main span length. Thus, the procedure is especially advantageous in bridges with a reasonably large width-to-span ratio of the deck.



**Figure 7.66** Self anchored cable stayed bridge erected by double-sided free cantilevering from the pylons

The erection procedure of Figure 7.66 will be most efficient if the distance between the cable anchor points is chosen so that the deck can be cantilevered from one cable anchor point to the next without requiring a temporary support (e.g. by temporary cables). This condition is often fulfilled in bridges with multi-cable systems.

It should be emphasized that to cantilever the deck of a self anchored cable stayed bridge it is essential to close all deck joints as soon as the deck segments are in place because an axial force is transferred during the subsequent tensioning of the stay cables.

The balanced free-cantilever method was used e.g. for the erection of the Alex Fraser Bridge at Vancouver, as illustrated by Figure 7.67. Here the concrete pylons were moment rigidly fixed to the main piers, and both the



**Figure 7.67** The Alex Fraser Bridge during erection



Figure 7.68 Model of the Sutong Bridge during free-cantilever erection of the deck

flexural and torsional stiffness of the pylons ensured stability in the construction phase so no temporary supports were required.

The double free-cantilever method was also applied for the Sutong Bridge for a length of 300 m on either side of the pylon until the nearest side span pier was reached, as seen in the model photo in Figure 7.68. Then the main span cantilever arm had to be further increased by 244 m to reach the main span centre, but, during the final cantilevering, stability was ensured by the support of the deck at both the pylon and the nearest side span piers. With its deck width of 41 m, the length-to-width ratio of the longest cantilever arm from the pylon to midspan was  $544/41 = 13.3$ .

In a number of cases the two erection procedures of Figures 7.63 and 7.66 have been combined so that the side spans are erected on temporary supports and the main span by a free cantilever, as shown in Figure 7.69.

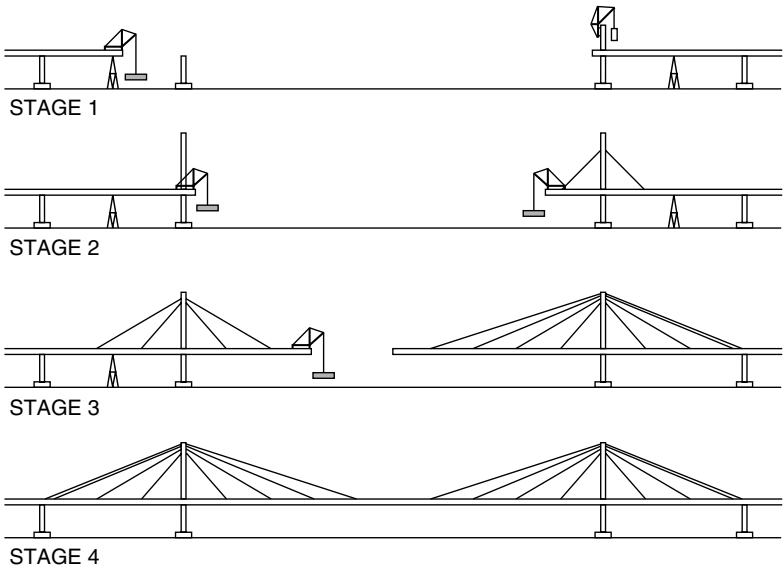


Figure 7.69 Self anchored cable stayed bridge erected by one-sided free cantilevering of the main span



**Figure 7.70** Initial erection of the deck on temporary supports at the pylon location (Photo credit: Arup)

In the four stages indicated, the following operations have to be performed:

- Stage 1* Erection of the deck in the side spans using temporary supports, followed by the erection of the pylons when the main piers are reached.
- Stage 2* One-sided free cantilever of the main span deck with installation of both the main span and the corresponding side span stay cable as the relevant anchor points in the main span are reached.
- Stage 3* After completion of one bridge half, the cantilever of the other half takes place.
- Stage 4* Closing of the bridge at the main span centre.

With this erection procedure the application of temporary supports is limited to the side spans where clearance requirements and water depths seldom will exclude such supports. At the same time the cantilever into the main span can start from a very stable position with the side span deck supported on both the main pier and the end pier. A temporary moment-rigid fixation to the main pier is therefore not required.

Figure 7.70 shows the initial erection of the deck in a bridge with a composite ladder deck (River Suir Bridge). Note that the plate girders are lifted into place by ordinary mobile cranes onto temporary supports. Special cranes were also not required during the subsequent free cantilever into the main span, as seen in Figure 7.71. Note that the relatively light longitudinal plate girders are cantilevered to reach the following anchor point before the cross beams are added. Then the new stay cables are installed and tensioned prior to adding the heavy concrete floor.

The principle of a one-sided cantilever in the main span will be especially advantageous if the side spans can be erected without requiring temporary supports in the side spans, e.g. in a cable stayed bridge with permanent intermediate supports in the side spans, as shown in Figure 7.72.

During erection of the two-span Severins Bridge (one of the very early cable stayed bridges), the main span was erected as a one-sided free-cantilever from the pylon to a temporary pier that could be allowed in the navigation channel opposite the pylon. Figure 7.73 shows the situation when all stay cables were erected and the deck close to completion. In this phase the deck was raised several metres by the temporary pier at the extremity of the cantilever arm. Therefore, a considerable part of the final cable tensioning took place during lowering of the deck prior to removal of the temporary pier.



Figure 7.71 Free cantilever of a ladder deck in a cable stayed bridge (Photo credit: Arup)

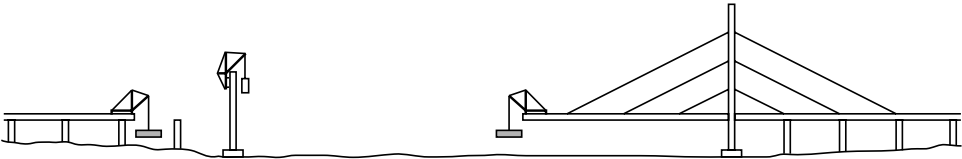
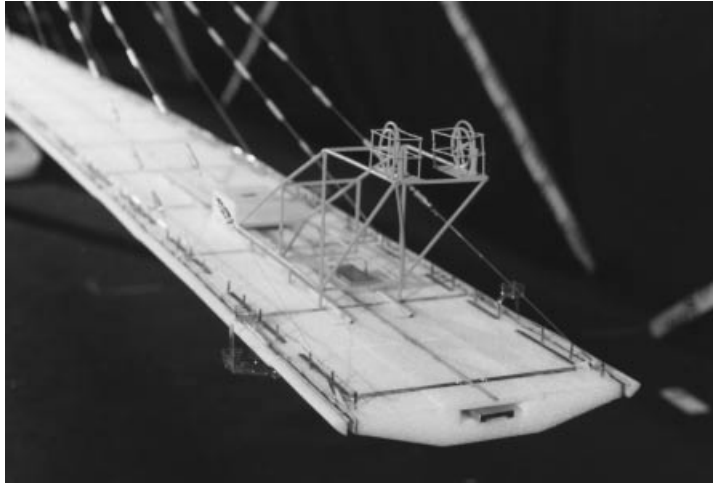


Figure 7.72 Erection procedure for a cable stayed bridge with a harp system and permanent intermediate supports in the side spans



Figure 7.73 The Severins Bridge under construction in 1959



**Figure 7.74** Wind tunnel model of the Normandy Bridge in the construction phase

In the case of the Normandy Bridge, the free cantilever had to be extended for a length of 428 m (= half the main span length) out from the pylons to midspan – corresponding to a cantilever-to-width ratio of approximately 20. With this, the longest cantilever at the time, a number of measures had to be taken to ensure the aerodynamic stability in the temporary stages.

First of all, the erection stages had to be carefully investigated both analytically and experimentally, e.g. by full model tests of the erection phase where the cantilever has reached midspan (Figure 7.74). Note that in this test the erection equipment, such as the purpose built crane, had to be carefully modelled.

The investigations revealed that the deck could be prone to lateral oscillations and it was therefore decided to install a large tuned-mass damper on the bridge deck to suppress these oscillations (Figure 7.75).

The principle of a one-sided free-cantilever in the central part of the main span was also applied during erection of the Farø Bridge in Denmark. However, in this bridge there were no intermediate supports in the side span so a temporary support 40 m from the pylon axis had to be established by fixing a large latticed bracket to the pylon. With this in place it was possible to erect a deck length of 80 m (corresponding to the span length used in all box girder approach spans) between the



**Figure 7.75** Tuned mass dampers on the deck of the Normandy Bridge





**Figure 7.76** 80 m long box girder element about to be pulled through the pylon during erection of the Farø Bridge

anchor pier and the tip of the bracket. Another 80 m segment was then pulled through the pylon to make up the remaining 40 m of the side span as well as a 40 m cantilever into the main span (Figure 7.76).

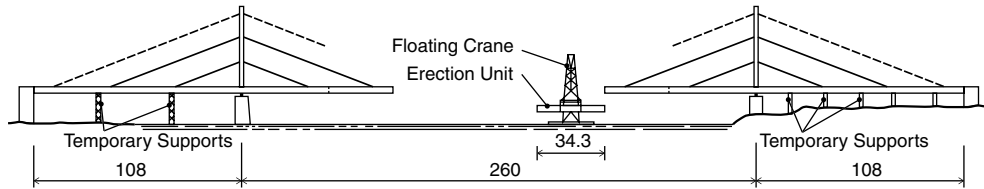
By this procedure it was achieved that the remaining  $290 - (2 \times 40) = 210$  m of the main span could be erected by a double free cantilever starting out from a very stable structural system.

A special problem arose during the erection of the narrow deck of the Karnali River Bridge in Nepal. In this two-span bridge the deck had to be cantilevered from one side only, and as the main span was 325 m long and the deck 10 m wide, the cantilever-to-width ratio was 32.5. At the same time the application of a stiffening truss implied that the drag forces were quite large. Therefore, it was necessary not only to stabilize by installation of a temporary tuned-mass damper (as in the case of the Normandy Bridge) but also to support the cantilever by two sets of horizontal guy cables attached to the deck at distances of 150 m and 239 m from the pylon and anchored on the opposite bank of the river [94.11].

The largest erection units are found within cable stayed bridges with the deck erected on temporary piers, as illustrated by the erection of the side span box girder of the Incheon Bridge (Figure 7.77).



**Figure 7.77** Erection of a truss element by two floating cranes during construction of the Incheon Bridge (courtesy of H. Tanaka, Samsung C&T)



**Figure 7.78** Erection of large deck segments with a floating crane (Theodor Heuss Bridge)

Floating cranes were also used during erection of one of the very first modern cable stayed bridges, the Theodor Heuss Bridge in Düsseldorf, and here the free cantilever method was used in the main span, as indicated in Figure 7.78. Each erection unit had a length corresponding to the distance between the cable anchor points in the deck. The weight of the erection units varied between 280 tonnes and 360 tonnes.

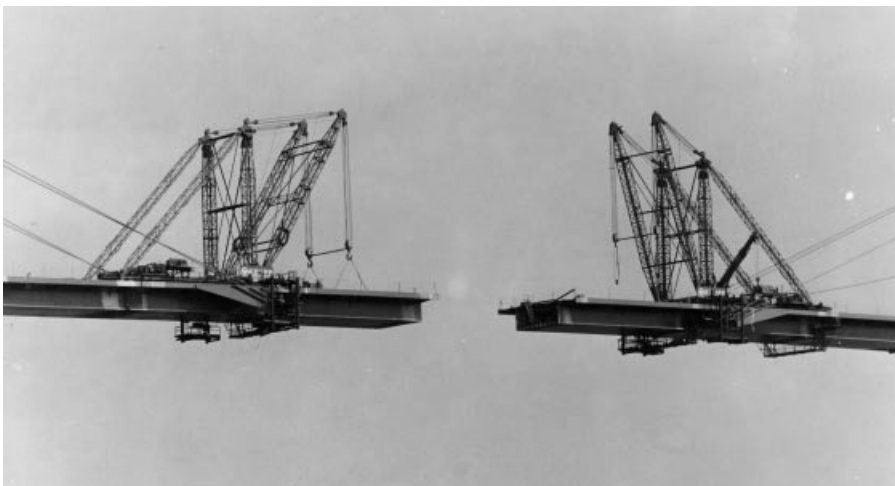
However, during the Theodor Heuss Bridge erection, a serious accident, leading to the destruction of an entire erection unit, occurred and this event inevitably caused repercussions for the procedure involving erection of large segments by floating cranes. Thus, in the following years it was generally preferred to use an erection procedure based on smaller units lifted by derrick cranes positioned at the tip of the already erected part of the deck (Figure 7.79).

Generally, the lifting capacity of standard derrick cranes is smaller than the capacity of lifting struts or floating cranes. Thus, the maximum lifting capacity of derrick cranes used for the erection of cable stayed bridges will hardly exceed 200 tonnes. It is therefore necessary to use smaller erection units and accept a larger number of erection joints.

In a number of cases special cranes have been constructed for the erection of decks in cable stayed bridges, e.g. for Farø Bridge, Normandy Bridge and Stonecutters Bridge (Figure 7.80).

For bridges with a concrete deck, special problems arise as the very favourable effect on the moment capacity due to the compressive force from the horizontal components of the stay cable pulls is non-existent at the tip of the deck during erection. At the same time the heavier concrete deck segments induce a larger cantilever moment than found in decks of steel.

During the Pasco-Kennebec Bridge erection the problems were overcome by application of a special erection traveller with its own temporary erection cable leading to the pylon top. By tensioning this erection cable simultaneously with the lifting of the heavy pre-cast segments weighing 270 tonnes, it was possible to release the cantilever moment in the previously erected segments to such an extent that overstressing was avoided. Furthermore, the pull of the erection



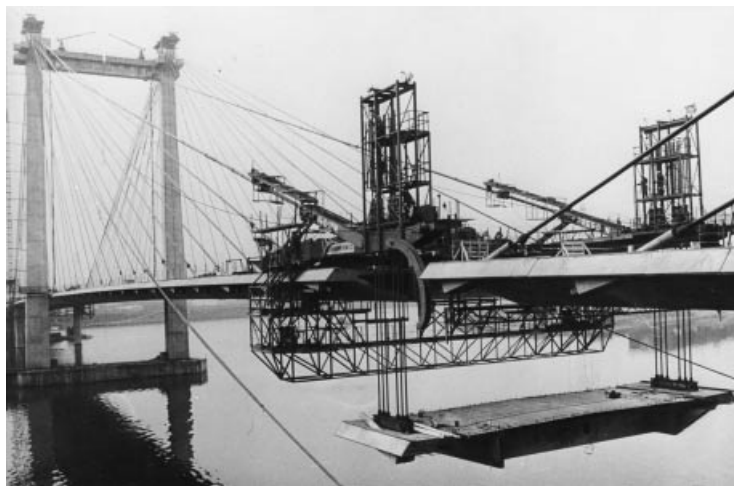
**Figure 7.79** Derrick cranes on the deck of the Tjörn Bridge



**Figure 7.80** Purpose-built crane for lift of deck segments in the Stonecutters Bridge (courtesy of Steve Kite, Arup)

cable favourably influenced the forces in the permanent stay cables that would otherwise have been seriously overstressed until the permanent stay cable of the new segment was installed and tensioned [78.1]. As seen in Figure 7.81, the erection traveller of the Pasco–Kennewick Bridge also contained the curved slides for the stay cable erection.

In cable stayed bridges with an *in situ* cast ladder deck (refer to Figure 4.42(g)), the deck is often cast by application of a form traveller attached to the completed part of the deck (Figure 7.82). With the modest depth of the edge girders generally found in these bridges the moment capacity of the deck is quite limited, so it will be necessary to cast the deck in relatively short segments with a length of typically 4–6 m and the full width of the deck. The form traveller has to be designed so that it can be moved forward and cantilevered after the newly cast concrete segment has hardened and the permanent stays installed and tensioned. With a reasonably short segment length in each casting, it will be possible to avoid temporary cables and be unnecessary to strengthen the edge girders for the loadings that appear during construction.



**Figure 7.81** The Pasco–Kennewick Bridge under erection



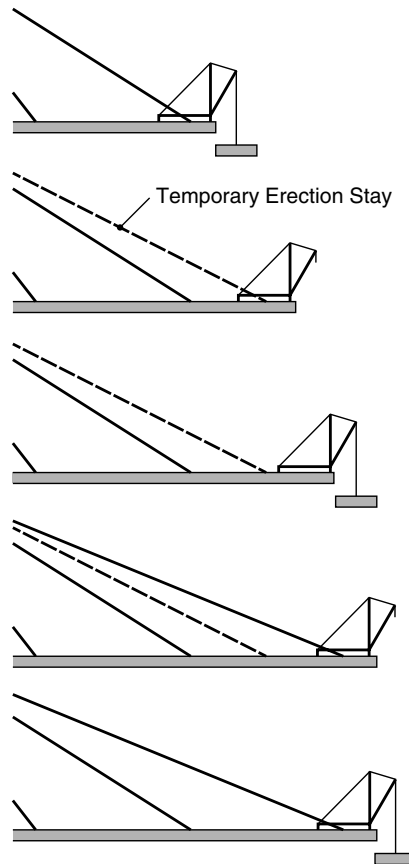
**Figure 7.82** Form traveller at the tip of an in situ cast ladder deck in concrete

The Barrios de Luna Bridge, record-holder for three years from 1983 to 1986, was designed with a 2.3 m deep box girder possessing a considerable moment capacity. It was, therefore, possible to cantilever from one stay cable anchor point to the next without any temporary supporting elements (Figure 7.83). The casting of the 8.16 m length between anchor points was, however, accomplished in two stages, each comprising casting of the full box width of 22.5 m and a length of 4.08 m. The Barrios de Luna Bridge constitutes a fine example of a cable supported bridge where the main structural system is chosen to fulfil the requirements in both the final operational phase and in the construction phase.

Temporary erection stays have also been used in cable stayed bridges with few stay cables, and consequently there is a considerable distance between the cable supported points of the deck. In these bridges an overstressing might occur either in the deck section or in the last erected stay cable during a free-cantilever from one cable anchor point to the next. In such a case a temporary erection stay, as shown in Figure 7.84, might be installed to reduce both the bending moments in the deck and the tension in the permanent stay cable.



**Figure 7.83** The Barrios de Luna Bridge during construction



**Figure 7.84** Application of a temporary erection stay during cantilevering from one permanent cable anchor point to the next

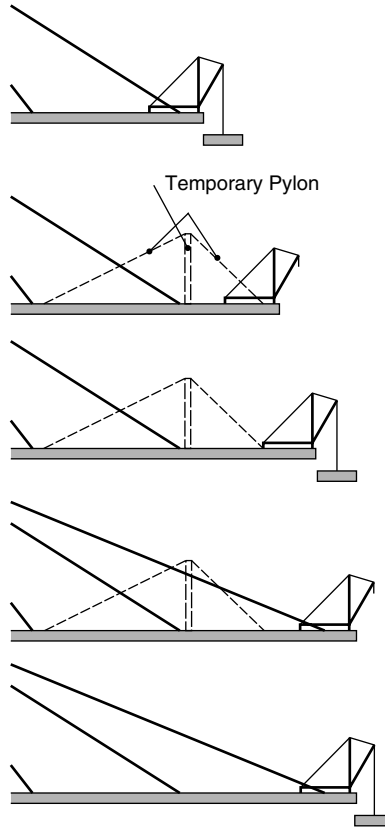
Alternatively, the cantilevered part of the deck might be supported by a secondary cable system comprising a temporary pylon, with a set of temporary erection stays, as illustrated in Figure 7.85. With this arrangement, the hogging moment in the deck is reduced, whereas the tension in the permanent stay cables remains practically unchanged. Thus, this arrangement is only applicable if the problem of overstressing is confined to the deck.

A secondary cable system as described above was used temporarily during the erection of the Rhine Bridge between Mannheim and Ludwigshafen (Figure 7.86).

In relation to the descriptions above it should be emphasized that temporary measures in the form of supports, stays, and pylons used only during erection are costly as they have to be fabricated, erected, and demolished before the construction is completed. It is therefore highly recommended that aspects regarding the erection are taken into consideration in the very early design stages so that the main layout of the structure can be chosen to minimize the amount of temporary structural members.

The descriptions of aspects related to the construction of cable supported bridges concludes by a brief description of the erection of the Millau Viaduct in southern France – one of the most spectacular bridge erections ever performed.

The erection of the deck in the Millau Bridge was especially challenging as the pre-fabricated segments could not be brought to the site and lifted vertically into place as generally occurs in cable supported bridges across waterways. Instead the superstructure was push-launched from both abutments to a closing point above the Tarn River 270 m below the deck. To give the necessary support during launching the permanent piers had to be supplemented by temporary piers at the



**Figure 7.85** Temporary cable system comprising a secondary pylon with a corresponding set of stay cables



**Figure 7.86** The Rhine Bridge between Mannheim and Ludwigshafen during erection



**Figure 7.87** The deck of the Millau Viaduct during the initial launching via a temporary support onto the first permanent pier



**Figure 7.88** The Millau Viaduct after completion of the launching. The deck is still partly supported by the temporary supports until the remaining pylons and cable systems will be added

centre of each span. However, as the closing point between the two launched deck sections was positioned at the centre of the span above the Tarn River, a temporary pier could be avoided where the deck is highest above the ground. As the Tarn River is closer to the north abutment than the south abutment, it was necessary to launch approximately 70% of the deck length from the south side and only approximately 30% from the north side (Figure 7.87).

To allow the cantilever at the tip to reach from the permanent pier support to the temporary pier support (or vice versa), the front pylon and the associated cable system had already been installed from the beginning of the launching process whereas the intermediate spans did not need a cable support as long as they could rest on the temporary piers. Most of the pylons and the stay cables were consequently not erected until the bridge deck had reached its final position (Figure 7.88).

# 8

## Aerodynamics

### 8.1 Historical Overview

#### 8.1.1 Nineteenth-century bridge failures

The first noteworthy example of a cable supported bridge failure due to wind is that of the first Dryburgh Abbey Bridge in Scotland (Figure 8.1). The cable stayed footbridge with a 79 m span was designed by John and William Smith and built in 1817. In January 1818, it collapsed when several of the stay connection hooks failed during a storm. The bridge is a noteworthy example, not because of its span or £550 construction cost, but because its failure – together with that of the Saale River Bridge in Germany in 1824 – led to the demise of the cable stayed bridge as a structurally efficient solution in the minds of designers for more than a century. This was reinforced by the ensuing condemnation of cable stayed bridges by one of its conceptual fathers, Claude Navier. Oddly, subsequent collapses of suspension bridges did not seem to have the same effect.

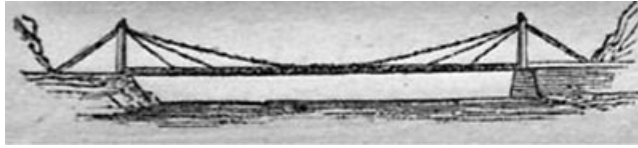
During the remainder of the century, several suspension bridge collapses and failures were witnessed during storms in Europe and North America, with a number of these scrupulously described by bystanders. In most cases the descriptions involved the words ‘undulation’, ‘twisting’ or ‘oscillation’, implying some form of dynamic motion of the bridge. Nevertheless, none of the bridges were designed for this type of action and wind-structure interaction was not even considered. Wind, when considered, was treated as an independent external static horizontal load.

For the Tay Bridge in Scotland, which collapsed in 1879, a wind pressure of 0.48 kPa was used as the static horizontal load. The bridge failed under a mean perpendicular wind velocity of approximately 28 m/s, while a train full of passengers was crossing it (Figure 8.2). This led C. Shaler Smith to publish an article in *Engineering News* two years later in 1881, in which he advocated that the loading of a bridge must also account for the loading generated by the wind acting on a passing train. He went on to reason that this load should not surpass 1.44 kPa, as he had calculated train overturning horizontal pressures to be 1.49 kPa. According to his reasoning, if a train were to overturn or derail due to the wind, it would take out the bridge anyway. Today, modern design codes and specifications require in most cases that static-equivalent horizontal wind pressures in excess of 3 kPa be considered for exposed members and traffic on truss decks and bridges – notwithstanding any aeroelastic instability. That is nearly twice what Smith advocated and six times what was used on the Tay Bridge. After the Tay Bridge collapse and to the bemusement of prominent fellow engineers, Sir John Fowler and Sir Benjamin Baker, designers of the Forth Bridge in Scotland, opted to consider a much higher wind pressure of 2.68 kPa for the design of their bridge. The 2528 m long tubular steel truss rail bridge, with main spans of 521.3 m, has been in service without major incident since 1890. As of 2006, it was carrying over 190 trains per day.

#### 8.1.2 Tacoma Narrows Bridge collapse

There is no doubt that the Tacoma Narrows Bridge collapse of 1940 proved to be a seminal moment in cable supported bridge design. Until that point, inadequate attention had been given to the theoretical and experimental understanding of the





**Figure 8.1** The first Dryburgh Abbey Bridge



**Figure 8.2** Tay Bridge after its collapse in 1879

effects of wind on these bridges, particularly when considering the scale and cost of the majority of them. This is not to say that designers did not consider wind loading to be an issue, but that there was a limited understanding of the mechanics behind dynamic wind–structure interaction.

Clearly, the static indeterminacy of these bridges, the absence of computing power, a lack of understanding of the nature of wind, and a tradition of designing and building based on experience alone greatly contributed to this. It might be surprising that more had not been done to understand the effects of wind on bridges, especially in light of the large number of bridge failures and large amplitude bridge deck oscillations that were attributed to wind preceding the Tacoma Narrows Bridge collapse. Table 8.1 lists the most prominent bridge failures and large amplitude bridge oscillations up to 1940.

**Table 8.1** Selected wind-induced bridge failures and oscillations until 1940

| Date | Bridge              | Location | Designer(s)   | Main span (m) | Incident     |
|------|---------------------|----------|---------------|---------------|--------------|
| 1818 | Dryburgh Abbey      | Scotland | J. & W. Smith | 79            | failure      |
| 1821 | Union Suspension    | England  | S. Brown      | 137           | oscillations |
| 1834 | Nassau              | Germany  | Lossen & Wolf | 75            | failure      |
| 1836 | Brighton Chain Pier | England  | S. Brown      | 78            | failure      |
| 1838 | Montrose            | Scotland | S. Brown      | 131           | failure      |
| 1839 | Menai Straits       | Wales    | T. Telford    | 176           | failure      |
| 1852 | Roche-Bernard       | France   | P. Leblanc    | 198           | failure      |
| 1854 | Queenston-Lewiston  | USA - CA | E. Serrell    | 259           | failure      |
| 1854 | Wheeling            | USA      | C. Ellet      | 310           | failure      |
| 1879 | Tay                 | Scotland | T. Bouch      | 75            | failure      |
| 1889 | Niagra-Clifton      | USA - CA | S. Keefer     | 386           | failure      |
| 1937 | Fykseund            | Norway   | A. Selberg    | 230           | oscillations |
| 1937 | Golden Gate         | USA      | J.B. Strauss  | 1280          | oscillations |
| 1938 | Thousand Islands    | USA - CA | D. Steinman   | 240           | oscillations |
| 1939 | Bronx-Whitestone    | USA      | O. Ammann     | 701           | oscillations |
| 1939 | Deer Isle Bridge    | USA      | D. Steinman   | 329           | oscillations |

The lack of focus on bridge aerodynamics up to 1940 is less surprising, however, when considering that the immediately preceding suspension bridge collapse due to wind occurred over 50 years earlier in 1889. Furthermore, unlike previous bridges, the size and the cost of the Tacoma Narrows Bridge led the prominent designers of the period to question their own designs, which in turn led to a plethora of research activity and a quest by designers to radically change existing bridge design concepts.

The Tacoma Narrows Bridge was built in a record time of 19 months with dimensional aspect ratios that had not been dared earlier. To save money and enhance the appearance of the bridge, its designer, Leon Moisseiff, advocated a narrower and shallower bridge deck and shorter pylons. The cable sag-to-span ratio of 1:12 was intended to provide greater horizontal stiffness due to the pendulum effect, while the 2.4 m-deep plate girder not only would reduce weight and bending moments, but also provided a smaller vertical surface area for the oncoming wind.

On 1 July 1940, the bridge was opened to the public with much fanfare. Immediately after the opening, there were reports of large amplitude vertical vibrations, something which had also been regularly observed by the builders during construction. Initially, the significance of the oscillations were played down and the public was generally unconcerned by them. The bridge was even nicknamed ‘Gallop Girtie’ and people often came to cross the bridge, just to experience the oscillations. The larger than expected levels of traffic prompted the Toll Bridge Authority to reduce the commuting tolls by 25% within the first month. In the background, however, concerns regarding the vibrations and the slenderness of the deck existed, with the Toll Bridge Authority having commissioned Professor F.B. Farquharson from the University of Washington to examine the dynamic behaviour of the bridge as early as 1939.

Farquharson made several dynamic models and was also able to perform some rudimentary wind-tunnel tests on a 1:20 scale section of the deck. They were the first of their type. From these, it was found that there were large fluctuating lift forces on the deck. By adding wind deflection panels or ‘fairings’ on the side of the model, he found that he could reduce the lift forces significantly. From these tests, he devised 23 cm-tall curved fairings that the Toll Bridge Authority proceeded to construct. In the meantime, the Toll Bridge Authority had already installed several vibrational countermeasures that mainly involved some form of girder ties.

Engineers decided to install the fairings at the first available opportunity, preferably just after a storm which had started on the evening of 6 November. Unfortunately, by early morning of 7 November, the very large amplitude vertical vibrations – now coupled with torsional vibrations – were starting to take their toll on the bridge. At 11:00 am on 7 November, a 183 m section of the deck collapsed into the waters below (Figure 8.3). Investigations into the collapse commenced immediately afterwards.



**Figure 8.3** Tacoma Narrows Bridge at the moment of girder failure. (Reproduced with permission from University of Washington Press)

### 8.1.3 The Carmody Board

A board of engineers was established to investigate the collapse of the bridge and to report their findings to the Federal Works Agency, then headed by John M. Carmody. The board, later referred to as the Carmody Board, was composed of eminent bridge designer Othmar H. Ammann, aerodynamicist Theodore von Kármán and Engineer of Design for the Transbay, Glenn B. Woodruff.

On 28 March 1941, less than five months after the bridge collapse, the Carmody Board published their findings. Surprisingly, one of the main conclusions of the report was that the vertical oscillations of the bridge were probably induced by the turbulent nature of the oncoming wind and not by some form of aeroelastic instability. It was later established that von Kármán was not in full agreement with the findings, as he was well aware of the effects of fluctuating vortices shed behind a structure and believed that these must have played a significant role in the vertical oscillation of the bridge. Nevertheless, von Kármán managed to squeeze several important points into the conclusions, including that further experiments and analytical studies should be made to investigate the action of aerodynamic forces on suspension bridges. Ammann, unconvinced of the phenomenon of aeroelastic instability, made sure that it was clear in the report that the evidence showing the fairings would have favourably affected the vertical oscillations was inconclusive. In fact, he went so far as to state that there was evidence that the fairings would have had an unfavourable influence on torsional stability.

### 8.1.4 The Fykkesund Bridge

Completed in 1937, the Fykkesund Bridge in Norway was much less remarkable for its span than for its original deck span to depth ratio of 511:1. This was much larger than any other major bridge of the time. From a statical point of view, this was not a problem. The deck and supporting cables were more than capable of carrying the design loads. But, periodically the bridge did suffer from severe wind-induced vibrations. Unlike many of his contemporaries, the bridge's designer, Arne Selberg, realized that the vibrations must be attributable to some form of aerodynamic instability. Selberg devised a series of measures to limit the vibrations, but was unable to implement them due to financial constraints and later due to the Occupation of Norway during World War II. In 1944, sectional model tests of the bridge were undertaken at the Norwegian Institute of Technology in Trondheim. The tests verified the propensity for oscillations and in 1945 countermeasures in the form of girder ties were installed. The ties are still in use today (see Figure 8.4).

After the war, Selberg decided to turn his attention to the understanding of bridge aerodynamics and, following the work of Friedrich Bleich and others, developed the well known empirical formulation for the critical flutter velocity of bridges. In the years after the Tacoma Narrows Bridge collapse, many other engineers and researchers became increasingly convinced of the phenomenon of aerodynamic instability and turned their attention to the field of bridge aeroelasticity.

## 8.2 The Bridge Deck and Pylon

### 8.2.1 Torsional divergence

In 1935, Norwegian physicist Theodore Theodorsen published a National Advisory Committee for Aeronautics Report (NACA 496) on aerodynamic instability and the mechanism for flutter. In this, he provided an exact solution to the equations governing the mechanics of flutter for an airfoil. It was to prove timely and several researchers used the theory to conservatively predict flutter velocities for bridge girders with a fair degree of success. Theodorsen's theory did not account for structural damping though and so A. G. Frandsen later went on to extend the theory to include structural damping. At the same time Frandsen presented a simplified theoretical framework for the understanding of both coupled flutter and torsional divergence of a thin airfoil.

The theory of thin airfoils constitutes an important tool in understanding the aeroelastic phenomena of both torsional divergence and coupled flutter, as will be shown in the following investigations.

The thin airfoil to be considered here is a plane plate of width  $b$ , having an infinitesimal thickness and an infinite length. With these idealizations the flow around the airfoil will be two-dimensional, which considerably eases the mathematical treatment.

For an airfoil, as shown in Figure 8.5, having a neutral position 1 parallel to the direction of the wind, a displacement to the deflected position 2 (characterized by a translation  $\delta$  and a rotation  $\theta$ ) introduces aerostatic pressures, having their resultant  $L$  acting at the windward quarter point, as indicated in Figure 8.5.

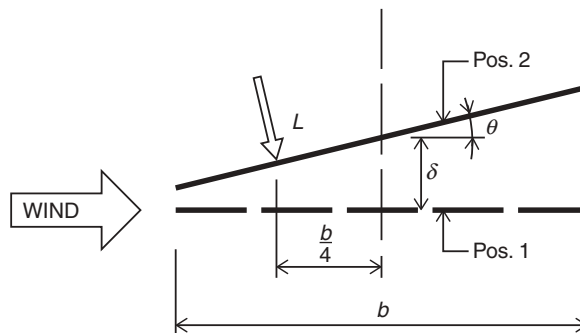


**Figure 8.4** Fyksesund Bridge, Norway (1937). Note girder ties

The action of the aerostatic pressures can be decomposed into a vertical force  $L$  and a moment  $M$ , for which the following expressions might be derived (assuming small values of the rotation angle  $\theta$ ):

$$L = -\pi\rho bU^2\theta \quad (8.1)$$

$$M = \frac{1}{4}\pi\rho b^2U^2\theta \quad (8.2)$$



**Figure 8.5** Airfoil in neutral position (1) and deflected position (2)

where  $\rho$  is the mass density of the air and  $U$  the oncoming wind velocity. The equations of motion of the airfoil ignoring damping can be expressed by introducing the formal spring constants  $K_v$  and  $K_t$  so that:

$$K_v \delta + \mu \frac{\partial^2 \delta}{\partial t^2} = K_v \delta + \mu \ddot{\delta} = L(t) \quad (8.3)$$

$$K_t \theta + I_m \frac{\partial^2 \theta}{\partial t^2} = K_t \theta + I_m \ddot{\theta} = M(t) \quad (8.4)$$

In these equations,  $L(t)$  and  $M(t)$  are the time-dependent active vertical force and active torsional moment, respectively.

With  $L(t) = M(t) = 0$ , the circular frequencies  $\omega_v$  and  $\omega_t$  become (refer to (3.119) and (3.120)):

$$\omega_v = \sqrt{\frac{K_v}{\mu}} \quad \text{and} \quad \omega_t = \sqrt{\frac{K_t}{I_m}} \quad (8.5)$$

where  $\mu$  is the mass of the girder per unit length and  $I_m$  is the corresponding mass moment of inertia.

The vertical and torsional spring constants  $K_v$  and  $K_t$  are then determined by the expressions:

$$K_v = \mu \omega_v^2 \quad \text{and} \quad K_t = I_m \omega_t^2 \quad (8.6)$$

Assuming that the airfoil is subjected to an external force  $P_0$  and an external moment  $M_0$ , equilibrium in the deflected state is expressed by (8.3) and (8.4), with  $\partial^2 \delta / \partial t^2 = \partial^2 \theta / \partial t^2 = 0$ ;  $P(t) = L_0 - \pi \rho b U^2 \theta$ , and  $M(t) = M_0 + 1/4 \pi \rho b^2 U^2 \theta$ :

$$K_v \delta = L_0 - \pi \rho b U^2 \theta \quad (8.7)$$

$$K_t \theta = M_0 + \frac{1}{4} \pi \rho b^2 U^2 \theta \quad (8.8)$$

leading to the following expressions for the deflection  $\delta$  and the rotation  $\theta$ :

$$\delta = \frac{1}{K_v} \left( L_0 - \frac{\pi \rho b^2 U^2}{K_t - \frac{1}{4} \pi \rho b^2 U^2} M_0 \right) \quad (8.9)$$

$$\theta = \frac{M_0}{K_t - \frac{1}{4} \pi \rho b^2 U^2} \quad (8.10)$$

From the above expression for  $\theta$ , it appears that the aerostatic pressure reduces the torsional stiffness from  $K_t$  to  $K_t - \frac{1}{4} \pi \rho b^2 U^2$ . Thus, the torsional stiffness will vanish completely for a wind velocity  $U_d$  determined by:

$$U_d = \frac{2}{b} \sqrt{\frac{K_t}{\pi \rho}} \quad (8.11)$$

The wind velocity  $U_d$ , called the divergence velocity, corresponds to the occurrence of a static stability problem, as even the smallest rotation of the airfoil from the neutral position will imply displacements without limits.

Immediately, (8.11) indicates that the divergence velocity is inversely proportional to the airfoil width  $b$ . However, it must be remembered that the torsional stiffness  $K_t$  also depends on the width  $b$ . Thus, for cable systems attached at the edges of the airfoil  $K_t$  will be determined by  $K_t = 1/2Kb^2$  (refer to (3.120)), and with this value, the expression for  $U_d$  becomes:

$$U_d = \sqrt{\frac{2K}{\pi\rho}} \quad (8.12)$$

Consequently, under these assumptions the divergence velocity becomes independent of the width  $b$ , but in reality both the spring constant  $K$  of each cable plane and the torsional stiffness of the girder section will change with the width  $b$  so that the relation between  $U_d$  and  $b$  becomes more complex.

The divergent wind velocity  $U_d$  of (8.12) can be determined without recourse to expensive and laborious wind-tunnel testing or analyses. Nevertheless, the assumption that a bridge deck can be represented to a fair degree by an airfoil is far from accurate in many cases. More appropriately, the divergence velocity can be calculated with knowledge of the aerodynamic moment coefficient of the deck for varying wind-angles of attack.

If the evaluated moment coefficient for bridge deck is  $C_t(\theta)$ , then the aerodynamic moment can be written as:

$$M_t(\theta) = \frac{1}{2}\rho U^2 b^2 C_t(\theta) \quad (8.13)$$

which can be expanded using a Taylor series, so that:

$$M_t(\theta) = \frac{1}{2}\rho U^2 b^2 [C_t(0) + \theta \cdot C_t'(0)] \quad (8.14)$$

The moment resistance is  $K_t\theta$ , so that in the state of equilibrium with an added external moment  $M_0$  it will hold that:

$$M_0 + \frac{1}{2}\rho U^2 b^2 [C_t(0) + \theta C_t'(0)] = K_t\theta \quad (8.15)$$

leading to:

$$\theta = \frac{2M_0 - \rho U^2 b^2 C_t(0)}{2K_t - \rho U^2 b^2 C_t'(0)} \quad (8.16)$$

$C_t'$  is the first derivative of the moment coefficient with respect to  $\theta$ .

From (8.16), it can be seen that stability is always met when  $C_t'(0) \leq 0$ . However, if  $C_t'(0) > 0$  then the divergence velocity is now found as:

$$U_d = \sqrt{\frac{2K_t}{\rho b^2 C_t'(0)}} \quad (8.17)$$

It should be noted that the divergence velocity of (8.17) is only valid when the aerodynamic moment coefficient is linear for the angles of attack of interest. If not, the nonlinear equilibrium equation below must be solved iteratively.

$$M_0 + \frac{1}{2}\rho U^2 b^2 C_t(\theta) - K_t\theta = 0 \quad (8.18)$$

### 8.2.2 Coupled flutter

For most cable supported bridges the divergence velocity  $U_d$  leading to static instability is of less interest than the divergent aeroelastic instability phenomenon known as flutter, which will occur for a lower wind velocity  $U_f$ , called the flutter velocity. Flutter vibration is a harmonic oscillation characterized by a coupling of the vertical and the torsional oscillations occurring when the frequencies of these two basic oscillations coincide.

Generally, cable supported bridges with two cable planes will have a larger torsional eigenfrequency  $f_t$  than vertical eigenfrequency  $f_v$ , but due to the equivalent reduction of the torsional stiffness under the action of the aerostatic pressure,  $f_t$  will decrease with increasing wind velocity. Frandsen [66.2] showed that for the airfoil, this leads to the airfoil flutter velocity:

$$U_f = U_d \sqrt{1 - \left(\frac{\omega_v}{\omega_t}\right)^2} \quad (8.19)$$

From this expression it is evident that the flutter velocity  $U_f$  is smaller than the divergence velocity  $U_d$ . It also appears that a low flutter velocity will result if the eigenfrequencies of the vertical and the torsional modes are close. Thus, it is generally desirable that torsional eigenfrequency  $f_t$  is more than twice as large as the vertical eigenfrequency  $f_v$  in larger cable supported bridges.

Frandsen's derivations leading to the above expression for the flutter velocity are of a very simplified nature as the expressions for the aerostatic pressures were used, thus disregarding the fact that flutter actually implies motion of the airfoil so that the wind is not locally stationary.

However, the simple expression of (8.19) agrees reasonably well with semi-empirical expressions adjusted by test results. Thus, Selberg [61.1] gives the following expression for the flutter velocity  $U_f$ .

$$U_f = 0.52U_d \sqrt{\left[1 - \left(\frac{\omega_v}{\omega_t}\right)^2\right] b \sqrt{\frac{\mu}{I_m}}} \quad (8.20)$$

An exact solution to the theoretical flutter equations with structural damping is provided by Frandsen. However, in a comparative investigation, it is shown that the Selberg expression, (8.20), will give adequate results for  $f_t/f_v > 1.5$ .

Again, the fact that the deck of a cable supported bridge has a much more complicated shape than a thin airfoil naturally implies that the critical wind velocity deviates from the flutter velocity of the airfoil. However, a deck of wide and slender box girders in streamlined shape will be characterized by having a critical wind velocity close to the theoretical flutter velocity, whereas bluff girders and trusses will show a larger difference between the critical wind velocity measured in the wind tunnel and the theoretical flutter velocity.

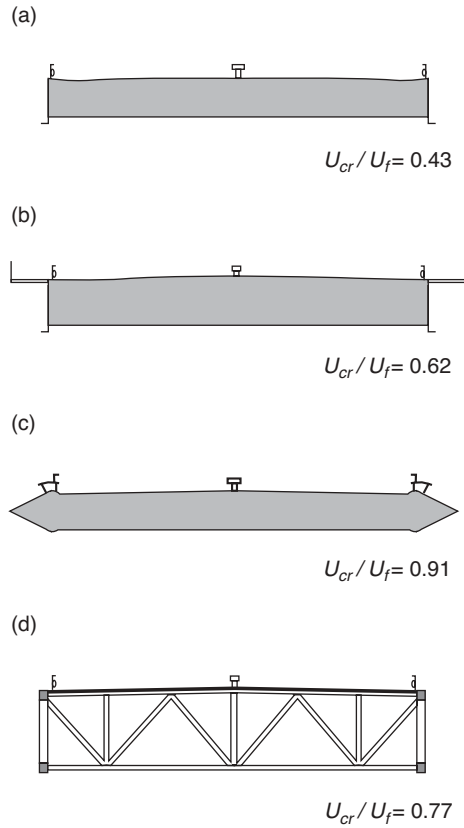
This feature is illustrated in Figure 8.6 showing cross sections of four models tested in a wind tunnel during the design process for the Little Belt Bridge in Denmark (from [66.4]). It appears that the streamlined box (c) is characterized by a critical wind velocity,  $U_{cr}$ , corresponding to 91% of the flutter velocity,  $U_f$ , whereas the critical wind velocity of the bluff box section (a) is only 43% of the flutter velocity. For the box with cantilevered deck areas (b) and for the truss solution (d), the results are between these two extremes.

During wind tunnel testing, models are in most cases subjected to wind blowing at different angles of incidence (e.g. within an interval from  $-5^\circ$  to  $+5^\circ$ ).

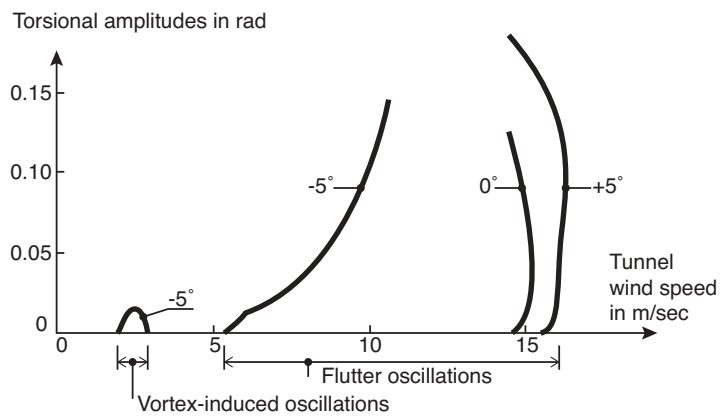
The result of a wind tunnel test with a model of a double-deck trapezoidal truss is shown in Figure 8.7 [78.3]. Note that small vortex-induced oscillations occurred for wind blowing from below ( $-5^\circ$ ) at wind velocities between 2 and 3 m/s.

It is evident from Figure 8.7 that the angle of incidence has a considerable effect. It should, however, be remembered that under normal topographic conditions the high and stationary wind velocities will only be found for an almost horizontal wind. Thus, at an inclination of  $5^\circ$  from the horizontal, measurements have shown that the maximum wind velocity amounts to only 20% of that found for horizontal wind.

A more accurate semi-empirical evaluation of the critical flutter velocity of a bridge girder was proposed by Scanlan and Tomko [71.3], in which empirically obtained velocity-dependent aeroelastic force coefficients or *flutter derivatives* are



**Figure 8.6** Four bridge models tested during the design of the Little Belt Bridge



**Figure 8.7** Results of wind-tunnel tests with a model trapezoidal double deck truss, investigated for the Storebælt Bridge in 1978



used to determine a bridge's propensity to exhibit flutter instability for increasing wind velocities. More specifically, the self-excited aeroelastic forces on a bridge girder vertically, torsionally and laterally will be:

$$L_{ae} = \frac{1}{2}\rho U^2 b \left[ \lambda_R H_1^* \frac{\delta}{U} + \lambda_R H_2^* \frac{b\dot{\theta}}{U} + \lambda_R^2 H_3^* \theta + \lambda_R^2 H_4^* \frac{\delta}{b} \right] \quad (8.21)$$

$$M_{ae} = \frac{1}{2}\rho U^2 b \left[ \lambda_R A_1^* \frac{\delta}{U} + \lambda_R A_2^* \frac{b\dot{\theta}}{U} + \lambda_R^2 A_3^* \theta + \lambda_R^2 A_4^* \frac{\delta}{b} \right] \quad (8.22)$$

$$D_{ae} = \frac{1}{2}\rho U^2 b \left[ \lambda_R P_1^* \frac{p}{U} + \lambda_R P_2^* \frac{b\dot{\theta}}{U} + \lambda_R^2 P_3^* \theta + \lambda_R^2 P_4^* \frac{p}{b} \right] \quad (8.23)$$

where the reduced circular frequency  $\lambda_R$  is the inverse of the reduced velocity, so that  $\lambda_R = 2\pi/U_R = (b\omega)/U$ .  $p$  is the lateral translation and  $H_1^* - H_4^*$ ,  $A_1^* - A_4^*$ , and  $P_1^* - P_4^*$  are the empirically obtained *flutter derivatives*.

As turbulence is generally found to raise critical wind velocities, flutter derivatives are usually obtained from section-model wind tunnel tests with smooth flow. The derivatives can be obtained through forced vibration tests, in which the scaled deck section is forced to move at specific displacements and velocities (or rotations and angular velocities), during which the aeroelastic forces in each motional degree-of-freedom are obtained after accounting for inertial forces. More commonly, the derivatives are obtained through free vibration tests, in which changes in girder stiffness and damping are recorded during free vibrations of the motional degree-of-freedom of interest.

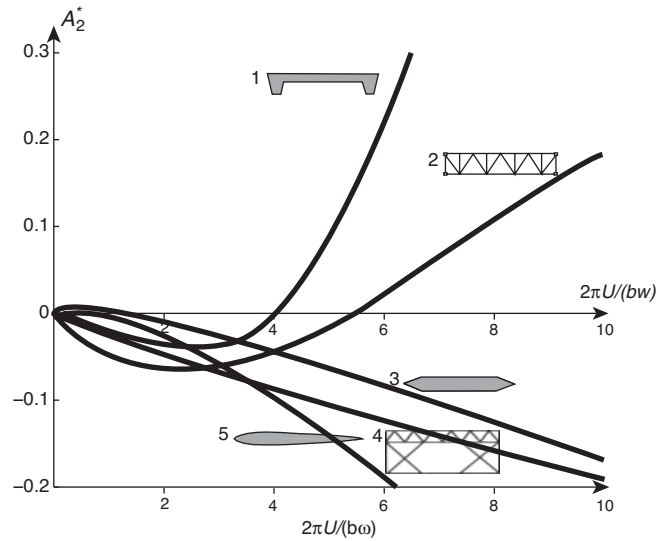
From (8.21)–(8.23) it can be seen that the derivatives are either associated with displacement proportional forces (stiffness related) or velocity proportional forces (damping related). Furthermore, each derivative is associated with a girder displacement or rotational degree of freedom. Changes in the equivalent girder stiffness due to the displacement proportional forces are considered to be of smaller significance. As such, focus is placed on the derivatives associated with velocity-proportional aeroelastic forces and, more importantly, their sign. The sign of a derivative is important as a positive velocity-proportional aeroelastic force will be equivalent to negative damping. The larger the level of negative damping, the larger the tendency for instability. For example, positive values of  $H_1^*$  might indicate some form of vortex-induced instability, while positive values of  $A_2^*$  would indicate the potential for classic torsional flutter. Positive values of  $H_2^*$  and  $A_1^*$  indicate strong aerodynamic coupling and the potential for coupled flutter. The flutter derivative  $A_2^*$  for several girder examples can be seen in Figure 8.8.

### 8.2.3 Buffeting

The successful design of a cable supported bridge for aerodynamic stability does not preclude large wind-induced oscillations of a different albeit self-limiting nature. The two most important mechanisms associated with these are wind *buffeting* and *vortex-shedding*. Figure 8.9 shows the progression of the dynamic response of a bridge structure under the different types of aerodynamic excitation, as a function of wind velocity.

Buffeting is the mechanism by which the fluctuations in the oncoming wind cause the bridge to vibrate. These vibrations are not usually of a catastrophic nature, but can be large enough to warrant closure of the bridge. Furthermore, the cumulative effect of these oscillations over the lifetime of the bridge could be the fatigue of various components of the bridge, often leading to the deterioration of the structural integrity of the bridge, accompanied by large maintenance and retrofit costs. Before venturing further into the description of buffeting though, it is prudent to describe the oncoming wind further.

The wind is generally described by the mean wind velocity within a given time interval (e.g. 10 minutes) and by the gust wind velocity (i.e. the peak value of the wind speed). The mean wind velocity depends on the local topography, and the presence of hills and valleys might diminish or increase the design wind velocity by as much as 50% compared to what would have been stipulated otherwise.

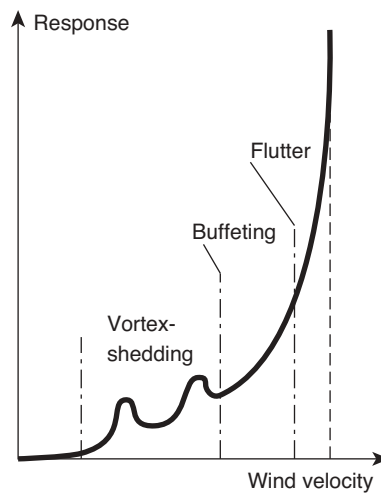


**Figure 8.8** Torsional flutter derivatives for different girder types [71.3] (1) unstable bluff box deck (2) trussed deck with instability (3) stable streamlined box deck (4) stable truss deck (5) thin airfoil

The wind velocity  $U$  varies with the height above the terrain and it is generally assumed that the mean wind velocity  $\bar{U}$  increases exponentially with height, as a function of a reference height, so that:

$$\bar{U}(h) = \bar{U}(h_{ref}) (h/h_{ref})^\alpha \quad (8.24)$$

where  $h_{ref}$  is a reference height often chosen as 10 m, and  $\alpha$  an exponent reflecting the roughness of the terrain under the incoming winds. For smooth terrain,  $\alpha$  will be 0.12 whereas a value as high as 0.40 can be found over very rough terrain. Under average terrain conditions,  $\alpha$  is often chosen to be 0.2.



**Figure 8.9** Dynamic response of a slender bridge structure under wind action

The gust or peak wind velocity  $\hat{U}$  will be characterized by a different variation with the height:

$$\hat{U}(h) = 1.41\hat{U}(h_{ref})(h/h_{ref})^{0.1} \quad (8.25)$$

For engineering purposes, both the mean and peak wind velocities are assumed constant and equal to their reference values for  $h < h_{ref}$ .

Two further quantities characterize the wind: turbulence and the integral (or turbulence) length scale. Turbulence describes the fluctuating components of the wind in three dimensions, while the integral length scale provides a measure of the average length of a turbulent wind eddy in a particular direction ( $x$ ,  $y$  or  $z$ ). The wind turbulence is described by a number of statistically averaged parameters in the streamwise direction ( $x$  direction), in the lateral direction ( $y$  direction), and in the vertical direction ( $z$  direction). The turbulence intensity  $I_{x,y,z}$  is expressed by:

$$I_{x,y,z} = \frac{\sigma_{x,y,z}}{\bar{U}} = \frac{U_{x,y,z}^{RMS}}{\bar{U}} \quad (8.26)$$

where  $\sigma_{x,y,z}$  is the standard deviation of the fluctuating wind velocity in all three directions.  $U_{x,y,z}^{RMS}$  is root-mean-square of the fluctuating components of the wind,  $v_{x,y,z}(t)$ , so that:

$$U_{x,y,z}^{RMS} = \sqrt{\frac{1}{T} \int_0^T (v_{x,y,z}(t))^2 dt} \quad (8.27)$$

Although the turbulence intensity has components in the  $x$ ,  $y$  and  $z$  directions, in most cases the streamwise component in the  $x$  direction is the most decisive. The streamwise component can vary from 1% on a very cold day over a cold water surface to over 40% over rough terrain on a warm day.

The length scale is more difficult to calculate, as it often requires on-site wind measurements and an evaluation of the autocovariance functions of the fluctuating wind components. As such, for engineering purposes, typical values for the three components of the scale are:

$$L_x = 150 \text{ m}, \quad L_y = 0.2L_x; \quad L_z = 0.4h$$

It should be noted though that the length scales also depend on the roughness of the terrain as well as the height above the ground.

Finally the fluctuations in the oncoming wind can be described in the frequency domain by the spectral density of each velocity component in relation to the frequency of fluctuation. This is often referred to as a wind spectrum. On-site measurement of the wind over an adequate period of time allows for the creation of such a spectrum, through Fourier decomposition of the measured wind velocity time-histories. When on-site measurements are not available, generalized wind spectra can be used. One of the most common spectra for wind over land is that of Davenport [61.2].

$$S_{x,y,z}(f) = \frac{4\kappa L_{x,y,z} \bar{U} \eta_{x,y,z}}{(1 + \eta_{x,y,z}^2)^{4/3}} \quad (8.28)$$

where  $S_{x,y,z}(f)$  represents the spectral density of the wind in the  $x$ ,  $y$  and  $z$  directions,  $\kappa$  is a factor often taken as 0.0025 for wind over open water, and  $\eta_{x,y,z} = fL_{x,y,z}/\bar{U}$ .  $L_x$  is often considered for this spectrum to be approximately 1200 m.

When plotting (8.28), Figure 8.10 is obtained. It is seen that the energy distribution of the wind as a function of frequency varies. By determining the area under the spectrum, the total energy associated with the oncoming wind can be found. Furthermore, integration of the spectrum over the entire frequency range is equal to the mean-square value (or variance) of the fluctuating velocity component, so that:

$$(U_{x,y,z}^{RMS})^2 = \int_0^\infty S_{x,y,z}(f) df \quad (8.29)$$

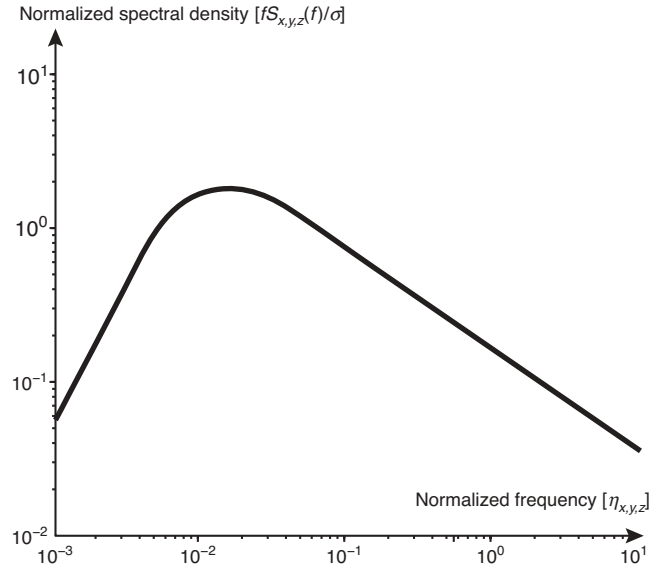


Figure 8.10 Davenport wind spectrum

The peak response of a bridge can be determined as a combination of the background response of the bridge to the fluctuations of the oncoming wind velocity and a combined resonant modal response resulting from the energy of the wind at the natural frequencies of the bridge [62.1]. The peak response of the bridge in a particular direction will be:

$$\hat{x} = \bar{x} + g_p \sqrt{(x_{RMS}^B)^2 + \sum (x_{i,RMS}^R)^2} \quad (8.30)$$

where  $\bar{x}$  is the mean response,  $g_p$  is the statistical peak factor,  $x_{RMS}^B$  is the root-mean-square background response and  $x_{i,RMS}^R$  is the resonant modal response. It should be noted that the terms referred to in (8.30) are general and could e.g. be displacements, stresses, moments or whatever other bridge response quantity that might be of interest. The mean vertical displacement can be found with knowledge of the static lift coefficient,  $C_z$ , of e.g. the bridge deck, which provides a mean force per unit length:

$$\bar{P} = \frac{1}{2} \rho \bar{U}^2 b C_z \quad (8.31)$$

Assuming that the wind velocity fluctuations can be defined as a random stationary process with a Gaussian distribution, the peak factor represents the maximum value of such a process over the root-mean-square of that process for a given return period. For structural response, the peak factor will also be dependent on the vibration of the structure. The peak factor is defined as:

$$g_p = \sqrt{2 \cdot \ln(vT)} + \frac{0.577}{\sqrt{2 \cdot \ln(vT)}} \quad (8.32)$$

where  $v$  is the cyclic vibration rate, often conservatively taken as the first natural frequency of the structure,  $f_1$ .  $T$  is the return period in seconds. A 10-min return period will give a value of  $T = 600$  sec. Clearly, the longer the return period considered, the larger the peak factor and the smaller the probability of exceeding the maximum value of the process.

For a bridge deck, the root-mean-square values of the vertical background and resonant modal responses can be found as:

$$(x_{RMS}^B)^2 = \left(\frac{1}{2}\rho\bar{U}^2 bC'_z\right)^2 I_z^2 \int_0^\infty \frac{\eta S_z(\eta)}{(U_z^{RMS})^2} A_z(\eta)^2 J_z(\eta)^2 d(\ln \eta) \quad (8.33)$$

$$(x_{RMS}^R)^2 \approx \left(\frac{1}{2}\rho\bar{U}^2 bC'_z\right)^2 I_z^2 \frac{\eta_i S_z(\eta_i)}{(U_z^{RMS})^2} A_z(\eta_i)^2 J_z(\eta_i)^2 \frac{\pi}{4(\zeta_{i,z}^s + \zeta_{i,z}^a(\eta_i))} \quad (8.34)$$

where  $C'_z$  is the first derivative of the deck's static lift coefficient with respect to wind angle of attack and  $S_z(\eta)$  is the spectral density of the vertical wind component as a function of reduced frequency, defined here as  $\eta = 1/U_R = bf/U$ .  $A_z(\eta)^2$  is the aerodynamic admittance function, which essentially characterizes the difference between the actual and quasi-steady forces acting on the bridge. This can be determined from wind-tunnel tests, but it has been found that by idealizing the girder as a thin airfoil, Sear's function may be used with sufficient accuracy for lift, so that:

$$A(\eta)^2 \approx \frac{2}{(7\eta)^2} [7\eta - 1 + \exp(-7\eta)] \quad (8.35)$$

$J_z(\eta_i)^2$  is the joint acceptance function that quantifies the ability of the wind load to excite that mode, by accounting for variations of the wind velocity over the length of the mode. The joint acceptance function for the lift force is:

$$J_z(\eta_i)^2 = \int_0^L \int_0^L \frac{S_z^{y_1, y_2}(\Delta y, \eta)}{S_z(\eta)} \phi_i(y_1) \phi_i(y_2) dy_1 dy_2 \quad (8.36)$$

With  $S_z^{y_1, y_2}(\Delta y, \eta)$  representing the cross-spectrum of the line-like wind load between two distinct points  $y_1$  and  $y_2$ , separated by  $\Delta y$ .  $S_z(\eta)$  is the line-like spectral density of the vertical wind component and  $\phi_i(y)$  is the mode shape for mode  $i$  over a length of  $L$ . For streamlined box-girders, an empirical approximation for the cross-spectrum over the line-like spectrum equivalent to the spanwise root coherence of the wind load is provided [95.19], so that:

$$\frac{S_z^{y_1, y_2}(\Delta y, \eta)}{S_z(\eta)} \approx \sqrt{\text{coh}_z(\Delta y, f)} = \exp\left(-\left(\Delta y \sqrt{c_2^2 + (c_3 f / \bar{U})^2}\right)^{c_1}\right) \quad (8.37)$$

The constants  $c_1$ ,  $c_2$  and  $c_3$  for lateral, lift and torsional force components are provided in Table 8.2.

$\zeta_i^s$  is the modal structural damping ratio and  $\zeta_i^a$  is the modal aerodynamic damping ratio. The aerodynamic damping for all three motional components is evaluated per unit length as:

$$\zeta_{i,x}^a = \frac{\rho C_x b \bar{U}}{4\pi f_i \mu} \quad (8.38)$$

$$\zeta_{i,z}^a = \frac{\rho C'_z b \bar{U}}{8\pi f_i \mu} \quad (8.39)$$

$$\zeta_{i,\theta}^a = \frac{\rho C_\theta b^3 \bar{U}}{8\pi f_i I_m} \quad (8.40)$$

**Table 8.2** Experimentally determined coefficient for the spanwise root coherence

| Force component   | $C_1$ | $C_2$ | $C_3$ |
|-------------------|-------|-------|-------|
| Lateral, $x$      | 1.0   | 4.21  | 5.47  |
| Lift, $z$         | 1.40  | 2.11  | 2.24  |
| Torsion, $\theta$ | 1.35  | 2.44  | 2.15  |

Changes in modal frequency, due to aerodynamic stiffness are considered small and so are ignored here.

To calculate the root mean square resonant vertical displacement of the bridge deck for the first vertical vibration mode, the root of the variance of (8.34) should be divided by the modal stiffness and multiplied by the mode shape.

Equations (8.33) and (8.34) can be modified to calculate the lateral response of the girder by replacing  $C'_z$  with  $2C_x$ . The torsional response can be found by replacing  $C'_z$  with  $C'_\theta$  and multiplying the right side of the equation with  $b^2$ .

It should be noted that although full-scale measurements of the buffeting response of bridges have been shown to generally be in good agreement with the predicted response obtained from the aforementioned theoretical framework, significant deviations due to uncertainties are not uncommon.

### 8.2.4 Vortex-shedding

Similarly to buffeting, vortex-shedding is a self-limiting wind-induced oscillation mechanism that is usually not of a catastrophic nature, but that can generate concerns regarding the bridge's serviceability and fatigue. Unlike buffeting, though, vortex-shedding involves a high degree of fluid-structure interaction, most often leading to oscillations that are harmonic in nature and with frequencies coinciding with those of the dominant eigenmodes of the bridge.

The critical vortex-shedding velocity is defined as:

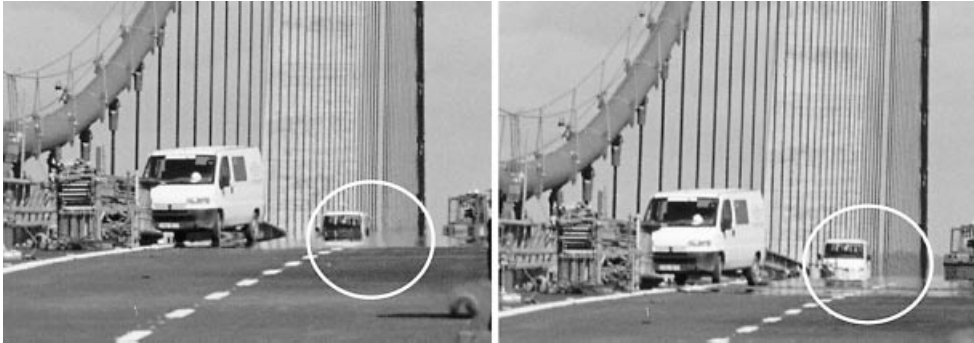
$$U_{cr} = \frac{f_i D}{St} \quad (8.41)$$

where  $D$  is the characteristic dimension of the structure. For a bridge girder this is often taken as the depth of the girder.  $St$  is the Strouhal number. For circular cylinders this is approximately 0.2. For the Storebælt Bridge, the mean Strouhal number for the bridge girder was found from scaled wind tunnel tests to be 0.133. For other deck shapes this number can vary greatly.

The critical vortex-shedding velocity does not indicate a velocity at which there is a definite propensity for a bridge to oscillate, but instead the wind velocity at which vortices shed at the same frequency as that of a particular eigenmode. For a bridge to oscillate, several additional conditions must be met, the most important of which are low structural damping and laminar wind flow with turbulence intensities typically below 5–8%. Furthermore, in the case of a bridge girder, the wind must be nearly perpendicular to the girder axis, within a range of  $\pm 20$  degrees. Finally, the critical wind velocity must occur at high enough wind velocities to have enough energy to excite the bridge, but also at low enough velocities that the narrowing of the wake does not disrupt the creation of vortices.

Most cable supported bridges do not suffer from vortex-shedding oscillations. Nevertheless, there are several reported cases of cable supported bridges that have exhibited these oscillations, either during construction or once completed. The Longs Creek Bridge experienced up to 200 mm amplitude of vibration for wind velocities between 4–11 m/s at a frequency of 0.6 Hz [92.4]. The Wye Bridge experienced much smaller vibration amplitudes of 44 mm for wind velocities between 7.2–8.0 m/s. The Storebælt Bridge experienced vortex-induced oscillations before and after completion of the bridge, with maximum root-mean-square values for vertical motion of 310 mm [01.1]. The successive pictures in Figure 8.11 provide an indication of the extent of the oscillations.

In the case of the Storebælt bridge, the propensity for vortex-induced oscillations had been identified from wind-tunnel tests (Figure 8.12). As such, provisions for guide vanes had been made and later fitted to the bottom corners of the deck. It is not completely apparent what the effect of the vanes is and wind tunnel tests have not been able to establish the exact mechanism resulting in their effectiveness. The most plausible explanation is that they streamline the flow, reducing the wake width and disturbing the formation of large vortices. A drawing of the guide vanes can be seen in Figure 8.13.



**Figure 8.11** Views of the Storebælt Bridge deck between alternating deck vortex-induced oscillations. (Courtesy of Aalborg Stiftstidende)

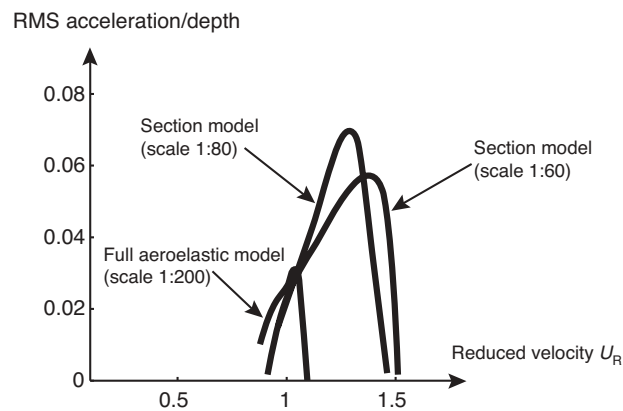
### 8.2.5 Wind tunnel testing

It is clear from the description of the various types of aerodynamic excitation that, in contrast to almost any other type of loading on a cable supported bridge, wind load depends not only on the main dimensions of the deck but also on its shape. In the early stage of the design process it is therefore essential to evaluate the aerostatic and aerodynamic properties of different cross sectional layouts for the deck, and here wind tunnel testing plays a dominant role.

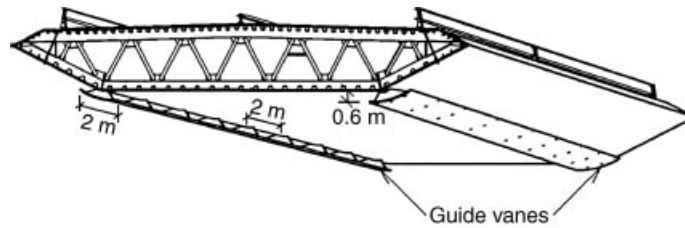
The influence of wind action on the design of the deck is seen very clearly in cable supported bridges with long spans. Here large cross sectional dimensions will result if bluff sections of the load-carrying elements are used, whereas a ‘streamlining’ of the girder will lead to reduced wind forces and smaller dimensions.

In smaller cable supported bridges, such as many of the present cable stayed bridges with relatively large depth-to-span and width-to-span ratios and efficient cable support, wind action is less decisive and its influence on the main layout is therefore considerably smaller.

It is important to distinguish between instability tendencies and actual instability when considering the aeroelastic problem [78.7]. Thus, a deck with an unfavourable shape in relation to aeroelastic instability will only lead to catastrophic oscillations if the structure is so flexible that its motion will allow the aeroelastic instability to develop fully at actual wind speeds.



**Figure 8.12** Vortex-induced oscillation of the Storebælt Bridge from wind tunnel tests [01.1]



**Figure 8.13** Storebælt Bridge guide vanes

In the case of the First Tacoma Narrows Bridge, the shape of the deck led to tendencies for aeroelastic instability, and as the structure was characterized by a significant flexibility due to its extremely slender dimensions, all conditions were fulfilled for the full development of aeroelastic instability.

Several recent cable stayed bridges have been constructed with decks having the same tendencies for aeroelastic instability (refer to Figures 4.43 and 4.47). But, as these structures are characterized by a much higher degree of structural stiffness, aeroelastic instability does not occur at actual wind speeds.

Since the Tacoma Narrows Bridge disaster, wind tunnel tests have become an important tool in investigations of aeroelastic stability. These wind tunnel tests are performed either on full models comprising the entire cable supported bridge with deck, pylons, and cable system, or on sectional models of a relatively small segment of the deck.

Full models offer the advantage of the most realistic reproduction of the interaction between the aerodynamic forces and all parts of the structure. On the other hand, full models have to be made to a relatively small scale to fit into the wind tunnels available, and this requires a very high degree of accuracy in manufacturing the model. Thus, it is generally expensive to use full models, and difficult to make modifications (Figure 8.14). Furthermore, scaling effects may be present.

Spring-mounted sectional models comprising a segment of the deck offer the advantage of a larger scale (typically between 1:25 and 1:100) and thereby a less demanding accuracy in manufacturing. The larger scale and the limited length of the sectional model also imply that it is relatively simple to modify the deck shape to test the effect of different configurations. This feature makes the sectional model very well suited for preliminary investigations (Figure 8.15).



**Figure 8.14** Full model of the Storebælt Bridge in the large 13.6 m wide wind tunnel at Danish Maritime Institute, Denmark



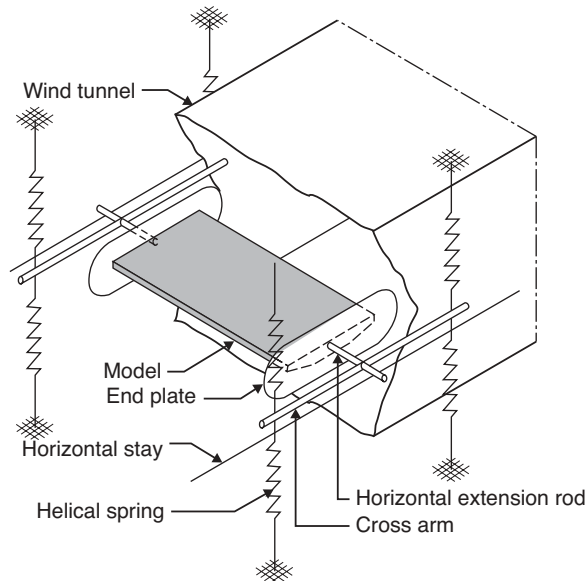


**Figure 8.15** Sectional model of the Øresund Bridge before erection in the wind tunnel

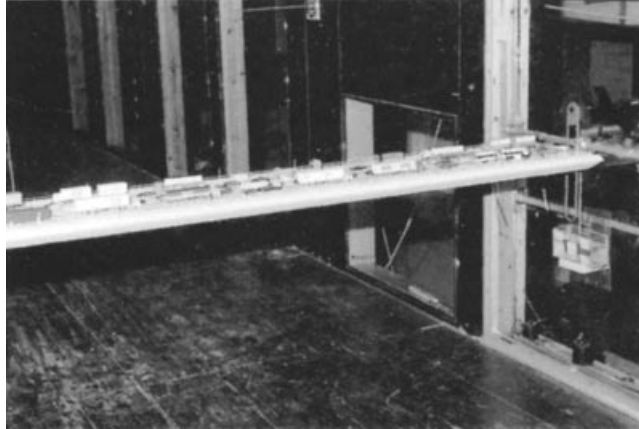
Furthermore, and more importantly, larger-scale sectional models are less prone to aerodynamic scale effects, such as Reynolds number effects.

The sectional model is manufactured with extension rods penetrating the side plates of the wind tunnel. Outside the tunnel the extension rods are supported vertically and torsionally by a system of helical springs through cross arms, and horizontally by stays, as illustrated in Figures 8.16 and 8.17.

Today, the sectional model is generally tested in both a smooth and turbulent airflow. The results obtained with the smooth airflow will in most cases be on the safe side for predicting the occurrence of aeroelastic instabilities. This is illustrated in Figure 8.18 (from [78.7]) showing results from comparative tests on a full model and a sectional model of the Lion's Gate Bridge in Canada.



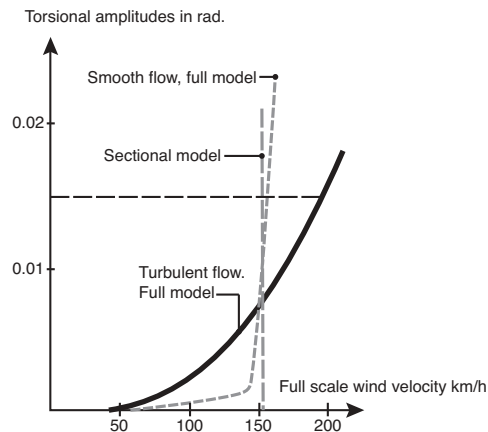
**Figure 8.16** Suspension of sectional model in wind tunnel on passive-dynamic test rig



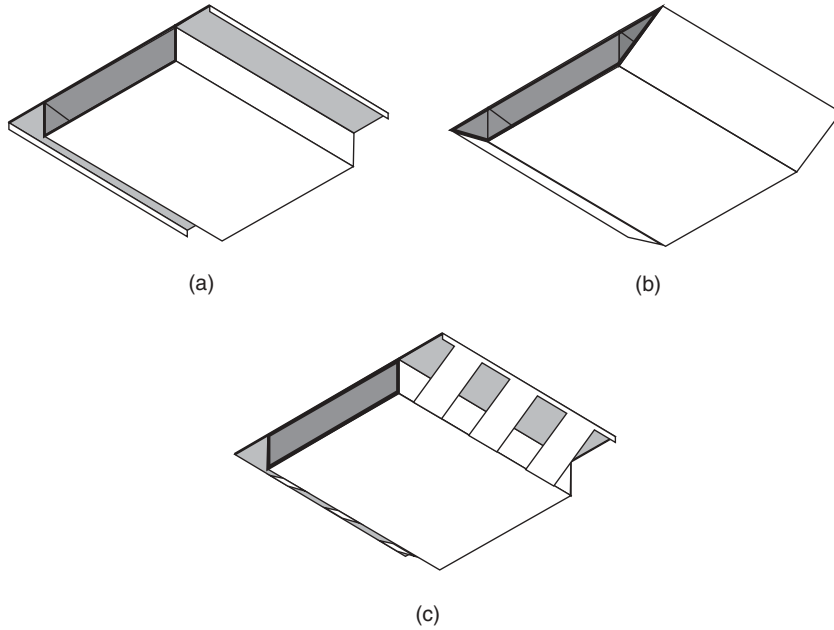
**Figure 8.17** Sectional model in the boundary layer wind tunnel at Danish Maritime Institute, Denmark

Based on the tests in the smooth flow of both the full and the sectional models, the prediction of the critical wind velocity (converted to full scale) would be approximately 150 km/h, but in turbulent flow the torsional deflection only reached 0.015 rad for a wind velocity of 195 km/h. On the other hand, in turbulent flow the oscillations were larger than in smooth flow for wind velocities in the range 30–150 km/h. However, it should be emphasized that the results illustrated in Figure 8.18 only apply to the particular bridge, so that quite a different behaviour might be experienced with other deck shapes and cable systems.

In the comparison between full and sectional models it should also be remembered that the system damping due to interaction between global and local oscillations in the cable system (as found e.g. in multi-cable fan systems) cannot be reproduced correctly in tests with sectional models. Consequently, in these cases the results of the sectional model tests might further underestimate the aeroelastic stability of the real structure.



**Figure 8.18** Torsional response of full model in smooth and turbulent flow, and of sectional model



**Figure 8.19** Three models tested during design of the Strømstein Bridge, Stavanger

In any case, wind tunnel tests with models of different configurations can often lead to results that could hardly be predicted theoretically. Thus, Figure 8.19 shows three of the models tested during the design process for a minor cable stayed bridge in Norway [75.1].

In configuration (a) the cross section consists of a rectangular box with a deck overhang, whereas configuration (b) is characterized by having inclined outer webs giving a more streamlined shape. Configuration (c) is a mixture between (a) and (b) as the inclined webs are discontinuous and only covering 33% or 50% (both values tested) of the total length. Immediately it would probably be anticipated that the best results were obtained with configuration (b) having the cleanest and most streamlined shape. However, the tests showed that configuration (c) had the most favourable vertical response, whereas all the configurations became unstable due to a torsional response of the catastrophic type. It was, therefore, essential to achieve a critical wind velocity considerably above those to be found at the actual construction site.

Finally, when scaling a bridge for wind tunnel testing, it is important to choose the correct type of scaling. Unfortunately, not all physical quantities can be appropriately scaled simultaneously and so the most important properties must take precedence in the choice of scaling. For sectional model testing, simple *length* and *velocity scaling* is often sufficient. The length and velocity scales are defined as:

$$\beta_L = \frac{D_m}{D_P} \quad \text{and} \quad \beta_V = \frac{U_m}{U_P} \quad (8.42)$$

where  $D_m$  and  $D_P$  are characteristic dimensions of the model and prototype, and  $U_m$  and  $U_P$  are the model scale and full-scale wind velocities. Based on this, it can be understood that the *frequency scale* will be:

$$\beta_f = \frac{\beta_V}{\beta_L} \quad (8.43)$$

with the *time scale* being the inverse of this.

For full cable supported bridge models, in which gravitational effects are important, length combined with velocity scaling is no longer appropriate. Here appropriate *gravitational scaling* together with Froude number similitude is employed, so that:

$$\frac{\beta_V^2}{\beta_L \beta_g} = 1 \quad (8.44)$$

where  $\beta_g$  is the gravitational scaling that in most cases will unavoidably be equal to 1. Consequently:

$$\beta_V = \sqrt{\beta_L} \quad (8.45)$$

This is often appropriate, as large enough wind tunnels to accommodate full bridge models, often operate with lower wind velocities. A bridge tested at 1:250 scale, will have a velocity scaling of approximately 1:16. If the critical flutter velocity is expected to be at 80 m/s full-scale, then the scaled critical flutter velocity will be at 5m/s. It should be remembered that, although bridge frequencies will be scaled, accelerations will not be. This allows for the direct measurement of expected full-scale accelerations during the tests.

### 8.2.6 During construction

Although most efforts in the determination of the effects of wind on the response of bridge structures are directed towards completed bridges, provisions must be made for the avoidance of excessive vibrations or aeroelastic instabilities of a catastrophic nature during construction.

Partially completed bridge girders can be extremely vulnerable to wind-induced vibrations. The main reason for this is the lack of torsional continuity of the girder before completion. Earlier, when examining the critical flutter velocity of an airfoil, it became apparent that it is desirable for a bridge girder's torsional and vertical frequencies to have a ratio greater than 2:1. For most cable supported bridges, vertical frequencies do not vary much during and after construction, as the girder's vertical stiffness is derived predominantly from the cable system. This is particularly true of suspension bridges. In contrast, a large percentage of the torsional stiffness comes from the girder itself. Consequently, the girder's torsional stiffness might be expected to increase by a factor of 2 or more from the beginning of construction until the end. This often leaves vertical and torsional frequencies dangerously close to each other during construction. The effect can be understood by examining the progression of first vertical and torsional frequencies of the Humber Bridge as a function of completed girder erection in Figure 8.20.

To increase the girder's critical wind velocities during construction of the Humber Bridge, adjustable water ballasts were placed on either side of the girder. When high winds were recorded and there was concern for the stability of the girder,

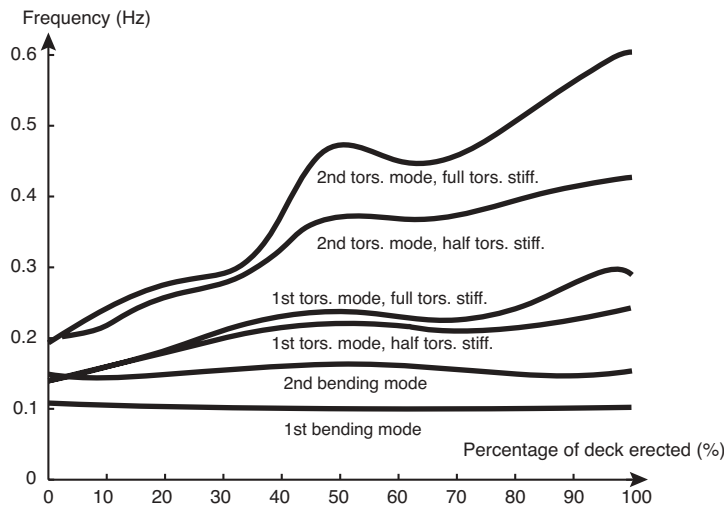
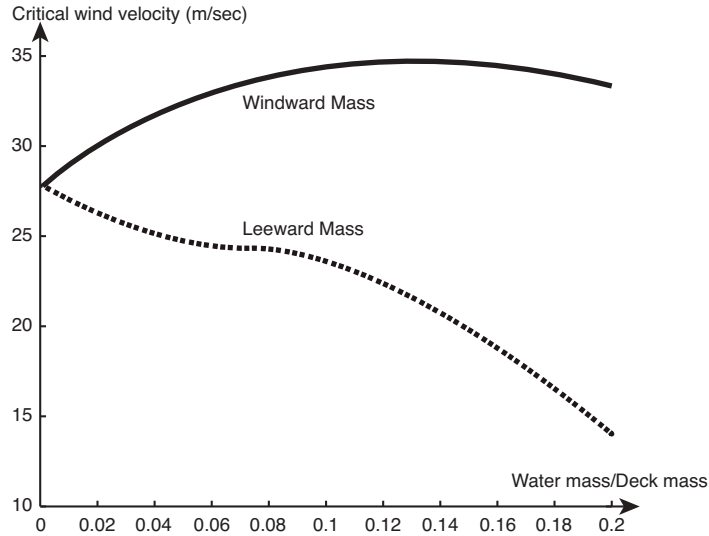


Figure 8.20 Evolution of the vertical and torsional frequencies of the Humber Bridge during girder erection. [92.15]



**Figure 8.21** Girder critical wind velocity as a function of water ballast for the Humber Bridge during construction [92.15]

ballasts on the windward side of the girder were filled. The effect of the ballast on the critical wind velocity as a function of water mass to deck mass ratio can be seen in Figure 8.21.

For the Storebælt Bridge, the effect of varying the construction scheme was also examined. It was found that erecting the girder at the pylons, while also erecting at midspan (Figure 8.22 (top)), helped to increase the critical wind velocity. This was achieved through the added stiffness in the main suspension cables due to the favorable distribution of mass. Critical wind velocities were increased from 35 m/s for the traditional erection scheme, where the girder is erected from the centre outwards (Figure 8.22 (bottom)), to 43 m/s for the simultaneous erection. When 4% of ballast was added to the edges of the girder, the critical wind velocity increased to 50 m/s. Ultimately, construction issues outweighed the aerodynamic benefits of the alternative scheme and so Erection Scheme B was applied.

### 8.2.7 Effects of vehicles

The aerodynamic properties are often influenced unfavourably by the presence of vehicles on the bridge deck. Whether this constitutes a real problem depends on the precautions taken during extreme wind conditions. Thus, it is a common procedure to close the larger bridges when the wind velocity reaches a certain magnitude (e.g. a cross-wind of 25 m/s), and under extreme wind (such as typhoons) the bridge will consequently be empty.

During wind tunnel tests for the Parana Bridges it was found that a flaring, as shown in Figure 8.23(a), had a very favourable effect on the aerodynamic behaviour of the empty bridge, whereas this measure had no effect when a train was placed on the bridge deck. In this condition solution (b) with a slightly inclined screen above the train had a more favourable effect. However, the inclined screen was never added.

### 8.2.8 Pylon aerodynamics

Wind-induced oscillations of bridge pylons are not uncommon, but tend to occur predominately during the construction phase, when the added bending and torsional stiffness from the cable system is not present.

One of the earliest reported examples is that of the Firth of Forth Road Bridge. During construction, the steel double-columned pylon oscillated on several occasions due to vortex-shedding. The problem was solved when the pylons were temporarily fitted with friction dampers until the main cable had been installed.

Free-standing steel pylons are particularly susceptible to wind-induced oscillations, due to the very low levels of inherent structural damping and mass. In Japan, where steel is used almost exclusively in the construction of bridge pylons,

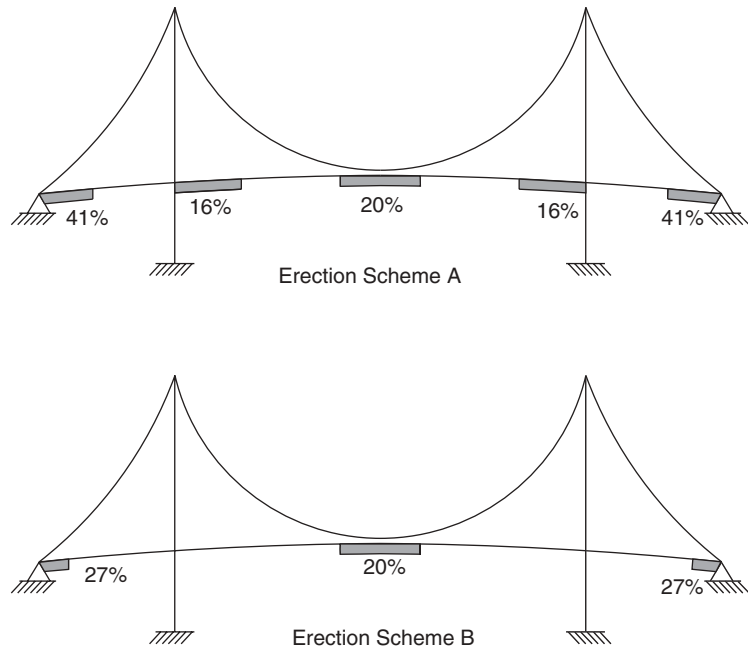


Figure 8.22 Erection schemes considered for the Storebælt Bridge [92.13]

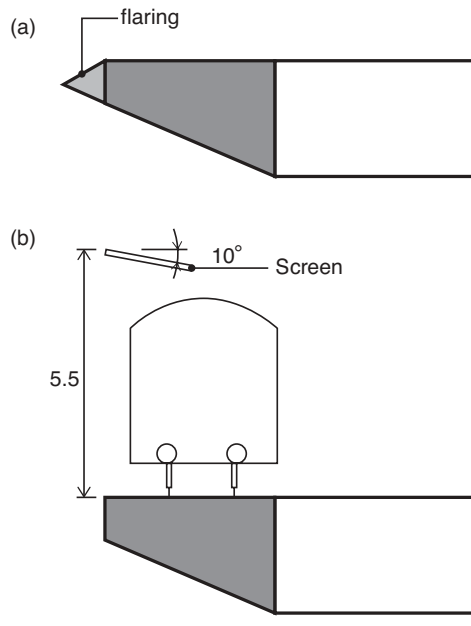
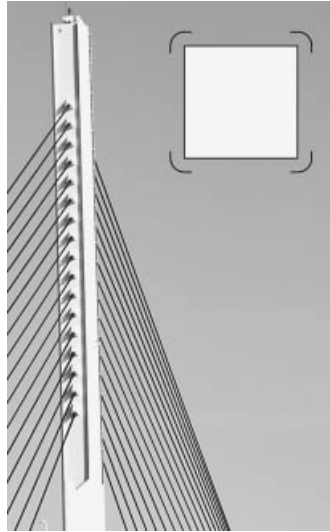


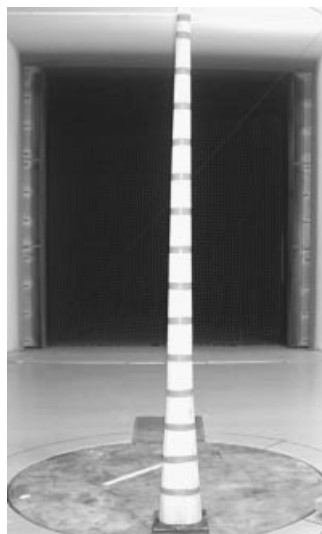
Figure 8.23 Modifications tested to improve the aerodynamic properties of the Parana Bridges



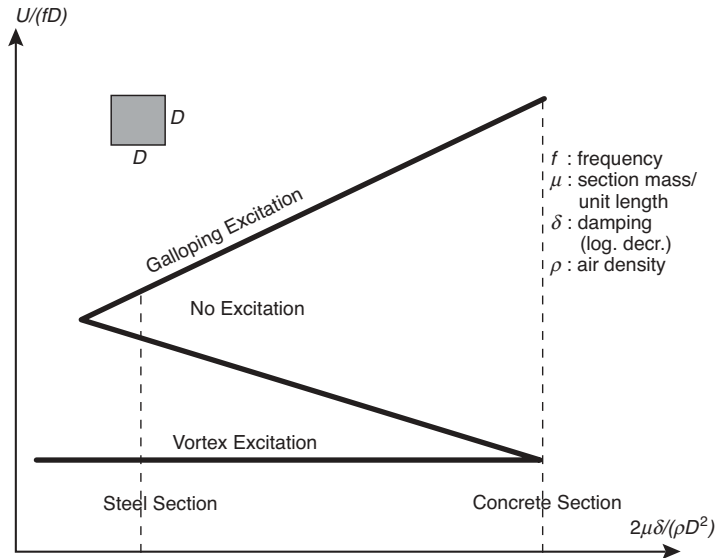
**Figure 8.24** Katsushika Harp Bridge pylon guide vanes with illustration of pylon cross section (Photo credit Ykanazawa)

numerous mitigation measures have been adopted for the avoidance of oscillations due to vortex-shedding or galloping. These include pylon shape modifications, guide vanes and dampers. Figure 8.24 shows the guide vanes added to the Katsushika Harp Bridge pylons to avoid wind-induced oscillations.

For larger cable supported bridges, free-standing pylons are tested at scale at appropriate wind-tunnel facilities. The results of these tests are generally accurate, as pylons are normally sharp-edged, allowing for the avoidance of Reynolds number effects when scaled. The testing of some pylons can be problematic, though. For the Stonecutters Bridge in Hong Kong, wind tunnel tests were undertaken on the pylon at a scale ratio of 1:100, to minimize the uncertainties involved in the testing of rounded sections (Figure 8.25). Fortunately, most rounded pylons are tapered towards the top, making it



**Figure 8.25** 1:100 scale tests of the Stonecutters Bridge pylon at the Velux Wind Tunnel Facility, Denmark (Photo credit Hong Kong Highways Department)



**Figure 8.26** Aerodynamic stability of squared pylons as a function of reduced velocity and the mass/damping parameter [92.2]

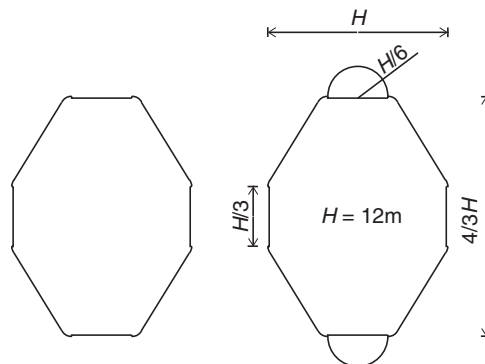
difficult for the wind to find a sufficiently long correlation length to generate large enough excitation forces. An added benefit for tall pylons is that the wind will normally vary significantly in velocity over height.

Figure 8.26 presents a generic aerodynamic stability diagram for square sectioned steel and concrete pylons, as a function of reduced velocity and the mass/damping parameter [92.2].

Scaled wind-tunnel tests undertaken on the proposed steel pylons for the Messina Straight Bridge showed a tendency for vortex-shedding oscillations at approximately 12 m/s during construction and then at 57 m/s, after the installation of the main suspension cables. To minimize the propensity for oscillations, added screens mainly on both sides of pylon perpendicular to the bridge axis were proposed, as viewed in Figure 8.27.

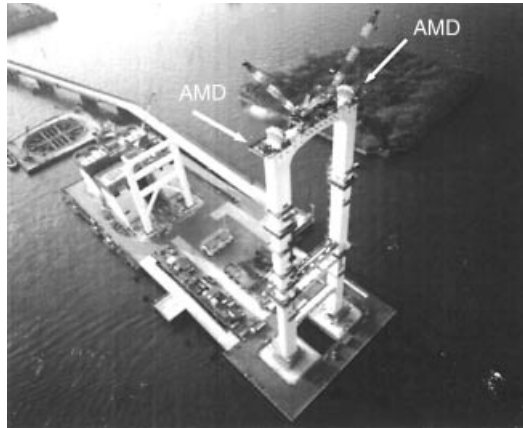
### 8.2.9 Vibration control

Wind tunnel tests and theoretical evaluations of the aerodynamic stability of decks and pylons do not always reveal a propensity for wind-induced oscillations. Furthermore, structural properties, such as damping and frequencies, are not always easily approximated before the completion of a bridge's construction. Even when the propensity for oscillations has been identified, aerodynamic shaping of the deck or pylon cannot always wholly eliminate them. In this case, traditional mechanical vibration control systems or guide vanes can be employed.



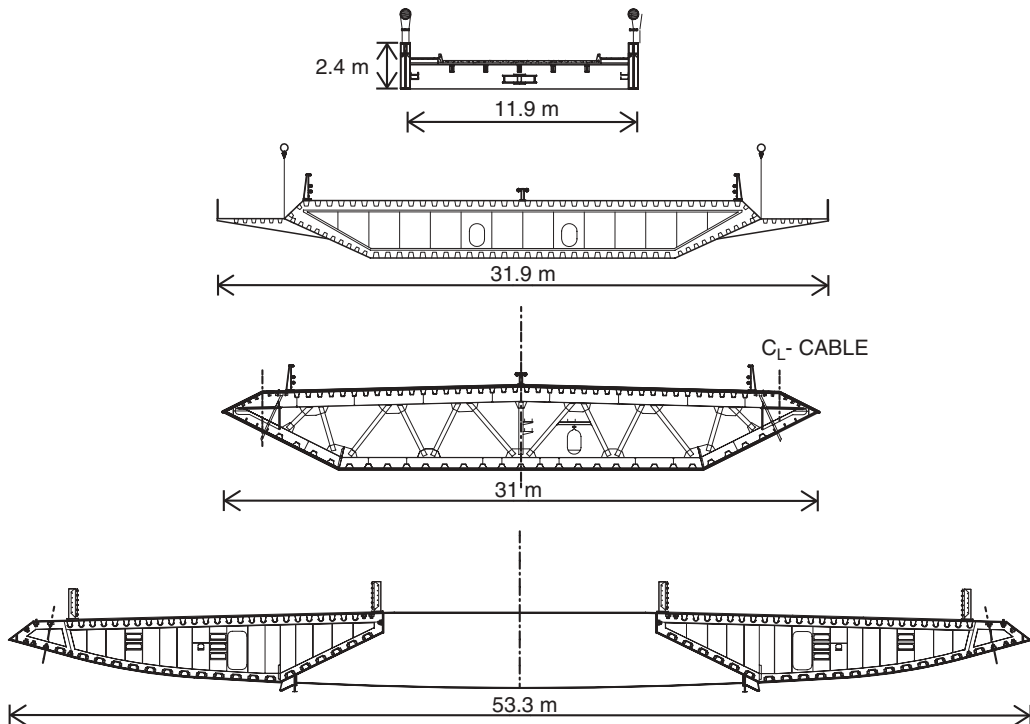
**Figure 8.27** Proposed vortex-shedding retarding screens for the Messina Straight Bridge [09.1]





**Figure 8.28** Tokyo Metropolitan Rainbow Bridge with actively controlled pylons. Active Mass Dampers (AMD) at pylon top outer edge (Photo credit Y. Fujino)

Vibration control systems are passive, semi-active or active in nature. They can be of the relative displacement or of the inertial type. For wind-induced vibrations, passive inertial systems are preferred, due to their reliability and low cost. Nevertheless, active inertial systems have been employed extensively in Japan. Ten of Japan's most recent cable supported bridges have active pylon control, including Akashi-Kaikyo. Tokyo's Rainbow Bridge was the first to employ active pylon control in 1991 to counteract wind-induced vibrations (Figure 8.28).

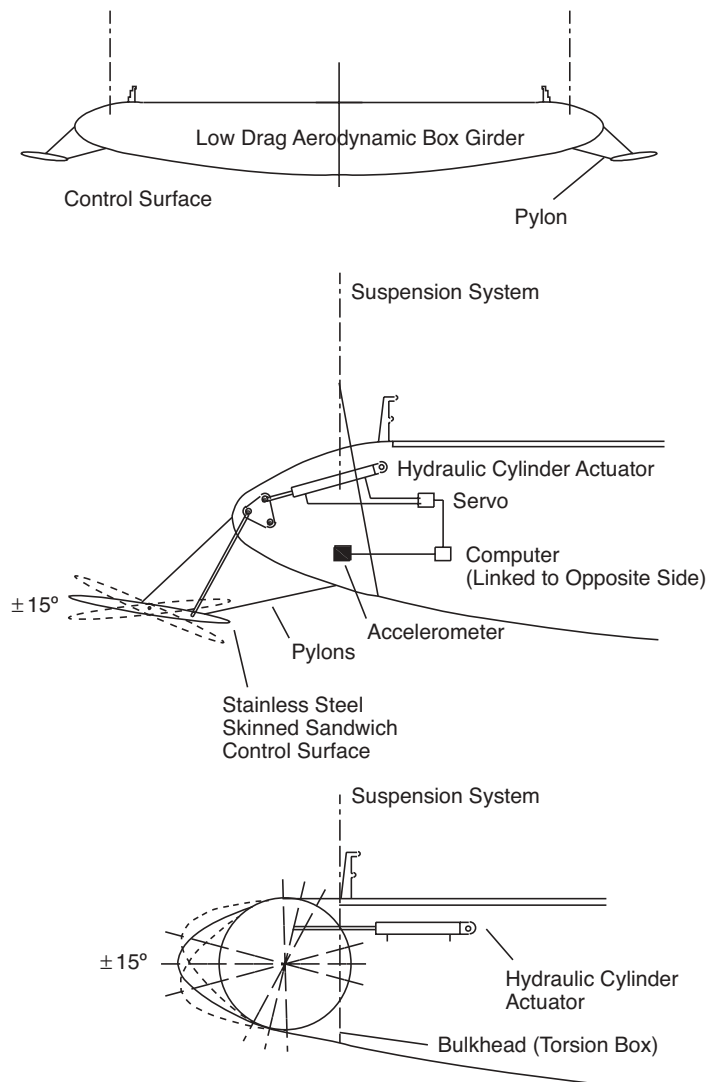


**Figure 8.29** Bridge girder evolution. (Top to bottom) Tacoma Narrows Bridge (1940), Severn Bridge (1966), Storebælt Bridge (1998) and Stonecutters Bridge, 2009 (Courtesy of COWI)

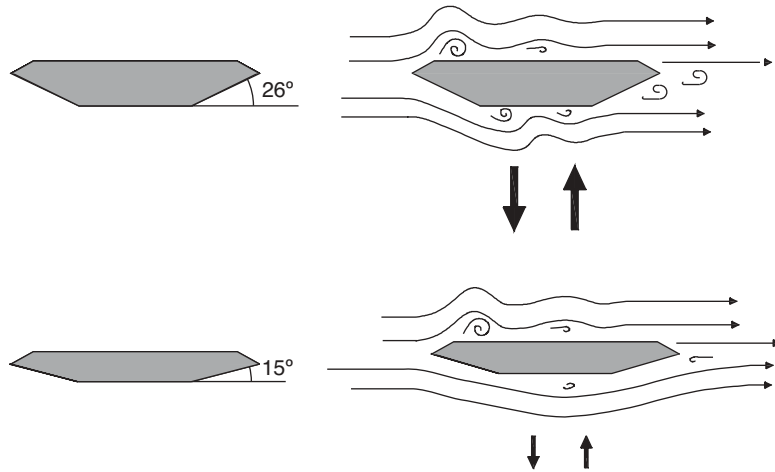
### 8.2.10 Future trends

Since the Tacoma Narrows Bridge collapse, bridge girder design has evolved, with an emphasis on aerodynamic stability. In the past few decades, several innovative design concepts for improved aerodynamic stability of bridges have emerged. In the late 1980s, British bridge engineer William Brown advocated the use of vented box girders for increased aerodynamic stability. Wind-tunnel verifications of his concept lead to the current design proposal for the 3,300 m Messina Bridge Crossing. Furthermore, several split box girder bridges with aerodynamic venting have recently been constructed. Hong Kong's 1018 m long Stonecutters Bridge is one such example. The four bridge girders of Figure 8.29 clearly show the evolution from Tacoma Narrows to Stonecutters.

The use of active control surfaces attached to the bridge deck to increase critical wind velocities has been proposed [92.2]. Due to their expense and complexity, they have not been implemented yet, but might be unavoidable for ultra-long bridge spans in future (Figure 8.30).



**Figure 8.30** Proposed active control surfaces for increased aeroelastic stability of bridge girders [92.2]



**Figure 8.31** Fine-tuning of leading edge angle for the elimination of vortex-shedding (Photo credit Allan Larsen)

More recently, a simpler and more cost effective means of improving bridge girder aerodynamic performance by means of shape fine-tuning has been proposed [09.2]. Wind tunnel tests of several deck shapes have shown that vortex-induced vibrations could be avoided without the traditional recourse to guide vanes. During tests in which five decks with bottom leading edge angles of between 12–26 degrees were tested (Figure 8.31), it was found that vortex-shedding was eliminated for a leading edge angle of 15 degrees.

## 8.3 Cables

### 8.3.1 Introduction

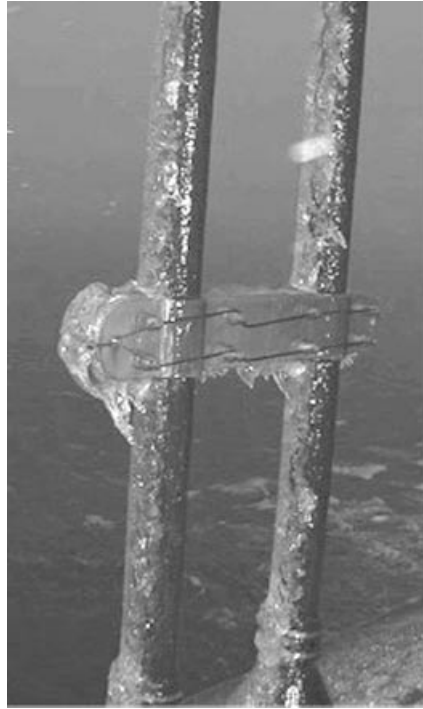
During the 1980s, a significant number of reported incidences of cable vibrations on both suspension and cable stayed bridges emerged. This period coincided with a large proliferation of cable supported bridges worldwide. Furthermore, the spans of these bridges were being pushed to new limits, leading to a natural growth in cable lengths. Initially, the causes of the vibrations were unknown, but it became increasingly apparent that most of them were being instigated by the wind or a combination of wind and rain. In some cases, the presence of sleet or ice was reported. The reports led to a significant research effort internationally, with the goal of understanding the vibration mechanisms.

The origins of the vibrations are now largely understood, although the exact mechanisms are still being studied. The vibrations can now broadly be grouped into those generated by the wind and those resulting from the loading of the bridge deck or pylons.

The vibrations resulting from the movement of the deck or pylons are often referred to as being ‘parametrically-induced’. This phrasing can be considered to be a misnomer, as it refers specifically to the case where excitation in the cable is brought about through a precise parameter combination of forcing frequency and cable natural frequency. In most cases, though, there is no independent bridge cable frequency, as the cable, deck and pylons are coupled in global bridge modes, making these precise parameter combinations unlikely. Bridge deck or pylon to cable mass ratios must be in the order of 500:1 or greater for independent frequencies to arise [05.2]. This will only occur on bridges with very heavy girders, as e.g. the Øresund Bridge. Nevertheless, cable vibrations resulting from girder or pylon excitation can be significant. Wind-induced cable vibrations can occur as a result of buffeting or, rarely, vortex-shedding. In most cases though, the larger amplitude vibrations occur due to dry galloping or galloping as a result of the presence of rain, sleet or ice.

### 8.3.2 Incidences of wind-induced cable vibrations

On 21 March 2001, 2 m amplitude hanger vibrations were measured on the Storebælt Bridge in Denmark [07.1]. This came as a surprise to many, as the bridge is of a similar design to the Lillebælt Bridge that had been built nearly 30 years earlier and for which until then there had been no reported hanger vibrations of any significance. Upon closer examination, two



**Figure 8.32** Hanger thin ice accretion (Courtesy of Storebælt Bridge A/S)

intriguing observations could be made. First, the vibrations occurred predominantly for the hangers with longer lengths than the hangers found on the Little Belt Bridge and, second, the vibrations coincided with conditions that on occasion generate thin films of ice on the hangers (Figure 8.32). Investigations narrowed the cause down to a change of cross sectional shape due to icing [09.3]. The change in shape causes significant changes in the aerodynamic force coefficients for specific wind-angles of attack. Naturally, longer cables are more susceptible to these vibrations, due to their greater wind exposure and lower damping values.

The hanger vibrations on the Storebælt Bridge are not unique though, as numerous other suspension bridges have experienced similar vibrations. Even so, the number of reported incidences on these bridges is much smaller than the number of reported incidences on cable stayed bridges over the past 30 years. Some well-known examples are summarized in Table 8.3.

From Table 8.3, one can see that most large amplitude cable vibrations result from dry galloping or rain- or wind-induced galloping. Rain-wind-induced cable vibrations most likely account for 95% of the reported and measured cases [03.1].

### 8.3.3 Rain-wind-induced vibrations

The exact mechanism involved in rain-wind-induced cable vibrations is not well understood, although there is enough experimental and observational evidence to suggest that the creation of one or two water rivulets along a significant length of the cable is responsible for an apparent modification in cable shape, leading to the initiation of galloping.

One of the first cases of rain-wind-induced bridge cable vibrations was reported in 1986, after observations of the mechanism on the Meiko-Nishi Bridge [86.03]. During the observations it was found that the wind-induced cable vibrations always occurred in the presence of rain and for relatively moderate wind velocities between 5–15 m/s. Furthermore, the cable oscillations did not occur in the cable's first mode of vibration, but at modes that had frequencies in the range of 1–3 Hz. Wind tunnel tests showed that the vibrations only occur when the cable is declining in the direction of the wind, so that the main water rivulet is generated on the 'top-side' of the cable.

**Table 8.3** Examples of cable stayed bridges with reported wind-induced cable vibrations

| Bridge            | Location    | Main span (m) | Excitation mechanism | Max amplitude (m) |
|-------------------|-------------|---------------|----------------------|-------------------|
| Normandy          | France      | 856           | vortex-shedding      | 1.0               |
| Øresund           | Denmark     | 490           | wet galloping        | 3.0               |
| Second Severn     | UK          | 456           | dry/wet galloping    | 1.5               |
| Kap Shui Mun      | Hong Kong   | 430           | wet galloping        | 1.5               |
| Meiko-Nishi       | Japan       | 406           | wet galloping        | 0.6               |
| Fred Hartman      | USA         | 381           | dry/wet galloping    | 2.0               |
| Tenpozan          | Japan       | 350           | wet galloping        | 1.0               |
| Dongting          | China       | 310           | wet galloping        | N/A               |
| Franjo Tudjman    | Croatia     | 304           | wet galloping        | 2.0               |
| Erasmus           | Netherlands | 284           | wet galloping        | 0.7               |
| Veterans Memorial | USA         | 195           | wet galloping        | 0.3               |
| Ponte del Mare    | Italy       | 172           | N/A                  | 2.0               |

Subsequent reports have confirmed to a large extent the initial observations, although there have been a few reports of vibrations generated on cables inclining towards the direction of the wind. Currently it is believed that rain-wind-induced vibrations can occur for wind velocities anywhere from 5–18 m/s, mainly on smooth lightly-damped cables declining in the direction of the wind and for modal frequencies in the range of 0.5–3.3 Hz. Wind velocities below the reported range are believed not to produce enough energy to excite a cable, while velocities above 18 m/s are too high for a rain rivulet to be sustained. Water rivulets are generally only sustainable for light to moderate rain fall in the range of 1–10 mm/h, although vibrations have been reported for greater values of rainfall. Finally, the relative yaw angles for which a cable is most susceptible to these vibrations is between 0° and 45°, where the cable relative yaw angle,  $\gamma$ , is defined as:

$$\gamma = \arcsin(\cos \phi \sin \beta) \quad (8.46)$$

where  $\beta$  is the horizontal yaw angle and  $\phi$  the stay cable angle of inclination, as shown in Figure 8.33.

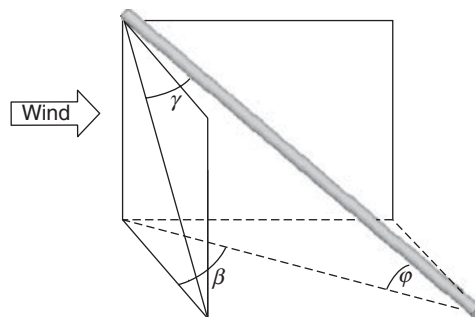
A graphical representation of a cross section of a cable with formed upper water rivulet is shown in Figure 8.34.

### 8.3.4 Dry galloping

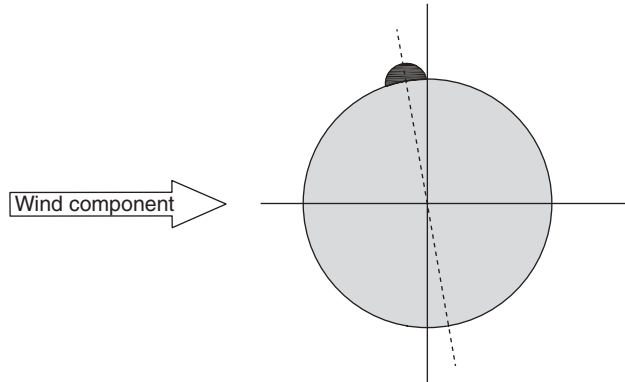
When wind is flowing perpendicular to a circular cylinder, the cylinder will experience a change in its drag coefficient with increasing wind velocity. Figure 8.34 shows this change, as a function of Reynolds number, defined as:

$$\text{Re} = \frac{UD}{\nu} \quad (8.47)$$

where  $D$  is the diameter of the cylinder and  $\nu$  is the kinematic viscosity of air (approximately  $1.5 \times 10^{-5} \text{ m}^2/\text{s}$  at 20 °C). The Reynolds number is a non-dimensional number that represents the ratio of fluid inertial forces to



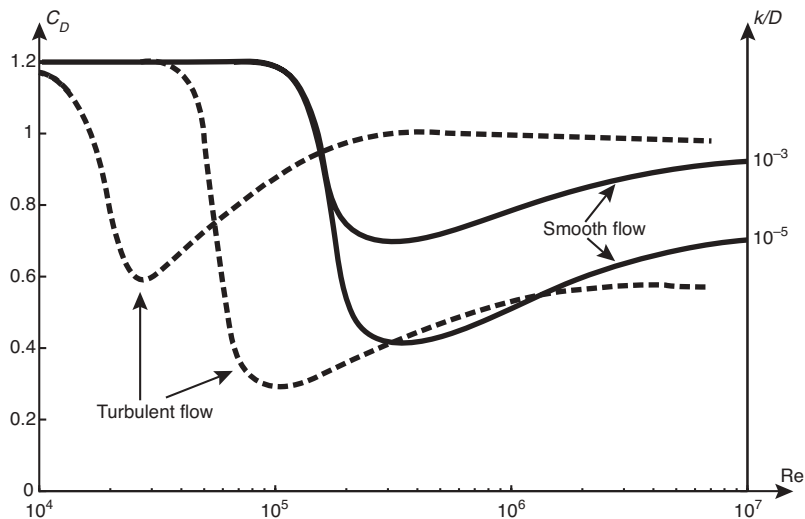
**Figure 8.33** Definition of cable relative yaw angle  $\gamma$



**Figure 8.34** Cross section of an inclined bridge cable with upper water rivulet

viscous forces. In Figure 8.35, several regions are defined. Each region is broadly characterized by a specific fluid behaviour, depending on this ratio. A large drop in drag, often referred to as *drag-crisis*, characterizes the ‘critical’ Reynolds number region. For smooth circular cylinders in laminar flow, the critical Reynolds number is in the region between  $1 \times 10^5$  and  $5 \times 10^5$ . In this region, several fluid flow transitions occur. It has been observed that lightly damped cylindrical structures exposed to wind and suffering from drag-crisis can vibrate violently. The drag-crisis leads to fluctuations in aerodynamic forces that can feed energy into the structure resulting in galloping vibrations. This form of galloping is otherwise known as *drag instability*. As these forces are for the most part velocity-dependent, they are often considered to be equivalent to ‘negative aerodynamic damping’. Lighting columns, traffic light poles, and cylindrical telecommunication towers are all examples of structures that can experience this type of vibration.

In the case of the inclined bridge stay-cable, the potential for a similar form of galloping is increased, as the cable can also experience a significant variation in lift coefficient with Reynolds number. This variation is due to the apparent cable shape ‘seen’ by the wind for varying relative cable yaw angles, an asymmetric flow that is often generated during flow transitions and the introduction of an axial flow along the cable due to its inclination.



**Figure 8.35** Cylinder drag coefficient as a function of  $Re$  and roughness  $k/D$ . [07.2]

If the reduced velocity,  $U_R = U/fD$ , is above 20, then it can be assumed that the motion of a bluff body in a fluidic medium can be analyzed in a ‘quasi-steady’ manner, i.e. the drag and lift forces are not altered by the frequency of vibration [11.1]. Therefore, for most cable vibrations at higher Reynolds numbers, a quasi-steady analysis of the motion could be considered reasonable, as reduced velocities are usually much higher.

Although no actual reports of full-scale dry galloping have ever been confirmed, several damaging events have been attributed to this phenomenon. It has been shown that dry galloping instability of a cable can be predicted through use of quasi-steady theory [06.1]. In its general form, an eigenvalue problem must be numerically solved to determine the level of negative aerodynamic damping or the necessary amount of structural damping to achieve aerodynamic stability. For two extreme cases, though, an analytical solution exists so that the galloping stability criteria can be determined readily. When the cable has significant sag, the first in-plane and out-of-plane frequencies are relatively far apart. In this case, they can be assumed to be independent and the condition for dynamic stability can be written as:

$$Z_s > \frac{-\text{Re}}{8\pi} \left[ g(C_D)\cos^2\theta - g(C_L)\sin\theta\cos\theta + \frac{1}{\sin\gamma} (C_D - C'_D\sin\theta\cos\theta + C'_L\sin^2\theta) \right] \quad (8.48)$$

$Z_s$  is a non-dimensional measure of structural damping defined as:

$$Z_s = \frac{\zeta_s \mu f_n}{v_d} \quad (8.49)$$

where  $\zeta_s$  is the structural damping ratio,  $\mu$  is the cable mass per unit length,  $f_n$  is the cable natural frequency and  $v_d$  is the dynamic viscosity. Furthermore:

$$g(C_F) = C_F \left( 2\sin\gamma - \frac{1}{\sin\gamma} \right) + \frac{\partial C_F}{\partial \text{Re}} \text{Re} \sin\gamma + \frac{\partial C_F}{\partial \gamma} \cos\gamma - \frac{\partial C_F}{\partial I_x} I_x \sin\gamma \quad (8.50)$$

$$h(C_F) = g(C_F) + \frac{2C_F}{\sin\gamma} \quad (8.51)$$

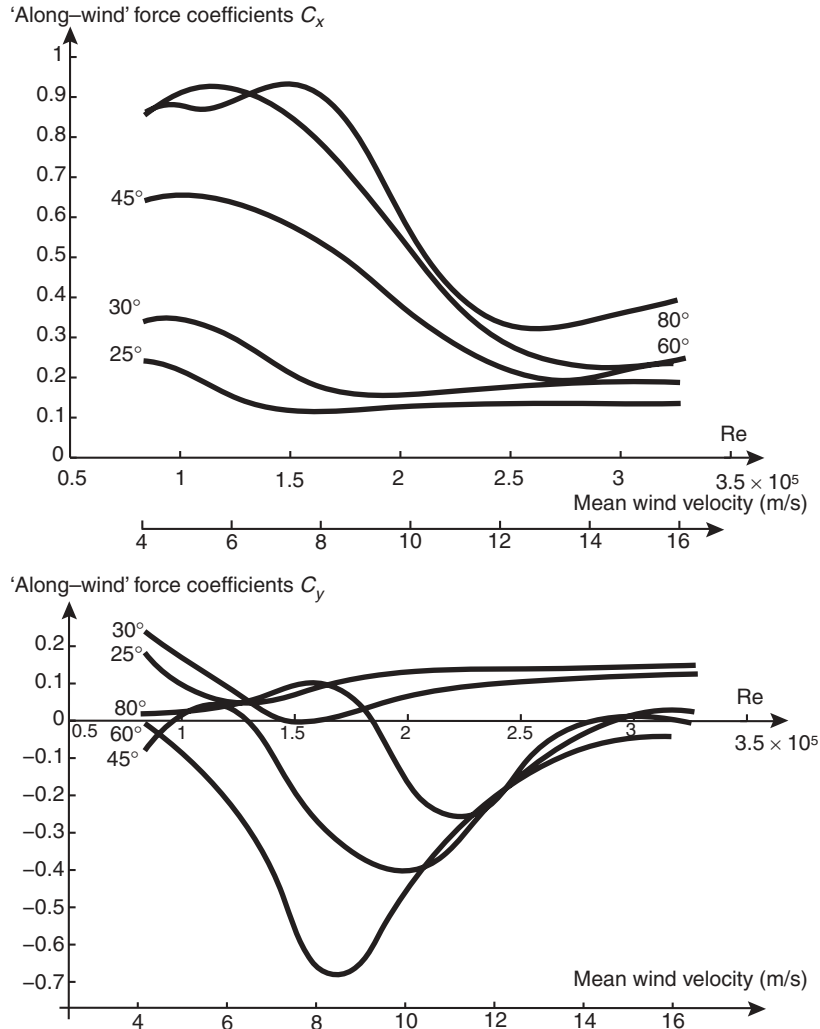
where:  $C_F = C_D$  or  $C_F = C_L$

When the cable natural frequencies are equal, the condition for dynamic stability can be written as:

$$Z_s > \frac{\text{Re}}{16\pi} \left[ - \left( h(C_D) + \frac{C'_L}{\sin\gamma} \right) + \Re \left\{ \sqrt{\left( g(C_D) - \frac{C'_L}{\sin\gamma} \right)^2 + \left( g(C_L) - \frac{C'_D}{\sin\gamma} \right)^2 - \left( h(C_L) - \frac{C'_D}{\sin\gamma} \right)^2} \right\} \right] \quad (8.52)$$

where the first derivatives are with respect to wind angle of attack  $\theta$  and  $\Re$  represents the real part of the enclosed expression.

Similar to dry galloping, rain-wind-induced cable vibrations are generally considered to be a form of galloping linked to large velocity-dependent changes in drag and/or lift coefficients of the cable with the presence of the water rivulet. In the case of the ‘wet’ cable, these changes are difficult to quantify. In the case of a dry inclined cable, these large changes are more easily quantifiable through static wind tunnel tests. Both drag and lift coefficients can be determined for varying cable relative yaw angles. The ‘along-wind’ and ‘across-wind’ force coefficients for a circular cylinder representing a bridge cable for decreasing yaw angles has been measured, as shown for selected angles in Figure 8.36.



**Figure 8.36** Selected along- and across-wind force coefficients for an inclined cable. [05.3]

Determination of the necessary damping for dynamic stability, with use of the force coefficients for an average bridge cable, shows that the particular vibrational instability can be avoided when overall damping is greater than 0.5% of critical, a value which is generally achievable on bridge cables.

### 8.3.5 Scruton number

Another non-dimensional number that is often used to evaluate the propensity of a cable to vibrate due to galloping or vortex-shedding is the Scruton number,  $Sc$ . The Scruton number is a mass-damping parameter that is often defined in terms of damping ratio as:

$$Sc_g = \frac{\mu \zeta}{\rho D^2} \quad (8.53)$$



The Scruton number is also defined in terms of the logarithmic decrement of damping,  $\Lambda \approx 2\pi\zeta$ , so that:

$$Sc_{\Lambda} = \frac{\mu\Lambda}{\rho D^2} \quad (8.54)$$

For both rain-wind-induced vibrations and dry inclined galloping, several recommendations regarding the appropriate Scruton number for the avoidance of these vibrations have been published. Both the US Federal Highway Administration (FHWA) and the Post-Tensioning Institute (PTI) recommend  $Sc_{\zeta} > 10$  for typical wind velocities and smooth cables. If aerodynamic countermeasures in the form of cable surface modifications, such as helical filets or dimples, are employed, then the recommended Scruton number is relaxed to the value of 5. In Japan, a stability limit criteria in relation to the critical wind velocity has been proposed [94.21], such that:

$$U_R \leq 14\sqrt{Sc_{\Lambda}} \quad (8.55)$$

An alternative proposal for the stability limit criteria is [95.20]:

$$U_R \leq 10(Sc_{\Lambda})^{2/3} \quad (8.56)$$

Generally, a smaller Scruton number is required for the avoidance of large amplitude vortex-shedding oscillations. The FHWA observed 'high reduced velocity' vortex-shedding vibrations on smooth cables during section model testing for  $Sc_{\zeta} < 3$ . As a result, vortex-shedding is not considered an issue, as long as a cable has this minimum Scruton number.

### 8.3.6 Wake galloping

Under special circumstances and for a narrow range of wind angles of attack, structures in the wake of another object can vibrate due to the special nature of the flow generated by the upstream object. This is commonly referred to as *wake galloping* or *wake buffeting*. On bridges, two situations in which this can occur are for the cables behind a bridge pylon and when cables are paired or bundled.

For the nearest cables behind a bridge pylon, the flow velocities of the oncoming wind can be amplified at specific wind angles of attack, while the spectrum of the oncoming flow can also be significantly altered. In special cases, a form of vortex resonance can occur, as a result of the coincidence of cable natural frequencies and pylon shedding frequencies (Figure 8.37). The velocity-dependent vortex-shedding frequency,  $f_s$ , can be determined by rewriting (8.41) so that:

$$f_s = \frac{UD}{St} \quad (8.57)$$

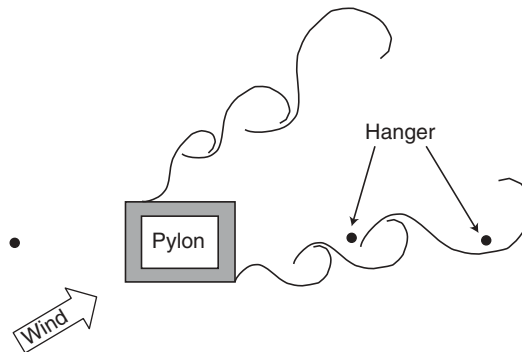
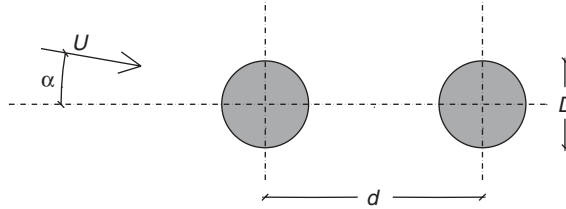


Figure 8.37 Vortex-street produced in the wake of a bridge pylon



**Figure 8.38** Bridge cable pair with critical wind angle and separation distance

where  $D$  here is the perpendicular width of the pylon with respect to the streamwise direction of the wind and  $St$  is the Strouhal number for the pylon. Even with the lack of resonance, the fluctuating changes of the wind velocities, as observed by the cables can cause a form of galloping that can be attributable to large variations of a cable's force coefficients at specific Reynolds numbers.

For cable pairs or groups, the problem is similar, with the exception of the distances and sizes of the objects. For most bridges with concentrated hanger or stay arrangements, cables are in pairs and connected with links. In a few cases, cable pairs are not linked. Cable groups, with three or more parallel cables, can be interconnected or independent.

In the case of the linked cable pair, as shown in Figure 8.38, Eurocode 1 (EC1) suggests the evaluation of several wake-induced vibration phenomena. For vortex resonance, the maximum expected vibration amplitudes will be conservatively 1.5 times the amplitudes calculated for the single cable, as long as the distance,  $d$ , between the cables is greater than one diameter and less than three diameters. EC1 outlines a detailed conservative procedure for the calculation of expected single cable vortex-shedding amplitudes. For wake galloping, the critical wind velocity at which pair galloping might be expected is defined as:

$$U_G = \frac{4\Lambda f_z \mu_T}{\rho D a_G} \quad (8.58)$$

where  $f_z$  is the cross-wind cable vibration frequency,  $\mu_T$  is the total mass per unit length of the cable pair and  $a_G$  is the galloping interference factor. The galloping interference factor takes the value of 1.5 for cable spacing,  $d$ , less than  $1.5D$ , a value of 3 for cable spacing greater than  $2.5D$  and is linearly interpolated in between. Furthermore, the critical galloping velocity should be higher than  $1.25U_m$ , where  $U_m$  is the maximum mean wind velocity calculated at the bridge height at which maximum galloping amplitudes might be expected. For the first cable mode of vibration, this would be expected to be near the cable mid-height.

For cable pair that is not linked, the critical wake galloping velocity can be estimated as:

$$U_G = 2.86 f_z D \sqrt{\frac{S c_g d}{D}} \quad (8.59)$$

The use of (8.59) is assumed valid as long as the distance between cable centres is not greater than  $3D$  and the wind angle of attack is between  $0^\circ$  and  $10^\circ$ . This does not imply that wake galloping will not occur outside of this range. On the contrary, there are two very distinct cable spacing ranges for which cable pair wake galloping has been observed. The first is  $1.5D - 4.5D$ , while the second is  $8D - 20D$ . Unlike the first range, for this second range it is only the downstream cable that usually oscillates, with the largest vibration amplitudes occurring when cable pair spacing is approximately  $10D$ . The larger range of spacing should be avoided and commonly is, as it is often impractical to create large cable pair spacing on actual bridges.

### 8.3.7 Aerodynamic countermeasures

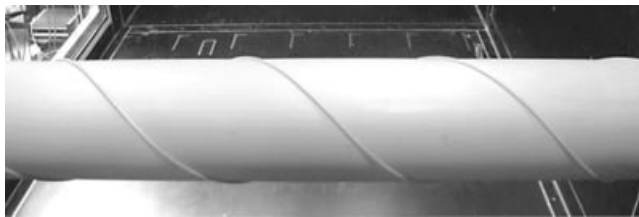
Several aerodynamic countermeasures, mainly in the form of cable HDPE surface modifications, have been proposed to avoid rain-wind-induced and vortex-shedding oscillations. The surface modification used predominantly in Europe and the Americas is the single or double helical fillet, as shown in Figure 8.39. In China and Japan, longitudinal channelling or protuberances and dimples or bumps are preferred.



**Figure 8.39** Cable surface modifications for the avoidance of wind-induced vibrations

The effectiveness of the helical filet in suppressing rain-wind-induced vibrations was reported after full-scale section model tests conducted in the large Climatic Wind Tunnel at CSTB [95.21]. The helix acts in disrupting the formation of the longitudinal water rivulet, which is generally assumed responsible for the observed aerodynamic instability. A double helix, 2 mm wide and 1.3 mm high, with a pitch length of 0.6 m was eventually applied on the Normandy Bridge. Furthermore, a drop in the supercritical drag coefficient to 0.64 was found, indicating a significant improvement in relation to the plain cylinder. An interesting observation from the tests at CSTB is that the rain-wind-induced instability was only seen when soot was rubbed onto the surface of the tubing. This was also confirmed in tests undertaken by the Danish Maritime Institute (now Force Technology) for the Øresund Bridge cables. HDPE tubing with single or double helixes has now been used on numerous cable stayed bridges, including the Øresund Bridge and the Owensboro and Maysville Bridges in the US. An example of a double-helixed HDPE stay tube can be seen in Figure 8.40.

Numerous tests have been performed on HDPE tubes with dimples and it has been found that specific pattern-indented surfaces are capable of suppressing rain-wind induced vibrations, while also stabilizing flow separation [03.2]. Furthermore, the same patterns have been found to reduce the cylinder drag coefficient to 0.61, although a value of 0.7 is used for design purposes. Here, the supercritical flow state is reached at a Reynolds number of  $0.5 \times 10^4$ , where the drag remains near constant through to the transcritical region. The final pattern used on both the Sutong and Stonecutters Bridges can be seen in Figure 8.41.



**Figure 8.40** Double-helixed HDPE stay tube



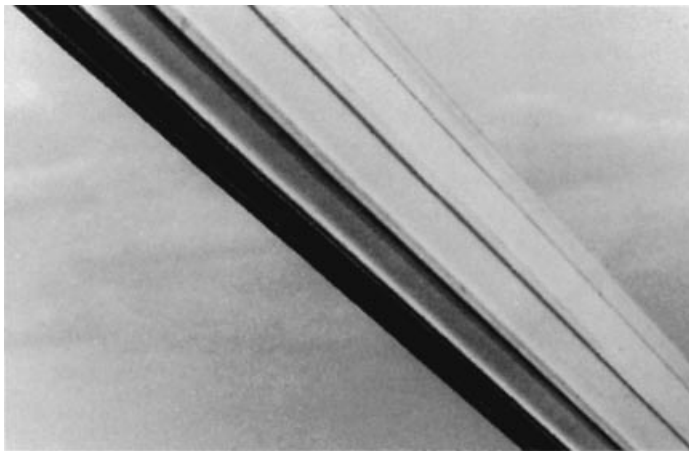
**Figure 8.41** Pattern-indentated HDPE tubing used on Sutong and Stonecutters Bridges

Cables with longitudinal grooving or protuberances have also been found to be able to suppress rain-wind-induced vibrations, although drag coefficients on cables with these countermeasures are generally higher than those of the plain cable. A HDPE tube with longitudinal protuberances, as applied on the Higashi Kobe Bridge, can be seen in Figure 8.42.

### 8.3.8 Mechanical damping

As the inherent structural damping in a cable is very low (in the order of 0.01–0.2% of critical), added dampers are often employed to aid in the suppression of wind-induced vibrations. The damper configurations include point viscous and friction dampers, anchorage neoprene and silicon radial dampers and tuned mass dampers. Point viscous dampers have been used on the longest hangers of the Storebælt Bridge (Figure 8.43), while, in their final configuration, radial viscous anchorage dampers in combination with tuned mass dampers (on the longest stays) were used for the Øresund Bridge stays (Figure 8.44).

Tuned liquid dampers are generally difficult to implement, due to the long stroke length necessary for their unimpeded operation. Consequently most bridges fitted with dampers employ relative-displacement viscous or friction point dampers positioned at the bottom end of the cable, near the anchorages. As might be readily understood, the closer the dampers are



**Figure 8.42** HDPE tube with axial protuberances, as applied on the Higashi Kobe Bridge



**Figure 8.43** Storebælt Bridge point viscous dampers

positioned to anchorage points, the less effective they become, leading to the issue of the maximum possible added damping that can be achieved with external point dampers.

The effectiveness of a point damper placed near the anchorage of a sagging cable has been thoroughly examined [02.1]. It has been found that for Irvine parameter,  $P_{ge} \leq 1$ , a sufficiently accurate estimate of damper effectiveness can be determined assuming the cable is a taut string, as in Figure 8.45.

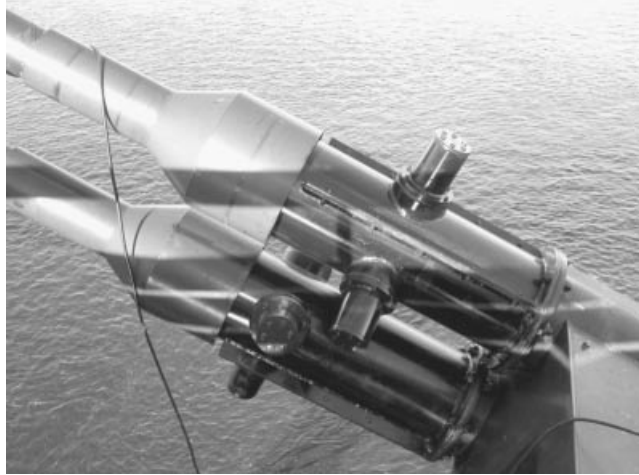
An approximate solution to the equations of motion of the cable-damper system, so that the modal damping ratio can be expressed as a function of distance of the point damper from the anchorage,  $x_d$ , leads to [00.1]:

$$\frac{\zeta_i}{x_d/l} = \frac{i\pi\eta x_d/l}{1 + (i\pi\eta x_d/l)^2} \quad (8.60)$$

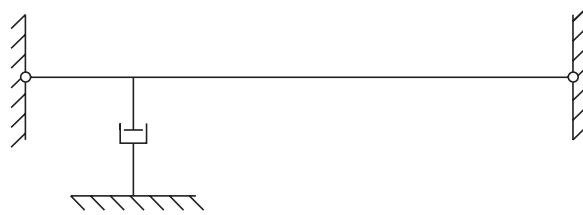
where  $l$  is the length of the cable,  $i$  is the mode number and

$$\eta = \frac{\pi c}{\mu l (2\pi f_1)} \quad (8.61)$$

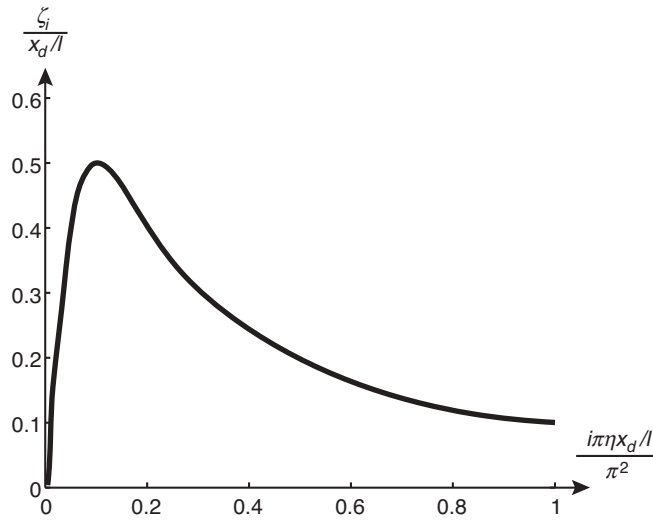
where  $c$  is the damping constant and  $f_1$  is the first natural frequency of the cable.



**Figure 8.44** Øresund Bridge anchorage viscous radial dampers (top) and tuned mass dampers (bottom) (Courtesy of Øresund Bridge A/S. Photo credit Lennart Emanuelsson)



**Figure 8.45** Taut string with point damper near support



**Figure 8.46** Universal damping curve for point damper near taut string support

Plotting (8.60) leads to the universal damping curve of Figure 8.46. From this it can be seen that the maximum achievable damping ratio is  $0.5x_d/l$ , noting that (8.60) is only valid for  $x_d/l$  values up to approximately 0.03. For values greater than this, the damping ratio is conservatively estimated, theoretically. It should also be noted that measured values of damping on site are often lower than those predicted by the universal damping curve. The reason for this may be found in the bending stiffness of the cable anchorage, which is often neglected [07.3]. Consequently, it is recommended the theoretically estimated achievable damping be halved for design purposes.

When an additional point damper is added symmetrically near the other end of the cable, the achievable damping is simply doubled.

Figure 8.47 shows the dampers that were erected on the Brotonne Bridge after it experienced severe oscillations of the stay cables. In this case, the dampers were made from ordinary shock absorbers similar to those used in automobiles. On the



**Figure 8.47** Shock absorbers erected to reduce local oscillations of the stay cables of the Brotonne Bridge

Brotonne Bridge the dampers were installed as part of a retrofit but in other cases, e.g. in the Sunshine Skyway Bridge, viscous dampers have been installed during construction and in these cases it has been possible to position the dampers more discretely inside the box girder.

### 8.3.9 Cable aerodynamic damping

It should be noted that in addition to the inherent structural damping, a bridge cable will be subject to positive aerodynamic damping outside the critical Reynolds number region. Similarly to the aerodynamic damping of the bridge deck, the along-wind and cross-wind modal aerodynamic damping of the cable per unit length will be:

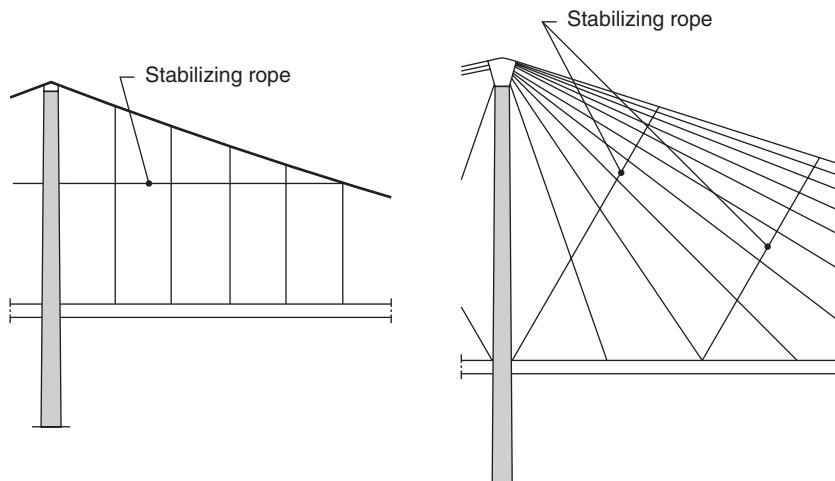
$$\zeta_{i,x}^a = \frac{\rho C_x D U_x}{4\pi f_i \mu} \quad (8.62)$$

$$\zeta_{i,z}^a = \frac{\rho C_x D U_x}{8\pi f_i \mu} \quad (8.63)$$

From (8.62) and (8.63), it can be seen that aerodynamic damping is velocity proportional and, as a consequence, increases with increasing wind velocities. This is very beneficial for the reduction of cable vibrations associated with wind buffeting at higher wind velocities, making large amplitude cable vibrations due to buffeting unlikely.

### 8.3.10 Cross ties

Another relatively successful cable vibration suppression technique involves the introduction of stabilizing ropes or *cross ties*, as shown in Figure 8.48. The cross ties are usually made of a strong fatigue-resistant material with a diameter significantly smaller than the diameter of the primary cables, so as not to noticeably influence the appearance of the total structure. Nevertheless, even with a few small diameter cross ties, the cable-deck modes of vibration can be altered drastically, as the single cable vibration length is shortened and it cannot oscillate without affecting the adjoining cables.



**Figure 8.48** Cross ties used for local cable vibration suppression





**Figure 8.49** Clamps with dampers at the connection between the main stays and the cross-lattice members on the Normandy Bridge

In most cases, this is beneficial, although there have been reports of cases for which the joining of cables with cross ties has had a negative influence on the vibrations of the bridge deck and at times have led to the previously unobserved vibration of the whole cable plane. It should be noted that the adequate design of the ties must involve the robust design of the cable-tie connectors, as they are often subject to large oscillating forces.

For the Normandy Bridge, with its very long stay cables, the stabilizing effect of the secondary ties was further increased by applying special cross-lattice members between the stays with dampers in the joints (Figure 8.49).

# 9

## Particular Issues

### 9.1 Pedestrian-Induced Vibrations

#### 9.1.1 Lateral vibrations

In recent years, there has been an ever-growing trend to design and build spectacular cable supported pedestrian bridges, serving as city landmarks and tools for urban regeneration. In June 2000, the 333 m long London Millennium Bridge, linking St Paul's Cathedral and the Tate Modern Art Gallery, was opened to pedestrian traffic (Figure 9.1). The bridge was the first to be built across the Thames in over a hundred years, leading people to flock to it on the opening day. It is estimated that up to 100,000 people crossed the bridge during the opening day celebrations, with up to 2000 people on the bridge at any one time [01.2]. Shortly after the opening, excessive lateral vibrations of the bridge were observed. The bridge was closed soon after and investigations were initiated to determine the cause of the large amplitude vibrations. The investigations led to the conclusion that the bridge vibrated due to synchronous lateral excitation (SLE), a phenomenon in which pedestrians 'synchronize' their walking motion to that of the bridge. This was not the first time that this type of pedestrian-induced vibration had been reported, though.

In 1989, the 179 m long cable-stayed Toda Park Bridge in Japan (Figure 9.2) experienced similar vibrations [93.3]. Measurements found that the bridge's first lateral frequency varied between 0.9–1.0 Hz, depending on the number of people on the bridge. This is in the range of the lateral walking frequency of pedestrians, and so it was hypothesized that some form of human–structure 'lock-in' was being observed. In support of this hypothesis, analysis of video footage revealed that the head motion of approximately 20% of the pedestrians was synchronous with that of the motion of the bridge.

Pedestrian tests undertaken on the Millennium Bridge after its closure led the bridge's designers, Arup, to similar conclusions and ultimately to the formulation of a stability criterion based on the notion of correlated velocity-proportional pedestrian forces. Back-calculations, using the response of the bridge and the number of people on the bridge, revealed an averaged equivalent velocity-proportional force coefficient of  $c = 300 \text{ N s/m}$  for each pedestrian. With this, the critical number of pedestrians,  $N_{cr}$ , needed to produce excessive lateral vibrations can be found as:

$$N_{cr} = \frac{4\pi L \zeta f m^*}{c \int_0^L \phi^2(x) dx} \quad (9.1)$$

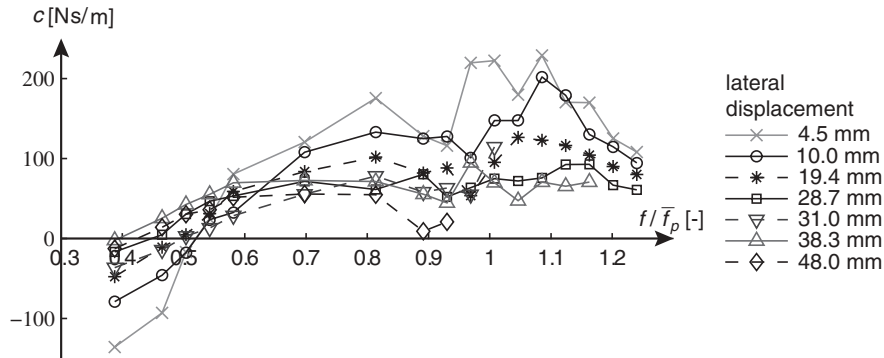
where  $L$  is the length of the bridge span,  $\zeta$  is the modal damping ratio,  $f$  is the frequency of the lateral mode of interest,  $m^*$  is the modal mass and  $\phi(x)$  is the mode shape. Effectively, the critical number of pedestrians is the number that will produce enough 'negative damping' to cancel a bridge's inherent structural damping.



**Figure 9.1** Millennium Bridge, London (Courtesy of Arup)



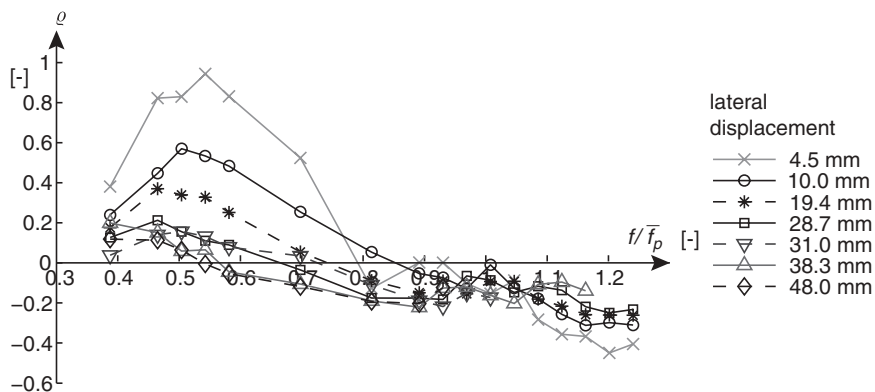
**Figure 9.2** Toda Park Bridge, Japan (Photo credit: Y. Fujino)



**Figure 9.3** Mean amplitude-dependent velocity-proportional force coefficients for pedestrians, as a function of normalized frequency [11.2]

More often than not, Arup's stability criterion is used to estimate a bridge's propensity to exhibit large amplitude lateral vibrations and to plan for possible countermeasures, in the form of e.g. dampers, rather than to determine the exact number of pedestrians for which instability might be expected to occur. There are several reasons for this. First, the average velocity-proportional force coefficient determined based on the Millennium Bridge tests is not necessarily applicable to other bridges. Second, humans tend to walk in a periodic manner, but not in a perfectly periodic way, i.e. pedestrian walking forces are a narrow-band random process. Strictly speaking, this means that the process cannot be treated deterministically. Third, it has been found that human 'lock-in' or synchronization is not a prerequisite for the generation of large amplitude lateral vibrations. It has been shown that pedestrians produce amplitude-dependent velocity-proportional lateral forces for bridge frequencies above approximately 0.3 Hz, irrespective of their level of synchronization with the lateral motion [11.2]. The mean amplitude-dependent velocity-proportional force coefficients,  $c$ , determined for pedestrians on a laterally moving treadmill, as a function of normalized frequency are provided in Figure 9.3.

Furthermore, as measured on the Toda Park Bridge, pedestrians will change the lateral frequency of the bridge when in motion, as they also produce lateral amplitude-dependent mass-proportional coefficients,  $\varrho$  as seen in Figure 9.4.



**Figure 9.4** Mean amplitude-dependent mass-proportional coefficients for pedestrians, as a function of normalized frequency [11.2]

Based on the values of Figure 9.3 and through use of (9.1), a more precise stability criterion can be formulated to determine the mean expected critical number of pedestrians for the onset of large amplitude lateral vibrations, through use of a frequency-dependent pedestrian load coefficient that can be defined as [11.2, 11.3, 11.4]:

$$c = -1602 \left( \frac{2f}{\bar{f}_p} \right)^3 + 2256 \left( \frac{2f}{\bar{f}_p} \right)^2 + 98 \left( \frac{2f}{\bar{f}_p} \right) - 463 \text{ Ns/m} \quad (9.2)$$

where  $\bar{f}_p$  is the mean pedestrian pacing frequency.

Although it is clear that human–structure synchronization is not a prerequisite for the onset of large amplitude lateral vibrations, the possibility of some level of synchronization cannot be precluded. Thus the coefficient formulated in (9.2) may not be conservative in cases where some level of human–structure synchronization might be present. In this case, it would be prudent to adjust the critical number of pedestrians for the onset of large amplitude lateral vibrations downwards.

### 9.1.2 Vertical vibrations

The well-publicized pedestrian-induced lateral vibrations of the Millennium Bridge also refocused the bridge engineering community's attention on the phenomenon of pedestrian-induced vertical vibrations. Towards the end of the previous century, several design codes and guidelines had incorporated methods for the calculation of vertical footbridge vibrations and provided suggestions for the corresponding Serviceability Limit States (SLS). Nonetheless, most were based on the calculations of the vibrations attributable to a single crossing pedestrian. Furthermore, all were deterministic in nature.

Several newer design codes and guidelines now incorporate methods for the calculation of vertical vibrations due to passing crowds, although most are still semi-probabilistic. More recently, researchers have suggested improved alternatives to these methods.

The Response Spectrum Method is a fully probabilistic method for the determination of the vertical response of a bridge due to crowd loading [08.1]. The method is based on the generation of a reference response spectrum for a 50 m long bridge from Monte Carlo simulations of pedestrian crowds with a flow rate of  $\lambda = 1$  pedestrian/s. The response obtained from the reference spectrum is then modified to take into account actual span length, bridge damping, pedestrian pacing frequency, variation on mode shapes, added pedestrian mass and damping, and predicted bridge-specific flow rates. Furthermore, the response is modified to account for a specific event return period.

The peak vertical acceleration,  $\hat{a}$ , of a footbridge can be determined as the Square Root Sum of Squares (SRSS) of each peak modal response, such that:

$$\hat{a} = \sqrt{\sum_{j=1}^n (\hat{a}_j)^2} \quad (9.3)$$

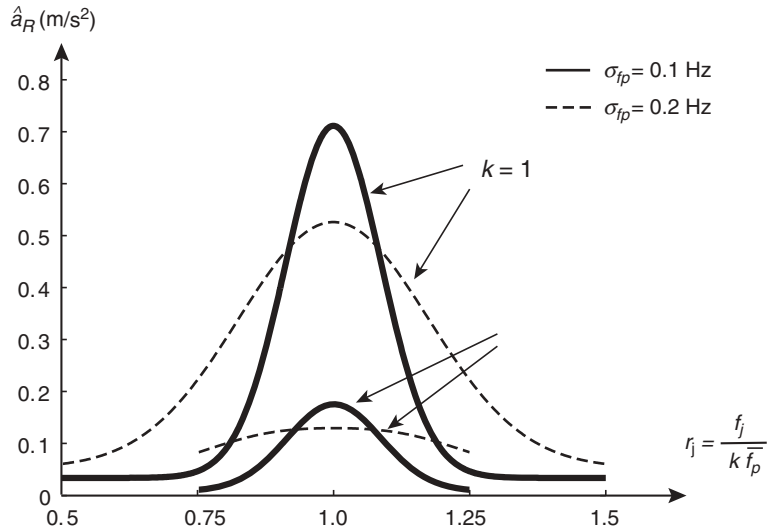
where  $j$  refers to the mode number. For footbridges with closely spaced modes, the Complete Quadratic Combination (CQC) of peak modal responses should be used.

The peak vertical acceleration,  $\hat{a}_j$ , for each mode can be readily determined as:

$$\hat{a}_j = \hat{a}_R \beta_L \beta_\zeta \beta_\phi \beta_M \beta_\lambda \beta_f R \quad (9.4)$$

where,  $\hat{a}_R$  is the reference peak acceleration,  $\beta_L$  is the span length factor,  $\beta_\zeta$  is the damping factor,  $\beta_\phi$  is the mode shape adjustment factor,  $\beta_M$  is the modal mass ratio,  $\beta_\lambda$  is the flow rate factor,  $\beta_f$  is the mean pacing frequency adjustment factor and  $R$  is the return period factor.

The reference peak acceleration,  $\hat{a}_R$ , is obtained directly from the reference response spectrum of Figure 9.5, for a mean pacing frequency of 1.8 Hz and standard deviations of either 0.1 or 0.2 Hz.



**Figure 9.5** Reference vertical acceleration response spectrum (mean pacing frequency  $\bar{f}_p = 1.8$  Hz)

The reference response spectrum for  $s_{fp} = 0.1$  Hz is described by the functions:

$$\hat{a}_R = 0.6113 \cdot \exp\left\{\frac{-(1-r)^2}{0.0151}\right\} + 0.0661 \cdot \exp\left\{\frac{-(1-r)^2}{0.0202}\right\} + 0.0338 \quad (9.5)$$

for  $0.5 < r_1 \leq 1.5$  (1st load harmonic,  $k = 1$ ) or

$$\hat{a}_R = 0.1501 \cdot \exp\left\{\frac{-(1-r)^2}{0.0146}\right\} + 0.0159 \cdot \exp\left\{\frac{-(1-r)^2}{0.0243}\right\} + 0.0097 \quad (9.6)$$

for  $1.5 < r_1$  (2nd load harmonic,  $k = 2$ ).

The 50 m long reference bridge is assumed simply supported with a fixed modal damping ratio of 0.5%. The modal mass for the bridge's first mode of vibration is 100,000 kg. A factor reflecting the effect of footbridge span deviation from 50 m is defined as:

$$\beta_L = \left(\frac{L}{50}\right)^{\eta_L} \quad (9.7)$$

where  $\eta_L = -0.11 + 0.622r$  if  $r = f/\bar{f}_p \leq 1$ , or  $\eta_L = 1.134 - 0.622r$  if  $r = f/\bar{f}_p > 1$

Span length parameters are also defined for other load harmonics in a similar manner by assuming the mean pedestrian walking frequency to be a multiple of the fundamental, so that:

$$r_j = \frac{f_j}{k \bar{f}_p} \quad (9.8)$$

where  $k$  denotes the load harmonic number. In all cases,  $r_j$  may take the values

$$0.5 \leq r_j \leq 1.5.$$

The damping parameter is also defined as a function of reference damping and footbridge frequency, such that:

$$\beta_{\zeta} = \left( \frac{0.005}{\zeta_T} \right)^{\eta_{\zeta}} \quad (9.9)$$

where,  $\zeta_T$  is the total bridge-specific damping ratio and  $\eta_{\zeta} = 1.25r - 0.743 \geq 0$  for  $r = f/\bar{f}_p \leq 1$  or  $\eta_{\zeta} = 1.758 - 1.25r \geq 0$  for  $r = f/\bar{f}_p > 1$ .

Similarly to the lateral vibrations, each pedestrian introduces amplitude-dependent damping to the bridge.

The total bridge-specific damping can be found as a combination of the bridge's structural modal damping ratio and the damping introduced by the pedestrians, so that:

$$\zeta_T = \zeta_j + \zeta_p \quad (9.10)$$

where

$$\zeta_p = \sum_{i=1}^N c_V \phi_j^2(x_i) \quad (9.11)$$

with  $c_V = 500 \text{ Ns/m}$  an average velocity-proportional force coefficient for moderate peak bridge amplitudes (i.e. approximately 10 mm).

The mode-shape correction factor is defined as:

$$\beta_{\phi} = \sqrt{\frac{\int_0^L \phi^2(x) dx}{\int_0^L \sin^2(\pi x) dx}} \quad (9.12)$$

The linear modal mass adjustment will be:

$$\beta_M = \frac{100,000 \text{ kg}}{m^* + m_p^*} \quad (9.13)$$

where  $m^*$  is the modal mass of the bridge and

$$m_p^* = 75 \text{ kg} \sum_{i=1}^N \phi_j^2(x_i) \quad (9.14)$$

The RMS response of a footbridge is proportional to the square-root of the mean pedestrian flow rate, assuming that pedestrian arrivals are random, i.e. follow a Poisson process. Consequently, the flow rate factor may be written as:

$$\beta_{\lambda} = \sqrt{\lambda} \quad (9.15)$$

The average pacing frequency of a population varies depending on their height, weight, age and cultural attitudes towards walking. As such, a mean pacing frequency adjustment factor is introduced that takes into account the increase of the first dynamic load factor with pacing frequency, so that:

$$\beta_f = 1 + 0.56(\bar{f}_p - 1.8) \quad (9.16)$$

**Table 9.1** Example pedestrian flow rate distribution

| Characterization | Mean flow rate (ped/s) | Daily duration (hrs) |
|------------------|------------------------|----------------------|
| Low              | 0.01                   | 14                   |
| Medium           | 0.1                    | 8                    |
| High             | 0.3                    | 2                    |
| Extreme          | 1.3                    | 20/year              |

The peak acceleration is dependent on the duration of the expected ‘event’, i.e. specific pedestrian flow rate. The reference response spectrum of Figure 9.5 has been obtained for an event duration of 10 minutes (600 s). For other response return periods,  $T_R$ , and return period factor  $R$  is defined as:

$$R = \left( 0.77 + \frac{\ln(T_R/60)}{10} \right) + \gamma \quad (9.17)$$

where  $\gamma = 0.3 \sin((\ln T_R)(2\pi)0.02 - 0.1) - 0.19$ , with  $10 < T_R < 10^{11}$  seconds.

On most footbridges, it can be expected that the flow rate will vary with time. To accommodate for this, the concept of a cumulative event period is introduced. With a cumulative event period, the various flow rates for a given period can be ‘binned’ or categorized, so that one peak acceleration is determined for each bin. On a typical footbridge, the flow rates might be categorized as e.g. low, medium, high or extreme. For each of these categories, a mean flow rate is defined and the times associated with all flow rates related to the mean are accumulated to produce a cumulative event period. A typical flow rate distribution may look similar to that presented in Table 9.1.

For a design life of e.g. 50 years, the cumulative event period for the low flow rate will be:

$$T_R^{Low} = 14 \times 60 \times 60 \times 365 \times 50 = 9.2 \times 10^8 \text{ s} \quad (9.18)$$

Similarly,  $T_R^{Medium} = 5.3 \times 10^8 \text{ s}$ ,  $T_R^{High} = 1.3 \times 10^8 \text{ s}$  and  $T_R^{Extreme} = 1.3 \times 10^6 \text{ s}$

Using an expected daily bridge flow rate, the concept of a cumulative event period allows for the more accurate establishment of the peak acceleration of the footbridge over its design lifetime. As a result, less frequented bridges will not be exposed to the same stringent design requirements as those that carry high volumes of pedestrians over long periods during an average day.

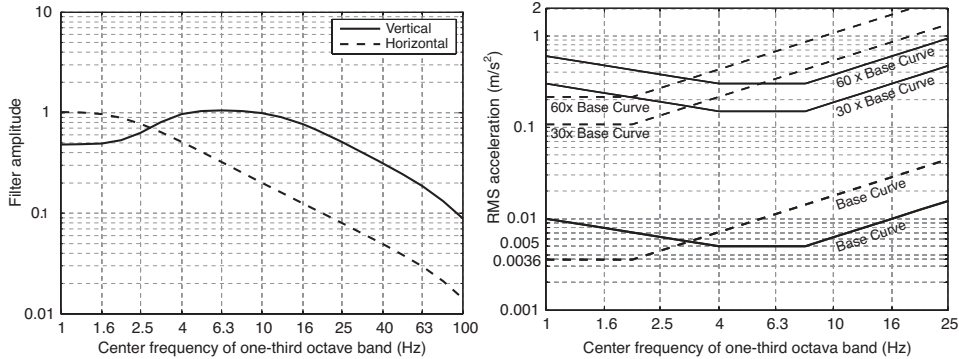
### 9.1.3 Serviceability limit states

Pedestrians who experienced the lateral vibrations on the opening day of the Millennium Bridge were asked how they felt when crossing the bridge. A few expressed anxiety, some concern, but for the majority, the experience was not at all negative. In fact, some people enjoyed the liveliness of the bridge. Similar accounts have been recorded on other bridges that have experienced comparable vibrations.

This underlines the problem that exists when trying to establish universally applicable SLS criteria. On footbridges, human vibration perception and anxiety are subjective and dependent on many parameters including gender, age, mood, time of day, weather, bridge setting and numbers of pedestrians. This makes the definition of a strict acceptable vibration amplitude threshold questionable. Nevertheless, for lack of a suitable alternative, several past and current design codes and guidelines have employed this type of limit with some success.

Notably, the superseded British Design Standard BS5400 – BD19/04 defined a frequency dependent vertical acceleration limit of  $\ddot{x}_{\max} = 0.5\sqrt{f}$  for the crossing of a single pedestrian. Similarly, the Danish Road Directorate defined a limit under the same circumstance of  $\ddot{x}_{\max} = 0.25f^{0.78}$ , while the Japanese Footbridge Design Code of 1979 defined a limit of  $1 \text{ m/s}^2$ . For crowd loading, Eurocode EN1990:2002/A1:2005 defines limits of  $0.7 \text{ m/s}^2$  for vertical vibrations and  $0.2 \text{ m/s}^2$  for horizontal vibrations. In exceptional crowd conditions, the horizontal limits are increased to  $0.4 \text{ m/s}^2$ . Several Eurocode national annexes provide the opportunity to modify the acceleration limits depending on the usage. The UK national annex introduced modification factors for ‘bridge function’, ‘route redundancy’ and





**Figure 9.6** ISO 10137:2007, Footbridge acceleration limits

‘bridge height’ above ground. In this way, bridges near hospitals or schools will have lower acceleration limits than rural bridges. Similarly, redundant bridges or those very close to the ground will have higher acceptable limits.

A more rational approach to the definition of SLS criteria might be to expand well-established acceleration limit criteria that focus on the acceptable limits for people standing or sitting in environments where vibrations might affect their work or wellbeing. This is the approach taken by the International Organization for Standardization (ISO). ISO 10137: 2007 provides a filter function (Figure 9.6 (left)) that should be used to filter a measured or computed 1s averaged multi-frequency component RMS bridge acceleration in either the vertical or horizontal direction. The filtered root-mean-quad value is then compared to lowest value of the base curve of Figure 9.6 (right). Alternatively, the single frequency component response can be compared the frequency-dependent comfort criteria of Figure 9.6 (right) directly.

The inability of all of the aforementioned codes and standards to account for the subjectivity of footbridge pedestrians often leads owners and designers to undertake full-scale pedestrian-induced vibration tests on completed bridges. For the 248 m long Tri-Countries Bridge between France and Germany, pedestrian tests were undertaken with up to 1000 volunteers at a time (Figure 9.7). The tests revealed the bridge’s propensity for lateral vibrations, with lateral



**Figure 9.7** Tri-Countries Bridge pedestrian-induced vibration testing (Courtesy of Leonhardt, Andrä und Partners)

accelerations reaching  $1.7 \text{ m/s}^2$ . Although this is significantly above the internationally defined SLS limits, when considering the reduced number of pedestrians that would be expected on the bridge at any one time, it was decided that dampers would not initially be installed on the bridge.

#### 9.1.4 Vibration control

When footbridge vibration amplitudes are found to exceed the acceptable levels, as defined by the relevant SLS criteria or by the client, vibration control measures are often used to reduce the vibration amplitudes. As it is usually difficult to fully anticipate not only the bridge response to pedestrians, but also the response of the pedestrians to the motion, footbridges are frequently designed to accommodate vibration control measures, even if not implemented from the opening of the bridge.

In most cases, due to the length of most bridges, stiffening does not result in a significant change in bridge response. Similarly, changes in mass are difficult to implement and often ineffectual. On the other hand, damping is much easier to increase, particularly as a cable supported bridge's inherent structural damping is often very low to start with.

Inertial passive damping systems are the preferred means for bridge vibration control, as they are effective even for small vibration amplitudes and are considered robust, owing to the fact that do not require an external power source to operate. For vertical vibrations, Tuned Mass Dampers (TMDs) are often employed. TMDs work on the principle of a moving secondary mass that acts to change the original vibration mode from a single-degree-of-freedom system to a bi-modal two-degrees-of-freedom system. This change, together with the optimal tuning of the secondary mass frequency and internal damping, allows for the successful augmentation of the original modal response. An example of an installed TMD is that of the Forchheim Bridge in Germany (Figure 9.8). For the vertical vibration control of the bridge, two TMDs were used, with masses of 1000 kg and 1660 kg.

A more advanced TMD is the semi-active TMD, in which the internal damping of the secondary moving mass is constantly adjusted to account for changes in the bridge's properties due to the pedestrians or cyclists crossing. This is often achieved through the use of a magneto-rheological fluid, the viscosity of which can be adjusted with a relatively small electrical current.

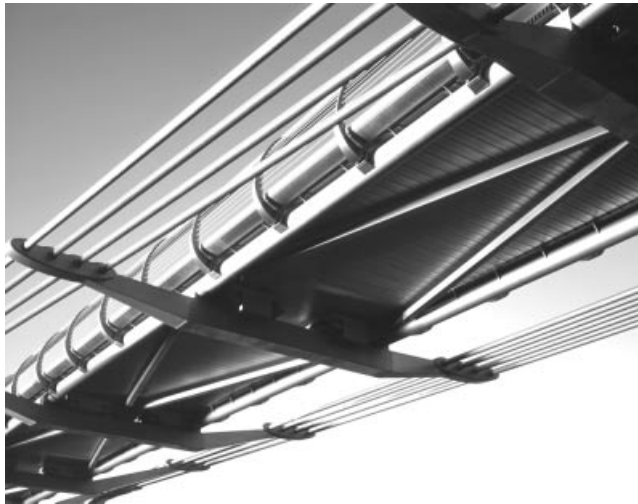
For lateral vibrations, TMDs are just as effective, but often rather expensive when compared with alternative damping systems. In this case, the Tuned Liquid Damper (TLD) is often used, as it is easy to implement and very cost-effective. This is exemplified by its use to dampen the lateral vibrations of the Toda Park Bridge. Here, plastic containers were bought from a local hardware store and then filled to the appropriate level with water for the proper frequency tuning of the system (Figure 9.9). In TLDs, the movement of water mass produces forces equivalent to those produced by the TMD mass and internal damping is usually achieved through the use of screens or baffles.



**Figure 9.8** Forchheim Bridge TMD (Courtesy of Maurer Söhne)



**Figure 9.9** Toda Park Bridge TLDs (Photo credit: Y. Fujino)



**Figure 9.10** London Millennium Bridge cross beam TMDs and viscous damper bracings (Courtesy of Arup)

In some cases inertial damping systems cannot be implemented due to their size and weight. In these cases, relative displacement damping systems are often employed. Relative displacement dampers work to dissipate energy through the generation of velocity-proportional forces between two points that are moving relative to each other. Relative displacement dampers can take many forms and be viscous, visco-elastic or friction in nature. One of the problems with relative displacement dampers is that it can often be difficult to find enough relative displacement between two points to produce a reasonable level of damping. In any case, a combination of relative-displacement dampers and TMDs has been employed on London's Millennium Bridge to dampen lateral and vertical vibrations, respectively (Figure 9.10).

## 9.2 Seismic Design

In regions where earthquakes are frequent and where one or several very large earthquakes might be expected during the lifetime of a bridge, special considerations must be made during the design phase to ensure the adequate performance of the bridge during an earthquake. In the absence of any seismic activity, dead, live, and wind loads dominate the design of a

**Table 9.2** Recommended performance-based design earthquake intensities

| Bridge significance | Earthquake intensity (probability of exceeding in 50 yrs) |          |       |
|---------------------|---|----------|-------|
|                     | Small   | Moderate | Large |
| Normal              | 20%   | 4%       | 1%    |
| Vital               | 10%   | 2%       | 1%    |

cable-supported bridge. If the seismic activity of the region in which the bridge is to be placed is considered to be relatively large, then seismic loading will dominate the design – if not for the whole bridge – at least for one or more key load-bearing elements, such as the deck or the pylon.

The main purpose of a bridge is to carry vertical live load. Therefore, cable supported bridges are often well equipped to handle vertical seismic accelerations. This is particularly true, as the probability of a seismic event occurring when a bridge's full live load capacity has been utilized is extremely small. Furthermore, it can be expected that the vertical component of the seismic motion will often be smaller than the components across and along the length of the bridge. For these reasons, particular attention must be given to the load effects from the lateral and longitudinal components of an earthquake.

### 9.2.1 Earthquake intensity

For most ordinary structures, it is considered reasonable to design the structure to avoid a total or partial collapse during an earthquake that has a 10% probability of exceedance in 50 years, i.e. a 1 in 475-year event. The seismic design loads for large cable supported bridges will differ from those of ordinary structures, as they should not only avoid collapse, but also continue to serve as vital transportation links after a large earthquake. Consequently, it is not unusual to consider an earthquake that only has a 2% probability of exceedance in 50 years, i.e. a 1 in 2475-year earthquake, for such a bridge. Alternatively, as a bridge might be subjected to several larger or smaller seismic events during its lifetime, it might be considered prudent to adopt a performance-based design approach, in which the rational design of a bridge's components is based on predetermined performance criteria. Performance criteria would in most cases translate into acceptable levels of damage.

The acceptable levels of damage should be directly correlated to the design for earthquake intensity. For smaller earthquakes, bridges should remain undamaged. For moderate earthquakes, damage should be limited and easily repairable, without the need for bridge closure. For larger earthquakes, significant damage can be allowed, as long as this does not lead to the collapse of the bridge or its closure to emergency response units. Subsequent repairs may require the closure of the bridge. Bearing this in mind, the performance-based earthquake intensities can be defined according to Table 9.2. [10.1].

The size and flexibility of most cable-supported bridges lead them to commonly exhibit natural frequencies that are nearly an order of magnitude smaller than those of common buildings. Therefore, unlike typical structures, their response is not characterized by large accelerations, but rather by large displacements. Thus, for small to moderate intensity earthquakes, larger cable supported bridges are generally capable of coping with the performance demands, even when the bridge has not been explicitly designed for seismic loading, as they are designed to allow for limited displacements in most directions. For larger seismic events, though, the optimal design of bridge members for an earthquake can often be in contrast to that for other traditional loads.

### 9.2.2 Pylon design

A good example of the contradiction in design requirements can often be found in the pylon design. For suspension bridges, parallel vertical pylon legs are preferred, as this eases the construction of the main suspension cables and the eventual transfer of load from the deck to the ground. For seismic loading, however, the split parallel pylon leg configuration is not optimal, as lateral accelerations in the deck will create moments about the vertical axis that will have to be resisted in part by the pylon legs. This will be particularly onerous for cable-stayed bridges, where there is a direct transfer of load from the deck to the pylons through the stay cables. Furthermore, the lateral forces generated by an earthquake will be resisted in a



**Figure 9.11** *New Oakland Bay Suspension Bridge (Copyright Caltrans)*

similar manner as for wind resistance, except that an additional vertical force must now be considered. This combination of forces may be difficult to resist economically using a portal frame or a braced portal frame pylon design.

To overcome this, a large singular central pylon, an A-frame pylon or a pyramidal pylon configuration may be considered beneficial. This has been found to be the case with several more recently designed bridges located in seismic regions. Examples include the Stonecutters Bridge, Sutong Bridge, Rion-Antirion Bridge, and the New Oakland Bay Suspension Bridge (Figure 9.11).

For the New Oakland Bay Suspension Bridge, the central pylon is composed of four legs that are linked by specially designed 'disposable' shear link beams capable of dissipating large amounts of energy during an earthquake. For the Rion-Antirion Bridge, the upper pyramidal pylon leg configuration was found necessary not only to withstand the lateral seismic loads, but also to be able to transmit the forces generated by the longitudinal seismic loads on the deck (Figure 9.12). This is generally not a problem for bridges in regions of low seismicity, even when considering substantial vehicle braking forces.



**Figure 9.12** *Rion-Antirion Bridge*

### 9.2.3 Deck design

The design of structures in seismically active regions dictates that mass is kept to a minimum, as all seismic loads are mass proportional. This should be rigorously pursued for the bridge deck, as its suspension will typically lead to large lateral and longitudinal displacements that will be difficult to restrain if heavy. Furthermore, the addition of mass will not significantly or positively alter lateral and longitudinal vibration frequencies, as they are primarily a result of pendulum effects. On the other hand, the lateral stiffness of the deck must be great, to resist the lateral bending moments. Thus, a correct balance between mass and stiffness must be achieved.

Naturally, it should be remembered that the deck restraints play an important role in the overall behaviour and load distribution of the deck and, as such, must be carefully planned. When coupled with specially designed seismic dampers, thermal expansion joints can be designed to move freely during normal use, but to restrain movement and dissipate energy during an earthquake. Conversely, it might be desirable to restrain lateral deck movements against wind or eccentric traffic loading, while allowing for the controlled movement during an earthquake. Lateral restraint of the deck during a seismic event will reduce deck displacement, but will simultaneously introduce undesirably large moments and shear forces into the deck and pylon.

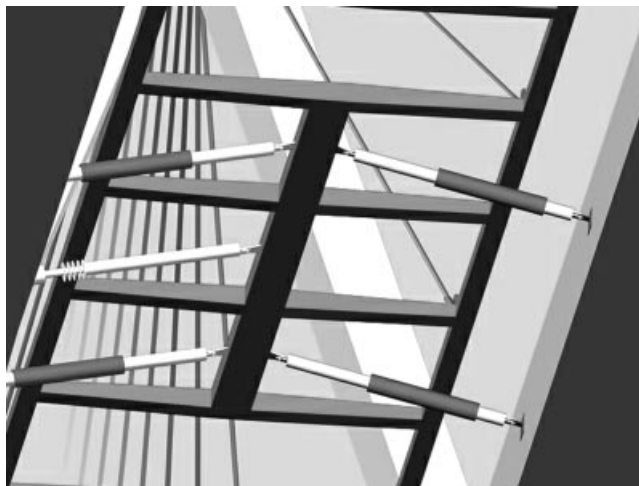
For the Rion-Antirion Bridge, a combined metallic fuse and damper system is used to laterally connect the deck to the pylons (Figure 9.13). The system restrains lateral movements during normal use, but then yields in a controlled manner to allow the engagement of dampers that dissipate energy. This has the effect of limiting deck and pylon forces, and deck displacements.

### 9.2.4 Foundations

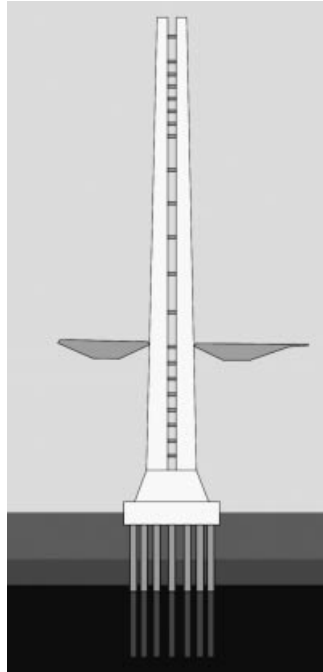
In the absence of a seismic isolation scheme, the bridge foundations must carry the total of all the lateral loads produced by an earthquake, through axial, shear and moment resistance. This places a large onus on the designer to ensure a robust foundation design.

When possible, foundations should ideally be placed on bedrock – not only to maximize pylon stiffness, but also to minimize the risk of soil amplification. This is not always possible though, as bridges are often built over water, where the underlying soil conditions are less than optimal. In this case, piles are required to enhance the soil stiffness and transfer the load effects to the stiffer soils below. A pylon foundation of this type is used on the New Oakland Bay Suspension Bridge (Figure 9.14).

When soft soil depths are too great, soil improvement coupled with seismic isolation might be a preferred solution. The pylon foundations of the Rion-Antirion Bridge lie on a bed of gravel to isolate them from the pile stiffened soft soil layers below (Figure 9.15).



**Figure 9.13** Rion-Antirion Bridge lateral deck restraint and dampers



**Figure 9.14** New Oakland Bay Suspension Bridge central pylon foundation

### 9.2.5 Seismic analysis

The length of most cable-supported bridges also creates a particularity in their seismic analysis that does not concern ordinary structures. If the distance between bridge pylons is greater than approximately 300–500 m, ground accelerations between pylons must be assumed to be partly or fully uncorrelated. This distance may be considerably reduced if the geological conditions have a large level of variability and/or if the terrain is very uneven. In this case, an ordinary Response



**Figure 9.15** Rion-Antirion Bridge foundation

Spectrum (RS) analysis is not suitable for the seismic response evaluation of the bridge. Instead a Multiple Support Response Spectrum Analysis (MSRS) should be employed, in which the correlation between the support motions – as well as between the bridge’s primary modes of vibration – is accounted for [92.16]. In some cases, where there is doubt about the ability of the bridge to perform in the prescribed or desired manner, e.g. with a uniform ‘behavioural’ or ductility factor, full structural time-history analyses with actually recorded or synthetically produced accelerograms should be employed. Synthetic accelerograms should be produced from site-specific response spectra and scaled for the appropriate expected peak ground acceleration.

### 9.3 Structural Health Monitoring

Structural health monitoring (SHM) can play a vital role in the maintenance and health evaluation of cable-supported bridges. In the past three decades, it has been used primarily and effectively for damage detection in bridges, especially where there is some doubt about the performance of a particular design or when the expected loading has been difficult to quantify in the design stages of the bridge. Storms, earthquakes, floods and accidents are examples of this type of loading.

SHM can be used not only for the detection of damage though. It can also be used for the quantification of the severity of damage and the locations of damage. Furthermore, SHM techniques have developed to the point where they can be used to evaluate the propensity for damage in a bridge.

These developments have led researchers and engineers to use existing SHM techniques and hardware for new purposes. It is not uncommon for SHM equipment to be used temporarily and selectively during the construction of a large bridge to evaluate the construction sequence and to provide data that will help improve the completion of not only the particular bridge, but also other similar bridges in future. SHM is also being used to obtain bridge population characteristics so that the health of any country’s bridge stock might be evaluated probabilistically based on structural configuration, location, usage and age. This is especially important for developed countries, where bridge stocks are ageing and stock management is vital. In the US, it is estimated that approximately 30% of the country’s bridge stock is deficient, with about half of this attributable to structural deficiencies. Finally, SHM is increasingly being used as a tool to evaluate the need for the retrofit of bridges with the goal of a fail-safe bridge design. In all cases it is clear that SHM is being used to help close the gap between the theoretical evaluation and the real-life performance of bridges.

#### 9.3.1 Equipment

The rational selection and placement of sensors form the most important aspect in the design of a successful bridge monitoring system. A thorough evaluation of the loads, load effects, structural properties and meteorological conditions that need to be measured should be made through dialogue between the SHM system designer and the bridge operator and engineers, always considering the particularities of the bridge and its location. Furthermore, the minimization of the amount of data acquired should be pursued to avoid resource expenditure on unnecessary processing of data. Similarly, sensors, the data transmission network and the data acquisition system should all be designed to cope with the roughest environmental conditions, while also providing for easy access of the data and maintenance.

An example of this is the Øresund Bridge SHM system, as shown in Figure 9.16. During the design, the future operators of the bridge, together with the engineers, decided it prudent to measure both the static and the dynamic

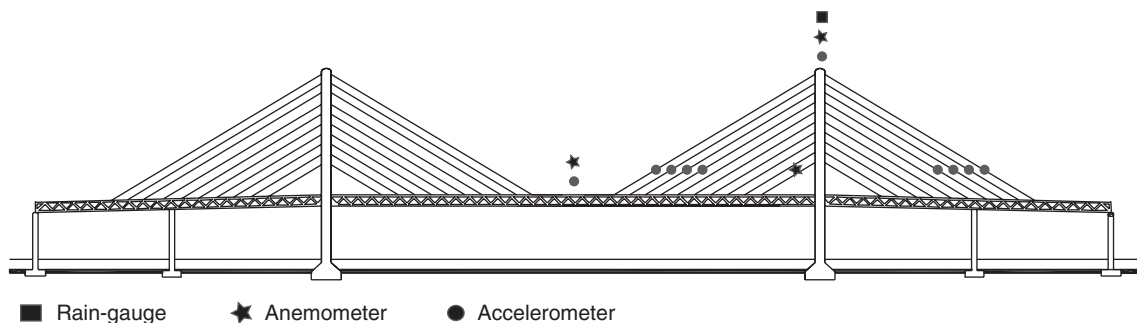
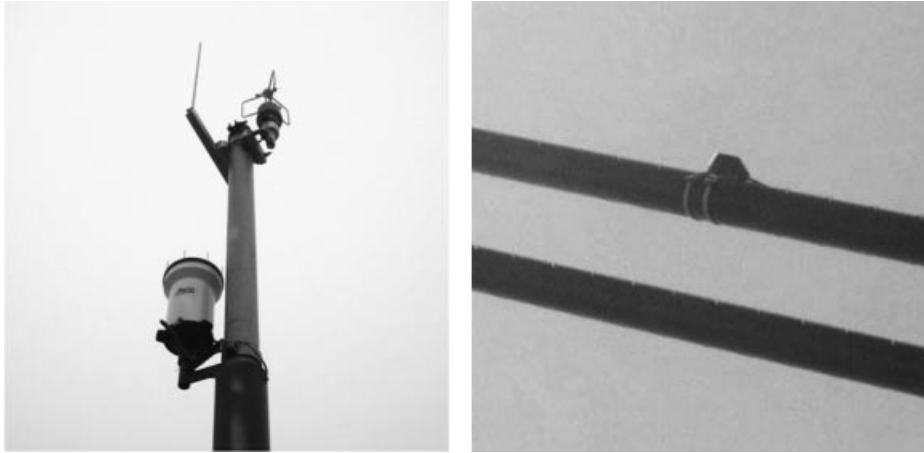


Figure 9.16 Øresund Bridge SHM sensors (phase II), Denmark-Sweden





**Figure 9.17** Øresund pylon meteorological station (left) and cable accelerometer (right). Rain gauge (lower left) and tri-axial ultrasonic anemometer with barometric pressure, temperature and humidity instruments (upper left) (Accelerometer photo courtesy of Geosig)

response of the bridge to passing vehicles and trains and the dynamic response of the stay cables to wind. Furthermore, strain gauge measurements were found to be of interest at the locations of maximum expected strain, around the cable outriggers and at several locations on the bottom chord of the bridge. More specifically, the bridge is fitted with 22 tri-axial force balance accelerometers, 19 strain gauges, several thermometers to correlate the strain gauge measurements with the variations in temperature, and two bi-axial ultrasonic anemometers to measure the oncoming wind velocities and turbulence intensities.

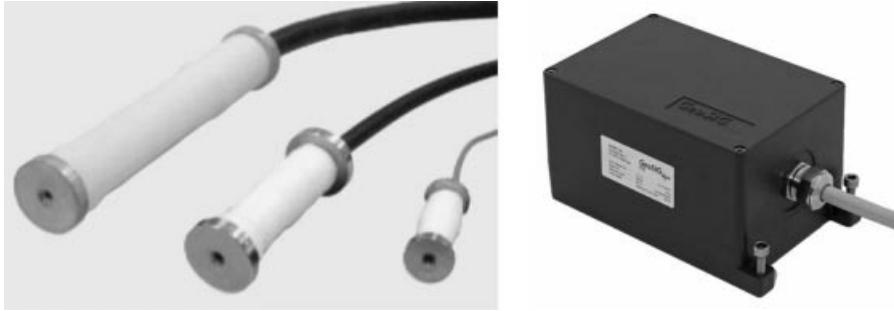
Since the bridge's opening in 2000, data from the accelerometers and strain gauges has been recorded and processed to deliver time-averaged quantities that can be compared to preset serviceability limit states. If a response threshold is passed, an alarm is triggered to inform the operators. Soon after its implementation, the system recorded large amplitude cable oscillations and high strain levels in the cable outriggers, as a consequence. This led to the design of a new cable damper system and the addition of structural support members for the outriggers.

To improve the monitoring of the cable system and an understanding of the flow fields around the cable, three new weather stations with heated tri-axial ultrasonic anemometers and rain gauges were installed by the Technical University of Denmark (DTU) in 2009 on the southeast pylon (Figure 9.17), in the deck midspan and between the first and second shortest cables on the southeast quadrant of the midspan (Figure 9.16). The data transmission system is now equipped with fibre optics, to avoid environmental noise and disturbances to and from Copenhagen's nearby Kastrup Airport. Power loss back-up systems have been implemented to record data, even during the unlikely event of a power outage, and data can be collected and monitored on-site or through a dedicated Internet connection worldwide.

The most common sensors used for bridge monitoring are strain gauges and accelerometers (Figure 9.18). Each respectively assists in the understanding of the bridge's static and dynamic response to traffic and environmental loading.

The static response might be global in nature or local, in the form of e.g. box girder distortion to a heavy passing train or vehicle. Based on these measurements, a more accurate evaluation of the structural performance can be made, together with more precise fatigue calculations.

The dynamic response of the bridge can also be evaluated globally or locally, often with the goal of determining structural properties that cannot be theoretically evaluated with any great degree of accuracy. These might include structural damping, cable tensions or bridge mode shapes and frequencies. Furthermore, as in the aforementioned case of the Øresund Bridge, the monitoring of the dynamic response of a bridge might reveal unexpected vibrations that can approach or surpass the serviceability limit state criteria defined for the bridge in question.



**Figure 9.18** Concrete strain gauges (left) and tri-axial force balance accelerometer (right) (Courtesy of Geosig)

Other sensors are often used to complement the data acquired from strain gauges or accelerometers, or to provide information unattainable using these traditional sensors. Alternative sensors might also be used when strain gauges or accelerometers are difficult or expensive to install.

Complementary sensors include cup or ultrasonic anemometers, thermometers, barometers, and hydrometers. Cup anemometers are used to measure mean wind velocities under all conditions, whilst ultrasonic anemometers measure wind velocities and turbulence intensities under most environmental conditions.

Alternative sensors include inclinometers, relative displacement transducers and, more recently, laser displacement transducers and Global Positioning System (GPS) equipment. Relative displacement transducers are often used to measure local deformations or bearing and expansion joint movements. Laser transducers offer the same capability, but without the need for contact between the measured surfaces. GPS equipment works relatively well in providing mean horizontal displacements, but not so well in providing vertical displacements.

A new promising SHM technology for the determination of both static and dynamic response is the combined Total Station (TPS) with powerful Laser Doppler Velocimetry (LDV) measurements (Figure 9.19). With this technology, measurements can be made on a bridge from a distance of up to 2 km with a very high degree of accuracy. A precise TPS can scan a large bridge quickly to allow a powerful laser to measure variations in the position of a bridge for any point on the bridge that the laser is in contact with. Shifts in modal properties, local distortions or global displacements can readily be logged.

## 9.4 Snow and Ice Removal and Prevention Systems

Between 2004 and 2007, the Storebælt Bridge was closed an average of 14.3 hours a year, 12 of which were due to falling ice and snow. The Øresund Bridge had to close six times between 2000 and 2010, due to ice and snow. Numerous other bridges throughout the Northern Hemisphere have had similar closures, including the Uddevalla Bridge in Sweden, the Severn Bridge in the UK, the Zakim Bunker Hill Bridge in the USA and the Hukacho Bridge in Japan.

Ice or heavy snow is generally not a problem for a bridge from a structural point of view. Most bridges can easily cope with the additional load introduced by the snow or ice mass. The problem lies in the melting phase, when large chunks of snow or ice are prone to fall onto the roadway below (Figure 9.20). Falling ice and snow endangers motorists and has often led to damaged windscreens and vehicles and, on occasion, accidents.

When the conditions are right, snow usually collects on all points of a bridge, while ice tends to collect predominantly on bridge members higher than 150 m above sea level. In all cases, several accretion removal or prevention systems are available for use on bridges [10.2].

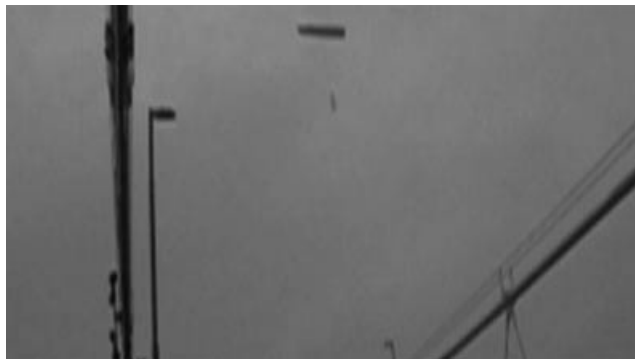
### 9.4.1 Mechanical removal

The mechanical removal of ice has traditionally been undertaken manually, with hoisted bridge maintenance workers beating the ice with ice picks or other similar implements. For the George Washington Bridge in New York, the baseball bat is the preferred implement for the removal of ice from the bridge hangers.



**Figure 9.19** Total station (TPS) with high power Laser Doppler Velocimeter (Photo credit: Y. Fujino)

Several more sophisticated electro-mechanical systems have been implemented recently on a few bridges. The Electro-Mechanical Expulsion De-icing System (EMEDS) and the Electromagnetic-Impulsive De-Icing (EIDI) system are the most well known of these systems. EMEDS works on the principle of electro-mechanical vibrations resulting from rapid current discharges into electromagnetic coils and leading to a discharge of surrounding ice. The EIDI system is similar in its philosophy, as high current DC pulses are run through a coil, leading to debonding and expulsion of ice due to the rapid acceleration and flexure of the icing surface.



**Figure 9.20** Falling ice from the Severn Bridge, UK (Courtesy of UK Highways Agency)



**Figure 9.21** The EIDI system installed on selective hangers of the Storebælt Bridge (Photo credit: E. Laursen)

The EIDI system was tested on the two longest hanger pairs of the Storebælt Bridge during a pilot project for a period of three years (Figure 9.21). The system was found to be very effective for light to moderate ice accretions, although road closures were still necessary during its operation, as the de-icing often resulted in a violent explosion of the ice. Towards the end of the trial period, a heavy 50 mm ice accretion rendered the system ineffective, leading to the eventual removal of the system.

#### 9.4.2 Thermal systems

An obvious way to avoid or remove accreted ice or snow is through some form of heating of the iced surface or the accretion itself. This is the basic principle employed in several existing thermal systems that have been tested on several bridges.

On the Hakucho Bridge, a comparative study between aluminium foil, sheet and hot water heaters was made. The aluminium foil heater was found to be the most effective and, although, as with all other thermal systems, it was found to consume copious amounts of energy, it still consumed the least amount when compared to the other two heaters.

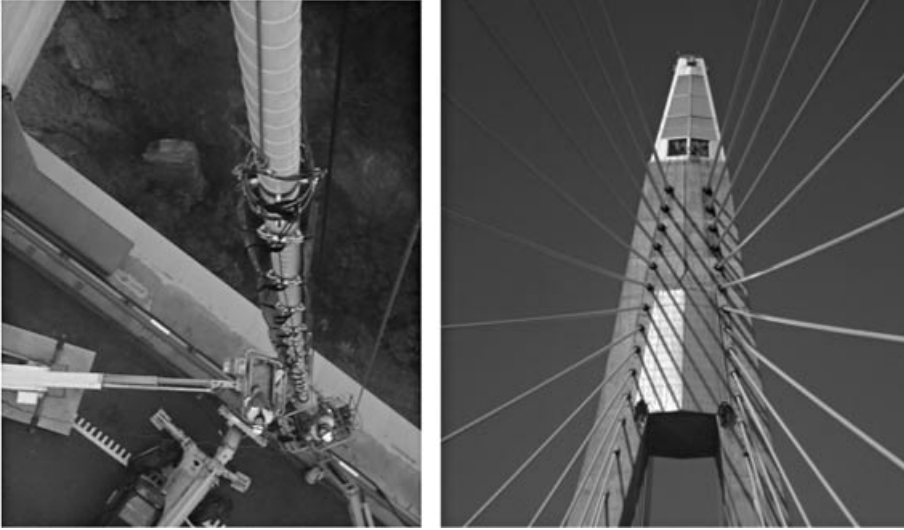
An alternative to the use of electricity or hot water involves the use of hot air. On the Uddevalla Bridge, a high-pressure hot air system has been employed on the bridge cables to avoid icing. The system pushes hot air through small holes on the HDPE tubing of the cable. Again, however, large amounts of energy are needed to operate this system.

A more successful accretion removal strategy employed on the Uddevalla Bridge involves the use of a thin electrical conductor film on surfaces where icing or heavy snow might be expected. Unlike the aluminium foil heater, electrical pulses are sent through the film for a short period of time to allow a thin water layer to develop, leading to the detachment of ice or snow. The system, also known as the Pulse Electro-Thermal De-icing (PETD) system, has been successfully applied to parts of the bridge's cables and the pylon (Figure 9.22).

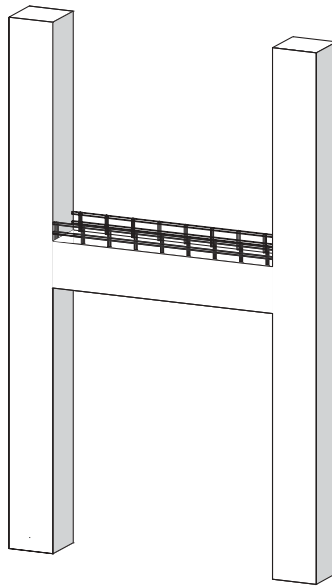
#### 9.4.3 Passive protection

In recent years, several passive protection systems have been devised to protect bridges against snow or ice accretions. Unlike the mechanical or thermal systems, passive systems need no external energy for their operation. Instead, they rely on their chemical or shielding properties to prevent accretion all together. Unfortunately, none of the passive systems are known to completely hinder the formation of ice or snow. In any case, several of these have been tested on bridges with a limited degree of success.

Passive systems that rely on their chemical properties include coatings that are hydrophobic, ice-phobic, thermally absorbent or highly lubricant. On the Storebælt Bridge, tests were undertaken using a coating that employs the *sol-gel* technology to avoid accretion. The tests were only partially successful and further development of the coating is ongoing. A similar picture emerges when examining the effectiveness of the other types of coating.



**Figure 9.22** PETD de-icing film applied to the Uddevalla Bridge cables (left) and pylon top (right) (Photo credit: E. Kuhn)



**Figure 9.23** Depiction of bridge pylon segment with snow retention screens

In other tests, success has been found in ‘trapping’ accreted snow or ice formed on the upper parts of the bridge from falling onto the roadway below. The technique involves the placement of lattice screens where the accretion is anticipated (Figure 9.23). The screens act to trap large chunks of snow or ice so that they do not fall when melting. Although, an interesting technology, it is clear that there are some cases in which accretion might be precipitated by the presence of the screens. Furthermore, the bridge’s aerodynamics might be affected in some manner.

# References

- 00.1 **Krenk, S.**, 2000. 'Vibrations of a Taut Cable with an External Damper', *Transactions of the ASME*, Vol. 67, December, pp. 772–776.
- 01.1 **Frandsen, J.B.**, 2001. 'Simultaneous Pressures and Accelerations Measured Full-Scale on the Great Belt East Suspension Bridge', *Journal of Wind Engineering and Industrial Aerodynamics*, Vol. 89, Issue 1, pp. 95–129.
- 01.2 **Dallard, P. et al.**, 2001. 'London Millennium Bridge: Pedestrian-Induced Lateral Vibration', *Journal of Bridge Engineering*, Vol. 6, Issue 6, pp. 412.
- 02.1 **Krenk, S. and Nielsen, S.**, 2002. 'Vibrations of a Shallow Cable with a Viscous Damper', *Proceedings of the Royal Society of London Series A*, Vol. 458, pp. 339–357.
- 03.1 **Wagner, P. and Fuzier, J-P.**, 2003. 'Health Monitoring of Structures with Cables', *Fifth International Symposium on Cable Dynamics*, 'Tutorial on Health Monitoring of Structures with Cables', Santa Margherita Ligure, Italy.
- 03.2 **Miyata, T.**, 2003. 'Historical View of Long-Span Bridge Aerodynamics', *Journal of Wind Engineering and Industrial Aerodynamics*, Vol. 91, Issue 12–15, pp. 1393–1410.
- 05.1 **Georgakis, C.T. and Taylor, C.A.**, 2005. 'Nonlinear Dynamics of Cable Stays. Part 1: Sinusoidal Cable Support Excitation', *Journal of Sound and Vibration*, Vol. 281, Issue 3–5, pp. 537–564.
- 05.2 **Georgakis, C.T. and Taylor, C.A.**, 2005. 'Nonlinear Dynamics of Cable Stays. Part 2: Stochastic Cable Support Excitation', *Journal of Sound and Vibration*, Vol. 281, Issue 3–5, pp. 565–591.
- 05.3 **Larose, G.L., Zasso, A. and Grappino, S.**, 2005. 'Experiments on a Yawed Stay Cable in Turbulent Flow in the Critical Reynolds Number Range', *Proceedings of the 6th International Symposium on Cable Dynamics*, Charleston.
- 06.1 **Macdonald, J.H.G. and Larose, G.L.**, 2006. 'A Unified Approach to Aerodynamic Damping and Drag/Lift Instabilities, and its Application to Dry Inclined Cable Galloping', *Journal of Fluid and Structures*, Vol. 22, Issue 2, pp. 229–252.
- 07.1 **Gjelstrup, H., Georgakis, C.T. and Larsen, A.**, 2007. 'A Preliminary Investigation of the Hanger Vibrations on the Great Belt East Bridge', *Seventh International Symposium on Cable Dynamics*, Vienna.
- 07.2 **Smith, B.W.**, 2007. *Communication Structures*, London. Thomas Telford Publishing.
- 07.3 **Hoang, N. and Fujino, Y.**, 2007. 'Analytical Study on Bending Effects in a Stay Cable with a Damper', *Journal of Engineering Mechanics*, ASCE, November.
- 08.1 **Georgakis, C.T. and Ingólfsson, E.T.** 'Vertical Footbridge Vibrations: The Response Spectrum Methodology', *Proceedings of Footbridge 2008*, Porto, July 2–4.
- 09.1 **Brancaleoni, F. et al.**, 2009. *The Messina Strait Bridge: A Challenge and a Dream*, The Netherlands. CRC Press/Balkema.
- 09.2 **Larsen, A.**, 2009. 'Winds of Change', *Bridge Design and Engineering*, Issue No. 56, Third quarter. Published by Hemming Information Services.
- 09.3 **Gjelstrup, H. and Georgakis, C.T.**, 2009. 'Aerodynamic Instability of a Cylinder with Thin Ice Accretion', *8th International Symposium on Cable Dynamics*, Paris.
- 10.1 **Calvi, G.M., Sullivan T.J. and Villani, A.**, 2010. 'Conceptual Seismic Design of Cable-Stayed Bridges', *Journal of Earthquake Engineering*, Vol. 14, Issue 8, pp. 1139–1171.
- 10.2 **Kleissl, K. and Georgakis C.T.**, 2010. 'Bridge Ice Accretion and De- and Anti-Icing Systems: A Review', *7th International Cable Supported Bridge Owners Conference*, May, Zhenjiang, China.
- 11.1 **Gjelstrup, H. and Georgakis, C.T.**, 2011. 'A Quasi-Steady 3-DOF Model for the Determination of the Onset of Bluff Body Galloping Instability', *Journal of Fluids and Structures*, doi: 10.1016/j.jfluidstructs.2011.04.006
- 11.2 **Ingólfsson, E.T. et al.**, 2011. 'Experimental Identification of Pedestrian-Induced Lateral Forces on Footbridges', *Journal of Sound of Vibration*, Vol. 330, Issue 6, pp. 1265–1284.

- 11.3 **Ingólfsson, E.T.**, 2011. 'Pedestrian-Induced Lateral Vibrations of Footbridges: Experimental Studies and Probabilistic Modelling', PhD Thesis, Technical University of Denmark, Department of Civil Engineering.
- 11.4 **Ricciardelli, F., Mafrici, M. and Ingólfsson, E.T.**, 2011. 'Motion-Dependent Lateral Walking Forces on Footbridges', *Proceedings of Footbridge 2011*, Poland.
- 32.1 **Moisseiff, L.S. and F. Lienhard**, 1932. 'Suspension bridges under the action of lateral forces', *Proc. ASCE*, March.
- 33.1 **Beggs, G.E., P.E. Davis and H.E. Davis**, 1933. 'Tests on structural models of proposed San Francisco-Oakland Suspension bridge', *University of California, Publ. Eng.* **3** No. 2.
- 37.1 **Timoshenko, S. and D.H. Young**, 1937. *Engineering Mechanics (Statics)*, McGraw-Hill, New York.
- 38.1 **Girkmann, K. and E. Königshofer**, 1938. *Die Hochspannungsfreileitungen*, Springer Verlag, Wien.
- 39.1 **Hardesty, S. and H.E. Wessmann**, 1939. 'Preliminary Design of Suspension Bridges', *Traus. ASCE*, **107**.
- 42.1 **Birdsall, B.**, 1942. The suspension bridge tower cantilever problem', *Trans. Asce*, **107**.
- 43.1 **Asplund, S.O.**, 1943. 'On the detection theory of suspension bridges', Uppsala.
- 45.1 **Selberg, A.**, 1945. 'Design of suspension bridges', *Det K. norske videnskabers selsk. skrift* No. 1.
- 49.1 **Dischinger, F.**, 1949. 'Hängebrücken für Schwerster Verkehrslasten', *Der Bauingenieur*, Heft 3.
- 49.2 **Schleicher, F.**, 1949. 'Die Verankerung von Drahtseilen', *Der Bauingenieur*, 5, 6.
- 50.1 **Bleich, F., C.B. McCuillough, R. Rosencranz and G.S. Vincent**, 1950. *The Mathematical Theory of Vibration in Suspension Bridges*, Bureau of Public Roads, Washington.
- 51.1 **Steinman, D.B.**, 1951. 'Der Entwurf einer Brücke von Italien nach Sizilien mit der grössten Spannweite der Welt', *Der Stahlbau*, Heft 3.
- 53.1 **Shirley Smith, H.**, 1953. *The World's Great Bridges*, Phoenix House Ltd., London.
- 57.1 **Steinman, D.B. and S.R. Watson**, 1957. *Bridges and Their Builders*, Dover, New York.
- 58.1 **Beyer, E.**, 1958. *Nordbrücke Düsseldorf* Springer Verlag, Berlin.
- 61.1 **Selberg, A.**, 1961. 'Oscillation and aerodynamic stability of suspension bridges', *Acta Polytech. Scand. Civil Eng. Build. Constr. Series No. 13, Trondheim*.
- 61.2 **Davenport, A.G.**, 1961. 'The Application of Statistical Concepts to the Wind Loading of Structures', *Proceedings of Institute of Civil Engineers*, Vol. 19, August, pp. 449–472.
- 62.1 **Davenport, A.G.**, 1962. 'Buffeting of a Suspension Bridge by Storm Winds', *Journal Struct. Div.*, ASCE, June.
- 63.1 **Wyatt, T.A.**, 1963. 'Secondary stresses in parallel wire suspension cables', *Trans. ASCE*, **128**, pt. II.
- 64.1 **Ellinger, M. and F. Chichocki**, 1964. 'Dehnungsfugen in Brückenfahrbahnen', *IABSE 7th Congr., Preliminary Publ.*
- 65.1 **Ernst, M.J.**, 1965. 'Der E-Modul von Seilen unter Besück-sichtigung des Durchhanges', *Der Bauingenieur*, **2**.
- 65.2 **Roberts, G.**, 1965. 'Design of the Forth Road Bridge', *Proc. Instn. Civ. Engrs.*, Nov.
- 66.1 **Durkee, Jackson, L.**, 1966. 'Advancements in suspension bridge cable construction', *Proc. Int. Symp. on Suspension Bridges, Lisbon*.
- 66.2 **Frandsen, A.G.**, 1966. 'Wind stability of suspension bridges, application of the theory of thin airfoils', *Proc. Int. Symp. on Suspension Bridges, Lisbon*.
- 66.3 **Gimsing, N.J.**, 1966. 'Anchored and partially anchored stayed bridges', *Proc. Int. Symp. on Suspension Bridges, Lisbon*.
- 66.4 **Ostenfeld, Chr., G. Haas and A.G. Frandsen**, 1966. 'Motorway bridge across Lillebælt, model tests for the superstructure of the suspension bridge', *Proc. Int. Symp. on Suspension Bridges, Lisbon*.
- 66.5 **Roberts, G.**, 1966. 'The Severn Bridge, a new principle of design', *Proc. Int. Symp. on Suspension Bridges, Lisbon*.
- 67.1 **Fukuda, T.**, 1967. 'Analysis of multispan suspension bridges', *Proc. ASCE, J. Structural Div.*, **93**(ST 3), June.
- 67.2 **Walshe, D. E.**, 1967. 'A resumé of the aerodynamic investigations for the Forth Road and the Severn Bridges', *Proc. Inst. Civil Engrs.*, May.
- 69.1 **Andrä, W. and W. Zellner**, 1969. 'Zugglieder aus Parallel-drahtbündeln und ihre Verankerung bei hoher Dauerschwellbelastung', *Die Bautechnik*, **8,9**.
- 70.1 **Jensen, M.**, 1970. *Motorway Bridge across Lillebælt — Publication XII: Erection of Steel Superstructures*, Chr. Ostenfeld and W. Jønsson, Copenhagen.
- 70.2 **Møllmann, H.**, 1970. 'Analysis of shallow cables. *Bygningsstatistiske Meddelelser*, **41**, No. 3.
- 70.3 **Ostenfeld, Chr., A.G. Frandsen, J.J. Jessen and G. Haas**, 1970. *Motorway Bridge across Lillebælt — Publication III: Design and Construction of the Bridge*, Chr. Ostenfeld and W. Jønsson, Copenhagen.
- 71.1 **Birdsall, B.**, 1971. 'Main cable of Newport Suspension Bridge', *J. Struct. Div.*, ASCE, **97**.
- 71.2 **O'Connor, C.**, 1971. *Design of Bridge Superstructures*. John Wiley, New York.
- 71.3 **Scanlan, R.H. and Tomko, J.J.**, 1971. 'Airfoil and Bridge Deck Flutter Derivatives', *Journal Eng. Mech. Div.*, ASCE, Vol. 97, pp. 1717–1737.
- 72.1 **Borelly, W.**, 1972. 'Nordbrücke Mannheim-Ludwigshafen', *Der Bauingenieur*, Heft 8, 9.
- 72.2 **Leonhardt, F. and W. Zellner**, 1972. 'Vergleiche zwischen Hängebrücken und Schrägkabelbrücken für Spannweiten über 600 m', *IVBH Abhandlungen, Band 32, Zürich*.

- 72.3 **Thul, H.**, 1972. 'Entwicklungen im Deutschen Schrägseil-brückenbau', *Der Stahlbau*, **6**, 7.
- 73.1 **Leonhardt, F. and J. Schlaich**, 1973. 'Vorgespannte Seilnetzkonstruktionen — Das Olympiadaach in München', *Der Stahlbau*, **3**.
- 74.1 **Andrä, W. and R. Saul**, 1974. 'Versuche mit Bündeln aus parallelen Drähten und Litzen für die Nordbrücke Mannheim-Ludwigshafen und das Zeltdach in München', *Die Bautechnik*, **9–11**.
- 75.1 **Hjorth-Hansen, E and Magnar Sigbjörnsson**, 1975. 'Aerodynamic stability of box girders for the proposed Strömstein Bridge', *Div. Struct. R. Mech. Norwegian Institute of Technology, Trondheim*.
- 75.2 **Irvine, H.M.**, 1975. 'Statics of suspended cables', *J. Eng. Mech. Div. ASCE*, August.
- 75.3 **Krishnaswamy, T.N. et al.**, 1975. 'Model observations of interference effects on oscillatory response on two identical stacks', *Proc. 4th Int. Conf. on Wind Effects on Buildings and Structures, Heathrow*.
- 76.1 **Brown, W.G., F. Parsons and H.S.G. Knox**, 1975, 1976. 'Bosporus Bridge', *Proc. Instn. Civ. Engrs.*, Nov. 1975, Aug. 1976.
- 76.2 **Gimsing, N.J.**, 1976. 'Multispan stayed girder bridges', *J. Struct. Div., ASCE*, October.
- 76.3 **Gimsing, N.J.**, 1976. *Skråstøtsbroer, Afdelingen for Bæende Konstruktioner*, DTH.
- 76.4 Honshu-Shikoku Bridge Authority, 1976. 'An outline of the Honshu-Shikoku Bridge Project'.
- 76.5 **Podolny, W. and J.B. Scalzi**, 1976. *Construction and Design of Cable-stayed Bridges*, John Wiley, New York.
- 76.6 **Weitz, F.R.**, 1976. 'Überspannungen aus Stahlseilen-Konstruktionsteilen für den modernen Grossbrückenbau', *Bauingenieur*, 51.
- 77.1 **Heughold, W.M. et al.**, 1977. 'Free vibrations of cable in three dimensions', *J. Struct. Div., ASCE*, **103**, May.
- 77.2 **Troitsky, M.S.**, 1977. *Cable-Stayed Bridges, Theory and Design*, Crosby Lockwood Staples.
- 78.1 **Clark, J.H.**, 1978. 'Relation of erection planning to design', *Cable Stayed Bridges, US Dept. of Transportation, Federal Highway Adm., Structural Engineering Series*, No. 4.
- 78.2 **Graham, H.J.**, 1978. 'Dames Point Bridge', *Cable Stayed Bridges, US Dept. of Transportation, Federal Highway Adm., Structural Engineering Series*, No. 4.
- 78.3 **Hjorth-Hansen, E. and R. Frederiksen**, 1978. 'Wind tunnel tests for the proposed Store Bælt Bridge', *SINTEF Rapport No. STF 71 F 78015*.
- 78.4 **Lin, T.Y. et al.**, 1978. 'Design of Ruck-a-Chucky Bridge', *Cable Stayed Bridges, US Dept. of Transportation, Federal Highway Adm., Structural Engineering Series*, No. 4.
- 78.5 **de Miranda, F.**, 1978. 'I'1 ponte strallato sull' Arno a Firenze in località FIndiano', *Costruziord Metalliche*, No. 6.
- 78.6 **Nogami, K. and F. Itoh**, 1978. 'Der Verlingerungssteifigkeit von Seilen unter Berücksichtigung des Durchhanges', *Mem Faculty Technol. Tokyo Metropolitan University*, No. 28.
- 78.7 **Scanlan, R.H. and R.L. Wardlaw**, 1978, 'Aerodynamic stability of bridge decks and structural members', *Cable Stayed Bridges, US Dept. of Transportation, Federal Highway Adm., Structural Engineering Series*, No. 4.
- 79.1 'The Great Belt Bridge — fatigue tests with cable models, 1st series of tests', *Statsbroen Store Bt*, 1979.
- 79.2 **Leonhardt, F. et al.**, 1979. 'Modellversuche für die Schräg-kabelbrücken Zárate-Brazo Largo über den Rio Parana (Argentinien)', *Bauingenieur*, **54**.
- 79.3 **de Miranda, F. et al.**, 1979. 'Basic problems in long span cable stayed bridges', *Dept. of Structures, University of Calabria, Report No. 25*.
- 79.4 **Modemann, J. and K. Tönnessen**, 1979. 'Die Neue Rhein-brücke Düsseldorf-Flehe/Neuss-Uedesheim', *Bauingenieur*, **54**.
- 80.1 **Frederiksen, R.**, 1980. 'Vindteknisk Vurdering av Lange Smale Hengebroer, ('Evaluation of long and slender suspension bridges exposed to wind'), *SINTEF Report, Trondheim*.
- 80.2 **Gimsing, N.J. and J. Gimsing**, 1980. 'Analysis of erection procedures for bridges with combined cable systems — cable net bridge concept', *ABK Report No. R 128*.
- 81.1 **Irvine, H.M.**, 1981. *Cable Structures*, MIT Press.
- 81.2 **Sofronie, R.**, 1981. 'The V-shaped cable-stayed bridges', *Rev. Roum. Sci Techn. Méc. Appl.*, **26**, Bucarest.
- 81.3 **Tscnemmernegg, F. and A. Obholzer**, 1981. 'Einfach abgespannte Seile bei Schrägseilbrücken', *Bauingenieur*, September.
- 82.1 **Birkenmaier, M. and R. Narayanan**, 1982. 'Fatigue resistance of large high tensile stay tendons', *Proc. IABSE Colloq. on Fatigue of Steel and Concrete Structures, Lausanne*.
- 82.2 **Gimsing, N. J.**, 1982. 'Preliminary design and optimization of cable systems for bridges', *Dialog 1–82, Miscellaneous Papers in Civil Engineering, Danish Engineering Academy*.
- 82.3 Bundesminister für Verkehr, 1982. 'Schäden aus Brücken und Anderen Ingenieurbauwerken', *Verkehrsblatt-Verlag Borgmann, Dortmund*.
- 86.1 Post-Tensioning Institute, 1986. 'Recommendations for Stay Cable Design and Testing', *Post-Tensioning Institute, Phoenix*.
- 86.2 **Roik, K.-H., G. Albrecht and U. Weyer**, 1986. 'Cable-stayed Bridges', *Verlag von Wilhelm Ernst & Sohn, Berlin*.
- 86.3 **Hikami, Y.**, 1986. 'Rain Vibrations of Cables of a Cable-Stayed Bridge', *Journal of Wind Engineering (Japan)*, Vol. 27, pp. 17–28.



- 87.1 **Gimsing, N.J.**, 1987. 'Structural Systems for Multispan Cable Suspended Bridges', *Proceedings of the Sessions at the Structures Congress '87 Related to Bridges and Transmission Line Structures*, ASCE, New York.
- 87.2 **Abdel-Ghaffar, A. M.**, 1987. 'Effects of Three-Dimensionality and Nonlinearity of the Dynamic and Seismic Behaviour of Cable-Stayed Bridges', *Proceedings of the Sessions at the Structures Congress '87 Related to Bridges and Transmission Line Structures*, ASCE, New York.
- 87.3 **Zan, S. J. and R.L. Wardlaw**, 1987. 'Wind Buffeting of Long Span Bridges with Reference to Erection Phase Behaviour', *Proceedings of the Sessions at the Structures Congress '87 Related to Bridges and Transmission Line Structures*, ASCE, New York.
- 87.4 **Gimsing, N. J.**, 1987. 'Parametric Studies of Cable-Stayed Bridges with Extreme Spans', *Proceedings of the International Conference on Cable-Stayed Bridges*, Bangkok.
- 87.5 **Finzi, L., A. Castellani and E. Baseciolla**, 1987. 'Cable Stays to Comply with Runnability Requirements in Long Span Suspension Bridges', *Proceedings of the International Conference on Cable-Stayed Bridges*, Bangkok.
- 87.6 **Como, M., A. Grimaldi and M. Lembo**, 1987. 'On the Static Behaviour of Cable Stayed/Suspension Bridges', *Proceedings of the International Conference on Cable-Stayed Bridges*, Bangkok.
- 87.7 **Yiu, P.K.A. and D.M. Brotton**, 1987. 'Mathematical Modelling of Cable-Stayed Bridges for Computer Analysis', *Proceedings of the International Conference on Cable-Stayed Bridges*, Bangkok.
- 87.8 **Parvez, S.M., M. Wieland**, 1987. 'Earthquake Behaviour of Proposed Multi-Span Cable-Stayed Bridge over Jamuna in Bangladesh', *Proceedings of the International Conference on Cable-Stayed Bridges*, Bangkok.
- 87.9 **Fujino, F., Pheinsusom, P. and M. Ito**, 1987. 'Galloping of Cable-Stayed Bridge's Tower with Closely-Spaced Natural Frequencies', *Proceedings of the International Conference on Cable-Stayed Bridges*, Bangkok.
- 87.10 **Combault, J.**, 1987. 'Retensioning the Cable Stays of the Brotonne Bridge', *Proceedings of the International Conference on Cable-Stayed Bridges*, Bangkok.
- 87.11 **Reseigh, C.S. and M.C. Tang**, 1987. 'Construction of the Sunshine Skyway Bridge', *Proceedings of the International Conference on Cable-Stayed Bridges*, Bangkok.
- 87.12 **Yamaguchi, H. et al.**, 1987. 'Design and Construction of the Yokohama Bay Bridge Superstructure', *Proceedings of the International Conference on Cable-Stayed Bridges*, Bangkok.
- 87.13 **Nonaka, K. and M. Sakate**, 1987. 'Design and Erection of the Meiko Nishi Bridge', *Proceedings of the International Conference on Cable-Stayed Bridges*, Bangkok.
- 87.14 **Ohno, S. et al.**, 1987. 'S-curved Cable-Stayed Bridge', *Proceedings of the International Conference on Cable-Stayed Bridges*, Bangkok.
- 87.15 **Christopher, D., R.A.C Freeman and T. Yokoi**, 1987. 'Dao Khanong Cable Stayed Bridge—Construction of the Superstructure', *Proceedings of the International Conference on Cable-Stayed Bridges*, Bangkok.
- 88.1 **Troitsky, M.S.**, 1988. 'Cable-Stayed Bridges, Second Edition', BSP Professional Books.
- 88.2 **Walther, R. et al.**, 1988. 'Cable-stayed Bridges', Thomas Telford, London.
- 91.1 **Gimsing, N.J.**, 1991. 'Cable-Stayed Bridges with Spatial Cable Systems', *Proceedings of the International Symposium for Innovation in Cable-Stayed Bridges*. Fukuoka.
- 91.2 **Virlogeux, M.**, 1991. 'Design and Construction of the Normandy Bridge', *Proceedings of the International Symposium for Innovation in Cable-Stayed Bridges*. Fukuoka.
- 91.3 **Wenzel, H.**, 1991. 'The Keelung Harbour Bridge', *Proceedings of the International Symposium for Innovation in Cable-Stayed Bridges*, Fukuoka.
- 91.4 **Petersen, A. et al.**, 1991. 'Outline Design and Special Studies for a 1200 m Cable-Stayed Bridge', *Proceedings of the International Symposium for Innovation in Cable-Stayed Bridges*. Fukuoka.
- 91.5 **Otsuka, H. et al.**, 1991. 'Fundamental Study for Design and Erection of Partially Anchored Composite Cable-Stayed Bridge with 900 m Center Span Length', *Proceedings of the International Symposium for Innovation in Cable-Stayed Bridges*. Fukuoka.
- 91.6 **Leonhardt, F. and W. Zellner**, 1991. 'Past, Present and Future of Cable-Stayed Bridges', *Proceedings of the Conference on Cable-Stayed Bridges, Recent Developments and their Future*, Yokohama. Elsevier Science Publishers B.V.
- 91.7 **Virlogeux, M.**, 1991. 'Erection of Cable-Stayed Bridges', *Proceedings of the Conference on Cable-Stayed Bridges, Recent Developments and their Future*, Yokohama. Elsevier Science Publishers B.V.
- 91.8 **Taylor, P.R.**, 1991. 'Precast and Composite Concrete Cable-Stayed Bridges', *Proceedings of the Conference on Cable-Stayed Bridges, Recent Developments and their Future*, Yokohama. Elsevier Science Publishers B.V.
- 91.9 **Ohashi, M.**, 1991. 'Cables for Cable-Stayed Bridges', *Proceedings of the Conference on Cable-Stayed Bridges, Recent Developments and their Future*, Yokohama. Elsevier Science Publishers B.V.
- 91.10 **Wyatt, T.A.**, 1991. 'The Dynamic Behaviour of Cable-Stayed Bridges: Fundamentals and Parametric Studies', *Proceedings of the Conference on Cable-Stayed Bridges, Recent Developments and their Future*, Yokohama. Elsevier Science Publishers B.V.

- 91.11 **Abdel-Ghaffar, A. M.**, 1991. 'Cable-Stayed Bridges under Seismic Action', *Proceedings of the Conference on Cable-Stayed Bridges, Recent Developments and their Future*, Yokohama. Elsevier Science Publishers B.V.
- 91.12 **Wardlaw, R.L.**, 1991. 'Cable Supported Bridges under Wind Action', *Proceedings of the Conference on Cable-Stayed Bridges, Recent Developments and their Future*, Yokohama. Elsevier Science Publishers B.V.
- 91.13 **Miyata, T.**, 1991. 'Design Considerations for Wind Effects on Long-Span Cable-Stayed Bridges', *Proceedings of the Conference on Cable-Stayed Bridges, Recent Developments and their Future*, Yokohama. Elsevier Science Publishers B.V.
- 91.14 **Tang, M.-C.**, 1991. 'Cable-Stayed Bridges in North America', *Proceedings of the Conference on Cable-Stayed Bridges, Recent Developments and their Future*, Yokohama. Elsevier Science Publishers B.V.
- 91.15 **Ito, M.**, 1991. 'Cable-Stayed Bridges in Japan', *Proceedings of the Conference on Cable-Stayed Bridges, Recent Developments and their Future*, Yokohama. Elsevier Science Publishers B.V.
- 91.16 **Takuwa, I. et al.**, 1991. 'Prestressed Concrete (PC) Cable-Stayed Bridge Constructed on an Expressway — the Tomei Ashigara Bridge', *Proceedings of the Conference on Cable-Stayed Bridges, Recent Developments and their Future*, Yokohama. Elsevier Science Publishers B.V.
- 91.17 **Maeda, K., A. Otsuka and H. Takano**, 1991. The Design and Construction of the Yokohama Bay Bridge', *Proceedings of the Conference on Cable-Stayed Bridges, Recent Developments and their Future*, Yokohama. Elsevier Science Publishers B.V.
- 92.1 'Guidelines for the Design of Cable-Stayed Bridges', ASCE, New York.
- 92.2 **Ostenfeld, K.H. and A. Larsen**, 1992. 'Bridge Engineering and Aerodynamics', *Proceedings of the First International Symposium on Aerodynamics of Large Bridges*, Copenhagen. A. A. Balkema Publishers.
- 92.3 **Scanlan, R.H.**, 1992. 'Wind Dynamics of Long-Span Bridges', *Proceedings of the First International Symposium on Aerodynamics of Large Bridges*, Copenhagen. A. A. Balkema Publishers.
- 92.4 **Wardlaw, R.L.**, 1992. The Improvement of Aerodynamic Performance', *Proceedings of the First International Symposium on Aerodynamics of Large Bridges*, Copenhagen. A. A. Balkema Publishers.
- 92.5 **Ito, M.**, 1992. 'Wind Engineering of Large Bridges in Japan', *Proceedings of the First International Symposium on Aerodynamics of Large Bridges*, Copenhagen. A. A. Balkema Publishers.
- 92.6 **Hjorth-Hansen, E.**, 1992. 'Section Model Tests', *Proceedings of the First International Symposium on Aerodynamics of Large Bridges*, Copenhagen. A. A. Balkema Publishers.
- 92.7 **Davenport, A.G., J.P.C. King and G.L. Larose**, 1992. Taut Strip Model Tests', *Proceedings of the First International Symposium on Aerodynamics of Large Bridges*, Copenhagen. A. A. Balkema Publishers.
- 92.8 **Irwin, P. A.**, 1992. 'Full Aeroelastic Model Tests', *Proceedings of the First International Symposium on Aerodynamics of Large Bridges*, Copenhagen. A. A. Balkema Publishers.
- 92.9 **Smitt, L.W. and M. Brinch**, 1992. 'A New Boundary Layer Wind Tunnel at the Danish Maritime Institute', *Proceedings of the First International Symposium on Aerodynamics of Large Bridges*, Copenhagen. A. A. Balkema Publishers.
- 92.10 **Virlogeux, M.**, 1992. 'Wind Design and Analysis for the Normandy Bridge', *Proceedings of the First International Symposium on Aerodynamics of Large Bridges*, Copenhagen. A. A. Balkema Publishers.
- 92.11 **Miyata, T. et al.** 'Wind Effects and Full Model Wind Tunnel Tests', *Proceedings of the First International Symposium on Aerodynamics of Large Bridges*, Copenhagen. A. A. Balkema Publishers.
- 92.12 **Muller, J.**, 1992. 'The Bi-Stayed Bridge Concept: Overview of Wind Engineering Problems', *Proceedings of the First International Symposium on Aerodynamics of Large Bridges*, Copenhagen. A. A. Balkema Publishers.
- 92.13 **Larsen, A. and S. Jacobsen**, 1992. 'Aerodynamic Design of the Great Belt East Bridge', *Proceedings of the First International Symposium on Aerodynamics of Large Bridges*, Copenhagen. A. A. Balkema Publishers.
- 92.14 **Gimsing, N.J.**, 1992. 'Large Bridges of the Future', *Proceedings of the First International Symposium on Aerodynamics of Large Bridges*, Copenhagen. A. A. Balkema Publishers.
- 92.15 **Brancaleoni, F.**, 1992. 'The Construction Phase and its Aerodynamic Issues', *Proceedings of the First International Symposium on Aerodynamics of Large Bridges*, Copenhagen. A. A. Balkema Publishers.
- 92.16 **Der Kiureghian, A. and Neuenhofer, A.**, 1992. 'Response Spectrum Method for Multi-Support Seismic Excitations', *Earthquake Engineering and Structural Dynamics*, Vol. 21, Issue 8, pp. 713–740.
- 93.1 **Jensen, G. and J. Jensen**, 1993. 'Asky Bridge. Erection of Suspended Superstructure', *Bygningsstatistiske Meddelelser*, **64**, No. 3–4.
- 93.2 **Morbech, K.B. and M.F. Olsen**, 1993. TParameterstudier af skråstagsbroer (Parametric studies of cable-stayed bridges)' (in Danish), Dept. of Struct. Eng., Techn. Univ. of Denmark
- 93.3 **Fujino, Y. et al.**, 1993. 'Synchronization of Human Walking Observed During Lateral Vibration of a Congested Pedestrian Bridge', *Earthquake Engineering and Structural Dynamics*, Vol. 22, Issue 9, pp. 741–758.
- 94.1 **Mathivat, J.**, 1994. 'Les ponts a câbles des origines a la conquête des grandes portées', *Proceedings of the Conference of Cable-Stayed and Suspension Bridges*. Deauville.

- 94.2 **Endo, T., K. Tada and H. Ohashi**, 1994. 'Development of Suspension Bridges — Japanese Experience with Emphasis on the Akashi Kaikyo Bridge', *Proceedings of the Conference of Cable-Stayed and Suspension Bridges*. Deauville.
- 94.3 **Jensen, G., A. Vangsn, J. Jensen**, 1994. 'Erection of the Steel Structure for the Askøy Suspension Bridge, Norway', *Proceedings of the Conference of Cable-Stayed and Suspension Bridges*. Deauville.
- 94.4 **Beard, A.S., C.K. Lau**, 1994. 'The Lantau Fixed Crossing', *Proceedings of the Conference of Cable-Stayed and Suspension Bridges*. Deauville.
- 94.5 **Jørgensen, G.R., L. Pettersson, A. Petersen and E.Y. Andersen**. 'Höga Kusten Bridge, Sweden', *Proceedings of the Conference of Cable-Stayed and Suspension Bridges*. Deauville.
- 94.6 **Flint, A.** 'The Strengthening and Refurbishment of the Severn Suspension Bridge, *Proceedings of the Conference of Cable-Stayed and Suspension Bridges*. Deauville.
- 94.7 **Howells, J., J. Bell and R. Hornby**, 1994. 'The Rhine Bridge at Köln-Rodenkrchen — Widening and Reconstruction of an Existing Suspension Bridge', *Proceedings of the Conference of Cable-Stayed and Suspension Bridges*. Deauville.
- 94.8 **Taylor, P.**, 1994. 'Composite Cable-Stayed Bridges', *Proceedings of the Conference of Cable-Stayed and Suspension Bridges*. Deauville.
- 94.9 **Svensson, H. and T.G. Lovett**, 1994. 'The Twin Cable-Stayed Baytown Bridge', *Proceedings of the Conference of Cable-Stayed and Suspension Bridges*. Deauville.
- 94.10 **Maury, Y., J. Macfarlane, D. Mizon and A. Yeoward**, 1994. 'Some Aspects of the Design of Second Severn Crossing Cable-Stayed Bridge', *Proceedings of the Conference of Cable-Stayed and Suspension Bridges*. Deauville.
- 94.11 **Arzoumanidis, S.G. and M. Kunihiro**, 1994. 'The Karnali River Bridge', *Proceedings of the Conference of Cable-Stayed and Suspension Bridges*. Deauville.
- 94.12 **Saul, R., T.G. Lovett and S. Hopf**, 1994. 'The Kap Shui Mun Bridge at Hong Kong', *Proceedings of the Conference of Cable-Stayed and Suspension Bridges*. Deauville.
- 94.13 **Enomoto, M. et al.**, 1994. 'Design and Study of the Tsurumi Fairway Bridge', *Proceedings of the Conference of Cable-Stayed and Suspension Bridges*. Deauville.
- 94.14 **Gimsing, N.J.**, 1994. 'Suspended Bridges with very Long Spans', *Proceedings of the Conference of Cable-Stayed and Suspension Bridges*. Deauville.
- 94.15 **Lacroix, E. et al.**, 1994. '3000 Metres. We Can Make It!', *Proceedings of the Conference of Cable-Stayed and Suspension Bridges*. Deauville.
- 94.16 **Castellani, A.**, 1994. 'The Project for the Bridge Over the Messina Strait', *Proceedings of the Conference of Cable-Stayed and Suspension Bridges*. Deauville.
- 94.17 **Walther, R. and D. Amsler**, 1994. 'Hybrid Suspension Systems for very Long Bridges: Aerodynamic Analysis and Cost Estimates', *Proceedings of the Conference of Cable-Stayed and Suspension Bridges*. Deauville.
- 94.18 **Larsen, S.V. and N, J. Gimsing**, 1994. 'Static and Dynamic Behaviour of Cable Supported Bridges with Small Width-to-Span Ratios', *Proceedings of the Conference of Cable-Stayed and Suspension Bridges*, Deauville.
- 94.19 **Flamand, O.**, 1994. 'Rain-Wind Induced Vibration of Cables', *Proceedings of the Conference of Cable-Stayed and Suspension Bridges*, Deauville.
- 94.20 **Miyata, T., H. Yamada and T. Hojo**, 1994. 'Aerodynamic Response of PE Stay Cables with Pattern-Indented Surface', *Proceedings of the Conference of Cable-Stayed and Suspension Bridges*, Deauville.
- 94.21 **Saito, T., Matsumoto, M. and Masahiko, K.**, 1994. 'Rain-Wind Excitation of Cables on Cable-Stayed Higashi-Kobe Bridge and Cable Vibration Control', *Proceedings of the Conference of Cable-stayed and Suspension Bridges*, (Vol.2), Deauville.
- 95.1 **Saeki, S. et al.**, 1995. 'Technology Aspects of the Akashi Kaikyo Bridge', *Proceedings of ASCE Congress XIII*, Boston
- 95.2 **Feng, M.R.**, 1995. 'Modern Suspension Bridges in China', *Proceedings of ASCE Congress XIII*, Boston.
- 95.3 **Tang, M.C.**, 1995. 'Multispan Cable-Stayed Bridges', *Proceedings of ASCE Congress XIII*, Boston.
- 95.4 **Podolny, W.**, 1995. 'Current Corrosion Protection Methods for Cable Stays', *IABSE Symposium: Extending the Lifespan of Structures*. San Francisco.
- 95.5 **Yuanpei, L.**, 1995. 'The Yangpu Bridge', *Proceedings of the International Bridge Conference: Bridges into the 21st Century*, Hong Kong.
- 95.6 **Beard, A.S. and Young, J.S.**, 1995. 'Aspects of the Design of the Tsing Ma Bridge', *Proceedings of the International Bridge Conference: Bridges into the 21st Century*, Hong Kong.
- 95.7 **Hunter, I.E.**, 1995. 'Tsing Ma Bridge — Superstructure Construction and Engineering Aspects', *Proceedings of the International Bridge Conference: Bridges into the 21st Century*, Hong Kong.
- 95.8 **Saul, R., T.G. Lovett and S. Hopf**, 1995. *Proceedings of the International Bridge Conference: Bridges into the 21st Century*, Hong Kong.
- 95.9 **Bergermann, P. et al.**, 1995. 'The Design of the Ting Kau Cable Stayed Bridge in Hong Kong', *Proceedings of the International Bridge Conference: Bridges into the 21st Century*, Hong Kong.

- 95.10 **Ostenfeld, K. H., A. Petersen and T. Forsberg**, 1995. 'Suspension Bridge Development Trends Based on Little Belt, Great Belt, Høga Kusten Bridge and the Gibraltar Crossing', *Proceedings of the International Bridge Conference: Bridges into the 21st Century*, Hong Kong.
- 95.11 **Pedersen, C.**, 1995. 'Construction of Superstructure of the Høga Kusten Bridge—Suspension Bridge in Sweden with a 1210 m Main Span', *Proceedings of the International Bridge Conference: Bridges into the 21st Century*, Hong Kong.
- 95.12 **Svensson, H.S. and T.G. Lovett**, 1995. 'The Twin Cable-Stayed Baytown Bridge', *Proceedings of the International Bridge Conference: Bridges into the 21st Century*, Hong Kong.
- 95.13 **Fletcher, M.S., Y. Maury and D.H. Mizon**, 1995. 'A New Crossing of the Severn', *Proceedings of the International Bridge Conference: Bridges into the 21st Century*, Hong Kong.
- 95.14 **Fuzier, J.-P.**, 1995. 'Long Stay Cables—Installation Technology for Easy Maintenance', *Proceedings of the International Bridge Conference: Bridges into the 21st Century*, Hong Kong.
- 95.15 **Kashima, S. et al.**, 1995. 'Design and Erection of Cables on the Akashi Kaikyo Bridge', *Proceedings of the International Bridge Conference: Bridges into the 21st Century*, Hong Kong.
- 95.16 **Jennings, A. and M. Aberle**, 1995. 'A Study of Cable Configurations to Support Multispan Bridges', *Proceedings of the International Bridge Conference: Bridges into the 21st Century*, Hong Kong.
- 95.17 **Brown, W.C. and Craig, S.**, 1995. 'Recent Developments in Deck Design of Suspension Bridges', *Proceedings of the International Bridge Conference: Bridges into the 21st Century*, Hong Kong.
- 95.18 **Lang, A.**, 1995. 'Current and Future-Bridge Cable Options', *Proceedings of the International Bridge Conference: Bridges into the 21st Century*, Hong Kong.
- 95.19 **Bogunovic Jakobsen, J.**, 1995. 'Fluctuating Wind Load and Response of a Line-Like Engineering Structure with Emphasis in Motion-Induced Wind Forces', PhD Thesis, The Norwegian Institute of Technology, Trondheim, Norway.
- 95.20 **Honda, A., Yamanaka, T., Fujiwara, T. and Saito, T.**, 1995. 'Wind Tunnel Test on Rain-Induced Vibration of the Stay-Cable', in *Proceedings of the International Symposium on Cable Dynamics*, Liège, Belgium.
- 95.21 **Flamand, O.**, 1995. 'Rain-Wind Induced Vibration of Cables', *Journal of Wind Engineering and Industrial Aerodynamics*, Vol. 57, Issue 2–3, pp. 353–362.

# Index

- Aerodynamic admittance, 530  
Aerodynamic countermeasures, 550, 551–553  
Aerodynamic damping, 530, 547, 548, 557  
Air-spinning method, 37, 47, 55, 58, 68, 70, 97, 413, 414, 475  
Akashi Kaikyo Bridge, 49, 50, 68, 69, 72, 82, 84, 89, 101, 110, 190, 292, 293, 380, 381, 420, 421, 438, 441, 465, 467, 472, 474, 481, 482, 493–495, 542  
Alex Fraser Bridge, 52, 53, 58, 59, 84, 312, 313, 384, 386, 504  
Alamillo Bridge, 61–62, 70  
Albert Bridge, 8, 9  
Ammann O.H., 15, 520  
Anchor block, 1, 3, 4, 8, 16, 27, 45, 55, 56, 67, 68, 70, 73, 77, 80, 104, 118, 148, 179, 188, 190–195, 199, 200, 236, 239, 257, 260, 261, 291, 341, 346, 348, 350, 351, 413, 452–461, 463, 470–473, 476, 478, 479, 481, 482, 489  
Anchor cable, 2–4, 63, 71, 72, 131, 174, 175, 176, 188, 202–208, 211, 213–215, 217–220, 225, 233, 242, 243, 249, 250, 260, 261, 263, 289, 298–301, 340, 341, 360, 361, 363, 365, 381, 388, 399, 426  
Askøy Bridge, 60, 61, 95, 198, 473, 500, 501  
A-shaped pylon, 6, 28, 29, 51, 60, 369, 370, 389–395, 396  
Asymmetric mode, 157–159, 161, 280
- Bar cables, 93, 94  
Barrios de Luna Bridge, 50, 84, 512  
Benjamin Franklin Bridge, 84, 456  
Bisan Seto Bridges, 55, 56, 88, 100, 196, 197, 239, 257, 335, 336, 380, 436, 437, 451, 457, 465  
Bosporus Bridge, 41, 42, 47, 58, 70, 100, 189, 198, 321, 322, 408–409, 465, 466, 481  
Bratislava Bridge, 210, 211  
Bronx–Whitestone Bridge, 19, 20, 23, 456, 518  
Brooklyn Bridge, 10–12, 15, 23, 24, 84, 103, 190, 191, 235–238  
Brotonne Bridge, 44, 52, 316, 317, 428, 556, 557  
Buffeting, 526–531, 544, 550, 557
- Cable band, 95, 97, 152, 153, 439, 490  
Cable net system, 222  
Cable saddle, 97, 149, 155–157, 382, 446, 448–451, 484  
Cable steel, 8, 66, 85, 86, 110, 111, 118, 139, 141, 148, 165–167, 169–172, 181–185, 188, 193, 206–210, 217–219, 221, 229, 231, 236, 247–249, 258, 260, 263, 264, 346–348, 366  
Cable vibrations, 343, 544–546, 548, 551, 557  
Carmody Board, 520  
Catenary, 127, 135–137, 139, 143–146, 289  
Catwalk, 261, 467, 472–475, 479–482, 485, 492, 496  
Central clamp, 152, 153, 162, 163, 193–197, 236, 247, 283, 284, 293, 498  
Centring device, 195, 236, 295  
Chain bridge, 22, 49  
Chao Phraya Bridge, 54–55  
Cincinnati–Covington Bridge, 10  
Clairborne Pell Bridge (Newport Bridge), 37–38  
Clark Bridge, 63, 64  
Clifton Suspension Bridge, 8  
Construction, 4, 8, 10, 11, 15, 17, 21–24, 30, 34, 35, 37, 38, 40, 41, 45, 48, 49, 51, 52, 55, 58, 60, 61, 65–67, 70, 73, 75, 77–79, 81, 83, 85, 88, 97, 100, 104, 106, 109, 185, 200–202, 216, 235, 239, 244, 255, 260, 261, 272–275, 300, 310, 327, 349, 353, 357, 358, 363, 373, 386, 396, 405, 409, 452, 463, 465, 466, 468–470, 473, 474, 488–491, 494, 495, 497, 502, 503, 505, 507–509, 511–513, 517, 519, 531, 536–538, 541, 557, 569, 571, 573  
Corrosion protection, 7, 44, 46, 87, 89, 93, 97, 102–109, 139, 209, 316, 421, 461  
Coupled flutter, 520, 524, 526  
Cross-ties, 221, 222, 557, 558
- Danube Canal Bridge, 37  
Davenport wind spectrum, 528, 529  
Dehumidification, 40, 69, 97, 104, 449, 458, 461  
Dischinger F., 24, 239

- Divergence speed, 523, 524  
 Drag instability, 547  
 Dry galloping, 544–546, 548  
 Dryburgh Abbey Bridge, 517, 518  
 Duisburg–Neuenkamp Bridge, 84  
 Duisburg–Ruhrort Bridge, 26–27  
 Düsseldorf–Neuss Bridge, 46  
 Dynamic behaviour, 22, 157, 158, 161, 324–327, 519, 538  
  
 Earthquake intensity, 569  
 Emmerich Bridge, 200, 333, 334  
 End link, 292, 293, 298, 300  
 Equivalent modulus of elasticity, 139–141, 221, 222, 261  
 Erasmus Bridge, 66  
 Erskine Bridge, 40, 95, 315, 316  
  
 Fan system, 2, 3, 25, 27, 66, 165, 167–172, 174–176, 201, 202, 204, 209, 210, 214, 216–218, 221, 223, 225–227, 229, 231, 233, 237–239, 249, 257, 269, 284, 364, 369, 370, 376, 384, 394, 399, 403, 442, 443, 501, 535  
 Farø Bridge, 51, 52, 107, 219, 220, 296, 297, 316, 317, 394, 395, 424, 445, 466, 470, 508–510  
 Fatigue strength, 44, 111, 420, 445  
 Fatih Sultan Mehmet Bridge, 58, 100, 189  
 Firth of Forth Road Bridge, 31, 33, 34, 380, 458, 475, 493, 538  
 Flehe Bridge, 46  
 Flutter derivatives, 524, 526, 527  
 Flutter velocity, 520, 524, 537  
 Forth Rail Bridge, 31–34, 82, 380, 458, 475, 482, 493, 538  
 Frandsen A.G., 520, 524  
 Fred Hartman Bridge, 63–65, 395  
 Freyssinet anchor, 421, 422  
 Friedrich Ebert Bridge, 35–37, 315  
 Fyksesund Bridge, 520, 521  
  
 George Washington Bridge, 15–19, 29, 31, 37, 190, 282  
 Gibraltar Strait Bridge, 246  
 Golden Gate Bridge, 16–20, 23, 30, 31, 84, 98, 192, 193, 310, 380, 382, 434, 435, 482, 518  
 Grand Pont Suspendu, 8, 84  
 Grant A, 45  
  
 Harp system, 2, 3, 38, 59, 165, 168–171, 176, 177, 222–234, 242, 285, 288, 289, 357, 365–367, 370, 377, 385, 403, 507  
 Helical Bridge Strands, 39, 85  
 HiAm socket, 41, 415, 417, 420  
 Higashi Kobe Bridge, 62, 234, 235, 333–335, 385, 387, 553  
 Hitsuishijima Bridge, 56, 57, 109, 509  
 Höga Kusten Bridge, 67, 77, 449, 450, 490, 491  
 Homberg H., 35, 54  
 Hukacho Bridge, 575  
 Humber Bridge, 46, 47, 58, 70, 77, 84, 190, 198, 321, 322, 377, 379, 384, 461, 465, 468, 474, 478, 483, 537, 538  
 Hysteresis of Helical strands, 35, 113–115, 198  
  
 Inclined hangers, 35, 47, 58, 113, 114, 198, 199, 201, 436, 474  
 Inclined pylon, 210, 211, 391, 396, 398  
 Indiano Bridge, 45  
 Innoshima Bridge, 49–51, 484  
 Intermediate supports, 3, 38, 55, 63, 68, 73, 79, 161, 176, 177, 219, 226, 227, 231, 232, 234, 309, 506–508  
 Irvine H.M., 158, 554  
 Iwagurojima Bridge, 56, 57, 74, 109  
  
 Jiangdong Bridge, 79, 80  
 Jiangyin Bridge, 71, 72  
 Joint acceptance function, 530  
  
 Kanmonkyo Bridge, 89  
 Kap Shui Mun Bridge, 68, 69, 74, 338, 546  
 Katsushika Harp Bridge, 53, 54, 540  
 Knie Bridge, 38, 39, 84, 232, 312, 313, 372, 373  
 Köhlbrand Bridge, 41–43, 52, 63, 105, 106, 299, 300, 318, 396, 397  
 Konaruto Bridge, 257  
 Konohana Bridge, 200–202  
 Kurushima Kaikyo Bridge, 73, 104  
 Kvarnsund Bridge, 60, 61, 84, 319, 320  
  
 Leonhardt F., 45, 46, 199, 200, 566  
 Leverkusen Bridge, 32, 33, 38, 95, 231, 232  
 Lillebælt Bridge, 39, 40, 86, 95–97, 193, 196, 283, 284, 294, 322, 323, 382, 383, 410, 411, 448, 449, 460, 461, 470, 471, 497–499, 544  
 Local oscillations, 284, 285, 535, 556  
 Locked-coil strands, 32, 35, 42, 54, 60, 87, 88, 95, 96, 98, 101, 102, 105, 106, 421, 445  
 London Millennium Bridge, 75, 76, 190, 559, 568  
 Ludwigshafen Bridge, 41, 178, 513, 514  
  
 Mackinac Bridge, 23, 24, 31, 37, 49, 496  
 Manhattan Bridge, 13, 15  
 Mannheim–Ludwigshafen Bridge, 41  
 Maracaibo Bridge, 29, 30, 106, 250, 254, 318, 319, 428, 429  
 Mariánský Bridge, 70, 71  
 Mechanical damping, 553  
 Meiko Nishi Bridge, 51, 391, 393, 545  
 Menai Bridge, 7, 84  
 Messina Strait Bridge, 22, 23, 83, 110, 325, 326  
 Millau Viaduct, 78, 252, 253, 399, 401, 513, 515  
 Miranda F. de, 46  
 Modified fan system, 364, 370, 377, 391  
 Mono-strand cable, 43, 88, 106, 218, 421, 423, 429, 444, 487  
 Moisseif L.S., 13, 16, 18, 519  
 Morandi R., 29, 30, 37  
 Multi-cable system, 4, 24, 35, 36, 40, 41, 44, 45, 88, 112, 169, 170, 218, 219, 268, 284, 288, 289, 294, 295, 303, 307, 427, 430, 433, 442, 444, 504  
 Multi-span bridges, 244, 246, 399  
 Multi-strand cable, 4, 94, 95

- Nanpu Bridge, 60, 63  
 Napoleon Bonaparte Broward Bridge (Dames Point Bridge), 59, 233, 314, 403, 404  
 Navier, C.L., 24, 25  
 Neuweid Bridge, 400  
 New PWS cables, 90, 91, 101, 102, 106  
 Niagara Bridge, 9  
 Nordereibe Bridge, 30–32, 98, 106, 368  
 Normandy Bridge, 65, 66, 72, 76, 84, 93, 275, 298, 299, 324, 325, 371, 396, 403, 422, 425, 426, 445, 447, 487, 488, 508, 509, 510, 552, 558  
 Novi Sad Bridge, 486
- Oberkasseler Bridge, 176, 177, 298, 316  
 Ohmishima Bridge, 57, 198, 322, 323  
 Ohnaruto Bridge, 50, 51, 55, 89  
 Ohshima Bridge, 57, 198, 322, 323  
 Øresund Bridge, 73, 74, 113, 114, 234, 235, 339, 340, 373–374, 411, 431, 445, 446, 468, 488, 503, 534, 544, 552, 553, 555, 573–575  
 Ostenfeld C., 39
- Papineau Bridge, 38, 39  
 Parallel-strand cable, 91–93, 101, 108, 112, 420, 425, 426, 487  
 Parallel-wire strand, 37, 38, 46, 87–90, 97, 100, 106–108, 114, 415, 419, 424, 445, 481, 485  
 Partially earth anchored systems, 339–351  
 Pasco–Kennewick Bridge, 45, 59, 108, 320, 321, 376, 442, 443, 510, 511  
 Pedestrian-induced vibrations, 559  
 Pipeline bridge at Barbara, 272, 273  
 Pylon, 1–4, 6, 8, 11, 15, 19, 23–33, 35, 40–42, 45–48, 50–53, 55, 57–63, 65–68, 70–74, 76, 77, 79, 81, 82, 84, 97, 104, 118, 124, 125, 148, 154, 161, 171–176, 178–180, 182, 184, 185–190, 192–194, 199, 200, 202–219, 221–225, 227–231, 233, 234, 236, 238, 239, 241–265, 268–271, 274, 277–280, 282–285, 287, 289, 291–299, 302, 310, 316, 326–328, 340–351, 353–411, 434, 442–449, 451, 463–474, 480–482, 486–490, 492–494, 496, 497, 499, 502–506, 508–510, 513–515, 519, 520, 533, 538, 540–544, 550, 551, 569–572, 574, 577, 578
- Rainbow Bridge, 463, 464, 542  
 Rain-wind-induced vibrations, 545, 546, 550, 552, 553  
 Rama VIII Bridge, 88, 396, 398  
 Rama IX Bridge, 54, 63  
 Record spans, 84  
 Reduced velocity, 526, 532, 541, 548, 550  
 Rees Bridge, 36  
 Rein chord system, 26, 27  
 Reynolds number, 534, 540, 546–548, 551, 552, 557  
 Rion Antirion Bridge, 77, 403, 570–572  
 Roberts G., 34  
 Roebing J.A., 8  
 Rokko Bridge, 43, 44, 333, 334, 377, 378, 502  
 Runyang Suspension Bridge, 78, 322
- Saale River Bridge, 517  
 St Nazaire Bridge, 42, 84  
 San Francisco–Oakland Bridge, 16, 55, 56, 239–241, 260, 331, 377  
 Save Bridge, 463, 519  
 Scaling, 533, 536, 537  
 Scanlan R.H., 524  
 Scruton number, 549, 550  
 Secant modulus, 131, 138–140  
 Second Bosphorus Bridge, 58, 70, 100, 189, 198, 481  
 Second Nanjing Bridge, 76  
 Second Severn Bridge, 108, 314  
 Second Tacoma Bridge, 21, 23, 24, 31, 49  
 Seismic design, 568, 569  
 Selberg A., 22, 518, 520, 524  
 Self-anchored system, 4, 5  
 Seven-wire strand, 44, 85, 86, 91–93, 102, 109, 420–422, 444, 486–488  
 Severins Bridge, 28–30, 38, 84, 95, 389–390, 506, 507  
 Severn Bridge, 34, 35, 39, 41, 47, 58, 97, 99, 108, 113–115, 198, 199, 314, 321, 322, 408, 436, 440, 452, 454, 497–500, 542, 575, 576  
 Shantou Bridge, 66, 67  
 Shimotsui Seto Bridge, 55, 100, 481  
 Snow and ice removal and prevention, 575  
 Socket, 18, 41, 87, 100, 101, 105, 109, 150, 301, 413, 416–421, 423, 429, 438, 439, 444, 452, 454, 461, 481, 487  
 Speyer Bridge, 370  
 Spinning wheel, 38, 475, 477–482  
 Splay chamber, 452, 457–461  
 Stability of cable system, 173–179  
 Steinman D.B., 12, 22, 23  
 Stonecutters Bridge, 79–81, 127, 326, 328, 369, 388, 425, 510, 511, 540, 542, 543, 552, 553, 570  
 Storebælt Bridge, 336, 476, 477, 497, 525, 531–533, 538, 539, 542, 544, 545, 553, 554, 575, 577  
 Strand shoe, 148, 413–415, 449, 452–454, 475, 477, 480, 481  
 Strömsund Bridge, 25–27, 37, 84, 94, 97, 218, 343, 358, 359  
 Structural health monitoring, 573  
 Sunshine Skyway Bridge, 52, 53, 59, 557  
 Sutong Bridge, 79, 81, 84, 343, 396, 505, 570  
 Symmetric mode, 157–161, 280, 282, 283, 285  
 Synchronous lateral excitation, 75, 559
- Tacoma Narrows Bridge, 18, 20, 517–520, 533, 542, 543  
 Tancarville Bridge, 27, 28, 31, 39, 95, 96, 194, 331, 332, 439, 441, 485  
 Tangent modulus, 101, 130, 131, 138–140, 261, 278  
 Tatara Bridge, 72, 73, 76, 84, 324, 325  
 Tay Bridge, 517, 518  
 Temposan Bridge, 394, 396  
 Theodor Heuss Bridge, 27, 29, 30, 84, 95, 365, 372, 510  
 Ting Kau Bridge, 71, 242, 243  
 Tjörn Bridge, 48, 49, 430, 510  
 Torsional divergence, 520  
 Torsional oscillation, 19, 35, 280, 281, 285, 524  
 Train loads, 70, 113, 114, 295, 335, 339

- Triangular pylon, 30, 246, 250–257, 262, 263, 399–401, 403  
Tsing Lung Bridge project, 326, 327  
Tsing Ma Bridge, 67, 68, 101, 192, 337, 338, 384–385, 465, 473, 479, 490, 497  
Tsurumi Tsubasa Bridge, 62, 63  
Tuned mass damper, 19, 468, 508, 509, 553, 555, 567  
20th April Bridge (Tagus River Bridge), 33, 34, 50, 190, 191, 196, 436, 482  
  
Verrazano Narrows Bridge, 30–32, 46, 332, 333, 405–407, 415, 436, 437, 454, 457, 463, 464, 475, 482, 496  
Vertical oscillation, 35, 280, 283, 285, 520  
Vibration control, 541, 542, 567  
Vibration serviceability limit state, 531, 562, 565, 574  
Vortex-shedding, 321, 526, 531, 538, 540, 541, 544, 546, 549–551  
V-shaped pylon, 365–367  
  
Wake galloping, 550, 551  
Wheeling Bridge, 8, 11, 84  
Williamsburg Bridge, 12, 13, 15, 18, 24, 84, 338, 339  
Wind-tunnel testing, 523  
Wöhler curve, 111–113  
  
Xihoumen Bridge, 68, 81, 82, 192, 327, 436, 438  
  
Yangpu Bridge, 63, 64, 84, 313, 321  
Yokohama Bay Bridge, 58, 59, 62, 385, 387  
Youngjong Bridge, 74  
  
Zakim Bunker Hill Bridge, 575  
Zarate-Brazo Largo Bridges (Parana Bridges), 46, 89, 90, 106, 107, 284, 319, 320  
Z-shaped wrapping wire, 104